Functional Analysis of the *mrd* Operon in *Salmonella*: Role in Biology and Pathogenicity

Anne Catherine Doble

Thesis submitted in partial fulfilment of the requirements of the regulations for the degree of Doctor of Philosophy (Integrated MRes/PhD)

Newcastle University
Faculty of Medical Sciences
Institute for Cell and Molecular Biosciences

September 2011

Abstract

Salmonella are major food-borne pathogens responsible for causing a broad spectrum of human disease, ranging from mild gastroenteritis to life-threatening systemic disease. We are interested in analysing the function of the putative *mrd* operon in *Salmonella*, whose gene products include PBP2 and RodA; two proteins which are involved in longitudinal cell wall synthesis and essential for rod shape-maintenance in *Salmonella*. Although PBP2 is fairly well described, surprisingly little is known about the function of RodA or the other *mrd* operon proteins.

This study aimed to characterise the *mrd* operon, elucidating its contribution to the biology and pathogenicity of *Salmonella*. Possible links between the structural integrity of the cell wall and the functionality of wall-spanning virulence organelles were also examined. Precise knockout mutations of the *mrd* operon genes were constructed in *Salmonella enterica* serovars Typhi and Typhimurium. A range of subsequent phenotypic analyses have revealed that the round-cell Δ*pbpA* (PBP2) and Δ*rodA* mutants, though viable and able to stably propagate, are defective in the expression of flagella and the *Salmonella* pathogenicity island 1 (SPI-1) type III secretion system (T3SS), although the SPI-2 T3SS remains active. These virulence defects were successfully complemented by expressing the major SPI-1 and flagella regulators *in trans* from inducible promoters. A transposon mutagenesis screen was subsequently developed to search for global regulators of the SPI-1 and motility phenotypes in round-cell mutants. This led to the identification of several candidate regulators, which ongoing work seeks to further analyse. This study has demonstrated that round-cell *mrd* mutants almost completely down-regulate the expression of key invasion-associated virulence genes, although the cell wall in these mutants remains sufficiently robust to enable the assembly and functioning of wall-spanning multi-protein complexes. Collectively these data provide important insights into both the physiological state of *mrd* operon mutants, and the function of *mrd* operon genes.

Acknowledgements

I would firstly like to thank my supervisor Dr Anjam Khan for his continual help, guidance and support throughout this study, which has been invaluable. Thanks also go to my co-supervisors Dr Richard Daniel and Professor Kenn Gerdes.

I would like to thank the other members of the Khan lab, past and present, for their patience, guidance, advice and friendship; in particular Dave Bulmer for his helpful assistance, provision of materials/constructs and help with the microarray work, Sonya Carnell, Michail Karavolos, Lubna Kharraz and Wei Chen for their continued encouragement, and Hannah Spencer for the provision of the Tn*10*d(Tc) lysate.

Considerable thanks go to Joe Gray, and Andrew Grant and Pietro Mastroeni, for their advice and assistance with LC/MS/MS and *in vivo* virulence assays, respectively, to which they dedicated a substantial amount of time.

I would also like to acknowledge our collaborators; Philip Aldridge for providing the TPA14 and Tn*10*d(Tc) phage stocks, Lawrence Rothfield for provision of the YFP-fusion protein constructs, David Holden for kindly donating various antibodies, strains and constructs, and Vassilis Koronakis and Brian Ahmer for providing antibodies and plasmid vectors respectively.

I am extremely grateful also to the Medical Research Council for funding my research.

Particular thanks go to my family, friends and church family for their unwavering love, support and prayers; I am especially thankful to Fran Doble, Joy Doble, Liz Evans, Clare Baker, Lynne Ranson and Ruth Whiteman for their assistance with proofreading.

Finally I am grateful to God, who loved me and gave himself for me, and who has not stopped providing me with everything I need.

Preface

This thesis is my own work and includes nothing which is the outcome of work done in collaboration, except where references are specially made; any work conducted previously, or by others, has been properly acknowledged. No material contained within thesis has been submitted for a degree or diploma or other qualification at this or any other university.

Anne Doble

Table of Contents

List of Figures

List of Tables

Abbreviations

µg	Microgram(s)
µl	Microlitre(s)
µm	Micrometre(s)
µM	Micromolar
A22	S-(3,4-dichlorobenzyl) isothiourea
amp^R	Ampicillin-resistance gene
APS	Ammonium persulphate
Aro	Aromatic amino acid mix
bp	Base pairs
BSA	Bovine serum albumin
c-di-GMP	Bis-(3´-5´)-cyclic dimeric guanosine monophosphate
cDNA	Complementary DNA
CFU	Colony-forming units
Cm^R	Chloramphenicol-resistance gene
DAPI	4',6-diamidino-2-phenylindole
DGC	Diguanylate cyclase
dH_2O	Deionised water
DNA	Deoxyribonucleic acid
DNase	Deoxyribonuclease
EDTA	Ethylenediaminetetraacetate
fmoles	Femtomoles
FRT	FLP recognition target site (238)
g	Gram(s)
H_2O_2	Hydrogen peroxide
HAP	Hook-associated protein
HPLC	High performance liquid chromatography
IFM	Immunofluorescence microscopy
Ig	Immunoglobulin
IPTG	Isopropyl β-D-1-thiogalactopyranoside
kan^R	Kanamycin-resistance gene
kbp	Kilo-base pairs
kDa	Kilodaltons
l	Litre(s)
LB	Luria-Bertani
LC/MS/MS	High-performance liquid chromatography with tandem mass spectrometry
LPS	Lipopolysaccharide
M	Molar

mA	Milliamps
MCS	Multiple cloning site
mg	Milligram(s)
min	Minutes
ml	Millilitre(s)
mM	Millimolar
mrd	*Mur*ein *D* region
mre	*Mur*ein *E* region
mRNA	Messenger RNA
ng	Nanogram(s)
nm	Nanometres
NTS	Non-typhoidal salmonellosis
OD	Optical density
OD600	Optical density at 600nm absorbance
PBP	Penicillin-binding protein
PBS	Phosphate-buffered saline
PCR	Polymerase chain reaction
PDE	Phosphodiesterase
PFA	Paraformaldehyde
pmoles	Picomoles
qPCR	Quantitative real-time RT-PCR
RNA	Ribonucleic acid
RNase	Ribonuclease
rpm	Revolutions per minute
rRNA	Ribosomal RNA
RT-PCR	Reverse transcriptase PCR
SCV	*Salmonella*-containing vacuole
SD	Shine Delgarno sequence
SD	Standard deviation
SDS-PAGE	Sodium dodecyl sulphate-polyacrylamide gel electrophoresis
SEM	Scanning electron microscopy
SEM	Standard error of the mean
SOC	Super optimal broth with catabolite repression
SPI	*Salmonella* pathogenicity island
T1SS	Type 1 secretion system
T3SS	Type 3 secretion system
T6SS	Type 6 secretion system
TAE	Tris-acetate EDTA
TCA	Trichloroacetic acid
TEMED	*N*,*N*,*N*′,*N*′-Tetramethylethylenediamine

Tet^{R}	Tetracycline-resistance gene
Tris	Tris(hydroxymethyl)aminomethane
tRNA	Transfer RNA
Tween®	Polyethylene glycol sorbitan monolaurate
Tyr	Tyrosine mix
UV	Ultra-violet
V	Volts
w/v	weight per volume
w/w	weight per weight
YFP/GFP	Yellow/Green fluorescent protein

Chapter 1. General Introduction

1.1 *Salmonella enterica* as an enteric pathogen

1.1.1 Introduction to *Salmonella enterica*

Salmonella enterica is one of only 2 recognised species of *Salmonella.* It is a Gram-negative bacterial pathogen responsible for widespread disease in humans and animals. The *Salmonella enterica* species itself comprises over 2500 closely related serovars, many of which are responsible for enteric disease, ranging from mild gastroenteritis to life threatening illness (1-4). The major disease-causing serovars in humans include *Salmonella enterica* serovar Typhimurium (*S.* Typhimurium), *S.* Enteritidis, *S.* Typhi and *S.* Paratyphi (4-7).

S. Typhimurium and *S.* Enteritidis generally cause mild self-limiting gastroenteritis in humans, which remains localised to the gut. *Salmonella* is a common cause of gastroenteritis, being responsible for approximately 1.4 million cases annually in the US, for example. Of these cases, approximately 26% are caused by *S.* Typhimurium (4, 8). Aside from gastroenteritis, *S.* Enteritidis, and more commonly *S.* Typhimurium, can also cause a serious systemic infection in an immunocompromised host. This disease is distinct from typhoid fever, being often more serious, invasive and recurrent (9). Systemic non-typhoidal salmonellosis (NTS) disease is increasingly becoming a major problem in parts of sub-Saharan Africa, particularly in AIDS patients, where NTS bacteraemia is associated with a mortality rate of up to 47%. In many countries where HIV infection is particularly prevalent, NTS accounts for the most common cause of bacteraemia (9-11).

Unlike *S.* Typhimurium and *S.* Enteritidis, which have a broad host range and hence retain a large reservoir outside humans, *S.* Typhi and *S.* Paratyphi infections are restricted to humans (4, 12). *S.* Typhi is the major cause of typhoid fever, a serious invasive disease in which the bacteria are able to evade host immune responses and survive inside macrophages, enabling them to spread beyond the gut, through the lymphoid tissues and the blood. Ultimately the bacteria set up a systemic infection in organs such as the liver, spleen and bone marrow. Around 22 million cases of typhoid fever are recorded worldwide, annually.

Of these cases, approximately 200,000 are fatal, although if untreated the fatality rate for typhoid fever is approximately 10-20% (1, 9, 11, 13, 14). A further problem associated with *S.* Typhi infections is the recent emergence of multidrug-resistant strains, which are now prevalent and endemic throughout Asia and South East Asia. A study conducted in 2008 found that of 204 clinical isolates taken from seven South Asian countries where typhoid fever is endemic, 41.2% were multidrug-resistant (resistant to at least 3 antimicrobials) (11, 15-18).

1.1.2 Major virulence determinants of *Salmonella enterica* and mechanisms of pathogenesis

Salmonella infections are acquired through the ingestion of contaminated food or water. In order to establish an infection in the host gut, *Salmonella* deploys a number of important virulence factors, many of which are essential for pathogenesis. Fundamentally, *Salmonella* infections involve the invasion of and survival inside intestinal epithelial cells or M cells. The establishment of a systemic infection is dependent upon intracellular survival and replication within adapted phagosomes, the so-called *Salmonella*-containing vacuoles (SCV), inside intestinal epithelial cells and macrophages (4, 19-21).

Salmonella Type 3 secretion systems (T3SSs)

A number of essential virulence factors have been recognised in *Salmonella*. Two of these encompass pathogenicity islands, each of around 40kb; Salmonella Pathogenicity Island 1 and 2 (SPI-1 and SPI-2), which both encode the apparatus and effector proteins of two type 3 secretion systems (T3SS) (12, 22, 23). The SPI-1 T3SS is essential in the initial stages of infection, enabling the bacteria to invade the host intestinal epithelium. SPI-1 effector proteins are injected directly into host epithelial cells, where they interfere with signal transduction and reorganise host cell actin filaments, therefore inducing phagocytosis of the bacterium. They also play a major role in assisting with colonisation of the intestine and modulating the host immunity to induce inflammatory responses, therefore causing gastroenteritis (4, 24, 25-28).

The roles of the major secreted SPI-1 effector proteins are fairly well characterised. Among the most significant SPI-1 effectors are the Sip proteins (SipA, SipB, SipC and SipD), the Sop proteins (SopA, SopB, SopD, SopE and SopE2), AvrA and SptP (4). The Sip proteins are SPI-1-encoded effectors. SipB, SipC and SipD together form the translocon element of the T3SS needle, which inserts into and thus form a pore in the host cell membrane, permitting the injection of effectors into the host cell cytoplasm (4, 29). SipA and SipC also function by directly binding host cell actin and promoting actin filament stability and polymerisation (4, 30, 31). In addition, SipB has been shown to activate the host inflammatory response, by inducing IL-18 and IL-1β (4, 32). The Sop effector proteins are encoded outside of SPI-1 (29). SopB, SopE and SopE2 function by activating host cell Rho GTPases. This results in the rearrangement of actin filaments, which in concert with the action of the Sip proteins causes subsequent membrane ruffling and induced phagocytosis of the bacterium (4, 29). The Sop proteins are also able to disrupt the tight junctions between epithelial cells, allowing *Salmonella* to gain access beyond the apical surface (4, 33). The SPI-1-encoded AvrA and SptP effectors also have roles in modulating the host inflammatory response. However, in contrast to the Sop proteins, AvrA suppresses the inflammatory response by inhibiting NF-κB and stabilising tight junctions between epithelial cells (34, 35). SptP encodes a tyrosine phosphatase, which also acts in opposition to the Sop proteins, reversing their effects on actin polymerisation after bacterial internalisation and reducing the inflammatory responses (4, 36).

Expression of the SPI-2 T3SS is induced after bacterial internalisation (between 2-24 hours after infection), possibly in response to the detection of, among other factors, a low magnesium concentration and a low pH, indicative of an intracellular phagosome environment (23, 37-39). The SPI-2 T3SS is therefore active at a later stage than SPI-1, and is required to help the bacterium survive and multiply intracellularly, in both epithelial cells and macrophages (4, 22, 23, 40-42). After phagocytosis into the host cell, *Salmonella* cells remain inside the uptake phagosomes, which are modified to form the *Salmonella*-containing vacuole (SCV). Maturation of the SCV may initially be implemented by SPI-1 effector proteins, although as the SPI-1 genes are downregulated shortly after internalisation, the majority of SCV maturation is thought to be directed by SPI-2 effectors (20, 21, 43).

The essentiality of the SPI-2 T3SS for infection has been widely demonstrated and SPI-2 mutants are severely attenuated for infection *in vivo* (11, 19, 23, 44, 45). In spite of this and despite recent advances in knowledge of the later stages in *Salmonella* infection, little remains known about the mechanisms involved to permit intracellular survival, and the precise roles of SPI-2 effector proteins (11, 23, 43). Some of the major functions of the SPI-2 effectors are thought to include promoting replication within the SCV, inducing changes in the SCV membrane to help it mature, and directing trafficking and fusion of vesicles towards/with the SCV, and trafficking of the SCV through the host cell (4, 11, 20, 43). Some research has indicated that additional functions of the SPI-2 effector proteins may include inducing delayed cell death of the host macrophage cell, avoidance of the oxidative burst or oxidative stress resistance, bringing about actin accumulation and polymerisation close to the SCV membrane, and recruiting cholesterol to the SCV membrane (4, 38, 41, 44, 46). Some research has indicated that SCVs may be able to fuse with lysosomes, suggesting the importance of resistance to lysosomal contents by *Salmonella* (4, 43). However, this remains disputed. Recent data suggests that SPI-2 and its effectors do not assist in bacterial resistance against host defence mechanisms, but rather aid specifically in bacterial replication inside the salmonella-containing vacuole (SCV) (19).

It was originally thought that the SPI-1 and SPI-2 systems acted in isolation, at separate stages of infection, with little if any overlap in gene expression or function. Only recently has it become clear that this model is too simplistic and that there is significant cross-talk between the two T3SSs (4, 20, 43). For instance, mutations in SPI-2 T3SS apparatus proteins were found to result in the downregulation of a number of SPI-1 T3SS genes (47). Also, a number of SPI-1 effector proteins are now known to persist and continue to be expressed long after bacterial internalisation. These effectors have a role in SCV maturation, a process originally attributed just to SPI-2 effectors. SipA is a SPI-1 effector protein involved in inducing internalisation of the bacterium through the binding and polymerisation of actin. However, Brawn et al. demonstrated that this effector protein persists on the cytosolic side of the SCV membrane after phagocytosis (20). From here it acts in concert with a major SPI-2 effector, SifA, to help direct the positioning of the SCV

within host cells. SipA is also important for bacterial replication within the SCV (4, 20, 43, 48).

Both T3S needles comprise multi-protein complexes made up of over 20 proteins, which span the cell wall (4, 29) (Figure 1.1). The complexity of these needle structures means that they must be expressed in an organised manner to ensure proper assembly. The assembly of both needles is tightly controlled at a number of levels and by several pathways (29). Work by Pucciarelli and Portillo showed that PrgH and PrgK, membrane components of the SPI-1 needle, were present in purified peptidoglycan fractions, suggesting that these proteins associate with peptidoglycan. These interactions were also necessary for correct assembly of the SPI-1 needle (49). T3SS assembly occurs in a sequential manner, and the needle components can only be assembled once the base and export apparatus of the structure are in place, as these are secreted in a Type 3-dependent manner (29).

Motility of *Salmonella*

Salmonella express peritrichous flagella, which although not essential for virulence, are recognised as virulence factors due to the observation that flagella-expressing *Salmonella* strains are more invasive than those lacking flagella (50-53). The bacterial flagellum is structurally related to the T3SSs, being made up of over 20 proteins which associate in a large cell wall-spanning multi-protein complex (4, 54, 55) (Figure 1.1). The assembly of this structure is also very tightly regulated, with over 50 genes involved in some aspect of assembly or function. The correct assembly of the flagellum is essential for its function (11, 56-59). *Salmonella* express between 5 and 10 flagella per cell, which are distributed all around the cell (42, 59, 60).

The flagellum apparatus structure itself can be divided into several distinct portions. At the base of the macromolecular structure is the cell-wall spanning basal body. This forms the T3SS-like structure, which is responsible for secreting the more distal structural components of the flagellum during flagellum assembly, including the hook proteins and the filament flagellin proteins. The basal body is also required to relay the rotational force generated by the motor, to the flagellum filament. It is made up of the MS, C, P and L rings, which reside in the inner

bacterial membrane, cytoplasm, periplasm and outer bacterial membrane respectively, as well as a central rod. These rings anchor the flagellum into the cell envelope (61, 62).

The MS ring, made up of FliF monomers, is the primary structure to be assembled into the cell wall. After this the C ring is built up, associating with the MS ring. The rod component connects to the MS ring of the basal body and spans the periplasm. This structure helps to transfer torque to the hook and filament structures as well as providing a central channel through which flagellar proteins are exported. Once assembled, the P and L rings form around the central rod, with the P ring physically associating with the peptidoglycan cell wall (61, 62).

The hook is assembled once the basal body structures are in place. This structure acts as a hinge and transfers torque from the basal body to the filament. The 120 FlgE monomers which make up the hook, along with the hook capping protein and three hook-associated proteins (HAPs) are secreted through the basal body T3S channel. The hook self assembles to the required length, at which point the cap protein is replaced by the HAPs, of which HAP2 forms the cap of the filament and is required for filament assembly. When the hook reaches a length of ~55nm, the T3SS specificity is switched irreversibly and filament assembly begins with the export of FliC flagellin monomers. Like the hook, FliC monomers self assemble into the filament, which grows from the tip to a length of up to 10-15μm (61, 62).

The stator region of the flagellum consists of a complex of the MotA and MotB proteins. This assembles around the flagellum rotor region in the cell cytoplasm. Rotational torque is generated through the interactions of the stator and rotor, formed by the C-ring. The stator itself is thought to be anchored to the peptidoglycan, through the C-terminus of the MotB protein, whilst MotA is involved in generating torque (62-65). The inner membrane-spanning Mot proteins are the final proteins to assemble into the flagellar structure, since rotational torque is only generated once the whole flagellar structure has been successfully assembled. Mutants of the *motA* or *motB* genes are able to assemble complete flagellum structures, but remain non-motile, whilst missense mutations in either protein are known to cause slow-rotation defects (65-68).

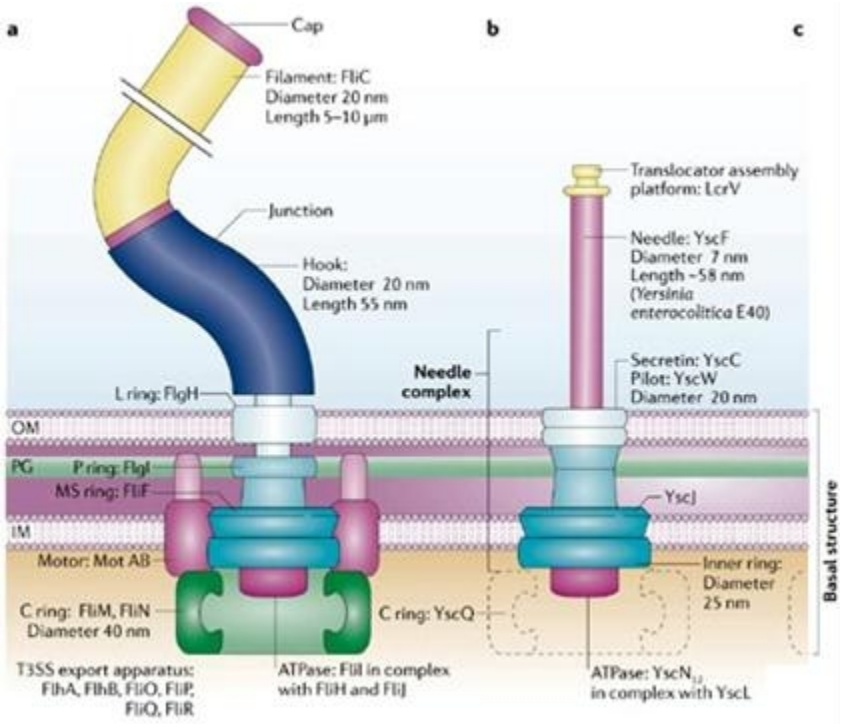

Figure 1.1: Molecular structure of bacterial flagella and type 3 secretion systems (T3SS): Schematic diagram to demonstrate molecular structure, and structural similarity of flagella and T3SSs. T3SS needle based on that of *Yersinia*. Both structures comprise complex wall-spanning macromolecular organelles, produced in many bacterial species including *Salmonella*. Figure taken from "The Type III Injectisome" (84).

1.1.3 Additional virulence determinants of *Salmonella* Typhi and *Salmonella* Typhimurium

Salmonella deploy a number of additional virulence determinants during the course of an infection, which although not essential, may play important additional roles in pathogenesis (1, 2, 12, 23, 69). These virulence determinants are directly involved in pathogenesis, being important for invasion or intracellular survival. The majority of these are encoded within one of the 14 horizontally acquired *Salmonella* pathogenicity islands (SPIs), that have to date been identified (12, 42). A brief overview of several significant factors which contribute directly to virulence in *Salmonella* is given below.

In addition, many factors could be described which are sometimes considered as virulence determinants due to their nature as housekeeping genes, nutrient acquisition genes, or stress response genes. These are needed to enable *Salmonella* to adapt and survive in a range of rapidly-changing environmental

conditions encountered in the host. However, in reality these factors are only indirectly related to virulence, and they play roles in the normal physiology of both *Salmonella* and many other non-pathogenic enteric bacteria (12).

Salmonella Typhi Vi capsular polysaccharide

The extracellular polysaccharide capsule, the Vi antigen, is expressed by *S.* Typhi almost exclusively among *Salmonella enterica* serovars (70). It is recognised as an important virulence factor, although not all clinical isolates of *S.* Typhi express Vi, and it is not essential for survival and spread within the host (70, 71). The capsule helps protect the bacteria from the host immunity, owing to its anti-phagocytic and anti-opsonic nature. It also may serve to reduce the inflammatory response of the host (11, 23, 72, 73). Genes for the regulation, synthesis and export of the Vi capsule are all located within SPI-7, a genomic pathogenicity island unique to Typhi.

Adhesins/Fimbriae

Salmonella express a number of types of cell surface fimbriae which are important for adhesion to and hence invasion of host epithelial cells. 14 separate fimbrial operons have been identified in *Salmonella*; these include the *bcf, csg (agf), fim, saf* (SPI-6)*, sef* (SPI-10)*, sta, stb, stc, std, ste, stg, sth* and *tcf* operons, as well as the *pil* operon within SPI-7, encoding type IV pili (1, 12, 23, 42, 74. 75). 12 are present within the *S.* Typhi genome, although Typhimurium lacks the *sef, sta, ste, stg, tcf,* and *pil* operons (23, 76). The specific complement of adhesive fimbriae expressed by Typhi may contribute to the host specificity of this serovar (3, 76, 77).

Virulence plasmids

Virulence genes and traits are often carried on virulence plasmids in bacterial pathogens. Serovars of *Salmonella enterica* belonging to Subspecies I (including *S.* Typhimurium, Enteritidis, and Paratyphi C but excluding Typhi, Paratyphi A and Paratyphi B) carry a self-transmissible plasmid termed *Salmonella* virulence plasmid, or pSLT. Contained within this plasmid are the genes for a fimbrial operon *pef* (plasmid-encoded fimbriae), and the *spv* locus; a 7.8kb region encoding 5 genes which plays a role in replication for intracellular *Salmonella*. This region is also known to be required for bacterial survival and replication within the

reticuloendothelial system. Aside from these genes, a number of other loci may also be present on pSLT which play various roles in infection. For example, the *rck* and *rsk* loci have roles in resistance to complement killing and serum killing respectively (42, 78-80).

Two plasmids harbouring multiple drug-resistance genes have been characterised in the CT18 strain of *S.* Typhi, including a large cryptic plasmid pHCM2, which has significant homology to a virulence plasmid of *Yersinia pestis*, and pHCM1 (1, 42). However, both pHCM1 and pHCM2 are absent from the majority of *S.* Typhi isolates, including the widely studied Ty2 strain, and the role of these plasmids in virulence remains unclear (1, 3, 42).

Toxins

Salmonella express a number of cytotoxins and enterotoxins which may play roles in virulence, although the complement of toxins expressed varies between serovars. Several *Salmonella* serovars express a variety of heat- and protease-sensitive cytotoxins, with recognised ability to kill mammalian cells. The most well characterised toxin of *Salmonella* is Stn, a heat-labile enterotoxin which is produced by several serovars, including Typhi and Typhimurium. Its exact role in virulence remains unclear, although Stn is known to bring about an increase in cAMP levels, as well as the synthesis and release of prostaglandins. Stn also causes an increase in fluid secretion into the gut lumen (42). This toxin displays homology at the amino acid level to both *Escherichia coli* (*E. coli*) LT-1 toxin, and the Cholera toxin subunits CT-A and CT-B (42, 81).

Serovars Typhi and Paratyphi A produce a pore-forming cytotoxin ClyA, sometimes termed ‘salmolysin’ due to its haemolytic activity (81). Several toxin or toxin-like genes have also been identified within a cluster on the *S.* Typhi genome, which are absent from other serovars. These *pltA*, *cdtB*, and *pltC* genes encode the A/B toxin ‘Typhoid toxin’, a cytolethal distending toxin which causes DNA damage, possibly bringing about cell death to fast-growing host cells (11, 82, 83). In addition *Salmonella* Typhi expresses at least 2 proteins with homology to RTX-like toxins (RTX: repeats in the structural toxin) along with T1SS apparatus proteins, which are encoded on SPI-4 and SPI-9 (1).

1.1.4 Comparisons between *Salmonella enterica* serovars Typhi and Typhimurium at the molecular level

Comparisons of the genome sequences of *S.* Typhimurium LT2 and *S.* Typhi CT18 or Ty2 strains have demonstrated a number of significant differences, in terms of both genome structure and the cohort of virulence genes (3, 80). The ~4.81 and ~4.86 mega base genomes of *S.* Typhi and *S.* Typhimurium, respectively, share over 90% of their DNA content. Within these conserved regions of the genome (including conserved SPI regions) the sequence identity between the two serovars is 97.6%, on average, at the DNA level. However ~10-12% (0.5-0.6 mega base pairs) of the *Salmonella* genome is generally unique to a given serovar. It is thought that these regions of the genomes are responsible for establishing the variable host specificities of different serovars, as well as bringing about different disease characteristics and stimulating specific immune responses within the host (1, 2, 11, 12, 18, 80).

Significant portions of the *S.* Typhi genome have, however, diversified from *S.* Typhimurium, as a result of major gene rearrangements, inactivations and insertions. Most significantly, of the 4599 genes of the *S.* Typhi genome, 204 are pseudogenes (~5%), resulting from single frame-shift mutations or the introduction of stop codons in the middle of open reading frames. 46 Typhi pseudogenes are known or at least thought to have been involved in virulence or host interactions prior to their inactivation. These include genes for several T3SS effector proteins such as *sseJ* (SPI-2), *sopE2*, and *sopA* (SPI-1), a flagellar methylation gene *fliB*, and several fimbrial operon genes. Of particular importance may be the *slrP* pseudogene of Typhi, encoding a T3SS-secreted protein which is involved in determining the host specificity. The *S.* Typhimurium genome shares only 23 pseudogenes with *S.* Typhi (1, 3). It is thought that the presence of such a large number of pseudogenes in *S.* Typhi, and particularly those involved in virulence or host interactions, is the major factor contributing to the host specificity and disease presentation of *S.* Typhi (1).

In addition to pseudogenes, *S.* Typhi possesses just over 600 unique genes. These appear to have been introduced as a result of the insertion of either

individual genes or whole blocks of genes. Significant insertions in Typhi include at least two additional pathogenicity islands, SPI-7 and SPI-10, several fimbrial operons (including one on SPI-10), homologues of *E. coli* and *Campylobacter* toxins haemolysin E and *cdtB* respectively, and toxin genes *ptxA* and *ptxB* from *Bordetella pertussis*. SPI-7 contains the Vi polysaccharide capsule biosynthesis and export genes, as well as the genes for a type IV pilus, as previously discussed. These may be significant factors involved in determining the presentation of clinical disease and host immune responses, particularly as the Vi capsule is known to dull the immune inflammatory responses (3). This may be directly through the expression of Vi itself, or through the downregulation of flagella expression by the SPI-7 regulatory protein TviA. Differing immune responses are made evident by the fact that the incubation period for *S.* Typhi can be up to 2 weeks, by which point the bacteria have spread beyond the gut. This is compared with an incubation period of 12-72 hours for Typhimurium infections, with subsequent sickness and diarrhoea (1, 3, 11, 12, 85).

1.2 Regulation of virulence in *Salmonella* Typhi and Typhimurium

Virulence gene expression in *Salmonella* is tightly controlled at a number of levels. In addition to specific virulence gene regulators (which, if inactivated, render the bacteria attenuated or avirulent) many upstream global gene regulators are involved in the control of virulence gene expression in response to environmental signals. The resulting regulatory networks, which are not yet fully defined, are highly complex, involving multiple factors and multiple levels of control.

1.2.1 Regulation of virulence gene expression

SPI-1 gene regulation: *hilA*, *hilC*, *hilD,* and *rtsA*

The regulatory pathways involved in the control of SPI-1 gene expression are as shown (Figure 1.2). Expression of SPI-1 genes is controlled by the HilA master regulator protein, a ToxR/OmpR family protein. HilA activates expression of the SPI-1 T3SS *prg*/*org* and *inv*/*spa* (encoding T3SS apparatus proteins), and *sic*/*sip* (encoding effector proteins) operons, as well as negatively regulating itself by an uncharacterised mechanism (86-88). In addition, HilA induces the expression of

further SPI-1 encoded transcriptional activators *invF* and *sicA*, which together activate the expression of the *sip* operon. InvF can also act independently of HilA to induce expression of important non-SPI-1-encoded effector protein genes *sopB* and *sopE* (87, 89, 90). That HilA is required for SPI-1 gene expression is illustrated by the fact that *hilA* mutants show a 10-fold decrease in SPI-1 gene expression, resulting in a massive reduction in both invasion (~150-fold), and in virulence in a mouse (~60-fold) (89).

hilA expression itself is induced by 3 upstream AraC-like positive transcriptional regulators, HilC, HilD and RtsA, which bind to the promoter region of *hilA* to activate it. Unlike the *hil* genes, *rtsA* is encoded outside of SPI-1. As well contributing in a feedback loop to positively regulate both their own expression and that of the other two AraC-like regulators, and inducing *hilA* expression, these regulators are able to induce SPI-1 activity independently of HilA. They activate expression of both the SlrP effector protein and a periplasmic disulphide bond isomerase which is needed for SPI-1 T3SS functionality (86-91).

Global regulation of SPI-1 gene expression

hilC, *hilD* and *rtsA* expression is controlled upstream both directly and indirectly by a number of global regulator proteins and systems encoded outside of SPI-1. These systems both activate and repress SPI-1 expression. The HilD protein is the most crucial regulatory factor in the activation of SPI-1 gene expression; environmental signals and global regulators which alter SPI-1 expression seem to converge on HilD. The regulation of HilD expression (and hence ultimately SPI-1 expression) appears to be predominantly post-transcriptional, brought about by altering translation or *hilD* mRNA stability. By comparison, *hilC* and *rtsA* expression (resulting from *hilD* activation) appear to amplify the HilD signal and further induce *hilA* expression. For instance, *hilD* mutants were found to be non-invasive (53-fold reduction in invasion of HEp-2 cells), lacking *hilA* expression (14-fold decrease in expression), whereas *hilC* mutants only displayed minor invasion defects, although the overexpression of *hilC* can increase SPI-1 expression and help compensate for the loss of *hilD* (87-89). *hilA* expression was decreased ~2-fold in both *rtsA* and *hilC* mutants (88, 89). Finally, although *hilC* and *rtsA* are able

to increase *hilD* expression, *hilD* expression is not reduced as a result of the loss of either *hilC* or *rtsA* (88).

A major global activator of SPI-1 expression is the BarA/SirA two-component system. Activated SirA binds directly to the *hilA* and *hilC* promoters to activate transcription. However, BarA/SirA is also known to post-transcriptionally regulate HilD expression through the *csr* system. This system comprises two small RNAs; *csrB* and *csrC*, which together are thought to bind and regulate the CsrA protein. CsrA post-transcriptionally regulates SPI-1 by binding to *hilD* mRNA near to the ribosome binding site and in doing so altering its translation. The concentrations of CsrA are thought to determine whether CsrA-mediated regulation is positive or negative; *csrA* is required for SPI-1 expression, although overexpression of CsrA causes a decrease in SPI-1 gene expression. In addition, *csrB* and *csrC* are needed for full SPI-1 expression. When phosphorylated, SirA activates *csrB* and *csrC* expression, which in turn tightly control and sequester CsrA, thereby de-repressing *hilD* translation and inducing SPI-1 gene expression (87, 89, 92).

A number of additional global regulators (encoded outside of SPI-1) feed in to the network to regulate SPI-1, including the PhoP/PhoQ and EnvZ/OmpR two-component systems, the ferric uptake regulator protein, Fur, CpxA, a flagellar protein FliZ, and HilE. These factors act upon *hilD* expression post-transcriptionally to regulate the expression of downstream SPI-1 genes. In addition, the flagella gene master regulator proteins FlhD and FlhC have been shown to activate *hilA* transcription (92). Whilst BarA/SirA, EnvZ/OmpR, Fur, and FliZ also all activate SPI-1, HilE appears to be the major repressor of SPI-1. HilE strongly represses HilD, potentially by binding directly to HilD, such that HilD-mediated SPI-1 expression is only brought about once activating signals are strong enough to overcome a threshold set by HilE suppression (93). Several global transcriptional regulators act directly through HilE to repress SPI-1 expression, including the PhoP/PhoQ and PhoR/PhoB two-component systems, and FimZY (87-89, 92, 94).

Other important repressors of SPI-1 virulence gene expression include several PhoP-activated genes (*pag* genes), the Lon protease which may digest HilD, the

DNA binding protein *hha* which binds *hilA* DNA and the Rcs phosphorelay system. In addition, the small secondary messenger molecule c-di-GMP suppresses SPI-1 effector protein secretion (95). The latter two factors are both involved in seemingly independent regulatory pathways which in response to environmental factors suppress invasion associated genes (e.g. SPI-1/flagella) and activate genes such as Vi and SPI-2, which are important for intracellular survival, as well as several colanic acid biosynthesis pathways (50, 86, 89, 95-97).

At the apex of these regulatory networks are environmental signals which are detected by various global regulators, such as osmolarity (EnvZ/OmpR), pH (EnvZ/OmpR, PhoP/PhoQ and Fur), Mg^{2+}/Ca^{2+} concentration (PhoP/PhoQ), bile, and nutrient starvation, which all indicate to the bacterium the nature of the environment and whether to express or repress invasion-associated genes (87, 89, 96, 98).

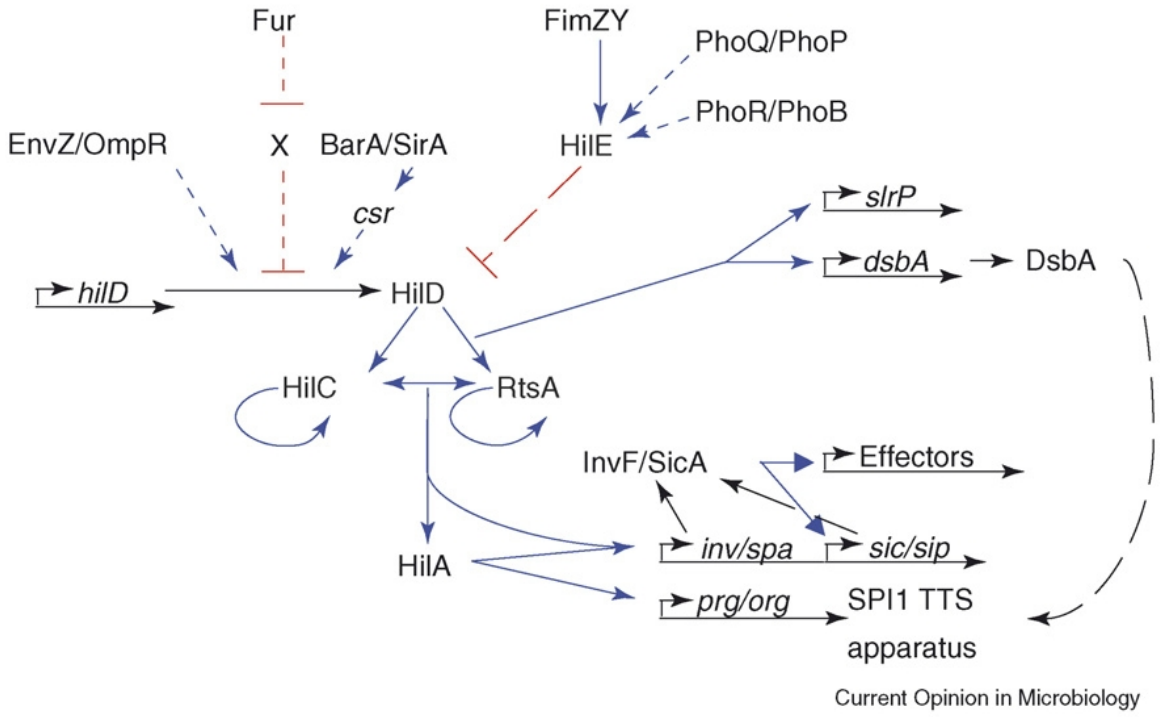

Figure 1.2: Regulation of SPI-1 gene expression: Diagram showing current models of the multiple levels of regulation involved in activating and repressing SPI-1 gene expression, along with major transcriptional regulator proteins. Taken from "Adaptation to the host environment: regulation of the SPI1 type III secretion system in *Salmonella enterica* serovar Typhimurium" (88).

SPI-2 gene regulation: the SsrA/B two-component system

Expression of both SPI-2 T3SS apparatus and effector protein genes is controlled by and dependent upon the SPI-2-encoded two component system SsrA/SsrB (11, 99, 100). In current models of SPI-2 gene regulation, the response regulator SsrB directly binds SPI-2 promoters to activate transcription of SPI-2 genes as well as the transcription of several effector proteins encoded outside of SPI-2, and other genes (11, 99-102) (Figure 1.3). SsrB is able to bind and thus activate transcription at all gene clusters within SPI-2, as well as auto-regulating itself. It has been demonstrated that the two components, SsrA and SsrB are divergently expressed. Also, the overexpression of SsrB is sufficient to stimulate SPI-2 gene expression, even with a lack of SsrA (101-104).

The mechanism of action of the SsrB response regulator is thought to differ from that of classical transcription factors. Analysis of SsrB DNA binding sites has shown that the location of these sites compared to the transcriptional start sites varies considerably at different gene clusters, being located either upstream, downstream or even overlapping the transcriptional start sites. In addition, a consensus sequence for the binding of the SsrB has been difficult to identify. Analysis of genes regulated by SsrB, including over 100 genes outside of SPI-2, revealed that the majority of SsrB-regulated genes appear to be horizontally acquired (11, 100, 102).

H-NS is a nucleoid-associated inhibitory protein which preferentially binds to A/T-rich regions of the genome, such as horizontally-acquired clusters of DNA. It is thought that this protein functions to protect the bacteria by suppressing the expression of foreign DNA. It is known that H-NS suppresses SPI-2 gene expression. However, recent work has shown that SsrB-mediated activation of SPI-2 genes is H-NS dependent; SsrB stimulates SPI-2 gene expression to a much lesser extent in *hns* mutants. Recent work has established that SsrB is likely to act by competitively inhibiting H-NS from binding to target DNA, and therefore relieving the DNA silencing brought about by this inhibitory nucleoid-associated protein. The authors suggested that when stimulated, SsrB competitively binds to SPI-2 DNA, causing the release of H-NS and therefore a relief in gene inhibition (11, 100, 102, 105).

Global regulation of SPI-2 gene expression

The expression of SsrAB is controlled by at least two upstream global regulators: SlyA and the OmpR/EnvZ two component system. These regulators are thought to respond to several environmental signals that are indicative of an intracellular environment, and go on to activate SPI-2 gene expression in an SsrA/B-dependent manner (Figure 1.3). OmpR directly binds to the *ssrAB* promoter, activating gene expression. The nature of the environmental signals which activate OmpR/SlyA-mediated SPI-2 activation remain elusive. *in vivo* data providing evidence on such signals is lacking, and much work *in vitro* has produced conflicting results. *In vitro*, SPI-2 gene expression is stimulated in stationary phase *Salmonella* cultures grown in minimal media (90). It has been variously suggested that the signals that induce SPI-2 gene expression include low osmolarity, low pH, and low Ca^{2+}, phosphate and Mg^{2+} concentrations. However more recent work has been unable to reproduce the effects of a low Mg^{2+} concentration on SPI-2 gene expression. Given that OmpR/EnvZ is known to be stimulated in response to osmolarity and pH changes, it is likely that these factors at least are important (38, 99, 102, 104, 106).

In addition to OmpR/EnvZ and SlyA, several other major regulators are thought to be involved in stimulating *ssrAB* expression, including the PhoP/PhoQ two component system, the major virulence gene global regulatory system which is essential for intracellular survival. This system directly activates genes (including *ssrAB*) needed for intracellular survival. PhoP/PhoQ also positively regulates the expression of SlyA (38, 96, 100, 102, 107). Negative regulators of SPI-2 gene expression are known to include nucleoid associated proteins H-NS and Fis, as well as YdgT (102). In general, much about the regulatory pathways involved in controlling SPI-2 gene expression remains to be fully elucidated.

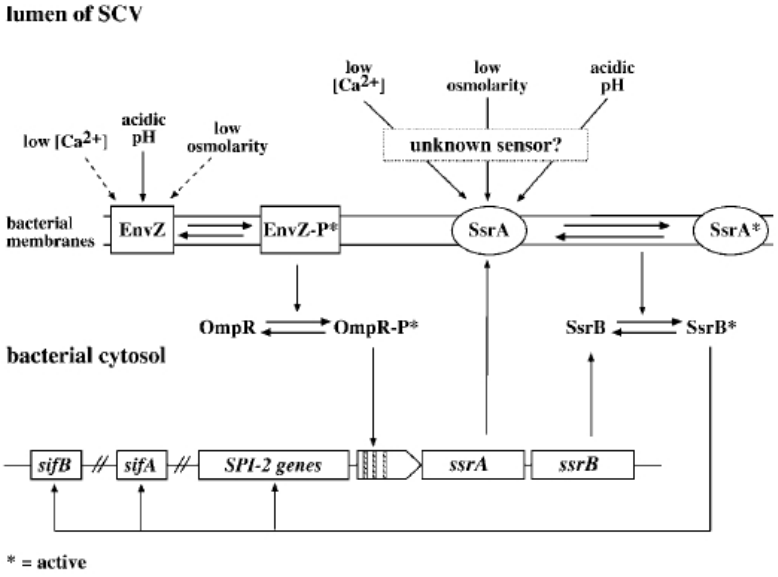

Figure 1.3: Regulation of SPI-2 gene expression: Diagram showing the major regulators, environmental signals and pathways involved in controlling the activation and repression of SPI-2 genes. Taken from "The roles of SsrA–SsrB and OmpR–EnvZ in the regulation of genes encoding the *Salmonella* typhimurium SPI-2 type III secretion system" (99).

Flagellar gene regulation: *flhDC*

The expression and assembly of the flagellar apparatus is highly complex, involving the tightly regulated and hierarchical expression of over 50 different genes contained within at least 17 operons. These operons, containing genes for the regulatory proteins, chaperones, basal body apparatus proteins and secreted flagellin subunits, are grouped into three separate gene classes according to the temporal regulation of their expression. Flagellar gene expression is tightly coupled with the assembly of the flagella structure. Flagellar genes are expressed in the order of their assembly into the flagellum structure, with each gene class corresponding to a distinct assembly stage. The expression of downstream classes of flagellar genes is completely dependent upon the successful expression and assembly of the preceding class of proteins. Hence, the so called 'late genes' encoding the secreted flagellin filament subunits are only expressed once the basal body structure of the flagellum is completely assembled. A schematic diagram demonstrating the hierarchical assembly of the flagellar structure is demonstrated below (Figure 1.4) (56, 58, 62).

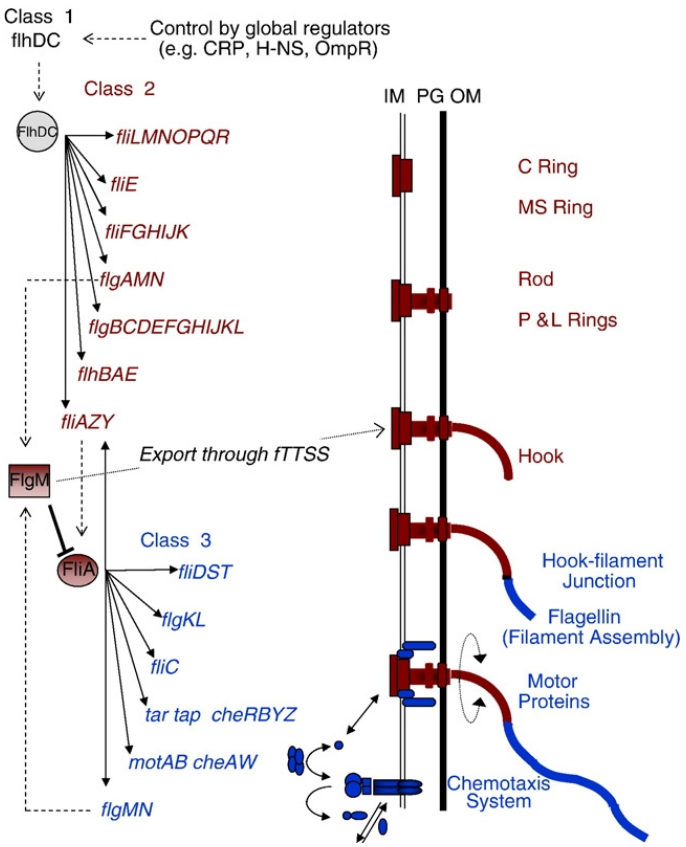

Figure 1.4: Hierarchical regulation of flagella gene expression: Schematic diagram showing the hierarchical control of flagella gene regulation and coupling of gene expression to flagella assembly, along with major transcriptional regulators involved in controlling flagella gene expression. Taken from "Bringing order to a complex molecular machine: The assembly of the bacterial flagella" (62).

At the peak of this temporal hierarchy is class 1, or the 'early' genes, comprising solely of *flhDC*. These genes encode the flagellar gene master transcriptional regulator, formed by a hetero-oligomer complex $FlhD_4C_2$. Transcription of the *flhDC* genes is induced in response to numerous signals involving both direct and indirect regulation from a number of global regulators. Environmental signals that regulate *flhDC* include temperature, osmolarity, carbohydrate and alcohol concentrations, and cell physiological signals such as cell cycle stage, the presence of certain heat shock proteins, growth phase and DNA supercoiling. A major regulator of *flhDC* expression is the cAMP-receptor protein CRP, which senses the cell state and activates *flhDC*. Other positive regulators of *flhDC* include H-NS, QseBC and several heat shock response proteins (DnaK, DnaJ and GrpE), whilst *flhDC* is negatively regulated by global regulators such as OmpR/EnvZ, HdfR, LrhA and the Rcs phosphorelay. All such factors signal directly

through FlhDC. *flhDC* expression is vital for the expression of all downstream flagellar genes and hence motility (56, 58, 62, 108-111).

The $FlhD_4C_2$ complex directly binds to class 2 gene promoters and interacts with RNA polymerase to activate transcription. Class 2 genes include those encoding the cell wall-spanning basal-body and hook components of the flagellum structure (Figure 1.4). The basal body elements together form a type 3 secretion structure through which the hook and filament protein subunits are secreted. Contained amongst the class 2 gene operons are also the transcriptional regulators for the class 3 genes, including *fliA* encoding the alternative sigma factor subunit of RNA polymerase, σ^{28}, and the anti-sigma factor anti-σ^{28}, FlgM. FliA (σ^{28}) is essential for class 3 gene expression. In order to ensure that the class 3 genes are not expressed until the hook-basal body structure is completed, however, FliA is repressed by FlgM until this stage. Upon completion of basal body assembly, the flagellar T3SS is able to secrete not only the flagellin filament subunits, but also the FlgM anti-σ^{28}. It is thought that the secretion of FlgM causes the de-repression of FliA, leaving it free to bind to and activate class 3 promoters. In this way, FlgM acts as a checkpoint, enabling the cell to sense completion of basal body assembly and switch to flagellin production (56, 58, 62).

Genes encoding the flagellin filament subunits, FliC and FljB (the latter being absent from *S.* Typhi), as well as chemotaxis genes and the motor proteins MotA and MotB, are all class 3 or 'late stage' genes. The expression of these genes is dependent upon σ^{28}. Flagellin proteins are then secreted through the flagellar T3SS and incorporated into the growing flagellum filament tail (56, 58, 62, 112).

In addition to the regulatory elements described here, more complex regulatory mechanisms and feedback loops are involved in fine-tuning flagellar gene expression. For instance, many flagellar genes are expressed from both FlhDC-regulated and σ^{28}–regulated promoters, albeit from different transcriptional start sites. FliA has been shown to activate transcription of both *flhDC* and class 2 genes when overexpressed. Under normal growth circumstances FlhDC negatively regulates itself, and so the presence of FliA is needed to increase *flhDC* expression. The FliZ protein, encoded within the same operon as *fliA*, is thought to

bind to the $FlhD_4C_2$ complex and increase its effect on class 2 gene activation (56, 58, 62, 111).

The regulation of flagella assembly also involves post-transcriptional regulatory mechanisms to bring about efficient, tight levels of control. In addition, mechanisms are in place to control both the length and number of flagella expressed on a cell. Further work remains to be carried out to fully delineate the flagellar gene regulatory complex (56, 113).

Vi capsule regulation

Genes responsible for the expression and assembly of the Vi capsule are located predominantly within the *viaB* locus. *viaB* is located on SPI-7 of the *S.* Typhi chromosome, a large 134kb pathogenicity island which is absent from *S.* Typhimurium (23, 70, 114). The locus consists of 11 genes, including *tviA*, a major regulatory gene, and other genes necessary for both the synthesis (*tviB-E* genes), and export (*vexA-E* genes) of the Vi polysaccharide subunits (23, 115, 116).

Upstream to *tviA*, which activates the *tvi* and *vex* genes, at least two other global regulators are involved in activating *viaB* locus expression, including OmpR/EnvZ, a two-component system that regulates gene expression in response to changes in osmolarity and pH (98, 116, 117). RcsB, the response regulator of the RcsCDB two component system (the Rcs phosphorelay), also positively regulates Vi capsule expression. These regulators both form important components regulating the stress responses in *Salmonella*, and respond to multiple environmental signals to regulate levels of Vi capsule production. TviA is also thought to form an auxiliary protein of the Rcs phosphorelay system, helping to regulate the expression of SPI-1 and flagella genes in *S.* Typhi in response to changes in osmolarity (85, 98, 114, 116-118). RpoS, another major stress response gene in *Salmonella*, may also be involved in Vi capsule regulation (85).

1.2.2 The role of global gene regulators in virulence gene regulation

As alluded to previously, many global regulators are involved in the direct activation or repression of SPI-1, SPI-2 and flagella genes. Many of these

regulators act conversely on SPI-1/flagella and SPI-2 genes, since they regulate genes involved in two very different states of infection. These global regulators are commonly found in both pathogenic and non-pathogenic *Enterobacteriaceae*. Their primary roles are not directly virulence-related, but in fact related chiefly in detecting environmental conditions and subsequently controlling physiological responses to external environmental stress. Thus these signalling pathways enable the bacteria to quickly respond and adapt to, and hence survive in rapidly changing conditions (98, 119-121).

The major *Salmonella* regulators which are responsible for controlling responses to environmental stress include the PhoP/PhoQ, OmpR/EnvZ and RcsCDB two-component systems, Fur, RpoE and RpoS. In addition, the Typhi-specific regulator TviA feeds into these regulatory networks. It is evident that in order to successfully establish an infection *Salmonella* must be able to detect and respond appropriately to environmental changes. This enables them to express virulence genes at the correct stages of infection, so that invasion-associated genes are expressed in the gut lumen, whereas genes essential for intracellular-survival are expressed after uptake into host cells. Thus the environmental stress response and virulence gene regulation in *Salmonella* are intimately linked and should not be considered in isolation of each other (98, 107, 116, 119).

The genetic networks are wired such that the environmental conditions which, through global regulators, stimulate SPI-1 expression (namely nutrient rich conditions, high osmolarity, low oxygen and a neutral pH) and SPI-2 expression (namely low Ca^{2+}/Mg^{2+}, low phosphate, low osmolarity and low pH) are those which are reminiscent of conditions found in the gut and intracellularly, respectively (87, 96, 98).

1.3 Cell shape determination and cell wall synthesis in rod-shaped bacteria

The mechanisms by which bacteria such as *E. coli*, *Bacillus* and *Salmonella* form and maintain a distinct rod shape have been the subject of considerable interest and debate in recent years. Much work remains to be done to fully elucidate these

mechanisms, although to date several models have been formulated. These will be discussed.

1.3.1 Bacterial cell shape determination

The bacterial peptidoglycan layer (sacculus) plays an essential role in providing mechanical support to the cell, both maintaining a distinct shape and resisting turgor pressure. The sacculus is a large macromolecule which surrounds the whole bacterial cell. It is made up of long glycan strands cross-linked by short peptide side chains. In Gram-negative bacteria the sacculus forms a fairly thin layer (~4-6nm thick), made up of 1-3 layers of peptidoglycan, which resides between the inner and outer membranes (122-125). Evidence suggests that the glycan strands and peptide cross-links are positioned so that they run perpendicular and parallel to the long axis of the cell, respectively. The peptide cross-links are fairly flexible, and thus thought to give the cell wall elastic properties, helping it to withstand external pressures and cell growth. Relaxed sacculi can be stretched up to 3-fold without breakage, because of the elastic nature of the molecule (125). When purified from the other cell components, the sacculus retains the distinct cell morphology, demonstrating that this molecule must be involved in physically constraining cell shape (125-127).

1.3.2 Cell wall synthesis in rod-shaped bacteria and *Salmonella*

Questions remain, however, as to how the cell walls in bacteria such as *E. coli* and *Salmonella* are synthesised, specifically with regard to the precise identity and functions of factors that must be involved in directing synthesis of the peptidoglycan sacculus during cell growth and division, so that it adopts a specific shape (122). After the translocation of peptidoglycan subunits across the inner membrane into the periplasm, the integration and polymerisation of peptidoglycan into the existing cell wall is brought about by the combined hydrolysis, transglycosylation and transpeptidation reactions. Current models hypothesise that the insertion of new wall material is brought about by the insertion of new glycan strands between existing strands, followed by the subsequent hydrolysis of old links, thus permitting growth of the cell wall without introducing breakages which may de-stabilise the cell wall (125, 126).

Cell shape determinant proteins of *Salmonella*

Whatever the mechanisms involved in cell wall synthesis, several proteins are now known to play essential roles in cell shape maintenance, through their direction of cell wall synthesis, by either their involvement in the control of peptidoglycan synthesis or by their nature as cytoskeletal elements (128, 129). The inactivation of any one of these proteins causes rod-shaped bacteria to become spheroid, and without compensatory mutations, to eventually lyse (95, 96). To date six such proteins have been identified; MreB, MreC, MreD, PBP2, RodA, and RodZ (122, 128, 130-132). That there are functional links between MreBCD, RodZ and PBP2/RodA is clear; cells treated with either the MreB-targetting A22 or PBP2-targetting mecillinam drugs exhibit exactly the same phenotypes in terms of the biochemical changes brought about in the sacculus structure and round-cell mutants also show identical phenotypes (126, 130).

The cytoplasmic MreB protein is now known to form a major cytoskeletal protein in non-spheroid bacteria (122, 132). This protein is highly structurally homologous to eukaryotic actin, despite lacking significant homology at the amino acid level. Electron microscopy (EM) studies demonstrated the ability of MreB (unlike eukaryotic actin) to self-polymerise in an ATP-dependent manner, into long filaments and filamentous bundles, and also form curved structures and rings, *in vitro* (126, 133). Fluorescent light microscopy in several rod-shaped bacterial species expressing GFP-MreB fusions have demonstrated that MreB localises just beneath the inner bacterial membrane, forming spirals or helices along the longitudinal axis of the cell (126, 132, 134, 135).

The *mreC* and *mreD* genes are located alongside *mreB*, within the same operon (131, 136). MreC and MreD are both integral membrane proteins. MreD is polytopic, whilst MreC is bitopic, possessing a large periplasmic domain. Both proteins have been observed to localise in a helical pattern along the length of the cell, MreC doing so independently of MreB (although long-term, the loss of MreB affects the localisation of MreC) (136, 137). Although some work has shown that MreC and MreB helices do not co-localise (138), bacterial two-hybrid and affinity chromatography experiments conversely demonstrated that MreC directly interacts with MreB, MreD and several high molecular weight peptidoglycan synthetic

enzymes, including PBP2 (131, 137, 139, 140). MreD and MreB did not, however, directly associate (84, 96). Furthermore, the helical localisation of MreB has been shown to be dependent upon the MreC and MreD proteins, as well as RodA, as depletion of either protein brings about the mislocalisation of MreB (126, 131). It was proposed that MreC and MreD may assist in anchoring MreB to the cytoplasmic membrane, although more recently, RodZ has emerged as a more likely candidate for this (141).

The *pbpA* gene encodes Penicillin-binding protein 2 (PBP2), the major transpeptidase enzyme involved in lateral cell wall synthesis in rod-shaped bacteria (130, 142-145). The 66 kDa PBP2 protein is a class B high molecular weight PBP, which catalyses the cross-linking transpeptidation reactions to link adjacent glycan strands by a pentapeptide bridge within the growing cell wall. PBP2 is the only transpeptidase known to be essential for lateral cell wall synthesis (125, 130, 146-149). The transpeptidation activity is contained within the large C-terminal penicillin-binding periplasmic domain of PBP2, whilst the protein is anchored into the cytoplasmic membrane via the transmembrane N-terminus of the protein. The N-terminal portion may also determine the localisation of PBP2 and interact with other proteins involved in elongation (130, 145, 150). Transglycosylation activity has not been detected in the PBP2 enzyme (126, 130).

The enzymatic activity of PBP2 is dependent upon the RodA protein (127, 143, 146). The *rodA* gene lies directly downstream of *pbpA*, within the same operon in many rod-shaped bacteria including *E. coli* and *Salmonella*. Given the contiguous nature of the two genes, and the dependence of PBP2 on RodA, it is likely that the two proteins directly interact (122, 146, 151-153). RodA is a 40 kDa polytopic membrane protein, containing at least 9 membrane-spanning helices (143, 153, 154). Various roles for RodA have been speculated, although none have been definitively demonstrated (126, 153, 155). Among the most widely recognised is the hypothesis that RodA forms the so-called flippase, responsible for the translocation of the lipid II peptidoglycan precursor across the cytoplasmic membrane into the periplasm, particularly given its structure. However, this process is thought to be coupled closely to transglycosylation, and it may be that the translocation of lipid II is coordinated by RodA as well as a number of

associated integral membrane proteins (126, 152, 156). It also remains unknown whether RodA possesses any enzymatic activity, although it has been speculated that RodA may have transglycosylase activity (127, 146).

As with the inactivation of other cell shape determinant proteins, treatment of Gram-negative rods such as *E. coli* and *Salmonella* with the PBP2-inhibiting antibiotic mecillinam, or the genetic inactivation of *pbpA* or *rodA*, results in the formation of spheroid cells, which divide asymmetrically and eventually lyse (127, 145). It is generally reported that growth of Δ*mre*, Δ*pbpA* or Δ*rodA* mutants is permitted in minimal media and at low temperatures (30°C), but that these cells are unable to grow and divide at high growth rates (i.e. in rich medium and at 37°C) unless the FtsA and FtsZ proteins, or the alarmone ppGpp are overproduced (126, 127, 130, 157). Similarly to the inactivation of *pbpA*, overexpression of *pbpA* in *E. coli* caused cells to become large and spheroid, and eventually lyse, although this effect was shown to be dependent upon the presence of the N-terminal membrane anchor, and not the transpeptidase domain (158).

The subcellular localisation of both PBP2 and RodA is helical, reminiscent of MreB, although PBP2 helices at least, are dependent upon MreB, MreC and MreD, and PBP2 co-localises with MreC (135-137, 159-161). Previous bacterial two hybrid work has also provided evidence that MreB and RodA directly interact, and that MreB localisation is dependent upon RodA, but not PBP2 (126, 131, 162, 163).

The well conserved RodZ protein was recently identified as an additional protein required for maintenance of rod-shape in bacteria, although one study has since suggested that RodZ is not necessary for this (128, 164-166). Both depletion and over-expression of RodZ, as with the other cell shape determinant proteins, cause a loss of rod-shape (128, 165). RodZ, encoded by the *rodZ* gene (formerly *yfgA*) is a bitopic membrane protein, containing both periplasmic and cytoplasmic domains. It was found to both directly bind and colocalise with MreB independently of all other cell shape determinants except MreB (141, 164). Bendezu et al. demonstrated that colocalisation of the RodZ and MreB helices was interdependent. In addition, a correct ratio of MreB:RodZ was shown to be important in maintaining cell shape (128, 164, 165, 167). However, another group

found that RodZ could localise helically independently of MreB (128, 164, 167). RodZ is also thought to interact with other cell shape determinants in the periplasm (128, 167). Although its precise function is still unknown, RodZ may be important in directing MreB localisation by anchoring MreB to the cytoplasmic membrane, and physically bridging MreB to the peptidoglycan synthetic enzymes (141). A recent study also brought to light a possible secondary role for RodZ, as an mRNA-binding protein which assists in post-transcriptional regulation (168).

1.3.3 Current models of peptidoglycan synthetic multi-protein complexes

All 6 cell shape determinant proteins have been shown to localise with a helical or banding pattern in the lateral cell wall of rod-shaped bacteria, in a manner reminiscent of MreB (126, 132, 135, 136, 163, 164). A number of protein interaction studies incorporating data from bacterial two-hybrid assays, affinity chromatography and X-Ray crystallography studies have also revealed that many of these proteins may directly interact. Thus, combined data from a number of studies has led to the formulation of a model, whereby cell wall synthesis in rod-shaped bacteria is coordinated by two separate multi-protein complexes, which are responsible for lateral and polar cell wall synthesis during cell elongation and cell division, respectively. These complexes contain the periplasmic penicillin-binding proteins (PBPs) and related proteins which coordinate the transpeptidation and transglycosylation reactions, integral membrane proteins, and associated cytoskeletal proteins. The latter components may form a track or a scaffold to direct the localisation of the complexes (Figure 1.5). It is thought that these complexes, and in particular the cytoskeletal elements, are responsible for determining cell shape (131, 136, 169, 122, 170, 171).

In terms of lateral cell wall synthesis specifically, all 6 cell shape determinant proteins along with other associated proteins, including lipid II synthesis enzymes (MraY and MurG), additional cell wall synthetic enzymes (PBP1A or PBP1B), and cell wall hydrolase enzymes, at least, may form a multiprotein complex to specifically coordinate longitudinal cell wall synthesis (125, 126, 139) (Figure 1.5). The cytoskeletal MreB protein may help determine cell shape by associating with this complex and forming a track to position the peptidoglycan synthesis

machinery in the cell membrane. This allows peptidoglycan to be synthesised in a spatially coordinated manner, permitting longitudinal cell wall growth (130, 131, 135, 169, 172). In this model, other cell shape determinants such as the membrane proteins MreC and MreD, or RodZ may tether MreB to the cytoplasmic membrane, or form the bridge between the MreB cytoskeleton and the peptidoglycan biosynthesis machinery, including PBP2 and RodA (Figure 1.5) (122, 130, 131, 169, 173). In support of this model, the incorporation of new peptidoglycan subunits into the cell wall occurs evenly and in a helical pattern across the lateral cell wall, in a manner which is disrupted upon the inactivation of MreB and the cell division protein FtsZ (122, 169, 171, 172, 174).

The protein complex responsible for bringing about septal cell wall synthesis and hence cell division, is coordinated by the tubulin homologue FtsZ. This protein forms a characteristic ring structure around the cell septum which contracts to bring about cell division. A large number of associated proteins, including at least 10 essential division proteins comprising the septal cell wall synthesis machinery are sequentially recruited by FtsZ to the septal ring before cell division (169, 172, 175-179) (Figure 1.5). Many of these proteins are essential for cell division, and their inactivation results in the formation of non-dividing filamentous cells. In this complex the PBP3 and FtsW proteins form the equivalents of the PBP2 and RodA proteins, coordinating septal peptidoglycan synthesis as the septal ring contracts (172, 175, 180). Experiments have demonstrated that the majority of PBPs form part of either the elongation or division complexes (126, 185).

The MreB- and FtsZ-coordinated multi-protein complexes involved in the direction of lateral and polar cell wall synthesis were originally thought to act independently of one another, and at different stages in cell growth (169, 181). The relative simplicity of this model has been brought into question by recent studies. Both FtsZ and MreB are dynamic proteins, with varying localisation patterns (122). MreB and associated proteins, for instance were shown to rearrange prior to cell division to form ring-structures flanking the mid-cell position, in a manner dependent upon FtsZ (135, 159, 160). This suggests an involvement of MreB and associated proteins in cell division. In non-dividing cells FtsZ re-localises, forming helices extending along the length of the cell (122, 182, 183). MreB and FtsZ may

potentially serve to re-localise cell wall synthetic complexes according to the required location of peptidoglycan synthesis (159, 182, 183). Furthermore, Varma et al. demonstrated that FtsZ may play a role in directing the incorporation of new peptidoglycan into the side wall of *E.coli*; inhibiting FtsZ brought about a significant reduction in the incorporation of peptidoglycan into sections of the side wall adjacent to the cell poles as well as alterations in the composition of the peptide side chains (172). This phenotype was exacerbated by the simultaneous inhibition of MreB (159, 169, 172). More recently the group demonstrated that the even distribution of peptidoglycan insertion into the *E. coli* side wall was disrupted with the inhibition of both MreB and FtsZ, but not MreB alone. The same disruption of insertion was also observed in *pbpA* mutants, suggesting that MreB and FtsZ may both act upon PBP2 to direct the localisation of the cell wall synthases (159, 169). Furthermore, FtsZ in *Caulobacter crescentus* contributes to cell elongation by mediating localisation of the lipid II synthase MurG, a protein that was coimmunoprecipitated with MreB and is recognised to form a part of the elongation complex, as well as localising to a mid-cell position prior to cell division (126, 184).

These pieces of evidence demonstrate that the two systems responsible for cell growth and division have significant overlaps in function which are necessary to bring about smooth transitions between cell elongation and division, and ultimately direct formation of rod-shaped cells (159). The complexes are highly dynamic, moving and relocalising according to the stage of growth. A number of proteins, including PBP1A, PBP1B, PBP2, MurG and MraY are also likely to form part of both complexes (122, 126).

Further questions about cell shape maintenance

MreB is thought to control cell shape by directly positioning cell wall synthetic complexes. However, it remains unclear as to precisely what directs the helical localisation of MreB, and hence which factors are involved first and foremost in determining rod-shape (122, 159). Some data suggests that contained within the MreB protein is the innate ability to rapidly self-polymerise into long filaments as required and direct cell shape (133). However, MreB helices are disrupted with the depletion of MreC, MreD, or RodA, but not PBP2 (131). Most recently, MreB localisation has been shown to require RodZ, although seemingly conflicting data

about the dependence of MreB localisation upon MreC and RodZ has been published (131, 138, 164). Thus, although the inter-dependence of the various protein complex constituents remains confusing, the localisation of MreB appears to be dependent on other cell shape determinants.

It also remains unclear as to precisely which proteins directly interact (or indeed how they associate) and form part of the proposed lateral cell wall synthetic complex (126, 135). The majority of data from protein interaction studies have come from bacterial two hybrid assays and co-immunoprecipitation studies, and hence do not provide definitive proof of actual protein interactions (126). It may be that the nature of the upstream factor(s) responsible for overall cell shape determination has yet to be realised, or that the models in place at present need to be refined as a result of further research.

An alternative model for the control of lateral cell wall synthesis

Recently the work of Swulius et al. has raised further questions about this widely accepted model of cell shape maintenance (134). This group used electroncryotomography to attempt to visualise MreB filaments residing near to the cytoplasmic membrane in various species of rod-shaped bacteria. This method provides a means of visualising cell ultrastructures at a high-resolution, whilst maintaining cells in a ‘near-native state’. Whilst FtsZ filaments were clearly visible, helical MreB filaments could not be detected despite a number of combinations and permutations tested. The authors concluded that long helical filaments of MreB do not form *in vivo*, as previously thought, suggesting that the observed helices from fluorescence microscopy studies may have resulted from the sample preparation method constraining soluble monomeric proteins including MreB and associated proteins into the available space between the nucleoid and cell membrane; hence the localisation of these proteins would appear helical because of the twisted morphology of the nucleoid. Alternatively, it was suggested that the observed helices may have resulted from small MreB complexes moving through the cell, combined with a long exposure time. However, Swulius et al. also recognised the possibility, if unlikely, of sample preparation in the cryotomography process causing long MreB filaments to depolymerise (134).

The group proposed an alternative model where the peptidoglycan cell wall itself forms a scaffold for further cell wall synthesis. They suggested that freely moving MreB-linked enzyme complexes may provide additional support to newly-synthesised sections of cell wall, lengthening and straightening them as they are incorporated into the existing cell wall. In addition, short filaments of polymerised MreB may play a role in forming a bridge between glycan strands (134).

However, this model does not explain several observations, including that of new wall insertion, which occurs in a helical fashion reminiscent of the proposed MreB localisation. In addition, the helical localisation of MreB and associated proteins is often seen to be dependent on at least one other cell shape-determinant protein, the absence of which causes the proteins to mislocalise, seemingly forming arcs and random linear filaments across the cell cytoplasm. A22 treatment also causes the observed helices to dissipate. Furthermore, MreB and associated proteins are known to re-localise to the cell septum before cell division. It is questionable as to whether these phenotypes would be detected if helical localisation was purely an artefact of sample preparation. Whatever the reason for the inability of Swulius et al. to detect MreB helices, both models warrant further investigation to more comprehensively elucidate the mechanisms of cell shape control in rod-shaped bacteria.

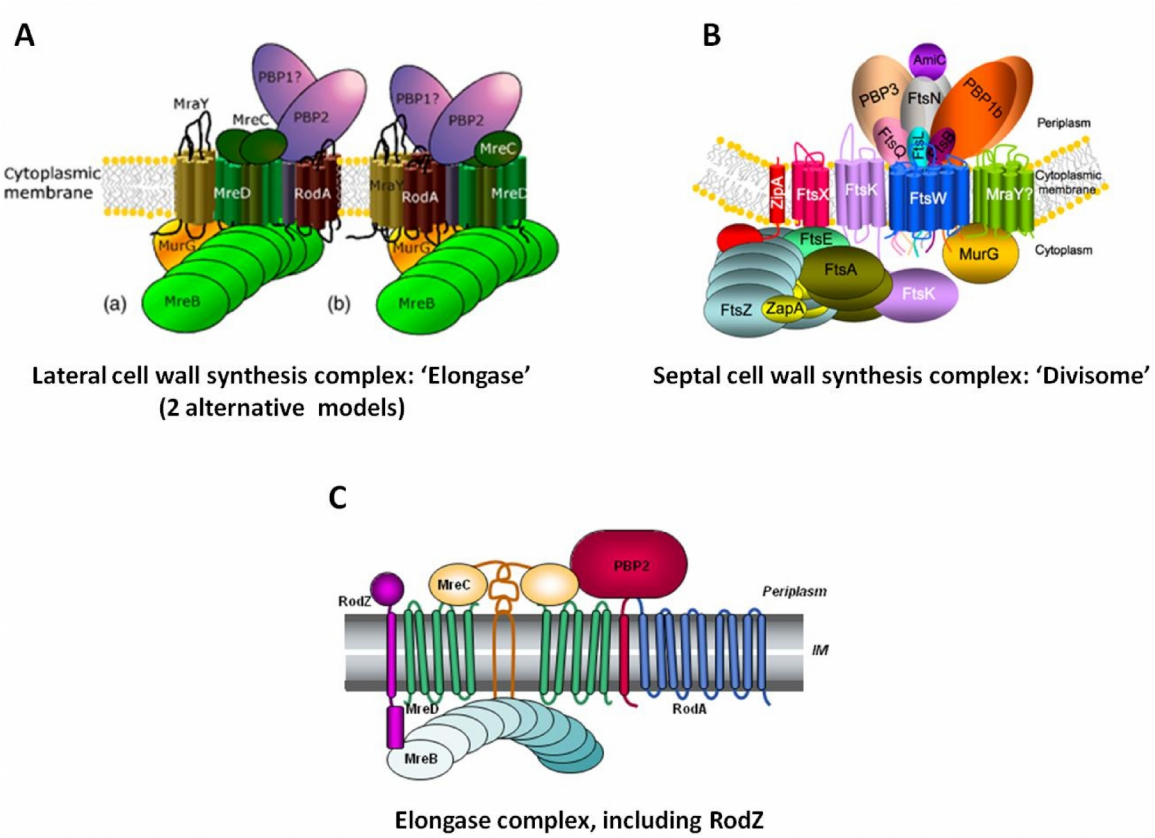

Figure 1.5: Putative multiprotein complexes responsible for lateral and septal cell wall synthesis: A and B taken from "Morphogenesis of rod-shaped sacculi" (126). Putative interactions (as shown) are based on data from bacterial two-hybrid assays and coimmunoprecipitation studies. Two alternative models of elongation complex given in A. C – additional model of elongation complex, adapted from figure in "The morphogenetic MreBCD proteins of *E. coli* form an essential membrane-bound complex" (131), to include RodZ.

1.4 The *mrd* operon of *Salmonella*

The cell shape determinant proteins PBP2 and RodA are encoded by the *pbpA* (*mrdA*) and *rodA (mrdB*) genes, respectively (155). These genes lie contiguously within the putative *mrd* (murein D) operon in many rod-shaped bacteria including *Escherichia coli*, and *Salmonella* (122, 142, 155). Studies show that the *mrd* operon is likely to consist of at least three other genes: *ybeB*, *ybeA*, and *rlpA* (Figure 1.6). The contiguous nature of *pbpA*, *rodA* and *rlpA*, along with the lack of transcriptional termination sequences between the *pbpA* and *rodA* genes, and the functional relationship of *pbpA* and *rodA* at least, suggests that these three genes are co-transcribed (142-144, 186). In addition, potential promoter sequences for this operon have been identified in the inter-genic region upstream of *ybeB*. Hence the two *ybe* genes may also form part of the operon (142).

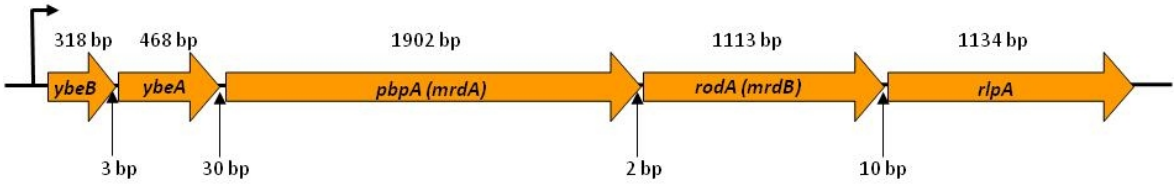

Figure 1.6: The putative mrd operon of Salmonella enterica serovar Typhi: Schematic diagram showing layout of *mrd* operon in *S.* Typhi, including gene sizes, spacing between genes, and position of putative *mrd* operon promoter upstream of *ybeB*. Operon layout as shown is identical in both Typhi and Typhimurium serovars, except for *rlpA* gene; length in *S.* Typhimurium is 1146 bp.

However, some evidence suggests that *rodA* and *rlpA* may be independently expressed. Putative promoter sequences were identified upstream of *rodA*, within the *pbpA* gene, although the activity of the promoter upstream of *ybeB* was much greater than that from the *rodA* promoter as shown by expression levels of a *rodA-lacZ* fusion construct, leading the authors to conclude that *pbpA* and *rodA* were likely to be co-expressed (143, 144). In addition, transposon mutagenesis of the *pbpA* gene did not have a polar effect on *rodA* expression, as would be expected for co-transcribed genes (144). Promoter-like sequences have also been identified upstream of the *rlpA* gene, within *rodA* although these may not constitute an actual active promoter, and *rlpA* is generally recognised as being co-transcribed with *rodA* (179, 186, 187).

ybeB encodes YbeB, a common, highly conserved protein (188, 189, 190). Relatively little is known about the function of YbeB, although it is homologous to Iojap, a plant protein required to maintain the stability of chloroplast ribosomes (189, 191). In 2007 Jiang et al. showed that YbeB is a 50S subunit ribosome-associated protein, possibly involved in ribosome biogenesis (189, 192, 193). Double mutants of *ybeB* and the *minCDE* genes were also isolated with a synthetic lethal phenotype in *E. coli*. The Min proteins are responsible for directing formation of the FtsZ ring at a mid-cell position, by inhibiting FtsZ polymerisation elsewhere. Double mutants isolated with a lethal or sick phenotype were therefore indicative of proteins potentially involved in cell division. However, the Δ*ybeB* Min$^-$ double mutants also harboured shape defects which were complemented with the recovery of *pbpA*/*rodA* expression *in trans*. The authors therefore suggested that the observed phenotypes were most likely due to a polar effect of the *ybeB* mutation on the expression of the downstream *pbpA* and *rodA* genes (188). YbeB

is not essential in *E. coli*, although given its highly conserved nature it is likely that this protein has some important function (188). That a *ybeB* mutation may have had a polar effect on *pbpA* and *rodA* expression also suggests that *ybeB* is indeed part of the *mrd* operon.

The *ybeA* gene is highly conserved in many bacterial species, and also present in archaeal and plant genomes (196). Recent work has identified YbeA (RlmH) as a methyltransferase involved in what is thought to be the final stage of ribosome assembly, which occurs as translation begins. In *E. coli*, dimeric YbeA specifically methylates a pseudouridine residue $m^3\Psi$1915, located within stem-loop 69 of the 23S ribosome subunit rRNA (194-196). This hairpin loop of rRNA is specifically important to ribosome function, playing a role in the initiation, elongation and accuracy of translation, as well as ribosome recycling. The three highly conserved pseudouridine residues contained within stem-loop 69 are important for translation termination in particular (195-197). Purta et al. speculated that YbeA may act as a checkpoint, indicating that translation initiation has proceeded (194). Aside from the effects on pseudouridine methylation in a Δ*ybeA* mutant strain, minor growth defects were reported for this strain when grown in rich medium at 37°C. However, the presence of additional morphogical defects, or polar effects on downstream gene expression in this mutant was either not noted or simply not reported (194, 196). It is therefore unknown whether *ybeB* and *ybeA* are in any way functionally related to the other *mrd* operon genes.

rlpA was found to encode a rare outer membrane lipoprotein (RlpA) (179, 186, 198). Due to close homology of the signal peptide sequence of *rlpA* with those of other peptidoglycan-associating lipoproteins including Braun lipoprotein (Lpp), it was suggested that RlpA may also associate with peptidoglycan in some way (124, 186). Further evidence supporting this came from analysis of the RlpA amino acid sequence using the SMART database (163, 199, 200). This identified a 70-amino acid sporulation-related (SPOR) domain close to the C-terminal of RlpA, which is found in several cell division proteins and may be involved in binding peptidoglycan. This domain is absent from the Lpp sequence. Gerding et al. demonstrated more recently that isolated SPOR domains from RlpA, as well as three other proteins (FtsN, DamX and DedD), bound peptidoglycan and localised

to the cell septum in *E. coli*, suggesting these domains are sufficient to direct septal accumulation. However, the full-length RlpA was found to localise at distinct foci along the side walls of both dividing and non-dividing cells, as well as at the cell septum, as has been observed in *Salmonella* (163, 179, 201). The authors concluded that SPOR domain proteins may form part of the septal cell division ring, although the precise role of RlpA in cell division, or other cell processes, remains unknown, since Δ*rlpA* mutants did not display any obvious growth or division defects in *E. coli* or *Salmonella.* It is possible, however, that some functional redundancy may exist, masking the effects of an *rlpA* mutation (163, 179, 201). RlpA is one of only two outer membrane lipoproteins so far recognised to localise at the cell septum. The outer membrane protein Pal is required for invagination of the outer membrane during cell division, and so it has been proposed that RlpA may bridge the outer membrane and peptidoglycan, playing a similar role to Pal, although this does not explain the side-wall localisation patterns. Given its presence within the *mrd* operon, it may also play a role linked with that of PBP2 and RodA (179, 186, 201, 202).

A study in 2002 also found that expression of *rlpA* was highly induced with hyperosmotic stress in *E. coli*, suggesting that RlpA may be involved to some extent in resistance to external stresses (203). Finally, Prc is a periplasmic protease which cleaves the cell division transpeptidase enzyme, PBP3. It is also important for resistance to both thermal and osmotic shock, since Δ*prc* mutants are lethal when cells are grown above 40°C in hypotonic media. A truncated RlpA (retaining just the N-terminal 102 amino acids of the full length protein) was able to suppress this lethality when overexpressed, potentially indirectly through the induction of another protease HtrA (198). This may point to another link, if indirect, between RlpA and cell division or stress resistance.

Another gene located 138 bp downstream of *rlpA*, *dacA*, may also form part of the operon (145, 204, 205). *dacA* encodes a non-essential D-alanine carboxypeptidase enzyme (PBP5), whose inactivation brings about morphological defects in *E. coli* (204, 206-208). Overproduction of PBP5 also caused *E. coli* cells to become spheroid and prone to lysis, and these cells had an altered peptidoglycan structure similar to that in ∆*pbpA* cells (209). This suggests a

functional link with other *mrd* operon cell shape genes. PBP5 has also been shown to localise both septally and in the lateral cell wall (126). However, PBP5 is the most abundant penicillin-binding protein expressed in bacterial cells, a feature which would not be expected for a gene located towards the 3' end of an operon (207, 210). In fact, PBP5 is much more highly expressed than PBP2, suggesting that expression of *dacA* is independent of *pbpA*, although this theory does not take into account the possible post-transcriptional regulation mechanisms to regulate both PBP2 and PBP5 protein levels (210). However, mutations in the *mrd* operon genes in *E. coli* did not affect PBP5 expression, and Δ*rlpA* mutants did not possess the morphological defects displayed by Δ*dacA* mutants, both suggesting that *dacA* is not co-transcribed along with the upstream *mrd* operon genes (179, 201, 211).

The precise complement of genes contained within the *mrd* operon is still not known and further experimental work is required to establish this. However, it is generally accepted that the *ybeB-rlpA* genes are likely to form one transcriptional unit, the putative promoter for the *mrd* operon being located upstream of the *ybeB* gene (142, 186, 187, 212).

1.5 Rationale for studying cell shape determinants and the *mrd* operon in *Salmonella*

The aims of this study focus on the further delineation of both the structure of the *mrd* operon, and the function of its constituent genes, within the enteric pathogen *Salmonella* Typhi specifically. In particular investigations will assess the potential wider roles of the *mrd* operon genes in the pathogenesis, as well as the general biology, of *Salmonella*. The rationale for studying the *mrd* operon in *Salmonella* is discussed below.

1.5.1 Cell shape determinant inactivation and effects on cell wall structure, integrity and general physiology in *Salmonella*

The peptidoglycan sacculus is widely recognised as the stress-bearing molecule of the cell, helping maintain cell shape and resist internal turgor pressure to prevent

cell lysis (124, 125, 213). Hence, disruptions to the cell wall structure caused by the genetic or drug-mediated inactivation of cell wall synthetic complexes, cause a loss of cell shape and eventual cell lysis. With the presence of additional compensatory mutations however, round cells are able to grow and divide indefinitely, although cell wall growth appears to be dependent upon the septal-specific peptidoglycan synthesis complex in cell shape determinant mutants (127). In addition, the cell wall integrity in these cells appears to be significantly affected. Several studies have noted increased sensitivity to various external stresses in cell shape-determinant mutants, including osmotic pressure, oxidative stress, drugs and antibiotics (211, 214). In mecillinam-treated cells, whilst growth and division rates remained at the same level as wild-type for at least one mass doubling, a 50% reduction in the rate of peptidoglycan synthesis was observed (127). This evidence suggests that the lateral cell walls of *pbpA* (and *rodA*) mutants have a significantly compromised cell wall structure, lacking both the physical strength to withstand osmotic pressure, and the structural integrity to act as an effective barrier against external stresses. Perturbations to the cell wall integrity are unlikely to be due to the constitutive synthesis of septal peptidoglycan, since the differences between septal and lateral cell wall peptidoglycan structure are very small (122, 201).

1.5.2 Cell shape determinant inactivation and effects on cell wall-spanning organelles

Besides the observed defects in cell wall structure and integrity, and cell morphology, the effects of *mre*, *mrd* and *rodZ* mutations upon the assembly and functioning of other cell wall components, including large cell wall-spanning multi-protein organelles, has not been widely considered (118, 166, 215). This has important implications in terms of virulence, since many major virulence determinants in pathogens such as *Salmonella* encompass such organelles, including flagella and type 3 secretion systems (T3SSs) (4, 11, 12, 216). Although two studies have noted motility defects in round-cell mutants, few, if any, have comprehensively analysed the effects of cell shape determinant inactivation upon flagella and T3SS function in *Salmonella* or other bacterial pathogens (118, 166).

The study of possible links between cell wall synthesis/integrity and wall-spanning organelle functionality could be significant for a number of reasons.

Involvement of peptidoglycan in assembly, stability and positioning of cell wall organelles

Cell wall-spanning multiprotein complexes such as flagella and T3SSs both traverse the peptidoglycan layer, directly associating with it. Such associations with the peptidoglycan may be necessary to help stabilise the flagellum/T3SS structures in the wall, and assist their function (213). For instance, the P ring of the flagellum basal body is a rigid, non-rotating structure consisting of 26 FlgI monomers. It is thought to specifically interact with the peptidoglycan layer, connecting the basal body to the cell wall, and in doing so, providing physical support and stability to the rotor (62, 217). Sequential regulation of flagellum assembly means that downstream elements of the flagellum structure are not expressed and assembled until the preceding elements are successfully assembled. Consequently, disruptions of FlgI cause flagellum assembly to halt at the assembly of the P ring (218). It may be that peptidoglycan-binding via the P ring is an important feature in flagella assembly. Flagellar rotation is extremely fast, having been measured at 100Hz. Such forces may make it necessary for the flagellum to be tightly secured within the cell wall (213). In addition to the P ring, the MotB flagellar protein is also involved in peptidoglycan binding. The C-terminus of MotB is thought to bind peptidoglycan in order to anchor and help stabilise the stator structure around the basal body (213, 63, 64). Amino acid substitutions in regions of the MotB protein within or close to the peptidoglycan-binding domain cause motility defects (213).

The loss of peptidoglycan-binding through mutations in peptidoglycan-binding regions of proteins within several bacterial wall-spanning secretion systems (including the SPI-1 T3SS, T2SSs and T6SSs) is linked with a loss of function (49). The PrgH, PrgK and InvH proteins of the SPI-1 T3SS also bind peptidoglycan directly. PrgH and PrgK are membrane proteins, forming part of the base of the SPI-1 needle structure, whereas InvH is an outer membrane lipoprotein which appears to form more stable cross-links with peptidoglycan. It was proposed that InvH, and its association with peptidoglycan, plays an important role in initiating

assembly of the SPI-1 needle, although InvH is not essential for needle assembly (49). In the same study, altered peptidoglycan structure caused an inhibition of these protein-peptidoglycan interactions along with a subsequent decrease in the number of SPI-1 needle complexes per cell, and hence decreased secretion and invasion. The peptidoglycan structural changes were brought about by the incorporation of D-methionine into the cell wall, resulting in changes including a significant reduction in the number of peptide cross-links (49, 219). SPI-1 structural protein expression however, was unaffected, and the same peptidoglycan modifications did not affect flagella assembly.

These data together demonstrate the importance of peptidoglycan-binding proteins and the integrity of the cell wall on the assembly and consequently the function of cell wall-spanning organelles. Peptidoglycan itself may function as a physical scaffold in the anchoring of such structures into the cell wall. Defects in the cell wall could therefore significantly affect organelle assembly and function (64, 67, 213, 220). The effects seen with alterations in peptidoglycan structure in these studies may be similar or amplified in cells with cell wall defects caused by the inactivation of the cell shape determinants.

Putative positioning of cell wall complexes by bacterial cytoskeletal proteins

Current models hypothesise that the MreB cytoskeleton and associated proteins act by directly positioning cell wall synthetic complexes within the cell wall to bring about spatially organised cell wall synthesis. It is therefore reasonable to consider that the same cytoskeletal elements may also be directly involved in the positioning and localisation of other multi-protein structures within the cell wall, including flagellar and T3SS basal body proteins. If this is the case, perturbations in the MreB cytoskeleton and/or associated proteins (since MreB localisation may be dependent on other cell shape determinant proteins) are likely to affect both the assembly and localisation of cell wall-spanning organelles.

Evidence to support this hypothesis has come from a study showing that the bacterial actin homologue, MreB, is involved in directing the polar localisation of several proteins, including, for example, secretion system proteins, virulence related proteins and cell surface receptors (173). In another example, motility in

the Gram-negative bacteria *Myxococcus xanthus* was shown to require MreB. Motility in this organism is mediated not by flagella, but using two separate motility systems to move across surfaces: S-Motility and A-motility. S-motility involves polar type-IV pili, which attach to surface polysaccharides and then retract to move the bacterium forward. A-motility is less well characterised but may comprise motor systems and adhesion complexes which display distinct localisation patterns along the length of the cell. Recently, Mauriello et al. demonstrated that treatment of *M Xanthus* cells with the MreB inhibitor, A22, blocked both A- and S-motility. Furthermore, localisation of the A-motility and S-motility protein complexes was disrupted in A22-treated cells. AglZ, a protein involved in A-motility, was localised in clusters along the length of the cell, in a manner reminiscent of MreB. Taking the results together, Mauriello et al. hypothesised that MreB is specifically involved in the localisation of motility complexes in this bacterium (221). Recently, another study in *Pseudomonas aeruginosa* found that the MreB cytoskeleton was directly involved in the polar localisation of type IV pili. In cells treated with A22, both the pili themselves and an important protein involved in pilus retraction mislocalised (222).

These studies are amongst the few that have considered both the importance of virulence determinant localisation in pathogens, and the possible role of the bacterial cytoskeletal elements in virulence determinant localisation (222). They provide clear evidence that the MreB cytoskeleton in particular may play an important role in the localisation and hence function of such systems.

Several cell wall-spanning organelles in *Salmonella* are known to have distinct localisation patterns. Wild-type *S. enterica* serovars are known to express between 4 and 8 flagella per cell, although some studies have reported numbers of between 6-10 flagella, or up to 15 per cell (113, 223-225). These peritrichous flagella are distributed around the whole of the cell surface, including the lateral cell walls and the poles (226). Nikolaus et al. demonstrated that SPI-2 needles have a polar localisation, with apparently few, or only one needle complex per cell (227, 228). By comparison, the SPI-1 T3SS appears to be distributed diffusely across the whole bacterial cell surface, with up to 200 needle complexes per cell (54, 227). It remains to be investigated whether the localisation of flagella, SPI-1

and SPI-2 organelles in *Salmonella* is coordinated by bacterial cell shape genes or the cytoskeleton, although their localisation is clearly significant for function (227).

1.5.3 Cell shape determinant inactivation and global effects on cell biology

The inactivation of cell shape determinant brings about stark defects in cell wall synthesis and integrity, indicated by morphological defects and increased sensitivity to external stress (229). Aside from these specific effects, the global effects in bacteria such as *Salmonella* have not been studied in detail. In particular, the increased exposure of *mrd*, *mre* or *rodZ* mutants to external stresses would have a potentially massive impact on global transcriptional and translational profiles. This would also be relevant in terms of virulence, given that virulence gene expression is tightly regulated by multiple environmental signals, so that virulence properties are expressed when the bacteria are in a particular state or environment. Increased exposure to certain environmental stresses which may trigger the activation of global regulatory pathways could certainly alter virulence gene regulation.

Hence there is a need to further investigate the global downstream effects of cell shape determinant inactivation. Doing so would provide a broader picture of both the general physiology and the responses involved in bacteria with cell wall defects, as well as providing further clues into the precise roles of both the cell wall, cell shape determinant proteins, and cell wall associated synthetic complexes.

1.5.4 The *mrd* operon in relation to the biology and virulence of *Salmonella*

The *mrd* operon genes are known to play an important role in lateral cell wall synthesis. However, the structure and regulation of the operon, as well as the precise roles of the constituent genes, are not well characterised. Much work is needed to delineate the functions of the cell shape determinant proteins PBP2 and RodA not only in cell wall synthesis, but also in the broader biology of rod-shaped bacteria such as *Salmonella*. Furthermore, the roles of the *ybe* and *rlpA* genes should be further investigated. *ybeB* and *ybeA* are known to be involved in ribosome assembly and stability, but whether their roles are linked with those of *pbpA* and *rodA* remains to be realised. Bacterial ribosomes in *B. subtilis* are

localised around the periphery of the cytoplasm and particularly at the cell poles (230, 231). If the same is true in *Salmonella* it is plausible that cell-shape determinant proteins may be involved in directing the localisation of ribosomes and associated proteins including YbeB and YbeA. An association between cell wall synthetic complexes and ribosomes may hint at a functional link between the *mrd* operon proteins (230). It was recently recognised that RlpA has a role in peptidoglycan binding, and may localise in a pattern reminiscent of the PBP2 and RodA helices, as well as at the division septum (163, 179, 201). These findings also may indicate a functional relationship between the *pbpA*, *rodA*, and *rlpA* genes which should be further investigated.

The high level of operon conservation suggests that there may be some conserved function between all 5 genes, that has until now not been recognised. That the conserved operon contains genes with seemingly unrelated functions may also point to the PBP2 and RodA proteins fulfilling more complex functions than currently proposed.

Finally, along with investigating the role of *mrd* operon genes in the functionality of important virulence determinants in *Salmonella*, it is important to establish whether *mrd* operon mutants of *Salmonella* remain not only viable, but virulent.

1.6 Outline of aims, progress and major results from this study

In conclusion, the major aims of this thesis were to systematically analyse the role of the *mrd* operon in the biology and pathogenicity of *Salmonella enterica* serovar Typhi. Specifically, this entailed the primary analysis of the *mrd* operon structure, followed subsequently by the construction of precise knockout mutants of each gene in *S. enterica* serovar Typhi, and comprehensive phenotypic analyses of these mutants. A wide range of phenotypic analyses were to be utilised to enable investigation of both the general physiology and biology of mutant cells, and the pathogenicity of these strains. This would be done with the hope of gaining a better understanding of the function of this operon, and in particular establishing whether there are any links between the function of these genes and pathogenicity in *Salmonella*. This aspect may be particularly significant, given the nature of

many major *Salmonella* virulence determinants as cell wall-spanning organelles, which may be dependent upon a certain level of cell wall integrity for their function, as previously discussed.

As work has progressed, initial results demonstrated clear effects of *mrd* gene inactivation on some but not all aspects of pathogenicity, due to the downregulation of invasion-associated virulence genes. As such, the focus of this project was developed, with additional aims of elucidating the regulatory mechanisms responsible for controlling the observed phenotypes and the overall behaviour of the mutants.

Work of this thesis has followed the aims closely, bringing about significant insights into the *mrd* operon genes. To date, the results of this work have shown that round-cell *pbpA* and *rodA* mutants, but not *ybeB*, *ybeA*, and *rlpA* mutants, have severe defects in invasion-associated virulence, such as SPI-1 and motility, whereas virulence factors involved in intracellular survival remained active in these mutants. More recent work has demonstrated that virulence can be recovered in round-cell mutants through the restored expression of the major SPI-1 and motility transcriptional regulators. Furthermore, several putative regulators of these phenotypes have been identified, suggesting that envelope stress response pathways are activated in round-cell mutants, as well as at least one other novel regulator. Together these regulators play a major role in controlling virulence gene expression in response to the inactivation of *pbpA* or *rodA*. The roles of the remaining 3 *mrd* operon genes have been investigated, and some data highlights potential functional links between the *mrd* operon genes.

Chapter 2. Materials and Methods

2.1 Materials

2.1.1 Chemicals, kits and reagents

General laboratory chemicals and antibiotics were acquired from Sigma-Aldrich® (Dorset, UK), or BDH® Chemicals (VWR International, Leicestershire, UK). Bacto™ Growth media was obtained from BD (Oxford, UK).

Restriction endonuclease enzymes and T4 DNA ligase used in this study were purchased from Promega UK (Southampton, UK) and Fermentas UK (York, UK). GoTaq® DNA Polymerase and Phusion® High-Fidelity DNA Polymerase were purchased from Promega UK (Southampton, UK) and Finnzymes (NEB UK, Herts, UK) respectively. RT-PCR reactions were performed using the Access RT-PCR System (Promega, Southampton, UK).

The Qiagen DNeasy Blood and Tissue Kit was used for genomic DNA preparation (West Sussex, UK). Additional DNA purification kits used in this study were obtained from Invitrogen™ (Life Technologies co., California, US), including the following: the Purelink™ Quick Plasmid Miniprep Kit, the PureLink™ PCR Purification Kit, and the PureLink™ Quick Gel Extraction Kit. The Ambion® Ribopure™-Bacteria Kit was used for RNA isolation (Life Technologies co., California, US). Lipopolysaccharide (LPS) extraction kits were obtained from iNtRON Biotechnology (Gyeonggi-do, Korea).

The NBS Biologicals SafeView Nucleic Acid Stain was used for detecting DNA/RNA in agarose gels (Cambridgeshire, UK). GeneRuler™1kb DNA Ladder and PageRuler™ Prestained Protein Ladder molecular weight markers were purchased from Fermentas UK (York, UK). Alternatively, 1kb DNA Ladder was purchased from Promega UK (Southampton, UK).

Finally, the “SilverSNAP” Pierce Silver Stain kit was obtained from Pierce Protein Research (Thermo Fisher Scientific, Illinois, US).

2.1.2 Antisera

Polyclonal horseradish peroxidise (HRP)-conjugated goat anti-rabbit and goat anti-mouse immunoglobulins, routinely used in western blotting, were purchased from Dako UK Ltd. (Cambridgeshire, UK). Alexa Fluor® 488 dye-labelled goat anti-rabbit IgG antibodies, for use in immunofluorescence microscopy, were purchased from Invitrogen™ (Life Technologies co., US).
HA.11 monoclonal IgG antibody was obtained from Covance Inc. (New Jersey, US).

Salmonella agglutinating sera for use with slide agglutination assays and immunofluorescence microscopy were obtained from Murex Biotech Ltd. (Dartford, UK).

The SPI-1 anti-SipA, anti-SipC and anti-SipD rabbit polyclonal antibodies used in western blots and immunofluorescence microscopy were kindly donated by Vassilis Koronakis (Cambridge University, UK). The SPI-2 anti-SseB rabbit polyclonal antibody was kindly donated by David Holden (Imperial College London).

2.1.3 Buffers, stock solutions, antibiotics and media

Buffers and stock solutions were prepared as follows. Final concentrations or working concentrations are shown in brackets. All growth media was sterilised before use by autoclaving. Buffers and solutions were sterilised as required, by autoclaving or filter sterilisation (pore size: 0.2 µm).

10x Phosphate-buffered saline (PBS)
80 g NaCl, 2 g KCl and 11.5 g Na_2HPO_4 made up to 1 litre with dH_2O, adjusted to pH 7.5.

10x SDS-PAGE running buffer
30.3 g Trizma® base (250 mM), 187.7 g glycine (2.5 M) and 10 g sodium dodecyl sulphate (SDS) (1%), made up to 1 litre with dH_2O.

6x SDS-PAGE sample buffer

100 µl 0.5 M Tris-HCl pH 6.8 (50 mM), 60 µl 10% SDS (0.6%), 50 µl 2% bromophenol blue (0.1%) and 400 µl glycerol (40%), made up to 1 ml with dH_2O. 10% 2-mercaptoethanol added before use.

2x SDS-PAGE sample buffer

200 µl 0.5 M Tris-HCl pH 6.8 (100 mM), 400 µl 10% SDS (4%), 100 µl 2% bromophenol blue (0.2%) and 200 µl glycerol (20%), made up to 1 ml with dH_2O. 10% 2-mercaptoethanol added before use.

Transfer buffer for western blotting

14.4 g glycine, 3.06 g Trizma® base and 200 ml methanol, made up to 1 litre with dH_2O. Freshly prepared and cooled to 4ºC before use.

Blocking solution for western blotting

3% bovine serum albumin dissolved in PBS-Tween (0.1% Tween). Freshly prepared before use.

Chloro-naphthol developer solution for western blotting

30 mg 4-chloro-1-naphthol, 10 ml methanol, 30 ml PBS and 60 µl hydrogen peroxide (30% w/w). Freshly prepared before use.

Coomassie® Brilliant Blue stain solution

0.2 g Coomassie® Brilliant Blue R, 80 ml methanol and 10 ml acetic acid, made up to 200 ml with dH_2O.

Coomassie® de-stain solution

300 ml methanol and 100 ml acetic acid, made up to 1 litre with dH_2O.

50x TAE buffer

242 g Trizma® base, 57.1 ml acetic acid and 100 ml 0.5 M EDTA, made up to 1 litre with dH_2O and adjusted to pH 8.0.

6x DNA loading buffer

1.25 ml 2% bromophenol blue (~0.25%), 4 ml glycerol (~40%) and 5 ml dH_2O (~50%).

4% Paraformalydehyde fixing solution

4% paraformaldehyde (PFA) dissolved in PBS.

1000x Ampicillin stock solution

100 mg ampicillin sodium salt dissolved in 1 ml dH_2O. Working concentration: 100 µg/ml.

1000x Kanamycin stock solution

50 mg kanamycin sulphate salt dissolved in 1 ml dH_2O. Working concentration: 50 µg/ml.

1000x Chloramphenicol stock solution

25 mg chloramphenicol dissolved in 1 ml 70% ethanol. Working concentration: 25 µg/ml.

100x Tetracycline stock solution

5 mg tetracycline hydrochloride dissolved in 1 ml 70% ethanol. Working concentration: 50 µg/ml.

100x Aromatic amino acid mix stock solution (Aro mix)

80 mg L-phenylalanine (40 µg/ml), 80 mg L-tryptophan (40 µg/ml), 20 mg 4-aminobenzoic acid (PABA) (10 µg/ml) and 20 mg 2,3-dihydroxybenzoic acid (DHBA) (10 µg/ml), dissolved in 20 ml dH_20.

100x Tyrosine stock solution (Tyr mix)

80 mg L-tyrosine dissolved in 20 ml 0.1 M HCl. Working concentration: 40 µg/ml.

100x Congo red solution

10 mg congo red dissolved in 1 ml 70% ethanol. Working concentration: 100 µg/ml.

Luria-Bertani (LB) broth

10 g tryptone, 5 g yeast extract and 10 g NaCl, made up to 1 litre with dH_2O. For 1.5% LB agar, 15 g of agar was added to 1 litre LB broth.

SOC media

20 g tryptone, 5 g yeast extract, 0.5 g NaCl and 10 ml 250 mM potassium chloride, adjusted to pH 7.0 and made up to 1 litre with dH_2O. 10 ml sterile 1 M $MgCl_2$ and 10 ml sterile 1 M glucose added before use.

M5.8 SPI-2-inducing minimal media

15.76 g Tris-HCl (100 mM), 0.1% casamino acids and 1.6 ml glycerol (0.16%), adjusted to pH 5.8 and made up to 1 litre with dH_2O. 10 µl sterile 1 M $MgCl_2$ (10 µM) and 10 ml sterile 4 mg/ml histidine (40 µg/ml) added before use.

Motility agar (0.3% agar)

10 g tryptone, 5 g NaCl and 3 g agar, made up to 1 litre with dH_2O.

2.1.4 Molecular size markers

DNA molecular size markers for agarose gels

The Fermentas GeneRuler™ 1 kb DNA Ladder (York, UK) or the Promega 1 kb DNA Ladder (Southampton, UK) were used as DNA molecular size markers for the separation of DNA in agarose gels (Figure 2.1).

Protein molecular size markers for SDS-PAGE

The Fermentas PageRuler™ Prestained Protein Ladder (York, UK) was used as a molecular weight marker during the separation of proteins by SDS-PAGE (Figure 2.2).

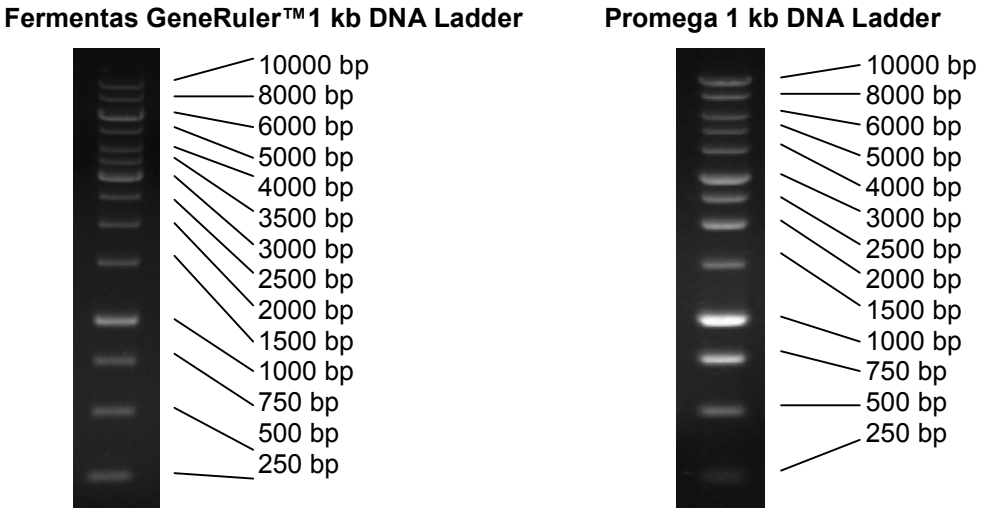

Figure 2.1: DNA molecular size markers: Indication of DNA fragment sizes for Fermentas and Promega DNA molecular size markers, as used in agarose gel electrophoresis with DNA.

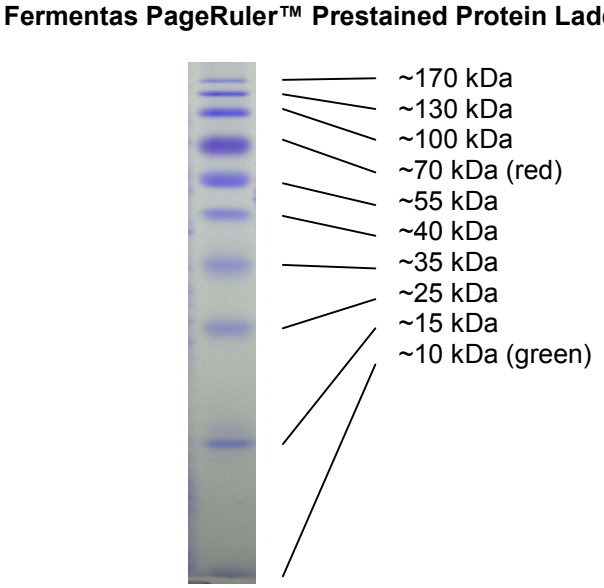

Figure 2.2: Protein molecular size markers: Indication of protein fragment sizes for the Fermentas PageRuler™ molecular size marker, as used in the separation of proteins by SDS-PAGE.

2.1.5 Bacterial strains and plasmids

The bacterial strains and plasmids used in this work, along with any relevant information, are outlined in Table 2.1.

Bacterial strains

Species	*Strain*	*Genotype/relevant information*	*Source/reference*
S. enterica serovar Typhi	BRD948	Derivative of Ty2 strain; Δ*aroC,* Δ*aroD,* Δ*htrA*	G. Dougan (Sanger institute, Cambridge) (232, 233)
	BRD948	Δ*ybeB*	This study
	BRD948	Δ*ybeA*	This study
	BRD948	Δ*pbpA*	This study
	BRD948	Δ*rodA*	This study
	BRD948	Δ*rlpA*	(163)
	BRD948	*pagN*::*cat* (Henceforth: Δ*pagN*)	This study
	BRD948	*rcsC*::*cat* (Henceforth: Δ*rcsC*)	This study
	BRD948	Δ*rodA* Δ*pagN*	This study
	BRD948	Δ*pbpA* Δ*rcsC*	This study
	BRD948	Δ*rodA* Δ*rcsC*	This study
S. enterica serovar Typhimurium	SL1344	Wild-type, derivative of LT2	(234)
	SL1344	Δ*spi1*	(235)
	NCTC 12023	Δ*ssaV* SPI-2 non-secretor	DW. Holden (47)
	SL1344	Δ*ssaV* SPI-2 non-secretor	Transduced from the above
	SL1344	*ybeB*::*kan* (Henceforth: Δ*ybeB*)	This study
	SL1344	*pbpA*::*kan* (Henceforth: Δ*pbpA*)	This study
	SL1344	*rodA*::*kan* (Henceforth: Δ*rodA*)	(163)
	SL1344	*rlpA*::*kan* (Henceforth: Δ*rlpA*)	(163)
	SL1344	TPA14 (P_{flhDC}*5451*::Tn*10*[del-25])	This study; transduced from phage stock given by PD. Aldridge (236)
	SL1344	Δ*pbpA* TPA14	This study; as above
	SL1344	Δ*rodA* TPA14	This study; as above
	SL1344	Tn*10*d(Tc)	H. Spencer (ICAMB, Newcastle)
	SL1344	*pagN10a*::Tn*10*d(Tc)	This study
	SL1344	*rcsC4a*::Tn*10*d(Tc)	This study
	SL1344	*rcsC9a*::Tn*10*d(Tc)	This study
	SL1344	*rodA::kan, pagN10a*::Tn*10*d(Tc)	This study
	SL1344	*rodA::kan, rcsC4a*::Tn*10*d(Tc)	This study
	SL1344	*rodA::kan, rcsC9a*::Tn*10*d(Tc)	This study
	SL1344	*pagN::cat* (*Cm*^{r}) (Henceforth: Δ*pagN*)	This study
	SL1344	*rcsC*::*cat* (Henceforth: Δ*rcsC*)	This study
	SL1344	Δ*pbpA* Δ*pagN*	This study
	SL1344	Δ*rodA* Δ*pagN*	This study
	SL1344	Δ*pbpA* Δ*rcsC*	This study
	SL1344	Δ*rodA* Δ*rcsC*	This study

	SL5338	*galE* r$^-$ m$^+$ (Rough LPS mutant)	(237)
E. coli	TOP10	F- *mcr*A Δ(*mrr-hsd*RMS-*mcr*BC) φ80*lac*ZΔM15 Δ*lac*X74 *rec*A1 *ara*D139 Δ(*araleu*) 7697 *gal*U *gal*K *rps*L (StrR) *end*A1 *nup*G	Invitrogen™ (Life Technologies co., California, US)
	MC1000	λ$^-$e14$^-$ *araD139* Δ(*araA-leu*)*7697 galE15 galK16* Δ(*codB-lac*)*3 rpsL150 mcrB1 relA1 spoT1*	L. Rothfield (University of Connecticut, US) (135)

Plasmids

Name	*Genotype/relevant information*	*Source/reference*
pKD46	Red helper plasmid. Derivative of pINT-ts, *araC-P$_{araB}$* and γ β *exo,* tL3 terminator downstream of exo. Encodes λ Red Recombinase gene. Ampicillin resistant (*amp^R*), temperature sensitive	(238)
pKD13	Template plasmid. Derivative of pANTSγ with kanamycin resistance (*kan^R*) gene flanked by FLP recognition target (FRT) sites, *amp^r*	(238)
pKD3	Template plasmid. Derivative of pANTSγ with chloramphenicol resistance (*Cm^R*) gene flanked by FLP recognition target (FRT) sites, *amp^R*	(238)
pCP20	*FLP$^+$,* λ cI857$^+$, λ $_{PR}$ Rep^{ts}, *amp^R, Cm^R*, temperature sensitive	(238, 239)
pMK1*lux*	Transcriptional luminescence reporter plasmid. pBR322 cloning vector with promoter-less *luxCDABE* operon (taken from pSB377) downstream of MCS. *amp^R*	(240-242)
pMK1*lux–PcobC*	499bp region, 27bp upstream of BRD948 *cobC* gene cloned into pMK1*lux* MCS between 5' ecoR1 and 3' BamH1 restriction sites	This study
pMK1*lux–PybeB*	499bp region, 29bp upstream of BRD948 *ybeB* gene cloned into pMK1*lux* MCS between 5' ecoR1 and 3' BamH1 restriction sites	This study
pMK1*lux–PybeA**	496bp region, 30bp upstream of BRD948 *ybeA* gene cloned into pMK1*lux* MCS between 5' ecoR1 and 3' BamH1 restriction sites	This study
pMK1*lux–PybeA*	289bp region, 30bp upstream of BRD948 *ybeA* gene cloned into pMK1*lux* MCS between 5' ecoR1 and 3' BamH1 restriction sites	This study
pMK1*lux–PpbpA*	499bp region, 33bp upstream of BRD948 *pbpA* gene cloned into pMK1*lux* MCS between 5' ecoR1 and 3' BamH1 restriction sites	This study
pMK1*lux–ProdA*	501bp region, 31bp upstream of BRD948 *rodA* gene cloned into pMK1*lux* MCS between 5' ecoR1 and 3' BamH1 restriction sites	This study
pMK1*lux–PrlpA*	500bp region, 30bp upstream of BRD948 *rlpA* gene cloned into pMK1*lux* MCS between 5' ecoR1 and 3' BamH1 restriction sites	This study
pMK1*lux–fliF*	Promoter region of *fliF* gene (499bp upstream of *fliF*, including first 18bp of *fliF*) cloned into pMK1*lux* MCS between 5' ecoR1 and 3' BamH1 restriction sites	This study
pMK1*lux–hilD*	Promoter region of *hilD* gene (504bp upstream of *hilD*, including first 24bp of *hilD*) cloned into pMK1*lux* MCS between 5' ecoR1 and 3' BamH1 restriction sites	This study
pRG38 (*flhD*)	Transcriptional luminescence reporter plasmid. *flhD* promoter cloned into promoter-less pSB401-based *luxCDABE* fusion plasmid to generate *flhD*::*luxCDABE.* (*Tet^R*)	BMM. Ahmer (Ohio State University, US) (243)
pWSK-*sseJ*2HA	*sseJ* (SPI-2 effector protein) and haemagglutinin (HA)	DW. Holden (244)

	tag sequences cloned into pWSK29 to generate C-terminal Haemagglutin-tagged (HA-tagged) SseJ	
pLE7	N-terminal Yfp fusion plasmid encoding *E. coli* MreB-YFP (P*lac-yfp*::*mreB*). (*amp*^{R})	L. Rothfield (University of Connecticut, US) (135)
pVP6	N-terminal Yfp fusion plasmid encoding *E. coli* PBP2-YFP (P*lac-yfp*::*pbpA*). Digested XbaI/HindIII site-flanked *pbpA* cloned into XbaI/HindIII-digested pLE7	L. Rothfield (135)
pVP3	N-terminal Yfp fusion plasmid encoding *E. coli* RodA-YFP (P*lac-yfp*::*rodA*). Digested XbaI/HindIII site-flanked *rodA* cloned into XbaI/HindIII-digested pLE7	L. Rothfield (135)
pLE-*ybeB*	N-terminal Yfp fusion plasmid encoding *S.* Typhi YbeB-YFP (P*lac-yfp*::*ybeB*). Digested XbaI/HindIII site-flanked *ybeB* cloned into XbaI/HindIII-digested pLE7	This study
pLE-*ybeA*	N-terminal Yfp fusion plasmid encoding *S.* Typhi YbeA-YFP (P*lac-yfp*::*ybeA*). Digested XbaI/HindIII site-flanked *ybeA* cloned into XbaI/HindIII-digested pLE7	This study
pJBT	Cloning vector derived from pBR322. 8 amino acid epitope tag '*Strep*-tag®' encoded downstream of MCS, all under control of an arabinose inducible pBAD promoter. Used to generate C-terminal *Strep*-tag® fusion proteins. *amp*^{R}	IBA International (Louvain-la-Neuve, Belgium) (241)
pJBT-*rlpA*	pJBT C-terminal *Strep*-tag® fusion plasmid encoding RlpA-*Strep*-tag®. Digested EcoRI/HindIII site-flanked *rlpA* cloned into EcoRI/HindIII-digested pJBT	(163)
pBAD24	Arabinose-inducible expression vector. Plasmid gene expression from MCS under control of arabinose operon P_{BAD} promoter. MCS contains optimised shine-delgarno (SD) sequence for efficient translation. *amp*^{R}	(245)
pBAD-*hilD*	pBAD24 expression vector encoding *S.* Typhimurium HilD protein under control of arabinose-inducible P_{BAD} promoter. Digested ecoRI/xbaI site-flanked *hilD* cloned into ecoRI/xbaI-digested pBAD24	DM. Bulmer (ICAMB, Newcastle, UK)
pBAD-*yciR*- *Strep*-tag®,	pBAD24 expression vector encoding N-terminal *S.* Typhi YciR- *Strep*-tag® fusion protein under control of arabinose-inducible P_{BAD} promoter. Digested ncoI/xbaI site-flanked *yciR* cloned into ncoI/xbaI-digested pBAD24-StrepN	This study

Table 2.1: List of bacterial strains and plasmids: Details and sources of bacterial strains and plasmids used in this study.

2.1.6 Synthetic oligonucleotide primers

Synthetic oligonucleotide primers were designed and then purchased from (Life Technologies co., US). Upon delivery, oligonucleotides were reconstituted in nuclease-free dH_2O to a final concentration of 100μM and stored at -20ºC till use. A comprehensive list of the primers used in this study, along with information on their usage, is given below (Table 2.2).

Primer name	*Nucleotide sequence (5' → 3' direction)*	*Usage, reference*
Check primers		
ybeB 5	ttataacgcaattattcacc	5' *ybeB* check primer
ybeB 3	cgacaagttgcagcttcacg	3' *ybeB* check primer
ybeA 5	gaactggaaaaactctggag	5' *ybeA* check primer
ybeA 3	ctgcttaatcttctcaagac	3' *ybeA* check primer
pbpA 5	gtaccgggcgtggagcatcac	5' *pbpA* check primer
pbpA 3	gatcgatatgaattttatccc	3' *pbpA* check primer
rodA 5	caacaacacccatttgcctg	5' *rodA* check primer (163)
rodA 3	agtagtactatccctgccgc	3' *rodA* check primer (163)
pagN 5	gggcttcgtttatgtaatcg	5' *pagN* check primer
pagN 3	ggcgcaggagtattcattac	3' *pagN* check primer
rcsC 5	cgtcatttaccgctaccta	5' *rcsC* check primer
rcsC 3	ggcctaccagtcgactcatc	3' *rcsC* check primer
Knockout primers		
ybeB P1	ttgcagggtaaagcactccaggattttgttatcgataaaa gtgtaggctggagctgcttc	P1 *ybeB* knockout primer
ybeB P4	agagtttttccagttcatacaggcggcgactttcttcctg attccggggatccgtcgacc	P4 *ybeB* knockout primer
ybeA P1	aagctgcaacttgtcgctgtcggcacgaagatgcccgact gtgtaggctggagctgcttc	P1 *ybeA* knockout primer
ybeA P4	tcacggtgataagggtggttggttgtgatgctccacgccc attccggggatccgtcgacc	P4 *ybeA* knockout primer
pbpA P1	aacgacaaaattcttttcgtgactatacggctgagtccgc gtgtaggctggagctgcttc	P1 *pbpA* knockout primer
pbpA P4	caggcaaatgggtgttgttgtcgcccagcatgatgtgatc attccggggatccgtcgacc	P4 *pbpA* knockout primer
rodA P1	catgacggataatccgaacaaaaaaaccttctgggataaa gtgtaggctggagctgcttc	P1 *rodA* knockout primer (163)
rodA P4	gacgcagattacaggcaactgcttacgcattgcgcacccc attccggggatccgtcgacc	P4 *rodA* knockout primer (163)
pagN P1	gaaacttgtcttttagcccaatattaaggcaggttctgaa gtgtaggctggagctgcttc	P1 *pagN* knockout primer (246)
pagN P2	cttcgggaacccacaggaccagctattttaccgatagtgt atgggaattagccatggtcc	P2 *pagN* knockout primer (246)
rcsC P1	gtcacactctatttacatcctgaggcggagcttcgcccct gtgtaggctggagctgcttc	P1 *rcsC* knockout primer (246)
rcsC P2	ttttacaggccggacaggcgacgccgccatccggcatttt atgggaattagccatggtcc	P2 *rcsC* knockout primer (246)
Mutant sequencing primers		
SEQybeB5	cacggcgtcccgccggaagg	5' Δ*ybeB* sequencing primer
SEQybeB3	atcagctcaaagggcatatc	3' Δ*ybeB* sequencing primer
SEQybeA5	tgactggattgtcgtcgatc	5' Δ*ybeA* sequencing primer

SEQybeA3	gcgaccagcgcccgacgcac	3' Δ*ybeA* sequencing primer
SEQpbpA5	gcgttaacgctccctcaccc	5' Δ*pbpA* sequencing primer
SEQpbpA3	gtcctggccgctggcgctcc	3' Δ*pbpA* sequencing primer
SEQrodA5	cggcgcaggcccggcagtag	5' Δ*rodA* sequencing primer (163)
SEQrodA3	cattacataccgcaggttgc	3' Δ*rodA* sequencing primer (163)
pMK1*lux* cloning primers		
pMK1lux-PcobC 5 ecoRI	gcggaattcgtcaacgcctcaagaatggc	5' P_{cobC} pMK1*lux* cloning primer
pMK1lux-PcobC 3 bamHI	gcgggatccaaacatgataatgcccctga	3' P_{cobC} pMK1*lux* cloning primer
pMK1lux-PybeB 5 ecoRI	gcggaattccgttcagcgattgccagaac	5' P_{ybeB} pMK1*lux* cloning primer
pMK1lux-PybeB 3 bamHI	gcgggatcctaacgatagaaaaaggcca	3' P_{ybeB} pMK1*lux* cloning primer
pMK1lux-PybeA* 5 ecoRI	gcggaattcggcgatgctttctgtgacgtg	5' P_{ybeA*} pMK1*lux* cloning primer
pMK1lux-PybeA 5 ecoRI	gcggaattcgcagggtaaagcactccagg	5' P_{ybeA} pMK1*lux* cloning primer
pMK1lux-PybeA 3 bamHI	gcgggatcccaggcggcgactttcttcct	3' P_{ybeA} pMK1*lux* cloning primer
pMK1lux-PpbpA 5 ecoRI	gcggaattccctgtatgaactggaaaaac	5' P_{pbpA} pMK1*lux* cloning primer
pMK1lux-PpbpA 3 bamHI	gcgggatccctcacggtgataagggtggt	3' P_{pbpA} pMK1*lux* cloning primer
pMK1lux-ProdA 5 ecoRI	gcggaattcggacggcaacgccgattcag	5' P_{rodA} pMK1*lux* cloning primer
pMK1lux-ProdA 3 bamHI	gcgggatccggttttccgcaggcaaatgg	3' P_{rodA} pMK1*lux* cloning primer
pMK1lux-PrlpA 5 ecoRI	gcggaattcgtggtttttcctgatgcacg	5' P_{rlpA} pMK1*lux* cloning primer
pMK1lux-PrlpA 3 bamHI	gcgggatccttttttctgtgggtgtggatc	3' P_{rlpA} pMK1*lux* cloning primer
pMK1lux-PdacA 5 ecoRI	gcggaattccgaccacgctggcgcctggc	5' P_{dacA} pMK1*lux* cloning primer
pMK1lux-PdacA 3 bamHI	gcgggatccccctactatagcaaaagcat	3' P_{dacA} pMK1*lux* cloning primer
pMK1lux-hilD 5 ecoRI	gcggaattctatatcagggagttgacctg	5' P_{hilD} pMK1*lux* cloning primer
pMK1lux-hilD 3 BamHI	gcgggatccacttacaaaggttacattttc	3' P_{hilD} pMK1*lux* cloning primer
pMK1lux-fliF 5 ecoRI	gcggaattcgcacctgaatccccatttgc	5' P_{fliF} pMK1*lux* cloning primer
pMK1lux-fliF 3 BamHI	gcgggatcccgatgcagtcgcactcatctc	3' P_{fliF} pMK1*lux* cloning primer
pMK1*lux* check primers		
Lux F	ctataaaaataggcgtatcac	5' pMK1*lux* check primer
Lux R	ctggccgttaataatgaatg	3' pMK1*lux* check primer
pBAD24 check primers		
pBAD-F	ggcgtcacactttgctatgc	5' pBAD24 check primer
pBAD-R	ctgatttaatctgtatcagg	3' pBAD24 check primer

pLE7 cloning primers		
pLE–ybeB 5	gcgtctagattgcagggtaaagcactccag	5' pLE-*ybeB* cloning primer
pLE–ybeB 3	gcgaagcttttaactccagagtttttccag	3' pLE-*ybeB* cloning primer
pLE–ybeA 5	gcgtctagagtgaagctgcaacttgtcgc	5' pLE-*ybeA* cloning primer
pLE–ybeA 3	gcgaagctttcactcacggtgataaggg	3' pLE-*ybeA* cloning primer
pLE7 check primers		
pLE7-F	gagagaccacatggtccttc	5' pLE7 & derivatives check primer
pLE7-R	gggttttcccagtcacgacg	3' pLE7 & derivatives check primer
RT-PCR primers		
RT cobD-C F	gtccgggtagcgctcaatgc	5' *cobD-cobC* primer
RT cobD-C R	ttctggcaatcgctgaacgc	3' *cobD-cobC* primer
RT cobC-ybeB F	tagaacagggatgctggagc	5' *cobC-ybeB* primer
RT cobC-ybeB R	taccctgaacatctaaggcg	3' *cobC-ybeB* primer
RT ybeB-A F	gcagggtaaagcactccagg	5' *ybeB-ybeA* primer
RT ybeB-A R	gtaacaatgcgattcttacc	3' *ybeB-ybeA* primer
RT ybeA-pbpA F	gcaaacgcggcaagaacgcg	5' *ybeA-pbpA* primer
RT ybeA-pbpA R	caaggggaatgccgttgcgg	3' *ybeA-pbpA* primer
RT pbpA-rodA F	ccaacgaaacgtacaatgcg	5' *pbpA-rodA* primer
RT pbpA-rodA R	cttggatattgcgccgaagg	3' *pbpA-rodA* primer
RT rodA-rlpA F	agagcgcaaactacatttgg	5' *rodA-rlpA* primer
RT rodA-rlpA R	ggaggcggttaaattactgc	3' *rodA-rlpA* primer
RT rlpA-dacA F	gccgtcagcgatcaaacgcg	5' *rlpA-dacA* primer
RT rlpA-dacA R	ccagaactttgccggagttg	3' *rlpA-dacA* primer
RT dacA-ybeD F	cgctgggcgtcgataaagac	5' *dacA-ybeD* primer
RT dacA-ybeD R	tttaccgtcggagagtaatc	3' *dacA-ybeD* primer
Tn*10*d(Tc) arbitrary PCR primers		
Tn10 arb1	ccacgcgtcgactagtacNNNNNNNNNNNgatat	Arbitrary primer 1 (1st round) (247)
Tn10 arb2	ccacgcgtcgactagtac	Arbitrary primer 2 (2nd round) (247)
Tn10-R	acctttggtcaccaacgctt	1st round Tn*10*d(Tc)-specific primer (248)
Tn10-I	gacaagatgtgtatccac	2nd round Tn*10*d(Tc)-specific primer (248)

Table 2.2: List of oligonucleotide primers: Details, sequences and sources of oligonucleotide primers used in this study.

2.2 Methods

2.2.1 Bacterial growth conditions

Bacteria were routinely cultured in LB broth at 37ºC with shaking (200 rpm). Where appropriate, culture media was supplemented with ampicillin, kanamycin, chloramphenicol or tetracycline at concentrations of 100 µg/ml, 50 µg/ml, 25 µg/ml and 50 µg/ml respectively. At these conditions SPI-1 and flagella genes are expressed whilst cells are actively growing. To induce SPI-2 gene expression, cells were cultured in M5.8 minimal media at 37ºC and 200 rpm, for at least 16 hours. *Salmonella* Typhi BRD948 was cultured in media supplemented with aromatic amino acids and tyrosine as described (163, 232). In addition, where appropriate growth media was supplemented with $MgCl_2$ to a final concentration of 20 mM, to facilitate growth of round-cell Δ*pbpA* and Δ*rodA* mutants.

2.2.2 Genomic DNA purification

Bacterial genomic DNA was isolated and purified using the Qiagen DNeasy Blood and Tissue Kit (West Sussex, UK). DNA purification was done according to the kit instructions. 5 ml of overnight culture (stationary phase cells) was harvested by centrifugation (4000 x g, 15 minutes, 4ºC) and the pellet resuspended in 180 µl Buffer ATL. 20 µl proteinase K was added to the suspension and mixed thoroughly by vortexing. Samples were then incubated at 56ºC for several minutes until the cells had lysed. After vortexing the samples for 15 seconds, 200 µl Buffer AL was added and mixed thoroughly. 200 µl 100% ethanol was subsequently added and mixed thoroughly. Samples were then transferred to DNeasy Mini spin columns, each in a collection tube, and centrifuged at ≥6000 x g for 1 minute. After replacing the collection tubes and discarding the contents, columns were washed with 500 µl Buffer AW1 and centrifuged as previously. The flow-through was discarded and the column washed in 500 µl Buffer AW2. Columns were then centrifuged at ~17000 x g for 3 minutes to dry the membranes, and transferred to clean 1.5 ml microcentrifuge tubes. Finally, 200 µl sterile dH_2O was pipetted onto the centre of each column and incubated at room temperature (~22°C unless stated otherwise) for 1 minute, before centrifuging for 1 minute at ≥6000 x g to elute the genomic DNA. Genomic DNA was stored at 4ºC until use.

2.2.3 RNA extraction and purification

The Ambion® Ribopure™-Bacteria Kit was used to isolate and purify DNA-free RNA for use in downstream reverse transcriptase PCR (RT-PCR). Work areas were thoroughly cleaned before commencing any RNA work, and all steps were done in using gloves, clean equipment and nuclease-free filter tips, to help prevent DNase or RNase contamination.

Bacteria were cultured to mid-log phase (OD600 ~1.2) and 10 ml each culture was harvested by centrifugation (4000 x g, 15 minutes, 4ºC). After completely removing the culture supernatants, cell pellets were resuspended in 350 µl RNAwiz by pipetting or vortexing. Cells were then transferred to individual screw-cap tubes containing 250 µl ice-cold Zirconia beads and vortexed at maximum speed for 10 minutes to lyse the cells. Lysates were centrifuged at ~17000 x g for 5 minutes to pellet the beads, then transferred to clean nuclease-free 1.5 ml tubes. 0.2 volumes of chloroform was added to each lysate, shaken vigorously for 30 seconds, and then incubated at room-temperature for 10 minutes. A further 5 minute centrifugation step at ~17000 x g enabled the aqueous phase (top layer) to be removed and transferred to a clean nuclease-free 1.5 ml tube. In the final RNA purification steps, 0.5 volumes 100% ethanol was added to the recovered aqueous phase and mixed well. Samples were then transferred to individual filter cartridges placed inside collection tubes, and centrifuged at maximum speed for 1 minute. After discarding the flow-through, columns were washed with 700 µl Wash Solution 1, and centrifuged as before. The flow-through was discarded, and the columns washed twice with 500 µl Wash Solution 2/3 and centrifuged as before. Cartridge membranes were finally dried by centrifugation at maximum speed for 1 minute. Columns were then placed into clean nuclease-free 2 ml collection tubes. To elute the RNA 25 µl preheated Elution Solution was added to the centre of each column and centrifuged at maximum speed for 1 minute. This elution step was repeated to obtain ~50 µl RNA.

An additional DNase treatment step was performed to remove any contaminating DNA. 4 µl DNase I and 5.5 µl 10x DNase buffer were added to the eluted DNA, before incubating at 37ºC for 30 minutes. 10 µl DNase Inactivation Reagent was

then added to each sample and incubated at room temperature for 2 minutes. Finally, samples were centrifuged at maximum speed for 1 minute, and the supernatants containing purified RNA were transferred to clean nuclease-free 1.5 ml tubes. Purified RNA was stored at -80ºC until use.

2.2.4 Plasmid DNA purification

Plasmid DNA was purified using the Invitrogen™ Purelink™ Quick Plasmid Miniprep Kit, according to kit instructions (Life Technologies co., California, US). 5 ml overnight cultures were first harvested by centrifugation (4000 x g, 15 minutes, 4ºC). After completely removing the supernatants, cell pellets were resuspended in 250 µl Resuspension Buffer and transferred to clean 1.5 ml microcentrifuge tubes. 250 µl Lysis Buffer was then added and mixed gently, and samples were incubated at room temperature for exactly 5 minutes. 350 µl Precipitation Buffer was added to each sample, shaken vigorously to mix, and samples were centrifuged at ~12000 x g for 10 minutes. Sample supernatants were then transferred onto individual spin columns placed within collection tubes. After centrifuging for 1 minute at ~12000 x g, 500 µl Wash Buffer W10 was added to each column and incubated for a minute at room temperature. The columns were centrifuged as previously, the flow-through discarded, and 700 µl Wash Buffer W9 added to each column. After centrifuging as before, the flow-through was again discarded and the columns centrifuged at maximum speed for 2 minutes to dry the membranes. The columns were then transferred to clean 1.5 ml elution tubes. 40-50 µl sterile dH_2O was pipetted onto the centre of each column and incubated at room temperature for 1 minute. Finally the columns were centrifuged at maximum speed for 1 minute to elute the purified plasmid DNA. Plasmid DNA was stored at -20ºC until use.

2.2.5 Purification of PCR products

The Invitrogen™ Purelink™ PCR Purification Kit was used to purify PCR products and other short linear DNA fragments, for use with downstream applications (Life Technologies co., California, US). Initially 4 volumes Binding Buffer with isopropanol was added to each DNA/PCR reaction mixture. After mixing, samples were transferred to individual spin columns and centrifuged at ~10000 x g for 1

minute. The flow-through was discarded, and then the spin columns washed with 600 µl Wash Buffer 1 before centrifuging as previously. The flow-through was again discarded and the spin columns were centrifuged at maximum speed for 1 minute to dry the membranes. The columns were then transferred to clean 1.5 ml microcentrifuge tubes. 40-50 µl sterile dH_2O was pipetted onto the centre of each column and incubated at room temperature for 1 minute. The columns were finally centrifuged at maximum speed for 1 minute to elute the DNA. Purified DNA was stored at -20ºC until use.

2.2.6 Purification of DNA fragments from agarose gels

DNA fragments excised from agarose gels were purified using the Invitrogen™ PureLink™ Quick Gel Extraction Kit (Life Technologies co., California, US). Purification of DNA was done according to the kit instructions with the exception of the initial solubilisation stage. After excision, gel slices of ~100 mg were solubilised by adding 300 µl Buffer QG (QIAquick Gel Extraction Kit, Qiagen) and incubating at 50ºC until fully dissolved. Once solubilised, samples were loaded onto individual Quick Gel Extraction Columns and centrifuged at ~12000 x g for 1 minute. The flow-through was discarded and the columns washed by adding 600 µl Wash Buffer W1 and centrifuging as previously. After discarding the flow-through, the column membranes were dried by centrifugation at ~12000 x g for 2 minutes. The columns were then transferred to clean 1.5 ml elution tubes and 40-50 µl sterile dH_2O was applied to the centre of each column. Purified DNA was eluted by centrifuging the columns at ~12000 x g for 1 minute.

2.2.7 Polymerase chain reaction (PCR)

A wide range of polymerase chain reaction (PCR) applications have been used in the course of this study. Each PCR technique is described below. In the case of all PCR applications, reaction mixtures were prepared on ice, in sterile nuclease-free 1.5 ml, 0.5 ml or 0.2 ml tubes. All reagents were added in order, as described. Thermal cycling conditions were also carried out as described. Where appropriate, PCR products were analysed by agarose gel electrophoresis and imaging, DNA sequencing, or restriction enzyme digestion.

GoTaq® PCR reactions

For standard non-fastidious PCR reactions, GoTaq® DNA polymerase, a formulation of the low fidelity *Taq* DNA polymerase, was used (Promega, Southampton, UK). Reaction mixtures were prepared according to kit instructions, as described.

Reaction mix:

Reagent (final concentration)	*Volume*
5x Green or Colourless GoTaq® Reaction Buffer (1x)	10 µl
Nuclease-free dH_2O	Up to final vol. of 50 µl
10 mM dNTPs (0.2 mM each dNTP)	1 µl
Upstream primer (1 µM)	0.5 µl
Downstream primer (1 µM)	0.5 µl
Template DNA (<0.5 µg/50 µl)	X µl
GoTaq® DNA polymerase 5 u/µl (1.25 u)	0.25 µl
	Final reaction volume: 50 µl

Thermal cycling conditions:

Step	*Temperature*	*Time*	
Initial denaturation	98ºC	5 minutes	
Denaturation	98ºC	30 seconds	x30
Annealing	55ºC	30 seconds	
Extension	72ºC	1 minute/kb	
Final Extension	72ºC	5 minutes	

Table 2.3: Reaction mix preparation and thermal cycling conditions for standard GoTaq® PCR

Colony PCR

Colony PCRs were performed by picking a small amount (<1 mg) of a bacterial colony with a sterile tip and transferring it to the bottom of a nuclease-free 0.2 µl PCR tube, for use as template DNA. The remainder of the colony was then patched onto LB agar containing relevant antibiotics, and cultured at 37ºC overnight. The thermal cycling conditions were done as for a standard GoTaq® PCR.

Reagent (final concentration)	*Volume*
5x Green or Colourless GoTaq® Reaction Buffer (1x)	10 µl
Nuclease-free dH_2O	37.75 µl
10 mM dNTPs (0.2 mM each dNTP)	1 µl
Upstream primer (1 µM)	0.5 µl
Downstream primer (1 µM)	0.5 µl
<1 mg Bacterial colony	-
GoTaq® DNA polymerase 5 u/µl (1.25 u)	0.25 µl

Final reaction volume: 50 µl*

*For colony PCR, 50 µl reaction mixtures were generally divided between 4 individual tubes to give ~12 µl reactions

Table 2.4: Reaction mix preparation for standard colony PCR

Phusion® polymerase PCR

Finnzymes Phusion® High-Fidelity DNA Polymerase (NEB UK, Herts, UK) was used to generate PCR products for applications such as cloning, to ensure a high quality PCR product. Reaction mixtures and cycling conditions were prepared according to the kit instructions, as described.

Reaction mix:

Reagent (final concentration)	*Volume*
5x Phusion® HF/GC Buffer	10 µl
Nuclease-free dH_2O	Up to final vol. of 50 µl
10 mM dNTPs (0.2 mM each dNTP)	1 µl
Upstream primer (1 µM)	0.5 µl
Downstream primer (1 µM)	0.5 µl
Template DNA (<0.5 µg/50 µl)	X µl
Phusion® DNA polymerase (0.02 u/µl)	0.5 µl
	Final reaction volume: 50 µl

Thermal cycling conditions:

Step	*Temperature*	*Time*	
Initial denaturation	98ºC	30 seconds	
Denaturation	98ºC	10 seconds	
Annealing	58ºC	30 seconds	x30-35
Extension	72ºC	0.5 minutes/kb	
Final Extension	72ºC	10 minutes	

Table 2.5: Reaction mix preparation and thermal cycling conditions for standard Phusion® polymerase PCR

Arbitrary PCR

Arbitrary PCR allows the amplification of DNA from a region where only part of the target sequence is known, using arbitrary primers in two separate rounds of PCR, as described by Knobloch et al. (247).

In this study arbitrary PCR was used to identify the insertion sites of the Tn*10*d(Tc) transposon during a mutagenesis screen, where only the TN*10*d(Tc) transposon sequence was known. The method was based on those from studies by Knobloch

et al., and O'Toole and Kolter (247, 249). The method used a specially designed forward arbitrary primer consisting of a specific 20 bp nucleotide 'tail' sequence at the 5' end, a mid-section containing a random 11 bp nucleotide sequence, and a specific 5 bp sequence at the 3' end (Figure 2.3, Table 2.2). The primer was designed such that on average the random sequence would anneal at sites within the template DNA at a given frequency. The arbitrary primer was coupled with a reverse primer complementary to a known target sequence within the 5' end of Tn*10*d(Tc). Thus the first round of PCR generated a mixture of products of varying lengths, all containing the 5' 20 bp tail sequence generated from the arbitrary primer. This was sometimes observed as a faint smear of DNA on agarose gels (Figure 2.3). In a second round of PCR, the products from the first round formed the template DNA. A second arbitrary primer was used consisting just of the 20 bp 5' tail sequence; this was coupled with another reverse primer complementary to a section of the Tn*10*d(Tc) sequence upstream from the first primer binding site (Table 2.2). The second round of PCR therefore generated several distinct products, typically of ~500-1000 bp in length, which were detected as distinct bands on an agarose gel. These products were purified and sequenced to determine the site of Tn*10*d(Tc) transposon insertion.

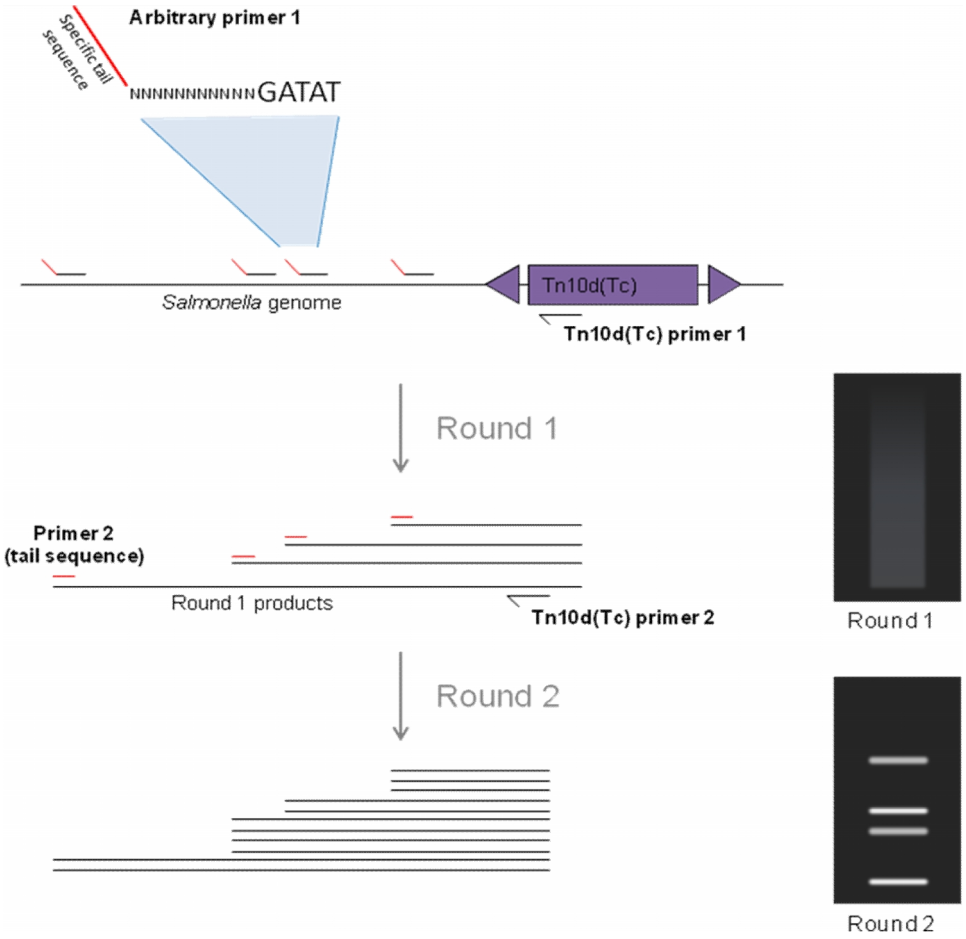

Figure 2.3 Arbitrary PCR to amplify regions of unknown sequence: Schematic diagram illustrating the arbitrary PCR method to amplify DNA, whereby only part of the target sequence is known. PCR products from successive rounds of PCR, as typically visualised on 1% agarose gels, are shown.

Arbitrary PCR reactions were performed using GoTaq® polymerase, with individual mutant colonies forming the template for the first round PCR reactions. After completion of the first round of PCR, 1 µl of the first round reaction mixture was directly transferred into the second round reaction mix as template DNA. PCR reaction mixtures were prepared and run as follows (Table 2.6).

Reaction mix:

Reagent	*Round 1*	*Round 2*
5x Green or Colourless GoTaq® Reaction Buffer	5 µl	10 µl
Nuclease-free dH_2O	18.875 µl	36.75 µl
10 mM dNTPs	0.5 µl	1 µl
Upstream primer	0.25 µl	0.5 µl
Downstream primer	0.25 µl	0.5 µl
Template DNA	<1 mg Colony	1 µl Round 1 product
GoTaq® DNA polymerase 5 u/µl	0.125 µl	0.25 µl
	Final reaction volume: 25 µl	Final reaction volume: 50 µl

Round 1 - Thermal cycling conditions:

Step	*Temperature*	*Time*	
Initial denaturation	95ºC	5 minutes	
Denaturation	95ºC	1 minute	x6
Annealing	30ºC	1 minute	
Extension	72ºC	1 minute 30 seconds	
Denaturation	95ºC	30 seconds	x30
Annealing	50ºC	30 seconds	
Extension	72ºC	1 minute 30 seconds	
Final Extension	72ºC	7 minutes	

Round 2 - Thermal cycling conditions:

Step	*Temperature*	*Time*	
Initial denaturation	95ºC	5 minutes	
Denaturation	95ºC	30 seconds	x30
Annealing	55ºC	30 seconds	
Extension	72ºC	1 minute	
Final Extension	72ºC	7 minutes	

Table 2.6: Reaction mix preparation and thermal cycling conditions for arbitrary PCR

Reverse transcriptase PCR (RT-PCR)

The Promega Access RT-PCR System (Southampton, UK) was used to detect the presence of certain RNA transcripts within *Salmonella* Typhi. The two-step system permits the generation and then amplification of cDNA from template RNA transcripts, with both AMV reverse transcriptase and *Tfl* DNA polymerase contained within one reaction mix. The resulting cDNA products can be detected by gel electrophoresis.

Reaction mixtures were prepared on ice in nuclease-free tubes, using clean equipment and work areas, according to the kit instructions. First and second strand synthesis steps were carried out as detailed in the kit protocol (Table 2.7).

Reaction mix:

Reagent (final concentration)	*Volume*
AMV/*Tfl* 5x Reaction Buffer	10 µl
Nuclease-free dH_2O	Up to final vol. of 50 µl
10 mM dNTPs (0.2 mM each dNTP)	1 µl
Upstream primer (1 µM)	0.5 µl
Downstream primer (1 µM)	0.5 µl
25 mM $MgSO_4$ (1 mM)	2 µl
AMV Reverse Transcriptase (0.1 u/µl)	1 µl

Tfl DNA Polymerase (0.1 u/µl)	1 µl
Template RNA (1 ng-1 µg)	X µl
	Final reaction volume: 50 µl

Thermal cycling conditions:

Step	*Temperature*	*Time*		
Reverse transcription	45ºC	45 minutes		1st strand cDNA synthesis
AMV RT inactivation, RNA/cDNA denaturation	94ºC	2 minutes		
Denaturation	94ºC	30 seconds	x40-45	2nd strand synthesis & cDNA amplification
Annealing	60ºC	1 minute		
Extension	68ºC	1 minute 50 seconds		
Final Extension	68ºC	7 minutes		

Table 2.7: Reaction mix preparation and thermal cycling conditions for reverse transcriptase PCR (RT-PCR)

2.2.8 Agarose gel electrophoresis

Nucleic acids were separated and analysed by gel electrophoresis. Agarose gels were prepared with TAE buffer and SafeView Nucleic Acid Stain (1:10000 dilution) (NBS Biologicals). To ensure good separation, 1% agarose gels were generally prepared for DNA fragments of ~250-2000 bp, whilst 0.7% agarose gels were prepared for larger fragments, or plasmid DNA. Gels were loaded with ~5 µl sample DNA or DNA molecular size marker per well (both mixed with loading buffer). Electrophoresis was performed at 100 V for 20-40 minutes, in TAE buffer. Gels were visualised under ultraviolet (UV) light and analysed using the GelDoc Molecular Analyst™ software (Bio-Rad, California, US).

2.2.9 Restriction enzyme digestion of DNA

Restriction enzyme digestion was generally performed at 37ºC for 1-2 hours. Reactions were prepared according to kit instructions, with recommended reaction buffers (Promega/Fermentas). Typical reaction mixtures comprised 40-50 µl DNA (0.5-1 µg/µl) and nuclease-free dH_2O, 4 µl 10x reaction buffer, and 1 µl restriction enzyme(s). For double-digest reactions with two restriction enzymes, 10x Fermentas Buffer Tango™ was routinely used. These reactions were performed in optimal conditions for the enzymes used, as recommended (Fermentas DoubleDigest™: http://www.fermentas.com/en/tools/doubledigest).

2.2.10 Ligation of DNA fragments

Ligation of restriction enzyme-digested DNA fragments was performed using T4 DNA ligase (Promega/Fermentas). Sticky-end ligation reactions typically consisted of 2 µl 10x T4 DNA Ligase Buffer, 20-100 ng digested DNA, 1 µl T4 DNA ligase, and dH_2O up to a total volume of 20 µl. Digested DNA fragments were added such that the molar ratio of vector to insert was approximately 3:1. Ligation reactions were incubated at 16-22ºC for 30 minutes.

2.2.11 DNA sequencing and mapping, and calculations of DNA/RNA concentration

DNA sequencing was carried out using the GATC Biotech and Dundee DNA sequencing services (www.gatc-biotech.com Germany, and www.dnaseq.co.uk, Dundee, respectively). *in silico* analyses and mapping of genes, operons, cloned plasmid constructs and mutants were performed with the aid of VectorNTI® version 10 software.

The concentration and purity of RNA/DNA samples were routinely measured using a Tecan Infinite® 200 PRO NanoQuant microplate reader. Concentrations were deduced from the average of at least two readings per sample.

2.2.12 Transformation of DNA into competent bacterial cells

Transformation of DNA into *E. coli* supercompetent cells (TOP10 cells)

Supercompetent One Shot® TOP10 chemically competent *E. coli* cells were obtained from Invitrogen™ (Life Technologies co., California, US). Transformations were carried out according to kit instructions. Briefly, vials of TOP10 cells were thawed on ice. 1-5 µl DNA or DNA ligation reaction mix (1 pg-100ng) was then added to each vial and mixed gently. Vials were incubated on ice for 30 minutes. After heat-shocking at 42ºC for 30 seconds, 250 µl sterile SOC medium was then added to each vial. Cells were recovered by incubating for 1 hour at 37ºC with shaking, before spreading 200 µl of each transformation mix onto agar plates containing the relevant antibiotics, and incubating overnight at 37ºC.

Transformation of DNA into electro-competent *Salmonella*

To create electro-competent cells for the transformation of plasmids and linear DNA fragments, 50 ml of LB broth was inoculated with a bacterial strain at 1:100 from an overnight culture, and incubated at 37ºC and 200 rpm till cells reached early log phase (OD600 ~0.4-0.5). Cultures were then incubated on ice for 30 minutes before harvesting by centrifugation (4000 x g, 20 minutes, 4ºC). The cells were washed 3-4 times by centrifugation and resuspension in decreasing volumes of sterile ice-cold dH_2O, before being finally resuspended in 400 µl sterile ice-cold 10% glycerol and divided into 100 µl aliquots.

To 100 µl of electro-competent cells, 5-10 µl plasmid/linear DNA was added and mixed gently. The cells were then incubated on ice for 30 minutes before electroporating at 2500 V and immediately adding 600 µl warm nutrient-rich SOC media. The cells were recovered by incubating at 37ºC for at least one hour, before spreading 100-200 µl cells onto agar plates containing the relevant antibiotics and incubating overnight.

In the generation of electro-competent Δ*pbpA* or Δ*rodA* mutants, cells were washed in decreasing volumes of sterile dH_2O with 20 mM $MgCl_2$. In addition, electroporation was carried out at 1800 V, and cells were recovered in SOC media containing 20 mM $MgCl_2$.

2.2.13 One-step gene disruption using the lambda-red system

Specific gene knockouts were created using the Lambda-red recombinase technique, as described by Datsenko and Wanner, and illustrated below (Figure 2.4) (238).

In order to create specific knockout mutants, short DNA cassettes containing kanamycin- or chloramphenicol-resistance genes were generated by PCR, for insertion into the parent strain genome. Upstream and downstream primers were designed, consisting of 40 bp of sequence from the 5' or 3' end of the target gene, alongside a 20 bp sequence from the template plasmid sequence, from which the antibiotic resistance gene-harbouring cassettes were amplified (Table 2.2). Hence,

the resulting DNA cassettes contained antibiotic resistance genes, flanked by short regions of homology to the target gene. Template plasmids pKD13 and pKD3 were used to create kanamycin-resistant *mrd* operon mutants, and chloramphenicol-resistant Δ*rcsC*/Δ*pagN* mutants respectively.

To generate mutants, the knockout cassettes containing kanamycin or chloramphenicol resistance genes flanked by short regions of specificity to the target gene, were introduced by transformation into parent strains expressing the Lambda-red recombinase enzyme (from the pKD46 plasmid). The cassettes were designed to insert specifically into the target gene by homologous recombination, resulting in the disruption and inactivation of the target gene (238). Where possible, knockout strains were then transformed with the FLP-recombinase enzyme-expressing plasmid, pCP20, which caused recombination to occur between the two FRT (FLP recognition target) sites. This resulted in the removal of the antibiotic resistance gene (238). This additional step had the advantage of decreasing any potential polar effects of the mutation on downstream genes. The creation of specific knockouts was checked by PCR and DNA sequencing.

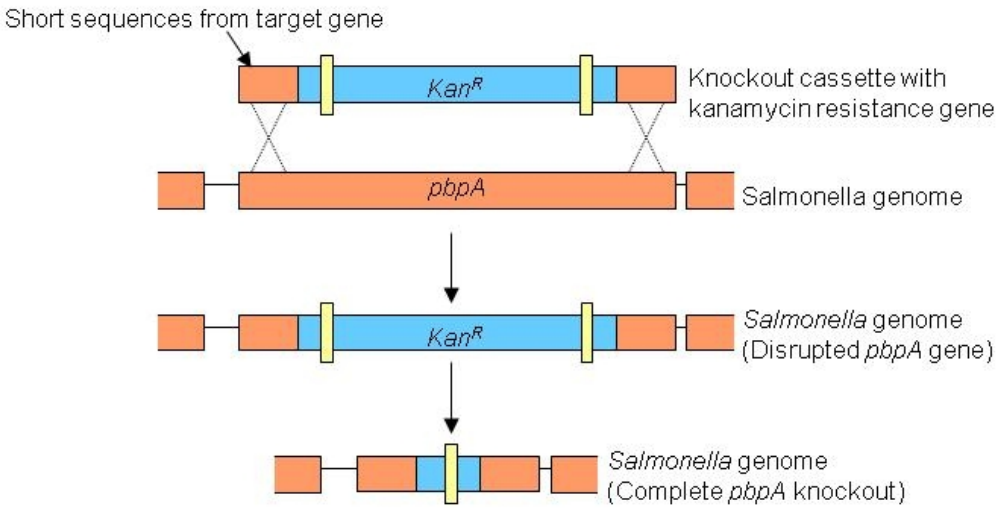

Figure 2.4: Generation of specific gene knockouts using the one-step gene disruption technique: Schematic diagram to illustrate the Lambda-red recombinase gene knock-out method, used to generate specific *mrd* operon knockouts. Adapted from "One-step inactivation of chromosomal genes in *Escherichia coli* K-12 using PCR products" (238).

2.2.14 Transduction with P22 phage

P22 lysate production

To reduce the risk of secondary mutations arising in the mutant strains, specific mutants were transduced into a fresh wild-type background. Lysates of the strains bearing the specific mutations were created by adding 10 µl P22 phage lysate to a 10 ml culture of the mutant strain, culturing overnight, and then lysing the cells with chloroform to harvest P22 phage harbouring the genetic lesion, as described (163).

Transduction of genetic lesions

To carry out transduction, 1 ml of overnight culture of wild-type *Salmonella* Typhimurium strain SL1344 was harvested by centrifugation and resuspended in 100 µl LB broth. To this, 10 µl of P22 lysate containing the genetic lesion was added. The cells were incubated at room temperature for 30 minutes before the addition of 1 ml warm LB and a further incubation at 37ºC for 30 minutes. The cells were then harvested and resuspended in 100 µl fresh LB before being spread onto agar plates containing the relevant antibiotic to select for transductants, and cultured overnight at 37^{o}C. All mutants created in *S.* Typhimurium SL1344 were transduced into a wild-type SL1344 background. However, due to the inability to transduce between *S.* Typhimurium and *S.* Typhi, this was not possible in the *S.* Typhi BRD948 mutants (439).

2.2.15 Transposition with Tn*10*d(Tc)

The Tn*10*d(Tc) mini transposon was used in the global mutagenesis screen to identify regulators of flagella gene expression. Initially a phage lysate was created from a parent donor strain of *Salmonella* which contained both Tn*10*d(Tc) and a plasmid-borne transposase, since Tn*10*d(Tc) alone is transposition-defective (251, 252). This initial phage lysate was kindly provided by Philip Aldridge (Newcastle University, UK), and was transduced into the wild-type *S.* Typhimurium SL1344. Transduced cells were grown overnight on plates containing tetracycline, to select for transductants where Tn*10*d(Tc) had randomly inserted into the genome by homologous recombination. 12000 transductant colonies were pooled into 10 ml fresh LB broth, and to this, 10 µl P22 phage stock was added. After incubating overnight at 37ºC, a P22 phage lysate was made, resulting in a phage pool

containing Tn*10*d(Tc) elements randomly inserted throughout the SL1344 genome (previous work of this lab). The phage pool consisted of Tn*10*d(Tc) insertions from the 12000 original transductant colonies so as to be sure of having complete coverage of the *Salmonella* genome. The global Tn*10*d(Tc) mutagenesis screen of this study was carried out using this P22 phage pool.

Global mutagenesis screen with Tn*10*d(Tc) P22 lysate

SL1344 Δ*rodA* cells expressing the transcriptional luminescence reporter plasmid pMK1*lux–fliF* were used in the global mutagenesis screen to identify transposon mutants with recovered *fliF* expression, as evident from a recovery in luminescence. The transduction method was the same as for the transduction of genetic lesions, although the process was scaled up; 5 ml of SL1344 Δ*rodA* pMK1*lux–fliF* overnight culture was transduced with 100 µl of the P22 Tn*10*d(Tc) lysate, and later recovered in 5 ml warm LB. Cells were then concentrated by centrifugation (4000 x g for 15 minutes, 4ºC) and resuspension in 500 µl LB. Cells were divided between and plated out on LB agar containing tetracycline, and grown overnight to select for Δ*rodA* mutants harbouring Tn*10*d(Tc).

The level of luminescence emitted from SL1344 wild-type (WT) cells expressing pMK1*lux–fliF* was such that it could be detected by eye, and by exposure to light-sensitive film. Thus, to conduct the screen to recover luminescent SL1344 Δ*rodA* pMK1*lux–fliF* Tn*10*d(Tc) mutants, transductant colonies and relevant WT/Δ*rodA* controls were patched in duplicate onto fresh LB agar containing ampicillin. After growth overnight, one of the two duplicate plates was blotted onto damp filter paper. This was covered in cling film and exposed to light-sensitive film in the dark for 20-30 seconds. The film was then developed to visualise luminescent colonies (Figure 2.5). Luminescent Δ*rodA* revertant colonies were re-patched from the second of the duplicate plates, so luminescence could be verified. Arbitrary PCR was then performed as described, from the re-patched colonies. PCR products were finally sequenced to identify the location of the Tn*10*d(Tc) insertions. In this way ~7000 mutant colonies have been screened to date.

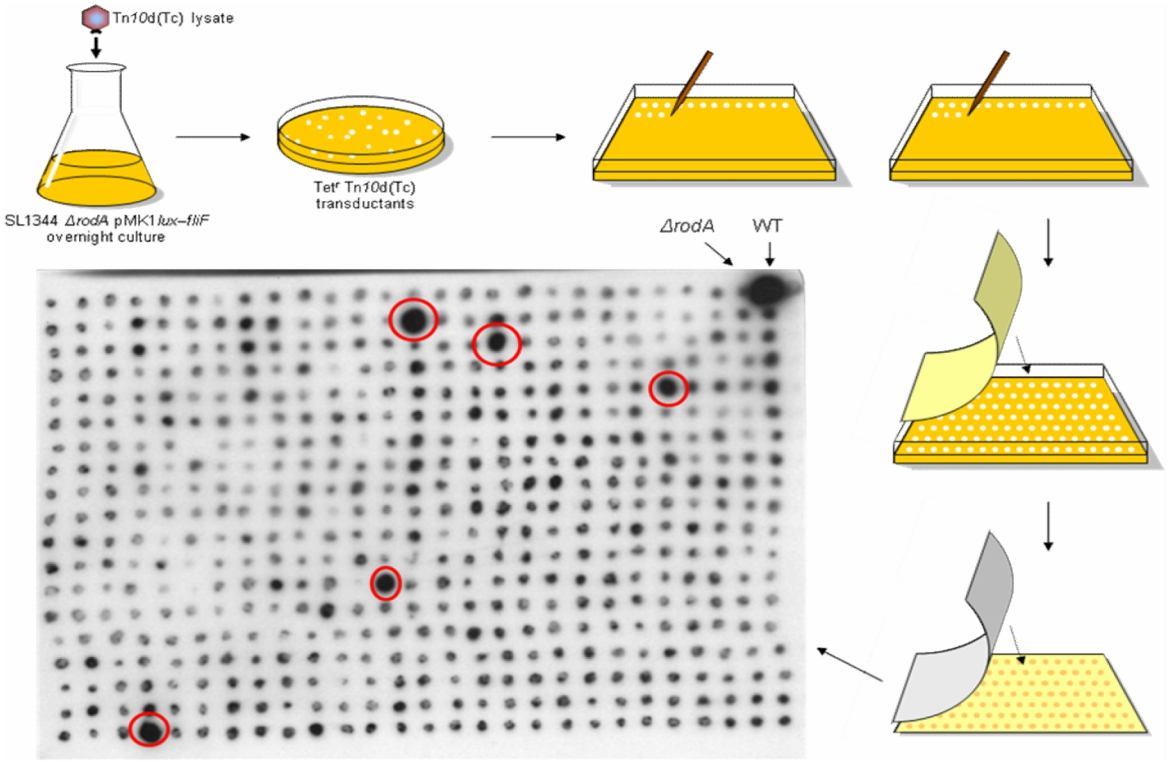

Figure 2.5: Tn10d(Tc) global mutagenesis screen: Schematic representation of the Tn*10*d(Tc) global mutagenesis screen method to identify luminescent revertants, and image of a typical film after exposure to patched Tn*10*d(Tc) mutant colonies. Controls and luminescent revertant colonies are indicated by arrows and red circles, respectively.

2.2.16 Analysis of bacterial growth and temperature sensitivity

Measurements of culture optical density (OD600) and generation of growth curves

To analyse the growth of *mrd* operon mutants as compared to wild-type (WT), WT and Δ*mrd* strains were subcultured 1:100 from overnight cultures into 50 ml fresh LB with the addition of relevant antibiotics, aro mix and tyrosine in the case of the *S.* Typhi BRD948 strain, and 20 mM $MgCl_2$. Strains were cultured in 250 ml flasks at 37ºC with shaking (200 rpm). Growth was assessed by measuring the optical density of the cultures at an absorbance of 600nm (OD600), every hour for at least 8 hours. The sensitivity of *mrd* mutants to growth at low temperatures was analysed by culturing WT and mutant strains at 30ºC with shaking (200 rpm), and measuring the OD600 every hour for at least 8 hours. Growth curves were produced by plotting growth (OD600) against time.

Haemocytometer counts

Total cell counts were carried out using a haemocytometer. Cells of a known wet weight, taken from agar plate cultures, were transferred to sterile microcentrifuge tubes and resuspended in 1 ml 4% paraformaldehyde (PFA) for around 15-20 minutes to fix. Cells were then centrifuged and carefully resuspended in 1 ml sterile dH_2O. Meanwhile a coverslip was fixed onto a clean haemocytometer slide, to ensure a depth of 0.1 mm between the slide and coverslip. ~5-10 µl of a fixed cell suspension, diluted 1:10, was then loaded into the prepared haemocytometer slide. The number of individual bacterial cells within a medium-sized haemocytometer square (comprising 16 small squares) was then carefully counted. This number was subsequently multiplied by 25 to attain the number of cells in 1 large haemocytometer square (equivalent to the number of cells $x10^4$ per ml). When multiplied by the dilution factor this gave the number of cells per ml of culture. Haemocytometer counts were each performed in triplicate per cell suspension, thoroughly cleaning and re-setting the haemocytometer slide between counts. Counts were then repeated 3 times with fresh cell suspensions. Averages of these counts were used to plot the number of cells per ml. The initial weighing of the cells, along with optical density (OD600) measurements of the cell suspensions enabled graphs to be produced, comparing wet weight, cell number, and OD600.

2.2.17 Analysis of bacterial motility

Motility of both the SL1344 and BRD948 WT and *mrd* mutants was investigated by measuring migration upon growth in semi-solid agar. 1-2 µl of overnight culture was inoculated into the centre of a petri dish containing semi-solid motility agar (0.3%). After incubation at 37ºC of 5-6 hours, the extent of culture spread (diameter) from the centre of the plate was measured as an indication of motility. Alongside motility assays, cells were observed by phase microscopy for signs of motility.

2.2.18 Analysis of Vi antigen expression in *S.* Typhi cells

Slide agglutination assays were performed to determine whether *S.* Typhi BRD948 cultures expressed the Vi capsular polysaccharide. 10 µl of culture was mixed on a

clean microscope slide, with 5-10 µl Vi-agglutinating serum and 5-10 µl PBS. After several minutes' incubation at room temperature, slides were observed for signs of agglutination, demonstrative of Vi capsule expression. *S.* Typhimurium SL1344 cultures were used as a negative control.

2.2.19 Analysis of antibiotic sensitivity

Antibiotic disc diffusion assays

Antibiotic disc diffusion assays were carried out to test the sensitivity of different bacterial strains to particular antibiotics. Molten LB agar (~46ºC) was inoculated with the required bacterial strains at 1:100 from an overnight culture. 5 ml of inoculated molten agar was then immediately poured into individual petri dishes containing 20 ml solid LB agar and cooled. Once set, sterile 5 mm filter paper discs were placed onto the agar surface and inoculated with 5 µl sterile dH_2O, or antibiotic stock solution, typically at a concentration of 10 mg/ml and 1 mg/ml. After growth overnight at 37ºC, zones of clearance in the bacterial lawns were measured. In this way, the sensitivities of both WT and *mrd* mutant strains to mecillinam, A22, rifampicin, erythromycin and streptomycin, were compared.

Antibiotic/oxidative stress sensitivity growth assays

Growth of both WT and *mrd* mutant strains in the presence of particular antibiotics or oxidative stress, was measured by inoculating LB broth containing the relevant antibiotics or hydrogen peroxide (30% w/w) 1:1000 from an overnight culture. The fresh cultures were then aliquoted between at least 3 wells of a sterile 96-well plate (200 µl per well) and cultured for 15-16 hours at 37ºC, with shaking, in a Tecan Infinite 200® spectrophotometer. The cycling conditions were set to measure the OD600 of each culture every 15-20 minutes. Growth curves were then constructed from the averages of OD600 values to compare growth of the different strains.

2.2.20 Luciferase transcriptional reporter assays

In order to test transcription levels of various genes in *S.* Typhi and *S.* Typhimurium, ~500 bp regions just upstream of the required genes, containing the gene promoter regions, were PCR amplified complete with appropriate restriction

enzyme sites and cloned into the promoterless luciferase transcriptional reporter plasmid, pMK1*lux*, between EcoR1 and BamH1 restriction enzyme sites (Table 2.1). Accurate cloning was checked by PCR and sequencing, and the newly constructed reporter plasmids were introduced into SL1344 and BRD948 wild-type and mutant strains. In this way, the following luminescence reporter plasmids were constructed in this study: pMK1*lux-fliF*, pMK1*lux-hilD*, pMK1*lux-PcobC*, pMK1*lux-PybeB*, pMK1*lux-PybeA*, pMK1*lux-PpbpA*, pMK1*lux-ProdA*, and pMK1*lux-PrlpA* (other pMK1*lux* plasmids were constructed previously – Table 2.1).

Luminesence and optical density (OD600) levels of cultures expressing the pMK1*lux* reporters were measured in 96-well plates in a Tecan Infinite 200® spectrophotometer. Fresh LB broth containing ampicillin was inoculated 1:1000 from overnight cultures expressing pMK1*lux* and aliquoted into individual wells, at least in triplicate. The plates were then cultured at 37°C overnight, with shaking. The OD600 and luminescence values of the cultures in each well were measured every 15-20 minutes. Averages from triplicate wells were calculated before deducing the relative luminescence (luminescence units per optical density) for each culture and plotting this as a function of time.

2.2.21 Preparation of proteins for analysis of protein expression

Preparation of total cell protein and secreted protein fractions

In order to prepare total cell protein and secreted protein samples for analysis, bacteria were routinely subcultured in 25-50 ml LB with appropriate additives, 1:100 from an overnight culture, and incubated at 37°C and 200 rpm till cultures reached mid-log phase (OD600: ~1.1-1.2). Cells were then harvested by centrifugation (4000 x g, 15 minutes, 4°C) and cell pellets were frozen at -20°C until use. Meanwhile, secreted proteins were precipitated by adding 10% trichloroacetic acid to filter-sterilised (pore size: 0.2 µm) culture supernatants and incubating overnight at 4°C. Secreted protein was then concentrated by centrifuging at 12000 x g for 30 minutes (4°C), and resuspending in 300 µl 2% sodium dodecyl sulphate (SDS). 1.2 ml acetone was added to each protein sample and mixed before being stored at -80°C overnight. The following morning, the secreted proteins were pelleted by centrifugation for 20 minutes at ~12000 x g.

The purified secreted protein and total cell protein pellets were finally resuspended in ≥25 µl or ≥500 µl PBS respectively, according to the optical densities of the cultures upon harvest so as to make sure the protein concentrations of each sample were standardised. This enabled comparisons to be made between the levels and composition of various protein preparations.

2.2.22 Preparation of bacterial lipopolysaccharide (LPS) from *Salmonella*

Bacterial lipopolysaccharide (LPS) was isolated from *Salmonella* cells using the iNtRON Biotechnology LPS extraction kit (Gyeonggi-do, Korea). This kit provided a rapid and effective method for preparing crude LPS from *Salmonella* cultures. LPS extraction was done according to kit instructions. *Salmonella* strains were grown at 37ºC till mid-log phase (OD600: ~1.1-1.2). 3 ml from each culture was then harvested by centrifugation (4000 x g, 15 minutes, 4ºC). The culture supernatants were completely removed, and the cell pellets were resuspended in 1 ml Lysis Buffer and vortexed well to mix. Cell lysates were transferred to clean 1.5 ml microcentrifuge tubes and 200 µl chloroform was added to each lysate, and mixed well by vortexing for 20 seconds. After 5 minutes' incubation at room temperature, samples were centrifuged for 10 minutes at ~17000 x g to separate the organic and aqueous phases. 400 µl from the aqueous phase (top layer) of each sample was then transferred to a clean 1.5 ml microcentrifuge tube. 800 µl Purification Buffer was added, and samples were incubated at -20ºC for 10 minutes. Samples were finally centrifuged at ~17000 x g for 15 minutes to pellet the purified LPS. After removing all of the supernatant, LPS pellets were washed by adding 1 ml 70% ethanol and inverting the tubes gently 2-3 times. LPS samples were then centrifuged at ~17000 x g for 3 minutes. The supernatant was completely removed, and the LPS pellets were allowed to dry. LPS samples were resuspended in 30-50 µl 10 mM Tris-HCl (pH 8.0), according to the original culture OD600 values upon harvest, in order to standardise the LPS concentration for each sample. The LPS pellets were dissolved by boiling the resuspended samples for ~2 minutes.

To further purify the LPS, removing any traces of protein, samples were treated with 2.5 µg proteinase K per 1 µg LPS. Assuming a yield of up to 45 µg LPS from

3 ml culture, samples were treated with 112.5 µg proteinase K from a 20 mg/ml stock solution. After adding proteinase K, the LPS samples were incubated at 50ºC for 30 minutes. Samples were finally boiled for 20-30 minutes to inactivate the proteinase K, and stored at -80ºC until use.

2.2.23 Separation of proteins/LPS by Sodium Dodecyl Sulphate-Polyacrylamide Gel Electrophoresis (SDS-PAGE)

Protein and LPS preparations from *S.* Typhi and *S.* Typhimurium cultures were analysed by SDS-PAGE.

12% Acrylamide gels were prepared as standard to enable the clear separation of proteins and LPS by SDS-PAGE. 12% separating gels and stacking gels were prepared as detailed (Table 2.8), thoroughly mixing the solution after the addition of successive reagents. Gels were cast immediately upon preparation. After casting the separating gels, 0.5 ml dH_2O was pipetted onto the top of each gel to remove any air bubbles and ensure the formation of a flat gel surface. When completely set excess water was removed from the top of each separating gel. The stacking gels were then prepared and immediately poured onto the separating gels. The required comb was also inserted into the stacking gel, avoiding the introduction of any air bubbles in the process. Stacking gels were continually topped up until the gels had set.

12% separating gels	*4x 3 ml 10-well mini gels (~9 cm)*	*1x large 30 ml 1 mm 15-well gel (~18 cm)*
Sterile dH_2O	5 ml	11 ml
1.5 M Tris-HCl (pH 8.8)	3.75 ml	8.25 ml
30% Acrylamide/bis-acrylamide	6 ml	13.2 ml
10% SDS	150 µl	330 µl
Fresh 10% Ammonium persulphate (APS)	75 µl	165 µl
N,*N*,*N*′,*N*′-Tetramethylethylenediamine (TEMED)	7.5 µl	16.5 µl

Stacking gels	*10 ml: 4x10-well mini gels or 1x large 1 mm 15-well gel*
Sterile dH_2O	6.35 ml
0.5 M Tris-HCl (pH 6.8)	2.5 ml
30% Acrylamide/bis-acrylamide	1 ml
Fresh 10% APS	50 µl

TEMED	10 µl

Table 2.8 Preparation of 12% acrylamide gels for separation of proteins and bacterial lipopolysaccharide (LPS)

After mounting the cast gels onto the gel electrophoresis apparatus, and filling the tank with 1x SDS running buffer (~300-500 ml for mini gels or 1.5 l for large gels), proteins were loaded onto the gels. 6x SDS loading buffer (with mercaptoethanol) was added to each sample, to a final concentration of 1x. 15 µl or 40 µl of each protein sample per well was then boiled for ~10 minutes, and loaded onto the mini and large 12% acrylamide gels respectively. 5 µl or 10 µl PageRuler™ Prestained Protein Ladder (Fermentas) was loaded alongside the samples, onto a mini or a large gel, respectively.

For the separation of LPS preparations by SDS-PAGE, 2x SDS loading buffer (without mercaptoethanol) was added to each LPS sample, to a final concentration of 1x. 30-40 µl sample per well was then loaded straight onto a large 12% acrylamide gel, alongside 10 µl PageRuler™ Prestained Protein Ladder.

Electrophoresis was carried out at 100 V for 1-1.5 hours for a mini gel, or overnight at 3-5 mA and 4ºC for a large SDS-PAGE gel.

2.2.24 Staining and analysis of SDS-PAGE gels

Staining with Coomassie® Brilliant Blue

After the separation of protein samples by SDS-PAGE, gels were carefully transferred to a clean dish and soaked in Coomassie® Brilliant Blue R stain solution for 1 hour at room temperature. The Coomassie® dye was removed and replaced with Coomassie® de-stain solution. Gels were incubated in de-stain until the protein bands became clearly visible.

Silver staining SDS-PAGE gels

LPS gels were stained using the “SilverSNAP” Pierce Silver Stain kit (Pierce Protein Research). Staining was carried out according to kit instructions; all steps were performed at room temperature. After electrophoresis, the gel was carefully removed from the casting plates, transferred to a large glass dish, and washed

twice in 50-100 ml sterile dH_2O for 5 minutes each. After removing the water, the gel was fixed in 100 ml 30% ethanol:10% acetic acid solution twice, for 15 minutes each. The fixing solution was discarded and the gel washed twice in 100 ml 10% ethanol, for 5 minutes each, then twice in 50-100 ml sterile dH_2O, for 5 minutes each. The gel was incubated in 50 ml freshly prepared Sensitizer Working Solution for 1 minute, before immediately washing twice in 50-100 ml sterile dH_2O for 1 minute per wash. 50 ml Stain Working Solution was then freshly prepared and applied. The gel was incubated in stain solution for at least 30 minutes. Prior to washing the gel again, the Developer Solution and 5% acetic acid stop solution were both pre-prepared. The gel was then briefly washed twice in 50-100 ml sterile dH_2O (20 seconds each), and developed by adding the Developer solution and incubating for 1-2 minutes. When the LPS bands reached the desired intensity, 100 ml 5% acetic acid stop solution was immediately added to the developer solution, until bubbles appeared in the solution. The developer solution was then replaced with a fresh 100 ml of stop solution and incubated for 10 minutes. The gel was finally washed in 50-100 ml sterile dH_2O for several minutes.

Western blotting

Proteins separated by SDS-PAGE were blotted onto nitrocellulose membranes. The 12% acrylamide gels were sandwiched together with nitrocellulose membrane between several layers of filter paper and sponge soaked in transfer buffer, set in a tank containing transfer buffer, and run at 150-200 V for 30 minutes on ice. After blotting, membranes were washed briefly in PBS and blocked in 3% bovine serum albumin (BSA) in PBS-Tween for 45 minutes. Primary antibody was then added to the block solution at 1:1000-10000 and the nitrocellulose membranes were incubated overnight in the block-antibody solution at 4ºC. The following morning, the membranes were incubated at room temperature for 30-40 minutes before washing 3 times in PBS (5 minutes per wash). Secondary antibody was then added to 20 ml fresh PBS at 1:10000. After 2 hours' incubation at room temperature, the membranes were washed as before and developed in chloro-naphthol developer solution. Freshly prepared developer solution was applied to the membranes, and incubated in the dark for 10-20 minutes until the protein bands reached the desired intensity. Membranes were then rinsed in water and dried.

2.2.25 Phase contrast, epifluorescence and electron microscopy

Preparation of cells and slides for microscopy

Both live and fixed bacterial cells were routinely viewed by phase contrast microscopy. Cells were fixed with 4% PFA for 30-60 minutes, before washing and resuspending in PBS, and storing at 4ºC until use.

Samples were mounted onto thin 1% agarose beds for viewing by microscopy. The agarose mounts were prepared by pipetting 500-750 µl melted 1% agarose (in PBS) onto the slide surface, and covering with another glass microscope slide to allow the agarose to form a thin gel layer. After 1-2 minutes, the covering slide was gently removed. 0.5 µl each sample was pipetted onto the surface of the agarose. Once dried, coverslips were placed over the samples.

Phase contrast microscopy

Cells were viewed by phase contrast microscopy at a 100x magnification, using a Nikon Plan 100x/1.25 Ph3 DL oil objective, on a Nikon Inverted Microscope Eclipse T*i*-E model microscope.

Epifluorescence microscopy

For immunofluorescence microscopy, 1-5 ml bacterial cultures were harvested and fixed as above. After washing thoroughly in PBS, cells were resuspended in 100 µl PBS containing the primary antibody; cells were probed with rabbit anti-SipD (kindly provided by Vassilis Koronakis, Cambridge), or rabbit anti-SseB (kindly provided by David Holden, UCL) at a 1:1000 dilution, or with rabbit anti-flagellin (Typhi/Typhimurium-specific) *Salmonella* agglutinating serum at a 1:20 dilution. Samples were then incubated for 1 hour at room temperature, washed as before, and probed with the secondary goat anti-rabbit antibody conjugated to the green-fluorescent Alexa Fluor® dye (Invitrogen, UK) at 1:1000 in 100 µl PBS. Samples were incubated in secondary antibody for 2 hours at room temperature, in the dark. After washing again in PBS, cells were finally resuspended in 100-300 µl 10% glycerol and stored at 4ºC, in the dark, until use.

Immunofluorescence microscopy samples or live cells expressing Green Fluorescent Protein (GFP) derivatives were viewed by epifluorescence microscopy at 100x magnification, using a Nikon Plan 100x/1.25 Ph3 DL oil objective.

Image processing

Images were captured using NIS-Elements Advanced Research (version 2.3) software. All image processing was done using NIS-Elements 2.3 and the ImageJ image processing software.

Electron microscopy

Scanning electron microscopy images were taken of *S.* Typhi BRD948 WT and mutant cells in collaboration with Newcastle University Electron Microscopy Research Services (Newcastle, UK). Appropriate strains were cultured to mid-log phase (OD600: 1.1-1.2) and harvested by centrifugation. After carefully removing all of the culture supernatant, cell pellets were resuspended in Sorenson's phosphate buffer with 2% gluteraldehyde. Samples were then taken to the Electron Microscopy Unit and processed further, to prepare them for scanning electron microscopy.

2.2.26 DNA Microarrays

NimbleGen gene expression microarrays were used to compare global gene expression between *S.* Typhimurium SL1344 wild-type and Δ*rodA* strains (Roche NimbleGen Inc., Wisconsin, US). 4x72000 multiplex arrays were used, consisting of 4 arrays per slide, and 72000 *S.* Typhimurium LT2-specific probes per array. These enabled the analysis of the gene expression of 4504 *S.* Typhimurium genes in both wild-type and mutant strains.

Strains were grown to mid-log phase (OD600 of ~1.0-1.2) in LB broth (without antibiotic or $MgCl_2$ supplementation) and harvested. The mRNA was then purified, processed and applied to the arrays. Statistical analysis of the array data was done using the DNASTAR ArrayStar® software. This work was kindly conducted by David Bulmer (ICAMB, Newcastle University).

2.2.27 Quantification of c-di-GMP by HPLC/Mass spectrometry (LC/MS/MS)

In order to directly quantify c-di-GMP levels from both wild-type and Δ*rodA* cultures of *S.* Typhi BRD948 a high pressure liquid chromatography (HPLC)-coupled mass spectrometry (MS) method (LC/MS/MS) was developed with the help of Joe Gray (Pinnacle, Newcastle University).

Cell lysates were initially prepared as follows. Overnight cultures of BRD948 wild-type and Δ*rodA* were subcultured into 25 ml fresh LB broth containing aro/tyr mix and 20 mM $MgCl_2$. Each strain was then cultured at 37°C and 200 rpm, till mid-log phase (OD600 of ~1.1-1.2). The two cultures were harvested by centrifugation (4000 x g, 20 minutes, RT) at an equal optical density. After thoroughly removing all culture medium, cell pellets were each resuspended in volumes of HPLC-grade dH_2O to standardise cell suspensions at an OD600 value of 2 (equivalent to 10^{10} wild-type/Δ*rodA* cells per ml). Cells were then cooled to 4°C, and lysed thoroughly by sonication (7-8 pulses, for 30 seconds each, at 10 microns). Optical densities were measured after sonication to ensure equal lysis. Cell lysates were subsequently centrifuged at 4000 x g, for ~20 minutes at room temperature to pellet the cell debris. 2 ml of supernatant from each strain was then transferred to an Amicon® Centriplus® centrifuge 10 kDa filter and centrifuged at 2000 x g until sufficient lysate had passed through the filters. This filtration step removed large molecules of >10 kDa, including proteins and genomic DNA, which may have interfered with the LC/MS/MS analysis. 1ml of each lysate was then recovered and stored in a sterile bijoux tube, at 4°C, until use. An additional 1 ml of filtered lysate from the wild-type strain was recovered and spiked with 10 pmoles of pure c-di-GMP, as a control.

The following steps were kindly carried out by Joe Gray (Pinnacle, Newcastle University). For LC/MS/MS analysis, 1ml lysates were dried *in vacuo* and reconstituted in 100 µl HPLC buffer A (5 mM dibutylamine acetate (DBAA) / 0.1% acetic acid). 5 µl sample was then injected onto the MS-coupled HPLC trap & column at a flow rate of 10 µl/minute for 2 minutes. The HPLC column used was a Waters Symmetry C18 Trapping Column, 5µm particle, dimensions 180 µm x 20 mm. This trap was then switched in-line with a resolving column; a self-packed

Reprosil™ C18-AQ, 5 µm capillary, dimensions 150 µm x 120 mm. A flow-rate of 2.5 µl/minute was used, along with a gradient of: T=0 - 2.5% Buffer B (80% Methanol (aqueous) with 5 mM DBAA/0.1% acetic acid), T=5 - 5.0% Buffer B, T=25 - 100% Buffer B, T=25.5 - 100% Buffer B, T=26 – 2.5% Buffer B. This was followed by a 10 minute re-equilibration step with 2.5% Buffer B. The eluate from the column was then sprayed directly into an LTQ FT Ultra mass spectrometer in negative ion mode (Thermo Fisher Scientific, Illinois, US). Scanning was done at a mass range of 300-1100 m/z. The c-di-GMP peak was detected at a m/z value of 689.17.

A calibration curve over a range of 0.05-5 pmoles (on-column loading) was initially constructed using integrated mass peak areas of a reference solution of c-di-GMP (BIOLOG Life Science Institute, Bremen, Germany). The calibration curve was used to determine unknown c-di-GMP concentrations from the MS response signals of biological samples. All measurements, both in the construction of the calibration curve, and measurement of wild-type/Δ*rodA* c-di-GMP levels, were performed in triplicate. Measured c-di-GMP levels in the spiked wild-type BRD948 sample were close to 10 pmoles (9.65 pmoles), verifying the accuracy of the calibration curve.

2.2.28 *in vivo* virulence assays

In order to study the virulence of the round-cell *mrd* operon mutants *in vivo*, C57BL/6 mice were each inoculated intravenously with 10^4 cells of either *S.* Typhimurium SL1344 wild-type or Δ*rodA* strains. *S.* Typhimurium infections in mice encompass a useful model of typhoid fever (250). The *in vivo* growth of both wild-type and Δ*rodA* strains was characterised by measuring the liver/spleen bacterial loads 6 hours, 1 day, 3 days, 6 days, 14 days and 28 days post-infection (colony-forming units (CFU) per organ). Data was based on the average bacterial load counts from 4 mice. This work was carried out in collaboration with Andrew Grant and Pietro Mastroeni (University of Cambridge, UK).

2.3 Statistical analyses of data

To ensure reproducibility and significance of results, assays in this study where possible were routinely conducted on at least three separate occasions, done in duplicate or triplicate where applicable. Data was then analysed with the calculation of both mean and standard deviation values, as presented on graphs.

In order to test the statistical significance of data generated in this study, student t-tests were carried out using Microsoft® Excel. Un-paired 2-tailed t-tests with unequal variance were routinely done to compare data generated from wild-type and mutant strains, whilst equivalent paired student t-tests were carried out to analyse the significance of differences between data from the same strain.

2.4 General definitions

Unless otherwise stated, the following definitions apply to the work carried out in this study:
'Room temperature' – equivalent to ~22-25°C
'Overnight' – 16 hours

Chapter 3. Analyses of the *mrd* operon structure

3.1 Introduction

The putative *mrd* operon is thought to consist of the 3 contiguous genes *pbpA*, *rodA*, and *rlpA*, as well as two upstream genes *ybeB* and *ybeA*, due to the presence of potential promoter sequences upstream of *ybeB*. However, the position of *rlpA* is in doubt and further experimental analyses are needed to characterise the promoter, and show whether *rlpA* and the downstream *dacA* gene form part of the operon (142, 143, 186, 187, 205). In this study, both experimental and *in silico* analyses were therefore implemented to enable characterisation of both the co-transcribed *mrd* operon genes and also the location(s) of *mrd* operon promoter(s).

3.2 *in silico* analyses of the *mrd* operon

3.2.1 Conservation of the *mrd* operon transcriptional unit

The *mrd* operon is thought to consist of 5 genes: *ybeB*, *ybeA* (*rlmH*), *pbpA* (*mrdA*), *rodA* (*mrdB*), and *rlpA* (142, 143, 186). Sequence analysis using the online "Kyoto Encyclopedia of Genes and Genomes" database demonstrated that the operon as a single unit is conserved in structure across Gram-negative species of both pathogenic and non-pathogenic bacteria, including *Escherichia coli*, *Shigella*, *Yersinia*, *Pseudomonas*, *Caulobacter*, *Vibrio*, and even the deep-sea marine bacteria *Photobacterium profundum* (253, 254). However, this is not so in Gram-positive organisms such as *Bacillus subtilis*, where *pbpA* and *rodA*, as well as homologues of *ybeB*, *ybeA* and *rlpA* (*yqeL*, *yydA*, and *lytD* respectively), are each encoded at completely separate loci within the genome. Furthermore, the *rodA* gene was shown to be monocistronic in *B. subtilis* (154, 253).

The structure of the *mrd* operon, in both open reading frames and intergenic regions, is well conserved between *Salmonella enterica* serovars Typhi and Typhimurium, as shown (Figure 3.1) (163). Basic Local Alignment Search Tool (BLASTn/megablast) comparisons of the relatedness of serovars Typhi and Typhimurium, in a previous study, showed that the 5 putative *mrd* operon genes

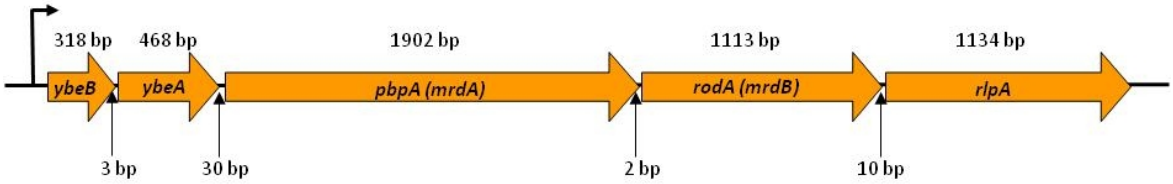

Figure 3.1: Putative mrd operon structure in S. enterica serovar Typhi: Layout of the *mrd* operon in *S.* Typhi, including gene sizes, size of intergenic regions, and position of the putative *mrd* operon promoter upstream of *ybeB* (187, 255). Genes drawn to scale. Operon layout as shown is identical in both Typhi and Typhimurium serovars, except for *rlpA* gene; length in *S.* Typhimurium is 1146 bp.

contain between 97% and 99% identity at the DNA level (163). BLAST sequence analysis of the whole operon (*ybeB-rlpA*) showed that the sequence identity between *S.* Typhi and *S.* Typhimurium is 99% (4931/4993 bp), at the DNA level.

3.2.2 Putative promoters of the *mrd* operon

The RegulonDB database contains comprehensive information on operon structure, and positional information on promoters, transcription factor binding sites and other sequences involved in gene regulation, in *E. coli* (212, 255, 256). The information based upon both bioinformatic and experimental data, and can be accessed through the online Ecocyc database (187, 255). Information from this database suggests that the *mrd* operon comprises the 5 genes in *E. coli*: *ybeB*, *ybeA*, *pbpA*, *rodA* and *rlpA*, the promoter being located upstream of *ybeB*.

There is little experimental evidence to demonstrate whether or not the putative promoter upstream of *ybeB* forms the true and sole promoter of the *mrd* operon, however, with predicted promoter sequences identified here, and upstream of both *rodA* and *rlpA* (142-144, 186). *in silico* online bacterial promoter prediction tools, the BDGP Fruitfly and Softberry BPROM programmes, were therefore used to identify putative promoter sequences within the region of the *mrd* operon in *S.* Typhi (257-259). *in silico p*romoter prediction methods are based upon experimentally derived consensus sequences for bacterial promoters. These include the conserved -35 and -10 sigma factor binding site hexamer sequences located upstream of the transcriptional start sites (TTGACA and TATAAT respectively) (260). They have inherent limitations, in that they can often result in the identification of false positives. Data from this work was therefore considered

with some caution (255). The Fruitfly programme predicts the presence of promoter sequences and transcriptional start sites within a region of DNA, whilst BPROM detects the presence of potential sigma factor 70 (σ^{70})-specific -10 and -35 sequences within sections of DNA, σ^{70} being the housekeeping sigma factor (255). For Fruitfly analyses the putative *mrd* operon including intergenic regions and upstream and downstream genes was analysed as a whole. BPROM promoter predictions were done by analysing individual 300 bp sections of genome immediately upstream of each putative *mrd* operon gene, along with genes immediately upstream and downstream of the proposed operon. This was done as advised, to improve accuracy (259). Using both the BPROM and Fruitfly programmes enabled the identification of several promoter-like sequences within this region of the *S*. Typhi genome. The results from these analyses were compiled and annotated, as shown (Table 3.1 and 3.2). Identified putative promoter regions are located as shown (Figure 3.2).

Transcriptional start sites are generally located between 20 and 40 nucleotides upstream of translational start sites (255). On this basis, and given the proximity between transcriptional and translational start sites as well as upstream sigma factor binding sites, a 300 bp cut-off point for putative promoter sequences was considered sufficient; any putative sequences identified further than 300 bp from the start of the proximal gene of an operon were discounted, being considered unlikely to constitute an actual promoter.

Putative promoters upstream of *ybeB*

Of major interest were any promoter-like sequences located upstream of *ybeB*, due to the findings of previous studies. Both *in silico* analyses and β-galactosidase reporter assays have identified a potential promoter for the *mrd* operon in the intergenic region upstream of *ybeB* in *E. coli*; the putative position of this promoter determined *in silico*, is as shown (Figure 3.3) (142, 143). The transcriptional start site was thought to be located 36 bp upstream from the start of *ybeB*, whilst the predicted -10 and -35 sequences were 48 bp and 75 bp upstream from the start of *ybeB* (142, 187) (Figure 3.3). Until now, the location of the *mrd* operon promoter has not been analysed in bacterial species other than *E. coli*.

Both BPROM and Fruitfly analyses of this region highlighted promoter-like sequences ~170-250 bp upstream of *ybeB*, although the identified promoter sequences did not overlap. The position of the predicted promoter in *E. coli* therefore differs considerably from the predicted promoters from BPROM and Fruitfly analyses of the *S.* Typhi genome sequence.

Nucleotide BLAST analysis of sequence conservation of the *ybeB* gene and upstream regions between *E. coli* and *S.* Typhi demonstrated that the *ybeB* gene sequences themselves are fairly well conserved between these two organisms (88% sequence identity). However, this is not the case with sequences upstream of *ybeB*; no significant sequence similarity was detected in the region of between 19 bp and 108 bp upstream of the start of *ybeB* in the *Salmonella* genome, although for sequences 0-19 bp and 109-200 bp upstream of *ybeB*, the sequence similarity was 100% and 77% respectively between *E. coli* and *Salmonella.* The lack of sequence similarity for the 89 bp stretch of sequence may be relevant, since within this region is located the proposed promoter of the *mrd* operon in *E. coli*. In *E. coli* this region lacking homology is 23 bp long and contains the putative transcriptional start site of *ybeB*. This may explain why *in silico* analyses of the Typhi genome sequences failed to recognise possible promoters in a similar position to the proposed *E. coli* promoter.

BDGP Fruitfly analysis of putative *mrd* operon and flanking genes

Promoter location	*Putative promoter sequence*	*Score*
P_{cobC}	5' ATGTTTTGCGCATTTAACCTCATGAGGAATACCATGCGATTGTGGCTGGT 3' (start = -33 bp from *cobC*)	0.91
P_{ybeB}	5' AGGCTTTTTTCACCTTGCAGAGCTTTGCAGAAATTGTTTTACAAAAATGG 3' (start = -253 bp from *ybeB*)	0.91
P_{ybeA}	None identified within 300 bp of *ybeA* start	
P_{pbpA}	None identified within 300 bp of *pbpA* start	
P_{rodA}	5' AGGTCTTTGGCCTGAAGGCCAACGAAACGTACAATGCGCATAAAATCGCC 3' (start = -259 bp from *rodA*)	0.97
P_{rlpA}	5' TCGCGTGATGGCTGGCGGATTAATGTTAATATTATTCGTTTATGTCTTCG 3' (start = -215 bp from *rlpA*)	0.94
P_{rlpA}	5' GGGATTGTGATGTCGATCCACACCCACAGAAAAATGTTGTCGAAAAGCGT 3' (start = -64 bp from *rlpA*)	0.98
P_{dacA}	5' TATGCTTTTGCTATAGTAGGGCTCTTTTTTAATTTCATCACGGACGTCGT 3' (start = -60 bp from *dacA*)	0.90

Table 3.1: BDGP Fruitfly promoter sequence searches: Results of BDGP Fruitfly analysis of *mrd* operon for putative promoter sequences within 300 bp of the start (5' end) of each gene. Putative transcriptional start sites indicated by underlined text. Probability score associated with each promoter sequence as shown.

Softberry BPROM analysis of promoter sequences upstream of *mrd* operon genes

Promoter location	*Putative promoter sequence*		*Position relative to translational start of gene*	*Score*
P_{cobC}	-10 box:	CGCTAAAAT	187	77
	-35 box:	TACCCA	208	4
P_{ybeB}	-10 box:	TGATAATCT	176	51
	-35 box:	TTTCTG	197	28
P_{ybeA}	-10 box:	CTGTATGAT	217	67
	-35 box:	TTCAGG	242	17
P_{pbpA}	None identified			
P_{rodA}	-10 box:	ACGTACAAT	233	59
	-35 box:	TGGCCT	252	19
P_{rlpA}	-10 box:	TGTTAATAT	192	72
	-35 box:	GTGATG	211	19
P_{dacA}	-10 box:	TGCTATAGT	52	64
	-35 box:	ATGCCT	72	26

Table 3.2: Softberry BPROM promoter sequence searches: Results of Softberry BPROM analysis of *mrd* operon for putative promoter sequences within 300 bp of the start (5' end) of each gene. Putative -35 and -10 boxes indicated, along with distance from start of each gene. Scores associated with each promoter sequence as shown.

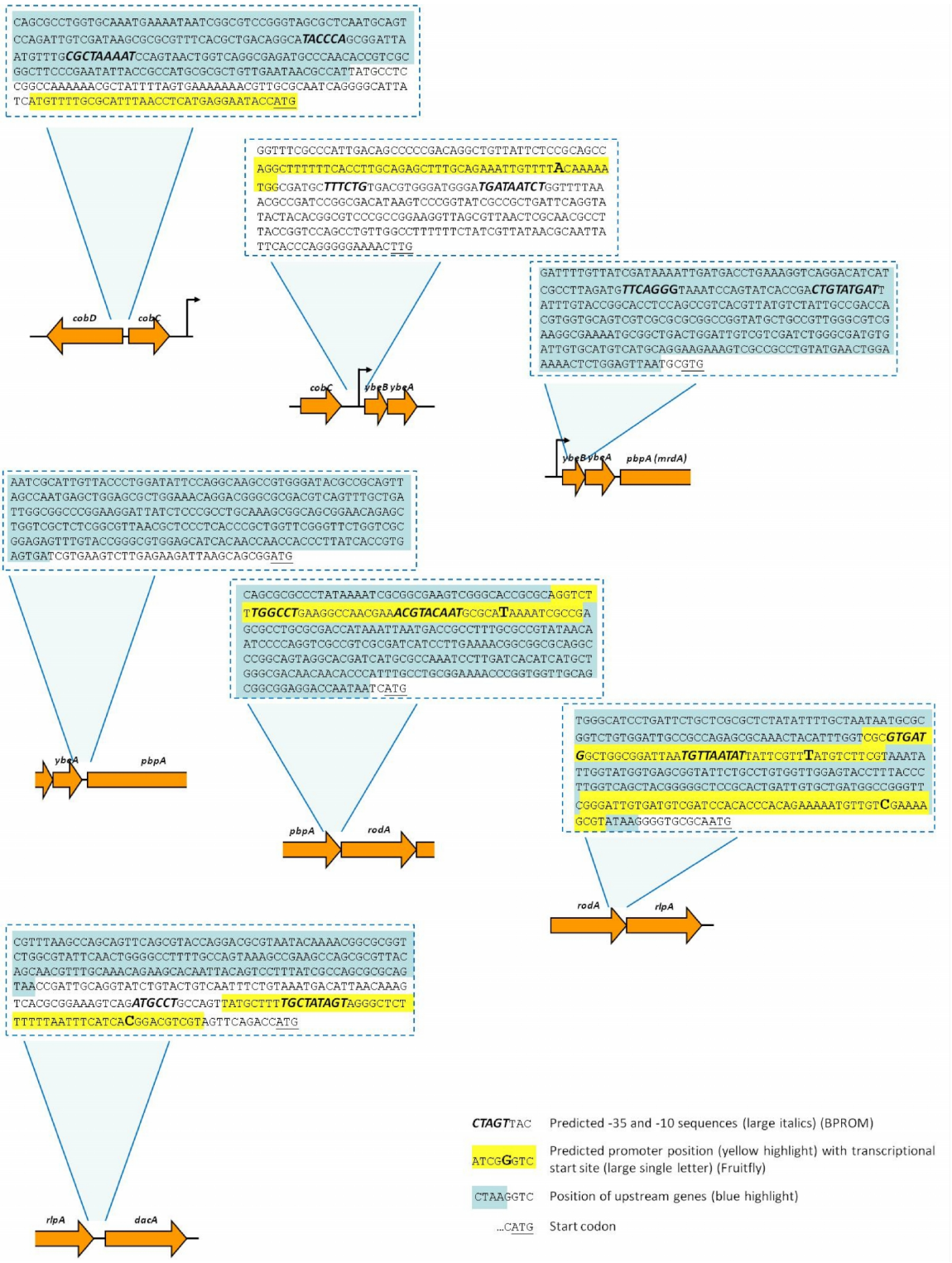

Figure 3.2: Location of putative promoter sequences within mrd operon region in S. Typhi: Compiled information from Fruitfly and BPROM analyses of putative promoter sequences to show locations of putative promoter sequences within 300 bp region upstream of *cobC*, *ybeB*, *ybeA*, *pbpA*, *rodA*, *rlpA* and *dacA* genes.

A

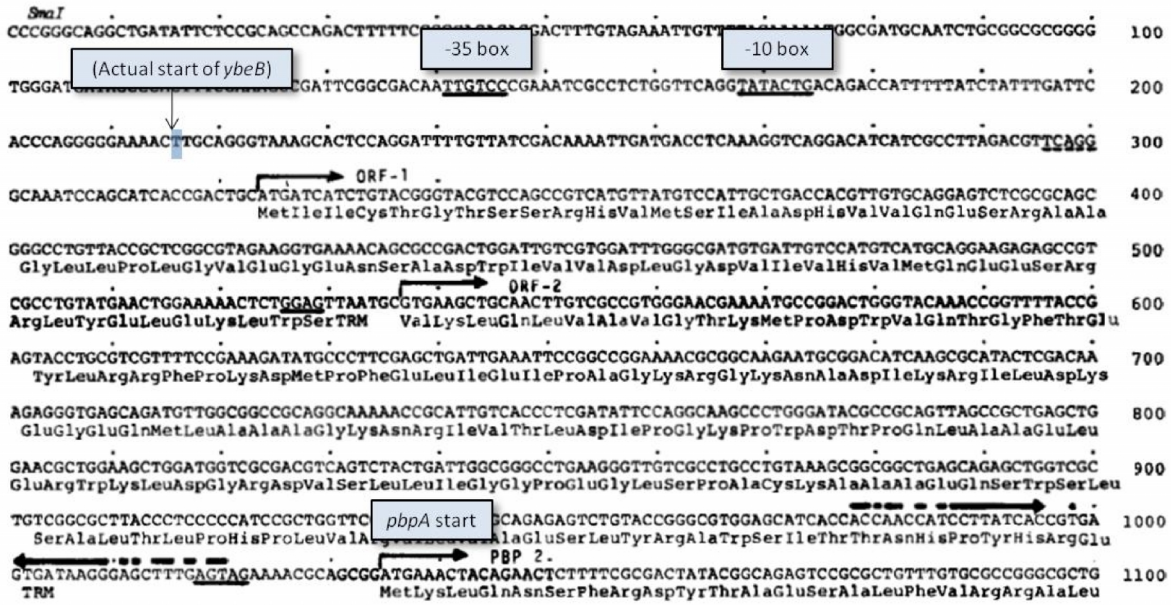

B

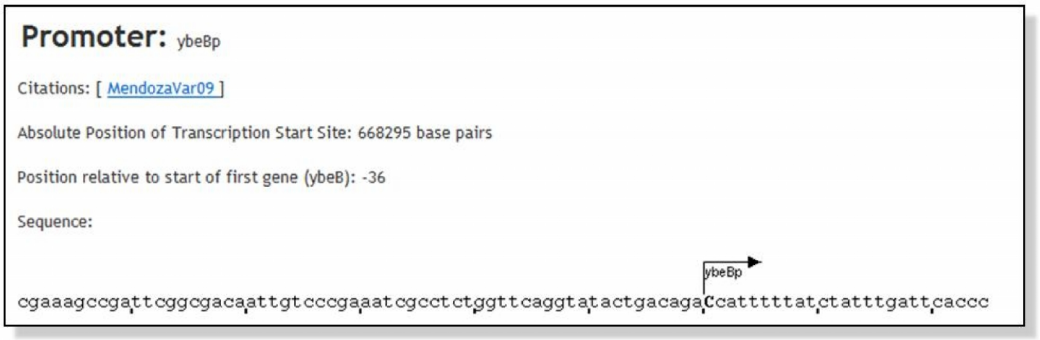

Figure 3.3: Predicted promoter sequences upstream of ybeB in E. coli: A – Predicted -35 and -10 box sequences upstream of *ybeB* start, taken from Asoh et al. "Nucleotide sequence of the pbpA gene and characteristics of the deduced amino acid sequence of penicillin-binding protein 2 of Escherichia coli K12" (142); 'ORF-1' indicates predicted start of *ybeB* gene. B – Putative position of *mrd* operon promoter and transcriptional start site upstream of *ybeB* in *E. coli*, taken from Ecocyc/RegulonDB database (187, 255).

Promoter-like sequences identified elsewhere within the putative *mrd* operon

The majority of putative promoters identified in this work, using either Fruitfly or BPROM, were located at some distance from the downstream genes, often being around 200 bp upstream of the translational start of a gene, whilst no putative promoters were identified upstream of *pbpA*. However, a few potentially significant sequences were also identified.

Putative promoter sequences were identified ~60 bp upstream from the start of *dacA* with both BPROM and Fruitfly. The identified sequences overlapped such that the putative -10 box was located 32 bp (5' end) upstream of the putative transcriptional start site. Promoter-like sequences were also identified ~60 bp upstream of *rlpA* in Fruitfly but not BPROM analyses. Also, although further upstream (~200 bp) from the gene start codons, overlapping promoter-like sequences were identified with both Fruitfly and BPROM, upstream of *rodA* and *rlpA*; in both cases, the putative -10 boxes were located a short distance upstream of predicted transcriptional start sites (14 bp and 16 bp respectively) (Tables 3.1 & 3.2, Figure 3.2).

The remaining promoter sequences identified in this work are less likely to form true promoters. For example, a promoter for *cobC* was identified in which the proposed transcriptional start site was located downstream of the start of the gene. Furthermore, promoter sequences identified upstream of *ybeA* and *rodA* were located a considerable distance from the start of these genes. From these results, the most likely candidates for actual promoter sequences seem to be those located close to the *rlpA* and *dacA* genes, and potentially the overlapping sequences located upstream of *rodA*.

Whilst *in silico* assays highlighted several putative promoter sequences, experimental analysis was necessary to validate these findings and demonstrate actual promoter activity within this region of the *Salmonella* genome.

3.3 Luciferase promoter reporter assays with pMK1*lux* to identify promoter activity within the *mrd* operon

3.3.1 Construction of *mrd* operon transcriptional reporter plasmids using luminescence reporter plasmid, pMK1*lux*

pMK1*lux* is high copy number transcriptional luminescence reporter plasmid. It contains the promoterless *Photorhabdus luminescens luxCDABE* operon, cloned downstream of the multiple cloning site (MCS) (240-242). The *lux* operon is required for luminescence in various bacterial species. The *luxAB* genes encode a

luciferase enzyme, which catalyses the oxidation of reduced riboflavin phosphate and a long-chain fatty aldehyde, resulting in the production of blue-green light. The LuxCDE proteins form the enzymatic complex required for the synthesis of the fatty aldehyde substrate (242, 261). Thus promoter activity can be detected by cloning the promoter regions from target genes into the MCS of pMK1*lux*. The relative luminescence of cultures expressing pMK1*lux* constructs gives an indication of *lux* gene expression, and therefore of promoter activity. In the promoter-less pMK1*lux* parent vector, the *lux* genes are not expressed.

To test experimentally for promoter activity within and upstream of the putative *mrd* operon, as detected in *in silico* analyses, ~500 bp regions immediately upstream of each putative *mrd* gene (as well as genes upstream and downstream of this region) were cloned into pMK1*lux*, to create pMK1*lux-PcobC*, pMK1*lux-PybeB*, pMK1*lux-PybeA**, pMK1*lux-PpbpA*, pMK1*lux-ProdA*, and pMK1*lux-PrlpA* (Figure 3.4). Promoter regions were cloned excluding the native Shine-Delgarno (SD) sequences, such that the pMK1*lux* promoter inserts were at an equivalent distance from the pMK1*lux*-encoded SD sequence, as they would be to that of the parent gene. Successful construction of each plasmid was verified by sequencing. A pMK1*lux-PdacA* construct was also engineered, although sequencing data demonstrated that the cloned sequence was incorrect, and so this plasmid was not used.

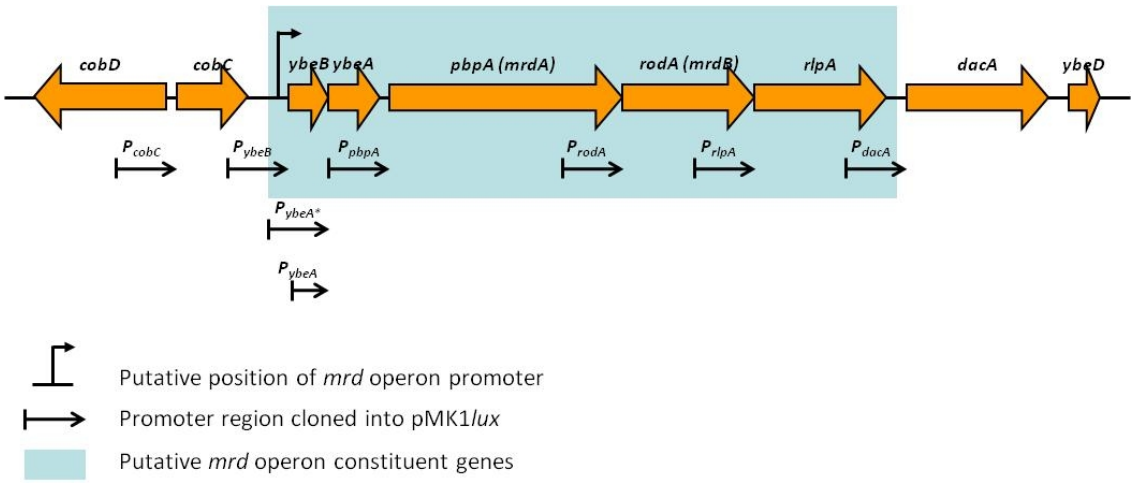

Figure 3.4: Construction of mrd operon transcriptional reporter plasmids using pMK1lux: Schematic diagram showing positions of promoter regions cloned into pMK1*lux* for each *mrd* operon gene, along with upstream and downstream genes, to create luciferase transcriptional reporter plasmids. ~500 bp regions upstream of each gene were

cloned into pMK1*lux*. Diagram drawn to scale. The pMK1*lux-PybeA** construct consisted of a ~500 bp region upstream of *ybeA* cloned into pMK1*lux*; the putative *ybeB* promoter was therefore included in construct. pMK1*lux-PybeA* contains a ~300 bp region upstream of *ybeA*, excluding putative *ybeB* promoter.

3.3.2 Luciferase promoter reporter assays

In order to assay for promoter activity upstream of each *mrd* operon gene, luminescence was detected from *S.* Typhi BRD948 cultures expressing the pMK1*lux* reporter constructs, whereby luminescence is proportional to expression levels of the *lux* genes, and hence activity from the promoter cloned into pMK1*lux*. Luminescence reporter assays were carried out as described.

Transcriptional luminescence reporter assays with the pMK1*lux* constructs showed high levels of relative luminescence in BRD948 cultures expressing both pMK1*lux-PybeB*, and pMK1*lux-PybeA** compared to the promoterless control, whereas negligible luminescence was emitted from cultures expressing the pMK1*lux–PpbpA* or pMK1*lux–ProdA* constructs (Figure 3.5 A), indicating little or no *lux* gene expression. The pMK1*lux-PybeA** construct was created so that the 500 bp cloned insert contained the whole of the *ybeB* gene, as well as 205 bp upstream of *ybeB*; a region containing both the putative *ybeB* promoter -10 and -35 box sequences, as identified by BPROM analyses, and the site of the putative *E. coli ybeB* promoter (Figure 3.4). As such, it was possible that the luminescence detected in cultures expressing pMK1*lux-PybeA** resulted from the activity of the putative *ybeB* promoter, rather than activity of another downstream *ybeA* promoter. To test this, an alternative luciferase reporter plasmid was constructed, whereby a 289 bp region upstream of *ybeA*, containing just the *ybeB* gene, was cloned into pMK1*lux*, to generate pMK1*lux-PybeA* (Figure 3.4). Subsequent luciferase transcriptional reporter assays with this construct demonstrated that there was no significant promoter activity upstream of *ybeA* within *ybeB* (Figure 3.5 B). It was therefore concluded that the promoter activity detected in pMK1*lux-PybeA** cultures resulted from the activity of the promoter upstream of *ybeB*.

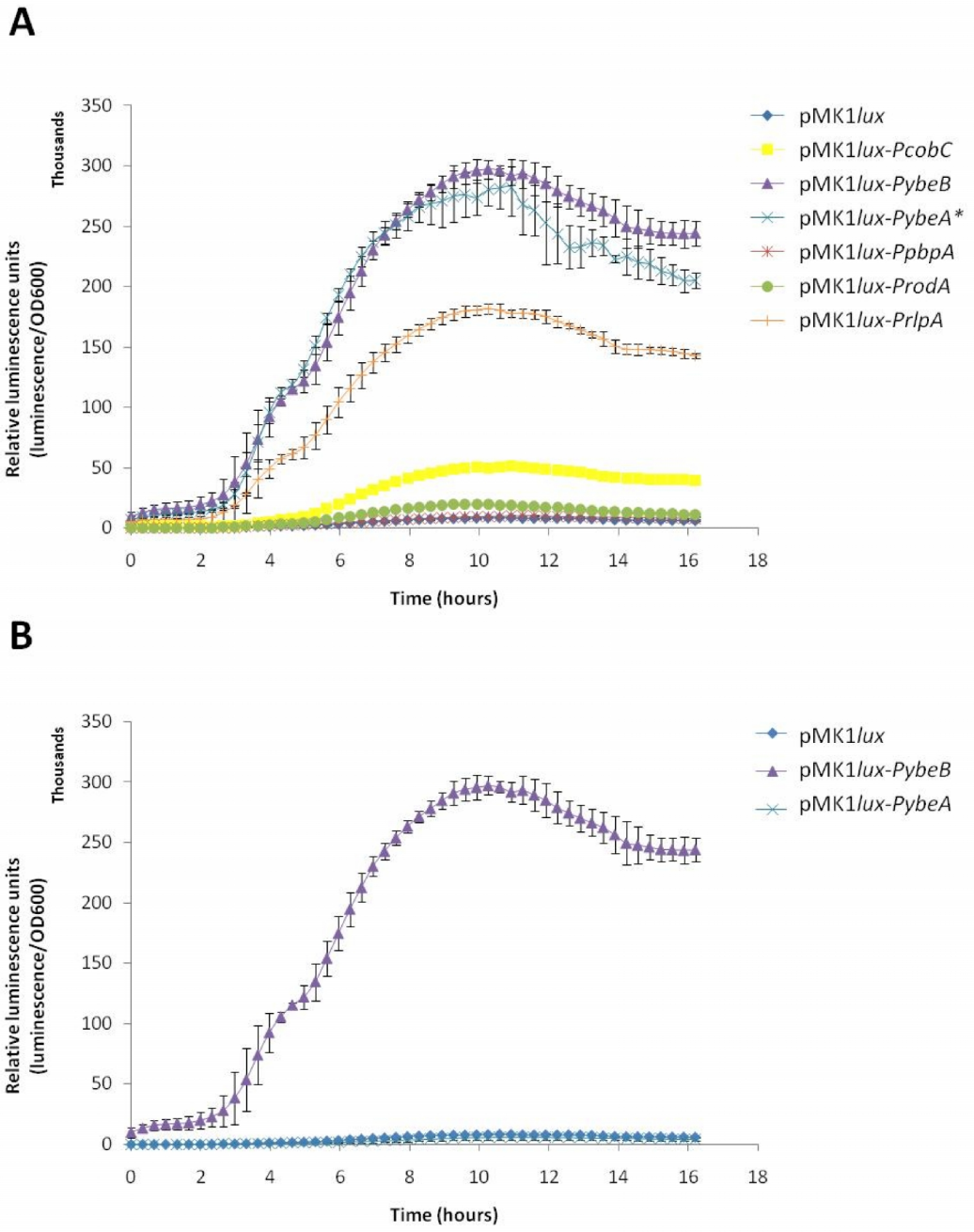

Figure 3.5: Luciferase transcriptional reporter assays for promoter activity upstream of mrd operon genes: A - Transcriptional luciferase reporter assays of BRD948 wild-type (WT) cells expressing ~500 bp *mrd* promoter fusions in the pMK1*lux* luminescence reporter plasmid. Activity of each promoter fusion measured as relative luminescence units (luminescence per culture optical density at 600 nm). B - Transcriptional luciferase reporter assays of BRD948 wild-type (WT) cells expressing *mrd* promoter fusions; pMK1*lux* (negative control), pMK1*lux-PybeB* (positive control) and pMK1*lux-PybeA* construct. The latter contained a 289 bp region upstream of *ybeA* cloned into pMK1*lux*. Cells were grown in LB medium at 37^{o}C with shaking. Growth rates of the strains were equivalent. Values show the means from 3 independent assays. Error bars = standard deviation.

Together this data suggests that the putative promoter sequences located in the intergenic region upstream of *ybeB* form a true promoter for at least the first 4 genes of the *mrd* operon, and hence the *ybeB*, *ybeA*, *pbpA*, and *rodA* genes are all cotranscribed. Furthermore, the *mrd* operon promoter was shown to be located within 205 bp (upstream) of the start codon of *ybeB* (TTG). As such, the -35 and -10 box promoter sequences detected using the BPROM programme could potentially form part of this promoter. Alternatively, sequences further downstream in an equivalent position to the putative *mrd* operon promoter in *E. coli* could form the true *mrd* operon promoter in *E. coli*. The lack of detectable promoter activity with strains expressing pMK1*lux-ProdA* is in contrast to previous studies, which suggested that a promoter for *rodA* may be located within *pbpA* (143, 144).

Significant luminescence was also emitted from cultures expressing pMK1*lux–PrlpA*, with relative luminescence generally reaching levels of at least 50% of that of the *ybeB* promoter (Figure 3.5 A). This result supports *in silico* searches of both this work and a previous study, which identified potential promoter sequences upstream of *rlpA* (186). This suggests that *rlpA* is transcribed independently of upstream genes, from its own promoter. However, given the reduced strength of this promoter, it should be considered that *rlpA* expression may be partially controlled by the *mrd* operon promoter.

The *cobC* gene lies upstream of *ybeB*. The size of the intergenic region between *cobC* and *ybeB*, along with the presence of the *ybeB* promoter, make it likely that this gene is not a part of the *mrd* operon. Some significant luminescence was measured from pMK1*lux–PcobC* cultures, supporting this hypothesis. Promoter activity upstream of *dacA* could not be assessed due to problems constructing a pMK1*lux–PdacA* reporter plasmid.

3.4 Reverse transcriptase PCR (RT-PCR) to identify co-transcribed genes

Further work was required to determine whether or not *rlpA* is co-transcribed along with the preceding genes, or expressed solely under the control of the putative promoter within *rodA*. To test this, RT-PCR was carried out to detect the presence of specific transcripts of mRNA from *S.* Typhi BRD948. RT-PCR primers were

designed to flank the short intergenic regions between the *mrd* operon genes, as shown (Figure 3.6 A), the resulting PCR products being approximately 500 bp in length. Purified DNase-treated BRD948 RNA was used as template for each RT-PCR reaction. Since each PCR product traversed the junction between two genes, the successful generation of PCR product should be dependent on the two primer binding sites being present within a single transcript, i.e. where two adjacent genes are co-transcribed.

RT-PCR reactions were performed as described, with an initial reverse transcription step followed by 45 cycles of cDNA polymerisation. Primer pairs for each reaction were designed for all putative *mrd* operon genes, including upstream and downstream genes, in order to help verify the full set of co-transcribed genes within the operon. The experiment was carried out at least 3 times, alongside negative-control reactions with RNase-treated RNA, to screen for DNA contamination.

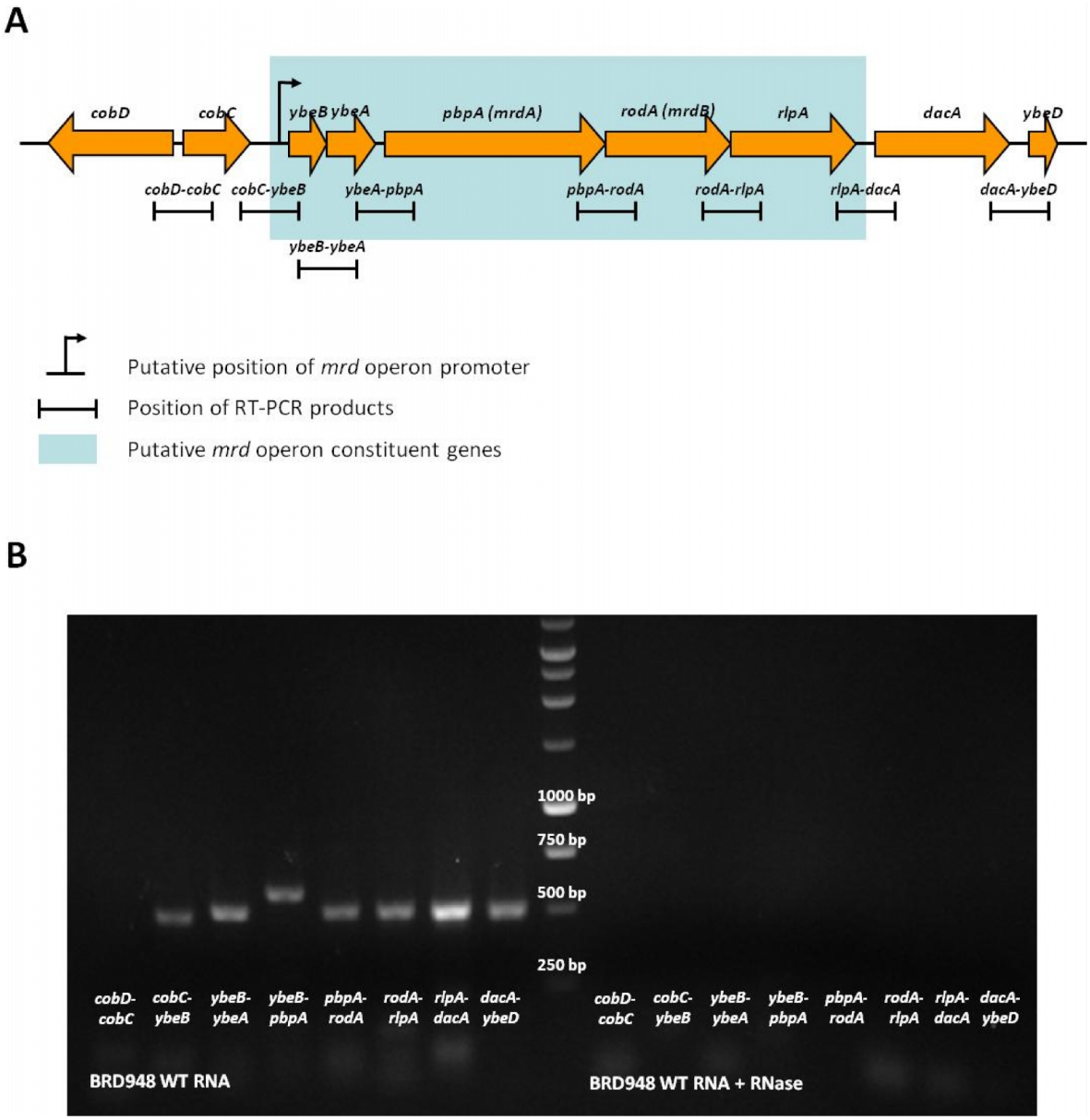

Figure 3.6 RT-PCR screen to identify co-transcribed genes: A - Schematic diagram showing primer design and subsequent positions of RT-PCR products. Primer pairs wer designed to be complementary to the 3' end of one gene and the 5' end of the adjacent downstream gene, such that PCR products flanked gene junctions, as shown. RT-PCR products were all approximately 500 bp in length. Diagram drawn to scale. B - 1% agarose gel showing PCR products from RT-PCR reactions to screen for co-transcribed genes. PCR products span the intergenic regions between genes of the *mrd* operon. Lanes to the left of the molecular weight marker contain PCR products from reactions with DNase-treated BRD948 wild-type RNA. Lanes to the right of the molecular weight marker contain PCR products from reactions with DNase- and RNase-treated BRD948 wild-type RNA as a negative control. Agarose gel shown is representative of 3 independent repeats with different RNA preparations.

The products of the RT-PCR reactions were run on 1% agarose gels, then visualised under UV light. A representative agarose gel is shown (Figure 3.6 B). Contrary to expectations, PCR products were detected for each adjacent *mrd*

operon gene, including the upstream *cobC* gene, and downstream *dacA* and *ybeD* genes. This would suggest that all 7 genes at least are co-transcribed, although this result does not agree with the findings of previous studies (187, 211). In addition, *in silico* analyses of the *Salmonella* genome and experimental luciferase reporter assays have demonstrated both the well conserved nature of the *ybeB-rlpA mrd* operon as a unit, as well as the presence of a strong promoter for the *mrd* operon genes upstream of *ybeB*, making it unlikely that both the upstream *cobC* and *ybeB* genes are co-transcribed.

A possible explanation for the findings of these assays is that various transcripts from this region of the genome may overlap in sequence. For instance, if the transcriptional start site of *ybeB* were upstream of a transcriptional termination signal of *cobC*, the resulting mRNA constructs would overlap, meaning that cDNA products would be generated bridging the *cobC-ybeB* junction in RT-PCR assays.

3.4.1 Transcriptional termination sequences within the *mrd* operon

Prokaryotic transcriptional termination sequences are recognised by their typical structure, consisting of a palindromic sequence which results in the formation of a hairpin loop in the DNA. This is generally followed by a uracil-rich region of DNA. The TranstermHP algorithm was designed to enable the *in silico* prediction of transcriptional terminator sequences within DNA (262, 263). This online tool was used to search for such sequences within the *S.* Typhi Ty2 genome, within 1 kb (downstream) of each putative *mrd* operon gene, as well as the flanking *cobC* and *dacA* genes (264). Previous studies had noted that transcriptional terminator sequences were lacking between the *pbpA* and *rodA* genes (142). The present *in silico* assays using TranstermHP identified transcriptional termination sequences downstream of both *cobC* and *dacA*, but not downstream of any of the intermediate genes in the *S.* Typhi genome (264). Both these termination sequences were located in the intergenic regions. The lack of obvious transcriptional termination signals elsewhere within this region of the genome would suggest that all 6 genes from *ybeB* to *dacA* are co-transcribed.

The proposed transcription termination sequences for *cobC* lay 171 bp downstream from the 3' end of *cobC*, 10 bp downstream of the putative -10 box of the *ybeB* promoter. As such mRNA transcripts from both genes may overlap slightly. This may also be the case for additional genes in the *mrd* operon, explaining why RT-PCR cDNA products were detected for all but the *cobC-cobD* junction. The *cobC* and *cobD* genes lie on opposite strands of the DNA; hence mRNA transcripts from these genes would not be complementary, preventing the generation of a cDNA product in RT-PCR assays. The results of the RT-PCR assay are therefore inconclusive and may be misleading in terms of identifying co-transcribed genes.

3.5 Discussion

Published research has produced conflicting theories concerning the structure of the *mrd* operon, as well as the position(s) of putative promoter(s). Little experimental data has been produced to support *in silico* analyses, and the majority, if not all work to date, has been conducted solely in *E. coli* (142, 143, 186, 187, 205). For this reason, both *in silico* and experimental analyses in this portion of work sought to characterise the structure of the *mrd* operon in *Salmonella*, focussing predominantly on the characterisation of both the position of the major promoter, and the cohort of co-transcribed genes.

Whilst the physical proximity of the *pbpA*, *rodA* and *rlpA* genes to each other may suggest that these genes are co-transcribed, more than one study has identified potential promoter sequences upstream of both *rodA* and *rlpA*, although the lack of transcriptional terminator sequences between *pbpA* and *rodA* led Asoh et al. to suggest that these genes at least are co-transcribed (142, 143, 186). *ybeB* and *ybeA* are also predicted to form part of the operon due to the presence of a predicted promoter upstream of *ybeB*, and *rodA* expression was shown to be strongly stimulated by the promoter upstream of *pbpA* (142, 143). Stoker et al. and others also suggested that the downstream *dacA* gene may be contiguous with the upstream genes, partly due to its functional relationship, being important for cell shape (155, 204, 205, 207). PBP5 is the most highly expressed of all the penicillin-binding proteins (265). Although this does not necessarily correlate to transcription

levels, it is unlikely that *dacA* transcription levels would be as high or higher than those of *pbpA* if it were part of the same operon, particularly being at the 3' end. Regulation of *dacA* expression is also distinct from *pbpA* expression (266). It therefore appears to be generally accepted that the *mrd* operon consists of just 5 genes: *ybeB*, *ybeA*, *pbpA*, *rodA* and *rlpA* in Gram-negative bacteria (143, 187).

The present work has identified that this putative 5-gene operon structure is indeed well conserved among *Salmonella* serovars, *E. coli* and more distantly related Gram-negative bacteria. However, a significant exception to this level of conservation was identified in an 89 bp stretch of DNA upstream of *ybeB* in *S.* Typhi, a region corresponding to the site of the putative *ybeB* promoter in *E. coli* (Figure 3.3). In contrast to the surrounding regions of DNA, no significant sequence similarity was identified between the *E. coli* and *Salmonella* genomes, in this stretch. This may be relevant in terms of the regulation of *mrd* operon expression.

In silico analyses of a ~7 kb region of the *Salmonella* Typhi (Ty2 strain) genome, containing the putative *mrd* operon identified promoter-like sequences for *ybeB* much further upstream of this site (~170-250 bp from *ybeB*) in *Salmonella*. Luciferase transcriptional reporter assays were utilised to verify these findings, assaying for promoter activity; 500 bp sections of DNA just upstream of each *mrd* operon gene were cloned into the luminescence reporter plasmid pMK1*lux*, introduced to the wild-type *S.* Typhi BRD948 strain, and examined for luminescence, indicative of promoter activity. Thus assays for promoter activity were carried out in a native background, to reflect natural conditions as much as possible. Significant promoter activity was detected in regions upstream of *ybeB*, *rlpA* and *cobC*, the strongest promoter being that located within ~200 bp upstream of *ybeB.*

Several conclusions may be drawn from these findings. Firstly, it is clear that a strong promoter exists upstream of *ybeB.* Assuming that the predicted promoter upstream of *ybeB* in *E. coli* forms a true promoter, the absence of an equivalent promoter in the *Salmonella* genome may indicate that expression of *ybeB* (and potentially downstream genes) is controlled by alternative promoter sequences

further upstream, as predicted by the BPROM and Fruitfly programmes. If this is the case, the differences in promoter sequences may result in dissimilar regulation of the expression of *mrd* operon genes between the two species. Alternatively, the true promoter of the *mrd* operon (or at least *ybeB*) is located within the conserved sequences further upstream in both *Salmonella* and *E. coli*. If this is the case, promoter-like sequences identified by BPROM and Fruitfly may form the true promoter in both organisms. Another possible conclusion is that the BPROM and Fruitfly programmes failed to identify the true promoter sequences upstream of *ybeB* within *S.* Typhi, which may be located in an equivalent position to the proposed promoter of *E. coli*.

The absence of detectable promoter activity upstream of *ybeA*, *pbpA* and *rodA*, along with a lack of putative transcriptional terminator sequences between *ybeB* and *rodA*, suggested that these genes are co-transcribed, being expressed under the control of the *ybeB* promoter. Furthermore, putative promoter sequences identified for these genes were located at some distance upstream of both *ybeA* and *rodA*, whilst no such sequences were found for *pbpA*, further supporting this hypothesis.

in silico analyses identified several putative promoters at positions upstream of the *rlpA* and *dacA* genes, and promoter activity was detected upstream of *rlpA* in luciferase reporter assays. The promoter activity identified upstream of *rlpA* is surprising since *rodA* is closely linked to *rlpA*, and the putative promoter sequences were located within the *rodA* gene. However, a previous study also recognised possible promoter sequences upstream of *rlpA*, although it was suggested that *rlpA* may yet be co-transcribed along with upstream genes (186). Promoter activity detected upstream of *rlpA*, however, may indicate that *rlpA* is not co-transcribed along with upstream genes, although the strength of this promoter was significantly lower than the *ybeB* promoter and no transcriptional terminator sequences were found downstream of *rodA*. It is possible that *rlpA* is expressed under the control of both its own promoter, and the upstream *ybeB* promoter, permitting a tighter level of control over RlpA levels.

The presence of promoter-like sequences upstream of *dacA* suggests that this gene is expressed independently of the *mrd* operon genes, although these findings could not be verified experimentally. The position of *dacA* within this operon was, however, made unclear by the absence of detected transcriptional terminator sequences between *rlpA* and *dacA*. *dacA* is thought to be unlikely to form part of the *mrd* operon due to its distance from *rlpA*, as well as the high levels of expression of the *dacA*-encoded PBP5 protein (210). As such, the identification of promoter sequences upstream of *dacA* was not surprising. Furthermore, in previous studies Δ*rlpA* mutants did not possess the morphological defects typical of Δ*dacA* mutants, as may be expected if these genes were co-transcribed, as an *rlpA* mutation could have polar effects on downstream genes of the same operon (163, 179, 207, 265, 266). Further experimental analyses are therefore needed, though results tend to suggest that *dacA* and *rlpA* are not co-transcribed.

RT-PCR assays were also designed to identify co-transcribed genes within this region. Primer pairs were designed to flank the junctions between adjacent genes, so that the successful amplification of specific cDNA product from an mRNA template would only occur if the genes were co-transcribed. However, contrary to other findings, the results of this assay suggested that at least 7 genes, from *cobC* to *ybeD* were all co-transcribed in *S.* Typhi. It was subsequently recognised that in some cases mRNA transcripts from divergently expressed genes may have overlapped, leading to false positive results in RT-PCR assays. As such, data from RT-PCR assays was disregarded, it likely being misleading.

Taken together, these results suggest that a strong promoter controlling expression of the *mrd* operon is located upstream of *ybeB* in *Salmonella*, although it remains to be shown whether or not the promoter is located in the same position as the putative *E. coli mrd* operon promoter. It is highly likely that at least *ybeB*, *ybeA*, *pbpA* and *rodA* are co-transcribed, due to a lack of likely promoter sequences or transcriptional terminator sequences within this region; putative promoter sequences identified for *ybeA* and *rodA* were located at a considerable distance from these genes, whilst no such sequences were found for *pbpA.* This finding was supported by luciferase reporter assays demonstrating an absence of detectable promoter activity upstream of *ybeA*, *pbpA* or *rodA*, although previous

work suggested that *rodA* possessed its own promoter (143). Likewise, the presence of the strong *ybeB* promoter, along with the identified transcription termination sequences for *cobC*, and the physical distance between *cobC* and *ybeB*, suggest that *cobC* is not part of the operon.

These analyses add further evidence to support the hypothesis that the *mrd* operon consists of 5 co-transcribed genes, whose expression is regulated by a strong promoter located upstream of *ybeB*. Although further work is needed to fully characterise the positions of *rlpA* and *dacA*, subsequent work in the present study has taken the tentative assumption that *rlpA*, but not *dacA*, forms part of the operon.

Chapter 4. Generation of and phenotypic analyses of specific knockouts of *mrd* operon genes

4.1 Generation of specific knockouts of *mrd* operon genes in *Salmonella* and complementation of knockout strains

4.1.1 Generation of specific non-polar mutants in *mrd* operon genes

Specific mutants of each of the *mrd* operon genes were successfully created in S. Typhi BRD948 using the Datsenko and Wanner method, as described (238). The Δ*rlpA* mutant was created previously (163). Briefly, kanamycin resistant knockout cassettes flanked by short FRT repeats and regions of homology to the target gene, were introduced into the BRD948 genome by homologous recombination, specifically replacing all but short sequences at the 5' and 3' ends of each of the wild-type *mrd* operon genes (Figure 2.4). In an additional step, the kanamycin resistance genes were removed to leave a single FRT site flanked by the short sequences remaining from the wild-type genes. Scar sequences were each 82bp, excluding the wild-type gene flanking sequences. This enabled the generation of specific non-polar mutants of each individual gene.

The successful generation of specific mutants was initially verified by PCR using primers specific to sequences just upstream and downstream of each target gene, as indicated by an alteration in PCR product size, from the removal of the wild-type gene (Figure 4.1). As such, PCR amplification of the regions covering each gene knockout resulted in a product of around 250 bp in size (Figure 4.1). In addition regions of the genome from around 100 bp upstream to 100 bp downstream of the target gene start and stop codons were amplified by PCR. These PCR products were then sequenced to confirm the correct construction of each mutant. Unlike *S.* Typhimurium mutants, mutants generated in *S.* Typhi BRD948 were not transduced back into a wild-type background due to the lack of a Typhi-specific phage.

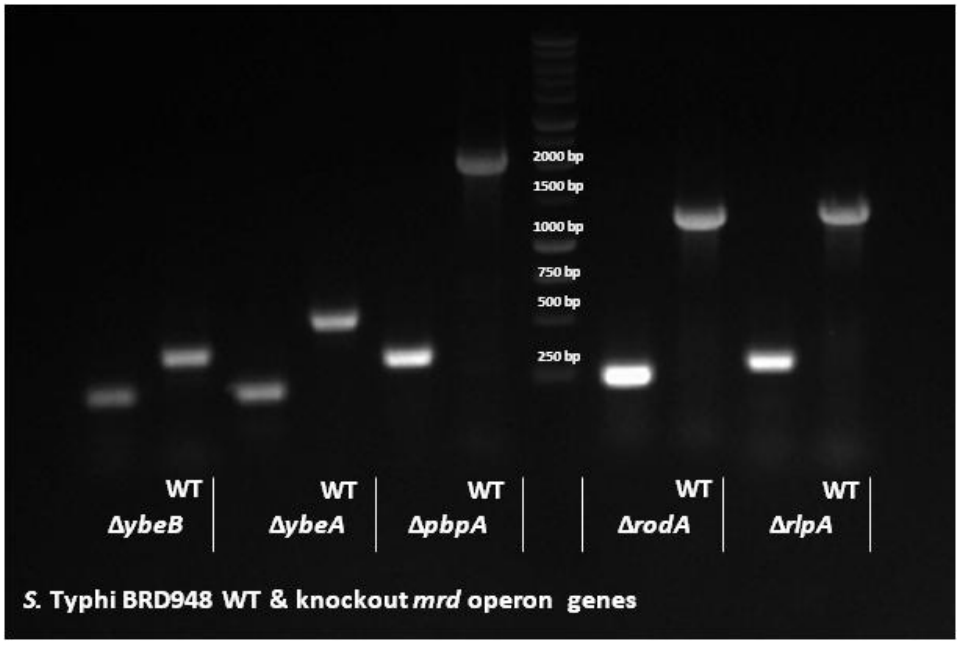

Figure 4.1: Construction of precise knockouts of mrd operon genes in S. Typhi: Agarose gel of PCR products from PCR check reactions of *mrd* knockout genes in BRD948. Complete knockouts were constructed in each *mrd* operon gene in BRD948, with removal of the kanamycin cassette, as demonstrated by a reduction in PCR product size, compared to the wild-type genes. Wild-type (WT) PCR fragment sizes: *ybeB* = 372 bp, *ybeA* = 522 bp, *pbpA* = 2035 bp, *rodA* = 1233 bp, *rlpA* = 1161 bp (Δ*rlpA* constructed in previous work (163)). Molecular size markers as indicated.

In addition to the *S.* Typhi *mrd* mutants, mutants of the *ybeB*, and *pbpA* genes were made in *S.* Typhimurium SL1344, with *rodA* and *rlpA* mutants having been generated in previous work (163). These mutations were transduced back into the wild-type SL1344 parent in order to reduce the risk of accumulating secondary mutations through the transformation process. Attempts were made to remove the kanamycin cassette in these mutants, but proved unsuccessful.

4.1.2 Evidence for non-polarity of mutations

It was important that the specific mutants generated in this work were non-polar, in order to ensure that any observed phenotypes were a direct result of the specific mutations, rather than a consequence of polar effects on the expression of downstream genes. Mutations of the *mrd* operon genes in this study were generated using the pKD13 plasmid as a template for production of the kanamycin cassette. Insertion of pKD13-specific knockout cassettes into bacterial genomes may cause polar effects on downstream protein expression, due to the lack of

translational signals within the scar sequence, such as ribosome binding site sequences (238).

However, should the *mrd* mutants have polar effects on downstream gene expression, one would expect the Δ*ybeB* and Δ*ybeA* mutants to display morphological defects, due to effects on downstream *pbpA* or *rodA* expression, as has been observed previously (188). This was observed in *S.* Typhi Δ*ybeB* and Δ*ybeA* mutants before removal of the kanamycin resistance gene; cells were spheroid, appearing identical in morphology to the Δ*pbpA* and Δ*rodA* mutants. However, upon removal of the kanamycin resistance gene, Δ*ybeB* and Δ*ybeA* cells reverted to a rod-shaped morphology (Figure 4.3). Thus it is likely that the *mrd* mutants generated in *S.* Typhi in this study are non-polar.

4.1.3 Morphology of *mrd* operon mutants

Morphological defects in each individual mutant were analysed by both phase contrast microscopy and scanning electron microscopy (SEM) (Figure 4.3 A and 4.7). In agreement with previous studies in various rod-shaped bacteria, Δ*pbpA* and Δ*rodA* mutants of *S.* Typhi displayed severe morphological defects (128, 130, 131, 163). Cells were spheroid, displaying significant heterogeneity of size and often appearing much larger than wild-type cells (Figure 4.3 and 4.4). There were no discernable differences in morphology between Δ*pbpA* and Δ*rodA* mutants. Division defects were also evident in these mutants, in both phase contrast and SEM images of dividing cells, as illustrated below (Figure 4.2). In round cells, septation and cell wall invagination originated at one side of the cell, before progressing around the whole cell. These asymmetric division patterns have been observed in round spheroid mutants in several studies, and appear to result from the formation of incomplete cell division FtsZ rings (127, 131, 182, 267, 268).

Figure 4.2: Asymmetrical division patterns of round-cell mutants: Schematic diagram to illustrate the progressive asymmetric division patterns in round-cell mrd mutants , as observed by phase contrast microscopy. Cell wall invagination begins and occurs predominantly at one side of the cell, eventually moving around the whole cell to bring about division.

In contrast, Δ*ybeB* and Δ*ybeA* cells retained a rod-shaped morphology, much as wild-type. However, the lateral cell walls of some Δ*ybeB* cells, and Δ*ybeA* cells to a greater extent, appeared to be on average slightly shorter than wild-type cells, although the cell diameter was unaffected (Figure 4.3 A and 4.7). Previous studies demonstrated that Δ*rlpA* mutants also retained the wild-type morphology (163).

4.1.4 Complementation of *mrd* mutant strains

BRD948 Δ*pbpA* and Δ*rodA* knockout strains were complemented with plasmid-encoded N-terminal YFP-fusion proteins of the respective genes from *E. coli*, which are expressed under the control of the *lac* promoter, and hence are isopropyl β-D-1-thiogalactopyranoside (IPTG) inducible. These vectors were a kind gift of Lawrence Rothfield (University of Connecticut, US) (135, 269). Previous work has demonstrated the ability of these vectors to complement Δ*pbpA* and Δ*rodA* mutants in *E. coli*, restoring rod-shape to such cells (135). Likewise, introducing the YFP-fusion proteins of PBP2 and RodA to *Salmonella* Typhi round-cell mutants successfully restored the wild-type morphology to Δ*pbpA* and Δ*rodA* mutants respectively (Figure 4.3).

The RodA-YFP fusion vector was introduced to both BRD948 Δ*pbpA* and Δ*rodA* mutants, as well as the wild-type parent. However expression of RodA-YFP in the Δ*pbpA* mutant did not restore rod-shape in these cells, demonstrating that both PBP2 and RodA have individual and essential functions in maintaining cell shape. The morphological defects observed in the Δ*pbpA* mutants are not simply due to polar effects on *rodA* expression (Figure 4.4).

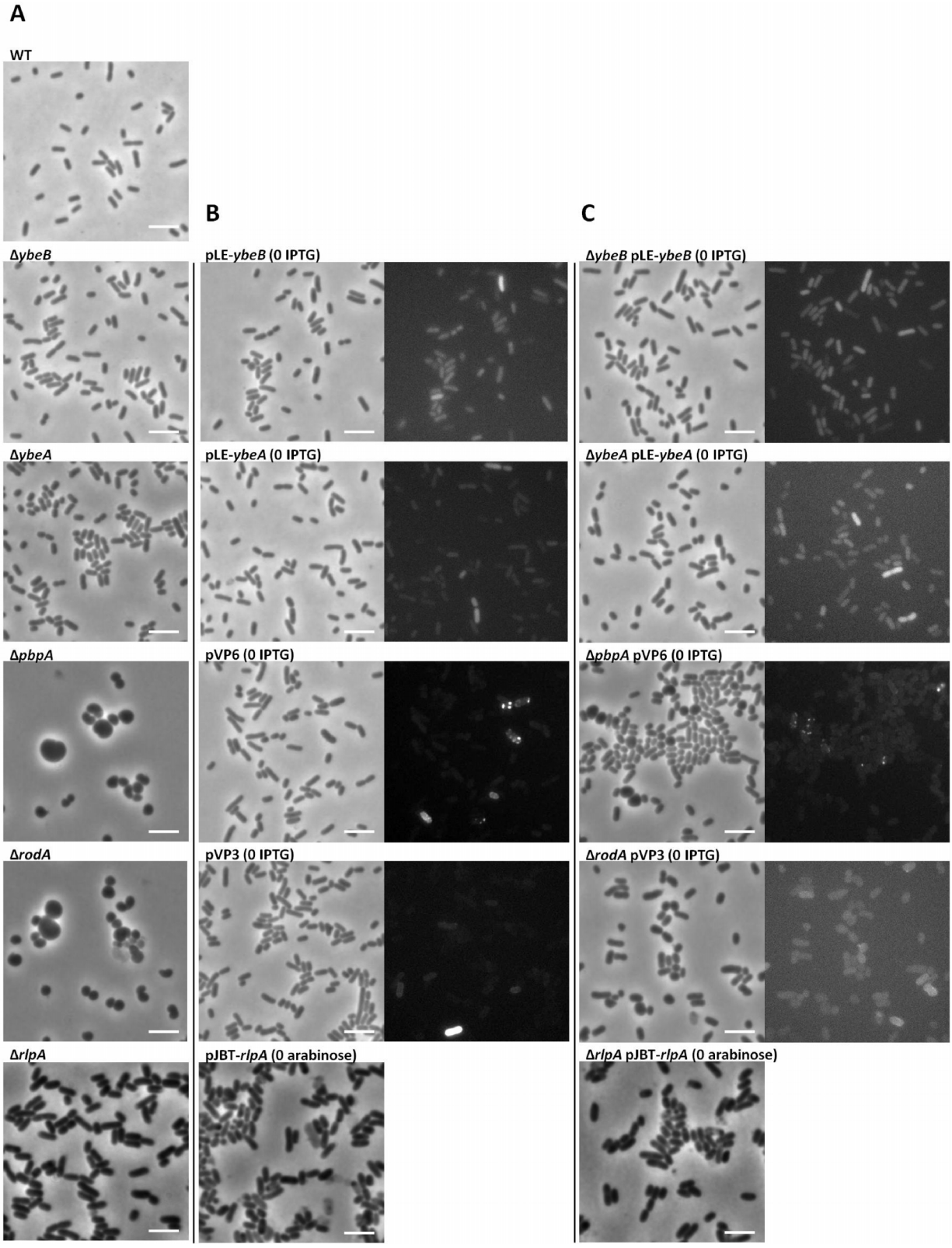

Figure 4.3: Phase contrast microscopy images of wild-type, mrd mutant and complemented mutants of S. Typhi: Phase contrast images of live *S.* Typhi BRD948 cultures; wild-type (WT) and *mrd* mutant strains (panel A), wild-type cells expressing *mrd* YFP-fusion proteins (panel B), and complemented *mrd* mutant strains (panel C). Phase contrast and epifluorescent microscopy images shown for YFP-fusion protein-expressing strains. Δ*rlpA* strain and pJBT-*rlpA* complementation plasmid constructed in previous work (163). Cells cultured in LB broth with aromatic amino acids and 20 mM $MgCl_2$, at 37°C and

200 rpm, harvested for microscopy at mid-log phase. Cells were grown without IPTG/arabinose supplementation (to induce plasmid expression). pLE-*ybeB*, pLE-*ybeA*, pVP6, and pVP3 encode YFP fusion proteins of YbeB, YbeA, PBP2, and RodA respectively. Scale bars indicate 5 µm.

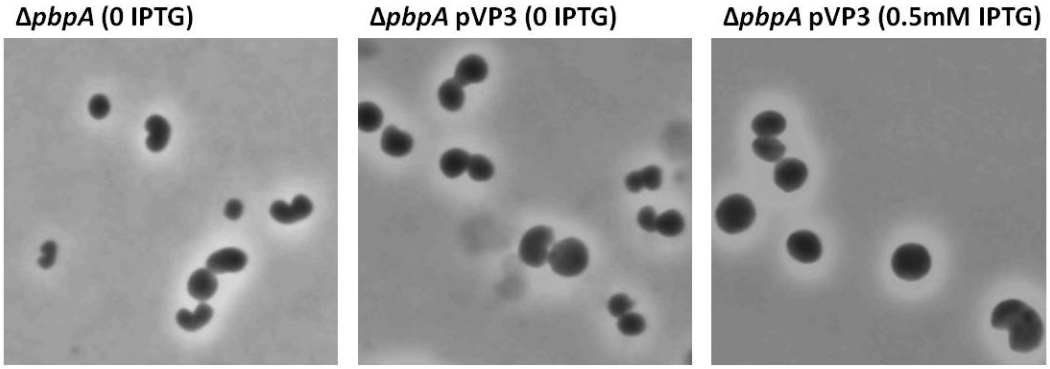

Figure 4.4: Overexpression of RodA in ΔpbpA cells: Phase contrast microscopy images of live *S.* Typhi BRD948 Δ*pbpA* cells and Δ*pbpA* cells expressing the RodA-YFP fusion protein (pVP3). Cells cultured in LB broth with aromatic amino acids and 20 mM $MgCl_2$, ± 0.5 mM IPTG, at 37°C and 200 rpm. Cells harvested for microscopy at mid-log phase. All images are to the same scale.

YFP-fusion proteins of the YbeB and YbeA proteins were constructed in this study using the Rothfield vectors. A parent MreB-YFP-expressing plasmid, pLE7 was digested with XbaI and HindIII enzymes to excise the *mreB* gene. The complete *ybeB* and *ybeA* genes (minus the stop codons) were then PCR-amplified from *S.* Typhi BRD948 genomic DNA, with specific primers to introduce XbaI and HindIII restriction sites into the resulting DNA fragments, flanking the *ybe* genes. These fragments were digested and ligated into the digested pLE7 vector. Accurate cloning was checked by DNA sequencing. The resulting plasmids were finally introduced to the BRD948 wild-type and *ybe* mutant strains. Attempts to construct an RlpA-YFP fusion proved unsuccessful. However, BRD948 Δ*rlpA* mutants from previous work were complemented with a plasmid-encoded *S.* Typhi RlpA fused to the *Strep*-tag® short epitope tag, also constructed in a previous study (163). This fusion protein is likely to be functional, given that immunofluorescence microscopy demonstrated its ability to localise specifically to both the cell septum and the lateral cell wall in a helical fashion, as observed in previous studies (163, 179). Successful complementation of both the Δ*ybe* and Δ*rlpA* mutants was difficult to establish, given the lack of obvious morphological defects in these strains (Figure 4.3).

Although the YFP-fusion proteins were able to reverse the cell shape defects in BRD948 Δ*pbpA* and Δ*rodA*, these fusion proteins may not be ideal since they encode *E. coli* proteins, which although clearly effective, have small differences in the amino acid sequences which may subtly affect protein activity between the two bacteria. The identity between the *Salmonella* Typhi and *E. coli* PBP2 and RodA sequences is 96% and 98% respectively, at the amino acid level. Furthermore, the pLE7 derivatives have a fairly high copy number, which may be problematic when attempting to restore protein levels that resemble the wild-type. Overexpression of cell-shape determinants has been shown previously to cause cell-shape defects similar to those seen in mutant cells (158, 164). Attempts were therefore made to clone the *S.* Typhi *mrd* operon genes into the low copy pNDM220 expression vector under the control of an inducible promoter (270), although to date this has proved unsuccessful.

4.1.5 Overexpression of *mrd* operon proteins

In both induced and un-induced cultures of YFP-fusion protein-expressing cells, the strength of the YFP signal varied considerably between cells. Hence, in a culture of Δ*pbpA* pVP6 or Δ*rodA* pVP3 cells, rod-shape was not restored in all cells. Concurrently, in those cells which remained spheroid there was usually very little, if any fluorescence, demonstrating that PBP2 or RodA expression in these cells was very low, or that the cells had lost the pVP plasmid (Figure 4.4 and 4.5). It is evident from both phase contrast and epifluorescence microscopy analyses that low levels of PBP2-YFP and RodA-YFP expression were, however, sufficient to restore a wild-type morphology in Δ*pbpA* and Δ*rodA* cells since rod-shaped morphology was restored even with a low fluorescent signal.

In the absence of IPTG, expression of low-levels of the appropriate plasmid-encoded YFP-fusion restored the rod morphology in BRD948 Δ*pbpA* and Δ*rodA* mutants (Figure 4.3). However, overexpression of the PBP2-YFP and RodA-YFP proteins through the prolonged growth of pVP6- and pVP3-expressing cells in the presence of at least 0.5 mM IPTG caused some morphological defects. PBP2- and RodA-overexpressing cells sometimes became larger or rounded, with an increased diameter, and a slightly distorted rod-shape (Figure 4.5). Similar

morphological changes caused by the overexpression of MreB, PBP2 and RodZ, have been observed previously, as well as the observed filamentation of cells from the overexpression of MreB (158, 164, 330). Similar defects were not observed with the overexpression of the YbeB-YFP, YbeA-YFP, and RlpA-*Strep* proteins (Figure 4.5) (163).

These observations were verified in further experiments to investigate how IPTG levels affected YFP fusion protein expression. BRD948 pVP6 and Δ*pbpA* pVP6 strains were cultured in varying concentrations of IPTG. Phase contrast microscopy and epifluorescence microscopy of these cultures demonstrated that increasing levels of IPTG clearly resulted in a much stronger YFP signal from the increased expression of PBP2-YFP. In addition, cells expressing relatively high levels of PBP2-YFP (particularly evident with growth in higher IPTG concentrations) often appeared bloated with an increased cell diameter. As within any population of cells, significant heterogeneity between individual cells was observed in terms of levels of PBP2-YFP expression (Figure 4.6).

Were the morphological defects in PBP2/RodA-overexpressing cells seen only in Δ*pbpA* and Δ*rodA* mutant strains, it could be argued that overexpression caused the YFP-fusion proteins to accumulate in inclusion bodies, preventing them from functioning properly. Such cells would be expected to revert back to a round-shape purely through a lack of functional PBP2/RodA, rather than through overexpression of these proteins causing direct morphological defects. However, the morphological defects were also seen in some wild-type cells overexpressing PBP2-YFP and RodA-YFP, providing evidence that overexpression of these cell shape proteins directly causes morphological defects. However, the possibility cannot be excluded that the YFP fusion protein itself somewhat perturbs PBP2/RodA function, causing morphological defects (Figure 4.6).

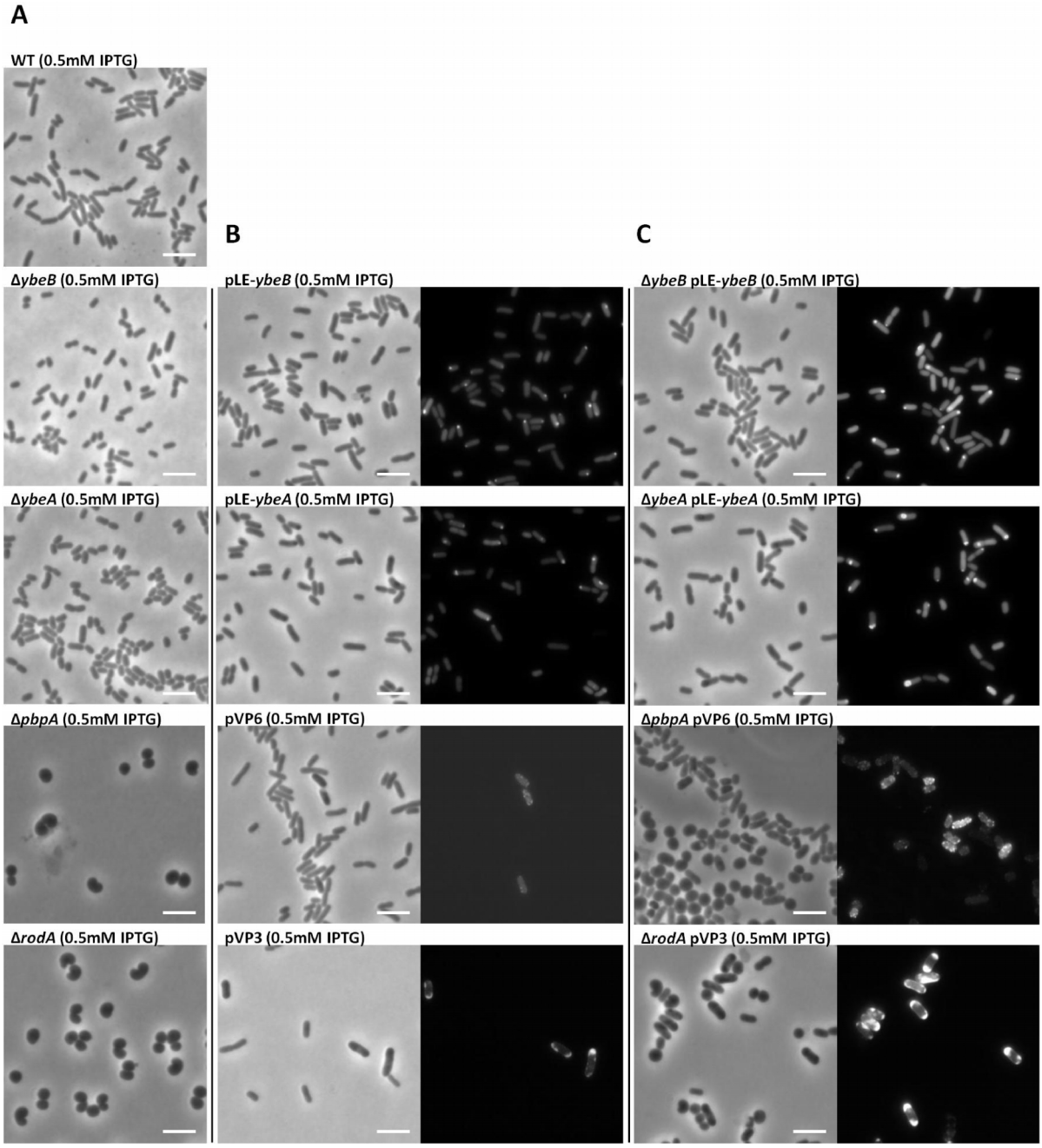

Figure 4.5: Overexpression of mrd operon YFP-fusion proteins: Phase contrast microscopy images of live *S.* Typhi BRD948 cultures; wild-type (WT) and *mrd* mutant strains (panel A), wild-type cells expressing *mrd* YFP-fusion proteins (panel B), and complemented *mrd* mutant strains (panel C). Phase contrast and epifluorescent microscopy images shown for YFP-fusion protein-expressing strains. Cells harvested for microscopy after 5 hours' growth (mid-log phase) in LB broth with aromatic amino acids, 20 mM $MgCl_2$, at 37°C and 200 rpm. Scale bars indicate 5 μm.

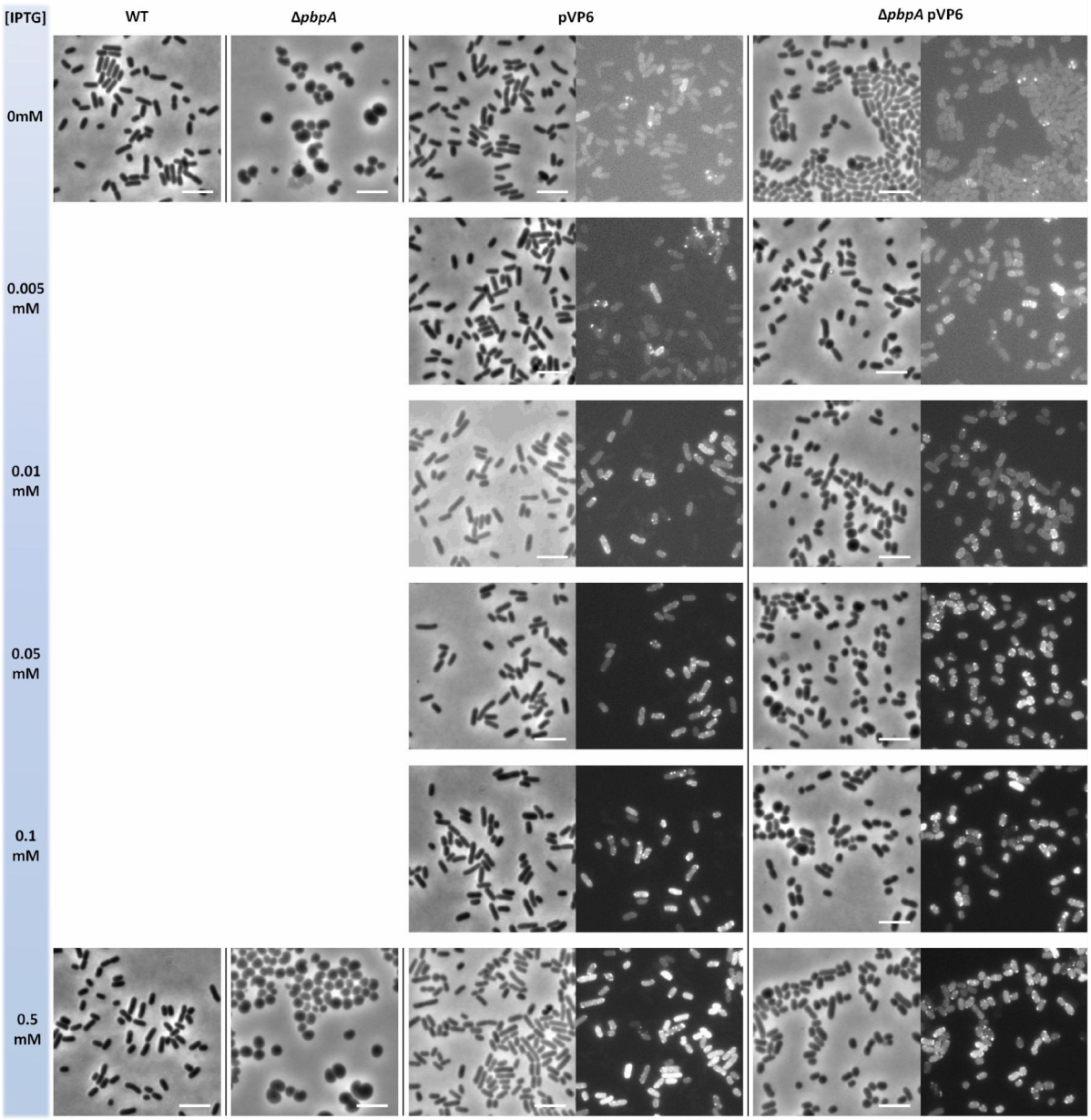

Figure 4.6: Overexpression of PBP2-YFP: Phase contrast microscopy images of live *S.* Typhi BRD948 wild-type (WT), Δ*pbpA* and WT/Δ*pbpA* cells expressing the PBP2-YFP fusion protein (pVP6). Phase contrast and epifluorescent microscopy images shown for YFP-fusion protein-expressing strains. Cells harvested for microscopy after 5 hours' growth (mid-log phase) in LB broth with aromatic amino acids and 20 mM $MgCl_2$, at 37°C and 200 rpm. Cultures supplemented with varying concentrations of IPTG to induce variable levels of plasmid expression and investigate *pbpA* overexpression. Scale bars indicate 5 μm.

4.1.6 Localisation of the *mrd* operon gene products by epifluorescence microscopy

The complementation of *mrd* gene mutants with YFP-fusions of the *mrd* operon proteins made it possible to investigate the subcellular localisation of each protein in *S.* Typhi cells by epifluorescence microscopy.

In cells where expression levels of PBP2-YFP and RodA-YFP were large enough to detect a fairly strong fluorescence signal, the PBP2 and RodA proteins were observed to localise at distinct foci along the lateral cell wall of *S* Typhi BRD948 (Figure 4.4 and 4.5). By altering the focus to look at different depths through the cell, these foci could be observed to form banding patterns, reminiscent of helices, as noted in previous immunofluorescence microscopy work (163). This is in line with other studies in *E. coli* and *C. crescentus*, which have demonstrated that both PBP2 and RodA localise in helices along the long axis of the cell (135, 136, 160).

In contrast, both the YbeB and YbeA proteins seemed to be evenly dispersed throughout the cell cytoplasm (Figure 4.4 and 4.5). Analyses of the protein sequence of both proteins have shown that the sequences lack both export signal sequences and putative transmembrane spans, suggesting that these proteins are indeed cytoplasmic (271, 272). In induced cultures overexpressing pLE-*ybeB* and pLE-*ybeA* cells, YbeB and YbeA sometimes appeared to localise in polar foci as well as throughout the cytoplasm. However, it is likely that this is a result of excess protein being gathered into inclusion bodies, particularly as in phase contrast microscopy images dark spots can be seen in these cells, which co-localise with the foci (Figure 4.5).

Likewise, it is likely that inclusion bodies formed with the overexpression of RodA, since RodA-YFP seemed to accumulate in large (usually) polar patches, which could also be seen in phase contrast images, particularly in IPTG-induced cells (Figure 4.5). The formation of inclusion bodies may have been caused by excess protein making the cells sick, the YFP fusion altering protein function, or expression of an *E. coli* protein in *S.* Typhi. It could be argued that the morphological defects seen with PBP2 and RodA overexpression are caused purely by the formation of large inclusion bodies, although such defects were also noticeable in PBP2-YFP-expressing cells, where inclusion bodies were not seen.

4.2 Scanning electron microscopy (SEM) of *mrd* operon mutants

Scanning electron microscopy (SEM) of each of the *mrd* operon mutants in *S.* Typhi was carried out to help further analyse the observed morphological defects

and investigate whether additional surface defects were evident in any mutant. Given that *pbpA* and *rodA* at least are involved in cell wall synthesis, mutations in these genes may be likely to affect cell surface structure and properties in a manner that could be detected by SEM. SEM images showed clearly both the morphological and asymmetric division defects evident in round-cell Δ*pbpA* and Δ*rodA* mutants (Figure 4.7 A). However, analysis of cells at a higher magnification did not reveal any obvious surface abnormalities in these mutants or in Δ*ybeB* or Δ*ybeA* cells (Figure 4.7 B).

By comparison, the surfaces of *S.* Typhi Δ*rlpA* cells appeared to be distinctly rough when compared to wild-type cells, with small irregular appendages extending from the surface (Figure 4.7 B). The surface pattern was comparable to cells treated with the antibiotic polymyxin B. A study by Lounatmaa et al. demonstrated that wild-type *Salmonella* Typhimurium treated with 30 µg/ml polymyxin developed dense 'rodlike projections' on the cell surface, resulting from excess folds of outer membrane extending out from the cell (273). Lounatmaa et al. suggested that polymyxin brought about these effects by integrating into the outer membrane, causing an increase in the outer membrane surface area which, combined with tight binding of the OM to the peptidoglycan, may have subsequently forced the formation of outer membrane appendages. RlpA is an outer membrane protein which may be involved in peptidoglycan binding (201). Further SEM analysis of WT and Δ*rlpA* cells was therefore carried out to investigate if the effects seen were significant, and similar to those seen with polymyxin treatment. In addition wild-type and Δ*rlpA* BRD948 cells were treated with 30 µg/ml polymyxin B to assess the effects of this drug on surface morphology. However, further SEM analysis of such cells proved inconclusive, since a fairly rough surface texture was seen in both wild-type and Δ*rlpA* cells, and the Δ*rlpA* mutant cells did not appear to have any distinguishing surface features. With polymyxin treatment cells appeared rougher, with the evident development of irregular appendages (Figure 4.8). Given the possible relationship between polymyxin B and RlpA function, it may be worth further investigation to determine whether or not the surface features observed initially were artefacts.

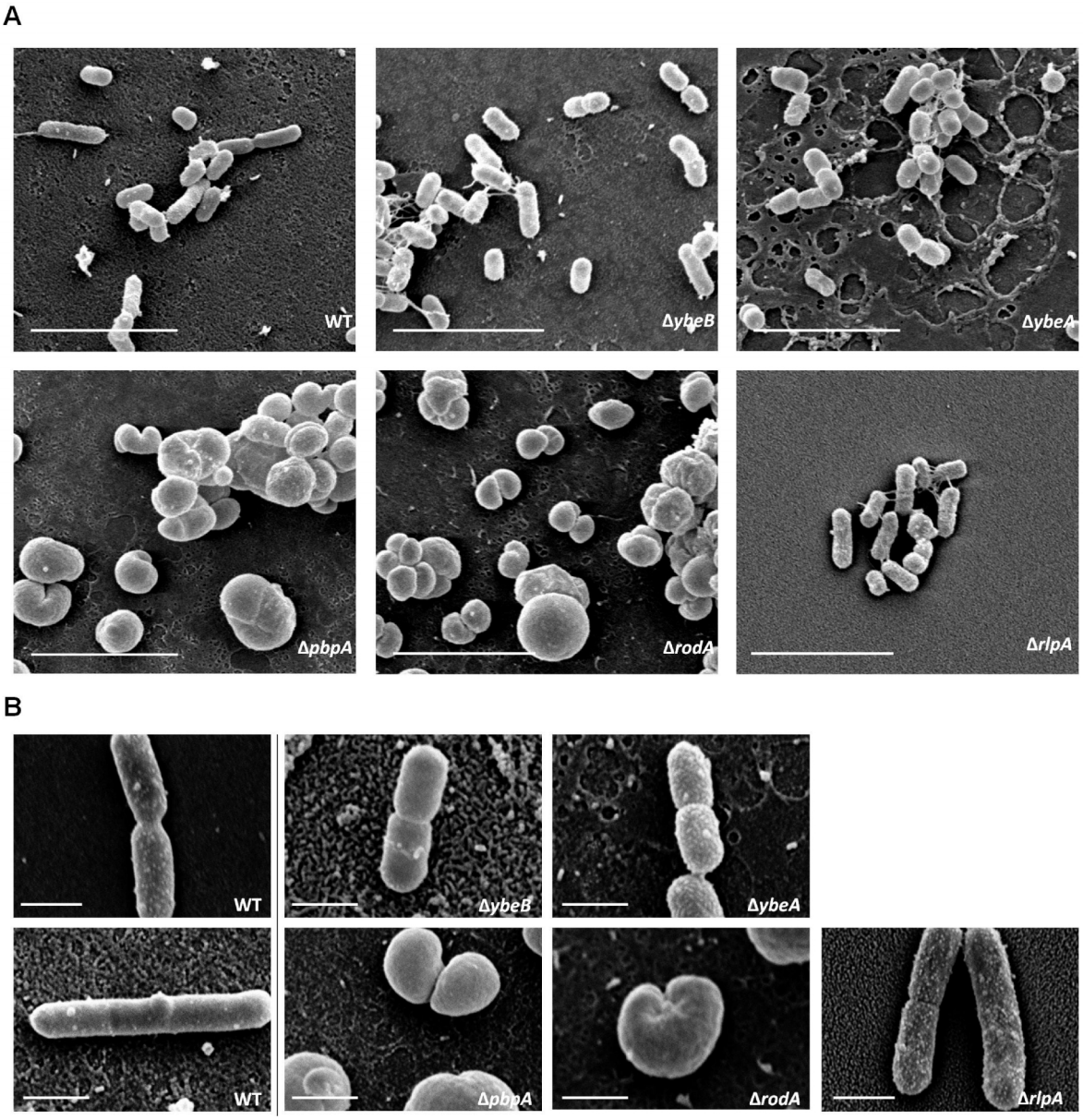

Figure 4.7: Scanning electron microscopy (SEM) images of wild-type (WT) and mrd mutant S. Typhi BRD948: Medium (A) and high (B) magnification SEM images of wild-type and mutant BRD948 cells. Cells harvested for microscopy at mid-log phase, after growth in LB broth with aromatic amino acids and 20 mM $MgCl_2$, at 37°C and 200 rpm. Scale bars indicate 5 µm (A) and 1 µm (B).

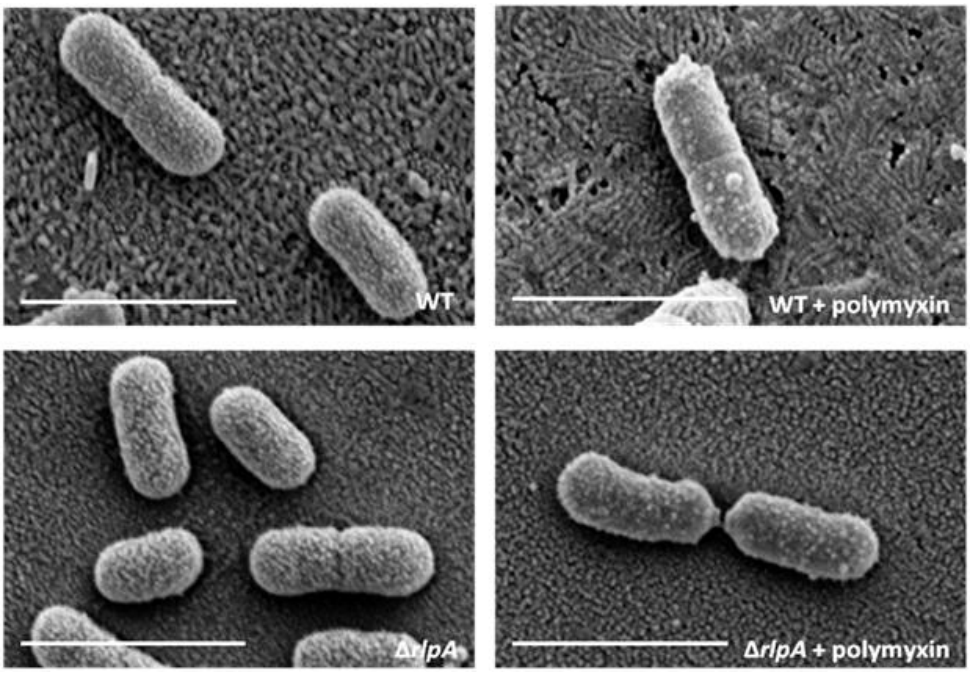

Figure 4.8: Scanning electron microscopy (SEM) images of wild-type (WT) and ΔrlpA S. Typhi BRD948 ± polymyxin B: Cells harvested for microscopy at mid-log phase, after growth in LB broth with aromatic amino acids and 20 mM $MgCl_2$. Strains grown ± 30 µg/ml polymyxin B at 37°C and 200 rpm. Scale bars indicate 2 µm.

4.3 General phenotypic analyses of *mrd* mutants

Once specific knockouts of the *mrd* genes were constructed in *S.* Typhi BRD948, phenotypic analyses were carried out in order to establish what effects each *mrd* gene mutation had upon the general health and physiology of the BRD948 cells, with the hope of providing more information about gene function.

4.3.1 Divalent cation dependent growth of *mrd* mutants

Upon initial generation of the *mrd* operon mutants in *S.* Typhi BRD948, it became evident that the round-cell Δ*pbpA* and Δ*rodA* mutants did not grow well on LB agar or in LB broth, even with the supplementation of the growth medium with aromatic amino acids and tyrosine. This is in contrast to the equivalent Δ*pbpA* and Δ*rodA* mutants of *S.* Typhimurium generated in this study and in a previous study, which displayed almost normal growth in LB medium at 37°C (163).

A study in 2005 by Formstone and Errington (229) demonstrated that Δ*mreB* mutants of *B. subtilis* were dependent upon high levels of magnesium and sucrose, their being major factors required for cell growth; growth in 2.5 mM $MgCl_2$ was

sufficient to restore a wild-type growth rate, whilst growth in 25 mM $MgCl_2$ almost completely restored the wild-type morphology. This was aided by concurrent sucrose addition and reversed upon removal of the magnesium and sucrose, something which caused cells to gradually expand and lyse. $CaCl_2$ addition had a similar effect, although it did not prove as effective as $MgCl_2$ (229). Much earlier studies have demonstrated similar dependencies of cell shape mutants upon magnesium in *B. subtilis* (274-276). It was suggested that magnesium and sucrose may act as osmoprotectants, helping prevent cell lysis in round cells, although sucrose appeared only to have a minor benefit. Alternatively, magnesium may instead act to stiffen the cell envelope, although the precise mechanism of magnesium action remains unknown (229). These studies were all carried out in *B. subtilis*, a Gram-positive organism. Thus it is recognised that similar effects may not be seen in organisms such as *Salmonella*.

However, in light of these studies, BRD948 round-cell mutants were initially cultured in medium containing 20 mM $MgCl_2$. When this was found to be effective in restoring growth, the addition of magnesium was titrated to determine the concentration of $MgCl_2$ required for optimum growth of *S.* Typhi Δ*pbpA* and Δ*rodA* mutants. The BRD948 Δ*pbpA* strain was sub-cultured into LB medium supplemented with $MgCl_2$ at various concentrations of between 0 mM and 30 mM. After 4 hours' growth at 37°C and 200 rpm, bacterial growth was assessed by measuring the optical density at 600 nm (OD600). The results of this assay demonstrate that addition of magnesium to the growth medium significantly improved growth of the Δ*pbpA* mutant, although not to the level of the wild-type. Magnesium addition did not significantly affect growth of the wild-type (Figure 4.9 A). 20 mM was shown to be an optimum level for growth in this assay, as higher concentrations of $MgCl_2$ did not significantly improve growth. As a result, 20 mM $MgCl_2$ was routinely added to BRD948 Δ*pbpA* and Δ*rodA* cultures and wild-type controls, to assist growth of the Δ*pbpA* and Δ*rodA* mutant strains. Growth of the Δ*rodA* mutant in the presence of 20 mM $MgCl_2$ was equivalent to that of BRD948 Δ*pbpA*.

Phase contrast microscopy analysis of both round-cell mutants demonstrated that unlike *B. subtilis* Δ*mreB* mutants, rod-shaped morphology was not restored in *S.*

Typhi or *S.* Typhimurium Δ*pbpA* or Δ*rodA* mutants with the addition of magnesium (Figure 4.10). This may reflect differences between bacterial species, or differences in function between the MreB, PBP2, and RodA proteins. However, microscopic analysis also showed that in BRD948 Δ*pbpA* and Δ*rodA* cultures grown in LB medium lacking, or containing low levels of additional magnesium, considerable numbers of both giant spheroid cells and lysed cells were apparent, as well as significant cell debris. With higher levels of magnesium, the vast majority of cells appeared to grow as small spheres, without significant numbers of lysed cells or evident cell debris (Figure 4.10). An increased magnesium concentration therefore appears to be associated with more stable healthy growth of round-cell *mrd* mutants, and perhaps with better regulation of cell diameter. Furthermore, wild-type BRD948 cell morphology appeared to change slightly with increasing magnesium concentrations; cells became slightly shorter in length, particularly when grown in media containing 20 mM or 50 mM $MgCl_2$, compared to cells grown without additional magnesium (Figure 4.10).

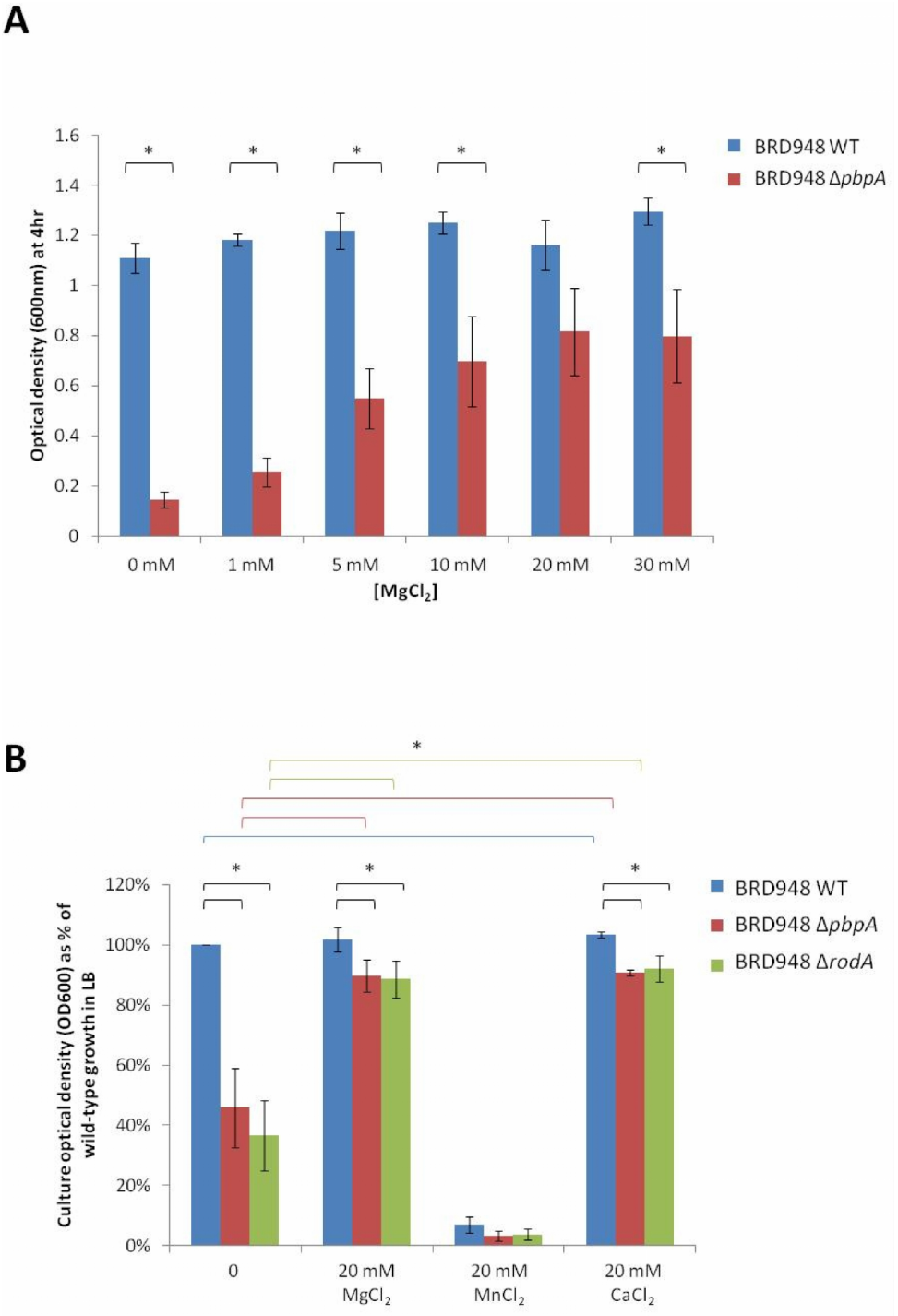

Figure 4.9: Divalent cation growth dependence of S. Typhi ΔpbpA and ΔrodA mutants: A - Growth of *S.* Typhi BRD948 wild-type (WT) and *ΔpbpA* in the presence of increasing concentrations of $MgCl_2$. Extent of growth measured as optical density (OD600) after 4 hours' growth in LB medium supplemented with aro/tyr mix, cultured at 37°C, and 200 rpm. B – Growth *S.* Typhi BRD948 WT *ΔpbpA* and *ΔrodA* mutants grown in the presence of 20 mM $MgCl_2$, $MnCl_2$, or $CaCl_2$, or in the absence of divalent cation supplementation. Growth (OD600 values) of each strain was measured as a percentage of the OD600 of wild-type strain grown in absence of additional divalent cations, after 4-5 hours' culture. Cells grown in LB medium supplemented with aro/tyr mix, at 37°C and 200 rpm. Both results show averages of 3 independent experiments. Error bars indicate standard deviation. Asterisks show significant differences, as determined using the Students t-test where P values of ≤0.05 were considered statistically significant.

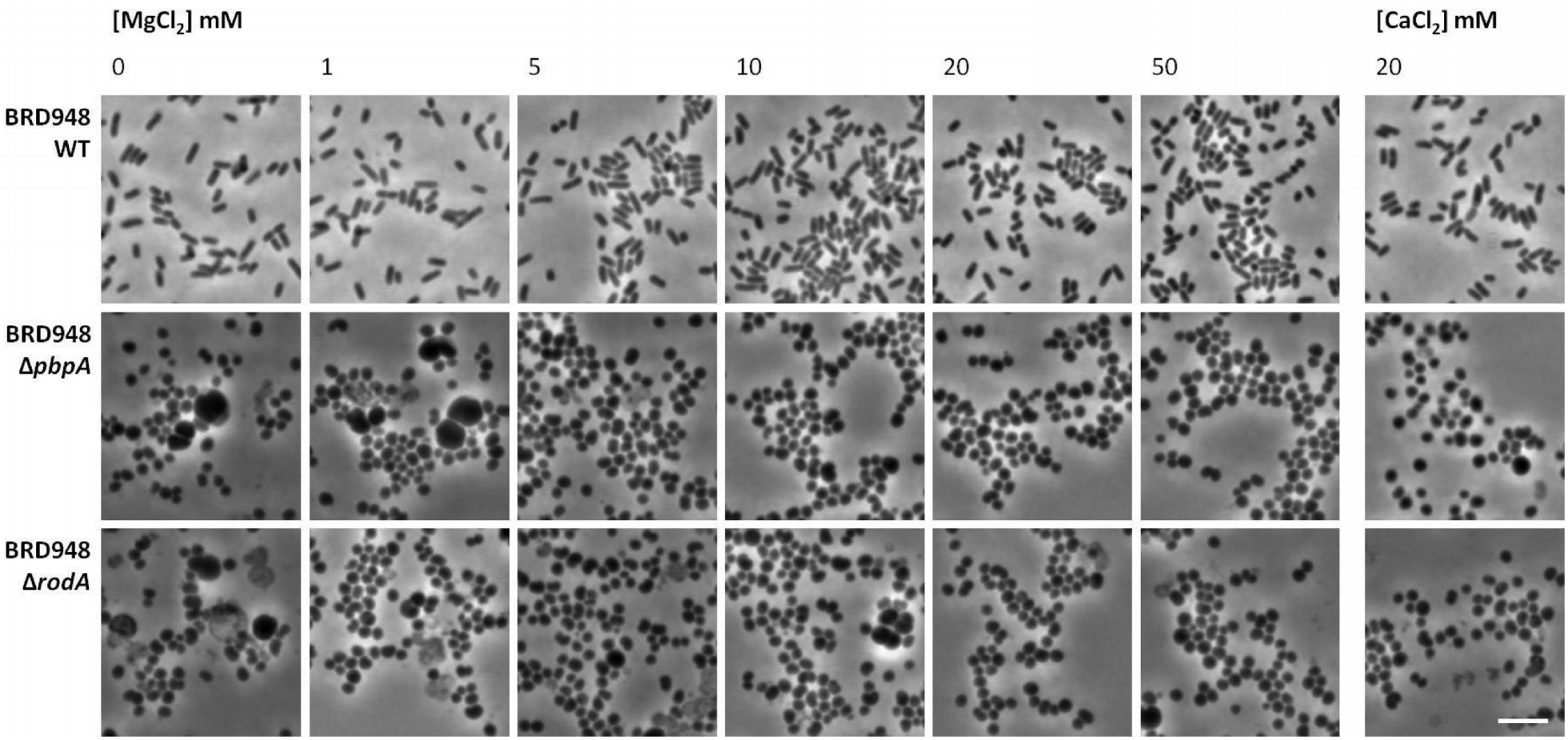

Figure 4.10: Magnesium dependence of *S.* Typhi Δ*pbpA* and Δ*rodA* mutants: Phase contrast microscopy of *S.* Typhi BRD948 wild-type (WT), Δ*pbpA*, and Δ*rodA* cells grown in the presence of increasing concentrations of $MgCl_2$ (or 20 mM $CaCl_2$). Cells cultured for 20 hours in LB broth with aro/tyr mix, at 37°C and 200 rpm. Scale bar indicates 5 μm; all images are to the same scale.

The dependence of round-cell *mrd* mutants on other divalent cations was tested, to determine if round-cell mutants specifically required magnesium. Wild-type *S.* Typhi BRD948, and Δ*pbpA* and Δ*rodA* mutants were therefore grown in LB media supplemented with $MgCl_2$, $MnCl_2$, or $CaCl_2$, each at 20 mM. Culture optical densities (OD600) were measured at mid-log phase, after 4-5 hours' growth.

The results of three independent assays were plotted as shown (Figure 4.9 B); OD values of each culture (wild-type and Δ*pbpA*/Δ*rodA*) were plotted as a percentage of that of the wild-type without the addition of any divalent cation to the growth medium. In this assay the addition of either $MgCl_2$ or $CaCl_2$ to the growth medium dramatically improved growth of both BRD948 Δ*pbpA* and Δ*rodA* mutants, with no significant differences between the effects exerted by either cation (Figure 4.9 B). Microscopic analysis of BRD948 strains grown in the presence of $MgCl_2$, and $CaCl_2$ reflect this, with no significant differences in the appearance of cells grown with either divalent cation (Figure 4.10). This suggests that the effect on growth in *S.* Typhi is not specific to magnesium, contrary to results seen in *B. subtilis*, where calcium did not exert as strong an effect on cell growth as magnesium (229). By comparison, addition of manganese to the medium drastically reduced growth of both wild-type and round-cell mutants, in a manner that may indicate that manganese is naturally toxic to *Salmonella* Typhi, since the effect on growth of the wild-type and mutants was similar.

Further work is needed to establish the mechanisms by which calcium and magnesium bring about the recovery of growth in *Salmonella* round-cell mutants. In addition to these assays, the successful preparation of electrocompetent Δ*pbpA* or Δ*rodA* cells of either Typhi or Typhimurium was found to be dependent upon the addition of 20 mM $MgCl_2$ to ice-cold dH_2O for each wash step. In the absence of additional magnesium, cells formed large clumps, and cell pellets became particularly viscous, possibly indicative of significant cell lysis.

4.3.2 Comparisons of growth measurements of *S.* Typhi wild-type and round-cell mutants

It was considered that the variable size, shapes and therefore also volumes of the round-cell mutants, compared to wild-type, may affect growth measurements such as optical density measurements of light scattering through a culture, or wet weight measurements. To determine how various measures of growth could be compared, and the best measure for enabling comparisons to be made between growth of wild-type and mutant cells, assays were carried out to compare the optical density (OD600), haemocytometer count and wet weight measurements between wild-type and round-cell *mrd* mutants of *S.* Typhi BRD948.

Haemocytometer counts, wet weight measurements, and optical density (OD600) measurements of wild-type and round-cell *mrd* mutants of BRD948

Experiments were conducted to investigate the relationships between cell number, OD600 values and wet weight, in BRD948 WT and Δ*rodA* cells. Total cell counts were carried out as described. Briefly around 3-4 mg cells from overnight agar plate cultures were transferred to a clean microcentrifuge tube using a sterile tip/loop, and carefully weighed. The cells were then fixed in 1 ml 4% paraformaldehyde (PFA), before being resuspended in 1 ml sterile dH_2O and diluted 1:10. Small volumes of each suspension were loaded onto clean haemocytometer slides, and cell counts were performed as described. Cell number was then calculated as a product of cell weight (wet weight). The data from these total cell counts show a clear increase in individual cell weight of round-cell Δ*rodA* cells compared to the wild-type, there being almost double the number of wild-type cells per mg of bacteria (wet weight) than Δ*rodA* cells (Figure 4.11 A). This is as expected for Δ*rodA* cells which often appear to have a volume at least twice that of the wild-type parent.

In addition, optical density (OD600) measurements of various cell resuspensions were taken at a range of dilutions, to enable comparisons between cell number, wet weight and OD600 values. The results of these comparisons were combined and plotted as shown (Figure 4.11 B,C, and D); cell number was calculated based on the average cell number per mg wet weight, as established in the preceding

assay (figure 4.11 A). Surprisingly, the shape defects and increased volume of Δ*rodA* cells appeared not to affect OD600 values, which were comparable to cell number for both wild-type and Δ*rodA* cells (based upon average values of cell numbers per mg bacteria) (Figure 4.11 C). Conversely, OD600 values were not comparable to bacterial weight, since the OD600 values of BRD948 Δ*rodA* cell suspensions were significantly lower than those of the wild-type cell suspensions, at an equivalent initial wet weight (Figure 4.11 B). Thus, measuring culture optical densities appears to constitute a more accurate means of measuring cell growth (increase in cell number) between wild-type and round-cell mutant cells. The relationship between wet weight and cell number, based on average numbers of cells per mg, is also illustrated (Figure 4.11 D).

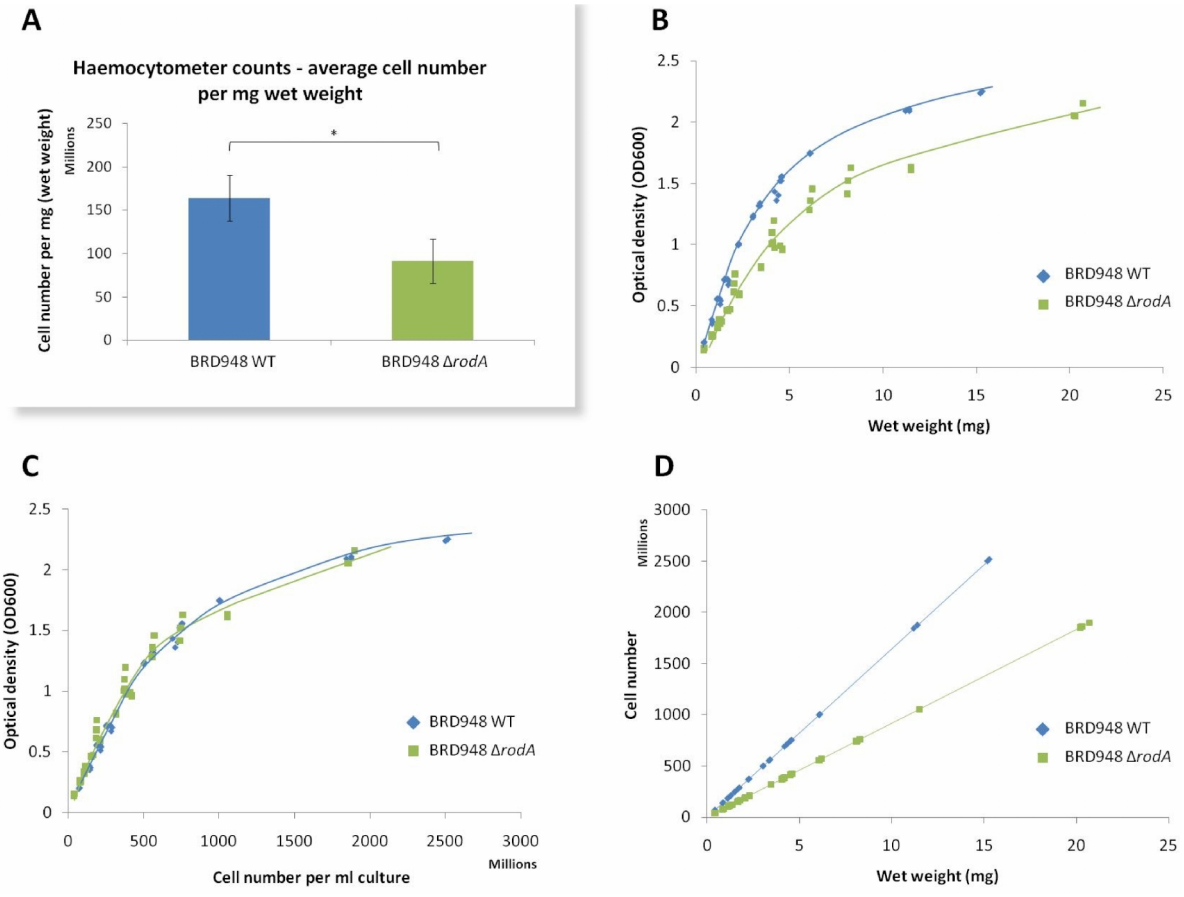

Figure 4.11: Comparison between haemocytometer counts, wet weight measurements and optical density (OD600) measurements of S. Typhi wild-type and ΔrodA cells: A – Haemocytometer total cell counts of number of bacterial cells per mg bacteria (wet weight) for *S.* Typhi BRD948 wild-type (WT) and Δ*rodA*. Assay conducted in triplicate on 3 separate occasions. Graph shows average values and standard deviation (Error bars). Students t-test conducted to determine statistical significance. B – Optical density (OD600) of *S.* Typhi BRD948 wild-type (WT) and Δ*rodA* 1 ml cell suspensions compared to wet weight (mg) before resuspension, with line of best fit as shown. C –

OD600 values compared with average cell number per ml of culture (based on average cell number per mg wet weight measurements (A) and measurements of OD600 values per mg wet weight, resuspended in 1 ml dH_2O (B)). Line of best fit as shown. D – Average cell number with increasing wet weight (mg) (based on average cell number per mg cells (A)).

4.3.3 Growth of *S.* Typhi wild-type and *mrd* mutants in rich medium at 37°C

Several studies of round-cell mutants have noted that in some bacteria including *E. coli*, round-cell mutants show a temperature sensitive phenotype; at fast growth rates (in nutrient-rich conditions at 37°C), round-cell mutants formed non-dividing giant cells, whereas the same cells propagated stably forming small spheres in slow growth conditions (i.e. growth in minimal media at 30°C) (130, 214, 277, 278). Growth was therefore analysed in *S.* Typhi mutants to see if the same was true. Growth of each *mrd* mutant strain in nutrient rich LB broth was analysed by measuring the optical density values (OD600) of flask cultures grown at 37°C and 200 rpm, hourly, over an 8 hour period (Figure 4.12).

Contrary to previous studies (130), unpublished work on a *Salmonella* Typhimurium Δ*rodA* mutant demonstrated that growth of this mutant at 37°C in rich medium was not significantly different from wild-type (163). Work on *S.* Typhi *mrd* operon mutants in the present study reflect this result, in that growth of both Δ*pbpA* and Δ*rodA* mutants of *S.* Typhi resembled that of the wild-type at 37°C in nutrient-rich medium (Figure 4.12 B). *S.* Typhi Δ*ybeB* and Δ*ybeA* mutants also grew almost as wild-type in LB medium at 37°C, with only a very slight reduction in the growth of BRD948 Δ*ybeA* (Figure 4.12 A). Previous work showed that the growth of BRD948 Δ*rlpA* was equivalent to the wild-type, in LB medium at 37°C (163).

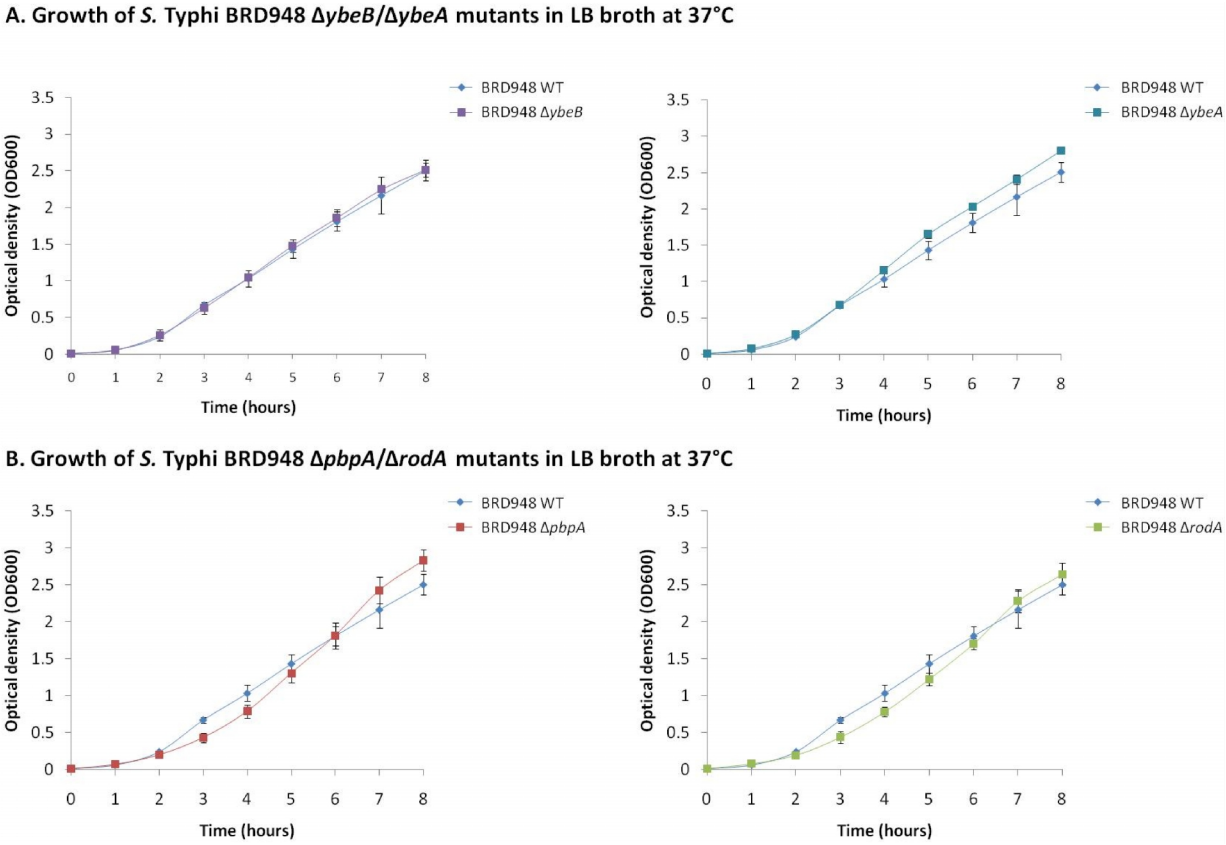

Figure 4.12: Growth of S. Typhi wild-type (WT) and mrd operon mutants in rich medium at 37°C: Growth curves of BRD948 wild-type (WT), Δ*ybeB* and Δ*ybeA* strains (A), and WT, Δ*pbpA* and Δ*rodA* strains (B); cells were cultured in flasks containing LB broth supplemented with aro/tyr mix and 20 mM $MgCl_2$. Optical density (OD600) values were measured hourly for 8 hours, with culture at 37°C, with shaking (200 rpm). Growth curves were generated from the average OD600 values of 3 independent experiments. Error bars indicate standard deviation values.

4.3.4 Growth of *S.* Typhi wild-type and *mrd* mutants in rich medium at 30°C

Potential temperature sensitivity in *S.* Typhi *mrd* operon mutants was considered by analysing growth of these mutants at 30°C. Growth of the *mrd* mutant strains was analysed over 9-10 hours by measuring the optical density values (OD600) of flask cultures grown in LB broth at 30°C and 200 rpm. As was previously seen in a Typhimurium Δ*rodA* mutant, growth was severely affected in *S.* Typhi round-cell mutants (Figure 4.13 B) (163). BRD948 Δ*pbpA* and Δ*rodA* cells grew considerably more slowly than the wild-type, reaching OD600 values of less than 1 after 10 hours, compared to values of up to 3 for the wild-type. These results are contrary to a previous study in *E. coli*, where growth of round-cell mutants was stable at 30°C but not 37°C (130). Both Δ*ybeB* and Δ*ybeA* strains grew as wild-type at 30°C

(Figure 4.13 A). Likewise, previous work demonstrated that *S.* Typhi Δ*rlpA* mutants grow as wild-type at 30°C in LB broth (163).

This data is in agreement with the extensive cell lysis observed when round-cell mutants were subjected to ice-cold temperatures during the generation of electrocompetent cells. Thus *Salmonella* Δ*pbpA* and Δ*rodA* mutants display significant sensitivity to cold temperatures.

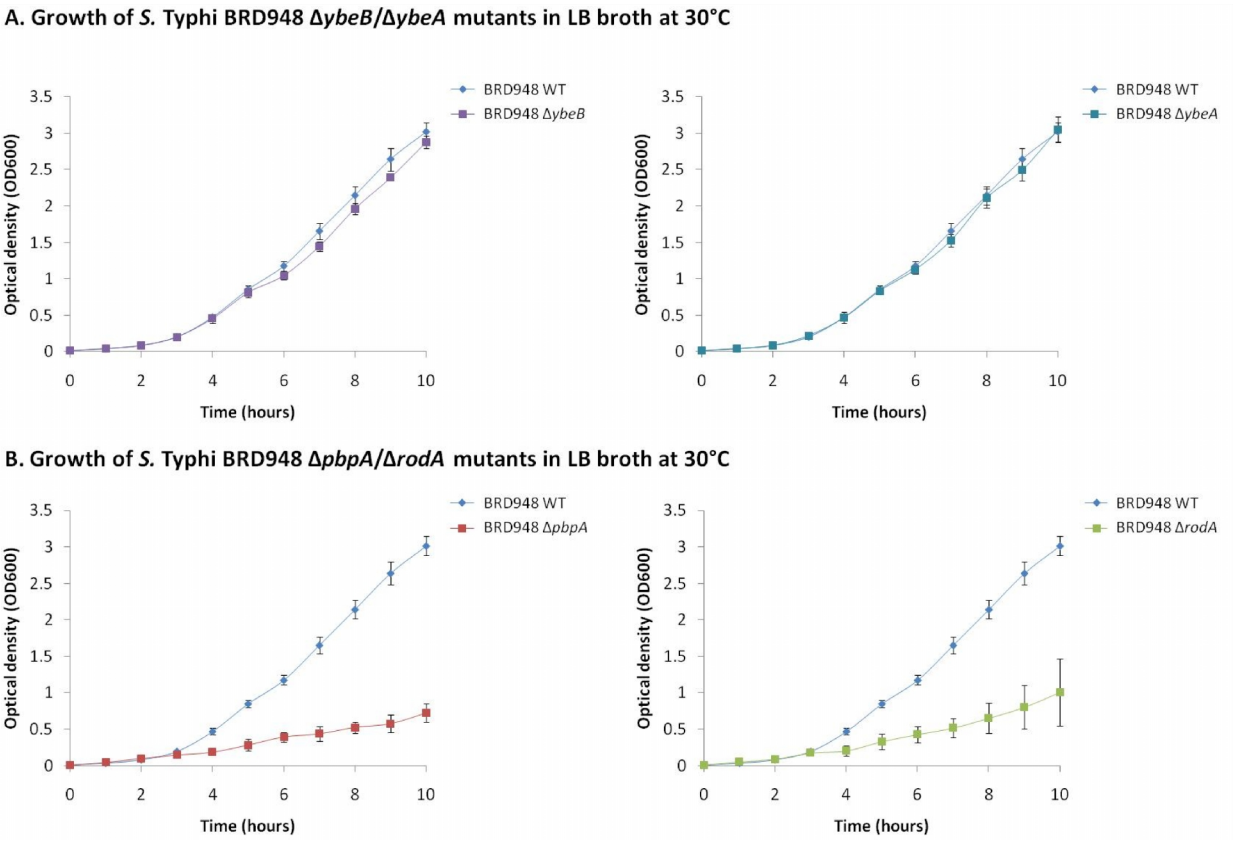

Figure 4.13: Growth of S. Typhi wild-type (WT) and mrd operon mutants in rich medium at 30°C: Growth curves of BRD948 wild-type (WT), Δ*ybeB* and Δ*ybeA* strains (A), and WT, Δ*pbpA* and Δ*rodA* strains (B); cells were cultured in flasks containing LB broth supplemented with aro/tyr mix and 20 mM $MgCl_2$. Optical density (OD600) values were measured hourly over 10 hours, with culture at 30°C, with shaking (200 rpm). Growth curves were generated from the average OD600 values of 3 independent experiments. Values for 10 hours' growth only indicate average values of 2 independent experiments. Error bars indicate standard deviation values.

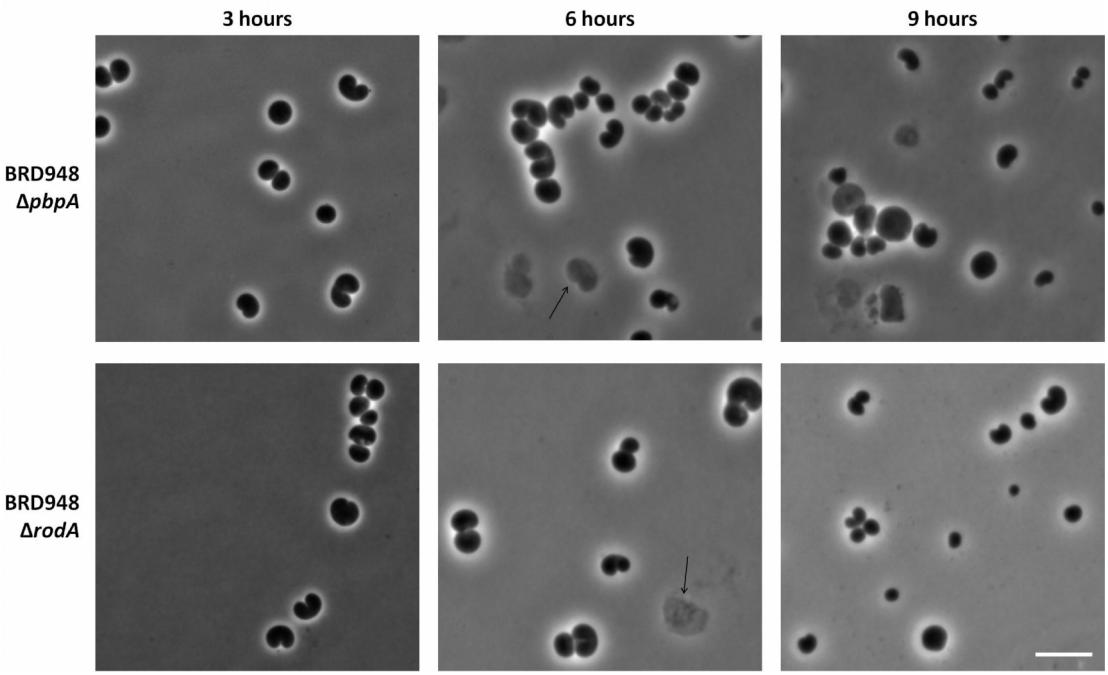

Figure 4.14: Growth of S. Typhi ΔpbpA and ΔrodA mutants at 30°C: Phase contrast microscopy images of BRD948 Δ*pbpA* and Δ*rodA* mutants after 3, 6 and 9 hours' growth in LB medium supplemented with aro/tyr and 20 mM $MgCl_2$, at 30°C with shaking (200 rpm). Arrows indicate lysed cells. Scale bar ~5 µm. All images are to the same scale.

Previous studies have highlighted division defects in round-cell mutants grown at higher temperatures (37°C), whereas at lower temperatures (30°C) cells formed small stably-dividing spheres (130). The morphology of *S.* Typhi Δ*pbpA* and Δ*rodA* mutants was therefore analysed with growth at 30°C. BRD948 Δ*pbpA* and Δ*rodA* cells appeared to grow and divide much the same at 30°C as in 37°C, cells being roughly the same size and morphology. However, with extended growth at 30°C, more cell debris and cell lysis became apparent in Δ*pbpA* and Δ*rodA* cultures, than at 37°C (Figure 4.14).

4.3.5 Mecillinam and A22 sensitivity of *mrd* mutants

Mecillinam sensitivity assays

Mecillinam is a beta-lactam antibiotic which specifically binds and inhibits PBP2 (279, 280). Mecillinam-treatment of wild-type *Salmonella* causes the formation of large spheroid cells, similar to Δ*pbpA* and Δ*rodA* mutant cells. Furthermore, both Δ*pbpA* and Δ*rodA* mutant strains are known to be mecillinam-resistant, demonstrating the functional relationship between these genes (281-283). *S.* Typhi *mrd* mutants were treated with mecillinam to determine whether Δ*ybeB*, Δ*ybeA*, or

Δ*rlpA* knockouts possessed any inherent mecillinam-resistance, which could be indicative of a functional linkage with *pbpA* and *rodA*.

The mecillinam sensitivity of both BRD948 *mrd* mutant and wild-type (WT) strains was examined by measuring antibiotic resistance in disc diffusion assays, as well as measuring growth of these strains in the presence of varying concentrations of mecillinam. Disc diffusion assays were conducted as described; mecillinam sensitivity was measured in terms of the size of zones of clearance around discs inoculated with 1 mg/ml or 10 mg/ml mecillinam.

As expected, BRD948 Δ*pbpA* and Δ*rodA* mutants were highly resistant to mecillinam treatment in these assays. Surprisingly, both Δ*ybeB* and Δ*ybeA* strains also exhibited significant resistance to mecillinam, although to a lesser extent than the round-cell mutant strains (Figure 4.15). BRD948 Δ*rlpA*, however, remained mecillinam-sensitive, suggesting that the activities of PBP2 and RodA may be directly connected with or dependent upon *ybeB* and *ybeA*, but not *rlpA*.

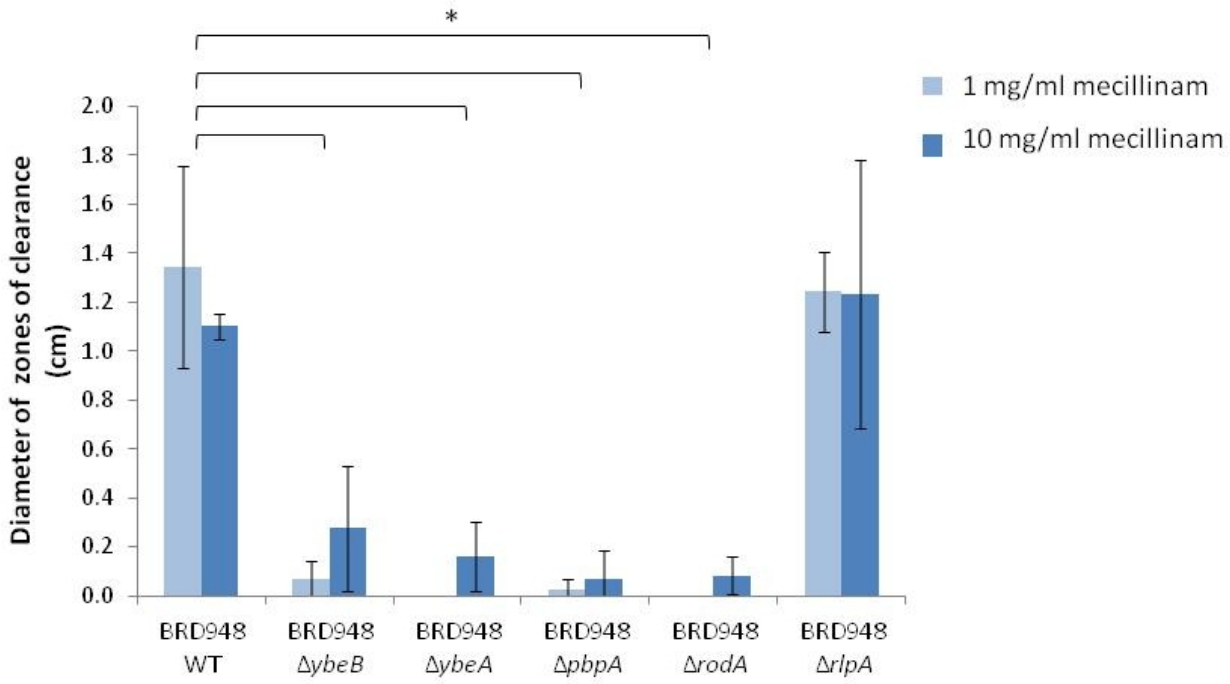

Figure 4.15: Sensitivity of S. Typhi mrd mutant strains to mecillinam: Graph indicates average diameter (minus disc size) of zones of clearance in WT and *mrd* mutant strain bacterial lawns, around mecillinam-containing filter paper discs. Discs were placed on LB agar containing the relevant strain, and inoculated with 5 µl sterile dH_2O, 1 mg/ml mecillinam or 10 mg/ml mecillinam. Zones of clearance were measured after growth overnight at 37°C. No zones of clearance were observed for any strain around discs inoculated with dH_2O (negative control). Assays were carried out in duplicate on 3

separate occasions. Error bars indicate standard deviation. Asterisks indicate statistically significant differences, as determined using the Students t-test, where P values ≤0.05 were considered significant.

A mecillinam growth assay was carried out in order to further analyse the effects of mecillinam on the *mrd* mutants which displayed some level of mecillinam-resistance, and to determine the concentration of mecillinam required to inhibit growth of each strain. BRD948 wild-type, Δ*ybeB*, Δ*ybeA*, Δ*pbpA* and Δ*rodA* cells were sub-cultured in LB broth containing mecillinam at between 0 µg/ml (negative control) and 50 µg/ml. Mecillinam sensitivity growth assays were subsequently carried out as described. The average values from 3 independent growth experiments were illustrated as growth curves (Figure 4.16). The assay was not conducted with BRD948 Δ*rlpA* cells as disc diffusion assays had indicated that this strain maintained a similar level of sensitivity to mecillinam as wild-type BRD948 cells.

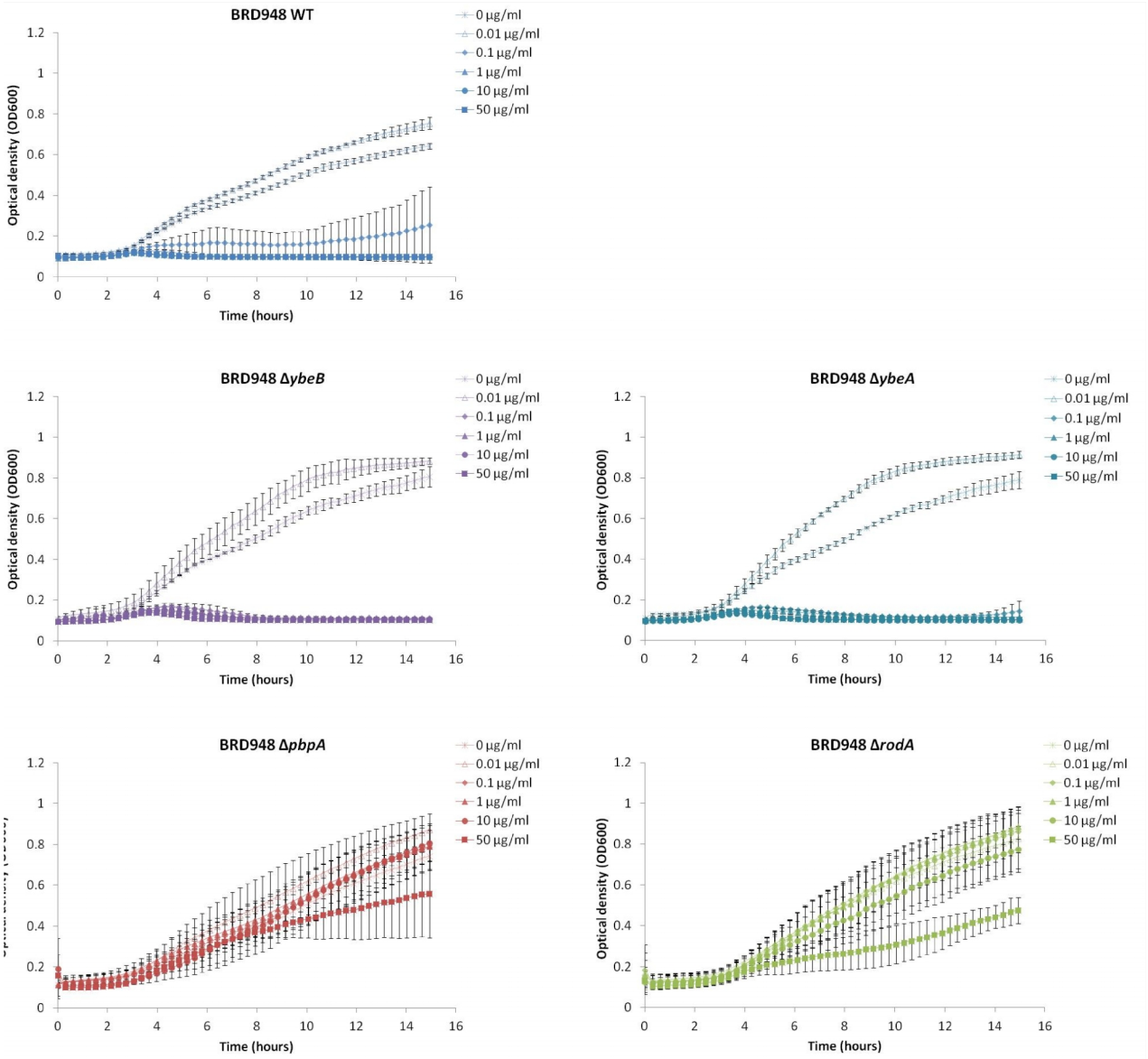

Figure 4.16: S. Typhi mecillinam sensitivity growth assays: Growth curves of *S.* Typhi wild-type (WT) and *mrd* mutants grown in LB media, in the presence of 0, 0.01, 0.1, 1, 10 or 50 µg/ml mecillinam. Cells were cultured overnight at 37°C, with shaking, in a Tecan Infinite 200® spectrophotometer. Growth (OD600) was measured every 15-20 minutes over 15 hours. Graphs show average OD600 values from 3 independent experiments. Error bars indicate standard deviation.

These growth assays demonstrated the extent of mecillinam resistance of the Δ*pbpA* and Δ*rodA* mutants; even at concentrations of up to 10 µg/ml bacterial growth was not significantly diminished. Growth of the round-cell mutants was slightly inhibited at 50 µg/ml mecillinam, although this may be a result of inherent toxicity from high levels of the drug, rather than specific effects on cell wall synthesis (Figure 4.16). Contrary to the results of disc diffusion assays, sensitivity of both the Δ*ybeB* and Δ*ybeA* mutants to mecillinam was equivalent to, if not

higher than the wild-type in this assay. In all three strains growth was almost completely inhibited with concentrations of mecillinam as low as 0.1 µg/ml. This is in stark contrast to the mecillinam-resistant Δ*pbpA* and Δ*rodA* strains. Surprisingly, and for unknown reasons, at low levels of mecillinam (0.01 µg/ml) growth rates seemed to be higher in WT, Δ*ybeB*, and Δ*ybeA* cells than equivalent growth rates in the absence of mecillinam.

A22 sensitivity assays

A22 is a drug which specifically binds MreB, blocking the binding of ATP and therefore inhibiting the polymerisation of MreB. *in vivo*, A22 disrupts filament formation, causing the disassembly and loss of the characteristic MreB helices, with an eventual loss of rod shape in various Gram-negative species, including *Salmonella* (281, 284, 285, 498). In *E. coli* A22 was shown to disrupt cell shape but not cause cell lysis, even at high concentrations, although given that disruption of cell shape determinants appears to be associated with the formation of giant cells and eventual cell lysis, A22 may indirectly bring about cell lysis (281). A22 also possesses inherent toxicity independent to its action upon MreB, having displayed MreB-independent growth inhibitory effects at high concentrations in a number of bacterial species and in an *E. coli* Δ*mreB* mutant (162, 286). Thus it may target other cellular functions besides MreB.

An early study on the A22 molecule found that mecillinam-resistant Δ*pbpA* and Δ*rodA* *E. coli* cells showed a reduced sensitivity to A22 (281). Very few if any studies have since investigated the sensitivity of Δ*pbpA* or Δ*rodA* mutant cells to A22, with a view to further investigating the functional relationships and interdependencies between cell shape determinants.

For this reason A22-sensitivity assays were performed for all 5 *mrd* mutant strains of *S.* Typhi; disc diffusion assays were carried out, whereby sterile filter paper discs, mounted on agar containing the relevant bacterial strains, were inoculated with either 1 mg/ml or 10 mg/ml A22. The resulting zones of clearance within the bacterial lawns were measured as an indication of A22 resistance.

Disc diffusion assays demonstrated that A22 had a minor detrimental effect on the growth of BRD948 wild-type and *mrd* mutant cells. Small zones of complete clearance of ~1-2 mm in diameter were observed around discs containing 10 mg/ml A22, for each strain. Larger zones of partial clearance in growth were also observed in these assays, as measured and recorded (Figure 4.17). This data reflected previous observations, in that no partial clearance of growth was observed around discs containing 1 mg/ml or 10 mg/ml A22 in Δ*pbpA* and Δ*rodA* bacterial lawns, whereas significant clearance of growth was seen in the other BRD948 strains (281). Unlike observations from mecillinam-sensitivity assays, the Δ*ybeB* and Δ*ybeA* mutants did not display any resistance to A22.

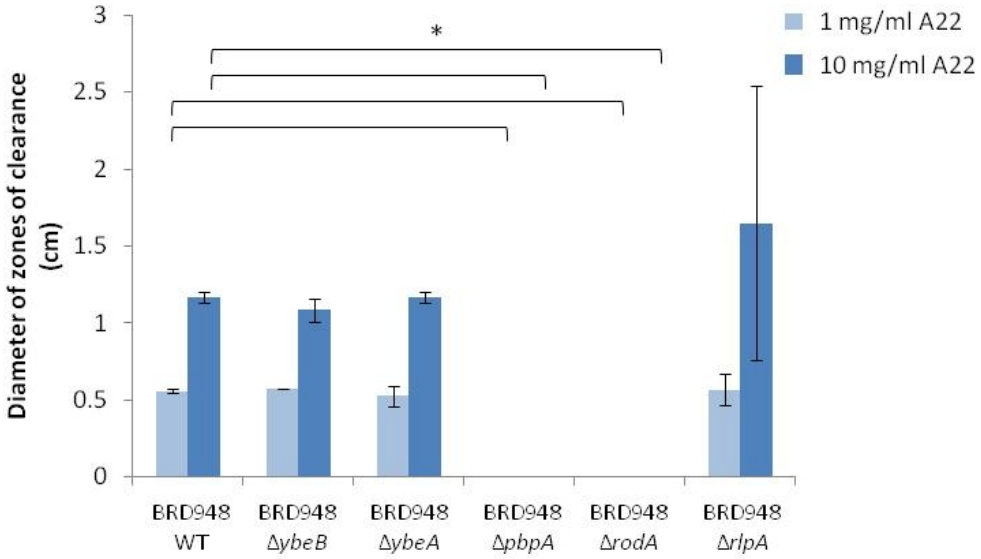

Figure 4.17: Sensitivity of S. Typhi mrd mutant strains to A22: Graph indicates average diameter (minus disc size) of zones of clearance in bacterial lawns containing WT and *mrd* mutant strains, around A22-containing filter paper discs. Discs were placed on LB agar containing the relevant strain and inoculated with 5 µl sterile dH_2O, 1 mg/ml A22 or 10 mg/ml A22. Zones of clearance were measured after growth overnight at 37°C. Observed zones of clearance showed only partial clearance. No zones of clearance were observed for any strain around discs inoculated with dH_2O (negative control). Assays were carried out in duplicate on 3 separate occasions. Error bars indicate standard deviation. Asterisks indicate statistically significant differences, as determined using the Students t-test, where P values ≤0.05 were considered significant.

It is likely that the small zones of complete clearance observed with each strain were the result of the inherent toxicity of A22, as demonstrated to be separate from its activity on MreB. However, partial zones of clearance were not observed in round-cell mutants. If this partial growth inhibition was also due to MreB-independent toxicity of A22, the round-cell mutants would be expected to show equivalent or even increased sensitivity to A22 due to the inherent weaknesses

possibly associated with these mutants. The partial growth inhibition may therefore be a result of specific activity of A22 on MreB, with the consequences of generating spherical cells with a liability to lyse.

4.3.6 Sensitivity of Δ*ybeB* and Δ*ybeA* mutants to a ribosome-targeting antibiotic

Both YbeB and YbeA are thought to be involved in ribosome binding, assembly, and possibly stability (189, 194). A number of major therapeutic antibiotics inhibit processes such as translation by targeting ribosomes (287). In order to investigate possible roles of the YbeBA proteins in ribosome stability and functionality, an assay was carried out to investigate the sensitivity of Δ*ybeB* and Δ*ybeA* mutants to ribosome-targeting antibiotics. For this assay the ribosome-targeting bactericidal aminoglycoside, streptomycin, was used. Streptomycin has been shown to bind specifically to the 'decoding centre' of the small 30S ribosomal subunit in *E. coli*, a region required for the correct reading of tRNA. The binding of streptomycin to this region brings about conformational changes in protein structure, resulting in the low-fidelity mis-reading of tRNA codons, and ultimately protein synthesis inhibition and cell death (288-290). A ribosomal protein S12 (*rpsL*) forms a crucial part of the ribosomal decoding centre. Furthermore, the majority of mutations causing streptomycin resistance were found to map to two highly conserved loops of this protein, the 'PNSA' and 'PGVRY' loops, which are physically located close by to the decoding centre and are involved in tRNA species recognition (290).

The sequences of the *S.* Typhi and *E. coli* S12 proteins were initially compared with those of both *S*. Typhi and *E. coli* YbeB and YbeA proteins to search for structural and possibly functional conservation between the proteins. Sequence analysis using the online Basic Local Alignment Search Tool (BLAST) 'blastp' algorithm revealed a small region close to the N-terminal of the YbeB protein with homology to S12. The 18 residue length of YbeB possessed 26% sequence identity, and 48% related 'positives', to a 23 residue region of S12. Further analysis showed that this region of YbeB slightly overlapped with the conserved 'PGVRY' loop region of S12 (Figure 4.18 A). Contained within this overlap were several amino acid residues which have been implicated in streptomycin

resistance (291). No significant sequence similarity to S12 was detected for YbeA in blastp searches.

Antibiotic disc diffusion assays were carried out with both wild-type and *mrd* mutant BRD948 strains to analyse the sensitivity of each strain to streptomycin. This assay was aimed in particular at testing the significance of sequence analysis data, determining whether YbeB and S12 may have some functional relationship. The results of this assay appear to show a slight decrease in streptomycin sensitivity in both Δ*ybeB* and Δ*ybeA* mutant strains compared to the wild-type, although student t-test analyses demonstrated that these differences in sensitivity were not statistically significant, with P values of 0.16-0.17 (at 10 mg/ml streptomycin), and 0.32-0.35 (at 100 mg/ml streptomycin) (Figure 4.18 B). However, this assay also showed that both Δ*pbpA* and Δ*rodA* mutants were significantly more sensitive than wild-type cells to killing by streptomycin at least at 100 mg/ml (Figure 4.18 B).

Further investigations could be worthwhile to determine whether the region of homology between YbeB and S12 is significant, and whether this N-terminal region is important to the function of YbeB. In terms of streptomycin resistance, although the differences were not statistically significant, it may be worth repeating this or a similar assay to better screen for streptomycin resistance in Δ*ybeB* and Δ*ybeA* mutants. However, any inherent streptomycin resistance in these mutants is clearly not substantial. It also remains to be explained why the Δ*pbpA* and Δ*rodA* show increased sensitivity to streptomycin, and whether this relates to the function of PBP2 and RodA.

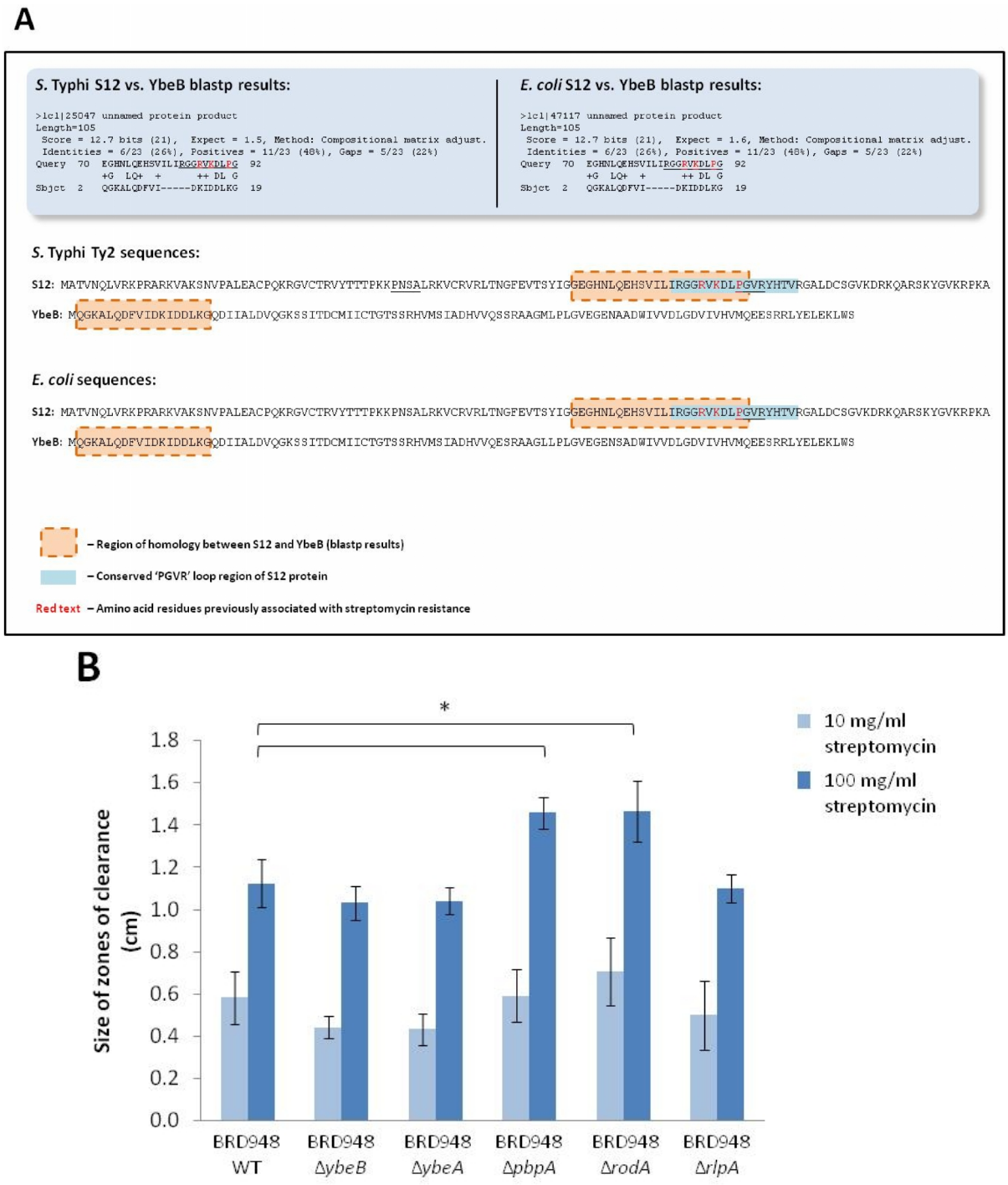

Figure 4.18: YbeB protein sequence analysis and sensitivity of S. Typhi mrd mutants to streptomycin: A – BLAST sequence comparisons between the S12 and YbeB proteins of *S.* Typhi and *E. coli*. *S.* Typhi protein sequences are shown, with highlighted sections showing conserved PGVR loop region of S12 and regions of homology between YbeB and S12. Amino acid residues previously shown to be involved in streptomycin resistance are highlighted in red (291). B – Streptomycin disc diffusion assays with wild-type and *mrd* mutant BRD948 strains. Streptomycin sensitivity measured in terms of average diameters of zones of clearance in bacterial lawns around antibiotic discs inoculated with 10 mg/ml or 100 mg/ml streptomycin, after growth overnight at 37°C. No zones of clearance were observed around discs inoculated with dH_2O (negative control). Assays were carried out in duplicate on 3 separate occasions. Error bars indicate standard deviation. Asterisks indicate statistically significant differences, as determined using the Students t-test, where P values ≤0.05 were considered significant.

4.3.7 Surface properties of *mrd* mutants and sensitivity to external stress

Mutations in cell shape-determinant genes clearly have significant effects on the structure of the bacterial cell envelope. The increased sensitivity of round-cell mutants to external stresses, as well their propensity to lyse, is indicative of a compromised cell wall structure and barrier function (125, 211, 214). Peptidoglycan integrity may also be significantly affected; a 50% decrease in peptidoglycan synthesis rate has been observed in round-cell mutants or mecillinam-treated cells (127, 292). The inactivation of cell shape determinant proteins leads to the constitutive activation of the septal cell wall synthetic machinery, and hence the synthesis of solely septal peptidoglycan synthesis. Unlike side-wall peptidoglycan, peptidoglycan at the cell poles is metabolically inert, potentially indicating differences between septal and side-wall peptidoglycan, although to date no chemical differences in septal and side-wall peptidoglycan have been characterised (122, 127, 201). Other cell envelope-associated defects have been observed in round-cell mutants besides those linked to peptidoglycan structure. For instance, Bendezú and de Boer found that both Δ*mre* and Δ*pbpA*/Δ*rodA* mutants in *E. coli* were unable to adjust the rate of phospholipid synthesis, despite altered cell wall synthesis and a decreased surface to volume ratio. This resulted in the production of excess cytoplasmic membrane, which folded inwards, forming extensive membrane involutions and vesicles (130).

A number of experiments were conducted to analyse the cell surface properties of *mrd* mutant cells, and investigate the effectiveness of the cell wall as a barrier to external stresses, particularly in the round-cell mutant strains.

Lipopolysaccharide (LPS) profiles of *mrd* mutants

The outer leaflet of the outer membrane of Gram-negative bacteria such as *Salmonella* is composed predominantly of the glycolipid, lipopolysaccharide (LPS), or ‘endotoxin’. This molecule is well characterised in terms of structure, and comprises 3 main sections: lipid A, a core oligosaccharide, and the outermost O-antigen made up of chains of polysaccharide (Figure 4.19) (293-295).

Lipid A forms the innermost hydrophobic component of LPS, acting to anchor LPS into the membrane (Figure 4.17). Lipid A is the only element of LPS known to be essential for growth and its structure remains fairly well conserved between bacterial species (294, 296, 297). It is also well characterised as the toxic element of LPS, contributing greatly to the activation of inflammatory responses and causing endotoxic shock in systemic Gram-negative infections (294, 298). The core oligosaccharide comprises two regions: the inner and outer cores (294, 299). The inner core, like Lipid A, is important for outer membrane integrity, and is well conserved between bacterial species (294, 299). Despite consisting of a conserved hexose backbone, the outer core is more variable due to various side-branch alterations. This results in variability between individual bacterial species. Two distinct core structures have been identified amongst *S. enterica* serovars (294, 299). 'Smooth-LPS' describes LPS which contains O-antigen linked to the core oligosaccharide region, as expressed by many Gram-negative bacteria including *Salmonella* and *E. coli*. Conversely, strains and mutants expressing LPS lacking this outer region are described as 'rough'. The outer O-antigen polysaccharide consists of repeating sugar units, which can vary considerably in structure and chain length between strains of the same bacteria (293-295). The O-antigen plays an important role in determining the serological specificity of the bacteria, as this region is exposed to the environment and host immunity (294).

The outer membrane as a whole, and in particular the core and O-antigen regions of LPS, have a major role in functioning as a physical barrier against environmental stress. LPS acts as a permeability barrier, preventing the diffusion of large molecules across the bacterial envelope, and due to its highly hydrophilic nature, effectively protecting against the diffusion of small hydrophobic molecules into the cell. This makes Gram-negative bacteria particularly resistant to hydrophobic antibiotics (301-303). Bacterial lipopolysaccharide is also recognised as a virulence factor, due to the properties of the O-chain polysaccharides which may enable bacteria to evade the host immune responses (294).

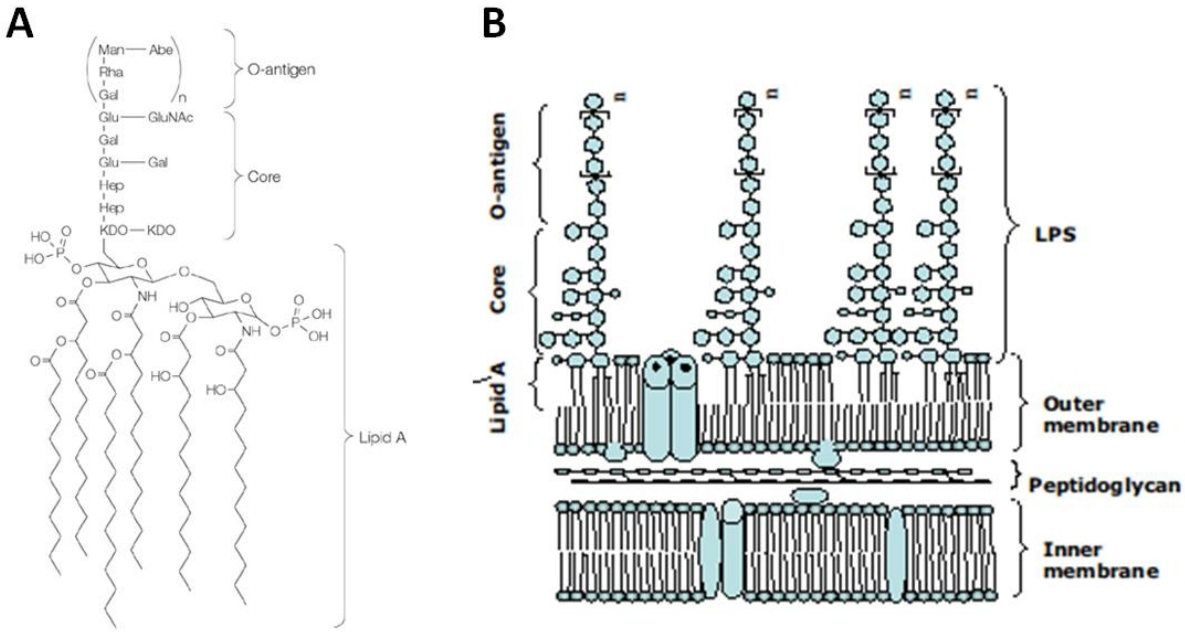

Figure 4.19: Structure of bacterial lipopolysaccharide (LPS): A - Generalised molecular structure of LPS, taken from "LPS, TLR4 and infectious disease diversity" (298). B - Schematic representation of smooth LPS and the bacterial cell wall structure, taken from *"Brucella spp* noncanonical LPS: structure, biosynthesis, and interaction with host immune system" (300)

The outer membrane is linked covalently to the peptidoglycan layer by at least one highly expressed outer membrane lipoprotein: Braun's Lipoprotein (Lpp). Additional outer membrane proteins are known to associate non-covalently with peptidoglycan, including peptidoglycan-associated lipoprotein (Pal) and RlpA (293, 304, 305). Furthermore, Pal and Lpp, along with outer membrane protein A (OmpA) are often co-purified with LPS (305).

The biosynthesis of all three LPS components and the linking of the lipid A and core regions occurs at the inner leaflet of the cytoplasmic membrane. Several factors are involved further in transporting the components across the inner membrane and through the periplasm to the cell surface (293). The latter process is mediated by the Lpt pathway, involving 7 Lpt proteins which together are thought to form a wall-spanning protein complex for the transportation of LPS (293). Interestingly, one of the Lpt proteins, LptE is regulated by sigma factor E (σ^E), a major regulator of the envelope stress response, which increases the expression of cell wall biosynthesis factors in response to envelope stress (293, 306, 307).

The importance of LPS to *Salmonella* physiology, its role in protection against environmental stress, its physical linkage with (and possible dependence upon) the peptidoglycan cell wall in particular, and also the observed regulatory pathways which appear to stimulate LPS production upon detection of envelope stress, together make it an important factor to be studied in the *mrd* mutants. The Δ*pbpA*, Δ*rodA* and Δ*rlpA* mutants in particular may have significant downstream effects on LPS expression and structure due to the putative effects of these mutations on the bacterial cell wall. In order to investigate LPS structure in the *S.* Typhi *mrd* operon mutants, LPS was isolated from cell lysates of each strain and analysed by SDS-PAGE separation on 12% acrylamide gels, as described. Gels were silver stained to visualise the LPS. LPS was also prepared in parallel from a *S.* Typhimurium rough LPS mutant, SL5338, as a negative control (237). Purified wild-type *S.* Typhimurium SL1344 LPS, prepared in previous work, was also run alongside the other samples.

No alterations in LPS structure, particularly in terms of O-antigen chain structure were seen in LPS samples from Δ*ybeB*, Δ*ybeA* or Δ*rlpA* mutants of *S.* Typhi, with laddering patterns appearing as wild-type in these strains, as observed by SDS-PAGE analysis (Figure 4.20). However, the laddering pattern of the O-antigen appeared somewhat different in round-cell *mrd* mutant strains. Although these mutants clearly expressed O-antigen, which appeared as wild-type at lower molecular weights, the laddering patterns at higher molecular weights (~55-170 kDa) were clearly affected, LPS bands appearing almost completely smeared on SDS-PAGE gels. However, a faint laddering pattern could just be seen flanking the smears in both strains (Figure 4.20). The presence of this smearing is not an artefact, given that it appeared in both Δ*pbpA* and Δ*rodA* strains, as well as in repeat experiments with fresh LPS preparations. However, it remains unknown whether the observed pattern is indicative of altered LPS structure/chain length in these strains, or whether another property of the round-cell mutants affected the preparation of LPS, leading to the observed patterns when separated by SDS-PAGE. It is also possible that LPS was overproduced in the round-cell mutants, leading to such a pattern.

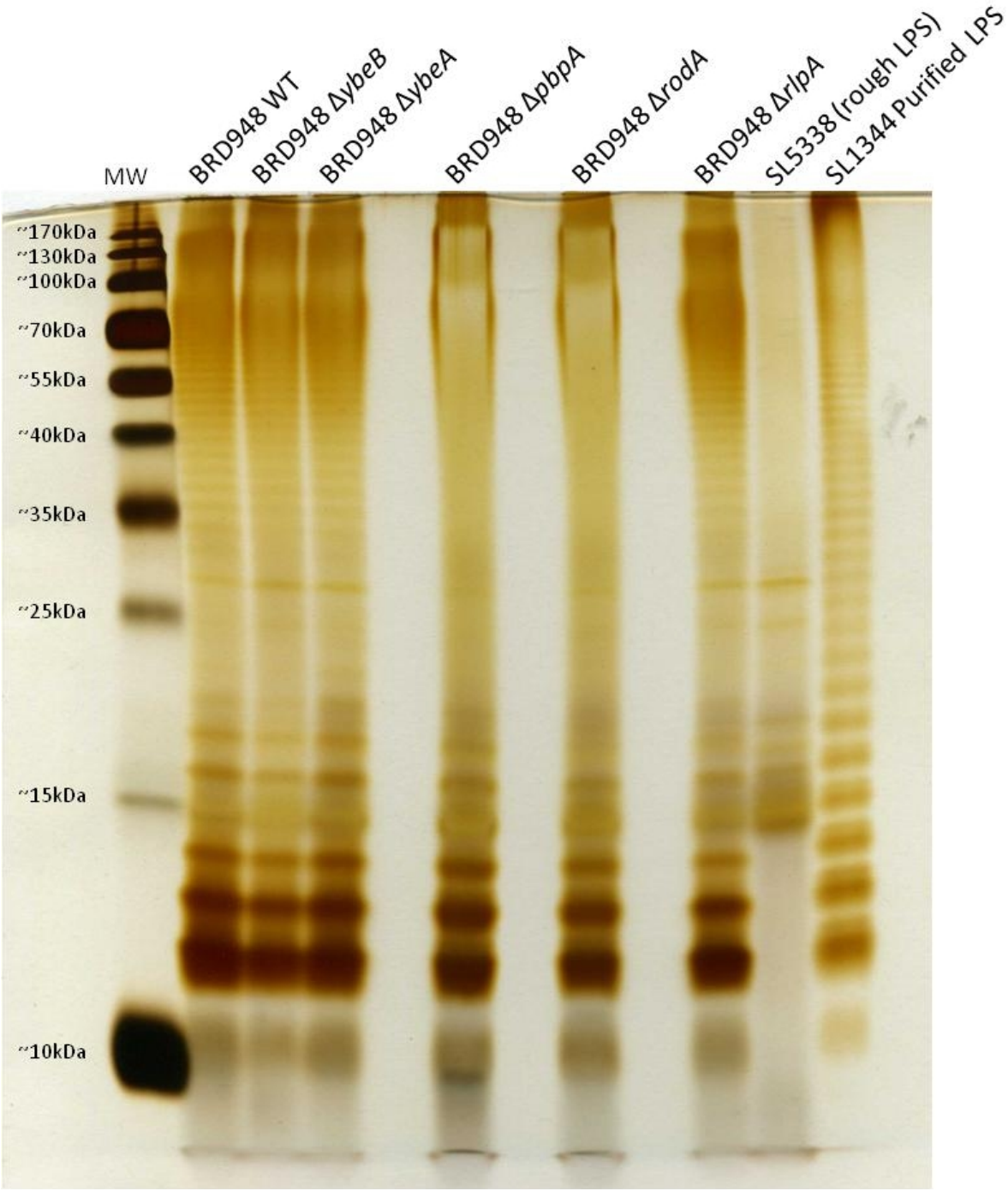

Figure 4.20: LPS structure in S. Typhi wild-type and mrd mutants: SDS-PAGE separation of LPS fractions isolated from BRD948 wild-type (WT) and *mrd* mutant cells, and the SL5338 rough LPS mutant strain. Purified LPS from WT *S.* Typhimurium SL1344 (from previous work) was run alongside other samples. Laddering patterns were indicative of O-antigen side chains of different lengths, and hence were missing from the rough SL5338 mutant. Consecutive 'rungs' are equivalent to an increase in chain length of one repeating O-chain unit (294). Cultures were grown to mid-log phase in LB medium at 37°C before harvesting and isolating LPS as described. The concentration of LPS in each preparation was standardised according to original culture optical density values.

Sensitivity of *mrd* mutants to hydrophobic antibiotics

The outer membrane and particularly expression of LPS in the outer leaflet in Gram-negative bacteria is known to afford significant protection against hydrophobic antibiotics such as rifampicin and erythromycin (302, 308, 309). Rifampicin is a large hydrophobic antibiotic, which specifically inhibits DNA-dependent RNA polymerase, thereby blocking transcription (301, 309). Comparisons between rifampicin potency against *E. coli* and the Gram-positive bacteria, *Staphylococcus aureus*, demonstrated that *E. coli* was intrinsically much more resistant to rifampicin; minimimum inhibitory concentrations (MICs) of rifampicin were 8 µg/ml for *E. coli*, compared to just 0.002 µg/ml for *S. aureus* (309). The authors attributed this to the outer membrane of *E. coli* cells forming a protective barrier against the drug (309). Erythromycin is another hydrophobic antibiotic which halts protein synthesis by binding to the 50S ribosomal subunit and bringing about the dissociation of peptidyl-tRNA complexes from the ribosome (310, 311).

Permeabilisation of Gram-negative outer membranes has proven effective at increasing sensitivity to hydrophobic antibiotics including rifampicin and erythromycin (118, 308). Mutations which alter outer membrane or LPS structure can also lead to an increase in the permeability of the outer membrane (301). In order to further screen for possible perturbations to the outer membrane and LPS in BRD948 *mrd* mutant strains, their sensitivity to the hydrophobic antibiotics rifampicin and erythromycin was tested. This was done by means of antibiotic disc diffusion assays, as described.

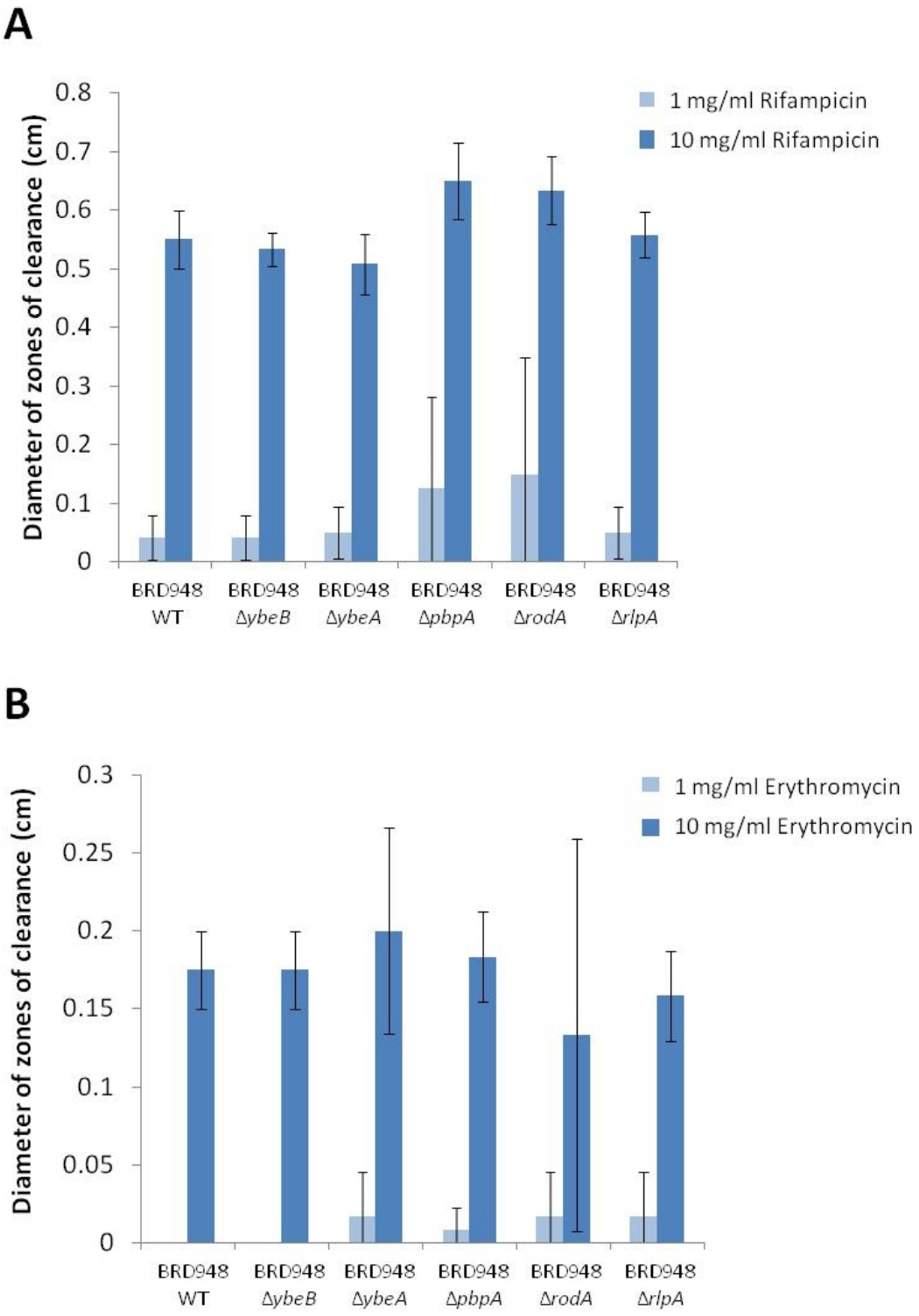

Figure 4.21: Sensitivity of S. Typhi mrd mutants to hydrophobic antibiotics: Disc diffusion assays with wild-type and *mrd* mutant BRD948 strains to screen for sensitivity to rifampicin (A) and erythromycin (B). Sensitivity measured in terms of average diameters of zones of clearance in bacterial lawns, around antibiotic discs inoculated with 1 mg/ml or 10 mg/ml rifampicin or erythromycin. Zones of clearance were measured after growth overnight at 37°C. No zones of clearance were observed for any strain around discs inoculated with dH_2O (negative control). Assays were carried out in duplicate on 3 separate occasions. Error bars indicate standard deviation. Students t-test were performed to test for statistical significance, where P values ≤0.05 were considered significant.

These assays showed a slight but statistically insignificant increase in sensitivity to rifampicin in the BRD948 Δ*pbpA* and Δ*rodA* strains compared to the wild-type, whereas no observable change in sensitivity to erythromycin was observed for these mutants. Likewise, no differences in sensitivity for the Δ*ybeB*, Δ*ybeA*, or Δ*rlpA* mutants were discernable for either antibiotic (Figure 4.21). However, in erythromycin sensitivity assays faint outer zones of partial clearance of ~0.5 cm in diameter, were visible on two occasions around 10 mg/ml discs for Δ*pbpA* and Δ*rodA* strains, besides the more distinct inner zones from which the data was presented. These partial zones of clearance were absent from any other strain.

These latter features may be indicative of a small increase in sensitivity of round-cell mutants to hydrophobic antibiotics, which may represent an effect on outer membrane permeability in these strains. However, there is insufficient evidence to make any firm conclusions. Conversely, the results suggest that the outer membrane barrier function of Δ*pbpA* and Δ*rodA* mutants remains generally intact. In agreement with this, mecillinam-treated *E. coli* cells did not show increased sensitivity to hydrophobic antibiotic treatment in a previous study (118).

Growth of *mrd* mutants on Congo red agar

Many enterobacteria, including *Salmonella*, produce an extracellular biofilm matrix, consisting of extracellular polysaccharides including colanic acid and cellulose, and curli and fimbriae. The biofilm is thought to help protect cells from external environmental stresses as well as from the host immunity (312, 313, 323, 326). Production of colanic acid, through expression of 19 *cps*/*wca* genes, is induced by the global regulatory RcsCB two-component system, which acts in response to environmental stimuli including envelope stress, osmotic stress and low temperature (96, 314-319). The Rcs phosphorelay controls the expression of around 150 genes, many of which have a function related to the bacterial cell surface (314, 320). A study in 2001 isolated mecillinam-resistant *S.* Typhimurium mutants which were also mucoid from overexpression of the colanic acid capsule (315). The majority of these mucoid strains contained mutations within the *mucM* gene, which acts through the Rcs phosphorelay to help regulate colanic acid. *mucM* mutations led to the de-repression of RcsB/RcsC and the subsequent

activation of RcsB-regulated genes, including *ftsZ* (321, 322). *mucM* mutant cells were often shorter in length than the wild-type parents, most likely due to overexpression of the *ftsZ* and *ftsA* genes. It was proposed that the *mucM* mutation and the resulting activation of the RcsBC-mediated phosphorelay led to the activation of both *wca* and *fts* genes. This consequently led to an increase in colanic acid biosynthesis, and mecillinam resistance, since increased FtsZ levels have been shown to suppress lethality in round-cell mutants and are required for mecillinam resistance in *E. coli* (315, 323, 324). A more recent study also noted that the majority of isolated mecillinam-resistant colonies were mucoid (325).

In a screen to identify genes whose overexpression led to changes in biofilm expression or appearance in *E. coli*, Tenorio et al. isolated several genes involved in cell wall synthesis or cell shape determination, including *mreB* and *ftsZ*, but not *pbpA* and *rodA*. MreB overexpression resulted in non-motile cells with an unusual biofilm architecture, whilst *ftsZ* overexpression resulted in the production of filamentous biofilm. Changes in biofilm structure or appearance were also associated with a concurrent reduction in motility in many of the isolated mutants (323).

It was important to assess capsular polysaccharide production in *mrd* mutant strains, particularly given the observed relationships between the expression of cell shape genes and biofilm formation, as well as the links between membrane stress and biofilm production. To test for overexpression of the extracellular polysaccharide cellulose in *mrd* mutant strains, each strain was spread onto LB agar containing the ‘Congo red’ dye at 100 µg/ml and incubated for ~24 hours at 37°C. Congo red binds cellulose with strong affinity. The growth of bacteria expressing high levels of a cellulose capsule on medium containing Congo red leads to extensive Congo red binding and the formation of so called ‘red, dry and rough’ or ‘rdar’ colonies (312, 326, 499). *mrd* mutants and wild-type strains were grown on LB agar containing Congo red to screen for the rdar phenotype.

When grown on LB agar containing Congo red (100 µg/ml), BRD948 Δ*pbpA* and Δ*rodA* mutant colonies had a significantly darker red appearance, compared to the wild-type and other *mrd* mutant strains, indicating that cellulose production was

somewhat increased in these mutants (Figure 4.22). An increased mucoid nature from excess cellulose or colanic acid production could also explain the tendency of these strains to form large clumps of cells in liquid culture.

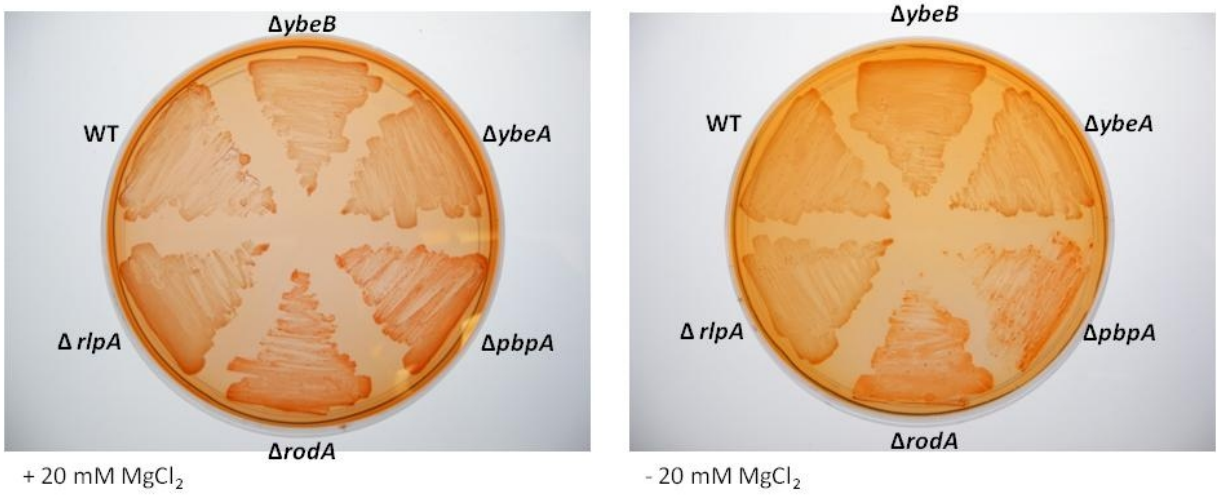

Figure 4.22: Growth of S. Typhi wild-type and mrd mutant strains on Congo red agar: BRD948 wild-type and *mrd* operon mutants were streaked onto LB agar with aro/tyr mix and ±20 mM $MgCl_2$, also containing 100 µg/ml Congo red dye to screen for excess cellulose production, as indicated by the development of darker red colonies; the rdar phenotype.

Oxidative stress sensitivity of *mrd* operon mutants

Bacteria possess many mechanisms to both detect and respond to various environmental stresses, including oxidative stress (98). In order to survive intracellularly, *Salmonella* must be also able to resist high levels of oxidative stress from the oxidative burst of macrophages (44, 327, 328). Perturbations to the cell surface of *Salmonella* may be linked to increased sensitivity to oxidative stress, having a significant impact on virulence; for instance, the inactivation of *rpoE*, the alternative sigma factor controlling responses to envelope stress, causes increased sensitivity to oxidative stress (329).

In order to investigate the effects of *mrd* operon mutations on sensitivity to oxidative stress, growth of both wild-type and *mrd* mutant strains in the presence of hydrogen peroxide was assessed. Strains were cultured in LB broth containing 10% sterile water or hydrogen peroxide (H_2O_2) at a range of 10-fold dilutions from a neat solution of H_2O_2 (30% w/w). Growth assays were then conducted as described and plotted as growth curves.

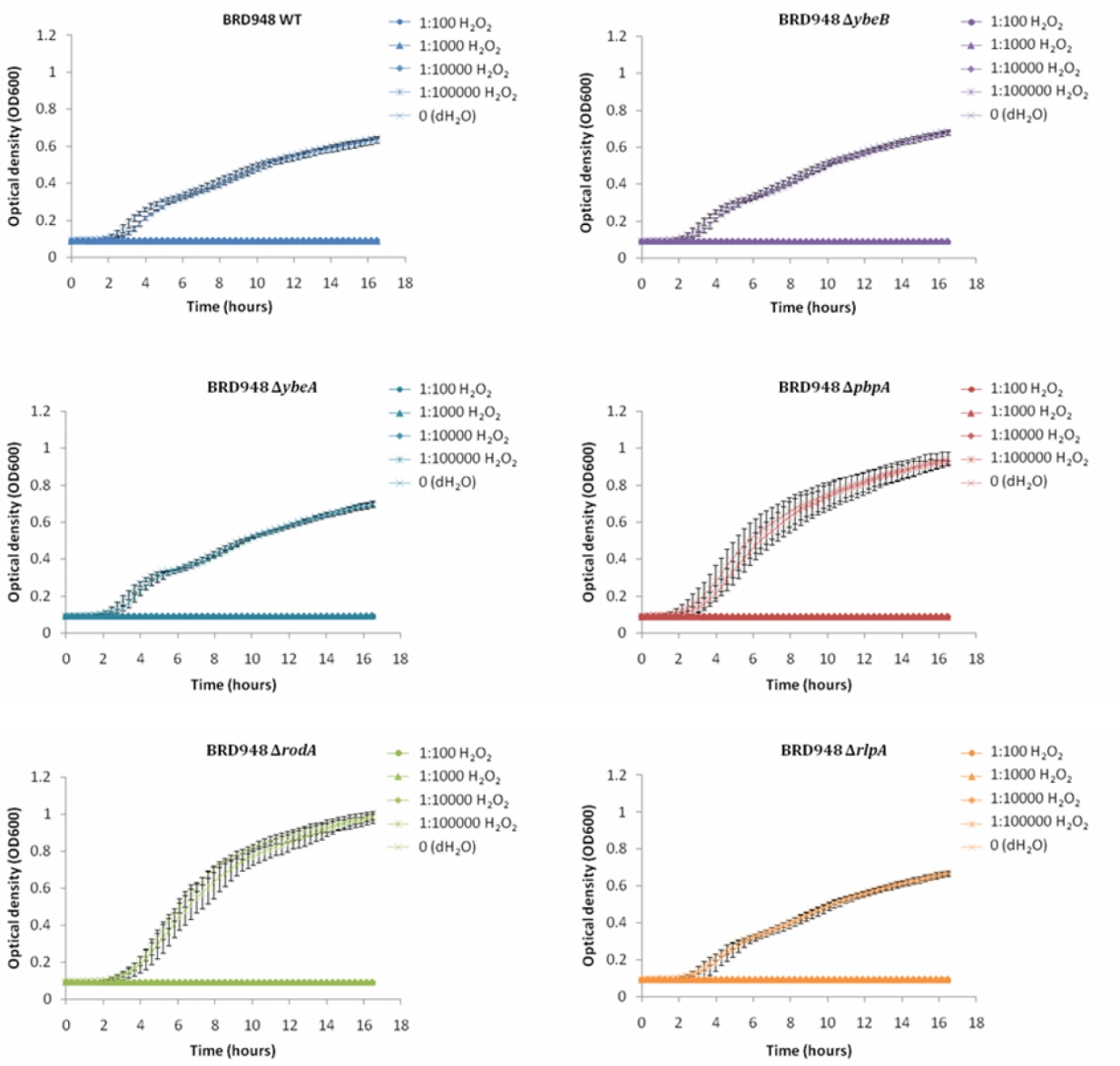

Figure 4.23: Sensitivity of S. Typhi mrd mutants to hydrogen peroxide: Growth curves showing growth of *S.* Typhi wild-type (WT) and *mrd* mutants in LB media, in the presence of hydrogen peroxide (H_2O_2), added at between 10^{-2} and 10^{-5} dilutions from a stock solution (30% w/w). Cells were cultured overnight at 37°C, with shaking in a Tecan Infinite 200® spectrophotometer. Growth (OD600) was measured every 15-20 minutes over 16 hours. Graphs show average OD600 values from 3 independent experiments. Error bars indicate standard deviation.

Growth assays demonstrated no significant change in sensitivity to hydrogen peroxide for any of the *mrd* operon mutants compared to the wild-type (Figure 4.23). All were alike, growing equally well in LB broth containing H_2O_2 at a 10^{-5} dilution as in LB broth containing water. Growth of all strains was completely inhibited in LB containing H_2O_2 at 10^{-4}, however. That the inactivation *pbpA* or *rodA*, as well as the other *mrd* operon genes, does not increase the sensitivity of these cells to oxidative stress, suggests that the cell wall structure and barrier

function may not be as compromised as was originally thought. Alternatively, oxidative stress response pathways may be upregulated in round-cell mutants to compromise for any defects in the barrier function of the cell wall, such that the oxidative stress sensitivity in these strains is equivalent to the wild-type cells.

4.4 Discussion

4.4.1 Construction and complementation of *mrd* operon mutants in *S.* Typhi

After examining the structure of the *mrd* operon in *Salmonella* using both *in silico* and experimental analyses, continuing work sought to investigate the functions of the individual *mrd* operon proteins further. To do this, precise knockout mutations were constructed using the method of Datsenko and Wanner, in the 5 putative *mrd* operon genes of *Salmonella* Typhi BRD948; namely, *ybeB*, *ybeA*, *pbpA*, *rodA* and *rlpA*. The latter mutant was constructed in previous work (163, 238). Complete gene knockouts were created for each gene, in which only a short scar sequence remained from the original insertion cassette along with short residual sequences from ends of the target gene.

The successful generation of each gene mutant was verified by PCR and DNA sequencing. Additionally the non-polarity of each mutant was demonstrated by several means. Firstly, both *S.* Typhi Δ*ybeB* and Δ*ybeA* mutants recovered a rod-shaped morphology after the removal of the knockout cassette, despite possessing severe morphological defects beforehand, suggesting that the cassette-containing mutations, but not the complete knockouts, brought about polar defects on the expression of downstream genes. Furthermore, complete Δ*pbpA* knockout mutants were complemented with a plasmid-encoded PBP2-YFP fusion protein, which was able to restore a rod-shape to these mutants, thus demonstrating that there were no significant polar effects on Δ*rodA* expression in these cells.

Δ*ybeB*, Δ*ybeA*, Δ*pbpA* and Δ*rodA* mutant strains of BRD948 were each complemented with YFP-fusion protein-expressing plasmids of the respective wild-type protein from *E. coli*. The PBP2-YFP and RodA-YFP plasmids were a kind gift

of L. Rothfield (University of Connecticut, US) (135, 269). The introduction of PBP2-YFP and RodA-YFP to Δ*pbpA* and Δ*rodA* mutants, respectively, successfully restored the wild-type morphology to these cells. Complementation of each mutant strain with a YFP-fusion protein also enabled localisation studies to be performed, showing, as previously, that PBP2 and RodA localise helically along the lateral cell wall (135, 136, 160, 163). However, significant overexpression of RodA-YFP, but not PBP2-YFP, tended to cause its accumulation into large polar inclusion bodies. This may be to do with the YFP fusion affecting protein structure. RodA is a highly hydrophobic membrane protein, containing at least 8 trans-membrane spans, which may be affected to a greater extent than PBP2 (which possesses only one or two trans-membrane spans) by the YFP fusion (154, 271).

Lower levels of PBP2 or RodA overexpression also occasionally brought about morphological defects to wild-type cells, in which the formation of inclusion bodies was not evident. It is possible that the YFP-fusion protein may have contributed to this defect, by significantly affecting the function of PBP2 and RodA. As such, overexpression of the YFP fusion proteins in wild-type cells may lead to an overall decrease in the proportion of fully-functional PBP2 or RodA molecules in the membrane, causing associated morphological defects. However, these YFP fusion proteins are known to be functional, given that they are able to complement Δ*pbpA* and Δ*rodA* mutations. The overproduction of MreB, RodZ, Mbl (*B.* subtilis), PBP2, and PBP5, at least, have been shown to cause morphological defects similar to those seen with the inactivation of the respective genes (158, 164, 209, 330). Thus it is more likely that the overproduction of PBP2 and RodA themselves led to defects in cell wall synthesis, with the observed morphological defects.

It is well accepted that the inactivation of either Δ*pbpA* or Δ*rodA* in bacteria such as *E. coli* and *Salmonella* results in severe and identical morphological defects. In Gram-positive organisms such as *B. subtilis*, the *pbpA* and *rodA* genes are located within separate loci on the genome. Hence in this organism morphology defects from the inactivation of *pbpA* are clearly not due to polar effects on *rodA* expression. Asoh et al., however, generated non-polar Tn5 transposon insertion mutants in *pbpA* and *rodA*, in *E. coli*, demonstrating that both genes were required for cell shape determination (144). Similarly the expression of PBP-YFP, but not

RodA-YFP in *S.* Typhi Δ*pbpA* was able to restore rod-shape, verifying that the cell shape defects in Δ*pbpA* mutants are not merely due to defective *rodA* expression.

YbeB-YFP and YbeA-YFP-expressing plasmids were generated in this work, from the same plasmid parent as the other YFP fusion vectors. The successful complementation of Δ*ybeB* and Δ*ybeA* was more difficult to ascertain, however, since few differences in phenotypes have been seen between these cells and the wild-type cells, both in the course of this study and in previous studies (188, 189).

Both YbeB-YFP and YbeA-YFP appeared to have a cytoplasmic localisation, in line with protein sequence analyses, which did not detect the presence of possible transmembrane helices in either YbeB or YbeA structures (253, 271). However, it is unknown whether these protein fusions retain their functionality.

4.4.2 Microscopic analysis of cell shape and surface features of *mrd* operon mutants in *S.* Typhi

The morphology and surface appearance of each *mrd* operon mutant was examined by both phase contrast and scanning electron microscopy. These observations reinforced those of previous studies; stark morphological defects were associated with Δ*pbpA* and Δ*rodA* mutants, which formed large spherical cells, which were often heterogeneous in size (127, 130, 157). As described previously, round-cell mutants were also shown to divide in an asymmetrical manner, with the formation of heart-shaped cells prior to cell division. It is thought that the increased diameter of these cells leads to the formation of an incomplete FtsZ division ring, such that constriction begins at one side of the cell and develops until cell division is permitted (127). Overexpression of the essential cell division proteins FtsA, FtsQ, and particularly FtsZ is known to help suppress lethality in round-cell mutants of *Salmonella* and *E. coli*. It was originally thought that high levels of these division proteins were needed to compensate for the increased diameter in the spherical cells, enabling cells to divide (130, 331, 332). A more recent model, however, suggests that excess production of the inner membrane in round-cell mutants causes FtsZ to mis-localise, preventing it from regulating cell division (130, 332). However, despite the putative increase in the

levels of the FtsZ, FtsA and FtsQ proteins, levels are clearly not sufficient to permit efficient symmetrical cell division.

The YbeB and YbeA proteins clearly do not play a direct role in cell shape determination, as microscopy in this study demonstrated that Δ*ybeB* and Δ*ybeA* mutants of *S.* Typhi retain wild-type morphology. However, in numerous assays average cell length appeared to be reduced in Δ*ybeA* cells compared to the wild-type cells, although the cell diameters were not affected.

Bacterial cell size is determined to a large extent by environmental factors, and primarily by the availability of nutrients (333). Nutrient-rich conditions (fresh growth medium, for example) cause an increase in growth rate (decreased mass doubling time) and an increase in cell size, whereas nutrient starvation (for example during stationary phase) results in a decrease in both growth rate and cell size (334, 335). Cell length in rod-shaped bacteria is also fundamentally determined by the rate of cell division. This in itself is coordinated by the FtsZ protein, which directs the formation of the FtsZ division ring and the recruitment of downstream division proteins. However, many of the signals which direct the rate of FtsZ ring formation, and hence cell division, remain to be characterised. These factors must form the link between environmental signals and the FtsZ protein (335, 336).

In round-cell mutants lethality is suppressed by the overexpression of cell division proteins, including FtsZ, as well as an increase in the concentration of the alarmone ppGpp (guanosine tetraphosphate and guanosine pentaphosphate), and a low growth rate (130, 331, 332). Although originally thought to simply prevent rRNA and tRNA synthesis with amino acid starvation, ppGpp is now known to function as a major global regulator of growth rate in response to various forms of nutritional starvation (337). In addition to regulating growth rate, ppGpp also regulates level of *ftsQAZ* transcription; *ftsQAZ* transcription varies with growth rate and cell cycle stage, and increased ppGpp levels led to an increase in FtsZ protein levels (338).

Overproduction of ppGpp in both wild-type and *mrd* operon mutants was previously shown to be associated with a decrease in cell size, from an increase in

cell division rate. Increased ppGpp levels also bring about mecillinam resistance (130, 331). Thus overproduction of ppGpp in round-cell *mrd* mutants may cause an increase in FtsZ levels, leading to a restoration of cell division. Given the observed decrease in cell size of Δ*ybeA* (and possibly Δ*ybeB*) mutants, it is possible that growth rate is also affected; an increase in ppGpp and FtsZ levels may cause the observed decrease in cell size of these mutants. Growth rate is associated with levels of ribosomal RNA and protein synthesis and growth rate regulation is mainly determined by regulating the levels of rRNA/tRNA and ribosomal protein synthesis (337). Since YbeB and YbeA are both involved in ribosome assembly and stability, it is possible that a mutation in either gene affects protein synthesis and with it growth rate, leading to a decrease in growth rate and cell size, as seen in wild-type cells with the reduction of nutrient availability.

Interestingly, the addition of magnesium or calcium to growth medium, to suppress lethality of the *pbpA* and *rodA* mutations in *S.* Typhi, decreased the prevalence of giant spherical cells, and also appeared to cause a slight reduction in cell length in wild-type cells. It was previously suggested that magnesium decreases lethality in round-cell mutants by stiffening the cell envelope, or acting as an osmoprotectant to reduce cell lysis (229). Calcium has been shown to induce ppGpp production in certain plant chloroplasts, whilst magnesium levels regulate the metabolism of ppGpp; activity of the ppGpp synthetic Rel enzymes is dependent upon magnesium, although high magnesium concentrations inhibit ppGpp synthesis (339-341). Magnesium is also involved in the binding of ppGpp to RNA polymerase in the regulation of transcription (373). However, manganese is required for the degradation of ppGpp (341). It would be interesting to assess whether the short-cell phenotype of magnesium-treated *S.* Typhi cells is linked to ppGpp and *ftsZ* expression, and therefore whether magnesium and calcium play a role in suppressing the lethality of round-cell mutants by increasing ppGpp synthesis and therefore increasing *ftsZ* transcription. Furthermore, magnesium ions were shown to induce the oligomerisation of FtsZ protein monomers *in vitro*, suggesting that magnesium may also assist with FtsZ ring formation, something which may be of significant importance in round-cell mutants (342). These

hypotheses, however, do not explain why the vulnerability of Δ*pbpA* and Δ*rodA* mutants to cold shock was reduced with the addition of magnesium.

Δ*rlpA* mutants retained their rod morphology, as previous work has shown (163, 201). However, initial SEM analyses highlighted potentially interesting surface features in these cells, which previous studies have not identified. The observed rough surface of Δ*rlpA* cells was reminiscent of surface appendages seen with polymyxin B treatment of wild-type *S.* Typhimurium (273). Although repeated SEM analyses of Δ*rlpA* and wild-type cells were inconclusive, the observations may still warrant future work. Polymyxin B is thought to act by incorporating into the outer membrane and therefore increasing its surface area. This, along with the tight binding of the outer membrane to the peptidoglycan, may have forced the excess sections of outer membrane outwards, forming the observed projections. RlpA is a peptidoglycan-binding outer membrane lipoprotein, which may be involved in linking the outer membrane to the peptidoglycan layer, along with other major outer membrane lipoproteins (201). As such Δ*rlpA* mutants may be expected to display visible surface defects such as those seen initially by SEM. If peptidoglycan-outer membrane associations were affected in this mutant, outer membrane projections could be observed, resulting from the disconnection in places of the outer membrane and the peptidoglycan layer. A number of major outer membrane lipoproteins are involved in linking the peptidoglycan layer to the outer membrane, including Pal and Lpp, indicating some possible redundancy of function (201). The variability in observed cell surface appearance of Δ*rlpA* cells in this study could potentially result from variability in Pal/Lpp expression between individual cells or cultures, such that increased levels of Pal/Lpp mask any cell surface defects caused by the Δ*rlpA* mutation.

4.4.3 Conclusions from general phenotypic analyses of round-cell *mrd* operon mutants of *S.* Typhi

In addition to those phenotypes already discussed, a number of other phenotypic screens were utilised to functionally analyse the *mrd* operon mutants. The sensitivity of the *mrd* mutants to a number of external stresses and antibiotics was assayed; furthermore, a number of cell surface features in these mutants were

assessed, given the role that PBP2 and RodA play in cell wall synthesis. Several previous studies have investigated cell wall synthesis in Δ*pbpA* and Δ*rodA* mutants and the sensitivity of these and similar mutants to environmental stress, suggesting that the cell wall integrity is somewhat compromised in round-cell mutants (127, 211, 214, 343).

The results of several phenotypic assays in this study highlighted some interesting features in Δ*pbpA* and Δ*rodA* mutants of *S.* Typhi. Although growth at 37°C in rich medium was not significantly affected, these mutants had an increased sensitivity to cold shock, and a slightly increased sensitivity to hydrophobic antibiotics. In addition, cells were prone to lysis. These results may be indicative of a significant weakening of the cell wall barrier function or structural integrity in round-cell mutants. Possible alterations to the surface structure were also highlighted with significant differences in the LPS profiles of Δ*pbpA* and Δ*rodA* mutants compared to the wild-type, as well as a noticeable increase in cellulose capsule production in these strains. However, it is possible that the alterations to LPS profiles resulted from the effects of *pbpA*/*rodA* mutations on LPS preparations, or levels of LPS expression rather than effects on LPS structure. Work by Matsuzawa et al. found that surprisingly, Δ*rodA* mutants were more resistant to UV irradiation than wild-type cells, reflecting results of several other studies (343). Similarly, despite Δ*pbpA* and Δ*rodA* mutations seemingly bringing about cell wall defects, these cells appeared no more sensitive to oxidative stress, from exposure to hydrogen peroxide, than wild-type cells.

Thus, it would appear that the cell wall barrier function and structure in Δ*pbpA* and Δ*rodA* mutants may not be as severely compromised as expected, although some changes in the overall cell envelope structure may be apparent. It is possible that *Salmonella* respond to the defects brought about by the inactivation of cell shape determinants by altering the expression of stress response pathways, and other cell surface-associated features, to compensate for a possible increase in sensitivity to external stress. A number of stress response pathways exist in *Salmonella*, which are activated in response to the detection of cell envelope stress. These pathways are regulated by a number of global regulators including CpxA/CpxR, RcsB, and RpoE (118, 344, 345). Further experimental analyses will

help establish whether these factors are involved in responding to the defects associated with *pbpA*/*rodA* inactivation, to maintain viability and resistance to environmental stresses. The possible upregulation of biofilm synthesis in round-cell mutants supports the hypothesis that envelope stress pathways may be involved (118).

As expected both Δ*pbpA* and Δ*rodA* mutants of *S.* Typhi were resistant to both mecillinam and the MreB-targetting molecule A22. The latter feature has been noted previously but not widely studied (281). MreB is thought to direct lateral cell wall synthesis through positioning the cell wall synthetic enzymes, including PBP2 and RodA, in the lateral cell wall (131). In addition, MreB localisation was shown to be dependent on RodA (131, 126). There are clear functional links between MreB, PBP2 and RodA, and in preventing MreB polymerisation and function A22 inhibits lateral cell wall synthesis (149). It is therefore not surprising that Δ*rodA* mutants at least are resistant to A22; if RodA is required for the correct localisation of MreB, MreB would already be mislocalised in Δ*rodA* mutants - the addition of A22 would not bring about any further effects. In terms of PBP2, although not essential for MreB localisation, lateral cell wall synthesis is already stalled in Δ*pbpA* mutants and so the addition of A22 would be ineffective at inhibiting lateral cell wall synthesis. These observations further reinforce the functional links between MreB, PBP2 and RodA, and their involvement in lateral cell wall synthesis.

In the course of these assays, no significant phenotypic differences were observed between the Δ*pbpA* and Δ*rodA* mutants of *S.* Typhi, suggesting they are closely linked in function. The activity of *pbpA* is known to be dependent on RodA (130, 146).

4.4.4 Conclusions from general phenotypic analyses of the Δ*ybeB*, Δ*ybeA*, and Δ*rlpA* mutants of *S.* Typhi

The functions of the three remaining *mrd* operon genes, *ybeB*, *ybeA*, and *rlpA,* in *Salmonella* remain less well characterised. It is also unknown whether they are in any way functionally linked to *pbpA* or *rodA*. Phenotypic analyses of mutants of

these genes sought to better characterise the roles of these proteins, and the reason for their placement within the *mrd* operon.

Experimental analysis of both the *ybe* mutants did not reveal any significant phenotypic traits; growth of these mutants at both 37°C and 30°C, and sensitivity to oxidative stress, A22, hydrophobic antibiotics did not differ significantly from the wild-type. In addition, LPS structure and extracellular cellulose synthesis were not affected in Δ*ybeB* or Δ*ybeA* mutants. Although additional work was carried out to assess virulence factor functionality in these strains, from these initial assays it was difficult to glean much useful information on the function of *ybeB* or *ybeA*.

However, several interesting features of these mutants were noted; firstly in terms of their slightly short-cell appearance, as already discussed. Also, antibiotic disc diffusion assays revealed increased resistance to mecillinam in both Δ*ybeB* and Δ*ybeA* strains. This would suggest a possible functional link between the *ybeB* and *ybeA* genes, and *pbpA* and *rodA*. Conversely though, the Δ*ybeB* and Δ*ybeA* mutants did not display any increased resistance to mecillinam in liquid growth assays.

The conflicting results seen with Δ*ybeB* and Δ*ybeA* cells in disc diffusion and growth rate assays may indicate differences in behaviour of these cells on solid and liquid medium. A study by Costa and Antón described round-cell mutants whose viability was somewhat dependent on growth medium; Δ*mre* and Δ*rodA* mutations were isolated which were lethal with growth on solid but not in liquid media (157). However, were the present results to reflect these results, one would expect the mecillinam resistance of Δ*ybeB* and Δ*ybeA* cells to be observed in liquid culture, rather than in disc diffusion assays. Alternatively, some polar effects of the Δ*ybeB* or Δ*ybeA* mutations on *pbpA* or *rodA* expression may be apparent in these mutants when grown on solid media, leading to significant mecillinam resistance. However, if this was the case it would be expected for the results of both assays to display similar resistance phenotypes, and no obvious polar effects on *pbpA* or *rodA* expression were otherwise noted in these mutants.

Analysis of the YbeB protein revealed a short sequence containing homology to the conserved 'PGVRY' loop region of the S12 ribosomal protein (290). The PGVRY loop of S12 is important for the recognition of specific tRNAs, enabling correct coding during protein synthesis. Furthermore mutations are often isolated within this loop, which confer streptomycin resistance (290). S12 itself is associated with the 30S ribosomal subunit. YbeB, however, is a 50S subunit ribosome-associated protein which may be involved in ribosome stability, but has no known role in the regulation of translation (189, 192, 193). Also, the sequences within the YbeB protein which direct the interaction with the 50S subunit have not been analysed (189). Streptomycin resistance assays resulted in only a negligible increase in resistance to streptomycin in Δ*ybeB* and Δ*ybeA* mutants. As such YbeB (and YbeA) appears not to be directly functionally connected to S12. Further work would be needed to establish whether the observed overlap in homology between YbeB and S12 is significant, or indicative of sequences within YbeB that are important for the function of YbeB, which may be analogous to the role of corresponding sequences within S12. It also remains to be assessed which portions of YbeB are involved in ribosome binding.

It is well established that YbeA functions to methylate a pseudouridine residue within stem-loop 69 of the 23S ribosomal subunit rRNA. This occurs in the final stages of ribosome assembly and may provide a signal to enable translation to begin (194-196). Similarly to the Δ*ybeB* mutants, streptomycin sensitivity assays showed that YbeA is not directly involved in translation functions which would normally by inhibited by streptomycin. YbeA is required prior to translation, so if mutations in *ybeA* were to affect translation, some resistance to translation-inhibiting antibiotics may be expected in Δ*ybeA* cells. As such, this mutation may not have a large inhibitory effect on protein synthesis.

Aside from the observed mecillinam resistance of Δ*ybeB* and Δ*ybeA* mutants, phenotypic analyses did not provide evidence of a functional link between these genes and *pbpA* or *rodA*. YFP-fusion proteins of YbeB and YbeA enabled the localisation of these proteins to be assessed. However, both YbeB and YbeA were spread diffusely through the cytoplasm. If YbeB or YbeA were linked with PBP2 and RodA they may be expected to co-localise with these proteins and the lateral

cell wall peptidoglycan synthetic complex. Studies in *B. subtilis* have shown that ribosomes were specifically localised around the cell periphery or at the cell poles (230, 231). It is possible that elements of the bacterial cytoskeleton may be involved in directing their localisation. However, no such localisation pattern was observed for the YbeB and YbeA ribosome-associated proteins in this study. Assuming the YFP-fusion constructs of these proteins are functional, it may be that these proteins exist freely in solution, as well as within ribosome complexes, in which case it is not possible to determine whether ribosome-associated YbeB and YbeA exhibit specific localisation patterns, which may be directed or linked to the bacterial cytoskeleton and associated proteins. It is also possible that the YFP protein fusion interfered with ribosome binding in both proteins, therefore masking any specific localisation patterns of these proteins.

The successful isolation of Δ*ybeB* and Δ*ybeA* mutants lacking obvious phenotypes demonstrates that these genes are not essential for viability in *Salmonella*. However, the observed mecillinam resistance in disc diffusion assays, along with the short-cell phenotypes, warrant further investigation to determine whether they relate specifically to the function of *ybeB* and *ybeA*.

RlpA is a peptidoglycan-binding outer membrane lipoprotein, which has been shown to localise both at the cell septum, and also at distinct foci along the lateral cell wall (163, 179, 201). Previous studies were unable to isolate a distinct phenotype associated with the Δ*rlpA* mutation, however, suggesting that its role is not important, or that significant functional redundancy exists (201). Likewise, microscopic analysis and general phenotypic analyses of the *S.* Typhi Δ*rlpA* mutant in the present study did not reveal any distinct features, besides those isolated by SEM. It might be expected that the cell morphology and structure of the outer surface of *S.* Typhi cells would be affected with the inactivation of *rlpA*; phase contrast microscopy and LPS profiles, though not comprehensive, did not highlight any changes, however. It may be that the simultaneous inactivation of other major peptidoglycan-associating outer membrane lipoproteins is required to reveal a phenotype for the Δ*rlpA* mutation. Further analysis of virulence determinant functionality in this mutant was also subsequently carried out.

If significant, the surface features noted in SEM analyses of Δ*rlpA* cells may highlight a role for RlpA in maintaining attachment of the outer membrane to the peptidoglycan cell wall. Given its localisation pattern, RlpA may be an important member of both the septal and lateral cell wall synthetic complexes at different stages of cell growth; it may be required, for instance, to maintain outer membrane-peptidoglycan associations in areas where active cell wall synthesis is occurring, or to establish those associations in newly incorporated peptidoglycan strands. It is recognised that a great deal more work will be needed to test these hypotheses.

Chapter 5. Phenotypic analyses of *mrd* operon gene knockout mutants to assess virulence factor functionality

5.1 Introduction and overview of major virulence determinants of *Salmonella*

Although many studies have investigated the roles of cell shape determinant proteins, few to date have considered the potential relationships between virulence and cell shape determination in rod-shaped bacterial pathogens. However, several studies have noted detrimental effects of cell shape determinant inactivation upon *flhDC* expression and motility (118, 166). A role for MreB in pili localisation has also been assessed (221, 222). This is significant, given that many crucial virulence determinants form cell surface or wall-spanning organelles, which may depend upon the cell wall structure for function.

Both *S.* Typhi and *S.* Typhimurium, along with the majority of *Salmonella* serovars, share a number of virulence determinants which are important for pathogenesis. Foremost among these are the two type 3 secretion systems (T3SS), which are both essential for virulence. The SPI-1 T3SS is required in the early stages of infection, where effector proteins injected into host epithelial or macrophage cells induce phagocytosis of the bacterium. Once *Salmonella* is internalised, the SPI-2 T3SS is required for intracellular survival and ultimately for systemic spread of *Salmonella* (4, 11).

Other significant surface-associated virulence determinants of *Salmonella* include flagella-mediated motility, which is known to assist in invasion potentially by physically bringing cells into closer proximity with host cells, as well as directing chemotaxis mechanisms (51, 53). *S.* Typhi and some Paratyphi serovars exclusively express an extracellular polysaccharide capsule, the Vi antigen. The capsule is anti-opsonic, assisting in the evasion and modification of host immune responses. The Vi capsule is thought to help particularly in systemic spread of *S.* Typhi (11, 70, 72, 114).

In the present study, a range of assays were used to assess the functionality of these major virulence determinants in each of the *mrd* operon mutants. As well as

providing useful information about the effects of *mrd* mutations on virulence, it was hoped that these analyses would provide further insights into the functions of the *mrd* operon genes.

5.2 Motility of *S.* Typhi *mrd* operon mutants

5.2.1 Microscopic analysis of *mrd* mutants

Initial observations of live *S.* Typhi BRD948 *mrd* mutant cells revealed that whilst the rod-shaped Δ*ybeB*, Δ*ybeA*, and Δ*rlpA* mutants appeared motile under the microscope, the vast majority of Δ*pbpA* or Δ*rodA* cells appeared completely non-motile. Amongst a large population of cells, only very few individual cells occasionally appeared motile.

5.2.2 Motility assays with *mrd* mutant cells

To assess the potential motility phenotype associated with round-cell *mrd* mutants, motility assays were performed, as described. After several hours of culture at 37°C, the extent of spread of wild-type and *mrd* mutant cultures through semi-solid agar was measured to give an indication of the motility functionality of each strain. A non-motile *S.* Typhimurium Δ*flhDC* strain was routinely used as a negative control in motility assays. Previous motility assays with BRD948 Δ*rlpA* demonstrated that there were no significant effects on motility in this mutant (163).

In line with previous observations in a *S.* Typhimurium Δ*rodA* mutant, both Δ*pbpA* and Δ*rodA* mutants in *S.* Typhi were completely non-motile in motility assays (Figure 5.1 C and D) (163). Motility assays were also carried out in BRD948 complemented strains in the presence or absence of 0.5 mM IPTG, to determine whether motility could be restored in Δ*pbpA* and Δ*rodA* strains expressing PBP2-YFP and RodA-YFP and to check that the observed motility defects were a direct result of the inactivation of *pbpA* and *rodA*. In the absence of IPTG, added to induce overexpression of the YFP-fusion proteins, around 50-70% motility was restored in BRD948 Δ*pbpA* and Δ*rodA* mutants expressing the relevant YFP-fusion complementation plasmids, pVP6 and pVP3 respectively (Figure 5.1 C and D). However, the addition of 0.5 mM IPTG to the motility agar was accompanied

by a complete loss of motility in the same cells. Overexpression of PBP2-YFP in wild-type BRD948 (with the addition of IPTG) also produced a slight but significant reduction in motility compared to the wild-type, although the equivalent measurement for RodA-YFP (pVP3) was not significantly different from the wild-type.

It is plausible that overexpression of PBP2-YFP and RodA-YFP caused detrimental effects to the cells; it has previously been seen that when overexpressed, RodA-YFP at least aggregates into inclusion bodies. Were this to occur, BRD948 Δ*pbpA* pVP6 and Δ*rodA* pVP3 cells grown in the presence of IPTG could revert to a spherical shape, with the concurrent loss of motility, as was seen. Alternatively, given that the overexpression of cell shape determinant proteins also causes morphological defects, it is possible that the motility defects are a result of overexpression of the functional proteins rather than a loss of functional PBP2/RodA.

In motility assays with BRD948 Δ*ybeB* and *ybeA* mutant strains, as well as those expressing the YbeB-YFP and YbeA-YFP fusion plasmids, generally no significant differences in motility were observed; only the Δ*ybeB* mutant displayed a small decrease in motility, being around 80% compared to the wild-type (Figure 5.1 A and B).

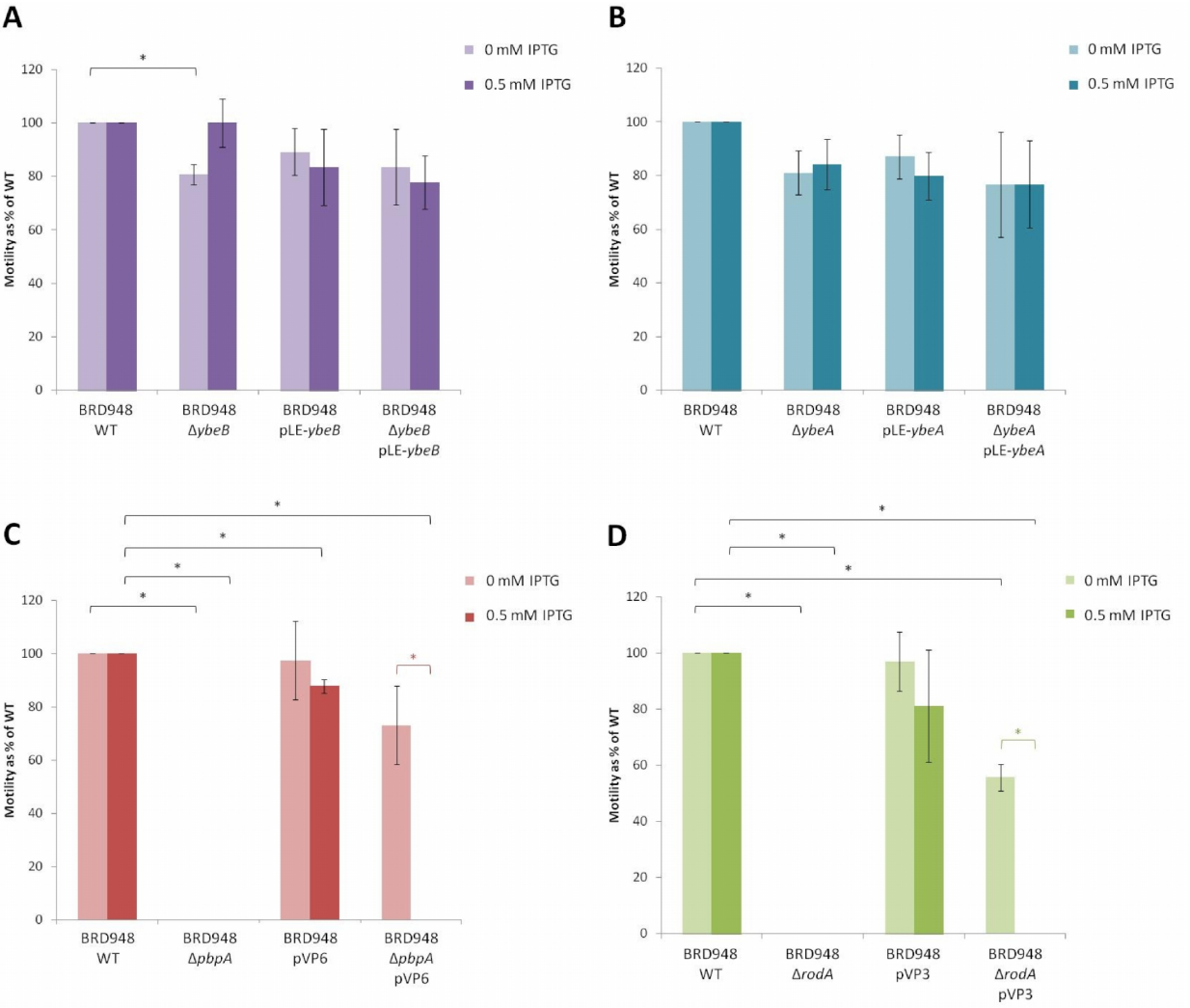

Figure 5.1: Motility assays of S. Typhi mrd operon mutants and complemented strains: Motility assay results for BRD948 Δ*ybeB* (A), Δ*ybeA* (B), Δ*pbpA* (C), and Δ*rodA* (D) mutants and YFP-fusion protein complemented strains. Cells were inoculated into semi-solid motility agar (with aro/tyr mix and 20 mM $MgCl_2$) and cultured at 37°C for at least 6 hours. Motility was measured in terms of extent (diameter) of culture spread through motility agar, as a percentage of that of wild-type cells. Results show averages from 3 independent assays. SL1344 Δ*flhD*, routinely used as a negative control, was completely non-motile in all assays. Error bars indicate standard deviations. Asterisks indicate statistically significant differences, where P values were ≤0.05 as determined by Students t-tests.

5.2.3 Motility assays with mecillinam-treated cells

Motility assays with round-cell *mrd* mutants demonstrated that these cells were completely non-motile. However, it remained to be seen whether or not the motility defects were the direct result of cell-wall and morphological defects in these mutants, with the resulting round cells becoming incapable of assembling or supporting structures such as flagella. If this were the case, the formation of round

cells would be associated with an immediate loss of motility, with a breakdown of flagella structures.

To investigate further the relationship between cell shape and motility, motility assays were carried out in semi-solid motility agar containing mecillinam at concentrations of 0, 0.001, 0.005, 0.01, 0.02, or 0.05 µg/ml. Motility assays were coupled with microscopic analysis to assess the concentrations of mecillinam required to both cause the formation of round cells and to inactivate motility function. These assays were carried out in parallel for each rod-shaped *mrd* mutant strain as well as the wild-type, to examine possible differences between the mutants. The results of motility assays in the presence of mecillinam are shown below (Figure 5.2 A). The motility of each strain was measured relative to the motility of that same strain in the absence of mecillinam.

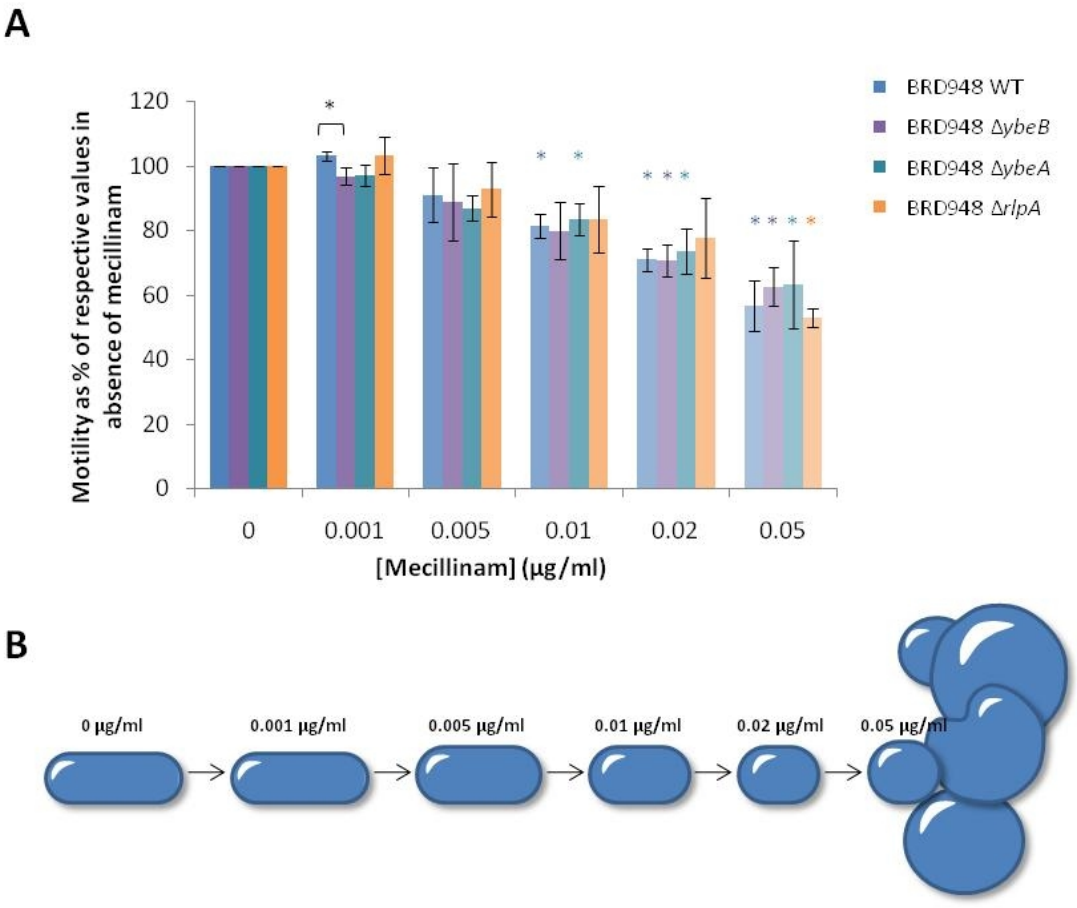

Figure 5.2: Motility of S. Typhi wild-type and mrd mutant strains in the presence of mecillinam: A - Motility assay results for BRD948 wild-type (WT), Δ*ybeB*, Δ*ybeA*, and Δ*rlpA* mutants in the presence of 0, 0.001, 0.005, 0.01, 0.02, or 0.05 µg/ml PBP2-inhibiting mecillinam. Cells were inoculated into semi-solid motility agar (with aro/tyr mix and 20 mM $MgCl_2$) containing mecillinam at a range of concentrations, and cultured at 37°C for ~6 hours. Motility was measured in terms of extent (diameter) of culture spread

through motility agar, as a percentage of that of the same strain grown in the absence of mecillinam. Results show averages from 3 independent assays. Error bars indicate standard deviations. Asterisks indicate statistically significant differences, where P values were ≤0.05 as determined by Students t-tests. Coloured asterisks demonstrate where the motility of a strain was significantly different to the motility of that strain in the absence of mecillinam. B – Schematic diagram representing the morphology of wild-type cells after 6-8 hours' growth in the presence of various concentrations of mecillinam, as observed by phase contrast microscopy of mecillinam motility assay cells.

Mecillinam motility assays demonstrated that increased mecillinam concentrations were accompanied by a concomitant decrease in motility in both wild-type and *mrd* mutant cells. However, even at concentrations of 0.05 µg/ml, 50-60% motility remained in all strains (Figure 5.2 A). In general no significant differences in motility between Δ*ybeB*, Δ*ybeA*, Δ*rlpA*, and wild-type strains were observed in this assay. Phase contrast microscopy analysis of these cultures demonstrated that mecillinam treatment was also associated with a loss of rod-shape, as represented (Figure 5.2 B). At low mecillinam concentrations, wild-type BRD948 retained a rod-shape. With increasing amounts of mecillinam, cells gradually became shorter, with a widened cell diameter, such that at 0.02 µg/ml the majority of cells were almost completely round. However, even at this concentration, both the cell size and diameter remained fairly regular between individual cells, although cells were slightly wider than the wild-type cells grown in the absence of mecillinam. At 0.05 µg/ml mecillinam cells were completely round and significant heterogeneity of size and diameter between individual cells was evident.

Despite the complete round morphology of all cells grown in 0.05 µg/ml mecillinam, these cells clearly retain some ability to swim. The motility observed was not simply 'residual' motility left from a number of cells in the culture which somehow remained rod-shaped, since no rod-shaped cells were observed by microscopy in cultures containing 0.05 µg/ml mecillinam. Furthermore many clearly motile spherical cells were seen by microscopy in these cultures. Thus, the motility defect seen in Δ*pbpA* and Δ*rodA* mutants is not a direct consequence of a loss of rod-shape; there in fact appears to be some delay between the loss of rod-shape and the complete loss of motility.

The isolation of completely spherical yet motile cells demonstrates that these cells, and significantly the cell walls, are able to support functional flagella, although it

may be that the number of flagella expressed by such cells is decreased. Alternatively, the slight reduction in motility may be caused by the loss of motility in some, but not all cells.

5.2.4 Luciferase promoter reporter assays to investigate flagella gene expression

Motility assays in this work showed that the round-cell *mrd* mutants were all non-motile, although the *ybeB* and *ybeA* mutants retained their motility. This supports the results of previous work (118, 163, 166). Transcriptional reporter assays were therefore carried out to further investigate the nature of the motility defect, by assessing flagella gene expression.

The promoter region of the flagella *fliF* gene was cloned into the pMK1*lux* reporter plasmid. *fliF* is a Class 2 flagella gene, in terms of the hierarchical regulation involved in the expression of the flagella structural genes. FliF is the first flagellar structural protein to be incorporated into the cell wall during flagella assembly, where it forms the MS basal body ring (346, 347). Thus *fliF* is expressed very early on in flagella assembly; the assembly of all subsequent basal body apparatus proteins and also expression of the downstream class 3 genes, is dependent upon the expression and assembly of the FliF MS ring (56, 62). It is for this reason that FliF was chosen as an ideal candidate to study flagella gene expression.

Luciferase transcriptional reporter assays were carried out in both wild-type and *mrd* mutant strains of BRD948 expressing the pMK1*lux-fliF* reporter plasmid, whereby relative luminescence of cultures expressing the reporter plasmid gave an indication of *fliF* expression. Strains were cultured in nutrient rich LB medium to stimulate flagella expression. As expected for the rod-shaped Δ*ybeB*, Δ*ybeA*, and Δ*rlpA S.* Typhi mutants, *fliF* expression remained at the level of the wild-type. However, transcription of *fliF* in both the Δ*pbpA* and Δ*rodA* mutants appeared to be almost completely downregulated (Figure 5.3 A-E).

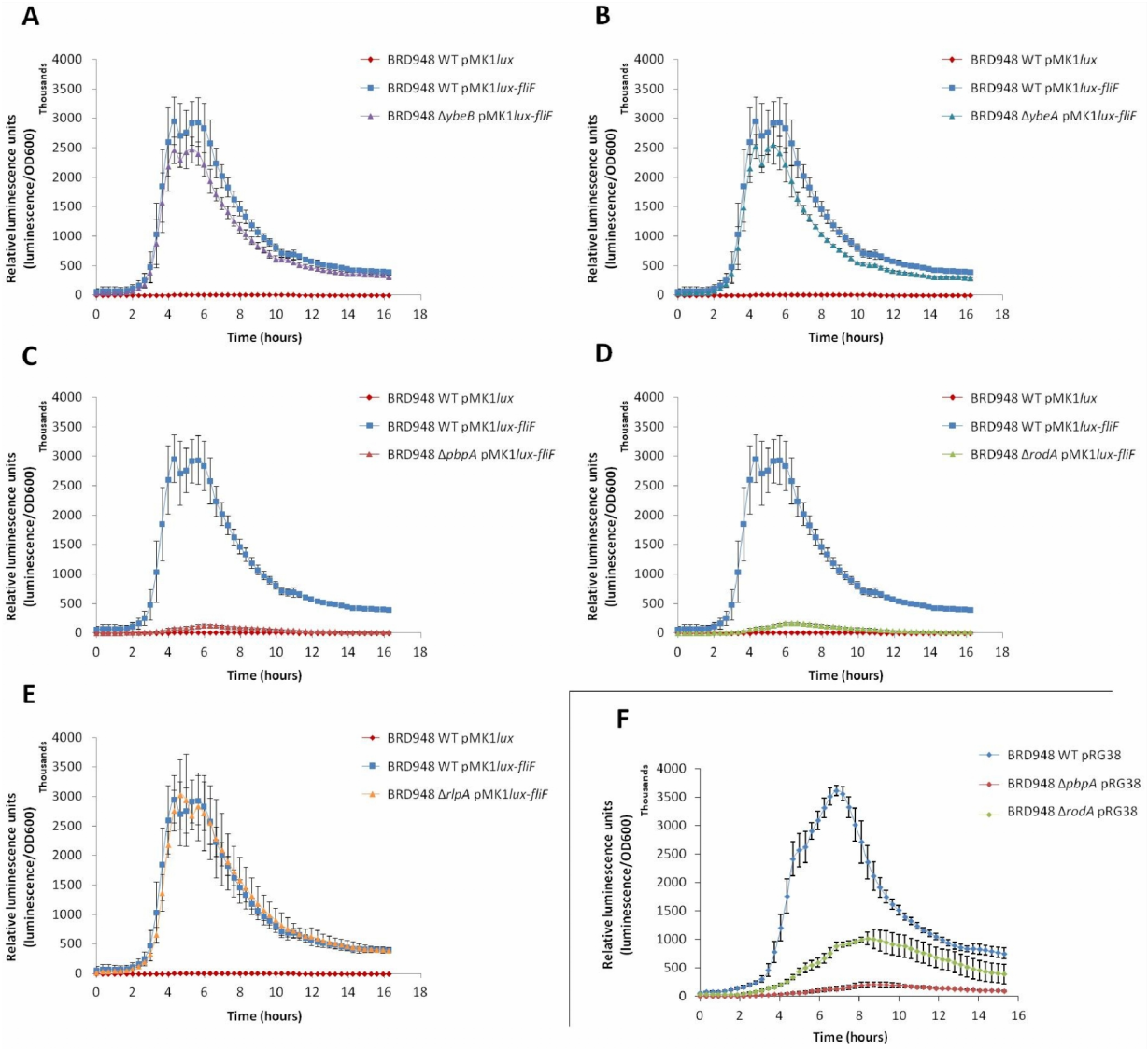

Figure 5.3: Motility gene expression in wild-type and mrd operon mutants of S. Typhi: A-E – Transcriptional luciferase reporter assays of BRD948 wild-type (WT) and *mrd* operon mutant cultures expressing a promoter fusion of the *fliF* gene, cloned into the pMK1*lux* luminescence reporter plasmid. Promoter activity was measured in terms of relative luminescence units (luminescence per culture optical density at 600 nm). Results are indicative of *fliF* transcription levels in WT and *mrd* mutant cells. F – Transcriptional luciferase reporter assays of BRD948 wild-type (WT), Δ*pbpA* and Δ*rodA* strains expressing pRG38; a promoter fusion of P_{flhDC} cloned upstream of *lux* genes (108). Promoter activity was measured in terms of relative luminescence units (luminescence per culture optical density at 600 nm). Results are indicative of *flhDC* transcription levels in WT and *mrd* mutant cells. Cells were grown in LB medium at 37^{o}C with shaking. Growth rates of strains were equivalent. Values show means of 3 independent assays. Error bars = standard deviation.

To further analyse flagella gene expression in these mutants, an *flhDC* luciferase transcriptional reporter plasmid, pRG38, was introduced into wild-type, Δ*pbpA* and Δ*rodA* BRD948 strains. The *flhDC* genes encode the major global transcriptional regulatory proteins which control flagella gene expression as well as the

expression of a number of other genes (56, 348-350). The pRG38 vector was a kind gift from Brian Ahmer (Ohio State University, US) (243). Luciferase reporter assays with this plasmid demonstrated that *flhDC* expression was significantly downregulated in the BRD948 Δ*rodA* strain and almost completely downregulated in Δ*pbpA* mutants (Figure 5.3 F). The difference in *flhDC* expression between the two round cell mutants may be significant, given that in all other assays conducted the phenotypes of these mutants have been indistinguishable.

5.2.5 Immunofluorescence microscopy of flagella expression in *mrd* mutant strains

Mid-log phase BRD948 wild-type and *mrd* mutant cultures were fixed and labelled with *Salmonella* agglutinating serum specific for Typhi-flagellin, followed by an anti-rabbit fluorophore-conjugated secondary antibody. Cells were then mounted onto slides and viewed by epifluorescence microscopy. Specific binding of the primary agglutinating serum to flagellin proteins permitted the visualisation of individual flagella expressed at the surface of cells.

The resulting images clearly show that long flagella filaments are expressed at the surface of both wild-type cells and rod-shaped *mrd* mutant cells. However, such filaments were not visible in Δ*pbpA* and Δ*rodA* cells. Fluorescent foci or very short flagellin tails were very occasionally observed at the surface, or around the cell wall in both mutants, possibly resulting from heterogeneous flagella protein expression between individual cells (Figure 5.4).

It is likely that during the preparation of the samples for immunofluorescence microscopy, some flagella filaments would have been physically sheared off the cells. This possibility is supported by the observation that wild-type cells contained within large clumps appeared to possess more flagella than individual cells, and explains why many cells of rod-shaped BRD948 strains appear to have no flagella. Alternatively, the anti-flagellin serum may have caused the agglutination and clumping of highly motile cells expressing large numbers of flagella filaments. Consequently, the cells which were seen not to form clumps may generally be those which are less motile. Hence, it is not possible to use this method to assess

levels of flagella expression between strains, although it effectively demonstrates whether flagella are expressed at all, as well as whether flagella generally appear relatively normal in terms of length, as demonstrated for Δ*pbpA* and Δ*rodA* mutants.

In conclusion, the results of various phenotypic assays have demonstrated that whilst BRD948 Δ*ybeB*, Δ*ybeA* and Δ*rlpA* mutants remained completely motile, motility was not only defective in *S.* Typhi round-cell *mrd* mutants, but completely downregulated from the level of transcription of the flagella master regulator operon, *flhDC* (163). Despite this, analyses of motility in mecillinam-treated cells suggested that round-cells with defective PBP2 remained physically able to support functional flagella.

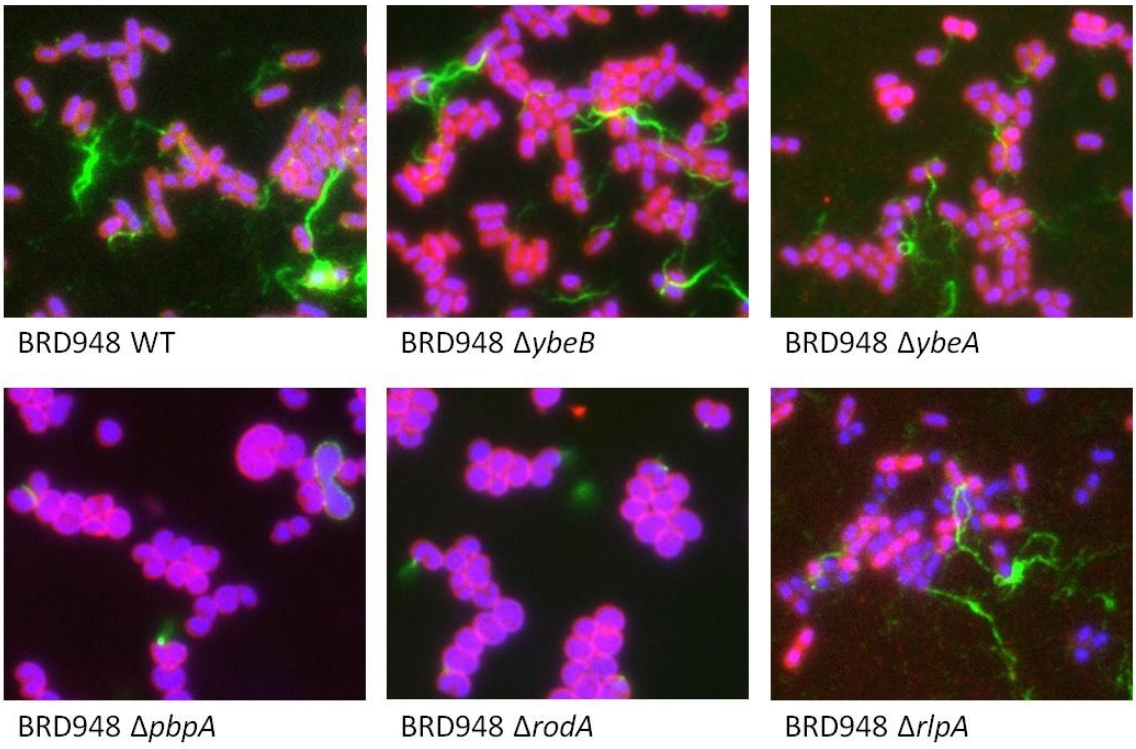

Figure 5.4: Flagella expression in wild-type and mrd operon mutants of S. Typhi: Epifluorescence microscopy of *S.* Typhi wild-type (WT) and mutant cells fixed and labelled with flagellin-agglutinating serum and a fluorophore conjugated secondary antibody, to enable visualisation of cell surface flagella by immunofluorescence microscopy. Cells further stained with DAPI DNA stain (blue) and Nile Red membrane stain (red). All images are to the same scale.

5.3 SPI-1 type 3 secretion system (T3SS) functionality in *S.* Typhi *mrd* operon mutants

5.3.1 Western blots and immunofluorescence microscopy with anti-SipD antibody

Expression and functionality of the SPI-1 T3SS was analysed in each of the *mrd* operon mutants in *S.* Typhi. Data from a previous study on an *S.* Typhimurium Δ*rodA* mutant strain had shown that the SPI-1 T3SS proteins were not expressed in this strain, whilst SPI-1 expression was active in both *S.* Typhimurium and BRD948 Δ*rlpA* mutant strains (163). For the purpose of testing SPI-1 functionality, strains were routinely cultured in nutrient-rich LB broth medium, which has been shown to stimulate SPI-1 gene expression (90).

SPI-1 T3SS protein expression and functionality were tested by means of western blots, immunofluorescence microscopy and luciferase reporter assays. Total cell protein and secreted protein fractions were isolated from mid to late exponential phase cultures of BRD948 wild-type and *mrd* mutant strains, as previously described. Protein samples were then subjected to SDS-PAGE, blotted onto a nitrocellulose membrane and labelled with antibodies specific to the SPI-1 secreted effector protein SipD. Along with SipB and SipC, this protein forms part of the SPI-1 needle translocon (351).

Western blot analyses demonstrated that the SPI-1 effector proteins were expressed both intracellularly and in the secreted protein fractions of wild-type Δ*ybeB*, Δ*ybeA* and Δ*rlpA* BRD948 cultures (163). However, similarly to the *S.* Typhimurium Δ*rodA* strain, SipD bands were absent from both total cell protein and secreted protein fractions of the BRD948 round-cell mutant strains (Figure 5.5 A) (163), suggesting that SPI-1 protein expression may be downregulated in Δ*pbpA* and Δ*rodA* mutants.

Immunofluorescence microscopy images supported these results. Mid-log phase cells of BRD948 *mrd* mutants were fixed and labelled with anti-SipD primary antibody, followed by a fluorophore-conjugated secondary antibody. The nature of

the SipD protein as a translocon protein means that it resides at the tip of the T3SS needle and can therefore be detected at the cell surface by immunofluorescence microscopy, whereby fluorescent foci indicate the location of SPI-1 needles. Whilst clear fluorescent foci were present in several copies along the lateral cell walls of wild-type, Δ*ybeB*, Δ*ybeA*, and Δ*rlpA* cells, such foci were completely absent from the surfaces of Δ*pbpA*, and Δ*rodA* mutant cells (Figure 5.5 B).

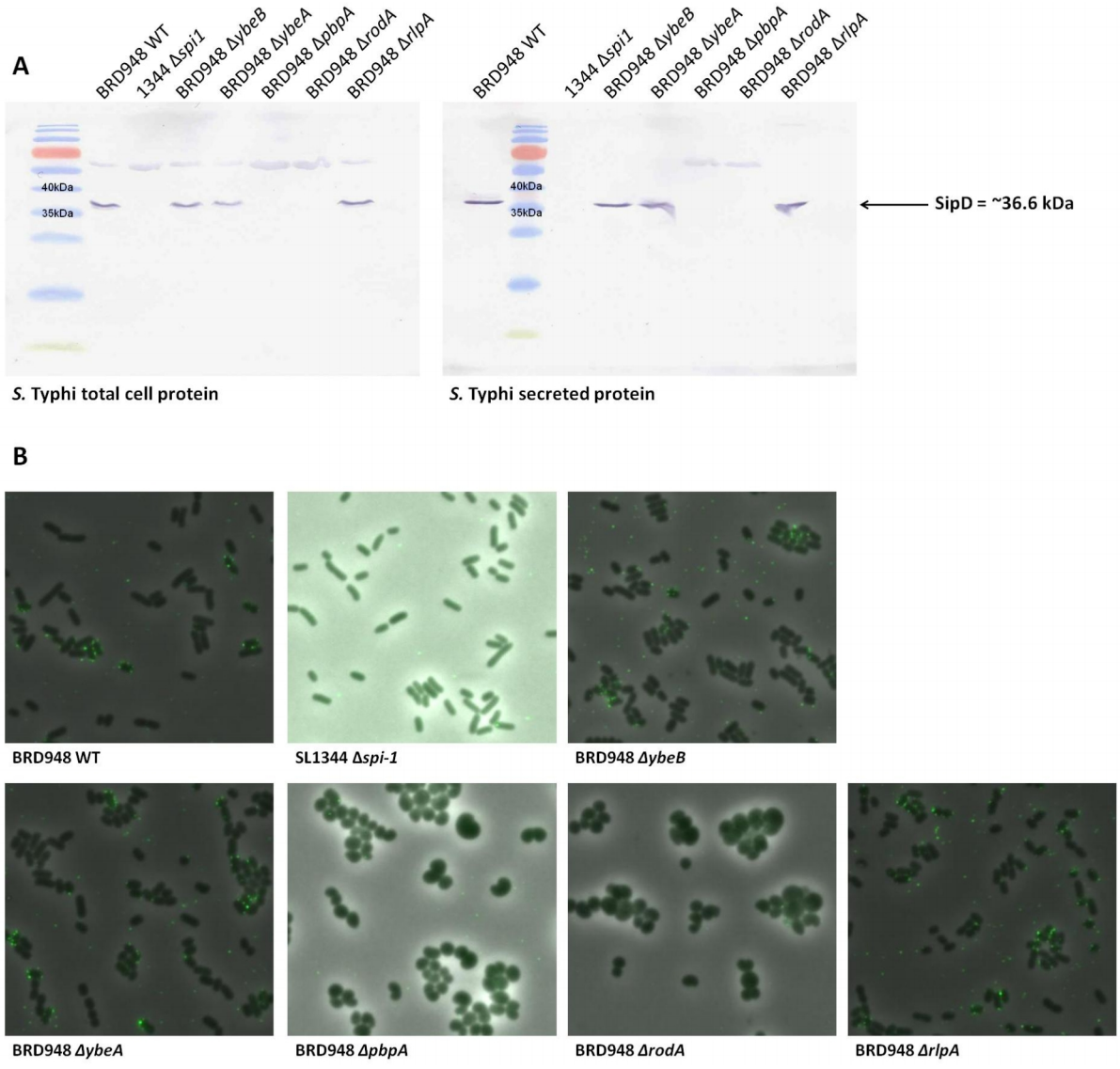

Figure 5.5: SPI-1 functionality in wild-type and mrd operon mutants of S. Typhi: A – Western blots showing expression of the SPI-1 SipD effector protein in total protein and secreted protein fractions of BRD948 wild-type and *mrd* mutant cultures, along with *S.* Typhimurium (SL1344) Δ*spi-1*, as a negative control. Western blots were repeated a number of times, using antibodies to other effectors including SipA and SipC. B - Immunofluorescence microscopy images of *S.* Typhi BRD948 wild-type (WT) and *mrd* mutant cells overlaid onto phase contrast images; samples labelled with anti-SipD

antibody and fluorophore-conjugated secondary antibody. All images are to the same scale.

5.3.2 Luciferase promoter reporter assays to investigate SPI-1 gene expression

HilD is the major SPI-1-encoded transcriptional regulator of the SPI-1 T3SS genes. Together with HilC it activates expression of HilA, which goes on to directly activate SPI-1 T3SS genes (352, 353). Expression of the SPI-1 genes is therefore dependent upon *hilD* expression (88). Western blot analyses showed that SPI-1 effector proteins were not expressed in round-cell *mrd* mutants. This, along with observed transcriptional repression of motility genes, hinted at the possibility that SPI-1 transcription may also be repressed in round-cell mutants. To test this, expression of *hilD* was investigated in the BRD948 wild-type and *mrd* operon mutant strains. The *hilD* promoter was cloned into the luciferase reporter plasmid pMK1*lux* and introduced into BRD948 wild-type and mutant strains. The relative luminescence of strains expressing pMK1*lux-hilD* was subsequently measured over 16 hours of growth in LB broth, as a measure of *hilD* expression. As was seen with expression of flagella gene regulators, *hilD* transcription was almost completely downregulated in the round-cell *mrd* operon mutants compared to the wild-type. In contrast, *hilD* expression remained largely unaffected in the Δ*ybeB*, Δ*ybeA* and Δ*rlpA* mutants, with only a slight depression of expression in Δ*ybeA* and Δ*rlpA* cells at 6-10 hours' growth (Figure 5.6).

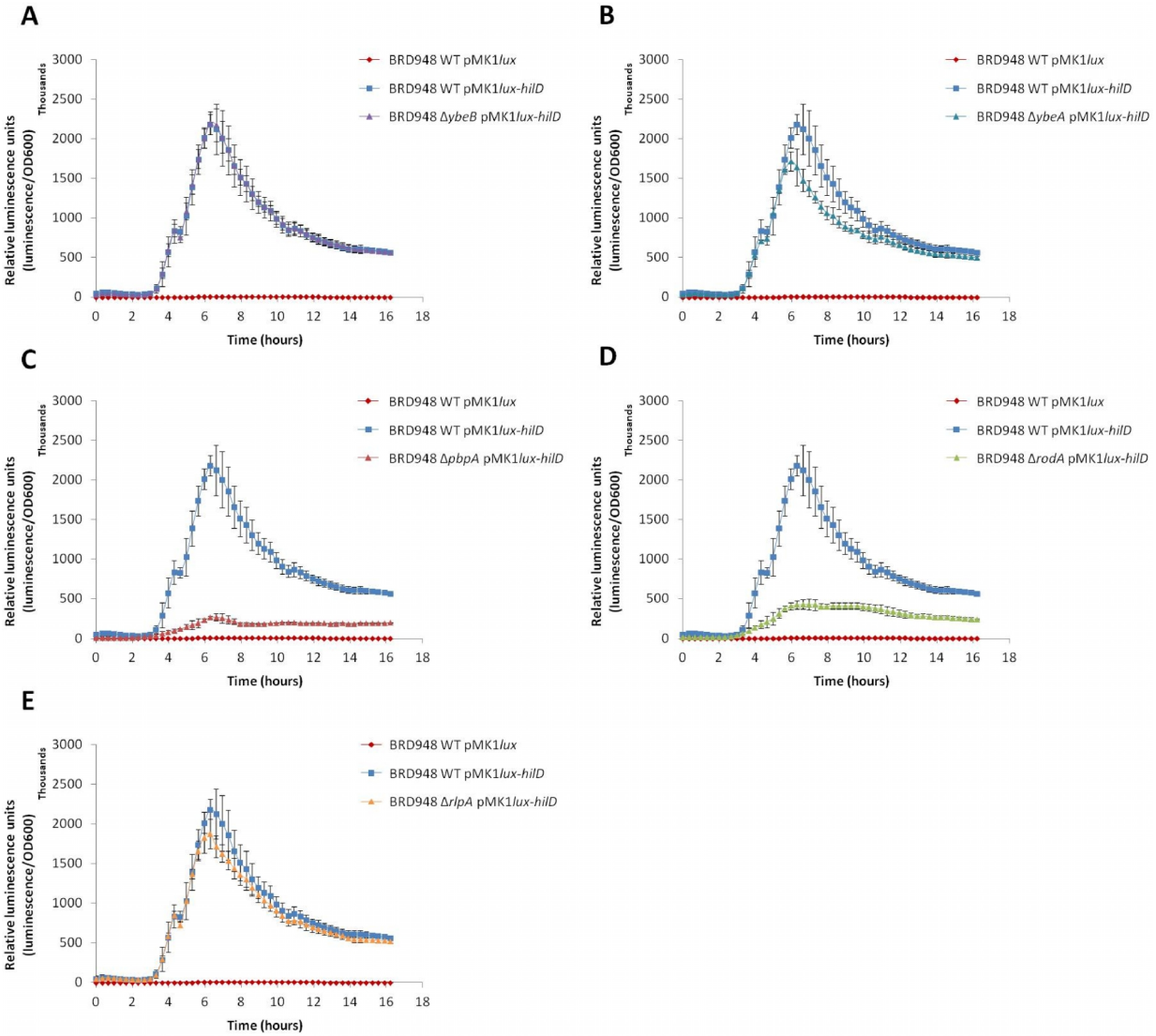

Figure 5.6: SPI-1 regulator gene expression in wild-type and *mrd* operon mutants of *S.* Typhi: A-E – Transcriptional luciferase reporter assays of BRD948 wild-type (WT) and *mrd* operon mutant cultures expressing a promoter fusion of the *hilD* gene, cloned into the pMK1*lux* luminescence reporter plasmid. Promoter activity was measured in terms of relative luminescence units (luminescence per culture optical density, at 600 nm). Results indicative of *hilD* transcription levels in WT and *mrd* mutant cells. Cells were grown in LB medium at 37°C with shaking. Growth rates of strains were equivalent. Values show means of 3 independent assays. Error bars = standard deviation.

5.4 Total cell protein and secreted protein profiles of *S.* Typhi *mrd* mutant strains in SPI-1 growth conditions

Global protein expression in the BRD948 wild-type and *mrd* operon mutants was assessed by separating both total cell protein and secreted protein preparations from each strain by SDS-PAGE. Proteins were separated on 12% gels and then stained using Coomassie® Brilliant Blue (Figure 5.7).

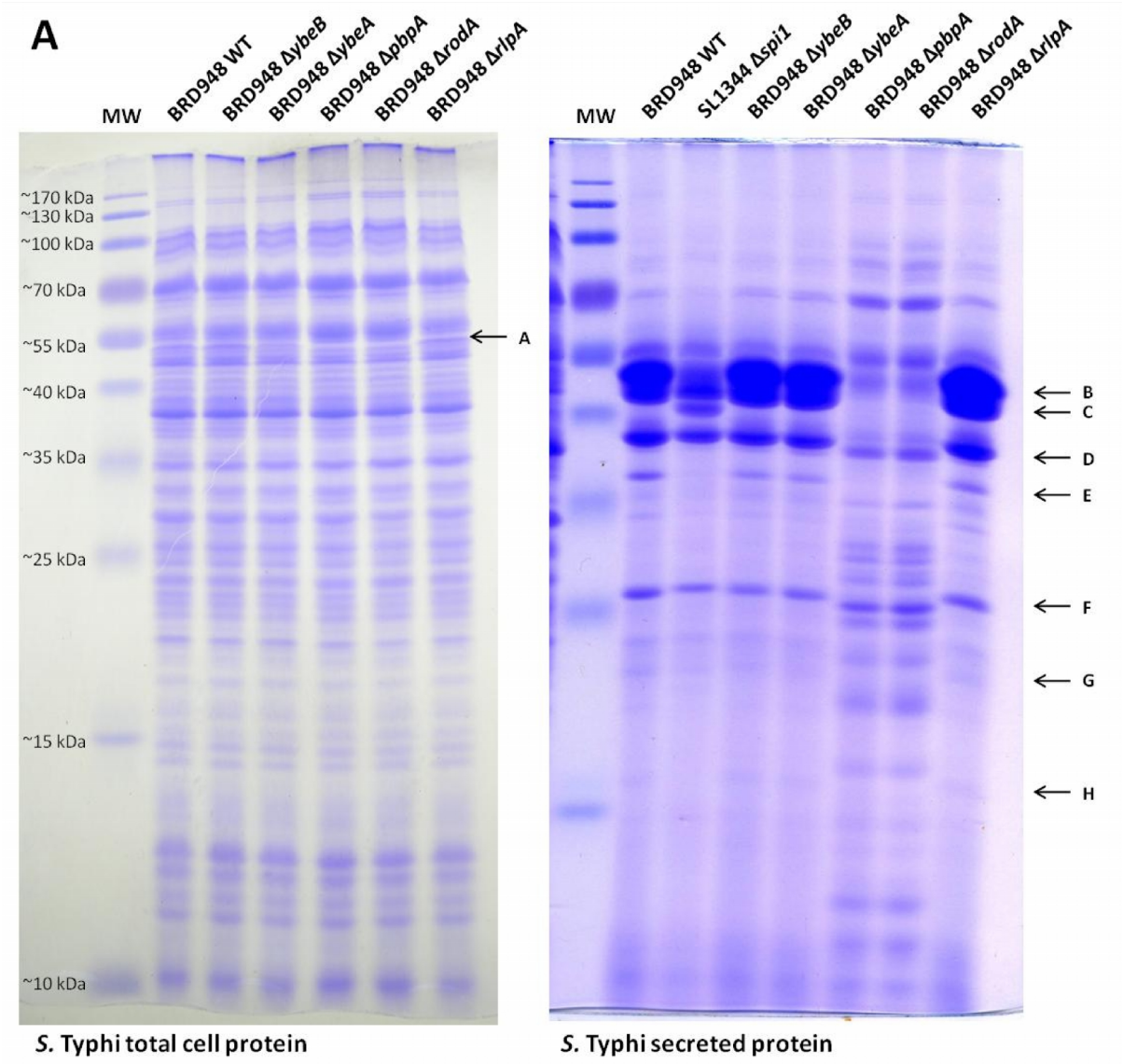

B

Protein Band	Protein Identity**
A	FliC[#] (~53.28 kDa)
B	FliC* (~53.28 kDa)
C	SipC* (~43.09 kDa)
D	SopD* (t2846[†]) (~36.16 kDa)
E	SipD* (~36.56 kDa)
F	SopE* (t4303[†]) (~26.69 kDa)
G	?
H	?

[#]Protein identity based upon identification by peptide mass fingerprinting

* Putative protein identity based upon protein size and published information on abundant *Salmonella* SPI-1 secreted effectors/flagella proteins (354, 355)

**Protein molecular weights estimated based upon calculations from amino acid sequence (253, 356)

[†]Effector encoded outside of SPI-1 region of genome (357)

Figure 5.7: Global protein expression in wild-type and mrd operon mutants of S. Typhi: A - Total and secreted protein profiles of BRD948 wild-type and *mrd* mutants grown in flagella/SPI-1-inducing conditions (LB nutrient rich conditions). SL1344 Δ*spi1* secreted protein profile included as negative control. Protein molecular weight (MW) marker sizes as indicated. Arrows indicate differentially expressed proteins between wild-type and round-cell *mrd* mutant strains. B - Putative identities of differentially expressed proteins based on molecular weight or peptide mass fingerprinting identification, as indicated by arrows in A.

The total cell protein profiles of BRD948 wild-type and *mrd* mutant strains appeared largely identical. The one exception seen in both Δ*pbpA* and Δ*rodA* lanes was the absence of a protein of approximately 50 kDa in molecular weight (arrow A) (Figure 5.7 A). Excision of this band from the lanes of both the wild-type and other rod-shaped *mrd* mutants, followed by peptide mass fingerprinting protein sequencing (done by Pinnacle, Newcastle University) revealed that the protein was the Typhi flagellin protein, FliC. Flagellin is one of the most abundantly expressed secreted proteins in *Salmonella* (358). The absence of FliC from total cell protein fractions of round-cell *mrd* mutants was echoed in secreted protein profiles where the strong bands, which are likely to be flagellin (arrow B), were missing from these strains (Figure 5.7 A).

Whilst the secreted protein profiles of Δ*ybeB*, Δ*ybeA* and Δ*rlpA* mutant strains appeared very similar to the wild-type, stark differences were seen in the profiles of round-cell Δ*pbpA* and Δ*rodA* mutants. Perhaps most notably was the presence of a large number of proteins in secreted protein fractions of Δ*pbpA* and Δ*rodA* cells, compared to wild-type cells. This is indicative of significant cell lysis in round-cell mutants, as observed previously (Chapter 4.3) (130), with the subsequent release into the culture supernatant of ordinarily non-secreted cytoplasmic proteins.

Several major secreted proteins, as indicated by the secreted protein profiles of the other strains, were also missing from the round-cell mutants (labelled arrows B to H). Whilst the most highly expressed of these proteins (arrow B) is likely to be the FliC protein, several other proteins are likely to encompass major SPI-1 effector proteins, since western blot analysis has shown that SPI-1 effectors, including SipA, SipC, and SipD, are not expressed by round-cell *mrd* mutant strains. SPI-1 effector proteins are normally highly expressed (358). Comparisons with both wild-type and Δ*spi1* secreted protein profiles, along with published

information on the major SPI-1 secreted effector proteins of *Salmonella*, enabled attempts to be made at identifying these proteins (Figure 5.7 B) (253, 354-357). Surprisingly, the higher molecular weight SPI-1 effectors (>55 kDa), including the most abundantly expressed SPI-1 effector, SipA, were not clearly distinguishable in any profile (354). However, lower molecular weight effectors, SipC and SipD are likely candidates for bands indicated by arrows C and E respectively, since they were absent from both Δ*spi1* and round-cell mutant lanes. Other putative effectors which were absent from the Δ*pbpA* and Δ*rodA* mutants may include SopD and SopE (arrows D and F). These proteins appeared in the Δ*spi1* profile, although SopD and SopE are both encoded outside of SPI-1, so it is possible that they were secreted independently of SPI-1 in the Δ*spi1* mutant, if indeed these proteins were SopD and SopE. Protein identification by peptide mass fingerprinting is required to unequivocally identify the proteins of interest. In addition, further two-dimensional SDS-PAGE assays would be needed for the comprehensive analysis of the proteomes of the *mrd* mutant strains.

5.5 SPI-2 type 3 secretion system (T3SS) functionality in *S.* Typhi *mrd* operon mutants

5.5.1 Preparation of strains for analysis of SPI-2 functionality

In order to test the functionality of the SPI-2 T3SS in BRD948 *mrd* mutants, strains were cultured in M5.8 minimal medium, which has been shown to induce expression of the SPI-2 genes, somewhat resembling conditions inside the macrophage *Salmonella*-containing vacuole (SCV). SPI-2 gene expression is thought to be induced by a number of factors, including an acidic pH and possibly a low magnesium concentration (90, 359). As such, cultures grown in SPI-2-inducing conditions were not supplemented with additional magnesium.

BRD948 wild-type and *mrd* mutant strains, as well as a SL1344 Δ*ssaV* SPI-2 non-secreting strain (360) (as negative control) were transformed with the pWSK-*sseJ*2HA expression plasmid. This was kindly given by David Holden (Imperial College London, UK) and encodes the SPI-2 effector protein SseJ conjugated to a double haemagluttinin epitope tag. SseJ-2HA is expressed under the control of its

own promoter (244). Strains expressing pWSK-*sseJ*2HA were cultured overnight in SPI-2-inducing conditions. From these cultures secreted protein fractions were prepared for analysis by SDS-PAGE and western blotting. Western blots were labelled with antibody specific for the haemagluttinin tag of the SseJ-2HA protein to assess expression of the SseJ effector protein.

5.5.2 Western blotting and immunofluorescence microscopy with SPI-2 effector protein and translocon antibodies

The western blot of secreted protein fractions from BRD948 wild-type and *mrd* mutant strains showed that SseJ was expressed and secreted in all *mrd* mutants, including the round-cell Δ*pbpA* and Δ*rodA* mutants (Figure 5.8 A). In wild-type cells, SPI-2 effectors are only secreted upon assembly of the needle complex; therefore the secretion of SseJ suggests that the SPI-2 T3SS may be functional (24). However, it has previously been demonstrated that round-cell mutants are liable to cell lysis. It could therefore be argued that the presence of SseJ-2HA within the culture supernatant was the result of lysis of Δ*pbpA* and Δ*rodA* cells rather than active secretion through the SPI-2 T3SS needle, particularly as SPI-2 effector protein expression is not dependent upon needle assembly (361). To test this, parent BRD948 wild-type and *mrd* mutant strains were cultured in SPI-2-inducing conditions. Cells were fixed and labelled with a polyclonal antibody specific for SseB, a SPI-2-encoded secreted effector protein, which forms part of the translocon component of the SPI-2 needle (228, 360). After labelling with a secondary fluorophore-conjugated antibody, cells were visualised by epifluorescence microscopy to look for the presence of cell surface SPI-2 T3SS needles.

Fluorescent foci, indicative of SPI-2 needles, were visible on the surface of all BRD948 strains, including Δ*pbpA* and Δ*rodA* cells, but were absent from negative control SL1344 Δ*ssaV* cells (Figure 5.8 B). The visualisation of cell surface SPI-2 needles provides evidence that unlike SPI-1, the SPI-2 T3SS remains actively expressed and functional in all *mrd* mutants. Immunofluorescence microscopy of α-SseB-labelled cells also demonstrated that SPI-2 T3SSs exhibit a polar

localisation, in contrast to SPI-1 T3SS which appeared to localise all around the lateral cell wall (Figure 5.5 B and 5.8 B).

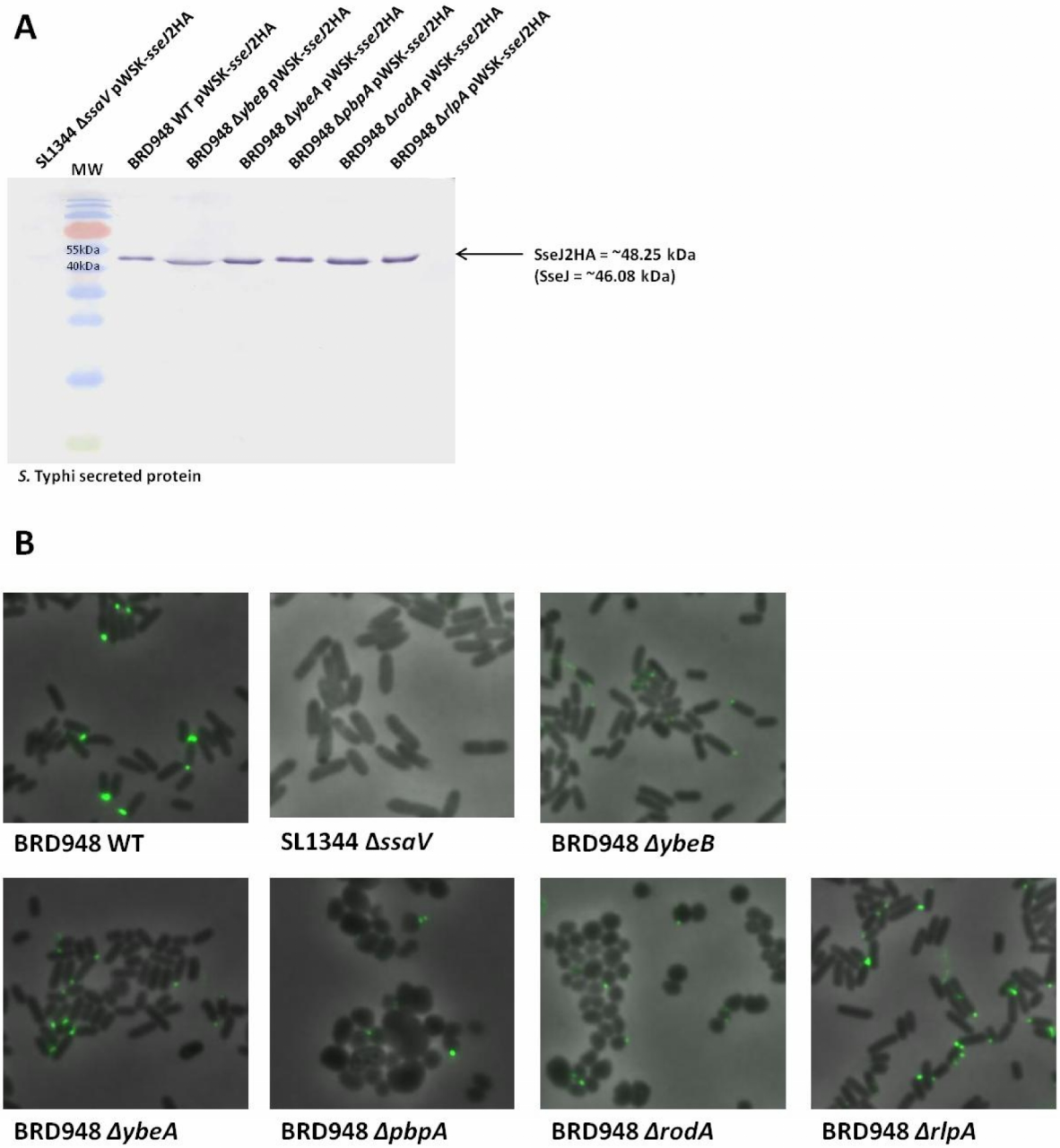

Figure 5.8: SPI-2 functionality in wild-type and mrd operon mutants of S. Typhi: A - Western blot of secreted protein fractions of BRD948 wild-type (WT) and *mrd* mutant strains expressing plasmid-encoded double haemagluttinin-tagged SseJ (pWSK-*sseJ*2HA) SPI-2 effector protein. SL1344 Δ*ssaV* expressing pWSK-*sseJ*2HA used as negative control. Δ*ssaV* mutants are attenuated and do not secrete SPI-2 effectors (27). SseJ-2HA expressed under the control of its natural promoter. B - Immunofluorescence microscopy images of *S.* Typhi BRD948 wild-type (WT) and *mrd* mutants, and SL1344 Δ*ssaV* cells overlaid onto phase contrast images; samples labelled with anti-SseB antibody and fluorophore-conjugated secondary antibody. All images are to the same scale. All cultures grown in SPI-2 inducing M5.8 media at 37°C, and 200 rpm, for 16 hours.

5.5.3 Total cell protein and secreted protein profiles of *S.* Typhi *mrd* mutant strains in SPI-2-inducing growth conditions

Global protein expression in BRD948 wild-type and *mrd* operon mutant strains was assessed in SPI-2-inducing conditions by separating both total cell protein and secreted protein preparations from each strain by SDS-PAGE. Proteins were separated by electrophoresis on 12% gels and then stained using Coomassie® Brilliant Blue dye.

Total protein profiles for both wild-type and *mrd* mutant strains grown in SPI-1 and SPI-2 conditions did not appear vastly different (Figure 5.7 and Figure 5.9). Likewise there were no apparent differences in total cell protein profiles between the wild-type and mutants grown in SPI-2-inducing conditions.

Whilst flagellin and SPI-1 effector proteins were highly expressed in SPI-1 secreted protein profiles, the equivalent protein bands were not clearly visible in SPI-2 secreted protein profiles. This was particularly noticeable with differences in flagellin expression. This demonstrates the differences in secreted protein expression in different growth conditions. Flagella and SPI-1 systems are generally differentially expressed to the SPI-2 T3SS (4, 90). Many global regulators responsible for SPI-1, SPI-2 and flagella gene expression are known to stimulate expression of one, whilst repressing expression of the other. This enables *Salmonella* to respond to the gut environment and express invasion-associated SPI-1 and flagella systems, and conversely to suppress invasion-associated genes in the relatively nutrient-starved intracellular niche whilst activating SPI-2 to aid with intracellular survival (90, 96, 98).

Unlike observations in SPI-1 inducing conditions, comparisons between the secreted protein profiles of wild-type and *mrd* mutant strains grown in SPI-2-inducing conditions did not reveal significant changes in protein expression between strains (Figure 5.9). Minor differences were apparent, possibly due to experimental error, with differences in the total amounts of protein loaded onto the gel (despite standardising protein preparations by OD600) rather than due to alterations in the expression of individual proteins. Surprisingly, the round-cell

Δ*pbpA* and Δ*rodA* mutant secreted protein profiles also appeared similar to the wild-type strain. Furthermore, significant cell lysis was apparent from Δ*pbpA* and Δ*rodA* mutants grown in SPI-1-inducing conditions, but not in SPI-2 secreted protein profiles.

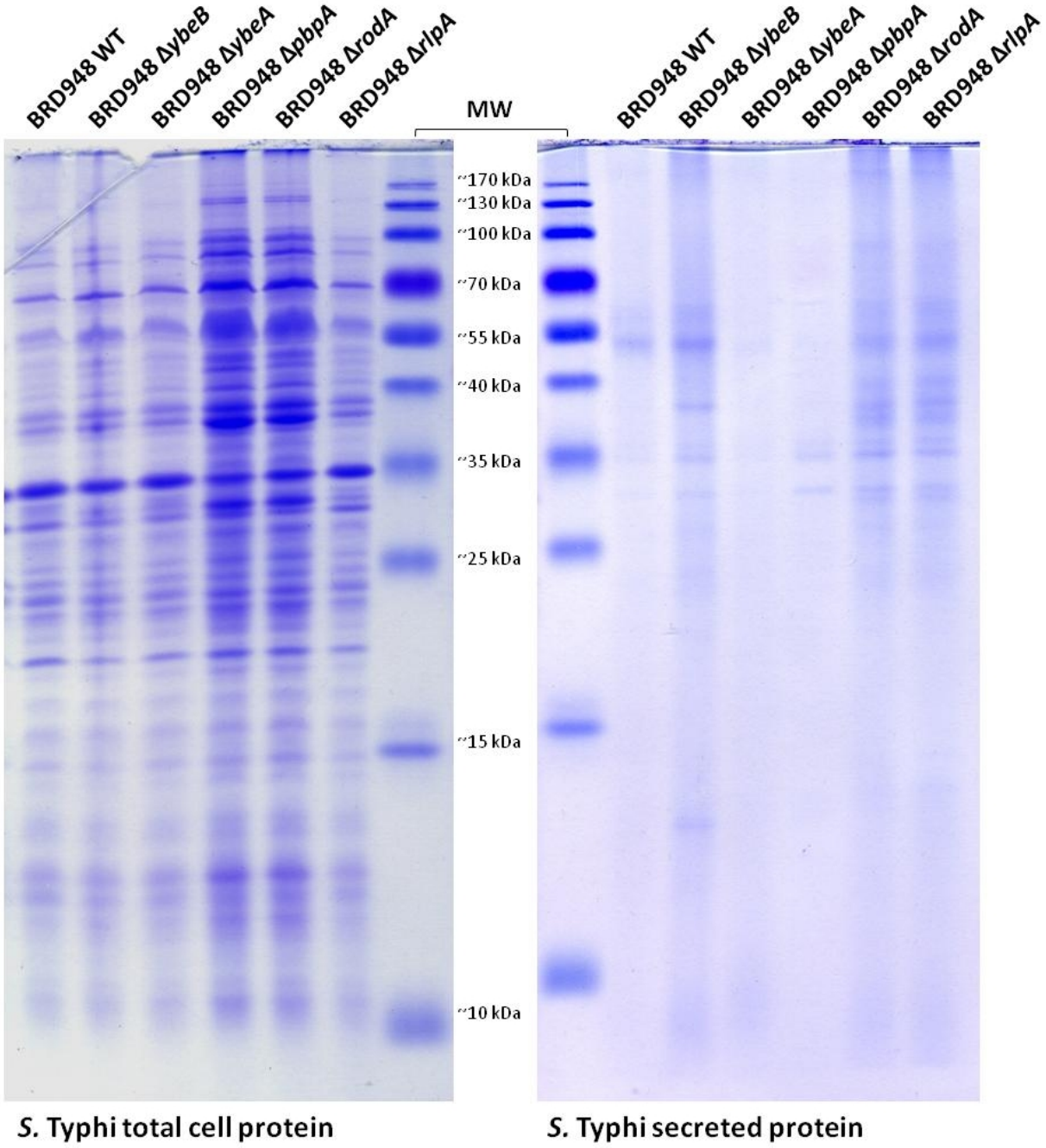

Figure 5.9: Global protein expression in wild-type and *mrd* operon mutants of *S.* Typhi in SPI-2-inducing conditions: Total and secreted protein profiles of BRD948 wild-type and *mrd* mutants grown in SPI-2-inducing M5.8 minimal medium. Protein molecular weight (MW) marker and sizes as indicated. All cultures grown in SPI-2 inducing M5.8 media (+ aro/tyr mix) at 37°C and 200 rpm, for 16 hours.

5.6 Vi antigen capsule expression in *S.* Typhi *mrd* operon mutants

5.6.1 Serum agglutination assays and immunofluorescence microscopy assays

Expression of the extracellular Vi antigen capsule was analysed in both wild-type and *mrd* mutant BRD948 strains by means of serum agglutination assays. Briefly, several microlitres of mid-log phase cultures were mixed with equal volumes of PBS and Vi antigen-typing agglutinating antisera on a clean microscope slide. After incubation for around 5 minutes at room temperature, slides were observed for signs of cell agglutination, which is indicative of Vi capsule expression. Slide agglutination assays were performed in parallel with wild-type and mutant BRD948 cells, as well as *S.* Typhimurium SL1344 cultures as a negative control. Extensive agglutination was observed in wild-type, Δ*ybeB*, Δ*ybeA*, Δ*pbpA* and Δ*rodA* BRD948 strains, but not in the SL1344 control, indicating that the Vi capsule is actively expressed in all BRD948 strains (Figure 5.10 A). Previous data has shown that Vi capsule expression is active in BRD948 Δ*rlpA* cells (163). Although this technique provides qualitative rather than quantitative data, Δ*pbpA* and Δ*rodA* cells appeared to agglutinate more quickly than other mutants or the wild-type, also forming larger clumps of cells. This may suggest that the Vi capsule is overexpressed in round-cell mutants, although further investigation is needed to verify this.

Alongside slide agglutination assays, immunofluorescence microscopy assays were done to visualise Vi capsule expression in each strain and examine whether the excess clumping of Δ*pbpA* and Δ*rodA* cells was due to visible Vi capsule overexpression. BRD948 wild-type/*mrd* mutant and SL1344 cultures were harvested after 5 hours' growth, fixed in 4% PFA and labelled with Vi-typing serum, followed by a fluorophore-conjugated secondary antibody. Samples were then visualised by epifluorescence microscopy. The resulting images of wild-type and *mrd* mutant cells clearly show Vi capsule expression around the periphery of both wild-type and mutant cells, but absent from SL1344 cells (Figure 5.10 B). Particularly bright fluorescent signals could be seen around the periphery of some, but not all Δ*pbpA* and Δ*rodA* cells, although overall there appeared not to be any

obvious Vi capsule overexpression in these cells compared to the wild-type (Figure 5.10 B).

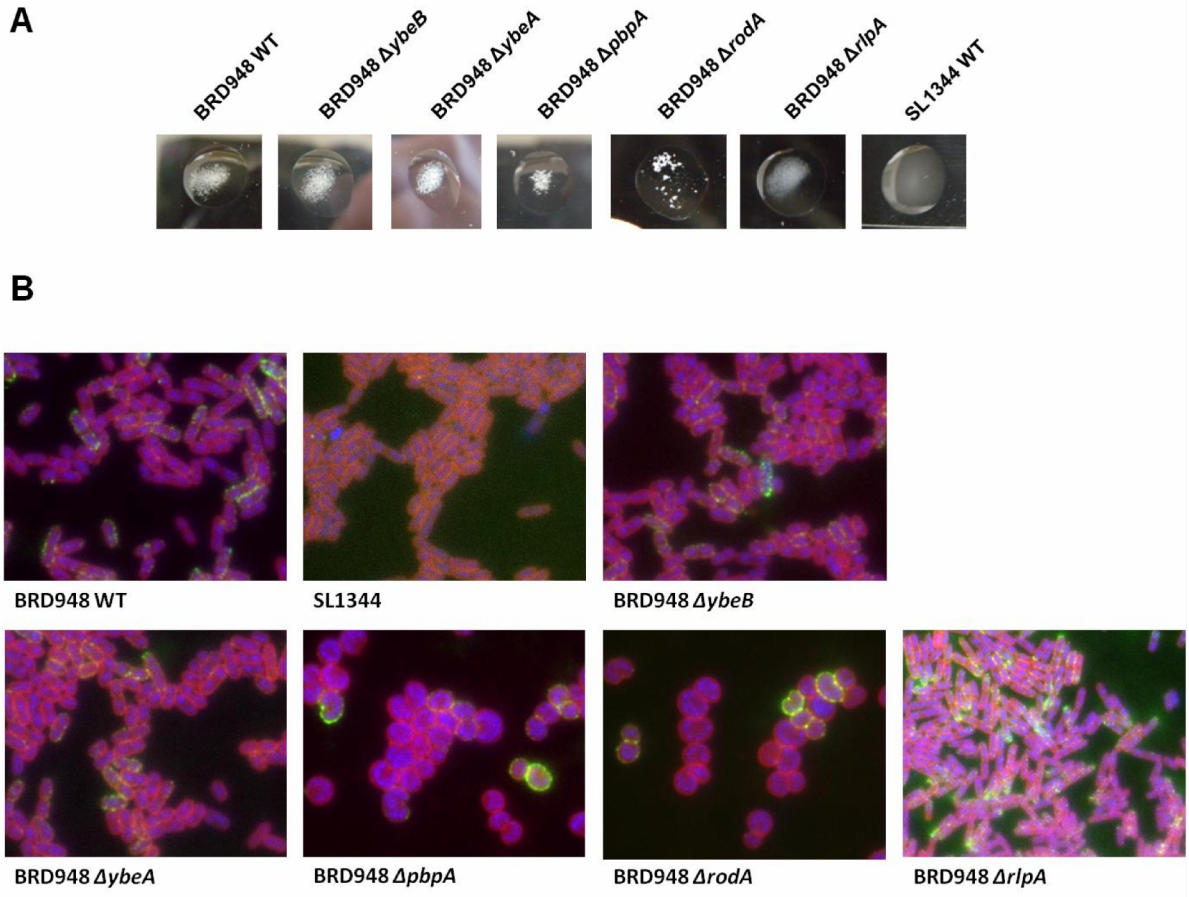

Figure 5.10: Vi antigen expression in wild-type and mrd mutant strains of S. Typhi: A - Slide agglutination assays with BRD948 wild-type (WT), *mrd* mutant strains and *S.* Typhimurium (SL1344) as negative control; Vi capsule-agglutinating antisera incubated with small culture volumes for 5-10 minutes and photographed. Images show signs of agglutination (cell clumping) for all BRD948 strains, but not for SL1344 (negative control), where cells remained evenly suspended. B - Epifluorescence microscopy of *S.* Typhi wild-type (WT) and *mrd* mutant cells fixed and labelled with Vi-agglutinating serum and a fluorophore conjugated secondary antibody to enable visualisation of the cell surface Vi capsule by immunofluorescence microscopy. Vi capsule shown by bright green signal around cell peripheries. Cells labelled with DAPI DNA stain (blue) and Nile Red membrane stain (red). All images are to the same scale.

5.7 Assessment of virulence of round-cell *mrd* operon mutants *in vivo*

Assays to investigate virulence factor functionality of each of the *mrd* operon mutants *in vitro* have demonstrated that in the round-cell Δ*pbpA* and Δ*rodA S.* Typhi mutants, SPI-1 and motility were completely inactive, whilst the SPI-2 T3SS remained actively expressed on the surface of these cells. These results do not necessarily correlate to actual virulence *in vivo*, where the situation is much more

complex. It was therefore important to test whether Δ*pbpA* and Δ*rodA* mutants remained virulent *in vivo*, given that SPI-2 remained active. The virulence of *S.* Typhimurium Δ*pbpA* and Δ*rodA* mutants was therefore investigated in the mouse model. These assays were kindly carried out by Andrew Grant (University of Cambridge, UK), as previously described (Chapter 2.2.28). Previous work has shown that the SPI-1, motility and SPI-2 phenotypes are identical in *S.* Typhi and *S.* Typhimurium round-cell mutants (unpublished data from this lab) (163). As such, *S.* Typhimurium strains were used in these assays, since *S.* Typhi is human-specific. *S.* Typhimurium infections of mice form a useful model for typhoid fever (12, 250).

Since SPI-1 is essential in the early stages of *Salmonella* infection for penetration of the gut epithelia, and is known to be repressed in these mutants, wild-type cells and Δ*pbpA* and Δ*rodA* mutants of *S.* Typhimurium were inoculated intravenously rather than orally, to bypass SPI-1 and test for SPI-2-mediated virulence (4). Growth of each strain *in vivo* was measured by recovering bacteria from the livers and spleens of infected mice. Viable counts (CFU counts) were performed to determine the bacterial load in each organ at 6 hours, 24 hours, 72 hours, 6 days, 14 days and 28 days post-infection. The results show the average counts (log_{10} CFU/organ) from 4 mice (Figure 5.11).

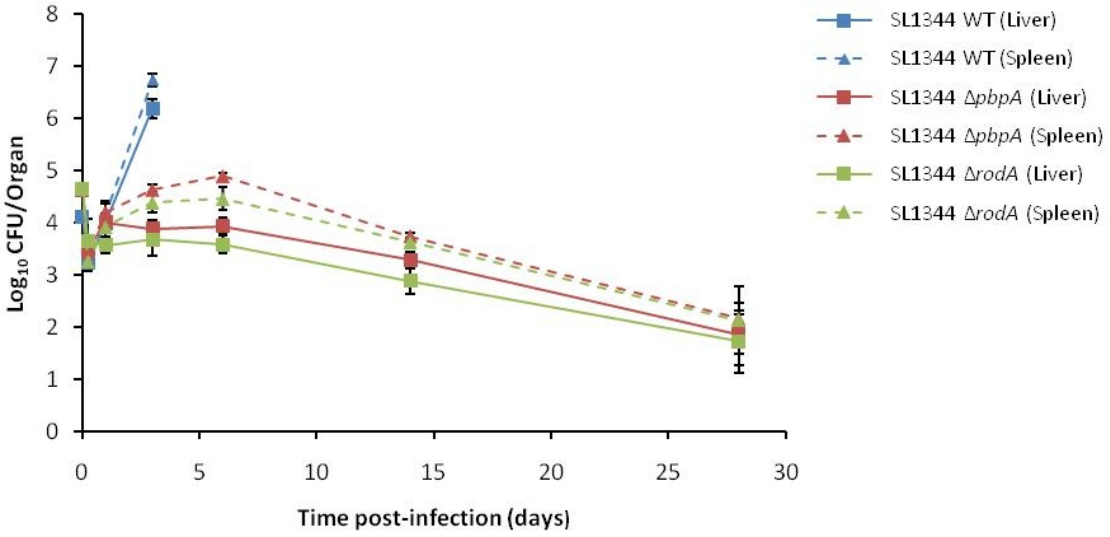

Figure 5.11 Virulence of S. Typhimurium ΔpbpA and ΔrodA in vivo: Mice were inoculated intravenously with 10^4 SL1344 wild-type (WT)/Δ*pbpA*/Δ*rodA* cells. Viable counts were performed 6 hours, 24 hours, 72 hours, 6 days, 14 days and 28 days post-infection to determine bacterial load for each strain in the liver and spleen. Mice infected

with wild-type SL1344 were euthanised at day 3. Results show average bacterial liver/spleen loads from 4 mice. Standard deviation indicated by error bars.

Viable counts showing average liver and spleen bacterial loads demonstrated that the Δ*pbpA* and Δ*rodA* mutants of *S.* Typhimurium were highly attenuated *in vivo.* After an initial kill, wild-type bacterial loads dramatically increased over 3 days. Similarly Δ*pbpA* and Δ*rodA* cells experienced an initial kill, followed by a slow recovery in cell numbers over 6 days, and a subsequent steady decline in bacterial load in both the liver and spleen (Figure 5.11). However, the mice were not able to kill the Δ*pbpA* and Δ*rodA* strains over the 28 days, suggesting that although significantly attenuated compared to the wild-type, these mutants were not completely avirulent. Intracellular survival and systemic spread is dependent upon SPI-2, and the SPI-1-dependent stages of infection were bypassed with intravenous injection of the bacteria. The observed attenuation therefore would be at the level of SPI-2 or related genes. The apparent attenuation of Δ*pbpA* and Δ*rodA* cells is therefore surprising, given that SPI-2 expression is active in round-cell *mrd* mutants. Interestingly, similar *in vivo* virulence assays with an *S.* Typhimurium Δ*mreCD* mutant showed very different results (368). In contrast to Δ*pbpA* and Δ*rodA* mutants, Δ*mreCD* bacterial loads gradually increased over 9 days, after an initial kill, until they reached lethal levels. This is the first instance where phenotypic differences have been observed between Δ*mre* and Δ*mrd* operon round-cell mutants. The reason for the increased attenuation in the Δ*pbpA* and Δ*rodA* mutants is unknown.

S. Typhimurium Δ*pbpA* and Δ*rodA* cells recovered from the livers and spleens of infected mice at 6, 14 and 28 days post-infection, were examined by microscopy, which showed no distinguishable differences between these and the pre-infection *S.* Typhimurium Δ*pbpA* and Δ*rodA* strains.

5.8 Discussion

Whilst investigating the factors which contribute to cell wall synthesis and cell shape determination, very few studies have considered the effects of these proteins on the assembly and functioning of large cell wall-spanning organelles, particularly those involved in virulence (215, 222). It is not known to what extent

the ability of flagella, pili and T3SSs to assemble and function is dependent upon cell shape determinant proteins and the integrity of the peptidoglycan cell wall. Many cell wall-spanning multi-protein complexes physically associate with the peptidoglycan layer in a manner which may be important for their assembly and stability (49, 63). Also, the bacterial cytoskeletal proteins are thought to specifically position synthetic complexes within the cell wall; it is therefore possible that they are involved in positioning other integral cell wall complexes, including virulence organelles, which are known to be specifically localised within *Salmonella* cells (222). Flagella are spread diffusely across the whole cell surface, as are SPI-1 type three secretion needles, whilst SPI-2 T3S needles have a polar localisation (Figure 5.4, 5.5, and 5.8) (54, 224, 226-228).

One of the major aims of this study was to investigate the ability of *mrd* operon mutants, and particularly Δ*pbpA* and Δ*rodA* mutants, to express and assemble functional virulence organelles including flagella and T3SS protein complexes.

5.8.1 Motility of *mrd* operon mutants of *S.* Typhi

A number of screens were utilised to assess both motility and flagella gene expression in each of the *mrd* operon mutants. Initial observations suggested that the round-cell Δ*pbpA* and Δ*rodA* mutants were non-motile, whilst the Δ*ybeB* and Δ*ybeA* mutants appeared motile under the microscope. Δ*rlpA* mutants of *S.* Typhi were known to remain motile from previous work (163). These observations were supported by both motility assays and immunofluorescence microscopy which showed that round-cell *S.* Typhi *mrd* operon mutants were completely non-motile, with the vast majority of cells lacking visible flagella. Total protein and secreted protein profiles of wild-type and *mrd* mutant strains grown in nutrient-rich conditions also demonstrated that flagellin expression was lost in Δ*pbpA* and Δ*rodA* strains (362). By comparison flagella expression and motility was largely unaffected in the other *mrd* operon mutants.

Complementation of Δ*pbpA* and Δ*rodA* mutants with the PBP2-YFP and RodA-YFP-expressing plasmids, pVP6 and pVP3 respectively, was sufficient to restore between 50% and 80% motility to these mutants, verifying that the observed

motility phenotypes are directly due to the inactivation of *pbpA* or *rodA* in these strains. Motility (and rod-shape) was restored in complemented cells grown without the addition of IPTG to induce overexpression of the YFP-fusion proteins, suggesting that low level background expression of these proteins was enough to cause both shape and motility to recover.

The heterogeneity of YFP-fusion protein expression, with morphological defects resulting from the loss of, or the overexpression of either PBP2-YFP or RodA-YFP, was observed previously in Δ*pbpA* and Δ*rodA* cells (Figure 4.3 and 4.5). Likewise, the lack of full motility recovery may be due to heterogeneous YFP-fusion protein expression between individual cells, whereby varying PBP2-YFP or RodA-YFP levels between cells affect morphology and consequently motility expression.

Thus, motility defects seen in this work were shown to be associated with a loss of cell shape. However, it remained to be shown whether or not the loss of motility was a direct result of the inactivation of *pbpA* or *rodA*, whereby the cell wall defects associated with a loss of function of lateral cell wall synthesis resulted in the direct dysfunction and perhaps disassembly of the flagella. If this were the case, one would expect the loss of rod shape to be quickly followed by a drop in motility function.

To test this, the motility of both wild-type and rod-shaped *mrd* mutant strains in the presence of varying concentrations of mecillinam was assessed. Mecillinam specifically binds PBP2, inhibiting its function and resulting in the formation of spherical cells, which appear identical to Δ*pbpA* mutants (145, 155, 363). These assays showed that exposure of all strains to increasing mecillinam concentrations was coupled with a reduction in motility. However, microscopic analysis demonstrated that at concentrations of mecillinam sufficient to render cells completely spherical, significant amounts of motility (~60%) were still retained. There was evidently a delay between the formation of spherical cells and the loss of motility, which may result from the active repression of motility in these cells, rather than an immediate loss in functionality from the formation of round cells.

The nature of the observed repression of motility was analysed in transcriptional reporter assays to assess flagella gene expression in the *mrd* operon mutants. As expected, flagella gene expression was as wild-type in Δ*ybeB*, Δ*ybeA* and Δ*rlpA* mutants. However, expression of both the class II *fliF* gene, and the *flhDC* master flagellar gene regulator was almost completely repressed in both Δ*pbpA* and Δ*rodA* mutants of *S.* Typhi. Since flagella gene expression and motility are dependent upon the expression of the *flhDC* operon, these results demonstrate that the motility phenotype of the round-cell *mrd* mutants resulted at least in part from the complete downregulation of flagella gene expression, at the level of *flhDC* (364). This is in agreement with a previous study, in which it was found that *flhDC* expression was decreased in *E. coli* cells treated with mecillinam (118).

Although mecillinam-treated spherical cells of *S.* Typhi were isolated which remained motile, further work is necessary to determine both whether motility can be recovered in round-cell mutants of *S.* Typhi and also why the flagella genes are completely repressed in these mutants.

5.8.2 SPI-1 and SPI-2 type 3 secretion system (T3SS) expression and functionality in *mrd* operon mutants of *S.* Typhi

It was evident from western blot data that the expression of both SPI-1 and SPI-2 effector proteins were unaffected in Δ*ybeB*, Δ*ybeA* and Δ*rlpA* (the latter mutant having been assessed in previous work (163)). In addition, SPI-2 effector protein expression was unaffected in Δ*pbpA* and Δ*rodA* mutants.

Expression of the SPI-1 and SPI-2 secreted effector proteins themselves was not sufficient to prove that the T3SS needle complexes were correctly assembled and functional in either wild-type or mutant cells. Unlike flagella assembly, which is sequentially regulated so that the flagellin proteins are only expressed upon completion of the basal body and hook assembly, SPI-1 gene expression appears to be not so tightly regulated, since the *hilA* master regulator directly regulates expression of both the SPI-1 T3SS apparatus proteins and the effector proteins, as well as indirectly activating the latter through InvF (62, 84, 86, 365, 366). Expression of SPI-2 effectors may also not be indicative of correct SPI-2 needle

assembly (361). However, various regulatory mechanisms of SPI-1 effector protein expression are thought to exist which enable *Salmonella* to alter the substrate specificity of secretion upon completion of needle assembly and contact with a host cell (84). The visualisation of cell surface-associated translocon subunits through immunofluorescence microscopy afforded better evidence that the T3SS needles were correctly assembled in the cell wall, suggesting that SPI-1 or SPI-2 T3SSs were functional in a particular strain. The translocon component comprises the tip of the T3SS needle, which is required to interact with and form a pore in the host cell membrane, permitting the translocation of other effectors into the host cell (228, 367). In SPI-1 the translocon consists of SPI-1-encoded SipB, SipC, and SipD, effector proteins which are also secreted (351). The SPI-2 translocon consists of the SPI-2-encoded SseB, SseC, and SseD proteins (228).

As such, the presence of both SPI-1 and SPI-2 needles at the cell surface of rod-shaped *mrd* operon mutants and wild-type *S*. Typhi cells suggested that both SPI-1 and SPI-2 were able to assemble and function in these strains. However, only the SPI-2 T3SS appeared to be expressed and functional in round-cell *mrd* operon mutants. SPI-1 effector proteins were not expressed intracellularly, or observed in secreted protein fractions of *S.* Typhi Δ*pbpA* and Δ*rodA* cells, as has been seen previously in a *S.* Typhimurium Δ*rodA* strain (163).

Investigation of SPI-1 gene expression in round-cell mutants of *S.* Typhi showed that, similarly to the motility defect, expression of *hilD*, the master regulator of the SPI-1 genes, was almost completely downregulated in both Δ*pbpA* and Δ*rodA* mutants; this suggests that the primary reason for SPI-1 non-functionality in these cells was the downregulation of SPI-1 expression, since *hilD* is required for SPI-1 gene expression (87-89).

5.8.3 Explanations for the observed virulence phenotypes

The interesting aspect of these results was that despite the downregulation of SPI-1 and motility, the SPI-2 T3SS remained actively expressed and functional in *S.* Typhi Δ*pbpA* and Δ*rodA* cells cultured in SPI-2 conditions. Whilst further work is

needed to establish why SPI-1 and motility expression is repressed yet SPI-2 remains active, there may be several explanations for these observations.

It may be that localisation of these virulence organelles affects functionality; SPI-1 and flagella are spread around the lateral cell wall, whilst SPI-2 needles are localised at cell poles. PBP2 and RodA are involved primarily in lateral cell wall synthesis, whilst polar peptidoglycan synthesis is controlled by a separate septal protein complex (126, 131). Furthermore, polar peptidoglycan is known to be inert once synthesis is completed (127). As such, it may be that in round cell mutants such as Δ*pbpA* and Δ*rodA*, cell wall structure and integrity at the cell poles remains intact. If cell wall integrity is important for the assembly and physical support of structures such as T3SS, it may follow that SPI-2 expression is unaffected in round-cell mutants because the cell wall at the poles remains able to support the SPI-2 T3SS whilst damage to the lateral cell wall may make it unable to support SPI-1/flagella assembly and functionality. Also, if, as previously suggested, the cell shape determinants are involved in directing the localisation of T3SSs and flagella, the SPI-1 and flagella defects may be caused by the disruption of cytoskeletal elements themselves, which regulate organelle localisation. SPI-2, with its polar localisation, may be organised by alternative factors, meaning it is not disrupted in round-cell mutants.

However, these data together demonstrate that the SPI-1 and motility defects of round-cell *mrd* operon mutants are at least primarily the result of SPI-1/motility downregulation at the level of transcription, although downstream features of round-cell mutants which affect SPI-1/flagella assembly and functionality may also play a part in bringing about the observed defects. It may be that an unknown regulatory factor detects lateral cell wall changes in the round-cell mutants and acts to downregulate SPI-1 and motility genes, whilst the same, or an alternative regulator, by a similar mechanism detects that the polar cell walls remain intact and therefore does not downregulate the SPI-2 genes.

The SPI-1 T3SS and flagella of *Salmonella* both comprise invasion-associated systems required for the invasion of host cells. As such, they are often co-regulated by some of the same global regulators in response to similar

environmental conditions, although the mechanisms controlling flagella and SPI-1 expression are not identical or completely understood (50, 362, 369-371). Furthermore, *flhDC* has been shown to positively regulate *hilA* (92). Invasion-associated genes appear to be activated in nutrient rich, aerobic conditions (362). Signals which activate the SPI-2 T3SS, however, are very different; being required for intracellular survival, SPI-2 is activated in response to low osmolarity, acidic pH and possibly low magnesium, all conditions indicative of an intracellular environment (4, 90, 318, 359). As such, the observed downregulation of both the SPI-1 and motility genes, but not SPI-2, in round-cell mutants may be the result of regulation from a common global transcriptional regulator; when activated in response to cell wall defects from the *pbpA*/*rodA* mutations, it may subsequently act to suppress invasion-associated genes, but activate stress-response genes, including those required for intracellular survival such as SPI-2 genes. Several global stress response regulators influence the expression of both SPI-1 and SPI-2 virulence genes, including the PhoP/PhoQ , RcsCDB and OmpR/EnvZ two-component systems (96, 98, 318).

In support of this, the Vi antigen capsule was also actively expressed in *S.* Typhi wild-type and *mrd* operon mutant strains, potentially being upregulated in the Δ*pbpA* and Δ*rodA* cells. Given that cellulose production was also increased in these latter mutants, it is plausible that biosynthesis of other extracellular polysaccharides such as colanic acid is also upregulated (Figure 4.20). Both colanic acid biosynthesis and Vi capsule synthesis, as well as the SPI-2 genes, are known to be upregulated by the RcsC and RcsB global regulators, part of the Rcs phosphorelay system which responds to envelope stress (50, 118).

5.8.4 Virulence of round-cell *mrd* operon mutants of *S.* Typhimurium *in vivo*

In the assessment of virulence determinant functionality in the *mrd* mutants, it was important to assess the actual virulence of these mutants *in vivo*. This was particularly important in round-cell mutants, where *in vitro* assays had demonstrated that virulence was significantly affected. Δ*pbpA* and Δ*rodA* strains of *S.* Typhimurium were inoculated into mice intravenously to determine whether these mutants remained able to both survive intracellularly and spread

systemically, features of infection which are dependent upon SPI-2. However, whilst data from *in vitro* assays suggested that SPI-2 remained active and functional in Δ*pbpA* and Δ*rodA* mutants, *in vivo* assays showed that these mutants were significantly attenuated. This result is in contrast to similar *in vivo* assays with *S.* Typhimurium Δ*mreCD* mutants; these mutants were slightly attenuated but still lethal to the mice, the infection lasting 10 days compared with 4 for the wild-type strain (368). This latter aspect is surprising since until now no significant differences in phenotype have been observed between round-cell *mrd* or *mre* mutants (130).

These results suggest that despite the active expression of SPI-2 in round-cell *mrd* mutants, the inactivation of *pbpA* or *rodA* results in more pronounced defects than those seen in Δ*mreCD* mutants. It is possible that the attenuation in these strains results from more serious perturbations to the cell wall structure which may leave these cells more vulnerable to external stress and host cell defences. However, these mutants did not show decreased resistance to oxidative stress *in vitro*, a feature which is particularly important for intra-macrophage survival. Therefore the increased attenuation of these strains may not be caused by increased sensitivity to killing by the macrophage oxidative burst. Also, the increased cellulose expression in these mutants may help to counteract any cell wall defects, helping protect the cells from external stress. It is possible that the increased surface expression of extracellular polysaccharides such as cellulose or colanic acid may make these mutants more vulnerable to targeting by the host immunity. However, capsular polysaccharides are reportedly poorly immunogenic and colanic acid overexpression may not occur intracellularly (372, 500).

Although SPI-1 and SPI-2 were once thought to act in isolation of each other, recent studies are establishing significant cross-over between the two systems. Several SPI-1-encoded effector proteins persist post-internalisation, and are important for SPI-2 function. It is possible therefore that the downregulation of SPI-1 genes, including those important during the later stages of infection, affects SPI-2 functionality and intracellular survival (4, 20, 48). However, if this were the case, the same attenuation phenotype would be seen in Δ*mreCD* mutant, in which SPI-1 was also downregulated (368).

It is possible that other factors affect SPI-2 expression in the Δ*pbpA* and Δ*rodA* mutants *in vivo*, which are not recognised *in vitro*. The structure of the cell wall and envelope may also be affected in as yet unrecognised ways in Δ*pbpA* and Δ*rodA* mutants, leading to increased killing *in vivo.* Whatever the reasons for the attenuation of the Δ*pbpA* and Δ*rodA* mutants*,* these results demonstrate differences in the downstream effects of *mrd* round-cell mutations compared to Δ*mreCD* mutants, which may suggest that the former genes play a more crucial role in cell wall synthesis and maintenance of the cell wall integrity.

5.8.5 Conclusions

Together these results suggest that virulence is severely affected in round-cell *mrd* operon mutants of *S*. Typhi, but not in Δ*ybeB*, Δ*ybeA* or Δ*rlpA* cells. The effects on virulence in the Δ*pbpA* and Δ*rodA* mutants are surprising, highlighting possible global regulatory pathways which may be activated in these mutants. Further work is needed to establish the identity of these pathways. Also the results of these assays did not definitively identify whether or not Δ*pbpA* and Δ*rodA* mutants could support functional flagella and SPI-1 T3SSs if *hilD* and *flhDC* expression were recovered in these cells. To answer this question would help in understanding more fully the mechanisms behind the motility and SPI-1 defects of round-cell mutants.

Chapter 6. Transcriptional profiling of *mrd* mutants

Transcriptional profiling was done to enable further analysis of the global effects of the Δ*pbpA* and Δ*rodA* mutations on the physiology of *Salmonella*, thus providing a more comprehensive picture of the role these cell shape determinant proteins play in the biology and pathogenicity of *Salmonella*. It was also hoped that microarrays would enable the identification of candidate global regulators involved in the control of the observed phenotypes in round-cell *mrd* operon mutants, such as flagella and SPI-1 gene regulation.

6.1 Microarrays to analyse transcriptional profile of wild-type and Δ*rodA S.* Typhimurium

Microarrays were performed to examine the global differences in gene expression between the wild-type and Δ*rodA* strains of *S.* Typhimurium SL1344. *S.* Typhimurium strains were used rather than *S.* Typhi strains, due to the lack of availability of Typhi-specific arrays at the time. The SL1344 Δ*rodA* strain used in this assay was generated in previous work (163). This was chosen above the Δ*pbpA* strain. As both strains retain the kanamycin resistant knockout cassette, it is likely that both mutations would have polar effects on downstream gene expression. Since *rodA* is downstream of the *pbpA* gene, the polar effects from this mutation are likely to be less pronounced than those from the Δ*pbpA* mutant, enabling results of transcriptional profiling to be more confidently attributed to the specific effects of the Δ*rodA* knockout. However, the results of this assay were treated with some caution; although distinct phenotypes associated with the *rlpA* mutation have yet to be recognised, it is possible that differences in gene expression profiles resulted from indirect effects on *rlpA* expression rather than the inactivation of *rodA*.

NimbleGen 4x72000 multiplex arrays were used as described, enabling the analysis of gene expression in 4504 *S.* Typhimurium genes. Data from the arrays was analysed using the ArrayStar® software and assessed for statistical significance using two-tailed Student's t-test. P values from gene expression data of ≤0.05 were considered statistically significant; thus, the expression data for

1608 genes was significant. Microarray results were examined to investigate the significant effects of the Δ*rodA* mutation on global gene expression and to identify genes with the greatest significant fold-change in expression in Δ*rodA* cells compared to the wild-type. The 100 most upregulated and downregulated genes in the Δ*rodA* mutant, compared to the wild-type, were hence plotted (Figure 6.1). Major alterations in gene expression in a number of distinct features and pathways in *Salmonella* will be discussed.

6.1.1 Analysis of major changes in gene expression between wild-type and Δ*rodA* strains; transcriptional downregulation

The microarray data highlighted numerous large changes in gene expression in the Δ*rodA* mutant, including 435 genes which were significantly downregulated at least 2-fold in Δ*rodA* cells compared to the wild-type. Analysis of just the 100 most downregulated genes revealed a clear pattern in terms of the effects of the Δ*rodA* mutation on the expression of several key classes of genes. The most common functional classes of genes which were affected are now outlined.

Flagella/chemotaxis

Amongst the 100 most highly downregulated genes in the Δ*rodA* mutant were 43 whose function related to motility or chemotaxis (Figure 6.1). Expression of these genes was downregulated at least 15-fold compared to gene expression in the wild-type. Flagella and chemotaxis genes were amongst the most common highly downregulated genes in the whole transcriptional profile, the majority of flagella/chemotaxis-related genes represented in this array being downregulated at least 10-fold (46/66 genes).

The range of flagella and chemotaxis genes represented amongst the most downregulated genes included structural proteins of the flagella basal body, rod and hook sections, as well as the flagellin and flagellar motor proteins and major chemotaxis regulators (Table 6.1). Knowing the hierarchical control of flagella gene expression and its coupling to flagella assembly, it was evident that the expression of both class 2 and class 3 flagella genes was highly downregulated in this mutant. Furthermore, the major transcriptional regulators of class 2 and class

3 genes were significantly downregulated, as well as the flagellar gene master regulator proteins, encoded by *flhD* and *flhC*, although the latter were downregulated to a much lesser extent. The downregulation of *flhDC* would, however, have led to the downregulation of all downstream flagella genes due to the hierarchical flagellar gene regulation (56).

Gene name	*Protein function*	*Fold change in gene expression in SL1344 ΔrodA compared to WT*
Hook and basal body structural proteins		
fliF (stm1969)	IM-spanning MS ring	-10.17
fliM (stm1976)	Cytoplasmic C ring	-22.56
fliN (stm1977)	Cytoplasmic C ring	-18.16
flgB (stm1174)	Rod protein	-21.33
flgI (stm1181)	Periplasmic P ring	-22.79
flgH (stm1180)	L ring	-19.89
fliJ (stm1973)	Rod-capping protein	-31.18
flgE (stm1177)	Hook protein	-16.04
Flagella filament proteins		
fljB (stm2771)	Flagellin filament protein	-72.18
fliC (stm1959)	Flagellin filament protein	-27.93
Flagella motor proteins		
motA (stm1923)	Flagellar motor protein	-28.87
motB (sttm1922)	Flagellar motor protein	-46.54
Flagella transcriptional regulators		
flhD (stm1925)	Class 1 gene. Master regulator of flagellar genes	-6.48
flhC (stm1924.S)	Class 1 gene. Master regulator of flagellar genes	-2.74
fliA (stm1956)	Sigma factor 28 (σ^{28}) – positive transcriptional regulator of class 3 genes	-41.02
flgM (stm1172)	Anti-σ^{28} repressor of class 3 genes	-28.71
fliZ (stm1955)	Activator of class 2 genes through altering $FlhD_2C_2$ promoter binding	-45.69
Chemotaxis proteins		
cheA (stm1921)	Sensor kinase of the CheA/CheB/CheY two-component system to regulate chemotaxis	-49.71
cheB (stm1917)	Part of two-component system to regulate chemotaxis	-61.57
cheY (stm1916)	Part of two-component system to regulate chemotaxis	-40.33
cheW (stm1920)	Part of two-component system to regulate chemotaxis; couples CheA to response regulators	-24.04

Table 6.1: Microarray expression data of major motility and chemotaxis genes in S. Typhimurium ΔrodA: Fold-change in gene expression as compared to wild-type. Unless otherwise stated, P values ≤0.05. Information on gene function taken from KEGG database (253).

SPI-1

The second most common class of genes found amongst the highly downregulated genes in the Δ*rodA* mutant were SPI-1-encoded genes. 38 out of the 43 SPI-1 genes represented were downregulated between 5-fold and 128-fold in this mutant. The two most highly downregulated genes in this array were also the SPI-1 genes stm2883 (*sipD*) and stm2871 (*prgK*) (Figure 6.1, Table 6.2). The SipD protein is a secreted effector protein which forms part of the translocon unit at the tip of the SPI-1 needle, needed to form pores in the host cell membrane. PrgK is a T3SS needle structural protein which together with PrgH forms a peptidoglycan-associated inner membrane-spanning ring (49, 374). SPI-1 genes whose expression was severely downregulated in the Δ*rodA* mutant included those encoding T3SS apparatus proteins, secreted effector proteins and chaperones. Expression of non-SPI-1 encoded secreted effector proteins, such as SopB and SopE2 was also affected, these effectors being downregulated 112.7-fold and 39.5-fold respectively in the Δ*rodA* mutant.

Genes encoding the major transcriptional activators of SPI-1 gene expression, *hilA*, *hilC*, *hilD* and *invF*, were downregulated 75.0-fold, 24.6-fold, 42.8-fold and 68.9-fold respectively, in the Δ*rodA* mutant. Interestingly, expression of the Hil master regulators of SPI-1 appeared to be more radically affected than expression of the *flhDC* flagellar gene regulators. Expression of SPI-1-encoded genes is known to be dependent upon expression of the upstream Hil transcriptional regulators, particularly HilD. Hence, in a similar manner to flagella gene expression, the repression of *hilA, hilC* and *hilD* gene expression would bring about the downregulation of SPI-1 gene expression in the Δ*rodA* mutant (87, 88).

The flagella and SPI-1 microarray expression data was supported by the observations of phenotypic tests, demonstrating that the SPI-1 and motility functionality defects in round-cell *mrd* operon mutants of *Salmonella* were caused by the almost complete downregulation of SPI-1 and flagella genes, brought about by the repression of expression of the upstream transcriptional regulators.

Gene name	*Protein function*	*Fold change in gene expression in SL1344 ΔrodA compared to WT*
SPI-1 T3SS structural proteins		
prgI (stm2873)	Major extracellular T3SS needle rod component	-82.00
invG (stm2898)	Outer membrane T3SS needle apparatus protein	-49.82
prgK (stm2871)	Inner membrane T3SS needle apparatus lipoprotein	-120.83
SPI-1 T3SS secreted effectors		
sipA (stm2882)	SPI-1-encoded T3SS effector; alters host actin polymerisation	-55.62
sipC (stm2884)	SPI-1-encoded T3SS effector; translocon component, alters host actin polymerisation	-33.01
sipD	SPI-1-encoded T3SS effector; translocon component, alters host actin polymerisation	-128.27
sopB (stm1091)	Non-SPI-1 secreted effector; actin filament rearrangement	-112.69
sopE2 (stm1855)	Non-SPI-1 secreted effector; actin filament rearrangement	-39.49
SPI-1 T3SS chaperone proteins		
sicA (stm2886)	SPI-1 chaperone required for effector secretion	-27.59
invB (stm2895)	SPI-1 chaperone required for effector secretion	-92.86
SPI-1 transcriptional regulators		
hilA (stm2876)	Master regulator of SPI-1 gene expression	-75.06
hilC (stm2867)	Activator of HilA to regulate SPI-1 genes	-24.59
hilD (stm2875)	Activator of HilA to regulate SPI-1 genes	-42.85
hilE (stm4509.S)	Repressor of SPI-1 gene expression	-1.29 (P value = 0.18)

Table 6.2: Microarray expression data of major SPI-1 genes in S. Typhimurium ΔrodA: Fold-change in gene expression as compared to wild-type. Unless otherwise stated, P values ≤0.05. Information on gene function taken from KEGG database (253).

SPI-4 and SPI-5

A number of genes from additional horizontally acquired pathogenicity islands, SPI-4 and SPI-5, were represented among the most highly downregulated genes in the SL1344 Δ*rodA* mutant (Figure 6.1). These included the SPI-5-encoded T3SS effector protein, SopB, which is secreted by SPI-1. The other significantly-downregulated SPI-5 gene, *pipC* (stm1090) is possibly encoded within the same operon as *sopB* (stm1091) (Table 6.3). PipC is thought to be a chaperone to SopB, aiding its secretion (375). stm1089, a small gene adjacent to *pipC*, was also significantly downregulated (4.56-fold) in the Δ*rodA* mutant. This gene encodes an

inner membrane protein of unknown function. Expression of the remaining 7 genes of the SPI-5 region of the chromosome, however, was not significantly affected in the Δ*rodA* mutant.

5 of the 8 SPI-4 genes found within this array were downregulated over 19-fold in SL1344 Δ*rodA* compared to the wild-type. Another SPI-4 encoded gene was downregulated 6.31-fold, expression of another gene was unaffected, and the remaining gene was upregulated just over 2-fold in the round-cell mutant (Table 6.3). The SPI-4 pathogenicity island encodes a type 1 secretion system (T1SS) along with an extremely large cognate T1SS-secreted adhesin, SiiE. This island is thought to assist in virulence by helping *Salmonella* to adhere to host gut epithelial cells and promoting the inflammatory response (376). The SPI-4 T1SS apparatus proteins, encoded by stm4259 (*siiC*), stm4260 (*siiD*) and stm4262 (*siiF*), were downregulated 33.0-, 42.2- and 6.3-fold in the Δ*rodA* microarray. The SiiE adhesin (stm4261) was downregulated 33.7-fold. The only upregulated SPI-4 gene was *yjcC* (stm4264), encoding a putative diguanylate cyclase EAL domain protein. Previous studies have shown that SPI-4 genes are co-regulated with the SPI-1 invasion genes and that their expression is regulated by HilA. Hence it is not surprising to find these genes downregulated in the Δ*rodA* mutant (376, 377). It was suggested that SPI-4-mediated adhesion to host cells may be linked to the subsequent functioning of SPI-1 (376).

Gene name	*Fold change in gene expression in SL1344 ΔrodA compared to WT*	*P value (<0.05 = significant)*
SPI-4 genes		
stm4257 (*siiA*)	-19.04	0.009
stm4258 (*siiB*)	-23.21	0.011
stm4259 (*siiC*)	-32.98	0.011
stm4260 (*siiD*)	-42.19	0.010
stm4261 (*siiE*)	-33.72	0.009
stm4262 (*siiF*)	-6.32	0.007
stm4263 (*yjcB*)	+1.14	0.352
stm4264 (*yjcC*)	+2.03	0.020
SPI-5 genes		
stm1096 (*copR*)	+1.13	0.135
stm1095 (*copS*)	-1.02	0.710
stm1094 (*pipD*)	-1.10	0.159
stm1093	+1.87	0.108
stm1092 (*orfX*)	+1.45	0.120
stm1091 (*sopB*)	-112.69	0.007
stm1090 (*pipC*)	-72.43	0.009

stm1089	-4.56	0.011
stm1088 (*pipB*)	-2.44	0.082
stm1087 (*pipA*)	+1.50	0.085

Table 6.3: Microarray expression data of SPI-4 and SPI-5 genes in S. Typhimurium ΔrodA: Fold-change in gene expression as compared to wild-type. P values as stated.

Nitrogen and amino acid metabolism

Interestingly, a significant number of the major downregulated genes were those with functions related to nitrogen metabolism. Transcription of these 8 genes was reduced between 16- and 25-fold in the Δ*rodA* mutant compared to wild-type. The 8 genes were clustered within one of three operons; the *nar*, *nap* or *nrf* operons (Figure 6.1).

Two of the isolated operons, *nar* and *nap*, encode two of the three individual nitrate reductase systems, as identified in *E. coli.* Nitrate reductase complexes are required for anaerobic growth, enabling bacteria to utilise nitrate as a terminal electron acceptor, and these are upregulated in anoxic conditions (378, 379). stm1762 and stm1763 encode the NarJ and NarH proteins respectively. These proteins form part of a membrane-bound heterotrimeric nitrate reductase complex, along with NarI (378, 380). Microarray data showed that stm1762 and stm1763 were downregulated 19.0-fold and 16.3-fold respectively in Δ*rodA*. The seven *nap* operon genes (*napA-H*) encode a periplasmic nitrate reductase complex, of which 4 (*napA-napD*) are essential in *E. coli*. The stm2255 (*napC*), stm2256 (*napB*) and stm2258 (*napG*) genes were downregulated 22.1-, 18.3- and 16.2-fold in the Δ*rodA* mutant, respectively. Similarly, the *nrfA* and *nrfB* genes encode a formate-dependent periplasmic nitrite reductase (378). The *nrf* operon is required for the reduction of nitrite to ammonia (381). The *Salmonella* homologues of *nrfA* (stm4277), *nrfB* (stm4278.S) and *nrfC* (stm4279), were downregulated in the Δ*rodA* mutant 23.1-, 25.6- and 19.7-fold, respectively.

A further 7 major downregulated genes were identified with related functions in the metabolism of lysine or arginine. These were included in three clusters of genes: stm2558 (*cadB*) and stm2559 (*cadA*), stm4465-4467, and stm0700 and stm0701. *cadA* encodes a lysine decarboxylase enzymes, whilst the upstream *cadB* gene encodes a lysine/cadaverine transporter. Expression of these genes is induced by

the presence of lysine combined with an extracellular reduction in pH (pH ≤5.8) (382, 383). The *cad* genes are involved in the acid tolerance response (ATR), which enables *Salmonella* to adapt to and survive in a highly acidic environment (pH ≤3.0) (383).

The stm4465-4467 genes comprise the *arcABC* operon. The *arcA* (stm4467), *arcB* (stm4465) and *arcC* (stm4466) genes encode three enzymes involved in the arginine fermentation pathway. The *arcABC*–encoded proteins are upregulated with growth in anaerobic conditions, permitting arginine to be used as an energy source in the absence of oxygen (379). The results of this array showed that expression of *arcA*, *arcB* and *arcC* was reduced in the Δ*rodA* mutant 73.3-fold, 19.0-fold and 40.2-fold, respectively.

Finally, stm0700 (*potE*) and stm0701 (*speF*) encode a putrescine/ornithine transporter protein and an ornithine decarboxylase, respectively. Similarly to *arcABC*, these genes appear to be involved in the adaptation of *Salmonella* to growth in anoxic conditions. *potE* and *speF* were previously shown to be activated by ArcA in *S.* Typhimurium, the response regulator of the ArcA/ArcB two-component system, an important global transcriptional regulator which responds to changes in oxygen levels and assists with adaptation to anaerobic growth (379, 384). In anaerobic conditions ArcA positively regulates genes involved in anaerobic respiration, as well as flagella genes, and suppresses aerobic respiration (384, 385). Confusingly, this *arcA* (stm4598) is a completely different gene from the stm4467/*arcA* gene (384). The present microarrays showed that *potE* and *speF* were downregulated 27.9-fold and 31.3-fold respectively, in Δ*rodA* cells.

These data show that several major factors involved in the utilisation of alternative carbon sources for anaerobic respiration were strongly repressed in the Δ*rodA* mutant, compared to the wild-type. The reason for the repression of anaerobic respiration genes in this mutant is unknown. FNR is a global regulator involved in detecting and responding to varying oxygen levels. Along with other regulators including the ArcA/ArcB two component system, or in isolation, FNR regulates gene expression to enable *Salmonella* to adapt to anaerobic growth (379, 385,

386). It was also shown to stimulate expression of both flagella and SPI-1 genes (386). Surprisingly, expression of both *fnr* (stm1660.S) and *arcA* (stm4598) in the Δ*rodA* mutant were not particularly affected, being only slightly increased by ~1.2-fold compared to their expression in the wild-type. However, two other transcriptional regulators, NarP and NarL, are also known to be important for controlling the use of nitrate/nitrite in anaerobic respiration (387). Expression of *narP* and *narL* was reduced 3.8-fold and 15.4-fold respectively in the Δ*rodA* mutant, although expression of their cognate sensor kinases was not significantly affected for either protein. The extent to which these regulators affected expression of nitrate utilisation genes is unclear, since NarL is known to repress both *nrf* and *nap* operons, whilst NarP activates these operons (387). It may be that other upstream transcriptional regulators are involved in the suppression of anaerobic respiration-related genes in Δ*rodA* cells.

Type I Fimbrial protein

The microarray data highlighted the stm0543 gene as being highly downregulated in the Δ*rodA* mutant. This gene encodes FimA, a Type I fimbrial major subunit protein (21). Type I fimbriae enable *Salmonella* to adhere to a number of different cell types, and are thought to assist with virulence (389-391). The immediately downstream *fimI* gene was also significantly downregulated in this array, although expression levels for the remaining *fim* operon genes were not significantly altered (Table 6.4). The *fim* operon is required for Type I fimbriae expression (391-393). Theoretically regulators which control the expression of SPI-1 and flagella genes in the Δ*rodA* mutant may also be responsible for the suppression of expression of Type I fimbriae.

fim operon genes	*Fold change in gene expression in SL1344 ΔrodA compared to WT*	*P value (<0.05 = significant)*
stm0543 (*fimA*)	-33.47	0.011
stm0544 (*fimI*)	-7.22	0.014
stm0545 (*fimC*)	-2.18	0.106
stm0546 (*fimD*)	-1.56	0.120
stm0547 (*fimH*)	-1.20	0.399
stm0548 (*fimF*)	-1.10	0.315

Table 6.4: Microarray expression data of fim operon genes in S. Typhimurium ΔrodA: Fold-change in gene expression as compared to wild-type. P values as stated.

stm1328

Of the 100 most highly downregulated genes, the remaining gene not belonging to any of the aforementioned functional classes was stm1328, whose expression was reduced 40.1-fold in the Δ*rodA* mutant, compared to wild-type. stm1328 (*lpxR*) encodes a putative outer membrane calcium-dependent 3'-O-deacylase enzyme, which covalently alters the structure of the Lipid A component of LPS, possibly functioning to assist in the evasion of host immunity (394). The downregulation of this Lipid-A modifying enzyme may bring about alterations in LPS structure in the *rodA* mutant, although it has previously been noted that LpxR-mediated lipid A deacylation is not commonly seen in standard culture conditions (394, 395).

6.1.2 Analysis of major changes in gene expression between wild-type and Δ*rodA* strains; transcriptional upregulation

Comparisons of gene expression between wild-type and Δ*rodA* cells showed that 464 genes were significantly upregulated at least 2-fold in SL1344 Δ*rodA*. As with downregulated genes, the 100 most upregulated genes were analysed. Expression of these genes was increased between 4-fold and 239-fold in SL1344 Δ*rodA*, although the majority of genes were not upregulated more than 50-fold (Figure 6.1). Several particularly prevalent functional classes emerged among the major upregulated genes, as discussed.

Transport proteins

23 genes were identified amongst the major upregulated genes of the Δ*rodA* mutant with functions related to the transport of substrates into or out of the cell, as summarised (Figure 6.1, Table 6.5). The majority of these genes encoded inner membrane transport proteins or components of transport protein complexes. An additional 4 SPI-1 genes, encoding an iron transporter, were also represented in this group (Table 6.8). These changes could illustrate both a significant alteration in the cohort of inner membrane proteins expressed in the round-cell mutant, and/or an increased requirement for the import of specific nutrients from the culture medium.

Transport-related genes	*Protein function*	*Fold change in gene expression in SL1344 ΔrodA compared to WT*
stm2787	Putative tricarboxylic transport inner membrane protein	+30.53
ydhC (stm1428)	Inner membrane transport protein; member of major facilitator superfamily (MFS)	+24.67
yqaE (stm2796)	Putative transport protein	+21.03
cysU stm2443	ABC superfamily inner membrane protein; sulphate/thiosulphate transporter; permease subunit	+19.56
fhuA (stm0191)	Outer membrane ferrichrome transporter protein	+14.96
stm2786	Putative tricarboxylic transport inner membrane protein	+14.80
nanT (stm3338)	MFS family sialic acid transporter	+11.69
nixA (stm2783)	Putative high-affinity nickel transporter	+11.55
cysW (stm2442)	ABC superfamily inner membrane protein; sulphate/thiosulphate transporter; permease subunit	+10.05
stm1494	ABC superfamily osmoprotectant transporter; permease subunit	+9.52
cysP (stm2444)	ABC superfamily inner membrane protein; sulphate/thiosulphate transporter; substrate-binding subunit	+8.97
sapB (stm1693)	ABC superfamily peptide transporter; permease protein	+7.78
sapC (stm1694)	ABC superfamily peptide transporter; permease protein	+7.14
chaA (stm1771)	Calcium/sodium:H^+ antiporter	+6.71
tehA (stm1609)	Potassium-tellurite ethidium and proflavin transporter	+5.80
narU (stm1576)	Inner membrane MFS transporter; nitrate extrusion transporter	+5.80
stm1492	ABC superfamily osmoprotectant transporter; permease subunit	+5.61
stm1491	Proline/glycine betaine transport; osmoprotectant transporter; ATP-binding subunit	+5.24
yjeH (stm4328)	APC super family inner membrane protein; basic amino acid/polyamine antiporter	+5.08
potF (stm0877)	Putrescine ABC transporter; periplasmic substrate-binding protein	+5.01
stm1493	ABC superfamily osmoprotectant transporter; periplasmic substrate-binding subunit	+4.87
exbB (stm3159)	Inner membrane iron-siderophore complex transporter protein	+4.72

Table 6.5: Microarray expression data of major upregulated transporter genes in S. Typhimurium ΔrodA: Fold-change in gene expression as compared to wild-type. Unless otherwise stated, P values ≤0.05. Information on gene function taken from KEGG database (253).

Stress response factors

Perhaps not surprisingly, the second most prevalent functional class of genes among highly upregulated genes were those related to responses to various types of environmental stress in *Salmonella* (Table 6.6, Figure 6.1). These included several heat shock or hyperosmotic shock related proteins, an oxidative stress regulatory protein, DNA repair enzymes, mis-folded protein repair proteins, a putative catalase, and a protease for the degradation of damaged proteins. The concert of stress-related genes identified here demonstrates something of the state of the round-cell mutants; it suggests that as expected, inactivation of cell shape determinants results in a compromised the cell wall structure and barrier function, leaving the mutants more susceptible to a range of environmental stresses, including heat, osmotic and oxidative stress.

Interestingly, the periplasmic protein CpxP encoded by stm4060, along with a similar periplasmic protein (stm1308) were upregulated 14.5-fold and 34.3-fold respectively in the Δ*rodA* mutant. This is unexpected given that CpxP is a repressor of the Cpx envelope stress response (253). The Cpx pathway is one of at least three envelope stress-detecting pathways, encompassing the CpxA/CpxR two-component system. In response to envelope stress and misfolded envelope proteins the CpxR response regulator activates the expression of genes involved in protein folding and protein degradation at the cell envelope (396). CpxP acts through CpxA to suppress the Cpx pathway (396). Little is known about stm1308/*spy*, although it was shown to be regulated directly by PhoP (397). BLAST alignment of the CpxP and Spy amino acid sequences showed that the two proteins have 29% identity with 50% positives in terms of related amino acid residues. The CpxA gene (stm4058), but not CpxR (stm4059), was also upregulated 2.25-fold in the Δ*rodA* mutant.

Another significant gene represented here was *htrA*, which was upregulated over 7-fold in the Δ*rodA* mutant. *htrA* encodes a serine endoprotease which is positively regulated by both RpoE (σ^E) and CpxA/CpxR. *htrA* is essential for both growth at high temperatures and virulence in *Salmonella*; Δ*htrA* mutants are unable to resist the oxidative burst and therefore cannot survive inside macrophages. HtrA

functions to remove mis-folded or damaged proteins by sequestering or degrading them (398).

Stress response-related genes	*Protein function*	*Fold change in gene expression in SL1344 ΔrodA compared to WT*
Heat shock genes		
(stm1251)	Similar to *E. coli* small heat shock protein. Putative molecular chaperone, similar to IbpA.	+15.38
ibpB (stm3808)	Chaperone protein IbpB: IbpA and IbpB protect aggregated proteins from denaturation and degradation	+15.27
ibpA (stm3809.S)	Chaperone protein IbpA	+11.57
htrA (stm0209)	Serine endoprotease Do: Degrades damaged proteins at high temperatures. Required for virulence.	+7.74
dnaJ (stm0013)	Hsp40: Molecular chaperone, prevents aggregation of denatured proteins in response to heat and hyperosmotic stress	+6.59
htpG (stm0487.S)	Hsp90: Molecular chaperone	+6.15
dnaK (stm0012)	Hsp70: Molecular chaperone, helps fold nascent polypeptide chains and re-fold mis-folded proteins	+4.96
Envelope stress-related genes		
spy (stm1308)	Function unknown, although similar to CpxP	+34.33
cpxP (stm4060)	Repressor of Cpx envelope stress pathway via CpxA	+14.51
DNA repair genes		
recN (stm2684)	DNA recombination and repair protein	+7.61
mutM (stm3726)	Formamidopyrimidine-DNA glycosylase; base excision repair of DNA damaged by oxidative stress or mutagens – recognises and removes damaged bases	+4.77
Other putative stress-related genes		
stm0581	Putative regulatory protein involved in resistance to oxidative stress	+19.51
osmB (stm1705)	Osmotically inducible lipoprotein B precursor	+8.11
stm2789	Hypothetical protein, induced by carbon starvation, σ^S-dependent.	+6.88
stm1731	Putative catalase	+5.25

Table 6.6: Microarray expression data of major upregulated genes related to stress responses in S. Typhimurium ΔrodA: Fold-change in gene expression as compared to wild-type. Unless otherwise stated, P values ≤0.05. Information on gene function taken from KEGG database (253).

Colanic acid biosynthesis

A large number of genes involved in colanic acid biosynthesis were significantly upregulated in the Δ*rodA* mutant. 16 genes related to synthesis of the colanic acid capsule were upregulated at least 2-fold whilst 11 were amongst the most upregulated genes in the Δ*rodA* strain, along with another biofilm-related gene (stm1564) (Table 6.7, Figure 6.1). This result was supported by phenotypic assays which showed that both Δ*pbpA* and Δ*rodA* mutants of *S.* Typhi expressed increased amounts of the cellulose polysaccharide capsule. Previous work has also identified mutants in cell shape determinant genes with increased mucoidy, from an increase in colanic acid biosynthesis (323). Treatment with beta-lactam antibiotics has also been shown to induce expression of colanic acid biosynthesis genes in *E. coli* (399). Furthermore, downregulation of the SPI-1 and flagella genes often appears to be associated with an increase in colanic acid capsule expression, regulated by a number of global regulators including the Rcs phosphorelay (RcsCDB), MqsR and the second messenger molecule cyclic diguanylate (c-di-GMP) (318, 400-402).

Colanic acid capsules are integral to mature biofilms, when, as a result of specific environmental conditions, bacteria are induced to form a multicellular state. In these conditions motility is not required, hence motility and colanic acid capsule related genes are inversely regulated (372, 403). The *wca*/*cps* gene cluster is responsible for colanic acid biosynthesis in *E. coli and Salmonella* (399, 404, 405). The products of these genes catalyse the biosynthesis, assembly, translocation and modifications of the colanic acid capsule, and they are essential for capsule expression (399, 405). Many of these genes were highly upregulated in the Δ*rodA* mutant (Table 6.7).

Little is known about the biofilm-related *yddX* gene, although it was induced in *E. coli* during stationary phase growth and its expression was regulated by RpoS (σ^S) (406).

Gene	*Protein function*	*Fold change in gene expression in SL1344 ΔrodA compared to WT*
Colanic acid biosynthesis gene cluster		
gmd (stm2109)	GDP-D-mannose dehydratase, contained within colanic acid biosynthesis cluster	+22.15
wcaD (stm2112)	Putative colanic acid polymerase, essential for colanic acid biosynthesis	+12.34
wcaE (stm2111)	Glycosyl transferase	+12.28
wcaA (stm2115)	Glycosyl transferase	+11.76
wcaG (stm2108)	GDP-fucose synthetase	+11.25
wcaF (stm2110)	Putative colanic acid biosynthesis acetyltransferase	+10.67
cpsG (stm2104)	Phosphomannomutase	+8.64
wcaM (stm2099)	Essential for biofilm formation, may be involved in colanic acid biosynthesis	+7.36
wcaB (stm2114)	Putative colanic acid biosynthesis acetyltransferase	+7.07
wcaL (stm2100)	Putative glycosyl transferase	+6.01
wcaK (stm2101)	Putative pyruvyl transferase	+5.57
Biofilm-related genes		
yddX (stm1564)	Biofilm-dependent modulation protein	+9.30

Table 6.7: Microarray expression data of major upregulated colanic acid biosynthesis genes in S. Typhimurium ΔrodA: Fold-change in gene expression as compared to wild-type. Unless otherwise stated, P values ≤0.05. Information on gene function taken from KEGG database (253).

SPI-1 *sit* operon

In stark contrast to all other SPI-1 genes represented in the microarray, four SPI-1-encoded genes were upregulated between 5.4-fold and 21.5-fold in SL1344 Δ*rodA* (Table 6.8). These genes, stm2861-stm2864, are contained within a distinct operon of SPI-1, and together encode an iron/manganese uptake ABC transporter which is common to SPI-1 in all *S. enterica* serovars. The GC content of this *sit* operon is higher than the rest of SPI-1 and more reminiscent of the rest of the *Salmonella* genome, suggesting that it may have a different origin from the remainder of SPI-1 (407-409). Also unlike other SPI-1 genes, expression of the *sit* genes is induced after uptake into epithelial cells and they are not required for invasion. Furthermore the *sit*-encoded iron transporter is known to assist in virulence *in vivo* (408, 410, 411). Expression of the *sitABCD* genes is repressed by the Fur and MntR transcriptional regulators in response to increasing iron and manganese levels (411).

Gene	*Protein function*	*Fold change in gene expression in SL1344 ΔrodA compared to WT*
sitA (stm2861)	Iron transporter; periplasmic binding protein	+21.51
sitB (stm2862)	Iron transporter; putative ATP-binding protein	+13.13
sitC (stm2863)	Iron transporter; putative integral membrane permease	+20.72
sitD (stm2864)	Iron transporter; putative integral membrane permease	+5.35

Table 6.8: Microarray expression data of upregulated SPI-1 genes in S. Typhimurium ΔrodA: Fold-change in gene expression as compared to wild-type. Unless otherwise stated, P values ≤0.05. Information on gene function taken from KEGG database (253).

The dissimilarity of both the functions and regulation of the *sit* operon genes compared to other SPI-1 genes, may explain why these genes are not downregulated along with the majority of SPI-1-encoded genes in the Δ*rodA* mutant. The reason for the increased expression of these genes in the Δ*rodA* mutant is unknown. Expression of the upstream Fur and MntR regulators was not significantly changed in this mutant, compared to the wild-type.

Outer membrane proteins

4 genes whose expression was increased over 4-fold in the Δ*rodA* mutant encoded integral outer membrane proteins or outer membrane lipoproteins, which did not function as transport proteins (Figure 6.1).

By far the most upregulated gene in this mutant was stm3031, encoding an outer membrane OmpX-like protein; stm3031 was upregulated just over 239-fold in SL1344 Δ*rodA*. Recent studies have implicated stm3031 in resistance to the cephalosporin antibiotic, ceftriaxone. Ceftriaxone-resistant strains expressed increased levels of this protein, whilst Δ*stm3031* mutants had reduced ceftriaxone-resistance (412, 413). Further evidence suggested that stm3031 may be involved in regulating levels of both the multidrug resistance efflux pump protein, AcrD, and the outer membrane porin OmpD; thus overexpression of stm3031 may lead to the increased export of ceftriaxone, along with a decreased permeability to the influx of drugs (412). However, the precise role of OmpX-like protein in *Salmonella* is not known. In *Yersinia pestis* OmpX-like protein, or Ail, is an outer membrane adhesin, required for successful Type III secretion (414, 415).

Outer membrane expression of stm3031 is associated with that of a putative inner membrane transporter encoded by *yjeH*, which may help to export OmpX-like protein (412, 416). Expression of stm3031 may also be regulated by the transcriptional regulator BaeR (413). In the present arrays, *yjeH* (stm4328) expression was increased ~5.1-fold in Δ*rodA* cells, although *baeR* expression was not significantly altered, being reduced ~1.7-fold. Notably, expression of stm3030, the gene immediately downstream of stm3031 encoding a hypothetical protein, was increased 93.0-fold in these arrays.

Like other beta-lactam antibiotics, ceftriaxone inhibits the penicillin-binding proteins, perturbing peptidoglycan synthesis (413, 417). It is possible that the overexpression of OmpX-like protein in the Δ*rodA* mutant is induced in order to protect cells from further cell wall damage, from the action of environmental stresses, drugs, antimicrobial molecules, or host immunity factors, for example.

Aside from OmpX-like protein, 3 putative outer membrane lipoproteins, encoded by stm1254, stm0080 and stm1561 were significantly upregulated in the arrays, 15.5-fold, 6.1-fold and 4.8-fold respectively (Figure 6.1). These significant changes in gene expression in the Δ*rodA*, particularly demonstrated by the vast increase in stm3031 expression, suggest that the outer membrane structure and composition is considerably affected in round-cell mutants. However, expression of the genes encoding two major outer membrane porin proteins, OmpA and OmpC, was not much changed in the Δ*rodA* mutant, although other porin genes *ompF* and *ompW* were downregulated 3.1-fold and 2.3-fold respectively.

SPI-2

Although the vast majority of SPI-2-encoded genes were not represented amidst the highly upregulated classes of genes in the Δ*rodA* mutant, the *ssrA* gene (stm1392), encoding the major regulator of the SPI-2 genes was upregulated ~5.8-fold (Figure 6.1). *ssrA* forms the histidine kinase component of the SsrA/SsrB two-component system, which is essential for the expression of SPI-2-encoded genes (99). *ssrB*, encoding the transcriptional activator, was not significantly upregulated in SL1344 Δ*rodA*, however.

Of the 49 SPI-2 encoded genes within the microarray, 2 genes were downregulated just over 2-fold in SL1344 Δ*rodA*, the expression of 5 genes was changed less than 1.5-fold, 4 genes were upregulated 1.5-2-fold and 5 genes were upregulated over 2-fold in SL1344 Δ*rodA* compared to the wild-type. Expression data for the remaining SPI-2 genes was not statistically significant. From these data it is difficult to gauge whether the expression of SPI-2 genes as a whole was significantly changed in the Δ*rodA* mutant compared to wild-type, although the microarray data echoes the results of phenotypic assays, showing that SPI-2 is clearly not repressed in this mutant. However, microarrays were conducted using RNA from cells grown in nutrient rich SPI-1-inducing medium. Hence it is hard to evaluate the effects on SPI-2 expression in the Δ*rodA* mutant, since SPI-2 is expressed at a low level in these conditions.

SPI-3 and SPI-6

Microarray data showed that of the 11 SPI-3 genes, 3 were significantly upregulated in SL1344 Δ*rodA* (Figure 6.1) (384). These included the co-transcribed stm3763 (*mgtB*) and stm3764 (*mgtC*) genes, which encode a magnesium transporter and a magnesium transport protein respectively. This operon is activated by PhoP/PhoQ in response to low magnesium levels, and is essential for intracellular growth in the macrophage (418, 419). *mgtB* and *mgtC* were upregulated 3.2-fold and 4.4-fold in the arrays. Furthermore, the *slsA* gene (stm3761) was upregulated 6.8-fold in the Δ*rodA* mutant. This gene encodes a putative inner membrane protein, which may be involved in virulence, as it is required for gut colonisation in chickens and calves (384, 420). Both the *mgtCB* operon and *slsA* are regulated by ArcA/ArcB. In anaerobic conditions, ArcA strongly repressed *mgtCB* expression, although it is thought to activate *slsA* (384).

The SPI-6 pathogenicity island is a region of between ~35-50kb, depending on specific serovars. In *S.* Typhi and Typhimurium SPI-6 encodes both a type 6 secretion system (T6SS) and the *saf* fimbrial operon, although the presence of pseudogenes within this region suggests that the T6SS may be non-functional in Typhi. In *S.* Typhi SPI-6 possesses an additional *tcf* fimbrial operon (421). Transcription of both the SPI-6 T6SS genes and the *saf* fimbrial operon was not significantly altered in the Δ*rodA* mutant from the present microarrays, although

two other SPI-6 genes were upregulated 2.9-fold (stm0306) and 8.7-fold (stm0307) in this mutant (Figure 6.1). stm0306 encodes PagN, a PhoP-activated outer membrane invasin, which is optimally expressed in SPI-2-inducing conditions and upregulated *in vivo* during mouse infections (422-425). PagN is able to mediate invasion of mammalian cells *in vitro* and assists with virulence *in vivo* (423, 425). The upstream stm0307 encodes a VirG-like protein, which is also thought to be involved in invasion or virulence (422). The *Shigella* VirG is an outer membrane protein which is involved in the recruitment of host cell F-actin, enabling the bacteria to move through the host cell cytoplasm, although the function of stm0307 is unknown (426).

Cell envelope-associated proteins

Although a number of integral membrane and periplasmic proteins have already been described whose expression was considerably increased in the Δ*rodA* mutant, it remains noteworthy that a large number of upregulated genes in the array were cell envelope associated. Of the 100 most highly upregulated genes, at least 45 are thought to encode inner membrane, outer membrane or periplasmic proteins (Figure 6.1). These included the transporter subunit proteins, outer membrane lipoproteins, adhesins, periplasmic stress-related proteins and other uncharacterised proteins, as well as others. This is highly significant and suggests that mutations which affect cell wall synthesis and cell shape bring about stark differences in the cell wall structure as a whole.

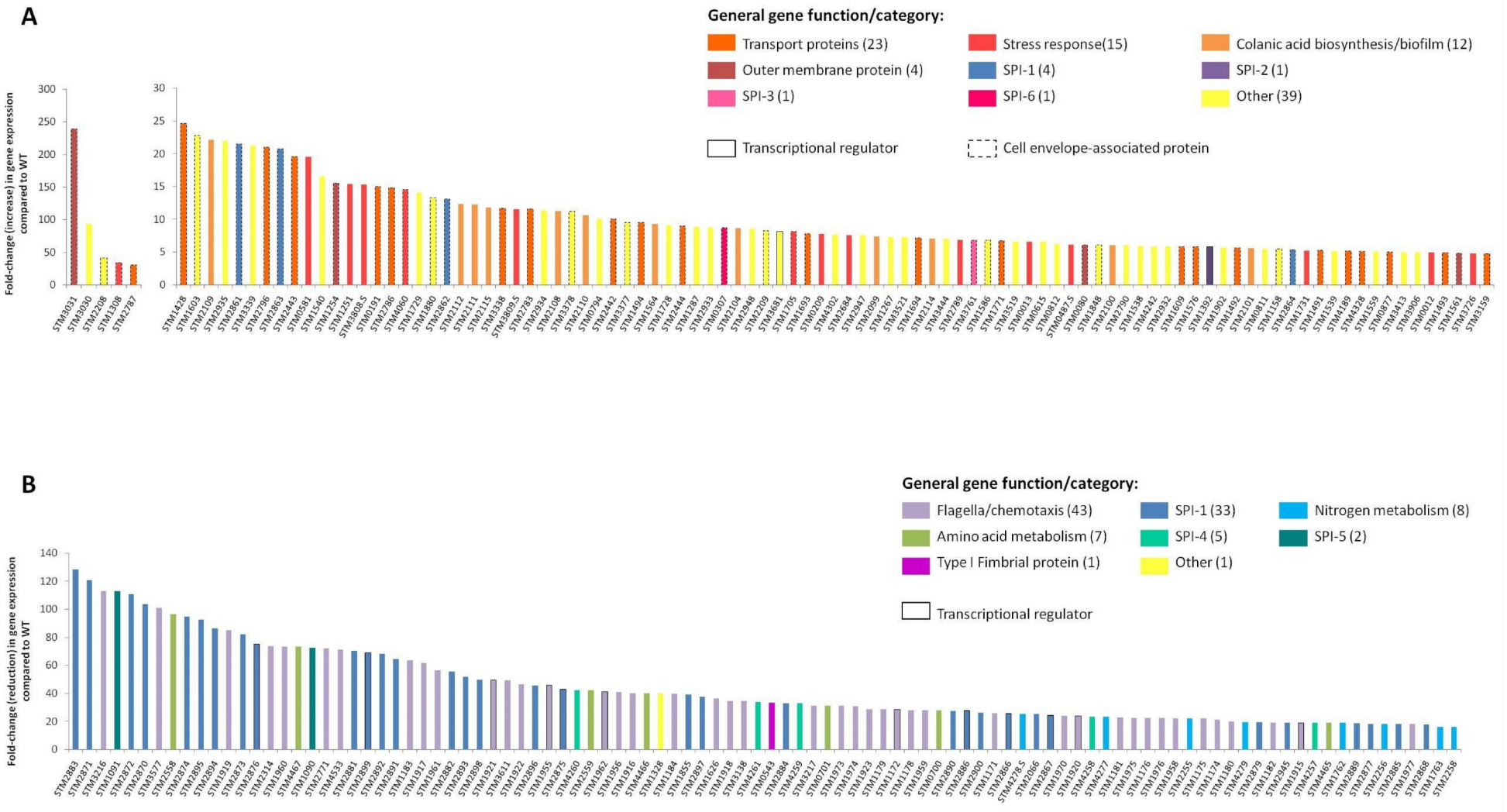

Figure 6.1: Microarray data showing major upregulated and downregulated genes in S. Typhimurium ΔrodA compared to wild-type: Data from NimbleGen 4x72000 multiplex arrays showing gene expression changes in SL1344 Δ*rodA* mutant as compared to wild-type. A - 100 most upregulated genes in SL1344 Δ*rodA*. B - 100 most downregulated genes in SL1344 Δ*rodA*. All gene expression data presented is statistically significant (P values ≤0.05, determined using two-tailed Student's t-tests)

6.1.3 Expression of global transcriptional regulators in SL1344 wild-type and Δ*rodA*

Microarray data concerning the expression levels of various major global transcriptional regulators were analysed in SL1344 Δ*rodA* as compared to the wild-type. This was done to provide a better overall picture of the patterns of gene expression in the Δ*rodA* mutant and to potentially identify any major regulators responsible for the observed virulence gene repression in round-cell mutants of *Salmonella*. In particular, the expression of global regulators involved in controlling responses to external environmental stress, was considered. The fold-changes in gene expression levels in Δ*rodA* for each gene are illustrated (Figure 6.2).

As previously discussed, the major transcriptional regulators of both SPI-1 and flagella genes were highly downregulated in the Δ*rodA* mutant. Furthermore the expression of the sensor kinase component of the SPI-2 major regulator, *ssrA*, was increased 5.8-fold. A number of global transcriptional regulators also showed considerable changes in gene expression in the microarrays. Global regulators whose expression was altered at least 2-fold compared to the wild-type included *cpxA*, *rpoE* and *rpoS*, which were upregulated 2.3-fold, 3.0-fold and 2.2-fold respectively, and *slyA*, *lrhA* and *cspA*, which were downregulated 2.5-fold, 7.0-fold and 4.1-fold respectively in the Δ*rodA* mutant (Figure 6.2). Although the expression data for a number of global regulators was not statistically significant, the expression of a number of other genes, though statistically significant, was altered less than 2-fold compared to the wild-type. These genes included *arcA*, *barA*, *ompR*, *fnr*, *csrA*, *baeR* and *baeS* (Figure 6.2).

The significant increases in both *rpoE* and *rpoS* transcription are perhaps not surprising. These two genes encode alternative sigma factors which control gene expression in response to external stresses, including high osmolarity, low pH and oxidative stress. As such they are needed in *Salmonella* for both stationary phase growth and also for intracellular survival. Furthermore, *rpoE* acts in response to the sensing of envelope stress (98, 307, 345, 427, 428). Perturbations in the cell wall structure from the inactivation of *rodA* are likely to be detected as envelope stress, leading to the activation of cell envelope stress-sensing mechanisms,

including *rpoE*, and hence the activation of envelope-stress/stationary phase associated genes. This is supported by the observation that *cpxA* was also upregulated in these arrays. This gene encodes the sensor kinase component of the CpxA/CpxR two-component system, which also responds to cell envelope stress, upregulating genes involved in periplasmic protein repair (307, 428, 429). Likewise, the increased sensitivity of this mutant to environmental stress could lead to the upregulation of general stress response pathways, regulated, for example, by *rpoS*. However, *slyA*, another stationary phase regulator whose regulon includes cell-envelope associated proteins and virulence factors, was found to be significantly downregulated in this array. SlyA is a major activator of the SPI-2 genes through SsrA/SsrB (38, 44).

Also contrary to expectations was the finding that *lrhA*, a repressor of *flhDC* transcription, was significantly downregulated in the Δ*rodA* mutant (437). However, it is recognised that the regulation of *flhDC* expression is complex and multifaceted. As such the downregulation of *lrhA* may not significantly affect *flhDC* expression. It also remains unknown whether the reduced expression of *cspA* is important, although CspA, the major cold-shock protein, activates H-NS, which goes on to downregulate SPI-2 expression. Hence it is possible that the downregulation of CspA indirectly affected the maintenance of SPI-2 expression in Δ*rodA* cells. Interestingly, two other related cold shock proteins CspC and CspE, were upregulated by 2.1-fold and 2.3-fold respectively in these arrays. This may be important, as both proteins have been shown to be involved in regulating the stress response; overexpression of these proteins led to increased levels of both *rpoS* mRNA and RpoS protein (427).

A number of other global regulators would be expected to play major roles in regulating the SPI-1 and flagella expression phenotypes in Δ*rodA* mutants, including the PhoP/PhoQ and OmpR/EnvZ two-component systems which both regulate virulence gene expression, and the Rcs phosphorelay sensor kinase and response regulator proteins RcsC and RcsB (99, 119, 397, 435). However no meaningful expression data was generated for these genes, since the microarray results were not statistically significant (Figure 6.2). Expression data for other important members of the Rcs phosphorelay, the cell-envelope stress-sensing

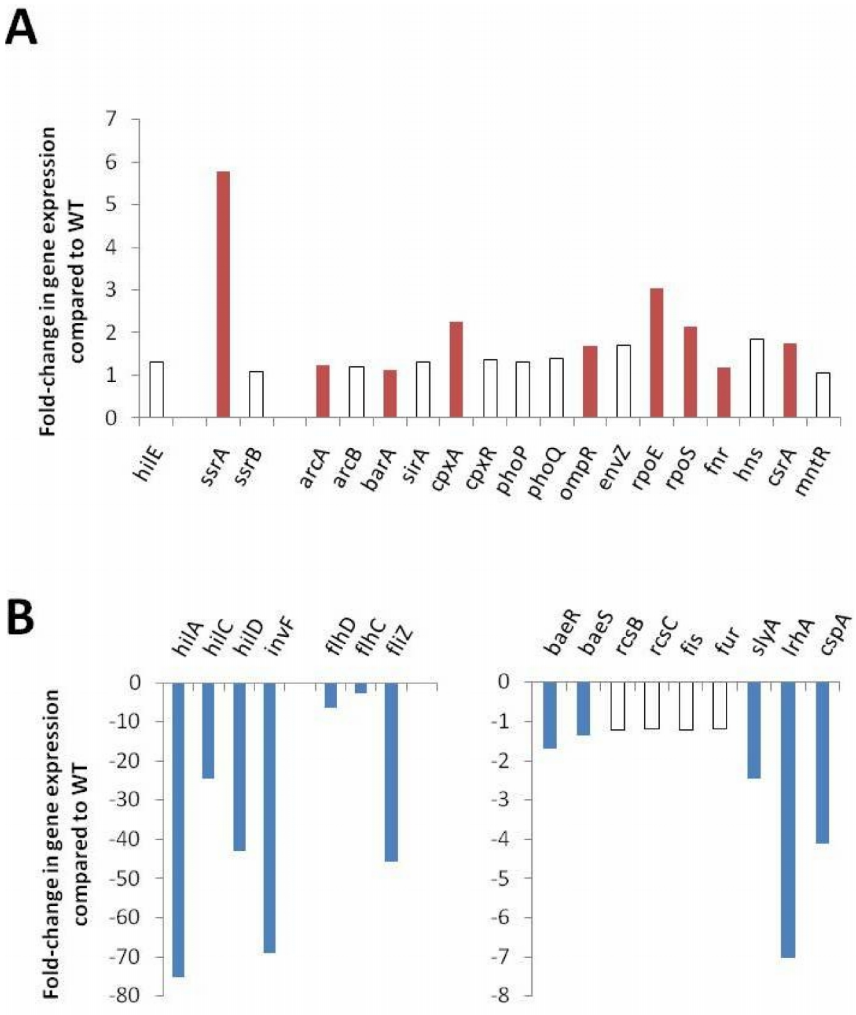

C

SPI-1 and Flagella gene major transcriptional regulators (56, 86, 87, 88, 93, 102)	
hilA	SPI-1 master regulator
hilC	SPI-1 regulation; activator of *hilA*
hilD	SPI-1 regulation; activator of *hilA*
hilE	SPI-1 regulation; repressor of HilD
invF	SPI-1 regulation; activates expression of *sip* operon and non-SPI-1 effectors
ssrA/ssrB	SPI-2 master regulator
flhD	Flagella gene master regulator
flhC	Flagella gene master regulator
fliZ	Activates flagella and SPI-1 genes

Global transcriptional regulators	
arcA/arcB	Responds to oxygen levels; activates anaerobic respiration and flagella genes in anaerobic conditions (384)
baeR/baeS	Activates multidrug resistance genes. Regulates flagella/chemotaxis genes (496)
barA/sirA	Positively regulates flagella and SPI-1 genes via CsrB (92)
cpxA/cpxR	Envelope stress response. Detects envelope stress and regulates proteins involved in folding/degrading mis-folded periplasmic proteins and assembly of cell wall structures (216, 307)
phoP/phoQ	Major virulence gene regulator. Responds to low Mg^{2+}; suppresses SPI-1, activates SPI-2. Essential for intracellular survival (98, 397)
ompR/envZ	Stationary phase and acid tolerance adaptation. Senses changes in osmolarity, regulates porin gene expression; activates SPI-1 in response to organic acid and SPI-2 in response to inorganic acid (98, 99)
rcsB, rcsC	Envelope stress response. Detects osmotic and membrane stress; suppresses flagella and SPI-1 genes, upregulates colanic acid biosynthesis and cell division genes. Regulates RpoS (118, 119)
rpoE	Heat shock sigma factor. Responds to cell envelope stress, regulates proteins involved in cell envelope synthesis and maintenance. Important in stationary phase (344, 345)
rpoS	Stationary phase sigma factor. Expressed *in vivo* or in conditions of high osmolarity, low pH, oxidative stress or nutrient starvation etc. Essential for intracellular survival and virulence (98, 438)
fis	Regulates expression of *hilA* and *invF*. Also regulates recombination, replication and transcription (102, 497)
fnr	Major regulator in oxygen sensing. Responds to aerobic/anaerobic conditions. Positively regulates motility and pathogenesis (386)
fur	Ferric uptake regulator. Activated by iron and manganese and required in acid tolerance adaptation (ATR); negatively regulates iron transport enzymes, activates SPI-1 expression through HilD protein, represses SPI-1 iron transporter (98, 352, 411)
Hns	Major global regulator. Negatively regulates expression of horizontally-acquired DNA including SPI-2 (102, 105)
csrA	Carbon storage regulator. Controls several processes including carbohydrate metabolism. Post-transcriptionally regulates SPI-1 by binding *hilD* mRNA (110)
slyA	Stationary phase gene regulation, independently of RpoS. Induced intracellularly, regulates expression of cell envelope-associated virulence factors including oxidative stress response. Essential for intracellular survival (38, 44)
lrhA	Transcriptional repressor of flagella/chemotaxis genes, type I fimbriae, and *rpoS*. (437, 438)
mntR	In presence of manganese represses SPI-1 iron transporter and manganese transporter (411)
cspA	Major cold shock protein, activates *hns* (427)

Figure 6.2: Microarray data showing expression of major global regulator genes in S. Typhimurium ΔrodA compared to wild-type: Data from NimbleGen 4x72000 multiplex arrays showing gene expression of major global regulators and stress response regulators in SL1344 Δ*rodA* mutant as compared to wild-type. A - Genes whose expression was upregulated in SL1344 Δ*rodA*. B - Genes whose expression was downregulated in SL1344 Δ*rodA*. Coloured bars indicate statistically significant gene expression data (P values ≤0.05, determined using two-tailed Student's t-tests). White bars indicate non-significant gene expression data (P values ≥0.05). C – Table summarising function of SPI-1 and flagella master regulators and global regulators (253).

RcsF protein and the intermediate protein in signal transduction, RcsD, was also non-significant. Further work will therefore be needed to assess whether these global regulators play a major role in regulating virulence genes in round-cell mutants.

6.1.4 Other significant changes in gene expression between SL1344 wild-type and Δ*rodA*

Several additional notable changes in gene expression were observed between the wild-type and Δ*rodA* strains, which will be briefly discussed.

Cell division genes

A large number of cell division-associated genes exist, encoding the major components of the septal cytokinetic ring machinery and the septal peptidoglycan synthesis complex. At least ten of these proteins play an essential role in cell division (175). Various studies have observed that the major cell division proteins FtsZ, FtsA and FtsQ (encoded by the *ftsQAZ* operon) are upregulated in round-cell mutants, and that upregulation of these proteins is essential to prevent cell lysis and restore viability to round-cell mutants (130, 131).

9 genes associated with cell division were upregulated at least 2-fold in the Δ*rodA* mutant (stm0119-stm0127), including the major cell division transpeptidase PBP3 (FtsI) and the cognate FtsW protein, as well as FtsL, another essential cell division protein (175). FtsQ was also upregulated 2.3-fold and FtsA expression was increased 1.9-fold in the Δ*rodA* mutant. However microarray data for *ftsZ* was not statistically significant. Overall, and in support of previous studies, proteins comprising the cell division machinery seem to be upregulated in this mutant.

mrd operon genes

As would be expected, the *rodA* gene was downregulated (8.3-fold) in the Δ*rodA* mutant, since the gene was completely inactivated in this strain and replaced by a kanamycin-resistance cassette. The *rlpA* gene, which lies immediately downstream of *rodA*, was also downregulated 10.3-fold in this mutant, suggesting that the Δ*rodA* mutation has a polar effect on downstream co-transcribed genes.

Alternatively, the effect on *rlpA* expression could result from the removal of the putative *rlpA* promoter with the removal of the *rodA* gene.

The expression of *dacA* was decreased only by 1.7-fold in the Δ*rodA* mutant, although this data was not statistically significant. The lack of a significant change in gene expression may indicate that *dacA* does not form part of the *mrd* operon, and hence its expression was not significantly perturbed in the Δ*rodA* mutant.

Expression of the *pbpA*, and the other upstream *mrd* operon genes was also not significantly affected in these arrays.

6.2 Discussion

6.2.1 Usability and verification of microarray data

Microarrays provide a highly useful tool for the comprehensive analysis of gene expression between wild-type and mutant strains. However, this technique has a number of inherent limitations and further *in vivo* experimental analyses are therefore required to fully validate microarray data. The microarray data presented here was well supported by previous phenotypic tests, which showed that the observed defects in SPI-1 and motility in round-cell mutants were at least in part a result of downregulation of the major flagella/SPI-1 regulators. Furthermore, the experimental observations of excess capsular polysaccharide production in the round-cell mutants may provide additional evidence to verify the overexpression of the colanic acid biosynthesis genes seen from the Δ*rodA* microarrays. Data from previous studies may also help to validate the current microarray data in terms of the expression of global stress regulators. Similarly to the data shown here, mecillinam-treated *E. coli* cells were shown to upregulate several major stress regulators, including *rpoE*, *cpxAR* and the Rcs phosphorelay (118). Ideally, given time the gene expression data generated in these arrays would best be verified with additional transcriptional reporter assays or quantitative real-time PCR (qPCR). Nevertheless, the phenotypic data provide strong evidence to support and verify the observations from microarray data, showing that it affords a reliable representation of the *S.* Typhimurium Δ*rodA* transcriptional profile.

It is important to note that although microarrays enabled a large-scale global analysis of gene expression, this data only represents one level of expression, not taking into account post-transcriptional and post-translational regulatory mechanisms which influence protein expression and function. As such the microarrays may not provide an accurate or complete representation of the physiological state of the Δ*rodA* mutant. However, the present microarrays have provided a wealth of information regarding global gene transcription in the Δ*rodA* mutant as compared to the wild-type.

Arrays were conducted using purified mRNA from mid-log phase cultures. Cultures were standardised according to culture optical densities (OD600). RNA concentrations were further standardised so that equal quantities of wild-type and mutant cDNA were hybridised to the arrays. This was done to enable comparisons to be made between the wild-type and Δ*rodA* mutant. As such, the results of these microarrays were used to compare gene expression between individual cells. It is recognised that some changes in gene expression may be the indirect result of cells compromising for the increase in both cell volume and quantity of cell membrane per cell in the Δ*rodA* mutant by increasing gene expression. However, if this were the case, one may expect that a large proportion of genes in the round-cell mutant would be upregulated.

6.2.2 Major gene expression changes in SL1344 Δ*rodA* mutant

DNA microarrays were carried out to characterise the major changes in gene expression in the round-cell *S.* Typhimurium Δ*rodA* mutant as compared to the wild-type, and hence to help gain a better understanding of the function of this gene. Several major changes in gene expression were evident in the mutant, the most pronounced of which being those seen in flagella and SPI-1 gene expression. In agreement with previous phenotypic assays, the vast majority of flagella/chemotaxis and SPI-1-encoded genes were highly downregulated in this mutant. Furthermore, expression of the major transcriptional regulators of these genes was also highly suppressed. The only exception was a SPI-1 encoded iron transporter, which was upregulated in the round-cell mutant. The DNA sequence of this operon is known to differ significantly from that of the rest of SPI-1 (407). In

addition, this operon is differentially regulated from the rest of SPI-1, and assists in intracellular survival rather than invasion (352, 410, 411). In reflection of phenotypic assays, a significant number of genes involved in colanic acid biosynthesis were also upregulated in the Δ*rodA* mutant.

A number of genes involved in responding to a variety of environmental stresses were upregulated in the Δ*rodA* cells. This may result from the upregulation of the global regulatory alternative sigma factors RpoE and RpoS, which are required in stationary phase particularly to regulate genes involved in stress resistance (98, 253, 345). As would be expected from a mutation which affects cell wall structure, pathways involved in reacting to cell envelope-associated stress also appeared to be upregulated in the Δ*rodA* mutant, including *rpoE* and *cpxA*. Furthermore, significant alterations were observed in the expression of several cell envelope-associated proteins, including a number of outer membrane proteins and integral membrane nutrient transporters. These features point towards significant changes in the general makeup and structure of the cell envelope and constituent proteins in round-cell mutants. Changes in the cell envelope as a whole have been noted in round-cell mutants. For example both round cell *mrd* and *mre* operon mutants have been seen to produce excess inner membrane from an inability to adjust the rate of phospholipid synthesis in response to an altered cell wall (130).

Round-cell mutants are known to have a decreased surface:volume ratio compared to wild-type cells, being considerably larger in diameter and volume than wild-type cells. This must be considered when analysing alterations in the expression of genes encoding membrane proteins. The upregulation of gene expression for a large number of membrane proteins may be a result of mutant cells responding to an increased overall quantity of cell envelope by concurrently overproducing important membrane proteins. As such the actual concentration of the majority of membrane proteins may not be much altered in Δ*rodA* cells. Alternatively the increased cell volume may lead to a decreased intracellular concentration of, among other things, essential nutrients. This may require Δ*rodA* cells to upregulate the expression of nutrient uptake transport proteins to enable cells to maintain the required intracellular concentration of essential nutrients.

A surprising feature of the Δ*rodA* mutant was a significant decrease in the expression of several genes associated with anaerobic respiration. This was echoed by the significant downregulation of two genes involved in the regulation of nitrate-associated anaerobic respiration, *narP* and *narL*, although these genes have opposing effects on the expression of nitrate reductase systems. Also, gene expression was not significantly altered in other important anaerobic respiration regulators, *arcA*, *arcB*, *fnr*, and *fur* (387, 430).

Genes important for intracellular survival appeared to be upregulated in the Δ*rodA* mutant, including the SPI-2 master regulator sensor kinase, *ssrA*. It is therefore surprising that anaerobic respiration genes should be downregulated in this mutant. Studies have shown that the ability of *Salmonella* to respire anaerobically is essential for intracellular survival; *S.* Typhi mutants that could not respire anaerobically were also less able to invade and replicate inside epithelial cells (431-433). This may suggest that anaerobic respiration genes would be upregulated or co-regulated along with other genes important for intracellular survival in Δ*rodA* cells. However, one study suggested that the *Salmonella*-containing vacuole (SCV) of the macrophage may not be completely anaerobic, as FNR and ArcA were not upregulated intracellularly (430). Also, FNR was shown to upregulate flagella and SPI-1 genes in anaerobic conditions, as well as the anaerobic respiration genes (386). Therefore anaerobic respiration genes may be co-regulated with invasion genes in the Δ*rodA* mutant, and as such the downregulation of both anaerobic respiration and invasion genes may result from the regulation of a common upstream factor.

6.2.3 Implications of major changes in gene expression and insights into the physiological state of the Δ*rodA* mutant

Taken together, these observations suggest that invasion-associated genes (e.g. flagella, SPI-1 and type I fimbriae) are almost completely repressed in round-cell mutants, whilst genes required in the later stages of infection for intracellular survival and resistance to external stresses, are activated. The latter class of genes are upregulated in conditions where cells are exposed to heightened levels of environmental stress, including a low pH, low magnesium, oxidative stress and

nutrient starvation, all of which are indicative of the intracellular environment (39, 96, 98, 434). Since such stress response pathways may be upregulated in the *rodA* mutant, it may follow that the observed virulence gene expression in this mutant is an indirect result of the upregulation of stress response pathways. These results provide further evidence that the mutation of cell shape determinant genes may affect the structure of the peptidoglycan cell wall, leaving cells more exposed to environmental stress, or alternatively that such mutants respond defensively to changes in the wall structure by upregulating stress response pathways regardless of any actual perturbation of barrier function. In support of these results, round cell mutants are known to show increased sensitivity to several stresses, and the presence of antibiotics (211, 214, 229).

These data provided important insights into the physiological state of the Δ*rodA* mutants. Potentially significant clues into the structure and expression of the *mrd* operon were also provided in this array, suggesting that *dacA* does not form part of the *mrd* operon, since its expression was not affected in the Δ*rodA* mutant.

6.2.4 Global transcriptional regulator expression in the Δ*rodA* mutant

Microarrays were conducted with the additional aim of identifying putative transcriptional regulator(s) which may be to a large extent responsible for the observed gene expression profile of the Δ*rodA* mutant. The expression of several major global transcription regulators was analysed, including those which regulate both essential housekeeping genes and virulence genes in response to environmental factors or stress. Several major transcription factors conversely regulate expression of both invasion-associated (e.g. SPI-1) and intracellular survival-associated (e.g. SPI-2) virulence genes in *Salmonella*, in a manner reminiscent of the observed phenotype in the Δ*rodA* mutant. Among these are the *rcsC* and *rcsB* genes, and *phoP*, and *phoQ,* which act to suppress flagella and invasion gene expression, whilst upregulating SPI-2. The Rcs phosphorelay genes also form a major activator of colanic acid biosynthesis (96, 98, 318, 435, 436). Another likely candidate could be the *lrhA* gene, which directly regulates flagella expression by binding to the *flhDC* promoter and inhibiting its expression, and represses type I fimbriae expression, although this gene also represses *rpoS*

expression and is repressed by the Rcs phosphorelay (437, 438). *lrhA* was significantly downregulated in the arrays, and hence it is unlikely to form a major regulator of the observed phenotypes. However, the more likely candidates, the *rcs* and *phoP/phoQ* genes were not significantly altered in expression between the wild-type and Δ*rodA* mutants. As such, the microarray data did not highlight any obvious candidates responsible for regulating the expression of SPI-1 and flagella genes in round cell *mrd* operon mutants. Further work will be needed to identify this/these regulator(s). It also remains to be seen to what extent other envelope stress response pathways, regulated by RpoE, CpxA/CpxR, and BaeS/BaeR, may influence the observed phenotypes in round-cell mutants (216, 428).

Chapter 7. Restoration of SPI-1 and flagella functionality through expression of major SPI-1/motility regulators *in trans*, in Δ*pbpA* and Δ*rodA* strains

7.1 Recovery of motility and SPI-1 functionality in complemented *mrd* mutants

Microscopic analysis of BRD948 *S.* Typhi Δ*pbpA* and Δ*rodA* mutants expressing plasmid-encoded YFP fusion proteins of the respective proteins demonstrated that these plasmids were able to restore rod-shape to the round-cell mutants (Figure 4.3). Subsequent assays for recovery of motility showed that around 50-70% motility was restored in both *S.* Typhi Δ*pbpA* pVP6 and *S*. Typhi Δ*rodA* pVP3 complemented strains, compared to the wild-type (Figure 5.1). Secreted protein profiles of these strains grown up to mid-log phase also clearly showed recovered flagellin expression (Figure 7.1 B).

The functionality of the SPI-1 T3SS was also assayed by western blot analysis of SPI-1 effector protein expression in the complemented strains. Secreted protein preparations from mid-log phase cultures of both wild-type, mutant and complemented strains were subjected to SDS-PAGE, blotted onto nitrocellulose and labelled with antibodies specific to the SPI-1-secreted effector protein, SopE. Although the resultant SopE band appeared faint, it was clearly present in both *S.* Typhi Δ*pbpA* pVP6 and *S*. Typhi Δ*rodA* pVP3 complemented strains. However, SPI-1 effector protein bands were not observed when the complemented strains were grown in the presence of 0.5 mM IPTG (Figure 7.1 A). This is reminiscent of motility assays, where the overexpression of *pbpA* and *rodA* in complemented strains caused a complete loss of motility (Figure 5.1). This is also seen in secreted protein profiles of these strains; the flagellin bands were significantly reduced with the addition of IPTG to complemented strains, as indicated (Figure 7.1 B).

Overexpression of the PBP2-YFP and RodA-YFP fusion proteins may have led to an accumulation of these proteins in inclusion bodies, resulting in a subsequent loss of morphology and with it a loss of motility and SPI-1 secretion in Δ*pbpA* and

Δ*rodA* strains. Alternatively, overexpression of these proteins may also lead to cell shape defects, as seen previously, along with an associated shut-down of SPI-1 and motility functionality (Figure 4.6) (158, 164, 330).

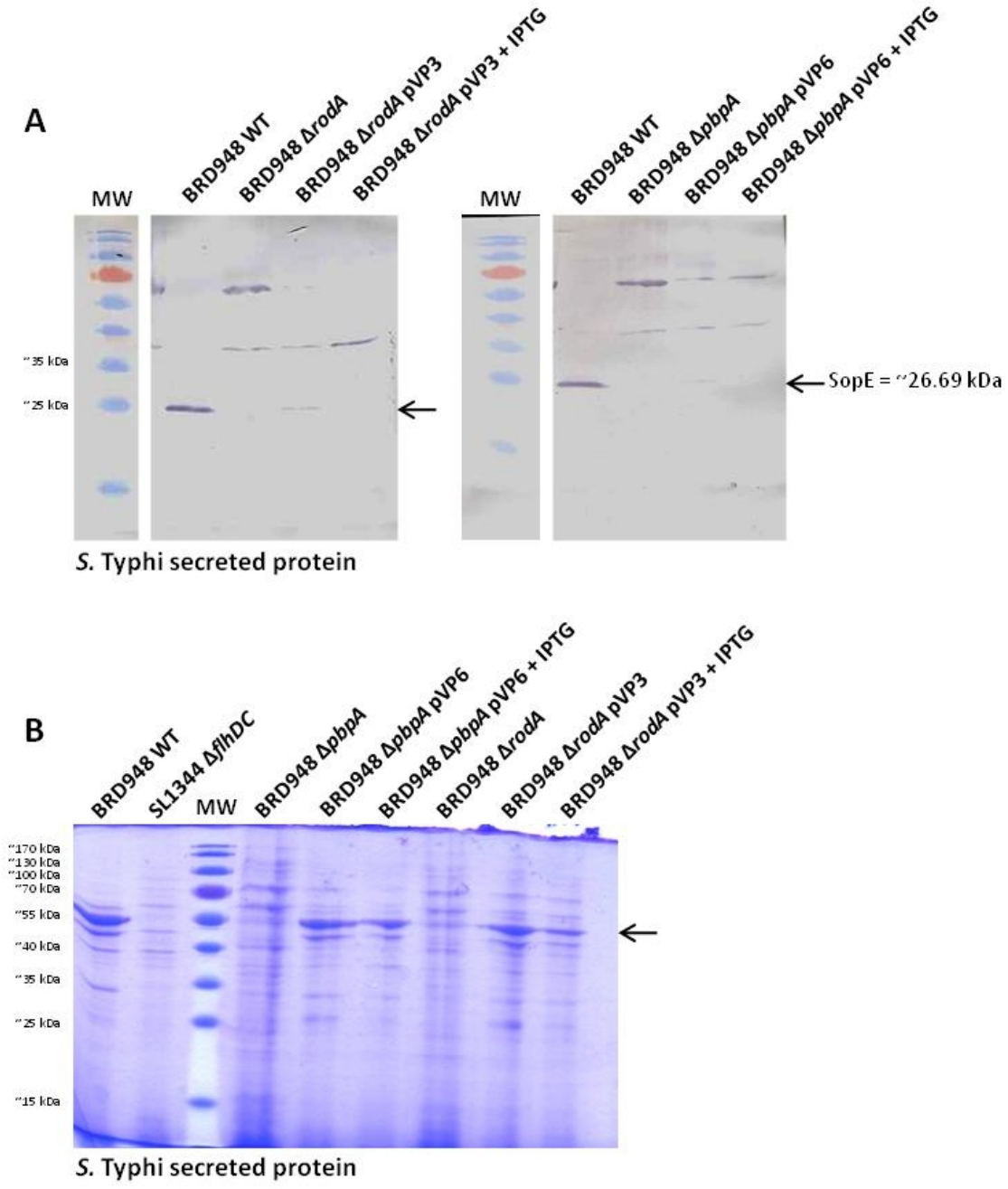

Figure 7.1: Recovery of motility and SPI-1 effector protein expression in complemented ΔpbpA and ΔrodA strains: A – Western blots showing expression of the SPI-1 SopE effector protein in secreted protein fractions of BRD948 wild-type, Δ*pbpA* and Δ*rodA*, and complemented mutant strains. Background protein bands likely due to antibody cross-reactivity to intracellular proteins; round-cell mutants are known to be prone to cell lysis (Figure 5.7) (130). B - Secreted protein profiles of BRD948 wild-type, Δ*pbpA* and Δ*rodA*, and complemented mutant strains. Arrow indicates flagellin band. Cultures grown in LB broth, harvested at mid-log phase. Protein molecular weight (MW) marker sizes as indicated.

The detection of SPI-1 effector proteins in secreted protein fractions may result from cell lysis with the release of non-secreted proteins into culture supernatant, and not active secretion through the SPI-1 T3S needle, particularly as round-cell mutants are prone to lysis (130). However, the clear functionality of motility in these complemented strains makes it probable that the SPI-1 T3SS is also functional. These data together demonstrate that the SPI-1 and motility defects observed with the inactivation of cell shape determinants such as *pbpA* and *rodA* are the direct results of the inactivation of these genes. This was important to establish, as it is plausible that the observed phenotypes may have resulted from the accumulation of secondary mutations through several passages of growth and the processes involved in the generation of specific *S.* Typhi *mrd* operon mutants.

Data from several phenotypic assays, as well as microarray analyses, demonstrated that both motility-related genes and genes encoding the SPI-1 T3SS were almost completely downregulated in round-cell *mrd* mutants of both *S.* Typhi and *S.* Typhimurium (Figure 5.3 and 5.6, Table 6.1 and 6.2). However, motility assays in the presence of mecillinam suggested that there was a significant delay between the loss of rod-shape and the shut-down of motility (Figure 5.2). Furthermore, in microscopic analysis of both Δ*pbpA* and Δ*rodA* mutants, within a population of cells a few motile round cells were occasionally noticed, likely due to natural heterogeneity within a population.

These observations, as well as the data showing that SPI-2 T3SS functionality remained intact in round-cell mutants, suggest that the motility and SPI-1 defects may be caused purely from the shutdown of gene expression and not from any additional incapacity to assemble the complex multi-protein structures in the cell wall of Δ*pbpA* and Δ*rodA* mutants. In order to test this hypothesis, it was necessary to attempt to restore expression of both SPI-1 and motility genes in these mutants, and assay for a parallel recovery of SPI-1 and motility functionality. Expression of the major SPI-1 and flagella gene transcriptional regulators was restored in each of the round-cell mutants by inducing their expression *in trans*, from heterologous promoters. These strains were subsequently assayed for motility and SPI-1 functionality.

7.2 Expression *flhDC* under the control of a tetracycline-inducible promoter in *mrd* mutant strains

7.2.1 Introduction of TPA14 tetracycline-inducible *flhDC* vector into *S.* Typhimurium Δ*pbpA* and Δ*rodA* mutants

Expression of all flagella and chemotaxis genes is tightly controlled by the upstream master regulator $FlhD_4C_2$, encoded by the *flhD* and *flhC* genes. Motility is therefore dependent upon expression of the *flhDC* operon (56, 62, 108).

In order to attempt to restore motility in round-cell *mrd* mutants, *S.* Typhimurium Δ*pbpA*, Δ*rodA* and wild-type cells were transduced with a P22 phage lysate stock containing 'TPA14', a chromosomally-encoded vector where the native promoter of the *flhDC* operon is replaced by a tetracycline-inducible P_{tetA} promoter with the insertion of a T-POP transposon (236). Hence, in cells harbouring TPA14 *flhDC* expression (and hence downstream motility) is no longer subject to the native regulatory mechanisms which may suppress *flhDC* with the inactivation of *pbpA* and *rodA*, but instead dependent upon addition of tetracycline to growth medium (236). The TPA14 phage stock was a kind gift of Philip Aldridge (Newcastle, UK). TPA14 was transduced into *S.* Typhimurium SL1344 wild-type, Δ*pbpA* and Δ*rodA* strains and tetracycline-resistant transductants were subsequently screened for recovered motility. This work was done in *S.* Typhimurium wild-type and mutant strains rather than BRD948 strains, due to the inherent inability to transduce *S.* Typhi with Typhimurium-derived P22 phage lysates (439).

7.2.2 Motility of *S.* Typhimurium WT, Δ*pbpA* and Δ*rodA* expressing TPA14

To test for recovery of motility in Δ*pbpA* and Δ*rodA* mutants expressing TPA14, tetracycline resistant TPA14 transductants and relevant negative controls were inoculated onto semi-solid motility agar, with or without the addition of 50 μg/ml tetracycline, and cultured for at least 6 hours at 37°C. The extent of culture spread was then measured as an indication of motility functionality in these strains. The motility of each strain was measured as a percentage of that of the wild-type harbouring TPA14 (Figure 7.2).

These motility assays demonstrated a clear and significant recovery of motility in Δ*pbpA* TPA14 and Δ*rodA* TPA14 cells, where *flhDC* was expressed under the control of the P_{tetA} promoter, compared to mutant strains lacking TPA14, in which *flhDC* was expressed from its natural promoter (Figure 7.2 A). In the absence of tetracycline Δ*pbpA* TPA14 and Δ*rodA* TPA14 cells recovered ~30-50% of the motility of wild-type SL1344 TPA14 cells. This suggests some low-level background expression of *flhDC* was evident, which was sufficient to restore significant amounts of motility to the Δ*pbpA* and Δ*rodA* mutants. However, in the presence of tetracycline, though some motility was restored to the round-cell mutants motility levels were highly variable in both Δ*pbpA* and Δ*rodA* strains expressing TPA14, making the results overall not statistically significant. Cell growth in motility agar appeared to be affected by the presence of tetracycline, being slightly diminished in both wild-type and mutant strains. As such, the variability in motility may be a result of either growth perturbation or variability in levels of *flhDC* expression.

Microscopic analysis of both wild-type and round-cell mutant cells of SL1344 confirmed that no overall differences in morphology were seen between wild-type, Δ*pbpA* and Δ*rodA* cells, and their TPA14-harbouring counterparts (Figure 7.2 B). Therefore, the recovery of motility in round-cell mutants was due specifically to a restoration of *flhDC* expression, with the downstream re-activation of flagella gene expression, rather than any secondary effects causing cells to regain a rod-shaped morphology. In addition, Δ*pbpA* TPA14 and Δ*rodA* TPA14 cells were clearly motile under the microscope, demonstrating that the observed spread of these strains in motility agar was due to active motility, and not just increased growth rates.

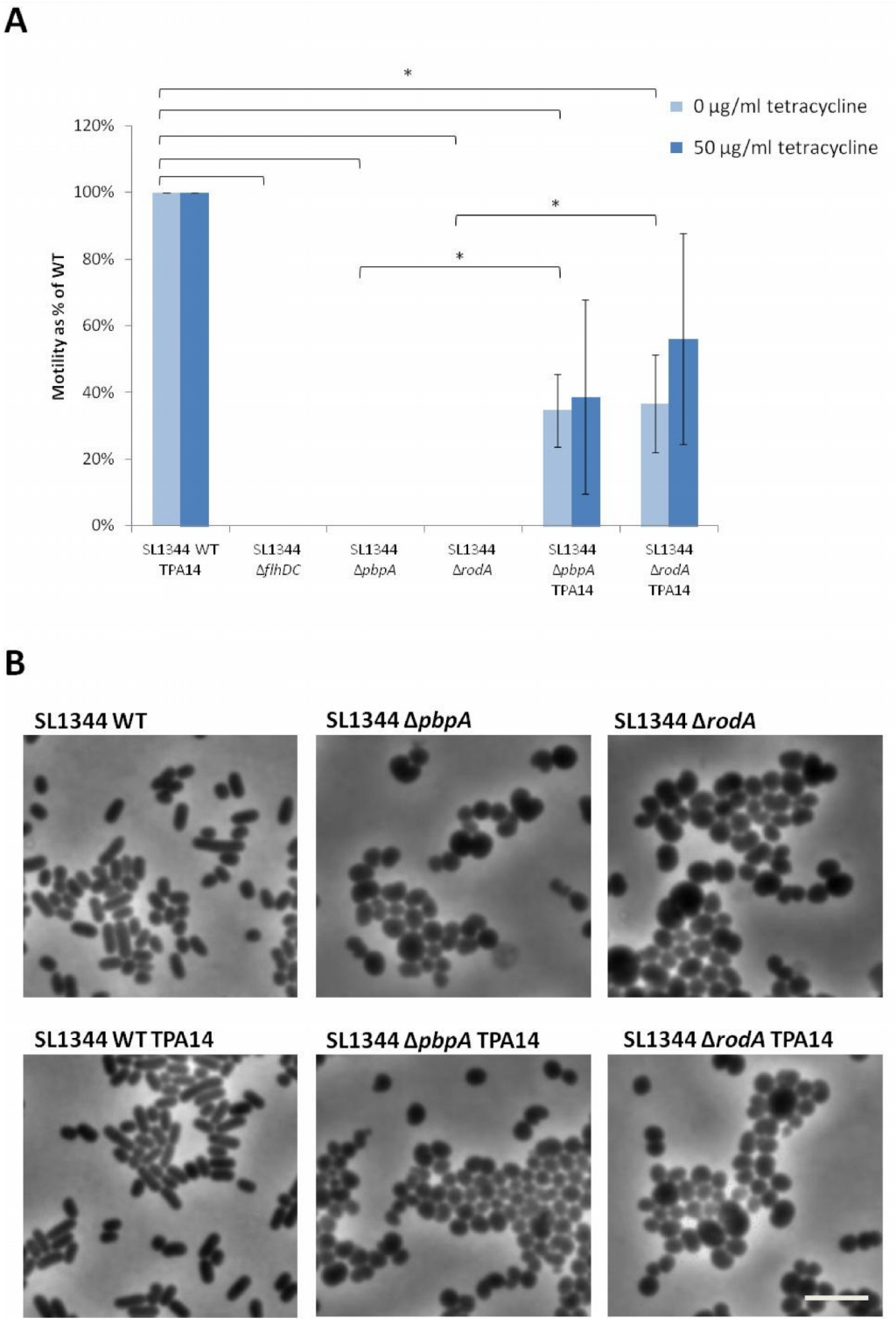

Figure 7.2: Motility assays of S. Typhimurium mrd operon mutants and TPA14 complemented strains: A **-** Motility assay results for SL1344 wild-type, Δ*pbpA* and Δ*rodA* strains expressing *flhDC* under the control of the native, or tetracycline-inducible P_{tetA} promoter (cells expressing TPA14). Cells were cultured in semi-solid motility agar at 37°C for ~6 hours. Motility was measured in terms of extent (diameter) of culture spread through motility agar, as a percentage of that of relevant wild-type strain. Results show averages from 3 independent assays. Error bars indicate standard deviations. Asterisks indicate statistically significant differences, where P values were ≤0.05 as determined by Students t-tests. B – Phase contrast microscopy images of the above strains. Scale bar ~5 µm; all images are to the same scale.

These results demonstrate that the motility defects seen in round-cell mutants, in *S.* Typhimurium are to a large extent due to the downregulation of flagellar genes, brought about from the repression of *flhDC* expression. Thus, motility defects do not result from an inability to assemble functional flagella in round-cell mutants. However, since motility was restored only up to ~50% in these cells through the recovery of *flhDC* expression (in the absence of tetracycline), it is possible that other regulators act on flagella gene expression further downstream of *flhDC* to diminish flagella gene expression. Also, it is possible that perturbations to the cell wall structure affect the assembly of flagella in these cells, reducing motility still further.

7.3 Expression of *hilD* from an arabinose-inducible pBAD vector in *mrd* mutant strains

7.3.1 Transformation of *S.* Typhi and *S.* Typhimurium Δ*pbpA* and Δ*rodA* mutants with pBAD-*hilD*

The expression of all SPI-1-encoded genes is essentially regulated by 3 SPI-1-encoded genes: *hilA*, *hilD*, and *hilC. hilA* is considered the master regulator of SPI-1, forming the point at which upstream regulatory inputs converge. However, *hilA* expression is dependent upon *hilC* and *hilD* and the vast majority of factors which regulate SPI-1 expression do so at the level of *hilD*, post-transcriptionally regulating its expression (86-89, 91). Furthermore, *hilD* expression was shown to be almost completely repressed in round-cell *mrd* mutants of *S.* Typhi (Figure 5.6). HilD may be the most crucial factor responsible for downregulating SPI-1 gene expression in these mutants; therefore in attempting to restore SPI-1 expression in the round-cell mutants it was necessary to attempt to restore *hilD* expression first and foremost.

The *hilD* gene, lacking its natural promoter, was cloned into the pBR322-derived expression vector pBAD24, such that it was expressed under the control of the arabinose-inducible *araBAD* operon P_{BAD} promoter (245). This vector was constructed and kindly provided by David Bulmer (Newcastle, UK). The pBAD-*hilD*

plasmid was introduced into wild-type, Δ*pbpA* and Δ*rodA* strains of both *S.* Typhi (BRD948) and *S.* Typhimurium by transformation.

7.3.2 SPI-1 functionality in *S.* Typhi and *S.* Typhimurium Δ*pbpA* and Δ*rodA* mutants expressing pBAD-*hilD*

Recovery of SPI-1 expression and functionality was initially tested in *S.* Typhi strains expressing *hilD* from the pBAD-*hilD* plasmid. Strains were cultured in LB medium supplemented with 1 mM arabinose to induce *hilD* expression, 1 mM glucose to repress expression of *hilD* from pBAD-*hilD*, as a negative control, or without supplementation. In the absence of arabinose, pBAD-*hilD*-containing cells may still express low levels of background *hilD* from the P_{BAD} promoter, potentially resulting in more native HilD proteins levels (440). pBAD24 is a relatively high copy-number expression vector and so supplementing cultures of pBAD-*hilD*-expressing strains with arabinose may lead to HilD overproduction. Secreted protein fractions were prepared from mid-log phase cultures and analysed by SDS-PAGE and western blotting.

Western blots of *S.* Typhi secreted protein fractions were labelled with antibody specific to the SipA effector protein (Figure 7.3 A). It was quickly evident from western blots that distinct SipA protein bands were present in both the wild-type *S.* Typhi and the wild-type *S.* Typhi pBAD-*hilD* strain. The addition of arabinose should induce P_{BAD}-regulated *hilD* expression whilst glucose addition should suppress *hilD* expression. As such, one would expect the effector protein expression, and hence SPI-1 expression as a whole, to be significantly increased in the presence of arabinose in pBAD-*hilD* expressing cells. Contrary to expectations, however, no observable alteration in the SipA band intensity was observed with growth in arabinose or glucose. A minor increase in SipA expression was observed for *S*. Typhi wild-type pBAD-hilD cells grown without the addition of glucose or arabinose, compared to wild-type, although this difference was only very slight. In fact, the SipA bands appeared more intense in both wild-type strains grown in the presence of glucose (Figure 7.3 A).

Furthermore, SipA was not detected in secreted protein fractions of Δ*pbpA* pBAD-*hilD* or Δ*rodA* pBAD-*hilD* strains, cultured in the presence of 1 mM arabinose, or in the absence of either arabinose or glucose. This suggests that restoring *hilD* expression does not lead to the recovery of SPI-1 expression and functionality in round-cell *S.* Typhi mutants – the propensity of round-cell mutants to lyse meaning that effector proteins would likely be observed in secreted protein fractions, regardless of active secretion. Surprisingly, faint SipA bands were observed in secreted protein fractions of *S.* Typhi Δ*pbpA* and Δ*rodA* strains, but not Δ*pbpA* pBAD-*hilD* and Δ*rodA* pBAD-*hilD* strains, grown in the presence of glucose.

The pBAD-*hilD* expression vector was also introduced to wild-type and mutant strains of *S.* Typhimurium SL1344. Wild-type, Δ*pbpA* and Δ*rodA* strains of SL1344 expressing pBAD-*hilD* were cultured in LB medium without the addition of glucose or arabinose, in order to attempt to keep HilD protein levels more closely resembling wild-type levels (440). Cells were harvested at mid-log phase, fixed and labelled with both anti-SipD antibody and a fluorophore-conjugated secondary antibody, and analysed by immunofluorescence microscopy. Meanwhile, secreted protein fractions were prepared from culture supernatants, subjected to SDS-PAGE and western blotting, and also labelled with antibody specific to the SipD effector protein.

In contrast to the results seen in *S.* Typhi cells expressing pBAD-*hilD*, SPI-1 secreted effector protein levels were significantly increased in *S.* Typhimurium wild-type cells overexpressing *hilD*, as shown by western blotting. In addition, SipD bands were clearly visible in both *S*. Typhimurium Δ*pbpA* pBAD-*hilD* and Δ*rodA* pBAD-*hilD* secreted protein fractions (Figure 7.3 B). Immunofluorescence microscopy analysis echoed these results, as SPI-1 needles were observed around the surfaces of many Δ*pbpA* pBAD-*hilD* and Δ*rodA* pBAD-*hilD* cells, suggestive of SPI-1 functionality, but were absent from the parent Δ*pbpA* and Δ*rodA* mutants. A significant increase in the number of cell-surface SPI-1 fluorescent foci was also observed in wild-type pBAD-*hilD* cells, showing that the overexpression of *hilD* led to an increase in SPI-1 T3SS expression (Figure 7.3 C).

These data demonstrate that in *S.* Typhimurium Δ*pbpA* and Δ*rodA* mutants, low levels of *hilD* expression from the pBAD-*hilD* vector, or rather the recovery of *hilD* expression, was necessary and sufficient to restore SPI-1 functionality. Also, SipD levels in Δ*pbpA* pBAD-*hilD* and Δ*rodA* pBAD-*hilD* cells were recovered approximately to that of the wild-type (Figure 7.3 B). This suggests that as expected, in *S.* Typhimurium at least, upstream regulators suppress expression of the SPI-1 genes in round-cell *mrd* mutants by regulating expression of the *hilD* SPI-1 regulator.

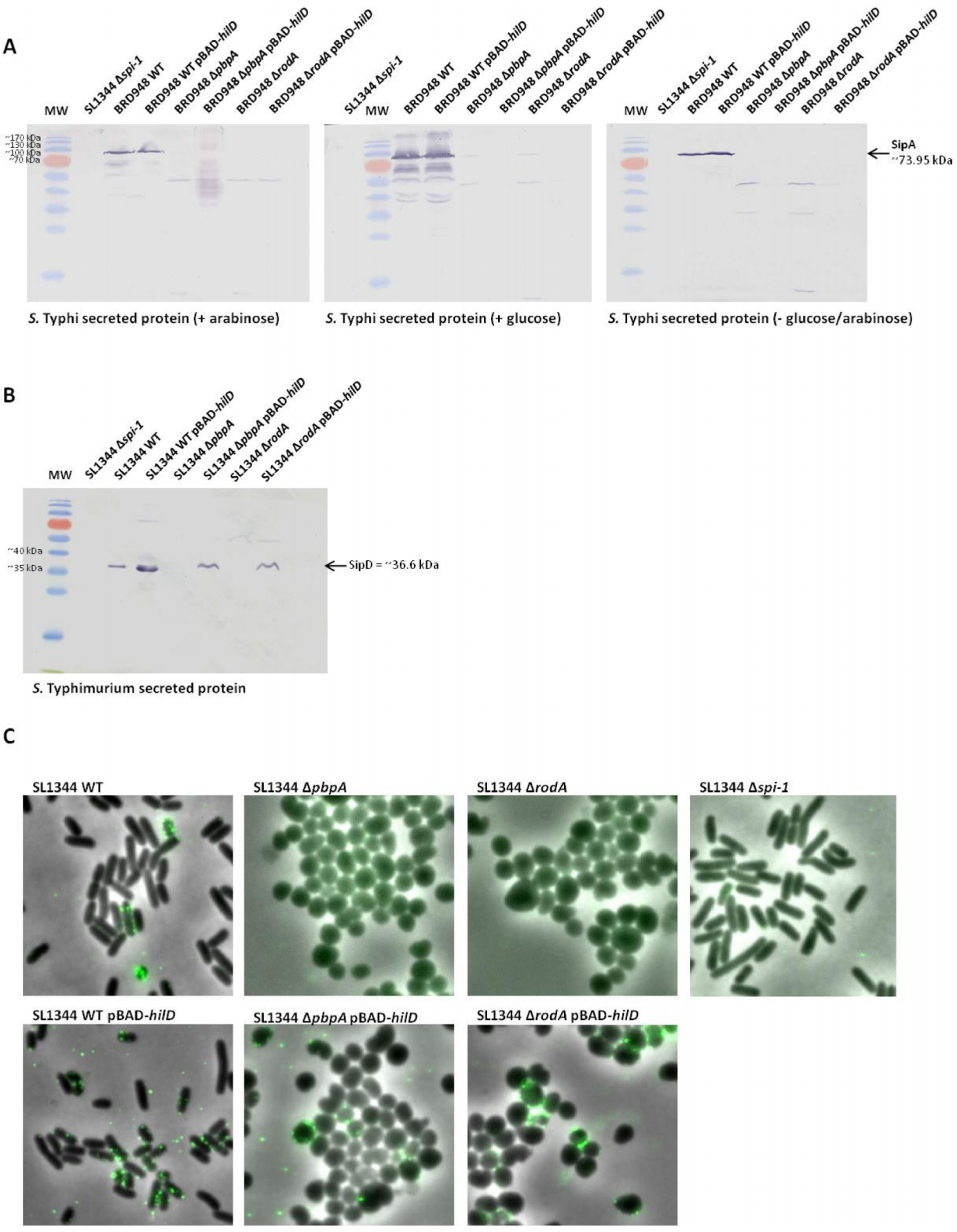

Figure 7.3: SPI-1 effector protein expression in ΔpbpA and ΔrodA mutants expressing pBAD-hilD: A – Western blots showing expression of the SPI-1 SipA effector protein in secreted protein fractions of BRD948 wild-type, Δ*pbpA* and Δ*rodA* strains ± pBAD-*hilD*. B – Western blot showing expression of the SPI-1 SipD effector protein in secreted protein fractions of SL1344 wild-type, Δ*pbpA* and Δ*rodA* strains ± pBAD-*hilD*. Background protein bands likely due to antibody cross-reactivity to intracellular proteins or aggregated Sip proteins. Protein molecular weight (MW) marker sizes as indicated. C - Immunofluorescence microscopy images of SL1344 wild-type (WT), Δ*pbpA* and Δ*rodA*

strains ± pBAD-*hilD,* overlaid onto phase contrast images; samples labelled with anti-SipD antibody and fluorophore-conjugated secondary antibody. All images are to the same scale. SL1344 Δ*spi-1* included as negative control. All cultures grown in LB broth at 37°C and 200 rpm, and harvested at mid-log phase. Where indicated, cultures were supplemented with 1 mM arabinose or glucose after 3 hours' growth.

7.4 Discussion

7.4.1 Introduction

Comprehensive analyses of major virulence determinant functionality in round-cell *mrd* mutants of *Salmonella* Typhi and Typhimurium have shown that the SPI-1 T3SS and flagella-mediated motility are non-functional in both Δ*pbpA* and Δ*rodA* mutants, whilst the SPI-2 T3SS remains active. These phenotypes were shown to be a direct consequence of the mutations in the *pbpA* or *rodA* genes. The SPI-1 and motility defects are thought to be at least in part due to the repression of expression of the major transcriptional regulators of the SPI-1 and flagella genes.

In order to further characterise the mechanisms behind the SPI-1 T3SS and motility defects, it was necessary to determine whether expression of both SPI-1 and flagella genes could be de-repressed in the round-cell mutants through recovered expression of the flagella and SPI-1 master regulators, and ultimately to determine whether this was sufficient to subsequently restore the functionality of these systems. For this reason the major transcriptional regulators of the SPI-1 and flagella genes, *hilD* and *flhDC* respectively, were expressed under the control of inducible heterologous promoters in round-cell *mrd* operon mutants of *Salmonella* in an attempt to restore flagella or SPI-1 gene expression (56, 62, 88). The resultant strains were assayed for functionality of SPI-1 or motility.

7.4.2 Recovery of SPI-1 and flagella gene expression with expression of SPI-1/flagella gene master regulators *in trans*

The recovery of *hilD* or *flhDC* expression *in trans* under the control of inducible heterologous promoters, was shown to restore SPI-1 functionality or motility respectively, in round-cell *mrd* mutants of *S.* Typhimurium. No significant differences in the expression levels of SPI-1 effector proteins, or actual numbers of SPI-1 needles were seen between Δ*pbpA* pBAD-*hilD* and Δ*rodA* pBAD-*hilD*

strains, and the wild-type. However, further work would be needed to accurately quantify levels of SPI-1 protein expression between wild-type and round-cell mutant strains expressing pBAD-*hilD*, to determine whether SPI-1 expression is reduced in the Δ*pbpA* and Δ*rodA* mutants.

However, although some motility was restored to round-cell mutants harbouring TPA14, motility remained significantly reduced in the Δ*pbpA* TPA14 and Δ*rodA* TPA14 strains, being on average less than 50% of that of the wild-type TPA14 strain. There may be a number of reasons for the observed reduction in the motility of round-cell mutants. It may indicate that other factors are involved in regulating flagella gene expression in round-cell *mrd* mutants, which act downstream of *flhDC*, at the level of the class II or class III gene promoters for example, to fine-tune flagella gene expression.

The FlgM and FliA proteins, encoding anti-σ^{28} and σ^{28} respectively, are important for the regulation of class III gene expression. FliA is naturally repressed by FlgM. With the removal of FlgM-mediated repression, on completion of basal body and hook assembly, FliA is enabled to activate expression of the class III genes, as well as class I and II genes (56, 62, 441). The ratio of FlgM to FliA molecules is also thought to be important in determining flagella number (441). *fliA* expression is dependent upon FlhD and FlhC, and a number of global regulators which induce *fliA* expression appear to act through $FlhD_4C_2$ (442, 443). However, a recent study in *E. coli* found that the transcriptional repressor NsrR specifically binds to the *fliA* promoter, inhibiting its expression, and ultimately reducing motility (444).

The finding that at least one transcriptional regulator can inhibit *fliA* expression, and with it motility, independently of *flhDC*, suggests that it is plausible that NsrR or a similar transcriptional repressor may also be involved in repressing motility at a level downstream of *flhDC* in round-cell *mrd* mutants, by decreasing the number of flagella per cell. FliA or FlgM form likely candidates as targets for such gene regulation, as they constitute the major regulators of genes involved in the later stages of flagella assembly which, importantly, act downstream of *flhDC*. Microarray data, however, showed that *nsrR* expression was not significantly

affected in the SL1344 *rodA* mutant, compared to the wild-type, being increased 1.23-fold compared to the wild-type (P value = 0.08).

Alternatively, defects in the cell wall structure of round-cell mutants may have restricted the successful assembly of the flagella apparatus, causing a reduction in the number of functional flagella expressed per cell. This explanation is unlikely when considering single cells, as flagella gene expression is tightly coupled to flagella assembly. A stalling in the assembly of the flagella apparatus results in the repression of downstream class III gene expression, and a complete loss of motility (56, 62). At a population level, however, variability between round-cell mutants may be such that motility is recovered in some, but not all Δ*pbpA* and Δ*rodA* cells. In some cells, the extent of defects to the cell wall structure may be sufficient to stall flagella assembly, preventing motility.

Although motility was reduced in Δ*pbpA* TPA14 and Δ*rodA* TPA14 strains, these results together demonstrate that round-cell mutants are able to assemble functional SPI-1 T3SS and flagella multi-protein complexes, the cell walls of these mutants remaining sufficiently robust to support such organelles. The inactivation of SPI-1 and motility systems appears to be caused, to a large extent, simply by the downregulation of *hilD* and *flhDC* gene expression.

Global responses to envelope-associated stress, caused by cell wall structural defects with the inactivation of *pbpA* or *rodA*, may lead to the inactivation of SPI-1 and flagella gene expression, although the major upstream regulators involved in mediating the Δ*pbpA* and Δ*rodA* motility/SPI-1 phenotypes remain to be identified. Future work will seek to isolate these regulators, and to further delineate the pathways involved in regulating SPI-1 and flagella genes in response to the inactivation of *pbpA* or *rodA*. This work will help better understanding into the global effects that the inactivation of cell shape determinants have on the physiology of *Salmonella*.

7.4.3 Recovery of SPI-1 expression in *S.* Typhimurium, but not *S.* Typhi Δ*pbpA* and Δ*rodA* mutants

Introduction of pBAD-*hilD* to Δ*pbpA* and Δ*rodA* mutants restored SPI-1 functionality in *S.* Typhimurium but not *S.* Typhi mutants. Furthermore, the addition of arabinose to *S.* Typhi cultures appeared to significantly inhibit growth of these strains. Increased sensitivity of *S.* Typhi to arabinose, from an inability to take up or utilise arabinose may be responsible for the growth defects in these strains. This may also have prevented arabinose from inducing expression of *hilD* from the P_{BAD} promoter in *S.* Typhi strains. However, background levels of uninduced *hilD* expression from the pBAD-*hilD* vector were also not apparent in these strains (in the absence of arabinose-mediated growth effects); effector protein expression was increased in uninduced *S.* Typhimurium cultures expressing pBAD-*hilD* (compared to the parent strain), but not in the equivalent *S.* Typhi strain. This may indicate that the *S.* Typhi strain was inherently unable to express pBAD-*hilD*.

Alternatively, differences between the Typhi and Typhimurium serovars may be such that low levels of *hilD* expression were insufficient to restore SPI-1 expression in *S.* Typhi round-cell mutants. If this is the case, it may highlight differences in the regulation of SPI-1 between *S.* Typhi and *S.* Typhimurium mutants.

Interestingly a small amount of SPI-1 expression was recovered in *S.* Typhi Δ*pbpA* and Δ*rodA* mutants lacking pBAD-*hilD* when grown in the presence of glucose. Further work is needed to establish how glucose was able to slightly alleviate suppression of SPI-1 gene expression.

Chapter 8. Global transposon mutagenesis screen to identify negative regulators of the motility phenotype in round-cell mutants and analysis of *mrd* mutant phenotype regulation

8.1 Introduction

Data from both phenotypic screens and complementation assays of the *Salmonella* Δ*pbpA* and Δ*rodA* mutants demonstrated that the expression of two major virulence factors, the SPI-1 T3SS and flagella-mediated motility, was almost completely downregulated in these mutants, at the level of the master regulator genes *hilD* and *flhDC*. However, the SPI-2 T3SS remained actively expressed in these mutants. Complementation of the expression of these genes *in trans* under the control of heterologous inducible promoters was sufficient to bring about a considerable recovery of SPI-1 expression and functionality, or motility, in both Δ*pbpA* and Δ*rodA* mutants. It is hypothesised that in round-cell mutants such as Δ*pbpA* and Δ*rodA*, the detection of envelope or other stress resulting from the inactivation of these genes results in the activation of transcription factors which repress the expression of both the SPI-1 and motility genes, but not SPI-2. It is likely that such regulators control the global stress response pathways. In order to better understand the regulatory pathways involved, which act upstream of *hilD* and *flhDC*, as well as to further characterise the effects that the inactivation of *pbpA* or *rodA* have on the cell wall and the general physiology of the cell, a screen was developed to enable the identification of upstream regulators which control *flhDC*, and possibly SPI-1, expression. Microarray data had not highlighted any specific candidate regulators with significantly altered expression in the Δ*rodA* mutant; therefore an alternative comprehensive screening strategy was required to identify putative regulators.

8.2 Global Tn*10*d(Tc) transposon screen in *S.* Typhimurium Δ*rodA* pMK1*lux-fliF* strain to identify luminescent revertants

8.2.1 Rationale for using a global transposon mutagenesis screen to identify major regulators of *flhDC*/*fliF* in Δ*rodA* mutants

A transposon mutagenesis screen was developed to enable the identification of putative regulators which are important for flagella gene regulation in Δ*pbpA* and Δ*rodA* mutants. Such a screen was considered ideal, since it permitted an unbiased and comprehensive coverage of the *Salmonella* genome. A global assay was needed whereby individual transposon-insertion mutants in the *Salmonella* Δ*pbpA*/Δ*rodA* genomes could be quickly screened for recovery of motility gene expression. The subsequent identification of the transposon insertion site would then identify genes whose functions were important for the repression of motility in round-cell mutants.

8.2.2 The Tn*10*d(Tc) mini transposon and generation of the Tn*10*d(Tc)-harbouring P22 phage library

Tn*10*d(Tc) is a 2640 bp transposition-defective derivative of the tetracycline-resistant Tn*10* transposon. It retains the *tetA* and *tetR* genes for tetracycline resistance, but lacks the transposase gene as well as the majority of the IS*10* inverted repeat sequences. Transposition of Tn*10*d(Tc) randomly into a host cell genome is therefore dependent upon the exogenous expression of the transposase protein from a plasmid (251, 252) (Figure 8.1). For use in the present screen, a phage lysate of a parent *Salmonella* strain (provided by Philip Aldridge, Newcastle, UK), which contained both Tn*10*d(Tc) and a plasmid-encoded transposase, was transduced into a wild-type SL1344 strain to enable the generation of individual transductant mutants with randomly inserted Tn*10*d(Tc) elements. These mutants were pooled to create a mutant library containing around 12000 individual mutants, allowing for good coverage of the *Salmonella* genome. A P22 phage lysate was then generated from the mutant library. This work was done prior to the present study (Hannah Spencer, Newcastle, UK). The P22 phage lysate of this Tn*10*d(Tc) mutant library was used for the present screen.

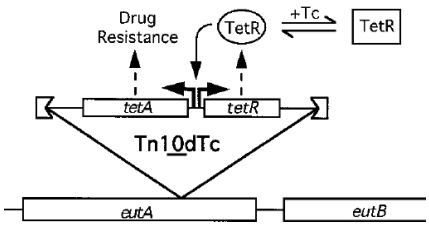

Figure 8.1: Structure of the mini transposon Tn10d(Tc): Schematic diagram illustrating the general structure of the Tn*10*d(Tc) Tn*10*-derived mini-transposon, including the *tetA*

and *tetR* genes. Image taken from "Transposition without Transposase: a Spontaneous Mutation in Bacteria" (252).

8.2.3 Use of pMK1*lux-fliF*-expressing strains for the detection of luminescent revertant Tn*10*d(Tc) mutants in global mutagenesis screen

Luciferase transcriptional reporter assays screening for *fliF* expression in *mrd* operon mutants of *S.* Typhi had shown that luminescence emitted from Δ*pbpA* and Δ*rodA* cultures was very low, indicating that *fliF* expression was highly downregulated compared to wild-type strains. The same assays were carried out in wild-type, Δ*pbpA* and Δ*rodA* strains of *S.* Typhimurium SL1344, producing almost identical results (Figure 8.2 A). Furthermore, the difference in luminescence emitted between the wild-type and round-cell mutant cells was clearly visible by eye from plate cultures of these strains, such that if exposed to light-sensitive film for as little as 20 seconds, the light emitted even from single colonies could be detected. The strong luminescence from the wild-type resulted in a large dark patch on light-sensitive film, whereas the signal from round-cell mutants was considerably weaker (Figure 8.2 B).

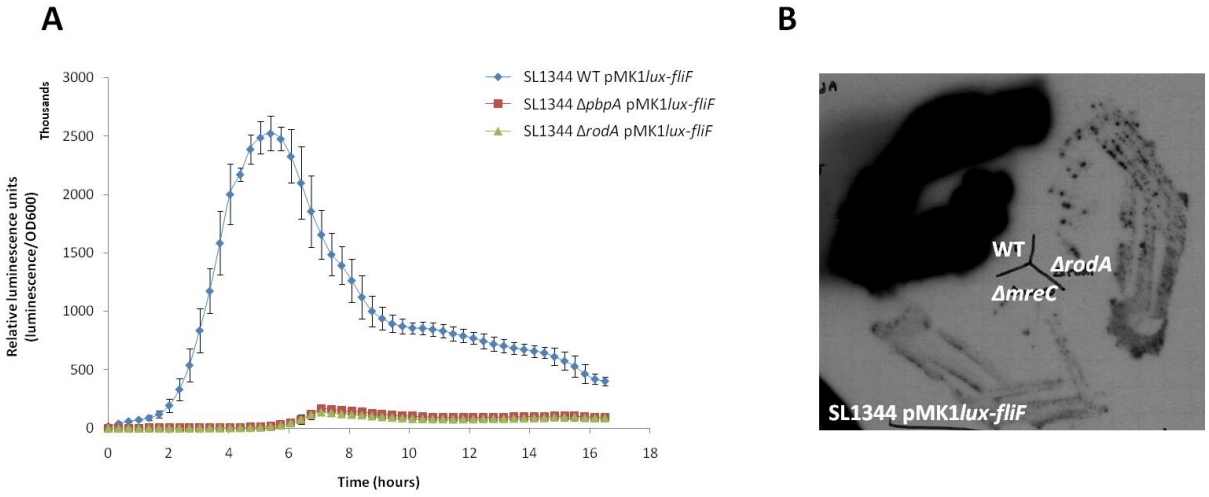

Figure 8.2: Expression of fliF in wild-type, ΔpbpA and ΔrodA strains of S. Typhimurium: A – Transcriptional luciferase reporter assays of SL1344 wild-type (WT), Δ*pbpA* and Δ*rodA* cultures expressing the luciferase promoter reporter plasmid pMK1*lux-fliF*. Promoter activity was measured in terms of relative luminescence units (luminescence per culture optical density at 600nm). Results indicative of *fliF* transcription levels in WT and *mrd* mutant cells. Cells were grown in LB medium at 37^{o}C with shaking. Growth rates of strains were equivalent. Values show means of 3 independent assays. Error bars = standard deviation. B – Image of light-sensitive film after exposure to plate cultures of SL1344 wild-type, Δ*rodA* and Δ*mreC* strains expressing pMK1*lux-fliF*, for ~20 seconds in the dark.

8.2.4 Global Tn*10*d(Tc) mutagenesis screen to recover luminescent revertants of *S.* Typhimurium Δ*rodA* with recovery of *fliF* expression

The strong luminescent signal emitted from the *fliF* promoter-luciferase plasmid in wild-type but not round-cell mutant strains enabled the development of a reporter system for the transposon mutagenesis screen; *S.* Typhimurium Δ*rodA* cells expressing the transcriptional reporter plasmid pMK1*lux-fliF* were transduced with the Tn*10*d(Tc) mutant phage library. After recovery and growth of the SL1344 Δ*rodA* pMK1*lux-fliF* Tn*10*d(Tc) mutant colonies, each of which harboured the Tn*10*d(Tc) transposon inserted somewhere into the genome, colonies were screened for recovery of luminescence, and hence *fliF* expression. Such revertant colonies were visualised by exposure to light-sensitive film, as previously described (Figure 2.5). Around 7200 transductant colonies have been screened in this way to date. Out of these, 21 luminescent revertants were isolated (0.29%). Arbitrary PCR, followed by DNA sequencing, was then used to identify the insertion sites of the Tn*10*d(Tc) transposon in all 21 revertants (Figure 2.3). The morphology of each luminescent revertant was also checked by microscopy. In all screens, wild-type and Δ*rodA* strains expressing pMK1*lux-fliF* were used as positive and negative controls, respectively.

S. Typhimurium strains were used in this screen rather than *S.* Typhi, due to the inability to transduce *S.* Typhi with P22, and the lack of an alternative Typhi-specific phage stock, although to date the phenotypes of Δ*pbpA* and Δ*rodA* mutants have been largely identical in both serovars (439). Also, the pMK1*lux-fliF* luminescence reporter plasmid was used rather than pRG38 (*flhDC*), as *flhDC* is thought to be a global regulator, controlling the expression of genes besides those involved in motility and chemotaxis (350). Measuring the expression of *fliF* therefore enabled a higher level of specificity, as the screen assayed for the recovery of motility specifically. However, since *fliF* is regulated by *flhDC*, a recovery of *fliF* expression would almost certainly be due to the upstream recovery of *flhDC* (56, 62). Finally the Δ*rodA* mutant was chosen over the Δ*pbpA* mutant for use in this screen, as it is likely that this mutant would have fewer polar effects on downstream gene expression than the Δ*pbpA* mutant, resulting from the kanamycin-resistance knockout cassette.

8.3 Identification of putative regulators of *fliF* expression and verification of revertant phenotypes

8.3.1 Re-screening of revertant colonies for luminescence and transduction of lesions into parent strains

In all, 21 luminescent Δ*rodA* pMK1*lux-fliF* Tn*10*d(Tc) mutant colonies have been recovered to date through the transposon mutagenesis screen. Each revertant retained its round-morphology, indicating that the recovery of luminescence was not from contamination, or a reversion in cell shape, but due to the specific recovery of *fliF* expression. The 21 revertants were each individually re-screened by exposing fresh re-patched plate cultures of each mutant to light-sensitive film. This was done to verify the luminescent phenotype. As such, 2 non-luminescent clones were rejected. The identity of the genetic lesions within each revertant is shown below (Table 8.1). The positions of each genetic lesion were mapped using the Vector NTI 10® software (Invitrogen™, California, US) (Figure 8.3).

Revertant clone	*Identity/location of Tn10d(Tc) genetic lesion*	*Gene function*	*Gene expression in SL1344 ΔrodA compared to WT**	*Revertant morphology (rod/round)*
4a	5' end of *rcsC* (stm2271)	Sensor kinase component of Rcs phosphorelay envelope stress response pathway; regulates flagella, colanic acid, and virulence gene expression.	-1.19 (ns)	Round
9a	5' end of *rcsC*			Round
9b	5' end of *rcsC*			Round
10a	Middle of *pagN* (stm0306)	PhoP-activated gene; outer membrane adhesin/invasin	+2.87	Round
15a	Middle of *rcsC*			Round
18a	5' end of *phsA* (stm2065)	Thiosulphate reductase	-11.00	Round
37a	3' end of *rcsC*	See above		Round
40a	Intergenic, upstream of *lrhA* (stm2330)	Transcriptional repressor of motility and chemotaxis genes	-7.03	Round
2a (b)	*rcsC* – As 15a	See above		Round
5a (b)	rcsC – As 15a	See above		Round
6a (b)	5' end of *dcm* (stm1992)	DNA cytosine methylase	-1.04 (ns)	Round
9a (b)	5' end of *rcsC*	See above		Round
13a (b)	Middle of *rcsC*	See above		Round
18a (b)	rcsC – As 4a	See above		Round
22a (b)	?			Round
22b (b)	?			Round
32a (b)	*rcsC* (un-mapped)	See above		Round

42a (b)	*rcsC* (un-mapped)	See above	Round
45a (b)	*rcsC* (un-mapped)	See above	Round

*Data from microarray analysis of gene expression of SL1344 Δ*rodA* compared to wild-type. 'ns' – non-significant, where P values were >0.05

Table 8.1: Identity of Tn10d(Tc) genetic lesions within the genome of luminescent revertants of S. Typhimurium ΔrodA: Position of genetic lesions identified by arbitrary PCR and sequencing, as described. Information on gene function taken from Kegg gene database (253).

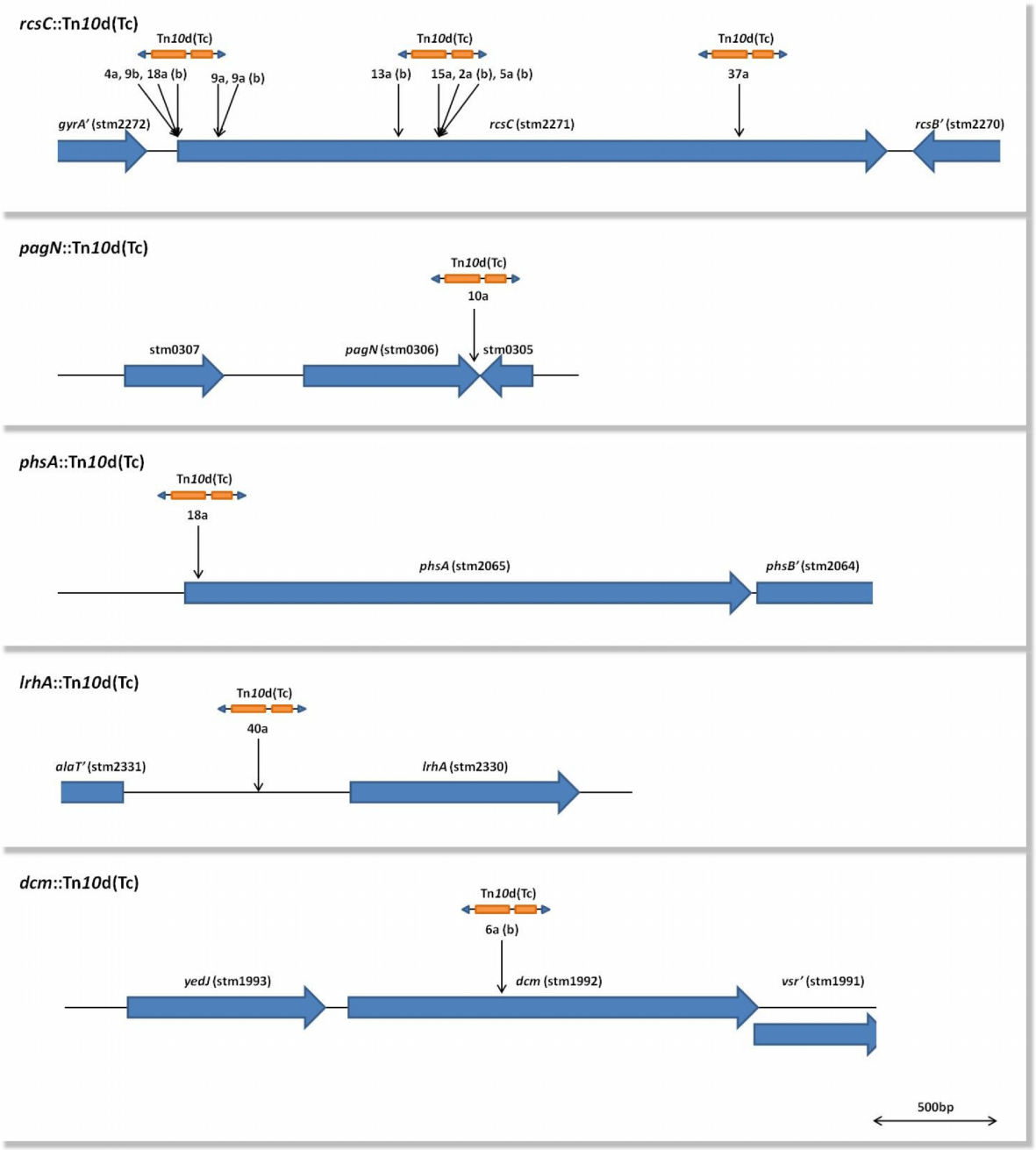

Figure 8.3: Mapped positions of S. Typhimurium ΔrodA pMK1lux-fliF Tn10d(Tc) luminescent revertants: Tn*10*d(Tc) insertion positions for each positive revertant were sequenced and mapped using Vector NTI 10® software, to illustrate their position within the genome. Insertion sites are indicated by black arrows, along with revertant names. Gene maps drawn to scale (2640 bp Tn*10*d(Tc) elements not drawn to scale).

In addition to re-screening each revertant for recovery of luminescence, to ensure the initial observations were not artefacts, the motility of each Δ*rodA pMK1lux-fliF* Tn*10*d(Tc) revertant strain was examined microscopically and in motility assays. These initial assays demonstrated that both the *prc*::Tn*10*d(Tc) and *lrhA*::Tn*10*d(Tc) mutants were non-motile or showed negligible motility. Since the screen aimed to identify major regulators of motility genes in round-cell mutants, ultimately it sought to identify revertants in which motility was also recovered. As such these two mutants were not further analysed.

P22 phage lysates were subsequently generated from each revertant strain. Both wild-type and Δ*rodA* parent strains of SL1344 were then transduced with each lysate and grown overnight on LB agar containing tetracycline to select for transductants in which the Tn*10*d(Tc) lesion was transferred back into the parent strain. The transduction of the genetic lesions back into the parent strains constituted a further step to ensure the recovered revertants were not false positives, through the accumulation of secondary mutations which may have altered *fliF* expression.

8.3.2 Insertional hot spots of Tn*10*d(Tc)

The Tn*10* transposon, and hence the Tn*10*d(Tc) derivative, preferentially targets particular DNA sequences, creating 'hot spots'; regions in the genome into which the transposon frequently inserts. The preferred consensus sequence helping determine the point of insertion of Tn*10*d(Tc) is a 6 base pair sequence: GCTNAGC, contained within a 9 bp symmetrical sequence which is cleaved and duplicated upon transposon insertion. This sequence is thought to be recognised by the transposase enzyme (445-447).

The tendency of Tn*10*d(Tc) to transpose into 'hot spot' regions, rather than randomly into the genome could affect the ability to achieve comprehensive genome-wide coverage within a global transposon mutagenesis screen. It was also considered that the repeated isolation of revertants with mutations at the same sites could be caused by the presence of strong hot spot sequences, rather than the identification of likely regulator candidates.

For this reason 12 randomly selected non-luminescent colonies of the SL1344 Δ*rodA pMK1lux-fliF* Tn*10*d(Tc) transductants were isolated, re-screened for luminescence, and sequenced to determine the insertion site of Tn*10*d(Tc). This was done to determine whether any specific mutants were isolated at a particularly high frequency, and to judge whether the frequent isolation of *rcsC* mutants was due to a high rate of transposition into this gene, rather than specifically because of recovery of luminescence. The 12 randomly picked transductants were sequenced and mapped, as shown (Figure 8.4). All were shown to lack any recovery of luminescence.

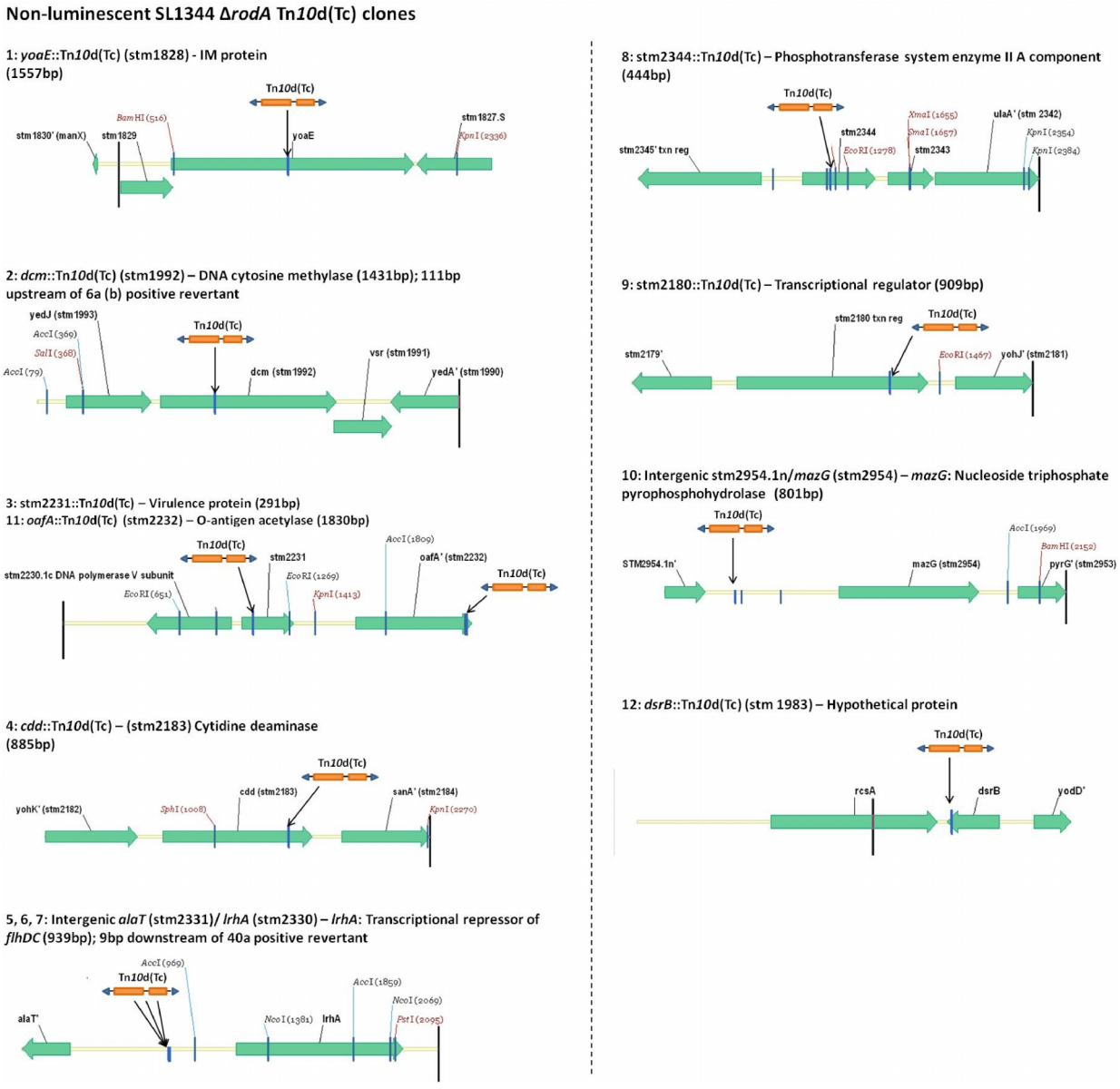

Figure 8.4: Mapped positions of randomly-selected S. Typhimurium ΔrodA pMK1lux-fliF Tn10d(Tc) non-luminescent mutants (negative controls): Tn*10*d(Tc) insertion positions for each randomly picked non-luminescent mutant were sequenced

and mapped using Vector NTI 10® software, to illustrate position within the genome. Insertion sites are indicated by black arrows. Individual gene maps drawn to scale (2640 bp Tn*10*d(Tc) elements not drawn to scale).

From this assay 3 non-luminescent transductants were identified with Tn*10*d(Tc) insertions located at an intergenic position between the transcriptional regulator *lrhA* (stm2330) and the *yfbQ* (stm2331) gene. These insertions were located at an almost identical position to the Tn*10*d(Tc) insertion in the 40a revertant strain (Table 8.1) and another isolated revertant (which was later rejected, due to a lack of recovered luminescence), as well as several luminescent revertants isolated in a parallel Δ*mreCD* transposon screen (unpublished work from this lab) (Figure 8.3 and 8.4). Thus it would appear that this region in particular constitutes a strong hot spot for the insertion of Tn*10*d(Tc). However, *lrhA* initially presented itself as a potential candidate for the regulation of flagella, since it encodes a transcriptional repressor of *flhDC*, and also due to its frequent isolation (437). However, the position of the insertion is likely to increase *lrhA* expression, which would be expected to decrease motility, as was observed previously in a similar transposon mutant (448). Subsequent motility assays and repeated luminescence screens with *lrhA*::Tn10d(Tc) mutants showed that these revertants were not in fact motile, or luminescent. An additional non-luminescent clone was isolated in which Tn*10*d(Tc) was inserted close to the Tn*10*d(Tc) insertion point in the positive revertant 6a (b), within the *dcm* gene (Figure 8.3 and 8.4). As such, both *lrhA,* and *dcm* were disregarded as potential regulator candidates.

The apparent frequency of Tn*10*d(Tc) insertion into hot spots clearly demonstrated that care must be taken when conducting this screen; it was essential to verify results, ensuring that luminescent revertants were not artefacts, but the result of the insertion of Tn*10*d(Tc) directly affecting the expression of *fliF* and downstream motility functionality. In these false positive strains, it may be that secondary mutations led to a significant increase in *fliF* expression and luminescence. During the screen to identify non-luminescent transductants, neither *rcsC* or *pagN* were isolated. In contrast, just over 60% of the positive luminescent revertants harboured Tn*10*d(Tc) insertions within *rcsC*. This combined with further verification which indicated that flagella gene expression and motility were significantly recovered in both *rcsC*::Tn10d(Tc) and *pagN*::Tn10d(Tc) mutants of Δ*rodA*,

provided evidence to suggest that these two genes may form true candidates for regulators.

8.3.3 Identification of *rcsC* and *pagN* as putative flagella gene regulators in *S.* Typhimurium Δ*rodA*

After excluding those revertants identified in the screen which appeared to be artefacts, two genes remained as possible candidates for involvement in the regulation of motility genes in round-cell mutants: *rcsC* and *pagN*. *rcsC* forms the sensor kinase component of the Rcs phosphorelay; a two component system which is one of the major global regulators of the stress response (118, 119). This system responds to certain stresses, including envelope stress, activating the expression of colanic acid biosynthesis, SPI-2 and Vi capsule biosynthesis genes, whilst downregulating transcription of flagellar and SPI-1 genes (50, 96, 118, 320). Furthermore, the Rcs phosphorelay activates the expression of the *ftsA* and *ftsZ* division genes in *E. coli* at least (119, 322). This points towards *rcsC* being a highly likely candidate for involvement in flagella gene regulation in round-cell mutants, particularly as it is known to respond specifically to peptidoglycan-associated stress, such as may be seen in *pbpA* and *rodA* mutants (118). The isolation of 13 luminescent revertants with genetic lesions at various positions within *rcsC* added further weight to the possibility that this gene may play a major regulatory role in the Δ*rodA* mutant. However, Tn*10*d(Tc) insertions were strangely isolated only in the *rcsC* and not within other important members of the Rcs phosphorelay, including the response regulator RcsB, the intermediate RcsD protein, or the outer membrane RcsF protein, which is thought to detect envelope stress and activate RcsC (119). Also, transcriptional data from microarrays in the present study did not provide meaningful information on the expression of *rcsC* or the other major Rcs phosphorelay genes in the Δ*rodA* mutant.

pagN (stm0306) may also be of some interest, potentially playing a role in motility regulation. Although a *pagN*::Tn*10*d(Tc) revertant was isolated just once in this assay, a parallel screen with round-cell Δ*mreCD* mutants has also isolated a *pagN*::Tn*10*d(Tc) luminescent revertant (unpublished work of this lab). Less is known about PagN, although it was recently characterised as an integral outer

membrane adhesin protein, which is encoded within the SPI-6 pathogenicity island of both *Salmonella* Typhi and Typhimurium (423, 449). PagN, a paralog of SapA, assists in adhesion to and invasion of mammalian cells, and hence may be important for virulence (397, 423, 425). Studies also demonstrated that *pagN* is maximally expressed in SPI-2-inducing conditions, being upregulated by the PhoP/PhoQ virulence gene master regulator as well as the virulence gene activator SlyA (38, 98, 422, 423, 450). Interestingly, the overexpression of PagN was shown to compensate for a lack of SPI-1. A possible explanation for this is that it is needed intracellularly to exit cells in situations where SPI-1 is not expressed (423). However, a role for PagN in the regulation of gene expression has not been identified. Microarray data from this study showed that *pagN* was upregulated ~2.9-fold in the *S.* Typhimurium Δ*rodA* mutant.

The positions of the Tn*10*d(Tc) insertions were all within the coding sequence of the *rcsC* and *pagN* genes, suggesting that gene function would be completely inactivated in these mutants. Furthermore, among the *rcsC* revertant mutants isolated, the position of the Tn*10*d(Tc) insertion varied between transductants, with insertions being isolated at the 5' end, the 3' end and in the middle of the *rcsC* coding sequence (Figure 8.3). This suggests that the motility reversion is not specific to the inactivation of a particular segment of the gene; rather that an insertion of Tn*10*d(Tc) in any part of *rcsC* is sufficient to disrupt its function, particularly in terms of motility regulation.

8.3.4 Motility of *S.* Typhimurium wild-type, Δ*rodA*, *rcsC*::Tn*10*d(Tc) and *pagN*::Tn*10*d(Tc) strains

Motility functionality in *S.* Typhimurium Δ*rodA* *rscC*::Tn*10*d(Tc) and *pagN*::Tn*10*d(Tc) transduced strains was assessed by culturing these cells in semi-solid motility agar containing 20 mM $MgCl_2$ and measuring the extent of culture spread in comparison to that of the wild-type and the wild-type *rscC*::Tn*10*d(Tc) and *pagN*::Tn*10*d(Tc) transduced strains. In addition, revertant strains were observed by phase contrast microscopy for signs of motility. Two individual *rscC*::Tn*10*d(Tc) strains were tested for recovery of motility, both strains

harbouring *rcsC* insertions at different positions within the 5' end of the *rcsC* gene ('4a' and '9a') (Figure 8.3).

Motility assays demonstrated that motility functionality in *rscC*::Tn*10*d(Tc) and *pagN*::Tn*10*d(Tc) strains, where the lesions were transduced into wild-type SL1344, was not significantly changed from the wild-type strain in which *rcsC* and *pagN* were functional. However, when compared to the SL1344 Δ*rodA* mutant strain, the Δ*rodA rscC*::Tn*10*d(Tc) (9a) and Δ*rodA pagN*::Tn*10*d(Tc) strains showed a significant increase in motility, up to around 50% of that of the wild-type. This was not the case for the Δ*rodA rscC*::Tn*10*d(Tc) (4a) strain, however, in which motility was not significantly greater than the parent Δ*rodA* strain (Figure 8.5 A). Interestingly, this parent strain appeared slightly motile, with motility assays demonstrating just under 20% of the motility of the wild-type. However, it is known that within a population of Δ*rodA* or Δ*pbpA* cells, a small proportion of cells remain motile. Thus the low level of motility in this strain, and perhaps the '4a' strain, may be due to this small proportion of motile cells. By microscopy, the vast majority of the Δ*rodA* parent cells appeared non-motile, and though the extent of spread throught motility agar was up to 20% of that of the wild-type, it was noted that the density of cells within this margin of spread was very low and faint compared to the wild-type.

The motility of the revertant Δ*rodA* strains remained significantly less than both the wild-type, and the wild-type *rscC*::Tn*10*d(Tc) and *pagN*::Tn*10*d(Tc) strains. This, along with the identification of two possible factors which influence motility in round-cell mutant strains, suggests that the control of flagella gene expression in round-cell mutants is more complex and multi-factorial, as would be expected given the number of global regulators known to influence flagella expression (110). However, the significant recovery of *fliF* expression, along with motility functionality, in *ΔrodA ΔrcsC* and *ΔrodA ΔpagN* double mutants, suggests that these two genes are indeed involved in regulating flagella gene expression in round-cell mutants. It may be that in the *ΔrodA rcsC*::Tn*10*d(Tc) (4a) strain, other factors were active to a greater extent in regulating flagella expression, possibly working to counteract the loss of *rcsC*.

The majority of Δ*rodA* *rcsC*::Tn*10*d(Tc) revertants, as well as the transduced Δ*rodA* *rcsC*::Tn*10*d(Tc) (9a) and the Δ*rodA* *pagN*::Tn*10*d(Tc) (10a) strains appeared highly motile by microscopy. In addition, from phase contrast microscopy images it was noted that cells of the revertant strains generally appeared significantly smaller in diameter than the parent Δ*rodA* strains, particularly with *rcsC*::Tn*10*d(Tc) (9a) and *pagN*::Tn*10*d(Tc) (10a) cells. This was also true of a large proportion of revertant strains, seen in both this screen, and in a similar screen with a SL1344 Δ*mreCD* mutant (unpublished work of this lab). Since the same phenotype was not as obvious in *rcsC*::Tn*10*d(Tc) 4a, it may be that motility is influenced by cell size and diameter, or that factors involved in regulating the size of these mutants, also act on motility genes (Figure 8.5 B).

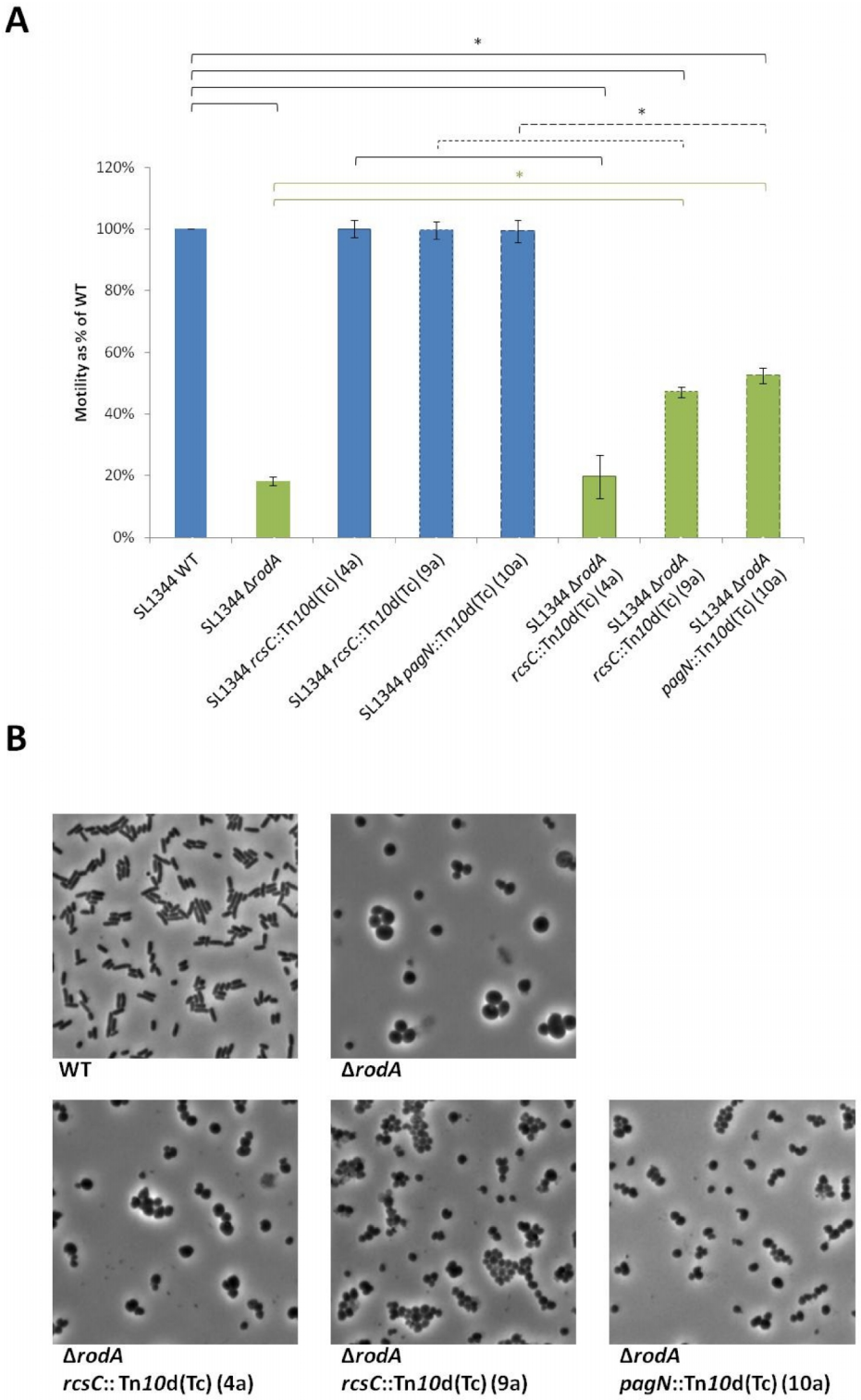

Figure 8.5: Motility assays and phase contrast microscopy of S. Typhimurium wild-type, ΔrodA, rcsC::Tn10d(Tc) and pagN::Tn10d(Tc) strains: A - Motility assay results for SL1344 wild-type, Δ*rodA,* and *rcsC*::Tn*10*d(Tc) and *pagN*::Tn*10*d(Tc) revertant strains (Tn*10*d(Tc) lesions transduced back into parent wild-type and Δ*rodA* strains). Cells were cultured in semi-solid motility agar containing 20 mM $MgCl_2$, at 37°C for ~6 hours. Motility was measured in terms of extent (diameter) of culture spread through motility agar, as a percentage of that of relevant wild-type strain. Results show averages from 3 independent assays. Error bars indicate standard deviation. Asterisks indicate statistically significant differences, where P values were ≤0.05 as determined by Students t-tests. B – Phase contrast microscopy images of the above strains. All images are to the same scale.

8.4 SPI-1 T3SS functionality in *S.* Typhimurium *ΔrodA rcsC*::Tn*10*d(Tc) and *ΔrodA pagN*::Tn*10*d(Tc) double mutants

In addition to examining the morphology and motility phenotypes of the Δ*rodA* *rcsC*::Tn*10*d(Tc) and Δ*rodA* *pagN*::Tn*10*d(Tc) revertant strains, it was important to analyse the expression of the SPI-1 T3SS in these strains, to determine whether the inactivation of *rcsC* or *pagN* was sufficient to restore SPI-1 expression, and thus whether these genes formed likely candidates for global regulators of the overall virulence phenotypes in round-cell *mrd* operon mutants.

Wild-type, Δ*rodA*, *rcsC*::Tn*10*d(Tc) and *pagN*::Tn*10*d(Tc) strains were grown to mid-log phase, harvested, fixed and labelled with anti-SipD antibody for visualisation by immunofluorescence microscopy. Secreted protein fractions were also prepared from culture supernatants and subjected to SDS-PAGE and western blotting with anti-SipD antibody.

Western blotting from secreted protein samples of *S.* Typhimurium wild-type, Δ*rodA*, *rcsC*::Tn*10*d(Tc), and *pagN*::Tn*10*d(Tc) cultures showed that there was considerable restoration of SipD expression in both the Δ*rodA* *rcsC*::Tn*10*d(Tc) (9a) and Δ*rodA* *pagN*::Tn*10*d(Tc) (10a) strains, as a reasonably strong SipD band was evident in these lanes. SipD was not expressed in the Δ*rodA* parent, or in the Δ*rodA* *rcsC*::Tn*10*d(Tc) (4a) strain (Figure 8.6 A). This result echoed motility assays, which showed that motility was recovered in the 9a and 10a revertants, but not in 4a. However, SipD protein expression levels in the Δ*rodA* 9a and 10a revertant strains were clearly not as high as those in the wild-type, or equivalent *rcsC*::Tn*10*d(Tc) and *pagN*::Tn*10*d(Tc) strains with a wild-type *rodA* gene, the intensity of the SipD band being much greater in the latter strains.

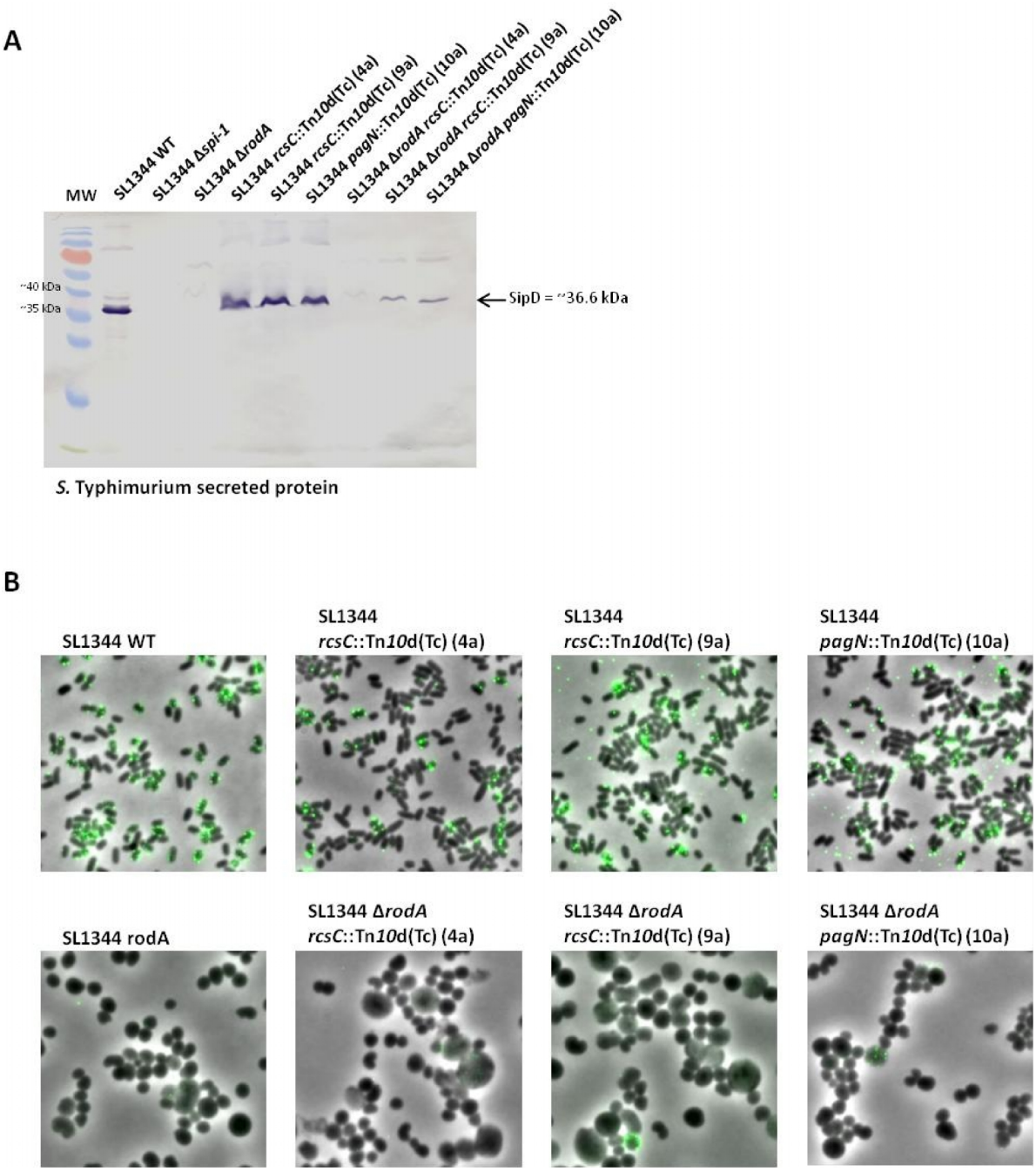

Figure 8.6: SPI-1 effector protein expression in S. Typhimurium wild-type, ΔrodA, rcsC::Tn10d(Tc) and pagN::Tn10d(Tc) strains: A – Western blot showing expression of the SPI-1 SipD effector protein in secreted protein fractions of SL1344 wild-type, Δ*rodA, rcsC*::Tn*10*d(Tc) and *pagN*::Tn*10*d(Tc), and Δ*spi-1* (negative control). Background protein bands likely due to antibody cross-reactivity to intracellular proteins or SipD translocon complexes. Protein molecular weight (MW) marker sizes as indicated. B - Immunofluorescence microscopy images of SL1344 wild-type, Δ*rodA, rcsC*::Tn*10*d(Tc) and *pagN*::Tn*10*d(Tc) cells, overlaid onto phase contrast images; samples labelled with anti-SipD antibody and fluorophore-conjugated secondary antibody. All images are to the same scale. All cultures grown in LB broth at 37°C and 200 rpm, and harvested at mid-log phase.

However, immunofluorescence microscopy analysis of SPI-1 functionality suggested that though SipD may be expressed in the Δ*rodA rcsC*::Tn*10*d(Tc) and *pagN*::Tn*10*d(Tc) revertant strains, the SPI-1 T3SS needle may not be functional in these cells; fluorescent foci indicative of SPI-1 T3S needles were clearly visible around the surface of all strains with a wild-type *rodA* gene, but not in any of the Δ*rodA* strains, including Δ*rodA rcsC*::Tn*10*d(Tc) (9a) and Δ*rodA pagN*::Tn*10*d(Tc) (10a) (Figure 8.6 B). Only occasionally were fluorescent foci observed at the surface of these cells. Interestingly, the average size of Δ*rodA* Δ*rcsC*/Δ*pagN* double mutant cells in these cultures did not appear significantly different from the parent Δ*rodA* strain.

In conclusion, the global transposon mutagenesis screen was clearly effective, enabling the identification of two possible regulators of flagella gene expression in the round-cell *mrd* operon mutants of *Salmonella*. Inactivation of either *pagN* or *rcsC* through the insertion of the mini transposon Tn*10*d(Tc) was shown to bring about significant recovery of *fliF* expression, actual motility and SPI-1 T3SS protein expression, although the SPI-1 T3SS may not be functional in these strains. The mechanisms behind the recovery of motility and SPI-1 expression in Δ*rodA rcsC*::Tn*10*d(Tc) and Δ*rodA pagN*::Tn*10*d(Tc) strains remain unclear. Whether or not, and how, the morphology and size of revertant cells is linked to the recovery of *flhDC* and motility, also remains to be elucidated.

8.5 Growth of *S.* Typhimurium Δ*rodA* Tn*10*d(Tc) motility revertants on Congo red agar

Another potentially interesting aspect of the revertant cells, and particularly those with *rcsC* mutations, was the level of extracellular polysaccharide expression in these strains, giving an indication of biofilm production (cellulose and colanic acid both form integral parts of mature biofilms (323, 471)). Growth of a number of the un-transduced revertant Tn*10*d(Tc) mutants (those expressing pMK1*lux-fliF*) on Congo red agar demonstrated that cellulose production in these strains was similar to that in the *S.* Typhimurium Δ*rodA* strain. Cellulose capsule expression appeared significantly greater than the wild-type in both the Δ*rodA* and Δ*rodA* Tn*10*d(Tc) revertant strains, as indicated by the more intense red colony

appearance (rdar phenotype) (Figure 8.7) (326). Given that the Rcs phosphorelay is a major activator of colanic acid biosynthesis, one may expect colanic acid production to be reduced in *rcsC*::Tn*10*d(Tc) strains particularly, although Congo red-binding gives an indication of cellulose, and not colanic acid production (119, 320). This result also reiterates the hypothesis that the regulation of extracellular polysaccharide biosynthesis and virulence phenotypes of round-cell mutants may be complex and multifactorial.

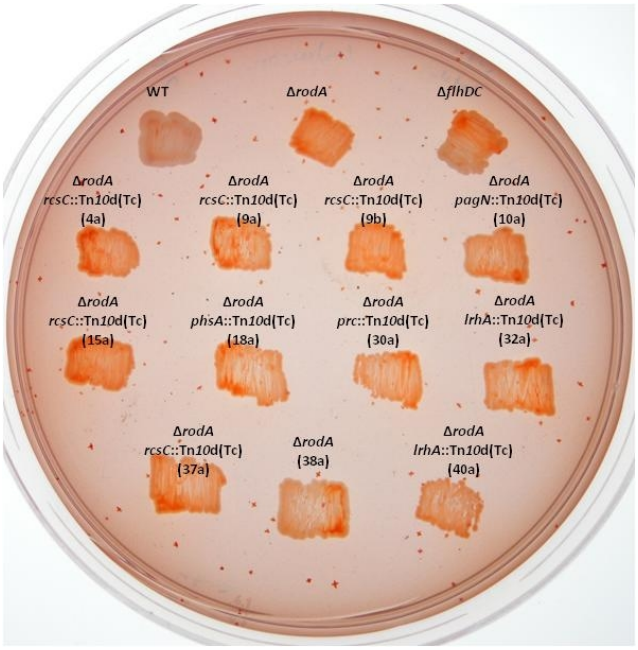

Figure 8.7: Growth of S. Typhimurium wild-type, ΔrodA and Tn10d(Tc) positive motility revertant strains on Congo red agar: SL1344 wild-type, Δ*rodA* and Tn*10*d(Tc) positive motility revertant strains were streaked onto LB agar containing 100 µg/ml Congo red dye to screen for excess cellulose production, as indicated by the development of red colonies; the rdar phenotype.

8.6 Generation and phenotypic analyses of specific Δ*pbpA*/Δ*rodA* Δ*rcsC*/Δ*pagN* double mutants in *S.* Typhimurium and *S.* Typhi

8.6.1 Generation of specific Δ*pbpA*/Δ*rodA* Δ*rcsC*/Δ*pagN* double mutants in *S.* Typhimurium and *S.* Typhi

In order to further investigate the role that *rcsC* and *pagN* may play in the regulation of virulence genes in round-cell *mrd* operon mutants of *Salmonella*, specific knockout mutants of the *pagN* and *rcsC* genes were constructed in wild-type, Δ*pbpA* and Δ*rodA* strains of both *S.* Typhi and *S.* Typhimurium, using the

Datsenko and Wanner method (238). In this instance the pKD3 template plasmid was used to generate chloramphenicol-resistance cassettes for specific insertion into each target gene. This enabled the construction of non-polar mutants of the *rcsC* and *pagN* genes. The successful generation of chloramphenical-resistant Δ*rcsC* and Δ*pagN* mutants was checked by both PCR and DNA sequencing. Using this method Δ*rcsC* mutants were created in wild-type, Δ*pbpA* and Δ*rodA* strains of both *S.* Typhi and *S.* Typhimurium. Δ*pagN* mutants were successfully created in wild-type, Δ*pbpA* and Δ*rodA* strains of *S.* Typhimurium, and in the wild-type and Δ*rodA* strains of *S.* Typhi. Chloramphenical resistance cassettes were not removed from the Δ*rcsC* or Δ*pagN* mutant strains, although due to the inherent stop codons and ribosome binding sites of the pKD3-encoded knockout cassette, mutants generated with these cassettes should be non-polar on the expression of downstream genes (238).

This creation of such mutants was necessary in order to verify that the observed phenotypes of the Δ*rodA rcsC*::Tn*10*d(Tc) and *pagN*::Tn*10*d(Tc) strains could be replicated, demonstrating that they were due specifically to the inactivation of *rcsC* or *pagN* and not due to polar or other effects brought about by the transposon insertion. It was also important to test whether the inactivation of *rcsC* or *pagN* was sufficient to restore at least some motility or SPI-1 gene expression in round-cell mutants of *S.* Typhi, as well as *S.* Typhimurium.

8.6.2 Phenotypic analysis of Δ*rcsC* and Δ*pagN* mutants in *S.* Typhimurium and *S.* Typhi

Motility assays

Motility of the wild-type, round-cell *mrd* mutant, Δ*rcsC*, Δ*pagN* and double mutant strains, of both *S.* Typhi and *S.* Typhimurium, was assayed by measuring the extent of spread of each culture after growth in semi-solid motility agar containing 20 mM $MgCl_2$ at 37°C for at least 6 hours. The motility of each strain was measured as a percentage of that of the wild-type.

These assays demonstrated that around 30% motility was restored in both Δ*pbpA* Δ*rcsC* and Δ*pbpA* Δ*pagN* double mutants of *S.* Typhimurium, as well as the Δ*rodA*

Δ*rcsC* strain, but not in Δ*rodA* Δ*pagN* cells. However, a difference in motility of statistical significance between these strains and the Δ*pbpA* or Δ*rodA* parent was only true for the Δ*pbpA* Δ*rcsC* cells, suggesting that the deletion of *rcsC* in Δ*pbpA* may restore some motility, if only low levels. This recovery of motility was much less evident than that seen in Δ*rodA* *rcsC*::Tn*10*d(Tc) (9a) and Δ*rodA* *pagN*::Tn*10*d(Tc) (10a) strains, where motility was recovered to around 50% of the wild-type motility levels (Figure 8.8 A and Figure 8.5A). In *S.* Typhimurium Δ*rcsC* and Δ*pagN*, motility was very slightly reduced compared to wild-type cells, although this was only statistically significant in the Δ*pagN* mutant (Figure 8.8 A).

Motility assays with the equivalent *S.* Typhi strains demonstrated that double mutants of both Δ*pbpA* and Δ*rodA* strains remained completely non-motile (Figure 8.8 B). Also, motility was slightly, but significantly reduced in both BRD948 Δ*rcsC* and BRD948 Δ*pagN* strains compared to the wild-type (Figure 8.8 B).

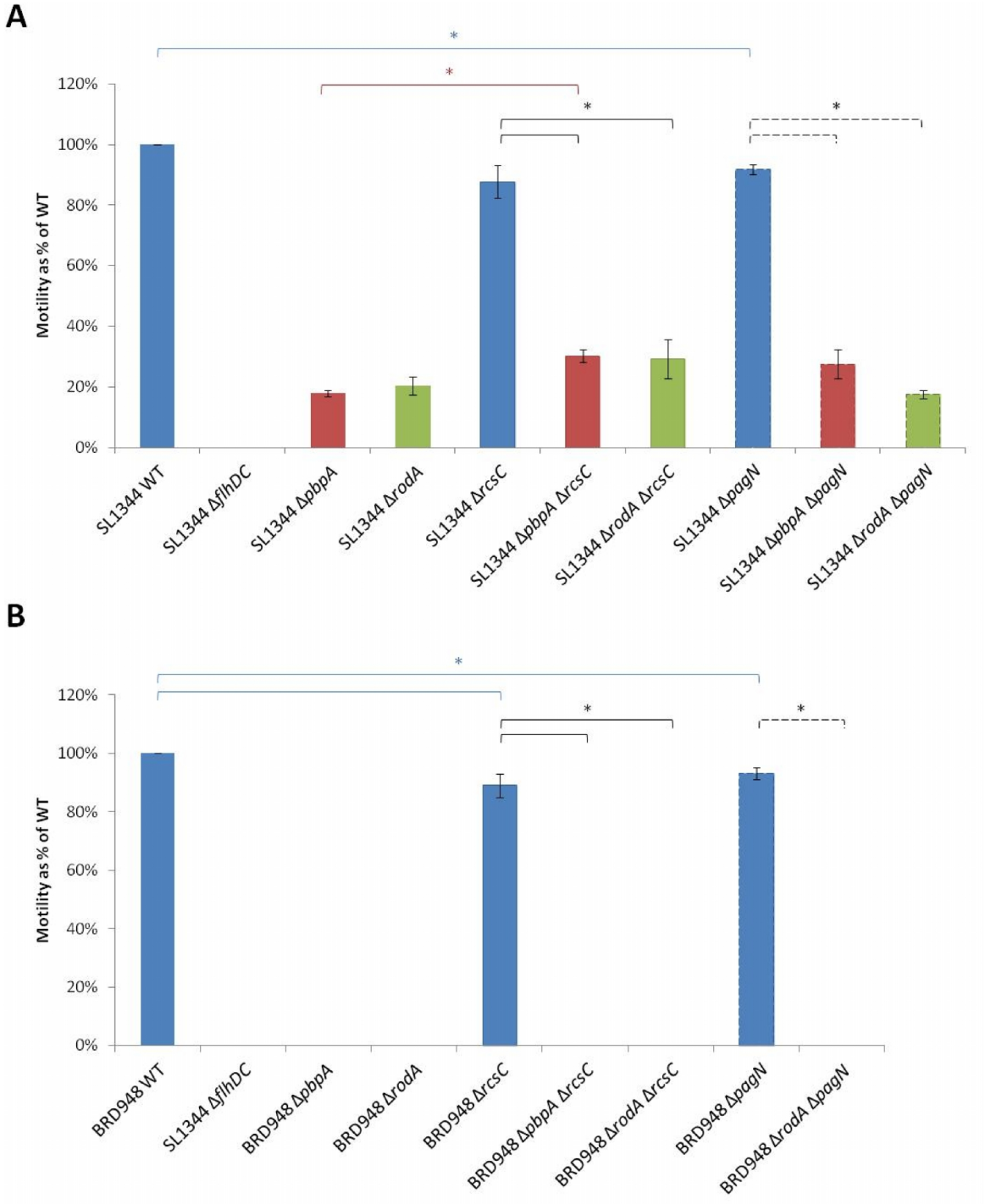

Figure 8.8: Motility assays with S. Typhimurium and S. Typhi wild-type, ΔpbpA/ΔrodA and ΔrcsC/ΔpagN mutants: A - Motility assay results for SL1344 wild-type, Δ*pbpA*/Δ*rodA* and Δ*rcsC*/Δ*pagN,* single and double mutants. B - Motility assay results for BRD948 wild-type, Δ*pbpA*/Δ*rodA* and Δ*rcsC*/Δ*pagN,* single and double mutants. Cells were cultured in semi-solid motility agar containing 20 mM $MgCl_2$, at 37°C for ~6 hours. Motility was measured in terms of extent (diameter) of culture spread through motility agar, as a percentage of that of relevant wild-type strain. Results show averages from 3 independent assays. Error bars indicate standard deviations. Asterisks indicate statistically significant differences, where P values were ≤0.05 as determined by Students t-tests.

SPI-1 T3SS functionality

To measure the expression of SPI-1 effector proteins and determine the functionality of the SPI-1 T3SS in Δ*rcsC* and Δ*pagN* double mutants, SDS-PAGE separation of mid-log phase secreted protein fractions, with western blotting, was carried out, along with immunofluorescence microscopy of fixed cells.

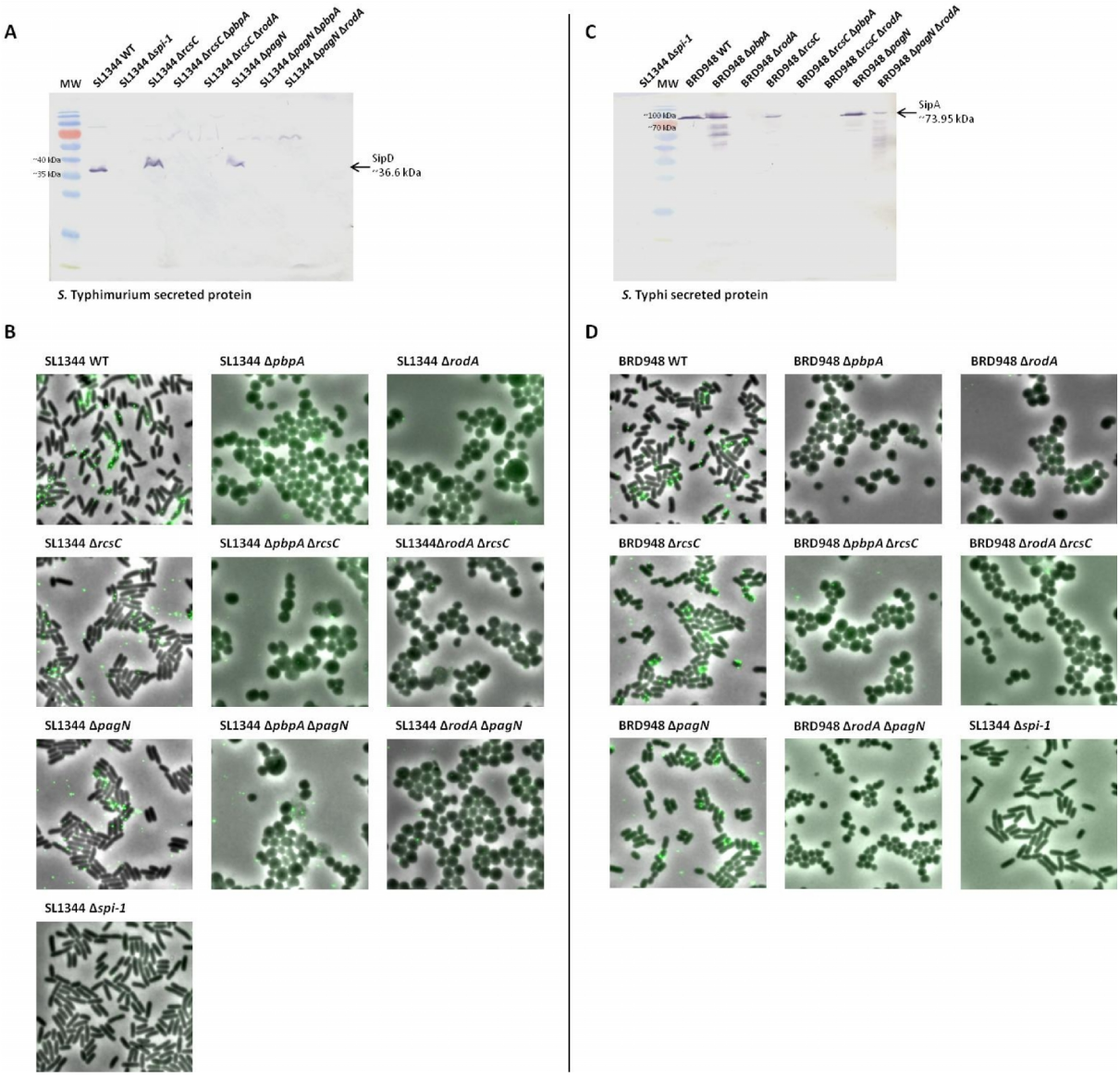

Figure 8.9: SPI-1 effector protein expression in S. Typhimurium and S. Typhi wild-type, ΔpbpA/ΔrodA and ΔrcsC/ΔpagN mutants: A & C - Western blots showing expression of the SPI-1 SipD (A) and SipA (C) effector proteins in secreted protein fractions of SL1344 (A) and BRD948 (C) wild-type, Δ*pbpA*/Δ*rodA* and Δ*rcsC* /Δ*pagN,* single and double mutants, and Δ*spi-1* (negative control) strains. Background protein bands likely due to antibody cross-reactivity to intracellular proteins or SipD translocon complexes. Protein molecular weight (MW) marker sizes as indicated. B & D - Immunofluorescence microscopy images of SL1344 (B) and BRD948 (D) wild-type, Δ*pbpA*/Δ*rodA* and Δ*rcsC*/Δ*pagN,* single and double mutants, and Δ*spi-1* (negative control) strains, overlaid onto phase contrast images; samples labelled with anti-SipD antibody

and fluorophore-conjugated secondary antibody. All images are to the same scale. All cultures grown in LB broth at 37°C and 200 rpm, and harvested at mid-log phase.

Both western blots and immunofluorescence microscopy images of round-cell Δ*rcsC*/Δ*pagN* double mutants showed that SPI-1 functionality was not restored in these strains. Whilst SPI-1 needles were clearly visible at the surface of both wild-type and Δ*rcsC*/Δ*pagN* single mutants, they were not found at the surface of either Δ*pbpA*/Δ*rodA* single mutants or Δ*pbpA*/Δ*rodA* Δ*rcsC*/Δ*pagN* double mutants, of *S.* Typhi or *S.* Typhimurium (Figure 8.9 B and D). The lack of a visible SipD band in secreted protein fractions of these strains suggests that these proteins were not expressed intracellularly, or secreted into the media; round-cell mutants are prone to lysis and so proteins expressed intracellularly are usually visible in secreted protein fractions (Figure 8.9 A and C). This contrasts the results seen with *rcsC*::Tn*10*d(Tc) and *pagN*::Tn*10*d(Tc) revertants, where SPI-1 effector proteins were clearly expressed at least intracellularly. A faint band of an equivalent size to the SipA effector protein band was present in the BRD948 Δ*rodA* Δ*pagN* double mutant in this western blot, although it was also present in the Δ*pbpA* mutant control, and as such this data may not be representative. This assay therefore remains to be repeated.

8.6.3 Conclusions

The present data from precise Δ*pbpA/*Δ*rodA* Δ*rcsC/*Δ*pagN* knockout strains suggested that although motility may have been slightly recovered in these mutant strains, SPI-1 functionality was not significantly altered with the inactivation of the putative regulators, *pagN* and *rcsC*, in round-cell *mrd* mutants. This differs considerably with the results of the Tn*10*d(Tc) transposon mutagenesis screen in which both SPI-1 functionality and motility were significantly restored in Δ*rodA* mutants with the inactivation of *rcsC* or *pagN*. It is possible that other factors or secondary mutations in the Tn*10*d(Tc) transposon mutant strains played a significant role alongside *rcsC* and *pagN* in producing the observed phenotypes, by further regulating *flhDC* or SPI-1 gene expression, or altering other aspects of the cell physiology (such as cell size), enabling flagella/SPI-1 functionality in these cells.

However, the transposon screen results, along with the repeated isolation of *rcsC*::Tn*10*d(Tc) mutants, suggest that *rcsC* at least plays a significant role in the down-regulation of both *flhDC* and the SPI-1 genes in round-cell *mrd* mutants of *S.* Typhimurium, and possibly *S*. Typhi. Extensive further studies may be needed to characterise the importance of both *rcsC* and *pagN* in the regulation of flagella/SPI-1. The present data suggested that *S.* Typhi and *S.* Typhimurium respond differently to *pbpA* and *rodA* mutations, or that the regulatory pathways activated by these mutants are different. Further investigation into these observed differences is therefore also required.

8.7 Investigation of c-di-GMP as a putative regulator of the round-cell *mrd* mutant phenotypes

8.7.1 c-di-GMP as a potential regulator of motility and SPI-1 in round-cell mutants

Although the transposon mutagenesis screen was partially successful in identifying putative transcriptional regulators responsible for the repression of flagella and SPI-1 genes in Δ*pbpA* and Δ*rodA* mutants, the results importantly highlight that other factors are also likely to be involved, in the transcriptional and/or post-transcriptional regulation of motility and SPI-1 in these mutants.

A likely candidate for involvement in the post-transcriptional regulation could be the second messenger molecule c-di-GMP, a universal global regulator among bacteria. Bis-(3´-5´)-cyclic dimeric guanosine monophosphate, or c-di-GMP, is a small cyclic di-nucleotide which is important in the regulation of motility and biofilm formation, helping to regulate the switch between two lifestyles; determining whether cells adopt a free-living motile state or a multicellular sessile state within a biofilm. c-di-GMP acts on numerous proteins to stimulate the production of extracellular adhesins and polysaccharides, and to repress motility (Figure 8.10) (95, 451-453). This molecule has also been shown to regulate virulence in various pathogens (95, 451, 453). In *Salmonella*, overproduction of c-di-GMP inhibited invasion; through the activation of the biofilm master transcriptional regulator CsgD, c-di-GMP was shown to inhibit the secretion of flagellin, and a SPI-1 effector

protein (95, 453). This occurred downstream of and independently of HilA regulation (95).

c-di-GMP acts post-transcriptionally to regulate biofilm and motility expression. The mechanisms by which it acts are complex and not fully understood. It is thought to directly bind and alter the structure of specific target effector proteins and RNAs, which are then enabled to act on and regulate the expression or activity of downstream genes and proteins (451, 454, 455). Four types of c-di-GMP-binding proteins have been described to date, including PilZ-domain proteins which act on downstream proteins, structurally un-related c-di-GMP-binding transcription factors, and proteins containing a c-di-GMP-binding 'I site' (451). In *E. coli* c-di-GMP regulates motility at least partially by binding the PilZ-domain protein YcgR. This protein targets the basal body of fully assembled flagella, interrupting motor function and reducing motility (451, 457).

c-di-GMP-mediated regulation of biofilm formation and motility depends on intracellular levels of this molecule, and as such high levels of c-di-GMP bring about biofilm production and an inhibition of motility (403, 451, 453). c-di-GMP levels are in turn regulated by the combined action of a large number of c-di-GMP-synthesising (diguanylate cyclases or DGCs) and c-di-GMP-degrading (phophodiesterases or PDEs) enzymes. DGC or PDE enzymatic activity is dependent upon two protein domains, the GGDEF and EAL domains, respectively. A third protein domain, HD-GYP, also possesses phosphodiesterase activity (403, 451-453). Many proteins possess both EAL/HD-GYP and GGDEF domains, although only one is usually enzymatically active (451, 453). Numerous bacterial GGDEF and EAL domain proteins have been identified and these proteins are extremely widespread among all bacteria. GGDEF/EAL domain proteins are also abundant within individual genomes (452, 453, 457). *Salmonella* Typhimurium itself expresses at least 20 c-di-GMP-metabolising enzymes, whilst Typhi expresses 21 (457-459). c-di-GMP-synthesising enzymes of major importance in *Salmonella* include AdrA and stm1987, whilst important c-di-GMP-degrading proteins include stm1827, YciR and YhjH (403, 95, 451, 452). The regulation of GGDEF/EAL-domain protein expression and activity is fundamental for regulating the intracellular levels of c-di-GMP (451, 453), and the overproduction of either

GGDEF or EAL proteins can significantly alter intracellular c-di-GMP levels (403, 451, 460).

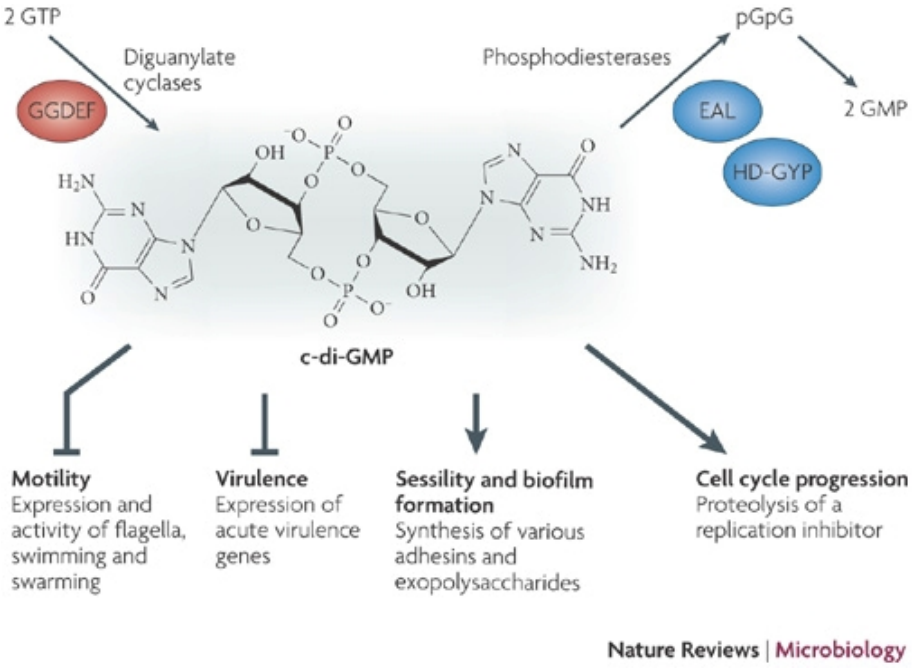

Figure 8.10: Summary of c-di-GMP biosynthesis/degradation, structure and function: Schematic diagram demonstrating the major aspects of c-di-GMP metabolism, and its major roles in regulating motility, sessility, virulence and cell cycle progression. Image taken from "Principles of c-di-GMP signalling in bacteria" (451).

In light of the observation that motility and biofilm formation appear to be significantly and inversely affected in round-cell *mrd* mutants, c-di-GMP has emerged as a potentially important regulator, which perhaps in conjunction with other regulators such as the Rcs phosphorelay, may play a major role in the control of motility and biofilm formation in Δ*pbpA* and Δ*rodA* mutants. In addition, whilst no genes involved in c-di-GMP metabolism were isolated in Δ*rodA* Tn*10*d(Tc) mutagenesis screens, such genes were isolated in a similar Δ*mreCD* Tn*10*d(Tc) screen (unpublished data). Whether and how c-di-GMP is involved in motility regulation in these mutants therefore warrants investigation.

8.7.2 Expression of *Salmonella* Typhimurium genes encoding GGDEF/EAL domain proteins in wild-type and Δ*rodA* mutants

Increased intracellular levels of c-di-GMP have been shown to suppress motility and activate biofilm formation, leading to the rdar phenotype on Congo red agar

(403, 451, 459). In order to investigate the role of c-di-GMP in motility regulation in round-cell *mrd* mutants, it was therefore important to determine whether the expression of both EAL and GGDEF domain-containing proteins was affected in these mutants, in a manner which could ultimately significantly alter c-di-GMP levels.

Microarray gene expression data from *S*. Typhimurium wild-type and Δ*rodA* strains was examined to assess whether the expression levels of GGDEF and EAL domain protein genes varied between *S*. Typhimurium Δ*rodA* and wild-type strains, since alterations in gene expression may give an indication of the downstream effects on c-di-GMP levels. The *S.* Typhimurium LT2 genome encodes 8 EAL domain proteins, 5 GGDEF domain proteins and 7 proteins with both EAL and GGDEF domains, but lacks any HD-GYP domain proteins (253, 458, 461). The expression of these genes in *S*. Typhimurium Δ*rodA* compared to the wild-type, as shown by microarray data, is illustrated below (Table 8.2).

Expression of many of the *Salmonella* EAL and GGDEF domain genes was not significantly affected in the Δ*rodA* mutant. However, *yciR*, *yjcC*, stm1827.S and *yhjH*, 4 genes which have been shown to play significant roles in c-di-GMP metabolism, were altered at least 2-fold in this mutant (403, 459). The former three were slightly upregulated, whilst *yhjH* was down-regulated over 40-fold (Table 8.2). All four of these proteins have been demonstrated to possess c-di-GMP phosphodiesterase activity, significantly reducing c-di-GMP levels and biofilm formation *in vivo* in *Salmonella*. They are also known to help regulate the expression of CsgD (403, 459). However, the proteins also may have distinct functions. For instance, YciR appeared to significantly affect biofilm formation, whereas YhjH played a more important role in the regulation of motility, having a lesser effect on biofilm formation (459). Another study also established a significant role for YhjH in motility regulation, and Δ*yhjH* mutants exhibited a motility defect (466). Considering that these proteins have related functions, it is surprising that they appeared to be inversely regulated in Δ*rodA* cells compared to the wild-type. However, the strong suppression of *yhjH* expression in this mutant may override the minor increases in the expression of the other three phosphodiesterases.

Gene	*Protein function (253)*	*Expression in ΔrodA compared to WT*
EAL domain-containing proteins		
stm0343	Hypothetical protein	+2.23 (P value = 0.07)
stm0468 (*ylaB*)	Hypothetical protein	+1.18 (P value = 0.19)
stm1344 (*ydiV*)	Hypothetical protein	+1.29
stm1827.S	Phosophodiesterase (459)	+2.33
stm2215 (*rtn*)	Hypothetical protein	+1.40
stm3611 (*yhjH*)	Phosophodiesterase (459); flagella/chemotaxis protein	-49.45
stm4264 (*yjcC*)	Phosophodiesterase (459)	+2.03
PSLT032	Putative phosophodiesterase	-1.08 (P value = 0.70)
GGDEF domain-containing proteins		
stm0385 (*adrA*)	Diguanylate cyclase	-1.09 (P value = 0.47)
stm1283 (*yeaJ*)	methyl-accepting chemotaxis protein	-1.38
stm1987	Inner membrane diguanylate cyclase	+1.96 (P value = 0.15)
stm2672 (*yfiN*)	Hypothetical protein	+1.38 (P value = 0.16)
stm4551	Hypothetical protein	+1.58 (P value = 0.14)
EAL & GGDEF domain-containing proteins (Major enzyme activity indicated, where known)		
stm1703 (*yciR*)	RNase II stability modulator, phosphodiesterase (459)	+3.61
stm2123 (*yegE*)	Diguanylate cyclase (460)	+1.97
stm2410 (*yfeA*)	Hypothetical protein	-1.25 (P value = 0.34)
stm2503	Diguanylate cyclase	+1.61 (P value = 0.16)
stm3375 (*yhdA*)	Regulatory protein CsrD	+1.64
stm3388	Signal transduction protein, diguanylate cyclase (460)	+1.69 (P value = 0.10)
stm3615 (*yhjK*)	Phosphodiesterase	-1.16 (P value = 0.54)

Table 8.2: Microarray expression data of EAL and GGDEF domain-containing genes in S. Typhimurium ΔrodA mutant: Data from NimbleGen 4x72000 multiplex arrays comparing gene expression of EAL- and GGDEF-domain proteins between SL1344 wild-type and Δ*rodA* strains. Fold-change in gene expression in Δ*rodA* compared to the wild-type as indicated. All data was statistically significant, as determined using two-tailed Student's t-test, with P values of ≤0.05, except where indicated. Information on gene function taken from the Kegg database and references shown (253, 458, 459, 461).

Interestingly, no c-di-GMP-synthesising GGDEF domain genes were significantly upregulated in the Δ*rodA* mutant, as may be expected since an increase in c-di-GMP production would lead to a similar motility/biofilm phenotype to that observed in this mutant (although some data was not statistically significant). However, the notable depression of *yhjH* transcription in the Δ*rodA* mutant may cause a pronounced increase in c-di-GMP levels and consequently increased biofilm expression, combined with decreased motility. It is plausible that this protein is therefore significantly involved in the regulation of the biofilom/motility phenotype in the Δ*rodA* mutant.

8.7.3 Analysis of c-di-GMP levels in wild-type and round-cell mutants of *S.* Typhi

To determine whether c-di-GMP plays a significant role in the regulation of motility and biofilm formation in round-cell *mrd* mutants, it was necessary to determine whether intracellular levels of c-di-GMP were significantly altered in these mutants.

In 2009 Simm et al. successfully developed a high-performance liquid chromatography (HPLC)–mass spectrometry-based method to directly quantify c-di-GMP levels between various species, and a wild-type and biofilm-overproducing mutant of *Salmonella* Typhimurium. This method enabled the detection of picomole or femtomole (pmole/fmole) levels of c-di-GMP within nucleotide extracts (457). The study produced data representative of actual physiological levels of c-di-GMP within cells. In the present study a liquid chromatography mass spectrometry (LC/MS/MS) method was developed to quantify c-di-GMP from cell lysates of wild-type and Δ*rodA* cultures of *S.* Typhi, allowing direct comparisons to be made between strains. Lysates were prepared as described, and samples were dried, reconstituted in dibutylamine acetate (DBAA) buffer and subjected to LC/MS/MS analysis. The LC/MS/MS assays were kindly developed and performed by Joe Gray (Pinnacle, Newcastle University).

The quantities of starting material for use in LC/MS/MS assays were calculated based on data from the New England BioLabs® and Epicentre® websites (http://www.neb.com/nebecomm/tech_reference/general_data/protein_data.asp and http://www.epibio.com/techapp.asp), which state that individual wild-type *Salmonella* cells have a wet weight of 0.95 pg. In this study 1 mg of wild-type *Salmonella* cells was therefore taken to be equivalent to around 10^9 cells. Analyses from the present study established that a 1 ml cell suspension containing 9.5 mg (wet weight) wild-type cells had an OD600 value of ~2 (Figure 4.11). Comparisons between cell-number and OD600 values had also shown that at a given OD600 value, cultures of an equal volume of wild-type and Δ*rodA* strains contained approximately equal cell numbers. These data were taken together to enable conservative estimates to be made concerning the amounts of cell lysates required for LC/MS/MS analysis. Both wild-type and Δ*rodA* cells were grown up to

mid-log phase, standardised to an optical density (OD600) of 2 in HPLC-grade dH_2O, lysed by sonication, then centrifuged and filtered to remove cell debris, large proteins and DNA from cell lysates. 1 ml lysate was then recovered for LC/MS/MS analysis, based upon the calculations indicating that 1 ml standardised lysate was equivalent to 10^{10} wild-type or Δ*rodA* cells. These considerations enabled comparisons to be made between wild-type and Δ*rodA* cells, based upon both cell number and cell mass. This was important given the observations that round-cell mutants are considerably larger than wild-type cells.

A

c-di-GMP calibration curve readings

On-column load (fmoles)	MS response value			Average	SD	SEM	SEM (%)
	1	2	3				
0	0	0	0	**0**	0	0	0.00%
50	12191	10104	11918	**11404.33**	1134	655	5.74%
100	29263	31615	30925	**30601**	1209	698	2.28%
500	131802	141569	123623	**132331.3**	8985	5187	3.92%
1000	325125	335662	323850	**328212.3**	6483	3743	1.14%
5000	2166374	2115169	2191934	**2157826**	39090	22569	1.05%

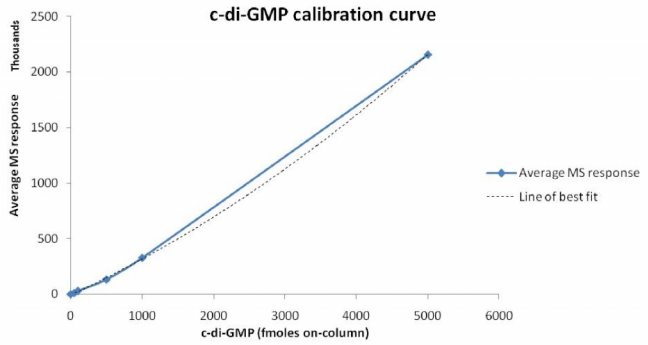

B

Data from initial c-di-GMP LC/MS/MS quantification assay

Sample	MS response value			Average	SD	SEM	SEM (%)	C-di-GMP on-column load (fmoles)	C-di-GMP per 1ml lysate (pmoles)	C-di-GMP per mg cells (pmoles)*
	1	2	3							
BRD948 WT	2337	1902	1835	**2024.67**	272.56	157	7.77%	7	**0.14**	0.0147
BRD948 Δ*rodA*	8700	6640	4655	**6665**	2022.62	1168	17.52%	23	**0.46**	0.0288
BRD948 WT (spike)	136373	135122	126614	**132703**	5310.20	3066	2.31%	483	**9.65**	1.0158

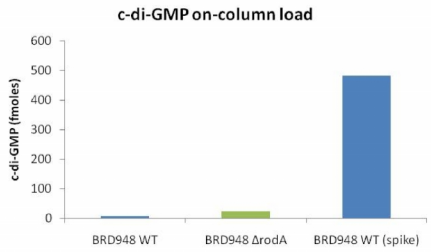

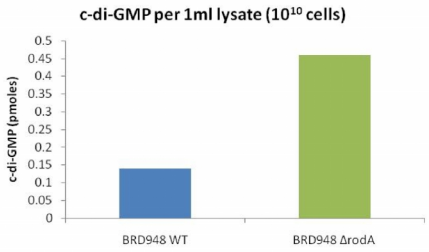

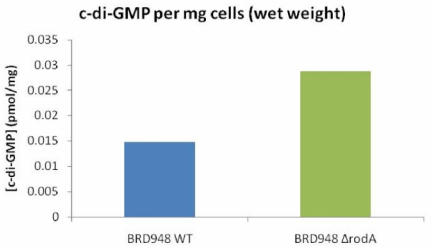

*Calculations based on the following estimates (Chapter 4.3.2 & http://www.epibio.com/techapp.asp):

10^{10} wild-type *Salmonella* cells = 9.5mg = OD600 of 2.0 in 1ml suspension
10^{10} Δ*rodA Salmonella* cells = 16.0mg = OD600 of 2.0 in 1ml suspension

Figure 8.11: Direct LC/MS/MS quantification of cellular c-di-GMP levels in S. Typhi wild-type and ΔrodA strains: Data from initial LC/MS/MS quantification assay of c-di-GMP levels in *S.* Typhi wild-type and Δ*rodA* strains. A – MS response values resulting from 0, 50, 100, 500, 1000 and 5000 fmoles pure c-di-GMP standard loaded onto the column. Resulting average MS response values were used to generate the calibration curve. B – MS response values were measured in triplicate from wild-type and Δ*rodA* cell lysates loaded on column. Average c-di-GMP levels for each sample were derived from

calibration curve values. Calculations of c-di-GMP concentrations per mg cells (wet weight) or per 10^{10} cells were based on previous estimates, as indicated. SEM = standard error of the mean. SD = standard deviation.

After developing and refining the c-di-GMP LC/MS/MS quantification method, an initial run was carried out using fresh lysates of BRD948 wild-type and Δ*rodA* cells, and an additional wild-type sample spiked with 10 pmoles/ml c-di-GMP. A calibration curve was prepared from injections of a fresh solution of pure c-di-GMP standard, at 0, 50, 100, 500, 1000 and 5000 femtomoles; as c-di-GMP levels in wild-type *S.* Typhimurium were previously measured at around 0.1-0.5 pmoles per mg cells (wet weight), this range for a calibration curve was considered suitable (457) (Figure 8.11 A). The average strength of the c-di-GMP peaks from MS spectra (average MS response) for both wild-type and Δ*rodA* lysates were then compared to the calibration curve to extrapolate c-di-GMP levels per mg cells (Figure 8.11 B). c-di-GMP levels measured from the spiked wild-type sample were close to the expected values (9.65 pmole c-di-GMP per ml lysate).

From this initial assay, the measured c-di-GMP levels in BRD948 wild-type and Δ*rodA* samples were much lower than expected, with less than 50 fmoles detected in each loaded sample (Figure 8.11 B). These figures were equivalent to values of around 0.015 pmoles c-di-GMP per mg wild-type cells (wet weight), which was around 10-fold lower than expected, from a previous study (457). The recorded c-di-GMP levels of the unspiked samples were lower than the minimum value of the calibration curve (50 fmole). This made it difficult to be sure of accurate c-di-GMP quantification in wild-type and Δ*rodA* lysates. However, these results provide information on relative c-di-GMP levels, demonstrating that c-di-GMP levels were approximately 3 times higher in Δ*rodA* lysates compared to the wild-type, per ml of original lysate. Since the samples were standardised by OD600 so that lysates generated from 1 ml of either wild-type Δ*rodA* cultures contained an approximately equal number of cells before lysis, this equates to c-di-GMP levels which were 3 times higher in individual Δ*rodA* cells, than in wild-type cells (Figure 8.11 B).

It could be argued that the perceived increase in c-di-GMP levels in Δ*rodA* cells was simply the result of the increased size and volume in round cell mutants. If the increase in c-di-GMP levels is proportional to the increase in volume, the overall

intracellular concentration of c-di-GMP may not differ much between wild-type and Δ*rodA* cells. However, when comparing c-di-GMP levels by wet weight, these figures showed that c-di-GMP levels were just under 2 times higher in Δ*rodA* than wild-type cells, per mg of cells (Figure 8.11 B). This data suggests that c-di-GMP levels were in fact significantly increased in Δ*rodA* mutant cells, to a greater extent than can be explained merely by an increase which simply compensates for the increased cell volume, leading to a fairly constant intracellular c-di-GMP concentration between wild-type and mutant cells.

As such, the combined data from both the microarray and initial LC/MS/MS results suggest that c-di-GMP may be involved in the regulation of motility and SPI-1 genes in round-cell mutants; in these cells, c-di-GMP levels appear to be increased, possibly as a result of the strong repression of expression of the major c-di-GMP-degrading phosphodiesterase, *yhjH*. Increased c-di-GMP levels are known to lead to the suppression of motility and virulence, combined with the activation of genes which promote a sessile lifestyle (403, 451, 453).

8.8 Discussion

8.8.1 Introduction

The purpose of work in this chapter was to identify putative regulators responsible for the downregulation of both motility and SPI-1 gene expression through the suppression of *flhDC* and *hilD* in the round-cell Δ*pbpA* and Δ*rodA* mutants of *S.* Typhi and *S.* Typhimurium. In addition work sought to determine the extent to which motility and SPI-1 functionality could be restored to these mutants through interrupting the regulatory pathways identified to be acting on *flhDC* and *hilD* expression. In doing so it was hoped to gain a better understanding of both the effects that these mutations have upon the cell wall and the physiological state inherent in the round-cell *mrd* mutants.

8.8.2 Identification and verification of RcsC and PagN as putative motility/SPI-1 regulators in round-cell *mrd* mutants

A global transposon mutagenesis screen using Tn*10*d(Tc), was developed and implemented in order to identify putative regulators of *fliF* expression in the *S.* Typhimurium Δ*rodA* mutant, whose inactivation through Tn*10*d(Tc)-mediated mutagenesis would bring about a restoration of *fliF* expression and motility. In the course of this work, over 7000 SL1344 Δ*rodA* Tn*10*d(Tc) mutants expressing the luminescence reporter plasmid pMK1*lux-fliF* plasmid were screened for recovery of luminescence, indicative of recovered *fliF* expression. This enabled good but not complete coverage of the *Salmonella* genome. The screening of at least 10,000 mutant colonies would be needed to ensure more comprehensive coverage of the *Salmonella* genome, or perhaps more, considering the tendency of Tn*10*d(Tc) to transpose into 'hot spots' within the genome, defined by a particular consensus sequence (445, 446). Due to time constraints and a requirement to further investigate positive revertants already isolated, the screen was not carried on further. However, it is recognised that further putative regulators may remain to be identified.

Of the 7000 mutants, 21 luminescent revertants were initially isolated in which *fliF* expression appeared to be recovered. These were rescreened for both recovered luminescence, recovery of motility and retention of the spherical morphology. As such several revertants were disregarded. In addition, two revertants were rejected, being unlikely to constitute actual positive revertants due to the isolation of non-luminescent mutants harbouring similar or identical Tn*10*d(Tc) insertions. It is likely that these latter revertants were false positives resulting from the high frequency of Tn*10*d(Tc) insertions within specific regions of the genome. This work culminated in the identification of two putative regulators of SPI-1 and motility in round-cell mutants: *rcsC* and *pagN*.

The vast majority of luminescent Δ*rodA* revertants were found to contain Tn*10*d(Tc) insertions within the *rcsC* gene. In addition, a single revertant was isolated in which the *pagN* gene was disrupted by Tn*10*d(Tc). Motility assays demonstrated that significant motility was restored in the *pagN*::Tn*10*d(Tc) revertants and some

rcsC::Tn*10*d(Tc) revertants. Furthermore, western blots demonstrated that SPI-1 protein expression was also recovered in these strains, indicating that these genes are involved in the regulation of both flagella and SPI-1 expression in round-cell mutants. However, SPI-1 needles were not visible at the surface of revertant cells, suggesting that though expressed, SPI-1 functionality may remain inactivated. Further *in vivo* analysis in the form of tissue culture invasion assays may be required to determine whether SPI-1 functionality is restored in these strains.

RcsC

RcsC is well described as the major sensor kinase component of the Rcs phosphorelay, which in response to various signals and activation by RcsF, phosphorylates the response regulator RcsB via RcsD. In response to envelope stress, the Rcs phosphorelay activates a global regulon, including SPI-2 genes, genes responsible for colanic acid biosynthesis and Vi capsule expression, whilst suppressing motility and SPI-1 gene expression (50, 96, 118, 119, 320). Knowing its major role in both motility and SPI-1 regulation, the isolation of numerous *rcsC*::Tn*10*d(Tc) mutants in this screen is not surprising, suggesting that the Rcs phosphorelay plays a major role in regulating motility and SPI-1 in response to mutations in *pbpA* and *rodA*. However, it is interesting that mutants were not also isolated within the *rcsB*, *rcsD* and *rcsF* members of the Rcs phosphorelay, or *rcsA*, encoding RcsA which in concert with RcsB binds the *flhDC* promoter and regulates its expression (119, 318). It was also surprising that motility was only significantly restored in one of the two *rcsC*::Tn*10*d(Tc) mutants tested.

Precise knockout mutants were constructed of the *rcsC* gene in the wild-type, Δ*pbpA* and Δ*rodA* strains of *S.* Typhi and *S*. Typhimurium, although neither motility nor SPI-1 expression was restored in these double mutant strains, with the exception of a slight recovery of motility in *S.* Typhimurium Δ*pbpA* Δ*rcsC* cells. The precise knockouts of both *pagN* and *rcsC* were generated to help verify that the observed phenotypes in Δ*rodA rcsC*::Tn*10*d(Tc) and Δ*rodA pagN*::Tn*10*d(Tc) mutants were not artefacts, resulting from the accumulation of secondary mutations or the effect of Tn*10*d(Tc) on downstream genes, for instance. There may be several explanations for the observed differences in *rcsC*::Tn*10*d(Tc) and Δ*rcsC* strains of Δ*pbpA*/Δ*rodA*.

It is possible that the isolated *rcsC*::Tn*10*d(Tc) mutants in these screens for recovery of *fliF* expression were simply artefacts, resulting from a high frequency of Tn*10*d(Tc) insertions into this gene. However, this is unlikely due to the repeated isolation of various different *rcsC*::Tn*10*d(Tc) mutants, whilst no *rcsC*::Tn*10*d(Tc) mutants were identified in screens for non-luminescent mutants. Another possible explanation is that the *rcsC*::Tn*10*d(Tc) insertions resulted in polar defects on the expression of downstream genes (a feature which would not be observed in the precise Δ*rcsC* knockouts, due to their non-polar nature), and that these, rather than the inactivation of *rcsC*, resulted in the recovery of flagella gene expression. The *rcsC* gene is located downstream of *rcsB* in both *Salmonella* and *E. coli*, but transcribed on the opposite strand, and independently expressed and regulated (462, 463). *rcsC* is thought to comprise a single transcriptional unit (187, 463). As such, it is unlikely that the inactivation of *rcsC* would affect the transcription of downstream genes such as *rcsB*.

Another more plausible explanation for the observed phenotypic differences is due to differences in the nature of the Tn*10*d(Tc) insertion mutants and the Δ*rcsC* complete knockout mutants. The RcsC protein contains a periplasmic N-terminal domain (298 amino acids) and a complex C-terminal 614 amino acid cytoplasmic region which contains both kinase and phosphatase activity (463-465). The majority of *rcsC*::Tn*10*d(Tc) mutants isolated in this screen contained Tn*10*d(Tc) insertions within the first 1.2 kilobase pairs of the *rcsC* coding sequence, encoding the N-terminal sensor region of RcsC, and just upstream of the histidine kinase and phosphatase regions (272, 463, 464). This clustering could result from the presence of hot spot regions within the 5' end of *rcsC*, or because this section of the protein is more relevant in the regulation of motility. It is thought that the Tn*10*d(Tc) insertions would completely disrupt *rcsC*, inactivating RcsC function. However, it may be that a truncated form of RcsC is expressed in *rcsC*::Tn*10*d(Tc) mutants, comprising just the C-terminal region, which may still retain some kinase and phosphatase activity. If this is the case, this may explain the slight differences in phenotypes observed between *rcsC*::Tn*10*d(Tc) mutants and Δ*rcsC* knockout mutants, where the full gene is inactivated. Thus the structure of the mutants may affect *rcsC* and hence Rcs phosphorelay activity.

In a previous study, point mutations within *rcsC* which increased expression of RcsC and hence activation of the Rcs phosphorelay as a whole, also increased colanic acid capsule production, whilst a Δ*rcsB* null mutant suppressed colanic acid synthesis and restored motility to these former *rcsC* mutant alleles (325). Another fairly recent study also found that the inactivation of *rcsB*, *rcsD*, or *rcsF* restored motility to non-motile mutants, through the suppression of the Rcs phosphorelay, although the inactivation of *rcsC* was not as effective at restoring motility. The RcsC sensor kinase is known to possess both kinase and phosphatase activity, and hence is able to activate or deactivate the response regulator RcsB, through RcsD. As such the authors suggested that the deletion of *rcsC* may have left some residual Rcs phosphorelay activity since RcsB could not be de-phosphorylated in Δ*rcsC* mutants (463, 466-468).

In a similar manner, differences in *rcsC*::Tn*10*d(Tc) and Δ*rcsC* knockout mutant phenotypes (and differences between individual *rcsC*::Tn*10*d(Tc) mutants) could result from differences in residual RcsC activity in these mutants. The inability to de-phosphorylate RcsB in Δ*rcsC* complete knockouts, from removal of the phosphatase, may result in the same incomplete reduction in the Rcs phosphorelay activity, preventing motility from being significantly restored in Δ*pbpA* Δ*rcsC* and Δ*rodA* Δ*rcsC* strains. By comparison, the recovery of motility in Δ*rodA rcsC*::Tn*10*d(Tc) may result from some residual phosphatase activity with the expression of a truncated RcsC.

PagN

The *pagN* gene is encoded within the SPI-6 pathogenicity island of *Salmonella* and is thought to be important for virulence. This outer membrane protein forms an invasin protein which can mediate invasion of mammalian cells. In addition *pagN* expression is activated in SPI-2-inducing conditions by the PhoP/PhoQ master regulators of virulence (397, 423, 425). Although *pagN* expression is upregulated in conditions along with other factors involved in the downregulation of motility and SPI-1, such as the Rcs phosphorelay, SPI-2 genes and PhoP/PhoQ, a link between PagN and motility regulation or functionality has not previously been identified. Also since PagN forms an outer membrane adhesin, it is unlikely to form a direct regulator of flagella gene expression.

It is possible that the inactivation of *pagN* leads to the activation of flagella gene expression, as seen in *pagN*::Tn*10*d(Tc) mutants, by indirect means. Considering its position in the outer membrane, it is possible that PagN may play a hitherto unrecognised role in sensing environmental conditions. PagN is known to assist in invasion; this role may involve more than simply the direct binding of host cells, and also comprise the consequent downstream signalling which informs the cell of the extracellular environment, bringing about the upregulation of genes involved in intracellular survival (423, 425). As such the inactivation of *pagN* would interrupt any such signalling pathway and affect the expression of genes involved in intracellular survival.

As with Δ*rcsC* complete knockouts, the Δ*pagN* knockout did not appear to bring about the recovery of motility in round-cell mutants seen in *pagN*::Tn*10*d(Tc) cells, although the recovery of motility in the latter mutants was not great. This may again result from differences in the nature of the mutants, whereby the possible expression of even a truncated version of PagN may cause different effects to the removal of the whole gene. Due to the position of *pagN* in the genome the inactivation of *pagN* is unlikely to affect the expression of downstream genes and so the effects on motility in either *pagN*::Tn*10*d(Tc) or Δ*pagN* mutants cannot be said to be due to polar effects on downstream genes.

The expression of *flhDC in trans* from an inducible promoter resulted in a recovery of around 40-60% motility compared to the wild-type, whilst the inactivation of *pagN* or *rcsC* resulted in a similar level of motility functionality in Δ*rodA* Tn*10*d(Tc) mutants. However, recovery of *hilD* expression *in trans* was sufficient to restore the surface expression of SPI-1 T3SS needles, although this was not seen in Δ*rodA rcsC*::Tn10d(Tc) or Δ*rodA pagN*::Tn10d(Tc) mutants. These observations, along with the isolation of two possible regulators of motility, suggest that the regulatory pathways involved in repressing motility/SPI-1 in round-cell mutants are more complex, involving input from a number of unidentified factors. This is highly likely considering the numerous regulatory pathways already characterised for their involvement in the regulation of motility and invasion genes in response to various environmental signals (56, 98, 119, 403, 437, 450). This may also explain the differences seen between Tn*10*d(Tc) mutants and complete knockout mutants

of *rcsC* and *pagN*. Motility revertants isolated in the Tn*10*d(Tc) mutagenesis screen may harbour secondary mutations or other properties, bringing about slight differences in motility gene regulation; for instance, in the different mutants other factors may input into the regulatory pathways to a greater or lesser extent.

8.8.3 Relationship between cell size and recovery of motility in round-cell Δ*rodA* revertants

It was noted that many of the revertant Δ*rodA* Tn*10*d(Tc) mutant cells, of various different identities, appeared significantly smaller in size and diameter than the parent Δ*rodA* cells. However, in one instance, with repeated culture during the preparation of cells for immunofluorescence microscopy, the difference in size appeared less significant. Interestingly, in these cells surface expression of the SPI-1 needles was not apparent. Smaller spherical cells also sometimes appeared more motile by microscopy. It is possible that the recovery of *flhDC* expression may itself be insufficient for full recovery of motility and that motility in these revertants was also dependent to some extent on cell size, regulated independently to the recovery of motility gene expression.

Motility functionality and cell size could be linked in a number of ways. For instance, motility recovery may be mediated to some extent, or even to a greater extent, by parallel effects of *rcsC*/*pagN* inactivation on cell size, rather than simply due to the direct de-repression of *flhDC* expression. It may be that a decreased cell size increases the stability in cell walls, rendering them more physically able to support flagella assembly. This may explain why motility was not significantly affected in the 4a *rcsC* mutants, even if *flhDC* expression was recovered.

The Rcs phosphorelay is known to activate *ftsZ* and *ftsA* expression (321, 322, 469). Since FtsZ and associated proteins play a major role in coordinating cell size, alterations in the expression of these proteins may significantly have affected the size of cells of the revertant strains (335, 336). However, since the Rcs phosphorelay increases *ftsZ* expression, an Δ*rcsC* mutation would be expected to result in a decrease in *ftsZ* expression, which would not lead to a reduction in cell size.

It is also possible that the reduction in cell size in these mutants may be due to a selection for secondary mutations which result in a decreased cell size, meaning that cells in which flagella gene expression was also recovered, were rendered more able to assemble functional flagella.

flhDC has also been shown to regulate cell division; it activates expression of *cadA*, and through the CadA protein acts to decrease rates of cell division during stationary phase, although this occurs independently of *ftsZ*. Furthermore, Δ*flhD* mutant cells were smaller than wild-type cells (349, 350). However, this is again contrary to expectations; if *flhDC* is significantly involved in regulating cell size and cell division in Δ*pbpA* and Δ*rodA* mutants, one would expect the recovery of *flhDC* expression to be associated with a decrease in cell division and an increase in cell size.

In conclusion, the present studies have isolated both *pagN* and *rcsC* as possible regulators of flagella and SPI-1 gene expression, which when inactivated in round-cell mutants, bring about a partial recovery of motility and SPI-1 protein expression at least. However, the mechanisms by which motility and SPI-1 expression are recovered remain to be characterised; it is likely that a number of factors are involved in the regulation of motility and SPI-1 in response to the inactivation of *pbpA* or *rodA*. It is also possible that other factors are involved in, or essential for, the recovery of actual motility and SPI-1 functionality downstream of flagella/SPI-1 gene expression. It was recognised that cell size may play a role in determining the functionality of flagella and SPI-1 in round-cell mutants. This is supported by the observations that only up to ~60% of the wild-type motility has been seen to be recovered in round-cell mutants, upon recovery of motility gene expression.

8.8.4 Identification of c-di-GMP as a putative motility/SPI-1 regulator in round-cell *mrd* mutants

Work which identified *pagN* and *rcsC* as regulators mostly considered these genes in terms of their function in the regulation of *flhDC* transcription. It has also been shown that the recovery of *flhDC* and *hilD* transcription is sufficient to restore significant motility and SPI-1 functionality to Δ*pbpA* and Δ*rodA* cells.

However, as previously discussed, it is likely that more than one factor may be involved in motility and SPI-1 functionality in round-cell *mrd* operon mutants. This regulation may also occur at a number of levels downstream of transcription. For this reason the secondary messenger c-di-GMP was considered as a possible additional regulator of motility and SPI-1 in round-cell mutants. c-di-GMP is quickly being realised as a major global regulator in bacteria, responsible for regulating transition from a free-living motile lifestyle, to a sessile multicellular lifestyle within a biofilm. c-di-GMP post-transcriptionally activates biofilm formation and represses motility and SPI-1 virulence through a number of mechanisms which are not well understood (95, 403, 453). c-di-GMP levels are regulated through the combined action of c-di-GMP synthesising and degrading enzymes; GGDEF and EAL domain-containing proteins respectively. The overexpression of GGDEF-domain diguanylate cyclases or EAL-domain phosphodiesterases results in the increase or decrease in intracellular c-di-GMP levels, with a consequent repression or activation of motility, respectively (403, 452, 453, 459, 460). *Salmonella* Typhimurium expresses 20 GGDEF and EAL domain proteins, whilst *S.* Typhi expresses 21 (458, 461).

Microarray data showed that a major EAL-domain protein of *Salmonella*, YhjH, was downregulated over 40-fold in a Δ*rodA* mutant compared to the wild-type. YhjH has been shown to decrease c-di-GMP levels *in vivo* in *Salmonella*, and is a major EAL domain protein affecting the regulation of motility (459). Furthermore, liquid chromatography with mass spectrometry (LC/MS/MS) analysis to compare c-di-GMP levels between *S.* Typhi wild-type and Δ*rodA* cells showed that c-di-GMP levels were significantly increased in the Δ*rodA* mutant. c-di-GMP levels in individual Δ*rodA* cells were approximately 3 times higher than levels in the wild-

type. Also, weight for weight, Δ*rodA* cells contained twice as much c-di-GMP as wild-type cells. These results suggest that the increase in c-di-GMP levels in the Δ*rodA* mutant is not simply due to the increased volume of the Δ*rodA* mutant cells, such that the overall concentration of c-di-GMP is equal. Thus, initial results suggest that c-di-GMP levels are actively increased in round-cell *mrd* operon mutants.

The accurate direct quantification of c-di-GMP levels in both *S.* Typhi wild-type and Δ*rodA* strains was difficult in the present work, as observed c-di-GMP levels fell below the minimum value of the calibration curve, that of 50 fmoles. In a recent study, c-di-GMP levels in the wild-type *S.* Typhimurium strain were detected at around 0.16-0.17 pmoles per mg cells (wet weight) (457). In contrast, c-di-GMP levels in the present study were around 10-fold lower in the wild-type, at 0.015 pmoles/mg. This result may highlight inherent problems with the present method, which led to the observed results.

Several factors may have affected c-di-GMP levels in *S.* Typhi wild-type cells, or the detection of c-di-GMP. Whilst differences between the two *Salmonella* serovars may result in varying c-di-GMP levels between *S.* Typhi and *S.* Typhimurium, a 10-fold reduction in c-di-GMP levels seems excessive. Simm et al. found that c-di-GMP levels varied up to 10-fold between *S.* Typhimurium and *Vibrio cholerae*. However c-di-GMP levels in *E. coli,* which is much more closely related to *S.* Typhimurium, were comparable to those in *S.* Typhimurium (2, 457). *S.* Typhi is still more closely related to *S.* Typhimurium (2). Minor differences between closely related serovars are unlikely to result in such major differences in c-di-GMP levels. However, it must be considered whether the attenuating mutations of the BRD948 Typhi strain could also significantly affect c-di-GMP levels. In particular, HtrA, which is inactivated in the BRD948 strain, is an envelope stress response protein, which is regulated by RpoE (232, 398). In addition, there is some evidence that RpoE, a major envelope stress regulator, may be involved in the formation of mature biofilms (470, 471). As such it is possible that the inactivation of *htrA* in BRD948 has some effect on biofilm formation and c-di-GMP signalling.

The specific phase of growth also may impact intracellular c-di-GMP levels, along with the culture medium and method of culture. In the study by Simm et al. cell lysates and nucleotide fractions were prepared from plate cultures of cells grown on LB agar without salt, rather than in liquid culture in LB medium, as was done in the present study. Elevated c-di-GMP levels are linked to biofilm overexpression, which is also associated with stationary phase (457, 470, 471). In the present study cells were cultured to mid-log phase, whereas in the 2004 study *S.* Typhimurium cells were cultured to a later growth phase. As such higher c-di-GMP levels may be expected in the latter cells (457). In another study different culture preparation methods, corresponding to different growth phases, were also shown to considerably affect c-di-GMP levels (457, 472). c-di-GMP levels from stationary phase BRD948 wild-type cells (after 16 hours' growth) have also been measured (unpublished results from this lab), being approximately double that of the mid-log phase cells. As such, growth phase appears to significantly affect c-di-GMP levels.

Sample purity is also an important factor which affects detection levels of c-di-GMP (457). Here again, differences may be evident between the study of Simm et al., and the present study; in the former, nucleotide extracts were analysed, whilst in this study cell lysates were centrifuged and filtered to remove cell debris and large molecules, using 10 kDa cut-off filters. The level of background noise seen in the LC/MS/MS spectra was quite high, resulting from the biological matrix mixed in with the c-di-GMP. This is likely to result from the extraction method. The biological matrix may have also partially blocked the column, preventing c-di-GMP loading and detection. It is therefore likely that a lower level of sample purity in this study considerably affected c-di-GMP detection.

A final possibility is that the c-di-GMP contained within cell lysates was somewhat degraded in the course of sample preparation. It was observed that reconstituted pure c-di-GMP degraded in solution at a rate of approximately 1% per day. Other factors present in cell lysate samples may have further increased the rate of c-di-GMP degradation, being retained even after filtering. It was intended that LC/MS/MS analysis would be done with as fresh samples as possible, to retain close to physiological levels. Although there was a slight delay (2-3 days) in the

preparation of samples and LC/MS/MS analysis due to unforeseen factors, calibration curves were generated on the same day as the samples were run.

Taking all these factors into consideration, the difference in c-di-GMP levels detected in the Simm study and the present study are most likely to be caused predominantly by differences in sample preparation and sample purity, although other factors may have affected c-di-GMP levels to a much lesser extent. Sample purity may need to be improved in future work, through the additional extraction of nucleotides from lysate preparations.

8.8.5 Motility/SPI-1 regulation in *S.* Typhi and *S.* Typhimurium round-cell *mrd* mutants

An important observation of this section of work was that whilst some recovery of motility was observed in Δ*pbpA*/Δ*rodA* Δ*rcsC*/Δ*pagN* double mutants of *S.* Typhimurium, no recovery was seen in the equivalent mutants in *S.* Typhi cells. This is likely to be caused by differences between the two serovars, or through the effects of the strain-specific mutations in the *S.* Typhi BRD948 strain. It may be that the same regulatory factors do not play the same, or as extensive roles, in *S.* Typhi; alternative or additional factors may be important in regulating motility in BRD948 Δ*pbpA* and Δ*rodA* mutants.

Comparisons between the genomes of *S.* Typhi and *S.* Typhimurium have shown that the two serovars share a large proportion of DNA content. Conserved regions, which make up around 90% of the genome of both serovars, share on average 97% homology at the DNA level (1-3, 18, 80). In addition, major global transcriptional regulator and regulatory pathways are conserved in both serovars, including the major stress response mechanisms and the Rcs phosphorelay (1, 2, 116, 253). In this respect it is expected that the regulatory pathways involved in SPI-1 and motility gene regulation in *S.* Typhi and *S.* Typhimurium round-cell *mrd* mutants would be the same. It is possible, however, that important global regulators exist in one serovar, but not the other (3, 80). *S.* Typhi is known to possess at least one major transcriptional regulator involved in virulence gene regulation, TviA, which is absent from *S.* Typhimurium. TviA is encoded within the

Typhi-specific SPI-7 pathogenicity island. It positively regulates expression of the SPI-7-encoded Vi capsule and negatively regulates motility and SPI-1 expression through suppression of *flhDC* and *fliZ* (116). Moreover, TviA is positively regulated by the Rcs phosphorelay, and also acts in concert with the response regulator RcsB to repress motility and SPI-1 gene expression. Unlike the situation in *S.* Typhimurium, both TviA and RcsB are required for SPI-1/motility suppression in *S.* Typhi. TviA is also able to regulate *flhC* independently of RcsB, in response to changes in osmolarity (116).

Thus, it is possible that TviA plays a major role in directing SPI-1 and motility gene regulation in *S.* Typhi mutants, leading to the observed phenotypic differences. The importance of TviA may be such that the inactivation of both the Rcs phosphorelay and TviA may be necessary to restore flagella and SPI-1 gene expression in round-cell mutants of *S.* Typhi; the inactivation of *rcsC* (or *pagN*) alone is clearly not sufficient for the restoration of motility and SPI-1.

The *S.* Typhi BRD948 vaccine strain harbours mutations in the *aroC*, *aroD*, and *htrA* genes, the latter of which encodes an important RpoE-regulated protein (232, 398). The inactivation of *htrA* in the BRD948 strain may also considerably affect SPI-1 and motility gene expression in round-cell mutants of this strain. *htrA* encodes a periplasmic protease which is involved in the envelope stress responses in *Salmonella* (216, 232, 398, 473, 474). However, *htrA* mutations do not affect invasion or adherence to host cells (233, 475). The BRD948 strain was used instead of the wild-type *S.* Typhi Ty2, to permit work and manipulation of *S.* Typhi at containment level 2 conditions.

It is possible that the Δ*htrA* mutation may have affected the detection of and responses to envelope stress caused by the inactivation of *pbpA* or *rodA* in BRD948 cells, resulting in alterations to the regulatory pathways involved in controlling SPI-1 and motility expression, such that flagella and SPI-1 genes were more strongly repressed in *S.* Typhi round-cell mutants. Δ*htrA* mutants are also known to be more sensitive to oxidative stress (473, 474). It is therefore also plausible that the inactivation of *htrA* rendered BRD948 cells more sensitive to envelope associated stress, leading to increased activation of alternative stress

response pathways, with the consequent tightened repression of SPI-1 and motility genes. The cell envelope in *S.* Typhi round-cell mutants may also be weaker than in equivalent *S.* Typhimurium mutants, leaving it naturally too compromised to permit the assembly of flagella or T3S needles, even if SPI-1/flagella gene expression were recovered.

Further work is required to characterise the extent to which *htrA* and *tviA* are involved in virulence gene regulation in round-cell *mrd* mutants of *S.* Typhi. The inactivation of both *tviA* and *rcsC* may help determine whether SPI-1 and motility expression and functionality can be restored in *S.* Typhi Δ*pbpA* and Δ*rodA* mutants.

8.8.6 Conclusions

The work of the present chapter has provided evidence that the Rcs phosphorelay plays a major role in the down-regulation of SPI-1 and motility gene expression in round-cell *mrd* operon mutants of *Salmonella* Typhimurium, such that the inactivation of the sensor kinase RcsC brings about the recovery of gene expression in Δ*pbpA* and Δ*rodA* mutants, and some recovery of functionality. This work has also identified the outer membrane adhesin PagN for its possible involvement in the regulation of SPI-1/motility genes in these mutants. Thus, the SPI-1 and motility defects in Δ*pbpA* and Δ*rodA* mutants are complementable, caused to a large extent by the repression of *flhDC* and *hilD* expression.

In addition, these results demonstrate that, in agreement with microarray data, major envelope stress response pathways are likely upregulated in these mutants, leading to the observed phenotypes. It is recognised that the regulation of SPI-1 and motility in response to the *pbpA* and *rodA* mutations is likely to be more complex, involving the interplay of a number of both transcriptional and posttranscriptional regulatory factors. Whilst evidence from this study suggests that c-di-GMP may also play a major regulatory role in round-cell mutants, considerable further work is required to further characterise identified regulators, to isolate other factors which contribute to flagella and SPI-1 regulation, and finally to establish how the various factors are interlinked.

In order to further elucidate the regulatory pathways involved in responding to *pbpA* or *rodA* mutations, future work will also need to assess possible regulators which work upstream of the Rcs phosphorelay (or related regulators), which in response to defects or certain properties in the cell wall of round-cell mutants, may activate this regulatory pathway. A possible important candidate would be RcsF, the outer membrane activator of the Rcs phosphorelay (119).

Chapter 9. General Discussion

9.1 Introduction

The *mrd* operon is thought to comprise the 5 contiguous genes: *ybeB*, *ybeA*, *pbpA*, *rodA* and *rlpA,* the putative operon promoter being located in the intergenic region upstream of *ybeB*. However, till now little experimental evidence has definitively shown this (142, 143, 155, 186, 187). *pbpA* and *rodA* encode PBP2 and RodA respectively, two proteins which play an essential role in longitudinal cell wall synthesis. Whilst PBP2 is known to be the major lateral cell wall transpeptidase in rod-shaped bacteria, the precise function of RodA is unknown, although it is required for PBP2 function (126, 130, 145, 155). Despite their location just upstream of *pbpA* and *rodA*, *ybeB* and *ybeA* appear to have completely unrelated roles, being involved in ribosome biosynthesis and stability (194, 189). The outer membrane lipoprotein RlpA is less well described. Evidence has shown that it localises to both the cell septum and at distinct foci along the lateral cell wall. It also is thought to bind peptidoglycan, although its precise role remains unknown (179, 201). Further experimental analysis is therefore required to elucidate the structure of the *mrd* operon and the functions of the *mrd* operon genes, particularly with respect to determining whether *ybeB, ybeA* and *rlpA* play any roles in cell wall synthesis and cell shape determination. The placing of these genes within close proximity and possibly within the same operon of *pbpA* and *rodA*, suggest that these genes are co-regulated and may share some functional relationship with *pbpA* and *rodA*.

In rod-shaped bacteria lateral and septal cell wall synthesis are thought to be directed by two cell wall-spanning multiprotein complexes, comprising the penicillin-binding proteins and associated proteins. The localisation patterns of these complexes, and hence the spatial organisation of peptidoglycan synthesis, are thought to be coordinated by the bacterial cytoskeleton proteins MreB and FtsZ, respectively. In this model PBP2 and RodA form an integral part of the lateral cell wall synthesis ‘elongase’ complex. Evidence suggests that these proteins are associated with, and spatially coordinated by MreB, MreC and MreD.

Along with RodZ, these five proteins all form major members of the elongase, being essential for rod shape maintenance (122, 126, 130, 131, 167).

The inactivation of any of the cell shape determinant proteins causes cells to form large spheres which are somewhat prone to cell lysis in the absence of either compensatory mutations, permissive growth conditions, or the addition of magnesium and sucrose to growth medium (130, 229). In these spherical mutants longitudinal cell wall synthesis appears to be replaced by constitutive activity of the septal cell wall synthesis complex (127). Cell wall structure and integrity may also be affected in these cells, with round-cell mutants showing increased sensitivity to external stress, as well as lysis (130, 157, 211, 214).

However, relatively few studies have investigated the possible roles of cytoskeletal proteins in the positioning of other cell wall-spanning multiprotein complexes, or in fact, on the effect of perturbations to lateral cell wall synthesis on the assembly, stability and functioning of other such organelles, which may depend on a certain level of cell wall integrity for their function (221, 222). In particular, the functionality of cell shape determinants and hence the integrity of the cell wall, may have major implications for the virulence of pathogens such as *Salmonella*, in which many of the major virulence determinants involve cell wall-spanning multi-protein organelles.

Thus, the major aims of this study encompassed the characterisation of the *mrd* operon in *Salmonella enterica* serovar Typhi. In particular the work aimed to better describe both the structure of the operon and the roles of the constituent genes in the biology and pathogenicity of *Salmonella*. To this end, *in silico* and experimental analyses have been implemented to characterise the *mrd* operon structure, along with the position of the *mrd* operon promoter(s). In addition, a large number of phenotypic screens have been employed to analyse the effects of the inactivation of each individual *mrd* operon gene on the general physiology of *Salmonella* and the functionality of major virulence factors.

Based on the results of these phenotypic screens, continuing work aimed to identify the major regulatory factors involved in the control of the observed

virulence phenotypes in response to *pbpA* or *rodA* inactivation. These latter studies, complemented by global transcriptional analyses, have provided further important insights into the effects of *pbpA* and *rodA* mutations on the physiology of *Salmonella*. The studies have also highlighted significant phenotypic differences between *S.* Typhi and *S.* Typhimurium round-cell mutants.

9.2 The structure of the *mrd* operon and constituent genes

Initial work investigated the structure of the *mrd* operon in *Salmonella* Typhi. *in silico* analyses to compare operon structure across various Gram-negative species showed that the proposed operon, as a putative 5 gene transcriptional unit, is well conserved in both pathogenic and non-pathogenic Gram-negative organisms, including *E. coli*, *Pseudomonas*, *Caulobacter*, *Yersinia* and *Vibrio* species, for instance. However, it is not conserved in Gram-positive organisms such as *B. subtilis*, where homologues of each of the *mrd* operon genes are dispersed across the genome (Chapter 3.2.1). *in silico* analyses of the *mrd* operon DNA sequence and flanking areas of the genome in *Salmonella* were also carried out to identify putative promoter sequences, as well as putative transcriptional terminator sequences within the region (Chapter 3.2.2 and 3.4.1).

These analyses were accompanied with luciferase transcriptional reporter assays to identify experimentally any active promoters within the *mrd* operon region (Chapter 3.3). 500 bp regions immediately upstream of each gene were cloned into the promoter-less luciferase reporter plasmid pMK1*lux*. The luminescence emitted from cultures expressing the resulting pMK1*lux* plasmids was then measured as an indication of promoter activity. Furthermore, RT-PCR assays were performed to identify co-transcribed genes of the *mrd* operon (Chapter 3.4).

Taken together, the data from these assays showed that a strong promoter for the *mrd* operon lies upstream of *ybeB*, within approximately 200 bp of the start of this gene. The lack of likely promoter sequences, transcriptional terminator sequences, or detectable promoter activity within the region between *ybeB* and *rodA* strongly suggests that these 4 genes at least are co-transcribed, under the control of the *ybeB* promoter. In support of this, both Δ*ybeB* and Δ*ybeA* mutants of *S.* Typhi and

S. Typhimurium generated in this study had morphological defects identical to those of Δ*pbpA* and Δ*rodA* mutants. These defects were reverted upon removal of the knockout cassette from *S.* Typhi mutants, suggesting that they were caused by polar effects on *pbpA* and *rodA* expression.

A putative promoter was previously mapped upstream of *ybeB* in *E. coli* (142). However, a 23 bp region in the *E. coli* genome shortly upstream of *ybeB*, proposed to contain this promoter, was not conserved between *Salmonella* and *E. coli*. In *Salmonella* this region was replaced by a ~90 bp stretch of dissimilar DNA (Chapter 3.2.2). By comparison, other regions of the *mrd* operon both upstream and downstream of these individual sections were conserved by around 88% at the DNA level between *E. coli* and *Salmonella*. It is possible that an alternative *mrd* operon promoter lies within this 90 bp section in *Salmonella*. If this is the case the differences in the promoter sequences between *Salmonella* and *E. coli* may be indicative of slight differences in the regulation of the *mrd* operon genes between *Salmonella* and *E. coli*, and also potential minor differences in gene function. The short sequences of DNA specific to *E. coli* and *Salmonella* genomes may contain specific promoter sequences for *ybeB.* Alternatively, it is possible that the true promoter for *ybeB* lies upstream of this region in *Salmonella*, and potentially also in *E. coli*, perhaps corresponding to other promoter-like sequences identified in this work.

In terms of the position of *rlpA* within the *mrd* operon, the close proximity of this gene to *rodA* would suggest that it may be co-transcribed along with *rodA*. However, significant promoter activity upstream of *rlpA* (within the *rodA* gene) was detected in luciferase transcriptional reporter assays, although the strength of this promoter was less than that of the *ybeB* promoter. In addition, several putative promoter sequences were identified upstream of *rlpA* in *in silico* analyses, both in the present work and in a previous study, although no transcriptional terminator sequences were identified downstream of *rodA* (186). For these reasons it is thought that *rlpA* also forms part of the *mrd* operon, although some *rlpA* expression may be controlled independently of the upstream genes through a separate *rlpA* promoter within *rodA*. RlpA is thought to play a role in cell division, having been visualised to have a septal localisation. This protein has also been

observed to localise along the lateral cell wall in a manner reminiscent of PBP2 and RodA (163, 179, 201). This evidence suggests a possible functional link between RlpA, PBP2 and RodA. Hypothetically, RlpA may function in both lateral and polar cell wall synthesis. Such a dual role may be differentially regulated, so that, for instance, *rlpA* expression is co-regulated with *pbpA* and *rodA* for involvement in lateral cell wall synthesis from the *mrd* operon promoter, whilst its cell division role may be independently regulated, through the control of the promoter immediately upstream of *rlpA*.

Microarray analysis of gene expression in the *S.* Typhimurium Δ*rodA* mutant demonstrated that *rlpA* transcription was downregulated around 10-fold compared to the wild-type (Chapter 6.1.4). This could be caused both by polar effects on *rlpA* expression from the insertion of a knockout cassette into the *rodA* gene, if indeed *rlpA* forms part of the *mrd* operon, or from the knockout of the *rlpA* promoter within *rodA* in this strain, disrupting *rlpA* expression..

It therefore remains unclear whether *rlpA* forms part of the *mrd* operon, or whether it may be expressed under the control of two separate promoters. In addition, despite the larger spacing between the *rlpA* and *dacA* genes, no putative transcriptional terminator sequences were detected between *rlpA* and *dacA*. Problems with cloning meant that the region upstream of *dacA* was not assayed for promoter activity. Furthermore, RT-PCR assays to identify co-transcribed genes proved unsuccessful. It is thought that the likely false-positive results generated in this assay may have resulted from overlapping mRNA transcripts of the *mrd* operon region causing the generation of PCR products which bridged the junction between adjacent, non-cotranscribed genes. However, putative promoter sequences were isolated a short distance upstream of *dacA*, *in silico*. In addition, microarray analyses showed that *dacA* expression was not significantly affected in the Δ*rodA* mutant. The retention of the kanamycin-resistance knockout cassette in both *S.* Typhi and *S.* Typhimurium mutants was shown to cause major polar effects on the expression of downstream operonic genes, as seen in Δ*ybeB* and Δ*ybeA* mutants. As such the absence of morphological defects in the Δ*rlpA* mutants of *S.* Typhi or *S.* Typhimurium prior to removal of the knockout cassette,

such as those associated with Δ*dacA* strains, suggests that *dacA* is not co-transcribed along with the upstream *mrd* operon genes (163, 207, 266).

Additional experimental analyses are needed to definitively identify whether *rlpA* and *dacA* form part of the *mrd* operon. Northern blot analysis, for instance, would form a useful assay to identify co-transcribed genes. Primer extension analyses would also be valuable in helping to accurately map the *mrd* operon promoter position(s) in *Salmonella*. Unfortunately it was not possible to conduct such assays within the course of the present study. For the purposes of this study it was assumed that *rlpA*, but not *dacA*, forms part of the *mrd* operon. As such *rlpA* was included in investigations into the functions of *mrd* operon genes.

9.3 Phenotypic characterisation of *mrd* operon gene mutants

9.3.1 Growth, morphology and division defects of the *mrd* operon mutants

Round-cell *S.* Typhi Δ*pbpA* and Δ*rodA* mutants

In order to further characterise the functions of the *mrd* operon genes, precise knockout mutants of the *ybeB*, *ybeA*, *pbpA*, *rodA* and *rlpA* genes were generated in *S.* Typhi (Chapter 4.1). Previous work has shown that the inactivation of *pbpA* or *rodA* in *Salmonella* or *E. coli* causes cells to lose their rod-shaped morphology and grow as spheres (130, 157, 163). Likewise, *pbpA* and *rodA* mutants of *S.* Typhi displayed identical morphological defects. These mutant cells were also considerably larger than wild-type cells, and much heterogeneity of size was evident between individual cells. Furthermore, significant numbers of lysed cells and cell debris were evident in cultures of round-cell mutants. Several studies have noted that the addition of magnesium, or calcium to a lesser extent, and sucrose, aided the growth of round-cell mutants of *Bacillus subtilis*, as well as helping to restore rod-shape (229, 274-276). In the present study, the addition of either 20 mM $MgCl_2$ or $CaCl_2$ was shown to greatly improve growth of both Δ*pbpA* and Δ*rodA* mutants of *S.* Typhi (Chapter 4.3.1). Although rod-shape was not restored in these cells, the extent of cell lysis was notably reduced. Furthermore cells appeared more uniform in size, with a reduction in the number of giant cells. Unlike previous studies, calcium appeared to have the same effect as magnesium

(229). Interestingly wild-type cells treated with 20 mM $MgCl_2$ also appeared slightly smaller in length than those grown without the addition of magnesium.

The round-cell Δ*pbpA* and Δ*rodA* mutants also displayed asymmetrical division defects, as observed previously (Chapter 4.1.3) (127). The general growth of round-cell *mrd* operon *S.* Typhi mutants was assessed in nutrient rich LB medium at both 37°C and 30°C. Significant growth defects compared to the wild-type were observed in round-cell mutants with growth at low temperatures (Chapter 4.3.4).

The general morphological defects, cell division defects and divalent cation-dependency of round-cell mutants have all been described previously, in organisms including *B. subtilis*, *E. coli*, *Caulobacter* and *Salmonella* (127, 130, 157, 229, 476). The phenotypes of mutants of all the cell shape determinant genes (i.e. *mreBCD*, *pbpA*, *rodA* or *rodZ*) are highly similar or indistinguishable (122, 126, 130). However, the observed temperature sensitivity of round-cell mutants in this study has not been much described in the literature, although a similar phenotype was also seen for *S.* Typhimurium Δ*pbpA* and Δ*rodA* mutants, in previous unpublished work (163). In contrast, several studies have shown that growth of round-cell *mrd* and *mre* mutants is rescued at conditions permitting slow growth rates (minimal media, and low temperatures, e.g. 30°C). Rather, growth in conditions permitting fast growth rates (nutrient rich media at temperatures >30°C) caused the formation of large non-dividing spherical cells which lysed (127, 130, 277, 278).

The reason for the stable growth of *Salmonella* round-cell mutants at 37°C in LB medium, (in apparently 'non-permissive' conditions), but not at 30°C is unknown. Furthermore, these mutants were particularly sensitive to low temperatures and extensive cell lysis was observed with incubation of these cells at 4°C. Two major cold-shock proteins, CspC and CspE, were also upregulated ~2-fold in *S.* Typhimurium Δ*rodA* microarrays (Chapter 6.1.3). It therefore appears that *S.* Typhi (and *S.* Typhimurium) Δ*pbpA* and Δ*rodA* mutants were particularly sensitive to cold-shock, being more so than previously characterised round-cell mutants in other bacteria, where lower temperatures assisted rather than hindered growth. It

is possible that features peculiar to *Salmonella* may be responsible for this difference in phenotype.

A number of factors are recognised as being required to rescue growth and prevent cell lysis in spherical cells, such as Δ*pbpA* and Δ*rodA* mutants. These include slow growth rates, as already mentioned, overexpression of the cell division proteins FtsZ, FtsA and FtsQ, and an increase in the levels of ppGpp, an alarmone which regulates growth rates and *ftsQAZ* transcription (130, 324, 331, 332, 337, 338). A widely held explanation for this is that the increase in the volume and diameter of round-cell mutants means that intracellular FtsZ levels are insufficient to form a complete septal ring to bring about division, something which the above factors help to alleviate (127, 130). The observation of asymmetric septation, with the formation of in-complete FtsZ rings, may support this model (127). However, Bendezú and de Boer suggested that the requirement for increased FtsZ levels is caused by the accumulation of FtsZ and associated proteins at non-division sites; excess inner membrane involutions and intracellular vesicle formation may cause FtsZ to be diverted from mid-cell, accumulating instead at these regions. For this reason, FtsZ levels are insufficient to coordinate symmetrical cell division (130).

It is likely that FtsZ levels are increased in *S.* Typhi Δ*pbpA* and Δ*rodA* mutants, as these cells appear to stably propagate. Also, microarray analysis of gene expression in the *S.* Typhimurium Δ*rodA* mutant showed that several genes involved in cell division were upregulated over 2-fold in this mutant, although *ftsZ* expression was not significantly altered (Chapter 6.1.4).

In addition, magnesium and calcium are known to help suppress cell lysis in round-cell mutants, although by an unknown mechanism (229, 274). Previous studies have hypothesised that magnesium, calcium and sucrose may act as osmoprotectants, preventing cell lysis in round-cell mutants in which cell wall integrity is compromised and so cells are unable to resist osmotic pressure. Alternatively it was suggested that magnesium somehow acts to physically stiffen the cell wall, preventing lysis (229, 274). Another possible explanation is that the addition of magnesium or calcium also affects FtsZ levels or FtsZ ring formation;

there is evidence that calcium and magnesium may both be involved in the regulation of ppGpp production or ppGpp activity, and as such they may affect *ftsZ* expression (339-341, 373). Furthermore, magnesium is able to induce FtsZ monomer oligomerisation *in vitro*. As such, it may also act to stabilise FtsZ ring formation in round-cell mutants (342). This is supported by the observation that the addition of magnesium slightly reduced cell length in wild-type cells. FtsZ is a major regulator of cell length, through its regulation of cell division rates (335, 336). As such, magnesium may have affected cell size through FtsZ in wild-type *S.* Typhi cells. However, magnesium is known to play a large number of roles in bacterial physiology, so the mechanism(s) by which it restores stability to round-cell mutants are likely to be complex (229). This hypothesis also does not explain why magnesium may be required for round-cell mutant viability at low temperatures, particularly at 4°C where the addition of magnesium was observed to significantly reduce cell lysis.

Rod-shaped *S.* Typhi Δ*ybeB*, Δ*ybeA* and Δ*rlpA* mutants

Until now, the morphology of Δ*ybeB* and Δ*ybeA* mutants has not been properly characterised. A previous study isolated Δ*ybeB* mutants with morphological defects similar to Δ*pbpA* or Δ*rodA* mutants, although these defects were likely due to polar effects on *pbpA* and *rodA* expression; a feature which was also seen in *S.* Typhi Δ*ybeB* and Δ*ybeA* mutants of this study, prior to removal of the kanamycin resistance cassette (188). Morphological defects in Δ*ybeA* mutants have not been noted, although minor growth defects in an *E. coli* Δ*ybeA* mutant were observed, with growth at 37°C in rich medium (194, 196).

The present study demonstrated that unlike Δ*pbpA* and Δ*rodA* mutants, *S.* Typhi Δ*ybeB* and Δ*ybeA* mutants retained a rod-shaped morphology, showing that these genes do not play a direct role in cell shape determination. Also, neither mutant displayed significant growth or division defects, or temperature sensitivity phenotypes. However Δ*ybeA* cells in particular appeared to have a slightly reduced length compared to wild-type cells (Chapter 4.1, 4.2 and 4.3.3).

As previously mentioned, cell size is regulated by the rate of cell division, and hence by the major cell division protein FtsZ. Overproduction of both FtsZ and

ppGpp cause a reduction in cell size (130, 331, 335, 336). Upstream of FtsZ, cell size is coordinated by environmental factors and nutrient availability. As such nutrient rich conditions cause an increase in cell size and growth rates, whilst nutrient starvation brings about the reverse (333-335). YbeA (or RlmH) is a methyltransferase, responsible for the methylation of a specific pseudouridine residue within the 23S ribosome subunit rRNA. This step occurs in the final stages of ribosome biosynthesis and may act as a checkpoint, allowing translation to proceed (194). The interruption of this step may cause downstream effects on protein synthesis, ultimately leading to a necessary reduction in growth rate, accompanied by the observed reduction in cell size. Alternatively, it is possible that the slight reduction in size of Δ*ybeA* mutants is caused by direct overproduction of FtsZ and/or ppGpp in these cells. This echoes the situation in Δ*pbpA* and Δ*rodA* mutants and may highlight a functional link between *ybeA* and *pbpA*/*rodA*, whereby mutations in each gene have certain similar effects, stimulating FtsZ overproduction. Similar growth defects were observed in Δ*ybeA* mutants and round-cell Δ*mrd*/Δ*mre* mutants in previous work, although in the present study growth of the Δ*ybeA* mutant was only very slightly reduced (Chapter 4.3.3) (194, 196).

Previous work demonstrated that Δ*rlpA* mutants of *E. coli*, *S.* Typhi and *S.* Typhimurium do not display morphological, growth or division defects, suggesting that this gene is not directly involved or essential in lateral cell wall synthesis (Chapter 4.1 and 4.3) (163, 179, 201). However, scanning electron microscopy analysis of *S.* Typhi Δ*rlpA* mutants in this study highlighted possible cell surface abnormalities on these cells, although further analysis is needed to verify these observations (Chapter 4.2). The rough surface appearance of some Δ*rlpA* cells may be suggestive of outer membrane protrusions, similar to those observed with polymyxin B treatment, an antibiotic which is thought to integrate into the outer membrane, increasing its surface area and therefore forcing excess membrane to project out of the cell (273). RlpA is an outer membrane protein involved in peptidoglycan binding (179, 201). If RlpA plays a significant role in maintaining peptidoglycan-outer membrane associations, the disruption of this role through the inactivation of *rlpA* may be expected to be associated with a loosening of outer

membrane-peptidoglycan connections, with a consequent extrusion of sections of the outer membrane, as has been observed.

9.3.2 Virulence factor functionality in *mrd* operon mutants

The expression and functionality of the major *Salmonella* virulence factors were tested in each *mrd* operon mutant of *S.* Typhi, by means of a number of phenotypic assays and microarray analysis (the latter being carried out in *S.* Typhimurium Δ*rodA*) (Chapter 5 and 6).

Examination of virulence factor functionality in the Δ*ybeB*, Δ*ybeA* and Δ*rlpA* mutants suggested that these mutants remained pathogenic, as wild-type (the majority of virulence screens for the Δ*rlpA* mutant were carried out in a previous study (163)). The major SPI-1 and SPI-2 type three secretion systems (T3SS), essential for invasion and intracellular survival respectively, remained actively expressed. Other important virulence traits, such as motility and Vi capsule expression, were also functional and actively expressed in these mutants (4).

However virulence was markedly affected in Δ*pbpA* and Δ*rodA* mutants of both *S.* Typhi and *S.* Typhimurium (163). The present study showed that major virulence determinants involved in initial invasion were completely down-regulated in these mutants in *S.* Typhi. Phenotypic assays were backed up by transcriptional reporter assays, showing that motility and SPI-1 genes were almost completely downregulated in these mutants from the level of the master transcriptional regulators of these systems, *flhDC* and *hilD*, respectively (Chapter 5.2.4 and 5.3.2). Microarray data also showed that the vast majority of SPI-1 genes and motility/chemotaxis genes were downregulated at least 5-fold in the *S.* Typhimurium Δ*rodA* mutant. Expression of *flhDC* and to a greater extent *hilD*, was also significantly reduced (Chapter 6.1.1). In contrast, the SPI-2 T3SS and the Vi capsule, virulence factors required later for intracellular survival and systemic spread, remained functional and actively expressed in these mutants (the former being expressed in SPI-2-inducing conditions). Microarray data also suggested that expression of the majority of SPI-2 genes was not affected in *S.* Typhimurium Δ*rodA*, and the sensor kinase regulator of SPI-2, *ssrA*, was upregulated in this

mutant (Chapter 5.5 and 6.1.2). In addition, a SPI-1 encoded iron transporter which aids intracellular survival but not invasion of *Salmonella*, was upregulated in the *S.* Typhimurium Δ*rodA* mutant (410).

It was speculated that the differences in SPI-1/motility and SPI-2 functionality in round-cell *mrd* operon mutants may relate to the spatial placement of these organelles within the cell wall. In agreement with previous work, immunofluorescence microscopy demonstrated that SPI-2 T3SS needles are expressed only at the cell poles in wild-type *Salmonella*. Conversely, SPI-1 and flagella organelles are spread across the whole surface of *Salmonella* cells (Chapter 5.2.5, 5.3.1 and 5.5.2) (54, 226-228). In light of the models of two modes of peptidoglycan synthesis, involving separate lateral and septal cell wall synthetic complexes, it is plausible that the localisation and functionality of the SPI-1 and SPI-2 needles may depend upon the functionality of the lateral and septal peptidoglycan synthase complexes respectively.

For instance, cytoskeletal elements such as MreB may be involved in the localisation of multiprotein complexes other than the cell wall synthesis machinery, such as virulence determinants (173, 222). If this is the case, the distribution of SPI-1 and SPI-2 T3SS needles may result from alternate cytoskeletal factors specifically directing their localisation. As such, the inactivation of Δ*pbpA* or Δ*rodA*, which may also disrupt MreB helices (126, 131), may have resulted in the mis-localisation and dysfunction of SPI-1, but not SPI-2 needles.

Alternatively, the disruption of lateral cell wall synthesis in round-cell mutants, and any associated lateral cell wall-specific structural defects, may lead to the perturbation of SPI-1, but not SPI-2 needle assembly. Furthermore any wall-contained signals directing SPI-1 and flagella organelles to localise in the lateral cell wall specifically, could result in the mis-localisation and mis-assembly of SPI-1/flagella structures in round-cell mutants, since in these mutants lateral cell wall synthesis is replaced with constitutive septal peptidoglycan synthesis. If SPI-2 needle assembly is associated specifically with areas of polar peptidoglycan, the constitutive activation of septal peptidoglycan synthesis may likewise cause SPI-2 assembly to remain unaffected. However, to date no structural or chemical

differences between septal and lateral cell wall peptidoglycan have been found, although polar peptidoglycan is known to be metabolically inert (122, 201, 477).

Further experimentation was needed to test the above hypotheses, initially by determining whether SPI-1 and motility functionality could be restored simply with the recovery of SPI-1 and flagella gene expression. It was subsequently demonstrated that the SPI-1 and motility defects in Δ*pbpA* and Δ*rodA* mutants were predominantly caused by downregulation of the SPI-1 and flagella genes; restoration of *flhDC* or *hilD* expression *in trans* was sufficient to restore significant motility functionality and surface expression of SPI-1 needles respectively, to both Δ*pbpA* and Δ*rodA* mutants of *S.* Typhimurium (Chapter 7). In addition, mecillinam-treated wild-type *S.* Typhi cells were recovered which retained significant ability to swim, despite being completely round in morphology (Chapter 5.2.3). These results importantly demonstrated that the motility and SPI-1 defects were not due to defects in the assembly of these organelles, either resulting from perturbations to the integrity of the lateral cell wall, or due to the disruption of cytoskeletal elements causing the mislocalisation of SPI-1 and flagella structures.

The demonstration that the SPI-1 and motility defects were caused by active downregulation of the motility and SPI-1 genes opened up further questions as to the nature and identity of the regulatory signals involved in repressing *flhDC* and *hilD* transcription, which further work sought to investigate.

9.3.3 Virulence of round-cell *mrd* operon mutants *in vivo*

In addition to testing virulence factor functionality *in vitro*, it was ultimately important to assess the actual virulence of *mrd* operon mutants *in vivo*, in the mouse model, particularly for the Δ*pbpA* and Δ*rodA* strains. *S.* Typhimurium Δ*pbpA* and Δ*rodA* were subsequently shown to be significantly attenuated for virulence *in vivo* (Chapter 5.7). This attenuation was independent of SPI-1, as bacteria were inoculated intravenously in order to bypass SPI-1-dependent stages of infection. This was done since *in vitro* data had demonstrated that invasion-associated virulence genes were downregulated. The observed attenuation of Δ*pbpA* and Δ*rodA* mutants was contrary to expectations, as data suggested that

the SPI-2 T3SS remained functional in these mutants, and that several genes involved in intracellular survival were upregulated. Also, *in vivo* assays with Δ*mreCD* mutants conducted previously had shown that these mutants remained virulent with intravenous inoculation (unpublished data) (368). This is one of the first indications of phenotypic differences between round-cell *mrd* and *mre* operon mutants (130). The attenuation of Δ*pbpA* and Δ*rodA* mutants may be explained by possible increases in the sensitivity of these cells to growth in the nutrient-starved *in vivo* environment, or to host cell defence mechanisms. However, the sensitivity of these strains to oxidative stress, such as would be experienced *in vivo* inside the macrophage, was shown to be equivalent to the wild-type *in vitro* (Chapter 4.3.9).

Several factors may account for the differences seen between the virulence of round-cell mutants *in vivo* and *in vitro*. The *in vitro* growth of the mutant strains, even in SPI-2-inducing conditions, cannot be well compared with the highly complex *in vivo* situation. It is also known that bacteria grown *in vivo* and *in vitro* in standard laboratory media, are very different in terms of their physiology and cell envelope composition in particular (480). As such, it may not come as a surprise that Δ*pbpA* and Δ*rodA* mutants appear to behave differently *in vivo*. In these conditions, many other factors will come into play, affecting the surface properties, and perhaps SPI-2 functionality in Δ*pbpA* and Δ*rodA* mutants. It may be that in these conditions, the general cell envelope integrity is so compromised in these mutants that it cannot well withstand environmental stress and host immune mechanisms. Also, though *in vitro* data showed that SPI-2 needles were actively expressed at the cell surface in round-cell mutants it is possible that, for whatever reason, these needle complexes remain non-functional or non-secretory, resulting in attenuation *in vivo*.

In the course of the *in vivo* assays, *S.* Typhimurium Δ*pbpA* and Δ*rodA* mutant levels in both the livers and spleens of the mice gradually dropped, although the mice were not able to clear the infection in the 28 days. It is possible that these mutants were not completely attenuated *in vivo*, although *in vivo* assays conducted for a longer period would be needed to determine this.

9.4 Regulation of virulence phenotypes in round-cell mutants

As well as demonstrating that invasion-associated virulence determinants were downregulated in round-cell *mrd* mutants, the various phenotypic assays and microarray analysis of the Δ*pbpA* and Δ*rodA* mutants also highlighted several interesting features concerning the physiology of these cells, particularly in terms of cell surface features. Further work was therefore necessary to identify global factors responsible for the regulation of both invasion genes and the general physiology of round-cell mutants.

9.4.1 Microarray analysis of global regulator expression in round-cell mutants

It was hoped that microarray transcriptional profiling data of *S.* Typhimurium Δ*rodA* cells would highlight potential global regulators involved in the control of virulence gene expression in round-cell mutants. The microarray expression data of several major global regulators, including the major stress response regulators, was therefore analysed (Chapter 6.1.3). Although several global regulators were significantly altered in this mutant, including genes such as *rpoE* and *cpxA*, involved in regulating envelope stress responses (*cpxA* also regulates SPI-1 expression (478)), expression of other major transcriptional regulators of motility or SPI-1 genes, such as the Rcs phosphorelay, OmpR, H-NS and CsrA, were surprisingly not significantly changed from the wild-type (≥2-fold difference from wild-type, with P values of ≤0.05) in these arrays (109, 110, 216). *lrhA*, a major transcriptional repressor of *flhDC*, was also downregulated in the Δ*rodA* mutant.

9.4.2 *rcsC* and the Rcs phosphorelay as a putative regulator of virulence gene expression in round-cell *mrd* operon mutants

In addition to analysing the microarray data, it was crucial to examine experimentally possible global regulators involved in controlling the virulence phenotypes of the round-cell mutants. A transposon mutagenesis screen was implemented to identify double mutants of the *S.* Typhimurium Δ*rodA* strain in which motility was recovered. This screen resulted in the identification of two

possible factors involved in motility and SPI-1 gene regulation in round-cell mutants: *rcsC* and *pagN* (Chapter 8.2).

Approximately 60% of the motile Δ*rodA* revertants isolated in the transposon mutagenesis screen contained mutations within *rcsC*, encoding the sensor kinase component of the Rcs phosphorelay two component system (Chapter 8.2) (119). In *S.* Typhimurium Δ*rodA rscC*::Tn*10*d(Tc) mutants, significant levels of motility and SPI-1 expression were recovered, although SPI-1 needles were not observed at the surface of these cells, and the level of motility recovered varied between individual *rscC*::Tn*10*d(Tc) mutants. Also, specific knockout mutants of *rcsC* were generated in Δ*pbpA* and Δ*rodA* strains of *S.* Typhimurium, in which motility was only slightly recovered, and SPI-1 effector protein expression was not observed (Chapter 8.6). RcsC and the Rcs phosphorelay as a whole presents itself as a likely candidate for involvement in motility and SPI-1 gene regulation in response to mutations in *pbpA* or *rodA.* The Rcs phosphorelay is well known as a global envelope stress response pathway in *Salmonella*; in response to osmotic and envelope stress the Rcs phosphorelay activates genes involved in survival in unfavourable conditions, including colanic acid biosynthesis and SPI-2 genes. It also represses both SPI-1 and flagella expression. As such the Rcs phosphorelay is also involved in intracellular survival (118, 119, 318, 400).

The repeated isolation of *rcsC* mutants in the transposon mutagenesis assay suggests that *rcsC* indeed plays a major role in regulating SPI-1 and flagella gene expression in Δ*pbpA* and Δ*rodA* mutants. The overexpression of colanic acid biosynthesis, combined with the SPI-1 and motility repression in round-cell mutants is in agreement with expectations from overexpression of the Rcs phosphorelay in these mutants. Furthermore, a study by Laubacher and Ades showed that expression of the *rcs* genes was induced specifically from the inactivation of PBP2 through mecillinam treatment of *E. coli* cells (118). Expression data of the *rcsB*, *rcsC*, *rcsD* and *rcsF* genes, major components of the Rcs phosphorelay, was however, not statistically significantly in the *S.* Typhimurium Δ*rodA* microarrays of the present work. The nature of this regulatory system as an envelope stress response pathway which responds to peptidoglycan stress, also makes it a highly likely candidate for involvement in the detection of

and responses to defects induced by the inactivation of Δ*pbpA* or Δ*rodA* (118, 119). In summary, it is proposed that in response to the inactivation of Δ*pbpA* and Δ*rodA* in *Salmonella*, cell wall and morphological defects lead to the activation of the Rcs phosphorelay, which goes on to play a significant role in the downregulation of SPI-1 and motility genes, resulting in the observed phenotypes.

However, the variable data concerning the extent to which SPI-1 and motility functionality could be restored in Δ*pbpA*/Δ*rodA* Δ*rcsC* double mutants sheds doubt on this hypothesis. Also it is interesting that mutations in the other major components of the Rcs phosphorelay were not isolated in this work. It is likely that other global transcriptional regulators, as well as post-transcriptional regulatory mechanisms are also involved in feeding into and the complex regulation and fine-tuning of SPI-1 and motility expression in Δ*pbpA* and Δ*rodA* mutants, leading to the variation seen. It must also be noted that *rcsC* functions both as a kinase and a phosphatase enzyme. As such, the inactivation of *rcsC* does not completely inactivate Rcs phosphorelay signalling (463-465). This factor may be another reason for the observed variability in the recovery of motility and SPI-1 in Δ*pbpA*/Δ*rodA* Δ*rcsC* double mutants.

9.4.3 *pagN* as a putative regulator of virulence gene expression in round-cell *mrd* operon mutants

The transposon mutagenesis screen also isolated a Δ*rodA pagN*::Tn*10*d(Tc) mutant of *S.* Typhimurium in which motility was recovered. Unlike *rcsC*, a *pagN* mutant was isolated only once in this assay and once in a parallel Δ*mreCD* Tn*10*d(Tc) mutagenesis screen (unpublished results of this lab). Similarly to Δ*rodA rscC*::Tn*10*d(Tc) mutants, motility and SPI-1 gene expression was recovered in Δ*rodA pagN*::Tn*10*d(Tc) mutants, but not significantly recovered in Δ*rodA* Δ*pagN* knockout mutants (Chapter 8.3, 8.4 and 8.6).

PagN is a SPI-6-encoded outer membrane adhesin protein which assists in invasion and virulence in *Salmonella* infections. It is positively regulated by PhoP/PhoQ, and as such is upregulated in the intracellular stages of *Salmonella* infection (38, 397, 422, 423, 425). In support of hypotheses that genes important

for intracellular survival remain actively expressed in round-cell mutants, *pagN* was shown to be upregulated nearly 3-fold in the Δ*rodA* mutant in microarrays (Chapter 6.1.2). PagN may also compensate for a lack of SPI-1 in some way, possibly assisting in the exiting of cells (423). A role for PagN in the regulation of virulence genes has not previously been recognised, however. The isolation of PagN in these assays is therefore of considerable interest. In its function as an outer membrane adhesin and invasin, it is possible that the interaction of PagN with host cells results in signalling to the bacteria, informing the cell of its position and therefore inducing invasion. In a similar light, PagN may be involved in passing information into the cell concerning environmental conditions, or cell wall factors specifically. However, a great deal of work is required to determine how PagN may be involved in motility and SPI-1 gene regulation in round-cell *mrd* mutants.

The isolation of both *rcsC* and *pagN* in this work provides further evidence that the pathways controlling virulence gene regulation in response to the inactivation of *pbpA* and *rodA* are complex, involving multiple factors.

9.4.4 c-di-GMP as a putative regulator of motility and SPI-1 functionality in round-cell *mrd* operon mutants

The complexity of these regulatory pathways was further established with the investigation of the role of c-di-GMP in motility and SPI-1 regulation in round-cell mutants (Chapter 8.7). c-di-GMP is a major post-transcriptional regulator of both biofilm formation and motility, whereby increased levels of this secondary messenger lead to an increase in biofilm formation and factors associated with a sessile lifestyle, and a concurrent decrease in motility. The mechanisms by which c-di-GMP controls motility are not fully understood (95, 403, 453). The expression of several major EAL domain proteins, responsible for the degradation of c-di-GMP, was altered in the *S*. Typhimurium Δ*rodA* mutant at the level of transcription. In particular, *yhjH*, encoding a major c-di-GMP phosphodiesterase in *Salmonella*, was downregulated nearly 50-fold in the Δ*rodA* mutant, according to microarray data (Chapter 8.7.2). This EAL domain protein has been shown to affect motility to

a greater extent than biofilm formation, through its influence on c-di-GMP levels (459, 466).

Furthermore, convincing preliminary data demonstrated that c-di-GMP levels in *S.* Typhi Δ*rodA* cells were significantly increased compared to the wild-type (Chapter 8.7.3). These results demonstrated that c-di-GMP may be involved as another level of control, in the regulation of SPI-1 and motility expression, as well as extracellular polysaccharide biofilm synthesis. The involvement of additional factors such as c-di-GMP may also explain why motility was not fully restored in round-cell mutants with the recovery of *hilD* or *flhD* expression, or through the inactivation of *rcsC* alone.

Further work is certainly needed to better establish the role of c-di-GMP, and YhjH in particular, in round-cell mutants, as well as determining whether any direct links exist between the c-di-GMP and Rcs (and other) regulatory pathways in these mutants.

9.5 Surface properties and physiology of the *mrd* operon mutants, and activity of the global stress response pathways

9.5.1 The cell envelope and global stress response pathways in *Salmonella*

In the course of this study, analyses sought firstly to phenotypically characterise the *mrd* operon mutants, and then secondly to further describe the regulatory mechanisms involved in controlling virulence in response to the inactivation of *pbpA* and *rodA*. As a result of these several interesting features have come to light concerning the physiological state of round-cell Δ*pbpA* and Δ*rodA* mutants of *Salmonella*, as will now be discussed.

The bacterial cell wall is crucial as a stress-bearing molecule which helps resist internal turgor pressure, preventing cell lysis (124, 125, 213). The cell envelope as a whole plays an essential barrier function in *Salmonella*, forming the first line of defence against exposure to harmful substances and environmental stress, including osmotic, oxidative and pH stress, as well as drugs, toxic molecules and

the host immunity. In addition, the ability of the cell envelope to sense environmental conditions is extremely important. As such, factors which disrupt cell wall synthesis and the general structure of the cell wall may have significant and wide-ranging effects on the sensitivity of *Salmonella* cells to environmental stress and host defence mechanisms (216, 428, 479, 480). Likewise, increased sensitivity to environmental stresses may be indicative of perturbations to the cell envelope structure (122, 173, 301, 302, 481). Furthermore, the major alternative sigma factor regulating the envelope stress response, RpoE, upregulates factors involved in cell envelope biosynthesis, in response to envelope stress (216, 293, 306, 307).

The importance of the cell envelope is such that a number of major regulatory systems are necessarily in place to detect and respond to perturbations to its structure and integrity. A number of envelope stress response pathways exist, and have been well characterised (216, 428). These responses are controlled by global regulators including the alternative sigma factor RpoE (σ^E), the phage stock response regulated by the *psp* operon genes, and various two-component systems including CpxAR, BaeSR, and the Rcs phosphorelay (118, 216, 428, 429). The CpxAR two component system is also able to regulate *rpoE* expression (428, 429). The environmental factors which contribute to the activation of these systems in *Salmonella* include heat/cold shock, oxidative stress, nutrient starvation, osmotic stress, acid stress, onset of stationary phase, and *in vivo* growth, as well as the presence of misfolded periplasmic proteins (428). The Rcs phosphorelay in particular is also able to respond to LPS- and peptidoglycan-associated stress, as already described (118).

The envelope stress response pathways are also directly connected with virulence in *Salmonella*; RpoE is required for intracellular survival and helps regulate SPI-2 genes, whilst *cpxA* regulates *hilA* expression and is required for virulence *in vivo*. The Rcs phosphorelay is known to activate SPI-2 expression and repress SPI-1 and motility (118, 216, 318, 428, 429, 482). The action of other major stress response pathways in *Salmonella* also affects virulence. For instance, PhoP/PhoQ and OmpR/EnvZ are both involved in SPI-1 and SPI-2 virulence regulation (98, 397).

Previous studies to have analysed round-cell mutants or cells treated with A22 or mecillinam, in various bacteria, have described several features of these cells indicative of significant perturbations to the cell wall/envelope structure and integrity, as would be expected from the inactivation of proteins essential for lateral cell wall synthesis. These features include morphological defects and a tendency of these cells to lyse, whilst increased sensitivities to various environmental stresses including temperature, osmotic stress, oxidative stress, and various drugs, have also been documented (127, 130, 211, 214). However, despite these observations, the activity of global stress response pathways have been largely overlooked, or at least not studied in detail, although one study noted that several major stress response pathways were upregulated in mecillinam-treated *E. coli* cells, including *rpoE*, *cpxAR*, *fur* and the Rcs phosphorelay (118). The consideration of global stress responses is important as these pathways have global impacts on the physiology and behaviour of the cell as a whole, and may provide further clues towards the function of cell shape determinant genes.

9.5.2 Surface properties of the *mrd* operon mutants and sensitivity to external stress

A number of phenotypic tests were applied to specifically ascertain what effects the inactivation of *mrd* operon genes had on the structure of the cell envelope as a whole, and the integrity its barrier function (Chapter 4.3.7). This work aimed to provide insights into both *mrd* gene function and the resulting downstream physiological states of each mutant, particularly in terms of identifying putative global stress response pathways likely to be involved in flagella and SPI-1 gene expression in the Δ*pbpA* and Δ*rodA* mutants.

Few studies to date have assessed the wider effects of Δ*pbpA* and Δ*rodA* mutants, or other *mrd* operon mutants on components of the cell envelope besides peptidoglycan structure (127, 130). In 2008 Bendezú and de Boer described effects of round-cell *mrd* and *mre* mutants on the inner membrane, whereby spherical mutants were unable to regulate rates of phospholipid synthesis. As such, these cells produced excess cytoplasmic membrane which folded inwards to form intracellular vesicles (130). These mutants also may have increased

sensitivity to external stress, possibly through alterations to the cell envelope barrier function (211, 214). A number of studies have also recognised that round-cell mutants or mecillinam-treated cells are often mucoid, indicative of excess colanic acid and biofilm production (315, 323, 325).

This latter feature was observed in Δ*pbpA* and Δ*rodA* mutants of both *S.* Typhi and *S.* Typhimurium in the current study, as previously noted. Growth of these mutants on Congo red agar demonstrated that biofilm or cellulose synthesis was significantly increased in round-cell mutants compared to the wild-type (Chapter 4.3.7). The tendency of these cells to form large clumps in liquid culture may also have been caused by excess biofilm formation. Furthermore, microarray analysis of the *S.* Typhimurium Δ*rodA* mutant showed that a number of genes involved colanic acid biosynthesis were strongly upregulated (Chapter 6.1.2). Colanic acid and cellulose are extracellular capsular polysaccharides, which form an integral part of mature biofilms in *Enterobacteriaceae* (313, 372, 401, 471, 483). This phenotype may be indicative of the involvement of regulatory pathways controlled by the Rcs phosphorelay, or c-di-GMP as already discussed (118, 119, 400, 484).

Lipopolysaccharide (LPS) forms the major constituent of the outer leaflet of Gram-negative outer membrane (294, 295). LPS provides innate defence against environmental stress and in particular prevents the diffusion of small hydrophobic molecules, such as antibiotics, into the cell. LPS biosynthesis is also upregulated with envelope stress (301-303). LPS O-side chain structure remained unaltered in Δ*ybeB*, Δ*ybeA*, and Δ*rlpA* mutants of *S.* Typhi, as demonstrated by SDS-PAGE analysis (Chapter 4.3.7). Δ*pbpA* and Δ*rodA* mutants of *S.* Typhi also seemed to express the full length O-side chains. However, LPS profiles of these mutants did appear slightly different to the wild-type, with significant smearing on LPS gels, possibly due to overproduction of LPS in these strains. Alternatively, other features of these mutants may have affected the purity of the LPS extracts, leading to the observed smearing. Hydrophobic antibiotic testing of each *mrd* operon mutant was carried out to further test for possible changes to LPS integrity. However, these results showed only a very slight increase in sensitivity of the round-cell mutants of *S.* Typhi to rifampicin and erythromycin, supporting LPS profiling and suggesting that LPS structure was not much affected or compromised in round-cell *mrd*

operon mutants. Furthermore, microarray analysis of the *lpt* genes, encoding proteins involved in transporting LPS components across the cell envelope to the outer membrane, showed that their expression was not significantly affected in the Δ*rodA* mutant of *S.* Typhimurium (293). Only *lptF*, encoding an inner membrane permease component of the LptBFGC LPS export complex, was upregulated nearly 2.5-fold in this mutant compared to the wild-type (P value = 0.054) (253). Interestingly, a previous study also noted that mecillinam-treated *E. coli* cells did not show increased sensitivity to hydrophobic antibiotics (118).

Other assays hinted at possible effects on the cell envelope structure in *mrd* operon mutants, although more work is needed to verify or quantify these findings. For instance, slide agglutination assays in the *S.* Typhi *mrd* operon mutants highlighted a possible upregulation of Vi capsule expression in round-cell mutants, as shown by the apparent increased rate and extent of agglutination of these strains in the presence of Vi-agglutinating antiserum (Chapter 5.6).

Potential differences in the composition of the outer membrane were noted from microarray data, which showed that the expression of a number of outer membrane proteins was significantly altered in *S.* Typhimurium Δ*rodA* cells (Chapter 6.1.2). This included an OmpX-like protein, encoded by stm3031, which was upregulated over 200-fold in the Δ*rodA* mutant. Microarrays with an Δ*mreCD* mutant and an A22-treated wild-type strain showed that stm3031 was also one of the most highly upregulated genes in each of these strains (unpublished work of this lab). OmpX-like protein is implicated in resistance to Ceftriaxone, an antibiotic which targets the penicillin-binding proteins (412, 413, 416, 417). As such, the overexpression of stm3031 may be indicative of a defence mechanism employed by *Salmonella* to protect against further cell wall stress. A large number of genes encoding cell envelope-associated proteins were upregulated in *S.* Typhimurium Δ*rodA*, as shown by microarray data. The majority of these were genes encoded components of nutrient transporters, such as the SPI-1-encoded iron transporter along with several transporters involved in osmoprotectant transport. Likewise, these data may be indicative of inherent defence mechanisms induced by round-cell mutants to protect cells against external stress and to maintain viability. It is also possible that the increased volume of Δ*pbpA* and Δ*rodA* mutant cells leads to

a requirement for increased nutrient uptake, with the subsequent increase in transporter gene expression. In addition, the microarray data highlighted potentially major changes in the protein composition of the inner and outer membranes of round-cell *mrd* operon mutants, although further work, such as 2D PAGE and outer membrane protein profiling is needed to further examine protein expression in these mutants.

Oxidative stress sensitivity assays were carried out in each *mrd* operon mutant, testing the susceptibility of each strain to hydrogen peroxide. These assays surprisingly showed that despite the potentially major effects of Δ*pbpA* or Δ*rodA* mutations on the cell wall structure, the sensitivity of these strains to oxidative stress was not significantly heightened.

9.5.3 Evidence for the upregulation of global stress response pathways in *Salmonella mrd* operon mutants and their effects on mutant phenotypes

Data from this study suggests that stress response pathways, and envelope stress response pathways in particular, play a major role in contributing to the phenotypes associated with round-cell Δ*pbpA* and Δ*rodA* mutants, and especially the virulence phenotypes in these strains.

It was initially predicted that the inactivation of *pbpA* or *rodA* would physically disrupt the localisation or assembly of virulence organelles such as the SPI-1/SPI-2 T3SSs and flagella, in the bacterial cell wall. However, it has become apparent that the SPI-1 T3SS and motility defects are caused by the downregulation of the major transcriptional regulators of these genes. This downregulation is thought to be mediated by several global stress response pathways. The isolation of motile Δ*rodA rcsC*::Tn*10*d(Tc) mutants suggests that the Rcs phosphorelay plays a major role in responding to envelope stress in round-cell mutants, acting to repress SPI-1 and motility genes, as previously discussed. Furthermore, microarray data demonstrated that both RpoE and CpxA were upregulated in the *S.* Typhimurium Δ*rodA* mutant. RpoS, another alternative sigma factor regulating global stress responses, was also upregulated ~2-fold in this mutant (98). Aside from global regulators, a large number of stress-related genes, including heat shock proteins,

DNA repair genes and envelope stress genes were also among the most highly upregulated genes in *S.* Typhimurium Δ*rodA* (Chapter 6.1.2). The active expression of SPI-2, Vi capsule production and colanic acid overexpression add further weight to this prediction, as many of the stress response pathways act to upregulate genes involved in intracellular or stationary phase survival in 'stressful' environmental situations, including SPI-2, Vi capsule and biofilm/colanic acid-associated genes (118, 318, 98, 397).

Furthermore, *ftsZ* is known to be overexpressed in round-cell mutants, helping to prevent cell lysis (130). *ftsZ* expression is regulated both directly and indirectly by the global stress response pathways, including RpoE, CpxAR, RcsCDB (211, 321, 322). Expression of *ftsZ* is also induced by the alarmone ppGpp, which itself is the regulator of RpoE (337, 338, 485, 486). The upregulation of *ftsZ* in round-cell mutants may be caused directly by the upregulation of upstream stress response pathways.

Previous studies have suggested that round-cell mutants displayed increased sensitivity to various forms of environmental stress, something which would be in line with the proposed activation of global stress response pathways (211, 214). Similarly, the sensitivity of round-cell mutants to cold-shock, along with the tendency to lyse, and the dependency of these mutants upon magnesium/calcium for growth, also point towards significant cell envelope defects and thus a likely upregulation of general and envelope stress response pathways. In addition, the overexpression of capsular polysaccharides and possibly the Vi capsule in *S.* Typhi, the formation of inner membrane vesicles as previously noted (130), upregulation of certain outer membrane proteins, and possible changes in LPS expression tend to suggest that the bacterial envelope as a whole is significantly affected in Δ*pbpA* and Δ*rodA* mutants.

However, the observation that the oxidative stress sensitivity of Δ*pbpA* and Δ*rodA* mutants was not significantly increased, along with the ability of these cells to assemble functional multi-protein wall-spanning complexes, and the generally retained structural integrity of the LPS layer, all may suggest that defects in the cell wall/envelope structure of Δ*pbpA* or Δ*rodA* mutants are not as severe as

originally proposed. Alternatively, it may be that the perturbations to the cell wall integrity in these mutants are counteracted by the upregulation of stress defence mechanisms, which are highly effective in restoring barrier function in these cells. However, more comprehensive studies are necessary to fully characterise cell wall defects in round-cell mutants.

In conclusion, these results reveal a situation whereby the inactivation of *pbpA* or *rodA*, and associated downstream peptidoglycan structural defects, are thought to bring about the activation of a number of global stress responses, including the major envelope stress response pathways such as the Rcs phosphorelay. It is the direct regulation from these responses which may bring about the observed phenotypes in round-cell mutants, leading to the suppression of SPI-1 and motility functionality. These pathways may also play a major role in maintaining viability in round-cell mutants, for instance by upregulating FtsZ to prevent cell lysis, and by effectively responding to increased stress-sensitivity.

9.6 Further analysis of *mrd* operon gene function

9.6.1 Physiology of round-cell mutants and clues into *pbpA* and *rodA* function

The observations concerning the upregulation of major stress response pathways in round-cell Δ*pbpA* and Δ*rodA* mutants may provide further clues as to the precise effects that the inactivation of *pbpA* or *rodA* have on cell wall structure, and hence the roles of these genes. However, the major global stress response pathways are each highly complex, and able to detect and respond to a number of factors. Hence, the activation of a particular stress response pathway cannot necessarily be said to result from the detection of any single feature, be it compromised peptidoglycan structure or increased sensitivity to certain environmental factors in the Δ*pbpA* and Δ*rodA* mutants. It is therefore difficult to determine from this study which precise features play a particular role in activating the stress responses.

The activation of the Rcs phosphorelay, however, may provide significant insights. The Rcs phosphorelay is able to detect and respond to peptidoglycan stress specifically, a property not yet recognised in other envelope stress response pathways. Activation of the Rcs phosphorelay resulting from perturbations to the peptidoglycan caused by the inhibition of PBP2, has been shown to involve RcsF, an outer membrane lipoprotein which induces Rcs phosphorelay signalling (118, 467, 487). The mechanism by which RcsF acts has not been characterised, although it is thought that in response to perturbations to the outer membrane, osmotic shock, or treatment with the antibiotic polymyxin B (which also affects the outer membrane), RcsF activates the Rcs phosphorelay (118, 484, 487, 488). The nature of the involvement of RcsF in the Δ*pbpA* and Δ*rodA* phenotypes has not been noted within the present study, and future work examining this further may be useful. However, should RcsF play a significant role, it may highlight important links between PBP2/RodA-mediated peptidoglycan synthesis and the structure and integrity of the outer membrane of *Salmonella*. As such, peptidoglycan synthesis and outer membrane integrity may be intimately linked. Microarray data suggested that the makeup of the outer membrane may be significantly affected or altered in Δ*rodA* mutants, supporting this hypothesis.

Phenotypic data in this study also supported previous work, showing that both Δ*pbpA* and Δ*rodA* mutants were resistant to A22 (Chapter 4.3.5) (281). The interdependence of cell shape determinant proteins is not fully understood, although to clarify this would help with establishing the function of each protein (131). Studies have also shown that PBP2 localisation was not affected with the disruption of MreB via A22 treatment of *C. crescentus* cells (137). In other work, the localisation of MreB helices was found to be dependent on RodA but not PBP2 (126, 131). These data suggest that the relationship between PBP2 and MreB differs from that of RodA and MreB in rod-shaped bacteria. As such, it may be surprising to find that both Δ*pbpA* and Δ*rodA* cells possess the same A22-resistance, perhaps indicating that PBP2 is more closely linked to MreB, along with RodA, than has been realised. Alternatively, the resistance of these strains to A22 may simply be due to the fact that since these cells are already round, with cell wall synthesis defects, the addition of A22 cannot do much to further impede cell wall growth.

The majority of studies have shown that the mutant phenotypes are similar, if not indistinguishable, between different round-cell *mrd*/*mre* knockout mutants (130). This has also been seen in the present study, where on the whole Δ*pbpA* and Δ*rodA* had identical mutant phenotypes. However, minor phenotypic differences may provide clues into the function of RodA in particular, whose function is unknown. As well as the different localisation dependencies already mentioned, data from this study highlighted significant differences in the virulence of Δ*pbpA*/Δ*rodA* and Δ*mreCD* mutants of *S.* Typhimurium. SPI-2 expression is active in Δ*pbpA*, Δ*rodA* and Δ*mreCD* mutants of *S.* Typhimurium. However, Δ*mreCD* mutants remained virulent *in vivo* when injected intravenously into mice (previous work of this lab) (368), whereas *in vivo* assays of Δ*pbpA* and Δ*rodA* mutants showed that these mutants were attenuated. This result may highlight hitherto unrecognised properties of PBP2 and RodA, such that mutants have a more marked effect on cell wall integrity, affecting virulence to a greater extent.

In addition, minor differences were seen in the level of *flhDC* repression between Δ*pbpA* and Δ*rodA* mutant cells. The greater suppression seen in Δ*pbpA* mutants may result from increased activation of regulatory pathways such as the Rcs phosphorelay, resulting from heightened damage to the cell wall. If this is the case, it may highlight the importance of PBP2 above RodA, in particular.

9.6.2 Further insights into *ybeB*, *ybeA*, and *rlpA* function

Experimental analyses conducted in this work sought to further describe the functions of *ybeB*, *ybeA* and *rlpA*, as well as *pbpA* and *rodA*, determining whether any functional relationships existed between the former and latter genes. Phenotypic assays of the Δ*ybeB*, Δ*ybeA* and Δ*rlpA* mutants showed that these strains generally behaved as wild-type, particularly in terms of virulence factor functionality. However, a number of observations were made, hinting towards the function of these genes.

ybeB and *ybeA*

Comparison of the *Salmonella* YbeB protein sequence with that of the *Salmonella* S12 ribosomal protein showed some significant similarities within a short region,

which in S12 mapped to the conserved 'PGVRY' loop of S12 (Chapter 4.3.6). This loop is implicated in streptomycin resistance and is important for tRNA recognition (290). S12 is also the target of streptomycin, which causes mis-reading of tRNA codons and ultimately a stalling of protein synthesis (288, 289). The YbeB protein is highly conserved even among distantly related species, suggesting that its function is important. The finding of this study may indicate that YbeB functions in a similar manner to S12 in *Salmonella*. However, the lack of a distinguishing phenotype for Δ*ybeB* mutants may point towards some redundancy of function. Furthermore, streptomycin sensitivity was not altered in Δ*ybeB* mutants, suggesting that this antibiotic does not target YbeB in addition to S12.

To date, a functional relationship between *pbpA*/*rodA* and the remaining *mrd* operon genes has not been established. Several portions of data from this study suggest that the 5 genes may not be completely unrelated. Transcriptional luciferase reporter assays from this study have confirmed hypotheses that *ybeB* and *ybeA*, at least, are co-transcribed along with *pbpA* and *rodA*. In addition, significant mecillinam resistance of both Δ*ybeB* and Δ*ybeA* mutants may be indicative of a functional relationship. The observation that Δ*ybeA* mutants were generally shorter in length than wild-type cells was suggestive of FtsZ overproduction, as previously discussed. Knowing that FtsZ production is also increased in round-cell mutants, this may present further evidence of a functional relationship whereby the inactivation of *ybeA* has some of the same effects on cell physiology as the inactivation of *pbpA* or *rodA*, if less severe.

Any functional link between the *ybe* genes and *pbpA* and *rodA* may also be related to the localisation of ribosomes, protein synthesis and RNA processing sites; in *B. subtilis* ribosomes were shown to localise to the cell periphery and the cell poles (230, 231). Whilst the localisation of ribosomes to the cell periphery, which is presumably important for protein synthesis, may occur independently, it is possible that the bacterial cytoskeleton and associated proteins are involved in directing ribosome localisation. The close proximity of bacterial ribosomes to the cell membrane may also indicate a link between active protein synthesis complexes and the cell wall synthetic complexes.

Expression of a major T3SS in *Shigella sonnei* is regulated post-transcriptionally through regulation of *invE* mRNA stability, so that in adverse conditions such as low temperature InvE is not expressed; InvE encodes the transcriptional regulator of the T3SS structural genes. *invE* mRNA is thus stable at 37°C but not at 30°C or low osmotic pressure. Mitobe et al. recently found that the cell shape determinant protein RodZ has a secondary function in *S. sonnei*; in directly binding *invE* mRNA, RodZ assists in regulating the stability of this molecule in a CpxA-dependent manner, directly affecting InvE expression. It was suggested that RodZ may function as an anchor, directing the localisation of mRNA species, helping constrain post-transcriptional regulation to regions close to the cell membrane (168). A number of recent studies also demonstrated that RNase E, a major component of the RNA degradosome, directly binds the cytoplasmic membrane in *E. coli*. RNase E also forms cytoskeletal-like structures which, along with other members of the degradosome, localises helically around the cell periphery in a manner reminiscent to MreB (489-492). Taken together, these results suggest that mRNA processing and perhaps general protein synthesis, are localised specifically at the cell periphery, and possibly associated with other cytoskeletal elements, along with the cell wall synthesis machinery.

If this is the case, any functional relationship between *ybeB*, *ybeA* and *pbpA*/*rodA* may be linked to the apparent associations between translation/mRNA processing and the bacterial cytoskeleton. For instance, YbeB and/or YbeA may play roles in directing the localisation of ribosomes. In its role as a possible 'checkpoint' methyltransferase, YbeA may also function to ensure that translation begins not only when ribosomes are correctly assembled, but also when they are correctly localised. However, YFP-fusion proteins of both YbeB and YbeA appeared to be spread diffusely through the cytoplasm in *S.* Typhi cells (Chapter 4.1.6). Assuming these protein fusions remained functional, this suggests that YbeB and YbeA do not play a role in ribosome localisation.

Whatever their role, *ybeB* and *ybeA* are co-regulated along with *pbpA* and *rodA*, suggesting that important links exist between the regulation of cell wall synthesis and ribosome assembly or protein synthesis. Given the conserved nature of these proteins, it is also clear that their function is important (189, 194). The putative

links between translation and the cytoskeletal proteins, or the cell wall synthesis machinery, warrant further investigation.

rlpA

Similarly to previous studies, an obvious phenotype for Δ*rlpA* mutants was also hard to find. However, some evidence suggests that it may be functionally related to *pbpA* and *rodA*. Both previous work of this lab and the work of Gerding et al. demonstrated that in certain situations RlpA localised in distinct helical-like foci along the lateral cell wall, reminiscent of PBP2 and RodA, as well as at the cell septum. The SPOR domain-containing RlpA protein is also known to bind peptidoglycan and may play a role in cell division, due to its septal localisation (163, 179, 201).

RlpA may play a significant role in directing associations between peptidoglycan and the outer membrane. The distinct localisation patterns of RlpA could indicate that such a role is specifically important during the course of both septal and lateral cell wall synthesis (201). Observations of the present study may support this. Several Δ*rlpA* mutant cells were noted with distinct surface features, similar to those seen with polymyxin B treatment (Chapter 4.2). If significant, the observed surface protrusions may result from significant dissociation of the outer membrane from the peptidoglycan layer as previously discussed. Alternatively the surface protrusions also may result from the production of excess outer membrane in Δ*rlpA* mutant cells. In round cell *mrd* mutants, it was noted that cells were unable to adjust the rate of cytoplasmic membrane synthesis, resulting in excess inner membrane production (130). In a similar manner, Δ*rlpA* mutants may be unable to regulate outer membrane production – speculatively, RlpA may play a role in helping cells to coordinate outer membrane growth according to rates of peptidoglycan synthesis and cell wall growth. The disruption of *rlpA* would, as such, interfere with this regulation, possibly leading to constitutive overproduction of outer membrane.

Additional work is needed both to verify these observations and to further investigate the function of RlpA. Also, the role of RlpA may be masked by functional redundancy, since several outer membrane lipoproteins are already

known to play crucial roles in linking the outer membrane to the peptidoglycan layer in Gram-negative bacteria, including Lpp and Pal, the latter of which is important in cell division (201, 202). Hypothetically, RlpA may play a temporary role, being important for maintaining peptidoglycan-outer membrane binding particularly during the breaking of old peptidoglycan strands and the incorporation of new peptidoglycan strands into the cell wall, before the more major and permanent Lpp and Pal proteins come into play.

It was previously noticed that the Rcs phosphorelay is induced by polymyxin B treatment (118, 488). It would be interesting to determine whether this stress response pathway is also induced in Δ*rlpA* mutants.

9.7 Comparisons between *S.* Typhi and *S.* Typhimurium *mrd* mutant phenotypes

Analyses of *S.* Typhi and *S.* Typhimurium *mrd* operon mutants from both this study and a previous study (163) showed that the phenotypes of Δ*pbpA* and Δ*rodA* mutants were largely indistinguishable between the two serovars, in terms of both growth and morphological defects, and virulence factor functionality. *S.* Typhi round-cell mutants, however, showed a more stringent requirement for $MgCl_2$ or $CaCl_2$ supplementation for survival and growth.

However, later results suggested that the regulation of the virulence phenotypes in response to *pbpA*/*rodA* inactivation may differ between the two serovars. Motility and SPI-1 functionality were recovered in *S.* Typhimurium round-cell mutants with restoration of *flhDC* and *hilD* expression respectively. The introduction of the pBAD-*hilD* expression vector into *S.* Typhi round-cell mutants, however, did not bring about a recovery of SPI-1 expression (Chapter 7.3.2). In this instance, it was thought that *hilD* expression from the pBAD vector may have been prevented in the *S.* Typhi strain, through either an inherent toxicity of this strain to arabinose, or an inability to express the pBAD-encoded proteins, particularly as SPI-1 expression levels were not increased in the wild-type strain expressing pBAD-*hilD*.

A possible role for both RcsC and PagN in the regulation of SPI-1 and motility was established in *S.* Typhimurium, but not *S.* Typhi round-cell mutants, where neither SPI-1 or flagella expression was recovered with the inactivation of *rcsC* or *pagN*. It is possible that in these strains expression of the SPI-1 and motility genes was recovered but protein expression or functionality remained suppressed, as transcription of SPI-1 and flagella genes was not assessed in *S.* Typhi round-cell Δ*rcsC*/Δ*pagN* cells. RcsC and PagN were identified as putative regulators from the recovery of flagella gene transcription in *S.* Typhimurium Δ*rodA* in *rcsC*::Tn*10*d(Tc) and *pagN*::Tn*10*d(Tc) transposon mutants. RcsC and PagN may play similar roles in both Typhi and Typhimurium round-cell mutants, but other factors may also be involved in *S.* Typhi, which prevent the downstream functionality of the motility or SPI-1 systems. It is also possible that the global regulation is significantly different between Typhi and Typhimurium. Whilst additional work is needed to establish at what level SPI-1 and motility defects are regulated in *S.* Typhi mutants, the reasons for the observed differences may be discussed. These may arise as a result of differences between the two serovars or from attenuations specific to the *S.* Typhi vaccine strain BRD948, for instance.

9.7.1 The nature of the BRD948 *S.* Typhi strain and the associated Δ*htrA* mutation

The BRD948 strain of *S.* Typhi harbours specific attenuating mutations in the *aroC*, *aroD* and *htrA* genes, making it suitable for use as a vaccine strain. Of these mutations, the Δ*htrA* mutation could be highly significant, affecting the phenotypes of *mrd* operon mutants in this study. HtrA (DegP) is a periplasmic protease which degrades mis-folded envelope proteins and is required for protection against oxidative stress and intracellular survival in *Salmonella*. HtrA expression is regulated by both the Cpx and *rpoE* envelope stress response pathways (216, 493-495). Interestingly, in *Yersinia htrA* expression was induced from overproduction of the outer membrane protein OmpX-like protein through the CpxAR pathway. However, in *E. coli*, which is more closely related to *Salmonella*, *htrA* activation through overproduction of outer membrane proteins was shown to occur through RpoE (494).

At least one envelope stress response pathway is thought to be significantly involved in the regulation of virulence in Δ*pbpA* and Δ*rodA* mutants. As such, and knowing the importance of HtrA in the stress response pathways, it is likely that HtrA is ordinarily overexpressed in Δ*pbpA* and Δ*rodA* mutants. This is supported by the observed upregulation of OmpX-like protein in *S.* Typhimurium Δ*rodA* cells, which would likely lead to *htrA* overexpression. Microarray data also showed that *htrA* itself was upregulated ~7-fold in *S.* Typhimurium Δ*rodA*. The absence of HtrA from *S.* Typhi may therefore have important consequences for the health of Δ*pbpA* and Δ*rodA* mutant cells. Any resulting perturbation to the health and general physiology of *S.* Typhi Δ*pbpA* or Δ*rodA* cells may affect their ability to express functional flagella or SPI-1 needles. It is also possible that the lack of HtrA significantly alters the envelope stress responses, and therefore influences *flhDC* and *hilD* expression in these mutants.

9.7.2 The *S.* Typhi serovar specific transcriptional regulator, TviA

TviA is a major SPI-7-encoded transcriptional regulator which is absent from the genome of *S.* Typhimurium. It is responsible for the expression of the Typhi-specific Vi capsule, but also regulates virulence genes outside of SPI-7. In conjunction with RcsB, TviA negatively regulates both motility and SPI-1 genes. This additional level of complexity of virulence gene regulation in *S.* Typhi, which is also related to the envelope stress response, may be at least partially responsible for the differences in phenotype seen in *S.* Typhi Δ*pbpA* and Δ*rodA* mutants (116). The inactivation of *rcsC* is known to not completely suppress the Rcs phosphorelay. Hence residual RcsB activation, combined with the action of TviA, may lead to the continued SPI-1 and motility repression seen in *S.* Typhi Δ*pbpA*/Δ*rodA* Δ*rcsC* double mutants (466, 467).

It is likely that both TviA and HtrA play considerable roles in establishing the observed phenotypes in *S.* Typhi round-cell *mrd* mutants, though further work will be needed in order to assess this. In terms of TviA, this would be made possible through the combined inactivation of both *tviA* and the Rcs phosphorelay, for instance, or through the inactivation of other members of the Rcs phosphorelay.

The phenotypic analysis of Δ*pbpA* and Δ*rodA* mutants generated from a wild-type *S.* Typhi strain, would also permit study into the effects of the *htrA* mutation.

9.8 Conclusions

A number of significant conclusions can be drawn from the results of this study. A considerable range of questions have also been raised through the course of this study, which form the basis of plans for future work.

From the outset, this study sought to better characterise the roles of the *mrd* operon genes in *Salmonella* Typhi. It was therefore important to initially characterise the *mrd* operon. Results of this study have shown that the *mrd* operon consists at least of *ybeB*, *ybeA*, *pbpA* and *rodA* in *Salmonella*, these genes being co-transcribed and co-regulated from a strong promoter located upstream of *ybeB*. *rlpA* may also be expressed under the control of the *mrd* operon promoter, as well as potentially from its own promoter, located inside the *rodA* gene.

In terms of gene function, the results of this study support those of previous studies, showing that *pbpA* and *rodA*, but not *ybeB*, *ybeA* and *rlpA*, are directly involved in cell shape determination. Several portions of evidence suggest that *rlpA* in particular may also play a role during cell wall synthesis, along with *pbpA* and *rodA*. A clear indisputable relationship between cell wall synthesis and cell shape, and the *ybe* genes has not yet been established, these genes appearing to play a major role in ribosome assembly and stability. However, the co-regulation of these genes with *pbpA* and *rodA*, along with a number of observations from this study and putative physical links between protein synthesis and cell wall synthetic machinery in the literature, permitted tentative hypotheses to be made concerning such a relationship. These therefore require further study.

The results of this study provide valuable information concerning the physiology and pathogenicity of round-cell Δ*pbpA* and Δ*rodA* mutants of *Salmonella* Typhi. It was firstly conclusively demonstrated that invasion-associated virulence factors are almost completely repressed in these mutants, at the level of transcription. The lack of repression of virulence factors required for intracellular survival, including

SPI-2, along with the ability to restore SPI-1 and motility expression through either recovery of *hilD* or *flhDC* expression, or the inactivation of upstream global stress response pathways, subsequently highlighted a number of important features of round-cell mutants, particularly concerning the regulation of the *mrd* mutant phenotypes:

- Round-cell *mrd* operon mutants retain their ability to assemble functional cell-wall spanning multi-protein organelles such as flagella, despite the apparent cell wall defects inherent in these mutants.
- The assembly, functionality and physical localisation of the T3SS and flagella organelles is not dependent upon bacterial cytoskeletal elements such as MreB, whose localisation is disrupted in Δ*rodA* mutants at least (131).
- SPI-1 and motility virulence factors are downregulated in Δ*pbpA* and Δ*rodA* mutants in response to the activation of a number of global stress response pathways, including envelope stress response pathways such as the Rcs phosphorelay, which in particular is thought to play a major role in virulence gene regulation in these mutants.
- The regulatory pathways activated in round-cell mutants result in a physiological state whereby invasion genes are repressed and genes required for intracellular survival and survival in adverse environmental conditions (e.g. stationary phase-activated genes) are upregulated. As such, the SPI-2 T3SS, the Vi antigen capsule and the cellulose and colanic acid capsular polysaccharides are all actively expressed or produced. These factors are thought to permit survival and growth/cell division of the round-cell mutants, and also are indicative of the effects that the inactivation of *pbpA* or *rodA* has on the cell envelope structure in particular.
- Although recovery of *flhDC* and *hilD* expression in round-cell mutants is sufficient to restore some motility and SPI-1 functionality to these mutants, full virulence is not restored. It is likely that a number of factors are involved in the complex regulation of virulence in response to the inactivation of *pbpA* and *rodA*. This regulation is also likely to occur at a number of levels. A potentially significant role for c-di-GMP in the post-transcriptional

regulation of motility and SPI-1 in round-cell mutants has also been established.

- A possible novel role for the outer membrane adhesin PagN in the regulation of virulence in round-cell mutants has been highlighted.
- Unlike studies with an Δ*mreCD* mutant, *in vivo* studies show that Δ*pbpA* and Δ*rodA* mutants remain attenuated despite the putative functionality of virulence factors required for intracellular survival. This result highlights the first instance of a significant phenotypic difference between different round-cell mutants.

Together these results enhance understanding of both the roles of each individual *mrd* operon gene in *Salmonella*, and the general physiology of round-cell *mrd* operon mutants. They also have provided important insights into the relationships between cell shape determination and virulence in *Salmonella*.

9.9 Outstanding questions and future work

In conclusion to this study, a number of outstanding questions remain unanswered, which future work aims to address. In addition, a number of hypotheses have been formulated from the results of this work which also require testing through further experimental analyses.

In terms of investigating the *mrd* operon as a unit, it would be useful to definitively map the *ybeB* promoter position, and also to clarify whether *rlpA* forms part of the operon, determining whether it is expressed predominantly under the control of its own promoter or from the *mrd* operon promoter upstream of *ybeB*. To test these points, northern blot or primer extension analyses would be useful, enabling a better definition of the full cohort of co-transcribed genes within the *mrd* operon. In addition, expression levels of *rlpA* could be investigated under the control of the putative *rlpA* promoter, by cloning the *rlpA* gene complete with upstream promoter sequences, or *ybeB* promoter sequences, into a promoter-less expression vector containing sequences encoding a 3' epitope tag, such that an easily traceable epitope-tagged RlpA protein would be expressed under the control of either promoter. This would enable comparisons of *rlpA* expression levels under the

control of either promoter, and also help determine the optimum conditions for *rlpA* expression with each promoter.

It would also be useful to investigate regulation of the *mrd* operon genes, by determining the conditions under which *mrd* operon genes are activated or suppressed. This would provide further information on the function of each gene and the operon as a whole.

Microarray analysis from this study provided extensive valuable insights into the gene expression profile of the Δ*rodA* mutant of *S.* Typhimurium. Whilst the large number of experimental analyses carried out alongside the microarrays helped to verify the microarray results, additional quantitative real-time RT-PCR (qPCR) experiments may be useful to fully verify these results. Initial qPCR analyses were attempted, but were not informative due to high levels of variation in the results, possibly due to experimental error. It may also be useful to conduct further microarrays in *S.* Typhi round-cell mutants, to provide important insights into the differences, particularly in the physiology and active regulatory pathways, between *S*. Typhi and *S*. Typhimurium round-cell mutants.

An important aspect of future work would be to investigate in more detail the regulatory mechanisms involved in the control of the virulence phenotypes of Δ*pbpA* and Δ*rodA* mutants. In particular, further work is needed to characterise the role of the Rcs phosphorelay in Δ*pbpA* and Δ*rodA* mutants, looking both at the expression levels of the major Rcs proteins in these mutants, and the extent to which they are responsible for SPI-1/motility repression, in both Typhi and Typhimurium mutants. Additional experiments are also needed to identify factors involved in the activation of the Rcs phosphorelay, upstream of RcsC or RcsB. RcsF constitutes a likely factor involved in the activation of the Rcs phosphorelay in response to peptidoglycan stress, although till now no evidence from this work has supported this hypothesis. To identify upstream regulatory signals would also help to define more precisely what effects the inactivation of *pbpA* of *rodA* have on the cell, and which features of the mutants cause the upregulation of such stress response pathways. Specifically, experimental work could focus on the systematic

generation and characterisation of knockout mutants of the major members of the Rcs phosphorelay in round-cell mutants.

The role of other major stress response pathways, and particularly those involved in the envelope stress response, also warrants further study, particularly as evidence suggests that *cpxA*, *rpoE* and *rpoS* at least were upregulated in round-cell mutants. It is likely that the regulatory pathways activated in round-cell mutants are complex, involving a large number of interacting factors. In particular the role of TviA in the regulation of virulence in round-cell *S.* Typhi mutants requires investigation. It would be interesting to test whether motility or SPI-1 functionality can be restored in Δ*pbpA*/Δ*rodA* Δ*tviA* double mutants.

Preliminary results of this study highlighted a role for c-di-GMP in the post-transcriptional regulation of virulence in round-cell mutants. In order to characterise the role of c-di-GMP further, it would be useful to repeat and refine the c-di-GMP LC/MS/MS assays, enabling the direct quantification of c-di-GMP in round-cell mutants. A number of EAL and GGDEF domain proteins which play a major role in the regulation of c-di-GMP levels, including AdrA, YciR, YhjH, and t3302 (stm3388) (95, 403, 451), have been cloned into the pBAD24 expression vector. These will be introduced into round-cell mutants of both *S.* Typhi and *S.* Typhimurium and induced, to determine the extent to which variation of c-di-GMP levels can affect motility/SPI-1 functionality in these mutants. Work is also needed to determine the mechanism by which c-di-GMP acts in round-cell mutants, and if its role is connected to that of the Rcs phosphorelay. Ultimately it would be useful to determine if SPI-1 and motility functionality can be fully restored in round-cell mutants, as well as virulence *in vivo*.

Additional experimental analyses are needed to further characterise the possible novel role of PagN in virulence gene regulation in round-cell mutants, be it direct or indirect. This could be done by the selective mutagenesis of short regions of the *pagN* gene to determine the downstream effects on virulence gene functionality, or by analysis of the transcriptional profile in Δ*pagN* mutants to identify regulatory pathways affected which may alter virulence gene expression, for example.

In global transposon mutagenesis screens a total of around 7000 individual colonies were assayed for recovery of motility gene expression. It may be useful to continue this screen, to be sure of more complete coverage of the *Salmonella* genome, enabling the identification of additional putative motility gene regulators.

Further phenotypic characterisation of the Δ*pbpA* and Δ*rodA* mutants may also be necessary to better describe the effects that these mutations have upon *Salmonella* biology and pathogenicity. For example, several assays conducted in this study highlighted significant alterations to the cell envelope structure in particular. Further work is needed to define the effects of *mrd* mutations on the outer membrane structure, through further analysing both LPS structure and the outer membrane protein profiles in these mutants. This is also applicable for the Δ*rlpA* mutant, in which possible major effects on the outer membrane structure were isolated.

In terms of *ybeB*, *ybeA* and *rlpA*, extensive further work is needed to better characterise the functions of these genes. In addition to examining the outer membrane in Δ*rlpA* mutants, it would be interesting to investigate expression of the Rcs phosphorelay in these mutants, along with other envelope stress response pathways which respond to perturbations in the outer membrane. This is particularly relevant since polymyxin B treatment is known to induce the Rcs phosphorelay, and would help to verify the surface phenotype observed in Δ*rlpA* mutants.

The putative links between protein synthesis and cell wall synthesis or the bacterial cytoskeleton also require investigation. The results of this study suggested that YbeB and YbeA are cytoplasmic proteins, with no particular pattern of localisation. However, it requires further analysis to ensure that the YFP-fusion proteins constructs of these genes are functional. It could also be interesting to determine whether the localisation of these proteins, along with other ribosome-associated proteins and proteins involved in translation, varies with cell growth, or as a consequence of Δ*pbpA*/Δ*rodA* mutations. This would help establish whether links exist between these elements and the cell shape determinant proteins.

The short-cell phenotype of Δ*ybeA* mutant cells was thought to result from the possible overexpression of *ftsZ* in these cells. This would need to be established experimentally through transcriptional reporter assays to analyse *ftsZ* expression, for example. Further work is also needed to investigate the reason for the short-cell phenotype of these cells. In addition, a possible link between cell size and motility/SPI-1 functionality in round-cell mutants was observed, which deserves further consideration, to determine whether motility functionality is directly related to cell size, or whether these two features are both independent consequences of upstream factors.

Finally, further assessment of the regulation of virulence in *S.* Typhi is required, to determine whether motility and SPI-1 functionality can be restored in Δ*pbpA* and Δ*rodA* mutants, as well as if and how regulation differs between the Typhimurium and Typhi serovars. In addition to examining TviA, the role of HtrA in contributing to the observed phenotypes in Typhi mutants should be assessed. As an extension to this study it may be useful to examine *mrd* gene function in a wild-type *S.* Typhi strain.

It is clear that the work of this study could be extended beyond the areas already discussed, and a large number of additional minor questions may also remain to be investigated. The cumulative results from this study, as well as future work, will no doubt provide extensive solid evidence and important insights into the roles of the *mrd* operon genes in both the biology and pathogenicity of *Salmonella*, the relationships between *mrd* operon genes, and the activity of global regulatory pathways. Ultimately this work provides useful insights into the biology of an important clinically relevant pathogen, particularly in terms of cell surface features which constitute important targets for future therapeutics. Much of this work is also applicable to related Gram-negative pathogens.

References

1. Parkhill, J. et al. Complete genome sequence of a multiple drug resistant *Salmonella enterica* serovar Typhi CT18. *Nature* **413**, 848-852 (2001).
2. McClelland, M. et al. Complete genome sequence of *Salmonella enterica* serovar Typhimurium LT2. *Nature* **413**, 852-856 (2001).
3. Baker, S. & Dougan, G. The Genome of *Salmonella enterica* Serovar Typhi. *Clinical Infectious Diseases* **45**, S29-S33 (2007).
4. Haraga, A., Ohlson, M.B. & Miller, S.I. *Salmonella*e interplay with host cells. *Nat Rev Microbiol* **6**, 53-66 (2008).
5. Kim, H.-J., Park, S.-H. & Kim, H.-Y. Comparison of *Salmonella enterica* Serovar Typhimurium LT2 and Non-LT2 *Salmonella* Genomic Sequences, and Genotyping of *Salmonella*e by Using PCR. *Appl. Environ. Microbiol.* **72**, 6142-6151 (2006).
6. Porwollik, S. et al. Characterization of *Salmonella enterica* Subspecies I Genovars by Use of Microarrays. *J. Bacteriol.* **186**, 5883-5898 (2004).
7. Tennant, S.M., Zhang, Y., Galen, J.E., Geddes, C.D. & Levine, M.M. Ultra-Fast and Sensitive Detection of Non-Typhoidal *Salmonella* Using Microwave-Accelerated Metal-Enhanced Fluorescence ("MAMEF"). *PLoS ONE* **6**, e18700 (2011).
8. Zhang, S. et al. Molecular Pathogenesis of *Salmonella enterica* Serotype Typhimurium-Induced Diarrhea. *Infect. Immun.* **71**, 1-12 (2003).
9. Gordon, M.A. *Salmonella* infections in immunocompromised adults. *J Infect* **56**, 413-422 (2008).
10. Gordon, M.A. et al. Epidemics of Invasive *Salmonella enterica* Serovar Enteritidis and *S. enterica* Serovar Typhimurium Infection Associated with Multidrug Resistance among Adults and Children in Malawi. *Clinical Infectious Diseases* **46**, 963-969 (2008).
11. Andrews-Polymenis, H.L., Baumler, A.J., McCormick, B.A. & Fang, F.C. Taming the Elephant: *Salmonella* Biology, Pathogenesis, and Prevention. *Infect. Immun.* **78**, 2356-2369 (2010).
12. Rhen, M., Maskell, D., Mastroeni, P. & Threlfall, J. *Salmonella*: Molecular Biology and Pathogenesis. (Horizon Scientific Press, 2007).
13. Everest, P., Wain, J., Roberts, M., Rook, G. & Dougan, G. The molecular mechanisms of severe typhoid fever. *Trends in Microbiology* **9**, 316-320 (2001).
14. Crump, J.A., Luby, S.P. & Mintz, E.D. The global burden of typhoid fever. *Bulletin of the World Health Organization* **82**, 346-353 (2004).
15. Mirza, S.H., Beeching, N.J. & Hart, C.A. Multi-drug resistant typhoid: a global problem. *J Med Microbiol* **44**, 317-319 (1996).
16. Chuang, C.H. et al. Surveillance of antimicrobial resistance of *Salmonella enterica* serotype Typhi in seven Asian countries. *Epidemiol Infect* **137**, 266-269 (2009).
17. Chau, T.T. et al. Antimicrobial Drug Resistance of *Salmonella enterica* Serovar Typhi in Asia and Molecular Mechanism of Reduced Susceptibility to the Fluoroquinolones. *Antimicrob. Agents Chemother.* **51**, 4315-4323 (2007).
18. Deng, W. et al. Comparative genomics of *Salmonella enterica* serovar Typhi strains Ty2 and CT18. *J Bacteriol* **185**, 2330-2337 (2003).
19. Helaine, S. et al. Dynamics of intracellular bacterial replication at the single cell level. *Proceedings of the National Academy of Sciences* **107**, 3746-3751 (2010).
20. Brawn, L.C., Hayward, R.D. & Koronakis, V. *Salmonella* SPI1 Effector SipA Persists after Entry and Cooperates with a SPI2 Effector to Regulate Phagosome Maturation and Intracellular Replication. *Cell host & microbe* **1**, 63-75 (2007).
21. Knodler, L.A. & Steele-Mortimer, O. Taking Possession: Biogenesis of the *Salmonella*-Containing Vacuole. *Traffic* **4**, 587-599 (2003).
22. Hansen-Wester, I. & Hensel, M. *Salmonella* pathogenicity islands encoding type III secretion systems. *Microbes Infect* **3**, 549-559 (2001).

23. Daigle, F. Typhi genes expressed during infection or involved in pathogenesis. *The Journal of Infection in Developing Countries* **2**, 431-437 (2008).
24. Hueck, C.J. Type III protein secretion systems in bacterial pathogens of animals and plants. *Microbiol Mol Biol Rev* **62**, 379-433 (1998).
25. Hayward, R.D., Hume, P.J., McGhie, E.J. & Koronakis, V. A *Salmonella* SipB-derived polypeptide blocks the 'trigger' mechanism of bacterial entry into eukaryotic cells. *Mol Microbiol* **45**, 1715-1727 (2002).
26. Hayward, R.D. & Koronakis, V. Direct modulation of the host cell cytoskeleton by *Salmonella* actin-binding proteins. *Trends Cell Biol* **12**, 15-20 (2002).
27. Tran Van Nhieu, G., Bourdet-Sicard, R., Dumenil, G., Blocker, A. & Sansonetti, P.J. Bacterial signals and cell responses during *Shigella* entry into epithelial cells. *Cell Microbiol* **2**, 187-193 (2000).
28. Daoguo, Z. Collective efforts to modulate the host actin cytoskeleton by *Salmonella* type III-secreted effector proteins. *Trends in Microbiology* **9**, 567-569 (2001).
29. Kimbrough, T.G. & Miller, S.I. Assembly of the type III secretion needle complex of *Salmonella* Typhimurium. *Microbes Infect* **4**, 75-82 (2002).
30. Hayward, R.D. & Koronakis, V. Direct nucleation and bundling of actin by the SipC protein of invasive *Salmonella*. *Embo J* **18**, 4926-4934 (1999).
31. Zhou, D., Mooseker, M.S. & Galán, J.E. Role of the S. typhimurium Actin-Binding Protein SipA in Bacterial Internalization. *Science* **283**, 2092-2095 (1999).
32. Dreher, D. et al. *Salmonella* virulence factor SipB induces activation and release of IL-18 in human dendritic cells. *Journal of Leukocyte Biology* **72**, 743-751 (2002).
33. Boyle, E.C., Brown, N.F. & Finlay, B.B. *Salmonella enterica* serovar Typhimurium effectors SopB, SopE, SopE2 and SipA disrupt tight junction structure and function. *Cell Microbiol* **8**, 1946-1957 (2006).
34. Liao, A.P. et al. *Salmonella* type III effector AvrA stabilizes cell tight junctions to inhibit inflammation in intestinal epithelial cells. *PLoS ONE* **3**, e2369 (2008).
35. Collier-Hyams, L.S. et al. Cutting Edge: *Salmonella* AvrA Effector Inhibits the Key Proinflammatory, Anti-Apoptotic NF-κB Pathway. *The Journal of Immunology* **169**, 2846-2850 (2002).
36. Murli, S., Watson, R.O. & Galán, J.E. Role of tyrosine kinases and the tyrosine phosphatase SptP in the interaction of *Salmonella* with host cells. *Cell Microbiol* **3**, 795-810 (2001).
37. Coombes, B.K., Brown, N.F., Valdez, Y., Brumell, J.H. & Finlay, B.B. Expression and Secretion of *Salmonella* Pathogenicity Island-2 Virulence Genes in Response to Acidification Exhibit Differential Requirements of a Functional Type III Secretion Apparatus and SsaL. *J Biol Chem* **279**, 49804-49815 (2004).
38. Linehan, S.A., Rytkonen, A., Yu, X.-J., Liu, M. & Holden, D.W. SlyA regulates function of *Salmonella* pathogenicity island 2 (SPI-2) and expression of SPI-2-associated genes. *Infect Immun* **73**, 4354-4362 (2005).
39. Deiwick, J., Nikolaus, T., Erdogan, S. & Hensel, M. Environmental regulation of *Salmonella* pathogenicity island 2 gene expression. *Mol Microbiol* **31**, 1759-1773 (1999).
40. Hensel, M. et al. Genes encoding putative effector proteins of the type III secretion system of *Salmonella* pathogenicity island 2 are required for bacterial virulence and proliferation in macrophages. *Mol Microbiol* **30**, 163-174 (1998).
41. Waterman, S.R. & Holden, D.W. Functions and effectors of the *Salmonella* pathogenicity island 2 type III secretion system. *Cell Microbiol* **5**, 501-511 (2003).
42. van Asten, A.J.A.M. & van Dijk, J.E. Distribution of “classic” virulence factors among *Salmonella* spp. *FEMS Immunology & Medical Microbiology* **44**, 251-259 (2005).
43. Olivia, S.-M. The *Salmonella*-containing vacuole—Moving with the times. *Curr Opin Microbiol* **11**, 38-45 (2008).

44. Buchmeier, N. et al. SlyA, a transcriptional regulator of *Salmonella* typhimurium, is required for resistance to oxidative stress and is expressed in the intracellular environment of macrophages. *Infect Immun* **65**, 3725-3730 (1997).
45. Klein, J.R. & Jones, B.D. *Salmonella* Pathogenicity Island 2-Encoded Proteins SseC and SseD Are Essential for Virulence and Are Substrates of the Type III Secretion System. *Infect. Immun.* **69**, 737-743 (2001).
46. Coombes, B.K., Wickham, M.E., Lowden, M.J., Brown, N.F. & Finlay, B.B. Negative regulation of *Salmonella* pathogenicity island 2 is required for contextual control of virulence during typhoid. *Proc Natl Acad Sci U S A* **102**, 17460-17465 (2005).
47. Deiwick, J. et al. Mutations in *Salmonella* pathogenicity island 2 (SPI2) genes affecting transcription of SPI1 genes and resistance to antimicrobial agents. *J Bacteriol* **180**, 4775-4780 (1998).
48. Sherry, A.E. et al. Characterisation of proteins extracted from the surface of *Salmonella* Typhimurium grown under SPI-2-inducing conditions by LC-ESI/MS/MS sequencing. *PROTEOMICS* **11**, 361-370 (2011).
49. Pucciarelli, M.G. & Garcia-del Portillo, F. Protein-peptidoglycan interactions modulate the assembly of the needle complex in the *Salmonella* invasion-associated type III secretion system. *Mol Microbiol* **48**, 573-585 (2003).
50. Arricau, N. et al. The RcsB-RcsC regulatory system of *Salmonella* typhi differentially modulates the expression of invasion proteins, flagellin and Vi antigen in response to osmolarity. *Mol Microbiol* **29**, 835-850 (1998).
51. Stecher, B. et al. Flagella and chemotaxis are required for efficient induction of *Salmonella enterica* serovar Typhimurium colitis in streptomycin-pretreated mice. *Infect Immun* **72**, 4138-4150 (2004).
52. Lockman, H.A. & Curtiss, R., 3rd *Salmonella* typhimurium mutants lacking flagella or motility remain virulent in BALB/c mice. *Infect Immun* **58**, 137-143 (1990).
53. Dibb-Fuller, M.P., Allen-Vercoe, E., Thorns, C.J. & Woodward, M.J. Fimbriae- and flagella-mediated association with and invasion of cultured epithelial cells by *Salmonella* enteritidis. *Microbiology* **145**, 1023-1031 (1999).
54. Kubori, T. et al. Supramolecular structure of the *Salmonella* typhimurium type III protein secretion system. *Science* **280**, 602-605 (1998).
55. Paul, K., Erhardt, M., Hirano, T., Blair, D.F. & Hughes, K.T. Energy source of flagellar type III secretion. *Nature* **451**, 489-492 (2008).
56. Chilcott, G.S. & Hughes, K.T. Coupling of flagellar gene expression to flagellar assembly in *Salmonella enterica* serovar typhimurium and *Escherichia coli*. *Microbiol Mol Biol Rev* **64**, 694-708 (2000).
57. Ikeda, J.S. et al. Flagellar phase variation of *Salmonella enterica* serovar Typhimurium contributes to virulence in the murine typhoid infection model but does not influence *Salmonella*-induced enteropathogenesis. *Infect Immun* **69**, 3021-3030 (2001).
58. Aldridge, P. & Hughes, K.T. Regulation of flagellar assembly. *Curr Opin Microbiol* **5**, 160-165 (2002).
59. Bonifield, H.R. & Hughes, K.T. Flagellar Phase Variation in *Salmonella enterica* Is Mediated by a Posttranscriptional Control Mechanism. *J. Bacteriol.* **185**, 3567-3574 (2003).
60. Lee, H.J. & Hughes, K.T. Posttranscriptional control of the *Salmonella enterica* flagellar hook protein FlgE. *J Bacteriol* **188**, 3308-3316 (2006).
61. Vonderviszt, F. & Namba, K. Fibrous Proteins - Structure, Function and Assembly of Flagellar Axial Proteins. (Landes Bioscience, 2008).
62. Apel, D. & Surette, M.G. Bringing order to a complex molecular machine: The assembly of the bacterial flagella. *Biochim Biophys Acta* **1778**, 1851-1858 (2008).
63. Hizukuri, Y., Kojima, S. & Homma, M. Disulphide cross-linking between the stator and the bearing components in the bacterial flagellar motor. *Journal of Biochemistry* **148**, 309-318 (2010).

64. Kojima, S. et al. Stator assembly and activation mechanism of the flagellar motor by the periplasmic region of MotB. *Mol Microbiol* **73**, 710-718 (2009).
65. Berg, H.C. The Rotary Motor Of Bacterial Flagella. *Annual Review of Biochemistry* **72**, 19-54 (2003).
66. Muramoto, K. & Macnab, R.M. Deletion analysis of MotA and MotB, components of the force-generating unit in the flagellar motor of *Salmonella*. *Mol Microbiol* **29**, 1191-1202 (1998).
67. Blair, D.F., Kim, D.Y. & Berg, H.C. Mutant MotB proteins in *Escherichia coli*. *J. Bacteriol.* **173**, 4049-4055 (1991).
68. Armstrong, J.B. & Adler, J. Complementation of nonchemotactic mutants of *Escherichia coli*. *Genetics* **61**, 61-66 (1969).
69. Salyers, A.A. & Whitt, D.D. Bacterial Pathogenesis. A Molecular Approach, Edn. 2nd. (ASM Press 2001).
70. Wain, J. et al. Vi antigen expression in *Salmonella enterica* serovar Typhi clinical isolates from Pakistan. *J Clin Microbiol* **43**, 1158-1165 (2005).
71. Hone, D.M. et al. A *galE* via (Vi antigen-negative) mutant of *Salmonella* typhi Ty2 retains virulence in humans. *Infect Immun* **56**, 1326-1333 (1988).
72. Looney, R.J. & Steigbigel, R.T. Role of the Vi antigen of *Salmonella* typhi in resistance to host defense in vitro. *J Lab Clin Med* **108**, 506-516 (1986).
73. Wilson, R.P. et al. The Vi-capsule prevents Toll-like receptor 4 recognition of *Salmonella*. *Cell Microbiol* **10**, 876-890 (2008).
74. Thoms, C.J. *Salmonella* fimbriae: novel antigens in the detection and control of *Salmonella* infections. *Br Vet J* **151**, 643-658 (1995).
75. Rank, D.L., Saeed, M.A. & Muriana, P.M. Cloning of *Salmonella enterica* Serovar Enteritidis Fimbrial Protein SefA as a Surface Protein in *Escherichia coli* Confers the Ability To Attach to Eukaryotic Cell Lines. *Appl. Environ. Microbiol.* **75**, 6622-6625 (2009).
76. Townsend, S.M. et al. *Salmonella enterica* Serovar Typhi Possesses a Unique Repertoire of Fimbrial Gene Sequences. *Infect. Immun.* **69**, 2894-2901 (2001).
77. Baumler, A.J., Tsolis, R.M., Ficht, T.A. & Adams, L.G. Evolution of Host Adaptation in *Salmonella enterica*. *Infect. Immun.* **66**, 4579-4587 (1998).
78. Garcia-Quintanilla, M., Ramos-Morales, F. & Casadesus, J. Conjugal Transfer of the *Salmonella enterica* Virulence Plasmid in the Mouse Intestine. *J. Bacteriol.* **190**, 1922-1927 (2008).
79. Rotger, R. & Casadesus, J. The virulence plasmids of *Salmonella*. *Int Microbiol.* **2**, 177-184 (1999).
80. Edwards, R.A., Olsen, G.J. & Maloy, S.R. Comparative genomics of closely related *Salmonella*e. *Trends in Microbiology* **10**, 94-99 (2002).
81. Oscarsson, J. et al. Characterization of a Pore-Forming Cytotoxin Expressed by *Salmonella enterica* Serovars Typhi and Paratyphi A. *Infect. Immun.* **70**, 5759-5769 (2002).
82. Spanò, S., Ugalde, J.E. & Galán, J.E. Delivery of a *Salmonella* Typhi Exotoxin from a Host Intracellular Compartment. *Cell Host & Microbe* **3**, 30-38 (2008).
83. Haghjoo, E. & Galán, J.E. *Salmonella* typhi encodes a functional cytolethal distending toxin that is delivered into host cells by a bacterial-internalization pathway. *Proc Natl Acad Sci U S A* **101**, 4614-4619 (2004).
84. Cornelis, G.R. The type III secretion injectisome. *Nat Rev Microbiol* **4**, 811-825 (2006).
85. Tran, Q.T. et al. The *Salmonella enterica* Serotype Typhi Vi Capsular Antigen Is Expressed after the Bacterium Enters the Ileal Mucosa. *Infect. Immun.* **78**, 527-535 (2010).
86. Lin, D., Rao, C.V. & Slauch, J.M. The *Salmonella* SPI1 Type Three Secretion System Responds to Periplasmic Disulfide Bond Status via the Flagellar Apparatus and the RcsCDB System. *J. Bacteriol.* **190**, 87-97 (2008).

87. Altier, C. Genetic and Environmental Control of *Salmonella* Invasion. *J Microbiol* **43**, 85-92 (2005).
88. Ellermeier, J.R. & Slauch, J.M. Adaptation to the host environment: regulation of the SPI1 type III secretion system in *Salmonella enterica* serovar Typhimurium. *Curr Opin Microbiol* **10**, 24-29 (2007).
89. Jones, B.D. *Salmonella* invasion gene regulation: a story of environmental awareness. *J Microbiol* **43**, 110-117 (2005).
90. Bustamante, V.H. et al. HilD-mediated transcriptional cross-talk between SPI-1 and SPI-2. *Proceedings of the National Academy of Sciences* **105**, 14591-14596 (2008).
91. Ellermeier, C.D., Ellermeier, J.R. & Slauch, J.M. HilD, HilC and RtsA constitute a feed forward loop that controls expression of the SPI1 type three secretion system regulator *hilA* in *Salmonella enterica* serovar Typhimurium. *Mol Microbiol* **57**, 691-705 (2005).
92. Teplitski, M., Goodier, R.I. & Ahmer, B.M.M. Pathways Leading from BarA/SirA to Motility and Virulence Gene Expression in *Salmonella*. *J. Bacteriol.* **185**, 7257-7265 (2003).
93. Saini, S., Ellermeier, J.R., Slauch, J.M. & Rao, C.V. The Role of Coupled Positive Feedback in the Expression of the SPI1 Type Three Secretion System in *Salmonella*. *PLoS Pathog* **6**, e1001025 (2010).
94. Pegues, D.A., Hantman, M.J., Behlau, I. & Miller, S.I. PhoP/PhoQ transcriptional repression of *Salmonella* typhimurium invasion genes: evidence for a role in protein secretion. *Mol Microbiol* **17**, 169-181 (1995).
95. Lamprokostopoulou, A., Monteiro, C., Rhen, M. & Römling, U. Cyclic di-GMP signalling controls virulence properties of *Salmonella enterica* serovar Typhimurium at the mucosal lining. *Environmental Microbiology* **12**, 40-53 (2010).
96. Garcia-Calderon, C.B., Casadesus, J. & Ramos-Morales, F. Rcs and PhoPQ Regulatory Overlap in the Control of *Salmonella enterica* Virulence. *J. Bacteriol.* **189**, 6635-6644 (2007).
97. Boddicker, J.D. & Jones, B.D. Lon Protease Activity Causes Down-Regulation of *Salmonella* Pathogenicity Island 1 Invasion Gene Expression after Infection of Epithelial Cells. *Infect. Immun.* **72**, 2002-2013 (2004).
98. Rychlik, I. & Barrow, P.A. *Salmonella* stress management and its relevance to behaviour during intestinal colonisation and infection. *FEMS Microbiology Reviews* **29**, 1021-1040 (2005).
99. Garmendia, J., Beuzón, C.R., Ruiz-Albert, J. & Holden, D.W. The roles of SsrA–SsrB and OmpR–EnvZ in the regulation of genes encoding the *Salmonella* typhimurium SPI-2 type III secretion system. *Microbiology* **149**, 2385-2396 (2003).
100. Worley, M.J., Ching, K.H.L. & Heffron, F. *Salmonella* SsrB activates a global regulon of horizontally acquired genes. *Mol Microbiol* **36**, 749-761 (2000).
101. Choi, J. et al. *Salmonella* pathogenicity island 2 expression negatively controlled by EIIANtr–SsrB interaction is required for *Salmonella* virulence. *Proceedings of the National Academy of Sciences* (2010).
102. Walthers, D. et al. The response regulator SsrB activates expression of diverse *Salmonella* pathogenicity island 2 promoters and counters silencing by the nucleoid-associated protein H-NS. *Mol Microbiol* **65**, 477-493 (2007).
103. Feng, X., Oropeza, R. & Kenney, L.J. Dual regulation by phospho-OmpR of *ssrA/B* gene expression in *Salmonella* pathogenicity island 2. *Mol Microbiol* **48**, 1131-1143 (2003).
104. Feng, X., Walthers, D., Oropeza, R. & Kenney, L.J. The response regulator SsrB activates transcription and binds to a region overlapping OmpR binding sites at *Salmonella* pathogenicity island 2. *Mol Microbiol* **54**, 823-835 (2004).
105. Lucchini, S. et al. H-NS Mediates the Silencing of Laterally Acquired Genes in Bacteria. *PLoS Pathog* **2**, e81 (2006).

106. Miao, E.A., Freeman, J.A. & Miller, S.I. Transcription of the SsrAB Regulon Is Repressed by Alkaline pH and Is Independent of PhoPQ and Magnesium Concentration. *J. Bacteriol.* **184**, 1493-1497 (2002).
107. Clements, M., Eriksson, S., Tezcan-Merdol, D., Hinton, J.C. & Rhen, M. Virulence gene regulation in *Salmonella enterica*. *Ann Med.* **33**, 178-185 (2001).
108. Wang, S., Fleming, R.T., Westbrook, E.M., Matsumura, P. & McKay, D.B. Structure of the *Escherichia coli* FlhDC Complex, a Prokaryotic Heteromeric Regulator of Transcription. *J Mol Biol* **355**, 798-808 (2006).
109. Kato, Y., Sugiura, M., Mizuno, T. & Aiba, H. Effect of the *arcA* Mutation on the Expression of Flagella Genes in *Escherichia coli*. *Bioscience, Biotechnology, and Biochemistry* **71**, 77-83 (2007).
110. Wei, B.L. et al. Positive regulation of motility and *flhDC* expression by the RNA-binding protein CsrA of *Escherichia coli*. *Mol Microbiol* **40**, 245-256 (2001).
111. Clarke, M.B. & Sperandio, V. Transcriptional regulation of *flhDC* by QseBC and σ^{28} (FliA) in enterohaemorrhagic *Escherichia coli*. *Mol Microbiol* **57**, 1734-1749 (2005).
112. Baker, S. et al. A linear plasmid truncation induces unidirectional flagellar phase change in H:z66 positive *Salmonella* Typhi. *Mol Microbiol* **66**, 1207-1218 (2007).
113. Aldridge, C. et al. The interaction dynamics of a negative feedback loop regulates flagellar number in *Salmonella enterica* serovar Typhimurium. *Mol Microbiol* **78**, 1416-1430 (2010).
114. Virlogeux-Payant, I. & Popoff, M.Y. The Vi antigen of *Salmonella* typhi. *Bulletin de l'Institut Pasteur* **94**, 237-250.
115. Virlogeux, I., Waxin, H., Ecobichon, C. & Popoff, M.Y. Role of the *viaB* locus in synthesis, transport and expression of *Salmonella* typhi Vi antigen. *Microbiology* **141**, 3039-3047 (1995).
116. Winter, S.E. et al. The TviA auxiliary protein renders the *Salmonella enterica* serotype Typhi RcsB regulon responsive to changes in osmolarity. *Mol Microbiol* **74**, 175-193 (2009).
117. Winter, S.E. et al. A Rapid Change in Virulence Gene Expression during the Transition from the Intestinal Lumen into Tissue Promotes Systemic Dissemination of *Salmonella*. *PLoS Pathog* **6**, e1001060 (2010).
118. Laubacher, M.E. & Ades, S.E. The Rcs Phosphorelay Is a Cell Envelope Stress Response Activated by Peptidoglycan Stress and Contributes to Intrinsic Antibiotic Resistance. *J. Bacteriol.* **190**, 2065-2074 (2008).
119. Huang, Y.-H., Ferrières, L. & Clarke, D.J. The role of the Rcs phosphorelay in *Enterobacteriaceae*. *Res Microbiol* **157**, 206-212 (2006).
120. Gao, H. et al. Phenotypic and transcriptional analysis of the osmotic regulator OmpR in *Yersinia pestis*. *BMC Microbiology* **11**, 39 (2011).
121. Perez, J.C. et al. Evolution of a Bacterial Regulon Controlling Virulence and Mg^{2+} Homeostasis. *PLoS Genet* **5**, e1000428 (2009).
122. Cabeen, M.T. & Jacobs-Wagner, C. Bacterial cell shape. *Nat Rev Microbiol* **3**, 601-610 (2005).
123. Labischinski, H., Goodell, E.W., Goodell, A. & Hochberg, M.L. Direct proof of a "more-than-single-layered" peptidoglycan architecture of *Escherichia coli* W7: a neutron small-angle scattering study. *J Bacteriol* **173**, 751-756 (1991).
124. Scheffers, D.-J. & Pinho, M.G. Bacterial Cell Wall Synthesis: New Insights from Localization Studies. *Microbiol. Mol. Biol. Rev.* **69**, 585-607 (2005).
125. Vollmer, W. & Bertsche, U. Murein (peptidoglycan) structure, architecture and biosynthesis in *Escherichia coli*. *Biochimica et Biophysica Acta* **1778**, 1714-1734 (2008).
126. Den Blaauwen, T., De Pedro, M.A., Nguyen-Distèche, M. & Ayala, J.A. Morphogenesis of rod-shaped sacculi. *FEMS Microbiology Reviews* **32**, 321-344 (2008).
127. de Pedro, M.A., Donachie, W.D., Holtje, J.V. & Schwarz, H. Constitutive septal murein synthesis in *Escherichia coli* with impaired activity of the morphogenetic

proteins RodA and penicillin-binding protein 2.[see comment]. *J Bacteriol* **183**, 4115-4126 (2001).
128. Shiomi, D., Sakai, M. & Niki, H. Determination of bacterial rod shape by a novel cytoskeletal membrane protein. *Embo J* **27**, 3081-3091 (2008).
129. Osborn, M.J. & Rothfield, L. Cell shape determination in *Escherichia coli*. *Curr Opin Microbiol* **10**, 606-610 (2007).
130. Bendezu, F.O. & de Boer, P.A.J. Conditional lethality, division defects, membrane involution, and endocytosis in *mre* and *mrd* shape mutants of *Escherichia coli*. *J Bacteriol* **190**, 1792-1811 (2008).
131. Kruse, T., Bork-Jensen, J. & Gerdes, K. The morphogenetic MreBCD proteins of *Escherichia coli* form an essential membrane-bound complex. *Mol Microbiol* **55**, 78-89 (2005).
132. Jones, L.J., Carballido-Lopez, R. & Errington, J. Control of cell shape in bacteria: helical, actin-like filaments in *Bacillus subtilis*. *Cell* **104**, 913-922 (2001).
133. Esue, O., Cordero, M., Wirtz, D. & Tseng, Y. The assembly of MreB, a prokaryotic homolog of actin. *J Biol Chem* **280**, 2628-2635 (2005).
134. Swulius, M.T. et al. Long helical filaments are not seen encircling cells in electron cryotomograms of rod-shaped bacteria. *Biochemical and Biophysical Research Communications* **407**, 650-655 (2011).
135. Vats, P., Shih, Y.-L. & Rothfield, L. Assembly of the MreB-associated cytoskeletal ring of *Escherichia coli*. *Mol Microbiol* **72**, 170-182 (2009).
136. Figge, R.M., Divakaruni, A.V. & Gober, J.W. MreB, the cell shape-determining bacterial actin homologue, co-ordinates cell wall morphogenesis in *Caulobacter crescentus*. *Mol Microbiol* **51**, 1321-1332 (2004).
137. Divakaruni, A.V., Loo, R.R.O., Xie, Y., Loo, J.A. & Gober, J.W. The cell-shape protein MreC interacts with extracytoplasmic proteins including cell wall assembly complexes in *Caulobacter crescentus*. *Proc Natl Acad Sci U S A* **102**, 18602-18607 (2005).
138. Dye, N.A., Pincus, Z., Theriot, J.A., Shapiro, L. & Gitai, Z. Two independent spiral structures control cell shape in *Caulobacter*. *Proc Natl Acad Sci U S A* **102**, 18608-18613 (2005).
139. Divakaruni, A.V., Baida, C., White, C.L. & Gober, J.W. The cell shape proteins MreB and MreC control cell morphogenesis by positioning cell wall synthetic complexes. *Mol Microbiol* **66**, 174-188 (2007).
140. Van Den Ent, F. et al. Dimeric structure of the cell shape protein MreC and its functional implications. *Mol Microbiol* **62**, 1631-1642 (2006).
141. van den Ent, F., Johnson, C.M., Persons, L., de Boer, P. & Lowe, J. Bacterial actin MreB assembles in complex with cell shape protein RodZ. *Embo J* **29**, 1081-1090 (2010).
142. Asoh, S. et al. Nucleotide sequence of the *pbpA* gene and characteristics of the deduced amino acid sequence of penicillin-binding protein 2 of *Escherichia coli* K12. *Eur J Biochem* **160**, 231-238 (1986).
143. Matsuzawa, H. et al. Nucleotide sequence of the *rodA* gene, responsible for the rod shape of *Escherichia coli*: *rodA* and the *pbpA* gene, encoding penicillin-binding protein 2, constitute the *rodA* operon. *J Bacteriol* **171**, 558-560 (1989).
144. Asoh, S., Matsuzawa, H., Matsuhashi, M. & Ohta, T. Molecular cloning and characterization of the genes (*pbpA* and *rodA*) responsible for the rod shape of *Escherichia coli* K-12: analysis of gene expression with transposon Tn*5* mutagenesis and protein synthesis directed by constructed plasmids. *J Bacteriol* **154**, 10-16 (1983).
145. Spratt, B.G. Distinct penicillin binding proteins involved in the division, elongation, and shape of *Escherichia coli* K12. *Proc Natl Acad Sci U S A* **72**, 2999-3003 (1975).

146. Ishino, F. et al. Peptidoglycan synthetic activities in membranes of *Escherichia coli* caused by overproduction of penicillin-binding protein 2 and RodA protein. *J Biol Chem* **261**, 7024-7031 (1986).
147. Ishino, F., Tamaki, S., Spratt, B.G. & Matsuhashi, M. A mecillinam-sensitive peptidoglycan crosslinking reaction in *Escherichia*, *coli*. *Biochemical and Biophysical Research Communications* **109**, 689-696 (1982).
148. Spratt, B.G. & Pardee, A.B. Penicillin-binding proteins and cell shape in *E. coli*. *Nature* **254**, 516-517 (1975).
149. Uehara, T. & Park, J.T. Growth of *Escherichia coli*: significance of peptidoglycan degradation during elongation and septation. *J Bacteriol* **190**, 3914-3922 (2008).
150. Goffin, C. & Ghuysen, J.-M. Multimodular Penicillin-Binding Proteins: An Enigmatic Family of Orthologs and Paralogs. *Microbiol. Mol. Biol. Rev.* **62**, 1079-1093 (1998).
151. García del Portillo, F. & De Pedro, M.A. Penicillin-binding protein 2 is essential for the integrity of growing cells of *Escherichia coli ponB* strains. *J Bacteriol.* **173**, 4530-4532 (1991).
152. Ehlert, K. & Holtje, J.V. Role of precursor translocation in coordination of murein and phospholipid synthesis in *Escherichia coli*. *J Bacteriol* **178**, 6766-6771 (1996).
153. Stoker, N.G., Pratt, J.M. & Spratt, B.G. Identification of the *rodA* gene product of *Escherichia coli*. *J Bacteriol* **155**, 854-859 (1983).
154. Henriques, A.O., Glaser, P., Piggot, P.J. & Moran Jr, C.P. Control of cell shape and elongation by the *rodA* gene in *Bacillus subtilis*. *Mol Microbiol* **28**, 235-247 (1998).
155. Tamaki, S., Matsuzawa, H. & Matsuhashi, M. Cluster of *mrdA* and *mrdB* genes responsible for the rod shape and mecillinam sensitivity of *Escherichia coli*. *J Bacteriol* **141**, 52-57 (1980).
156. Van Dam, V. et al. Transmembrane transport of peptidoglycan precursors across model and bacterial membranes. *Mol Microbiol* **64**, 1105-1114 (2007).
157. Costa, C.S. & Anton, D.N. Conditional lethality of cell shape mutations of *Salmonella* typhimurium: *rodA* and *mre* mutants are lethal on solid but not in liquid medium. *Curr Microbiol* **38**, 137-142 (1999).
158. Legaree, B.A., Adams, C.B. & Clarke, A.J. Overproduction of Penicillin-Binding Protein 2 and Its Inactive Variants Causes Morphological Changes and Lysis in *Escherichia coli*. *J. Bacteriol.* **189**, 4975-4983 (2007).
159. William, M. Sculpting the Bacterial Cell. *Curr Biol* **19**, R812-R822 (2009).
160. Den Blaauwen, T., Aarsman, M.E.G., Vischer, N.O.E. & Nanninga, N. Penicillin-binding protein PBP2 of *Escherichia coli* localizes preferentially in the lateral wall and at mid-cell in comparison with the old cell pole. *Mol Microbiol* **47**, 539-547 (2003).
161. Carballido-Lopez, R. The Bacterial Actin-Like Cytoskeleton. *Microbiol. Mol. Biol. Rev.* **70**, 888-909 (2006).
162. Karczmarek, A. et al. DNA and origin region segregation are not affected by the transition from rod to sphere after inhibition of *Escherichia coli* MreB by A22. *Mol Microbiol* **65**, 51-63 (2007).
163. Doble, A. The role of cell shape determining proteins in the biology and pathogenicity of *Salmonella.* Institute for Cell and Molecular Biosciences, Masters of Research dissertation (Newcastle University, Newcastle; 2008).
164. Bendezu, F.O., Hale, C.A., Bernhardt, T.G. & de Boer, P.A.J. RodZ (YfgA) is required for proper assembly of the MreB actin cytoskeleton and cell shape in E. *coli*. *Embo J* **28**, 193-204 (2009).
165. Alyahya, S.A. et al. RodZ, a component of the bacterial core morphogenic apparatus. *Proc Natl Acad Sci U S A* **106**, 1239-1244 (2009).
166. Niba, E.T.E., Li, G., Aoki, K. & Kitakawa, M. Characterization of *rodZ* mutants: RodZ is not absolutely required for the cell shape and motility. *FEMS Microbiol Lett* **309**, 35-42 (2010).

167. Gerdes, K. RodZ, a new player in bacterial cell morphogenesis. *Embo J* **28**, 171-172 (2009).
168. Mitobe, J. et al. RodZ regulates the post-transcriptional processing of the *Shigella sonnei* type III secretion system. *EMBO Rep* **12**, 911-916 (2011).
169. Varma, A. & Young, K.D. In *Escherichia coli*, MreB and FtsZ Direct the Synthesis of Lateral Cell Wall via Independent Pathways That Require PBP 2. *J Bacteriol* **191**, 3526–3533 (2009).
170. Carballido-López, R. et al. Actin Homolog MreBH Governs Cell Morphogenesis by Localization of the Cell Wall Hydrolase LytE. *Developmental Cell* **11**, 399-409 (2006).
171. Daniel, R.A. & Errington, J. Control of cell morphogenesis in bacteria: two distinct ways to make a rod-shaped cell. *Cell* **113**, 767-776 (2003).
172. Varma, A., de Pedro, M.A. & Young, K.D. FtsZ directs a second mode of peptidoglycan synthesis in *Escherichia coli*. *J Bacteriol* **189**, 5692-5704 (2007).
173. Shih, Y.-L. & Rothfield, L. The Bacterial Cytoskeleton. *Microbiol. Mol. Biol. Rev.* **70**, 729-754 (2006).
174. de Pedro, M.A., Quintela, J.C., Holtje, J.V. & Schwarz, H. Murein segregation in *Escherichia coli*.[see comment]. *J Bacteriol* **179**, 2823-2834 (1997).
175. Goehring, N.W. & Beckwith, J. Diverse Paths to Midcell: Assembly of the Bacterial Cell Division Machinery. *Current biology : CB* **15**, R514-R526 (2005).
176. Buddelmeijer, N. & Beckwith, J. Assembly of cell division proteins at the *E. coli* cell center. *Curr Opin Microbiol* **5**, 553-557 (2002).
177. Dajkovic, A. & Lutkenhaus, J. Z ring as executor of bacterial cell division. *J Mol Microbiol Biotechnol.* **11**, 140-151 (2006).
178. Errington, J., Daniel, R.A. & Scheffers, D.-J. Cytokinesis in Bacteria. *Microbiol. Mol. Biol. Rev.* **67**, 52-65 (2003).
179. Gerding, M.A. et al. Self-Enhanced Accumulation of FtsN at Division Sites and Roles for Other Proteins with a SPOR Domain (DamX, DedD, and RlpA) in *Escherichia coli* Cell Constriction. *J. Bacteriol.* **191**, 7383-7401 (2009).
180. Datta, P. et al. Interaction between FtsW and penicillin-binding protein 3 (PBP3) directs PBP3 to mid-cell, controls cell septation and mediates the formation of a trimeric complex involving FtsZ, FtsW and PBP3 in mycobacteria. *Mol Microbiol* **62**, 1655-1673 (2006).
181. Canepari, P., Signoretto, C., Boaretti, M. & Lleò, M.D.M. Cell elongation and septation are two mutually exclusive processes in *Escherichia coli*. *Archives of Microbiology* **168**, 152-159 (1997).
182. Thanedar, S. & Margolin, W. FtsZ Exhibits Rapid Movement and Oscillation Waves in Helix-like Patterns in *Escherichia coli*. *Curr Biol* **14**, 1167-1173 (2004).
183. Peters, P.C., Migocki, M.D., Thoni, C. & Harry, E.J. A new assembly pathway for the cytokinetic Z ring from a dynamic helical structure in vegetatively growing cells of *Bacillus subtilis*. *Mol Microbiol* **64**, 487-499 (2007).
184. Aaron, M. et al. The tubulin homologue FtsZ contributes to cell elongation by guiding cell wall precursor synthesis in *Caulobacter crescentus*. *Mol Microbiol* **64**, 938-952 (2007).
185. Alaedini, A. & Day, R.A. Identification of Two Penicillin-Binding Multienzyme Complexes in *Haemophilus influenzae*. *Biochemical and Biophysical Research Communications* **264**, 191-195 (1999).
186. Takase, I. et al. Genes encoding two lipoproteins in the *leuS-dacA* region of the *Escherichia coli* chromosome. *J Bacteriol* **169**, 5692-5699 (1987).
187. Keseler, I.M. et al. EcoCyc: A comprehensive view of *Escherichia coli* biology. *Nucleic Acids Res* **37**, D464-D470 (2009).
188. Bernhardt, T.G. & De Boer, P.A.J. Screening for synthetic lethal mutants in *Escherichia coli* and identification of EnvC (YibP) as a periplasmic septal ring factor with murein hydrolase activity. *Mol Microbiol* **52**, 1255-1269 (2004).

189. Jiang, M. et al. Identification of novel *Escherichia coli* ribosome-associated proteins using isobaric tags and multidimensional protein identification techniques. *J Bacteriol* **189**, 3434-3444 (2007).
190. Galperin, M.Y. & Koonin, E.V. 'Conserved hypothetical' proteins: prioritization of targets for experimental study. *Nucleic Acids Res* **32**, 5452-5463 (2004).
191. Walbot, V. & Coe, E.H. Nuclear gene iojap conditions a programmed change to ribosome-less plastids in *Zea mays*. *Proc Natl Acad Sci USA* **76**, 2760-2764 (1979).
192. Jiang, M. et al. The *Escherichia coli* GTPase CgtAE Is Involved in Late Steps of Large Ribosome Assembly. *J. Bacteriol.* **188**, 6757-6770 (2006).
193. Kaczanowska, M. & Ryden-Aulin, M. Ribosome Biogenesis and the Translation Process in *Escherichia coli*. *Microbiol. Mol. Biol. Rev.* **71**, 477-494 (2007).
194. Purta, E., Kaminska, K.H., Kasprzak, J.M., Bujnicki, J.M. & Douthwaite, S. YbeA is the m3Psi methyltransferase RlmH that targets nucleotide 1915 in 23S rRNA. *Rna* **14**, 2234-2244 (2008).
195. Ero, R., Leppik, M., Liiv, A. & Remme, J. Specificity and kinetics of 23S rRNA modification enzymes RlmH and RluD. *Rna* **16**, 2075-2084 (2010).
196. Ero, R., Peil, L., Liiv, A. & Remme, J. Identification of pseudouridine methyltransferase in *Escherichia coli*. *Rna* **14**, 2223-2233 (2008).
197. Ejby, M., Sørensen, M.A. & Pedersen, S. Pseudouridylation of helix 69 of 23S rRNA is necessary for an effective translation termination. *Proceedings of the National Academy of Sciences* **104**, 19410-19415 (2007).
198. Bass, S., Gu, Q. & Christen, A. Multicopy suppressors of *prc* mutant *Escherichia coli* include two HtrA (DegP) protease homologs (HhoAB), DksA, and a truncated RlpA. *J Bacteriol* **178**, 1154-1161 (1996).
199. Letunic, I. et al. SMART 5: domains in the context of genomes and networks. *Nucleic Acids Res* **34**, D257-D260.
200. Schultz, J., Milpetz, F., Bork, P. & Ponting, C.P. SMART, a simple modular architecture research tool: Identification of signaling domains. *Proceedings of the National Academy of Sciences* **95**, 5857-5864 (1998).
201. Arends, S.J.R. et al. Discovery and Characterization of Three New *Escherichia coli* Septal Ring Proteins That Contain a SPOR Domain: DamX, DedD, and RlpA. *J. Bacteriol.* **192**, 242-255 (2010).
202. Gerding, M.A., Ogata, Y., Pecora, N.D., Niki, H. & De Boer, P.A.J. The trans-envelope Tol–Pal complex is part of the cell division machinery and required for proper outer-membrane invagination during cell constriction in *E. coli*. *Mol Microbiol* **63**, 1008-1025 (2007).
203. Kanesaki, Y., Suzuki, I., Allakhverdiev, S.I., Mikami, K. & Murata, N. Salt stress and hyperosmotic stress regulate the expression of different sets of genes in *Synechocystis* sp. PCC 6803. *Biochem Biophys Res Commun* **290**, 339-348 (2002).
204. Spratt, B.G., Boyd, A. & Stoker, N. Defective and plaque-forming lambda transducing bacteriophage carrying penicillin-binding protein-cell shape genes: genetic and physical mapping and identification of gene products from the *lip-dacA-rodA-pbpA-leuS* region of the *Escherichia coli* chromosome. *J Bacteriol* **143**, 569-581 (1980).
205. Stoker, N.G., Broome-Smith, J.K., Edelman, A. & Spratt, B.G. Organization and subcloning of the *dacA-rodA-pbpA* cluster of cell shape genes in *Escherichia coli*. *J Bacteriol* **155**, 847-853 (1983).
206. Matsuhashi, M. et al. Isolation of a mutant of *Escherichia coli* lacking penicillin-sensitive D-alanine carboxypeptidase IA. *Proc Natl Acad Sci U S A* **75**, 2631-2635 (1978).
207. Nelson, D.E. & Young, K.D. Penicillin binding protein 5 affects cell diameter, contour, and morphology of *Escherichia coli*. *J Bacteriol* **182**, 1714-1721 (2000).

208. Spratt, B.G. Deletion of the penicillin-binding protein 5 gene of *Escherichia coli*. *J Bacteriol* **144**, 1190-1192 (1980).
209. Markiewicz, Z., Broome-Smith, J.K., Schwarz, U. & Spratt, B.G. Spherical *E. coli* due to elevated levels of D-alanine carboxypeptidase. *Nature* **297**, 702-704 (1982).
210. Dougherty, T.J., Kennedy, K., Kessler, R.E. & Pucci, M.J. Direct quantitation of the number of individual penicillin-binding proteins per cell in *Escherichia coli*. *J Bacteriol* **178**, 6110-6115 (1996).
211. Philippe, N., Pelosi, L., Lenski, R.E. & Schneider, D. Evolution of penicillin-binding protein 2 concentration and cell shape during a long-term experiment with *Escherichia coli*. *J Bacteriol* **191**, 909-921 (2009).
212. Gama-Castro, S. et al. RegulonDB (version 6.0): gene regulation model of *Escherichia coli* K-12 beyond transcription, active (experimental) annotated promoters and Textpresso navigation. *Nucleic Acids Res* **36**, D120-124 (2008).
213. Scheurwater, E.M. & Burrows, L.L. Maintaining network security: how macromolecular structures cross the peptidoglycan layer. *FEMS Microbiol Lett* **318**, 1-9 (2011).
214. Iwaya, M., Goldman, R., Tipper, D.J., Feingold, B. & Strominger, J.L. Morphology of an *Escherichia coli* mutant with a temperature-dependent round cell shape. *J. Bacteriol.* **136**, 1143-1158 (1978).
215. Biondi, E.G. et al. Extended phenotype of an *mreB*-like mutant in *Azospirillum brasilense*. *Microbiology* **150**, 2465-2474 (2004).
216. Raivio, T.L. MicroReview: Envelope stress responses and Gram-negative bacterial pathogenesis. *Mol Microbiol* **56**, 1119-1128 (2005).
217. Hizukuri, Y., Kojima, S., Yakushi, T., Kawagishi, I. & Homma, M. Systematic Cys mutagenesis of FlgI, the flagellar P-ring component of *Escherichia coli*. *Microbiology* **154**, 810-817 (2008).
218. Kubori, T., Shimamoto, N., Yamaguchi, S., Namba, K. & Aizawa, S. Morphological pathway of flagellar assembly in *Salmonella* typhimurium. *J Mol Biol* **226**, 433-446 (1992).
219. Caparros, M., Pisabarro, A.G. & de Pedro, M.A. Effect of D-amino acids on structure and synthesis of peptidoglycan in *Escherichia coli*. *J. Bacteriol.* **174**, 5549-5559 (1992).
220. Togashi, F., Yamaguchi, S., Kihara, M., Aizawa, S.I. & Macnab, R.M. An extreme clockwise switch bias mutation in *fliG* of *Salmonella* typhimurium and its suppression by slow-motile mutations in *motA* and *motB*. *J. Bacteriol.* **179**, 2994-3003 (1997).
221. Mauriello, E.M.F. et al. Bacterial motility complexes require the actin-like protein, MreB and the Ras homologue, MglA. *Embo J* **29**, 315-326 (2010).
222. Cowles, K.N. & Gitai, Z. Surface association and the MreB cytoskeleton regulate pilus production, localization and function in *Pseudomonas aeruginosa*. *Mol Microbiol* **76**, 1411-1426 (2010).
223. Lino, T. Assembly of *Salmonella* flagellin *in vitro* and *in vivo*. *Journal of Supramolecular Structure* **2**, 372-384 (1974).
224. Neidhart, F.C. et al. *Escherichia coli* and *Salmonella*: cellular and molecular biology, Vol. 1, Edn. 2. (American Society for Microbiology, 1996).
225. Stafford, G.P. & Hughes, C. *Salmonella* typhimurium *flhE*, a conserved flagellar regulon gene required for swarming. *Microbiology* **153**, 541-547 (2007).
226. Fujii, M., Shibata, S. & Aizawa, S.-I. Polar, Peritrichous, and Lateral Flagella Belong to Three Distinguishable Flagellar Families. *J Mol Biol* **379**, 273-283 (2008).
227. Chakravortty, D., Rohde, M., Jager, L., Deiwick, J. & Hensel, M. Formation of a novel surface structure encoded by *Salmonella* Pathogenicity Island 2. *Embo J* **24**, 2043-2052 (2005).
228. Nikolaus, T. et al. SseBCD proteins are secreted by the type III secretion system of *Salmonella* pathogenicity island 2 and function as a translocon. *J Bacteriol* **183**, 6036-6045 (2001).

229. Formstone, A. & Errington, J. A magnesium-dependent *mreB* null mutant: implications for the role of *mreB* in *Bacillus subtilis*. *Mol Microbiol* **55**, 1646-1657 (2005).
230. Errington, J. Dynamic proteins and a cytoskeleton in bacteria. *Nat Cell Biol* **5**, 175-178 (2003).
231. Mascarenhas, J., Weber, M.H.W. & Graumann, P.L. Specific polar localization of ribosomes in *Bacillus subtilis* depends on active transcription. *EMBO Rep* **2**, 685-689 (2001).
232. Hone, D.M., Harris, A.M., Chatfield, S., Dougan, G. & Levine, M.M. Construction of genetically defined double *aro* mutants of *Salmonella* typhi. *Vaccine* **9**, 810-816 (1991).
233. Chatfield, S.N. et al. Evaluation of *Salmonella* typhimurium strains harbouring defined mutations in *htrA* and *aroA* in the murine salmonellosis model. *Microb Pathog* **12**, 145-151 (1992).
234. Hoiseth, S.K. & Stocker, B.A. Aromatic-dependent *Salmonella* typhimurium are non-virulent and effective as live vaccines. *Nature* **291**, 238-239 (1981).
235. Murray, R.A. & Lee, C.A. Invasion Genes Are Not Required for *Salmonella enterica* Serovar Typhimurium To Breach the Intestinal Epithelium: Evidence That *Salmonella* Pathogenicity Island 1 Has Alternative Functions during Infection. *Infect. Immun.* **68**, 5050-5055 (2000).
236. Karlinsey, J.E. et al. Completion of the hook–basal body complex of the *Salmonella* typhimurium flagellum is coupled to FlgM secretion and *fliC* transcription. *Mol Microbiol* **37**, 1220-1231 (2000).
237. Brown, A. et al. An Attenuated aroA *Salmonella* typhimurium Vaccine Elicits Humoral and Cellular Immunity to Cloned β-Galactosidase in Mice. *The Journal of Infectious Diseases* **155**, 86-92 (1987).
238. Datsenko, K.A. & Wanner, B.L. One-step inactivation of chromosomal genes in *Escherichia coli* K-12 using PCR products. *Proc Natl Acad Sci U S A* **97**, 6640-6645 (2000).
239. Cherepanov, P.P. & Wackernagel, W. Gene disruption in *Escherichia coli*: TcR and KmR cassettes with the option of Flp-catalyzed excision of the antibiotic-resistance determinant. *Gene* **158**, 9-14 (1995).
240. Karavolos, M.H. et al. Adrenaline modulates the global transcriptional profile of *Salmonella* revealing a role in the antimicrobial peptide and oxidative stress resistance responses. *BMC Genomics* **9**, 458 (2008).
241. Sutcliffe, J.G. Complete Nucleotide Sequence of the *Escherichia coli* Plasmid pBR322. *Cold Spring Harb Symp Quant Biol* **43**, 77-90 (1979).
242. Winson, M.K. et al. Engineering the *luxCDABE* genes from *Photorhabdus luminescens* to provide a bioluminescent reporter for constitutive and promoter probe plasmids and mini-Tn*5* constructs. *FEMS Microbiol Lett* **163**, 193-202 (1998).
243. Goodier, R.I. & Ahmer, B.M.M. SirA Orthologs Affect both Motility and Virulence. *J. Bacteriol.* **183**, 2249-2258 (2001).
244. Freeman, J.A., Ohl, M.E. & Miller, S.I. The *Salmonella enterica* serovar typhimurium translocated effectors SseJ and SifB are targeted to the *Salmonella*-containing vacuole. *Infect Immun* **71**, 418-427 (2003).
245. Guzman, L.M., Belin, D., Carson, M.J. & Beckwith, J. Tight regulation, modulation, and high-level expression by vectors containing the arabinose PBAD promoter. *J. Bacteriol.* **177**, 4121-4130 (1995).
246. Yamamoto, N. et al. Update on the Keio collection of *Escherichia coli* single-gene deletion mutants. *Mol Syst Biol* **5** (2009).
247. Knobloch, J.K.M. et al. Establishment of an Arbitrary PCR for Rapid Identification of Tn*917* Insertion Sites in *Staphylococcus epidermidis*: Characterization of Biofilm-Negative and Nonmucoid Mutants. *Appl. Environ. Microbiol.* **69**, 5812-5818 (2003).

248. Horswill, A.R., Dudding, A.R. & Escalante-Semerena, J.C. Studies of Propionate Toxicity in *Salmonella enterica* Identify 2-Methylcitrate as a Potent Inhibitor of Cell Growth. *J. Biol. Chem.* **276**, 19094-19101 (2001).
249. O'Toole, G.A. & Kolter, R. Initiation of biofilm formation in *Pseudomonas fluorescens* WCS365 proceeds via multiple, convergent signalling pathways: a genetic analysis. *Mol Microbiol* **28**, 449-461 (1998).
250. Mastroeni, P. & Sheppard, M. *Salmonella* infections in the mouse model: host resistance factors and in vivo dynamics of bacterial spread and distribution in the tissues. *Microbes and Infection* **6**, 398-405 (2004).
251. Way, J.C., Davis, M.A., Morisato, D., Roberts, D.E. & Kleckner, N. New Tn*10* derivatives for transposon mutagenesis and for construction of *lacZ* operon fusions by transposition. *Gene* **32**, 369-379 (1984).
252. Rappleye, C.A. & Roth, J.R. Transposition without transposase: a spontaneous mutation in bacteria. *J. Bacteriol.* **179**, 2047-2052 (1997).
253. Kanehisa, M. et al. KEGG for linking genomes to life and the environment. *Nucleic Acids Res* **36**, D480-484 (2008).
254. Vezzi, A. et al. Life at depth: *Photobacterium profundum* genome sequence and expression analysis. *Science (New York, N.Y.)* **307**, 1459-1461 (2005).
255. Mendoza-Vargas, A. et al. Genome-Wide Identification of Transcription Start Sites, Promoters and Transcription Factor Binding Sites in *E. coli PLoS ONE* **4**, e7526 (2009).
256. Salgado, H. et al. RegulonDB (version 3.2): transcriptional regulation and operon organization in *Escherichia coli* K-12. *Nucleic Acids Res* **29**, 72-74 (2001).
257. Reese, M.G. Application of a time-delay neural network to promoter annotation in the *Drosophila melanogaster* genome. *Computers & Chemistry* **26**, 51-56 (2001).
258. Reese, M.G. BDGP: Neural Network Promoter Prediction. *http://www.fruitfly.org/seq_tools/promoter.html* (2008).
259. Solovyev, V. & Sagitov, V. SoftBerry - BPROM. *http://linux1.softberry.com/berry.phtml?topic=bprom&group=programs&subgroup=gfindb* (2007).
260. Hawley, D.K. & McClure, W.R. Compilation and analysis of *Escherichia coli* promoter DNA sequences. *Nucleic Acids Res* **11**, 2237-2255 (1983).
261. Meighen, E.A. Molecular biology of bacterial bioluminescence. *Microbiol. Mol. Biol. Rev.* **55**, 123-142 (1991).
262. Ermolaeva, M.D., Khalak, H.G., White, O., Smith, H.O. & Salzberg, S.L. Prediction of transcription terminators in bacterial genomes. *J Mol Biol* **301**, 27-33 (2000).
263. Kingsford, C.L., Ayanbule, K. & Salzberg, S.L. Rapid, accurate, computational discovery of Rho-independent transcription terminators illuminates their relationship to DNA uptake. *Genome Biol.* **8**, R22 (2007).
264. Kingsford, C.L. TranstermHP. *http://transterm.cbcb.umd.edu/query.php* (2006).
265. Pucci, M.J. & Dougherty, T.J. Direct Quantitation of the Numbers of Individual Penicillin-Binding Proteins per Cell in *Staphylococcus aureus*. *J. Bacteriol.* **184**, 588-591 (2002).
266. Santos, J.M., Lobo, M., Matos, A.P.A., De Pedro, M.A. & Arraiano, C.M. The gene *bolA* regulates *dacA* (PBP5), *dacC* (PBP6) and *ampC* (AmpC), promoting normal morphology in *Escherichia coli*. *Mol Microbiol* **45**, 1729-1740 (2002).
267. Begg, K.J. & Donachie, W.D. Cell shape and division in *Escherichia coli*: experiments with shape and division mutants. *J Bacteriol* **163**, 615-622 (1985).
268. Pas, E., Einav, M., Woldringh, C.L. & Zaritsky, A. Perpendicular planes of FtsZ arcs in spheroidal *Escherichia coli* cells. *Biochimie* **83**, 121-124 (2001).
269. Vats, P. & Rothfield, L. Duplication and segregation of the actin (MreB) cytoskeleton during the prokaryotic cell cycle. *Proceedings of the National Academy of Sciences* **104**, 17795-17800 (2007).

270. Grønlund, H. & Gerdes, K. Toxin-antitoxin systems homologous with *relBE* of *Escherichia coli* plasmid P307 are ubiquitous in prokaryotes. *J Mol Biol* **285**, 1401-1415 (1999).
271. Claros, M.G. & von Heijne, G. TopPred II: an improved software for membrane protein structure predictions. *Comput Appl Biosci* **10**, 685-686 (1994).
272. Finn, R.D. et al. The Pfam protein families database. *Nucleic Acids Res* **38**, D211-D222 (2010).
273. Lounatmaa, K., Makela, P.H. & Sarvas, M. Effect of polymyxin on the ultrastructure of the outer membrane of wild-type and polymyxin-resistant strain of *Salmonella*. *J. Bacteriol.* **127**, 1400-1407 (1976).
274. Rogers, H.J., Thurman, P.F. & Buxton, R.S. Magnesium and anion requirements of *rodB* mutants of *Bacillus subtilis*. *J Bacteriol.* **125**, 556-564 (1976).
275. Rogers, H.J. & Thurman, P.F. Temperature-sensitive nature of the *rodB* maturation in *Bacillus subtilis*. *J Bacteriol* **133**, 298-305 (1978).
276. Murray, T., Popham, D.L. & Setlow, P. *Bacillus subtilis* Cells Lacking Penicillin-Binding Protein 1 Require Increased Levels of Divalent Cations for Growth. *J. Bacteriol.* **180**, 4555-4563 (1998).
277. Joseleau-Petit, D., Thévenet, D. & D'Arl, R. ppGpp concentration, growth without PBP2 activity, and growth-rate control in *Escherichia coli*. *Mol Microbiol* **13**, 911-917 (1994).
278. Barbour, A.G., Mayer, L.W. & Spratt, B.G. Mecillinam Resistance in *Escherichia coli*: Dissociation of Growth Inhibition and Morphologic Change. *The Journal of Infectious Diseases* **143**, 114-121 (1981).
279. Spratt, B.G. The mechanism of action of mecillinam. *J Antimicrob Chemother* **3**, 13-19 (1977).
280. McDowell, T.D., Buchanan, C.E., Coyette, J., Swavely, T.S. & Shockman, G.D. Effects of mecillinam and cefoxitin on growth, macromolecular synthesis, and penicillin-binding proteins in a variety of streptococci. *Antimicrob. Agents Chemother.* **23**, 750-756 (1983).
281. Iwai, N., Nagai, K. & Wachi, M. Novel S-Benzylisothiourea Compound That Induces Spherical Cells in *Escherichia coli* Probably by Acting on a Rod-shape-determining Protein(s) Other Than Penicillin-binding Protein 2. *Bioscience, Biotechnology, and Biochemistry* **66**, 2658-2662 (2002).
282. Antón, D.N., Micheli, A.T.d. & Palermo, A.M. Isolation of round-cell mutants of *Salmonella* typhimurium. *Canadian Journal of Microbiology* **29**, 170-173 (1983).
283. Amaral, L. Effect of Subminimal Inhibitory Concentrations of Mecillinam on the Synthesis of DNA, RNA, and Protein of *Salmonella* typhimurium: A Proposed Mechanism of Action. *Review of Infectious Diseases* **1**, 813-820 (1979).
284. Bean, G.J. et al. A22 disrupts the bacterial actin cytoskeleton by directly binding and inducing a low-affinity state in MreB. *Biochemistry* **48**, 4852-4857 (2009).
285. Gitai, Z., Dye, N.A., Reisenauer, A., Wachi, M. & Shapiro, L. MreB Actin-Mediated Segregation of a Specific Region of a Bacterial Chromosome. *Cell* **120**, 329-341 (2005).
286. Takacs, C.N. et al. MreB Drives De Novo Rod Morphogenesis in *Caulobacter crescentus* via Remodeling of the Cell Wall. *J. Bacteriol.* **192**, 1671-1684 (2010).
287. Poehlsgaard, J. & Douthwaite, S. The bacterial ribosome as a target for antibiotics. *Nat Rev Micro* **3**, 870-881 (2005).
288. Hancock, R.E. Aminoglycoside uptake and mode of action-with special reference to streptomycin and gentamicin. II. Effects of aminoglycosides on cells. *The Journal of antimicrobial chemotherapy* **8**, 429-445 (1981).
289. Luzzatto, L., Apirion, D. & Schlessinger, D. Mechanism of Action of Streptomycin in *E. coli*: Interruption of the Ribosome Cycle at the Initiation of Protein Synthesis. *Proc Natl Acad Sci U S A* **60**, 873-880 (1968).

290. Sharma, D., Cukras, A.R., Rogers, E.J., Southworth, D.R. & Green, R. Mutational Analysis of S12 Protein and Implications for the Accuracy of Decoding by the Ribosome. *J Mol Biol* **374**, 1065-1076 (2007).
291. Gregory, S.T., Cate, J.H.D. & Dahlberg, A.E. Streptomycin-resistant and streptomycin-dependent mutants of the extreme thermophile *Thermus thermophilus*. *J Mol Biol* **309**, 333-338 (2001).
292. Licht, J., Gally, D., Henderson, T., Young, K. & Cooper, S. Effect of mecillinam on peptidoglycan synthesis during the division cycle of *Salmonella* typhimurium 2616. *Res Microbiol* **144**, 423-433.
293. Ruiz, N., Kahne, D. & Silhavy, T.J. Transport of lipopolysaccharide across the cell envelope: the long road of discovery. *Nat Rev Micro* **7**, 677-683 (2009).
294. Raetz, C.R.H. & Whitfield, C. Lipopolysaccharide Endotoxins. *Annual Review of Biochemistry* **71**, 635-700 (2002).
295. Rietschel, E.T. et al. Bacterial endotoxin: molecular relationships of structure to activity and function. *The FASEB Journal* **8**, 217-225 (1994).
296. Galloway, S.M. & Raetz, C.R. A mutant of *Escherichia coli* defective in the first step of endotoxin biosynthesis. *J Biol Chem* **265**, 6394-6402 (1990).
297. Onishi, H.R. et al. Antibacterial Agents That Inhibit Lipid A Biosynthesis. *Science* **274**, 980-982 (1996).
298. Miller, S.I., Ernst, R.K. & Bader, M.W. LPS, TLR4 and infectious disease diversity. *Nat Rev Micro* **3**, 36-46 (2005).
299. Heinrichs, D.E., Yethon, J.A. & Whitfield, C. Molecular basis for structural diversity in the core regions of the lipopolysaccharides of *Escherichia coli* and *Salmonella enterica*. *Mol Microbiol* **30**, 221-232 (1998).
300. Cardoso, P.G., Macedo, G.C., Azevedo, V. & Oliveira, S.C. *Brucella* spp noncanonical LPS: structure, biosynthesis, and interaction with host immune system. *Microb Cell Fact.* **5** (2006).
301. Nikaido, H. Molecular Basis of Bacterial Outer Membrane Permeability Revisited. *Microbiol. Mol. Biol. Rev.* **67**, 593-656 (2003).
302. Vaara, M. Antibiotic-supersusceptible mutants of *Escherichia coli* and *Salmonella* typhimurium. *Antimicrob. Agents Chemother.* **37**, 2255-2260 (1993).
303. Trent, M.S., Stead, C.M., Tran, A.X. & Hankins, J.V. Invited review: Diversity of endotoxin and its impact on pathogenesis. *Journal of Endotoxin Research* **12**, 205-223 (2006).
304. Hellman, J. et al. Outer Membrane Protein A, Peptidoglycan-Associated Lipoprotein, and Murein Lipoprotein Are Released by *Escherichia coli* Bacteria into Serum. *Infect. Immun.* **68**, 2566-2572 (2000).
305. Hellman, J., Tehan, M.M. & Warren, H.S. Murein Lipoprotein, Peptidoglycan-Associated Lipoprotein, and Outer Membrane Protein A Are Present in Purified Rough and Smooth Lipopolysaccharides. *The Journal of Infectious Diseases* **188**, 286-289 (2003).
306. Dartigalongue, C., Missiakas, D. & Raina, S. Characterization of the *Escherichia coli* σ^E Regulon. *J Biol Chem* **276**, 20866-20875 (2001).
307. MacRitchie, D.M., Buelow, D.R., Price, N.L. & Raivio, T.L. Two-component signaling and Gram negative envelope stress response systems in, Vol. 631. (ed. R. Utsumi) 80-110 (Springer New York, 2008).
308. Savage, P.B. Multidrug-resistant bacteria: overcoming antibiotic permeability barriers of gram-negative bacteria. *Ann Med.* **33**, 167-171 (2001).
309. Williams, K.J. & Piddock, L.J. Accumulation of rifampicin by *Escherichia coli* and *Staphylococcus aureus*. *J Antimicrob Chemother* **42**, 597-603 (1998).
310. Tenson, T., Lovmar, M. & Ehrenberg, M. The Mechanism of Action of Macrolides, Lincosamides and Streptogramin B Reveals the Nascent Peptide Exit Path in the Ribosome. *J Mol Biol* **330**, 1005-1014 (2003).

311. Gotoh, N., Tanaka, S. & Nishino, T. Supersusceptibility to hydrophobic antimicrobial agents and cell surface hydrophobicity in *Branhamella catarrhalis*. *FEMS Microbiol Lett* **50**, 211-213 (1989).
312. Solano, C. et al. Genetic analysis of *Salmonella* enteritidis biofilm formation: critical role of cellulose. *Mol Microbiol* **43**, 793-808 (2002).
313. Stevenson, G., Andrianopoulos, K., Hobbs, M. & Reeves, P.R. Organization of the *Escherichia coli* K-12 gene cluster responsible for production of the extracellular polysaccharide colanic acid. *J. Bacteriol.* **178**, 4885-4893 (1996).
314. Van Houdt, R. & Michiels, C.W. Role of bacterial cell surface structures in *Escherichia coli* biofilm formation. *Res Microbiol* **156**, 626-633.
315. Costa, C.S. & Antón, D.N. Role of the *ftsA1p* promoter in the resistance of mucoid mutants of *Salmonella enterica* to mecillinam: characterization of a new type of mucoid mutant. *FEMS Microbiol Lett* **200**, 201-205 (2001).
316. Gottesman, S., Trisler, P. & Torres-Cabassa, A. Regulation of capsular polysaccharide synthesis in *Escherichia coli* K-12: characterization of three regulatory genes. *J. Bacteriol.* **162**, 1111-1119 (1985).
317. Stevenson, G., Lan, R. & Reeves, P.R. The colanic acid gene cluster of *Salmonella enterica* has a complex history. *FEMS Microbiol Lett* **191**, 11-16 (2000).
318. Wang, Q., Zhao, Y., McClelland, M. & Harshey, R.M. The RcsCDB Signaling System and Swarming Motility in *Salmonella enterica* Serovar Typhimurium: Dual Regulation of Flagellar and SPI-2 Virulence Genes. *J. Bacteriol.* **189**, 8447-8457 (2007).
319. Römling, U., Sierralta, W.D., Eriksson, K. & Normark, S. Multicellular and aggregative behaviour of *Salmonella* typhimurium strains is controlled by mutations in the *agfD* promoter. *Mol Microbiol* **28**, 249-264 (1998).
320. Ferrières, L. & Clarke, D.J. The RcsC sensor kinase is required for normal biofilm formation in *Escherichia coli* K-12 and controls the expression of a regulon in response to growth on a solid surface. *Mol Microbiol* **50**, 1665-1682 (2003).
321. Gervais, F.G., Phoenix, P. & Drapeau, G.R. The *rcsB* gene, a positive regulator of colanic acid biosynthesis in *Escherichia coli*, is also an activator of *ftsZ* expression. *J Bacteriol* **174**, 3964-3971 (1992).
322. Carballès, F., Bertrand, C., Bouché, J.-P. & Cam, K. Regulation of *Escherichia coli* cell division genes *ftsA* and *ftsZ* by the two-component system *rcsC–rcsB*. *Mol Microbiol* **34**, 442-450 (1999).
323. Tenorio, E. et al. Systematic characterization of *Escherichia coli* genes/ORFs affecting biofilm formation. *FEMS Microbiol Lett* **225**, 107-114 (2003).
324. Navarro, F., Robin, A., D'Ari, R. & Joseleau-Petit, D. Analysis of the effect of ppGpp on the *ftsQAZ* operon in *Escherichia coli*. *Mol Microbiol* **29**, 815-823 (1998).
325. García-Calderón, C.B., García-Quintanilla, M., Casadesús, J. & Ramos-Morales, F. Virulence attenuation in *Salmonella enterica rcsC* mutants with constitutive activation of the Rcs system. *Microbiology* **151**, 579-588 (2005).
326. Römling, U. Characterization of the rdar morphotype, a multicellular behaviour in *Enterobacteriaceae*. *Cellular and Molecular Life Sciences* **62**, 1234-1246 (2005).
327. Fields, P.I., Swanson, R.V., Haidaris, C.G. & Heffron, F. Mutants of *Salmonella* typhimurium that cannot survive within the macrophage are avirulent. *Proc Natl Acad Sci U S A* **83**, 5189-5193 (1986).
328. Halsey, T.A., Vazquez-Torres, A., Gravdahl, D.J., Fang, F.C. & Libby, S.J. The Ferritin-Like Dps Protein Is Required for *Salmonella enterica* Serovar Typhimurium Oxidative Stress Resistance and Virulence. *Infect. Immun.* **72**, 1155-1158 (2004).
329. Skovierova, H. et al. Identification of the σ^E regulon of *Salmonella enterica* serovar Typhimurium. *Microbiology* **152**, 1347-1359 (2006).
330. Carballido-López, R. & Errington, J. The Bacterial Cytoskeleton: In Vivo Dynamics of the Actin-like Protein Mbl of *Bacillus subtilis*. *Developmental Cell* **4**, 19-28 (2003).

331. Vinella, D., Joseleau-Petit, D., Thevenet, D., Bouloc, P. & D'Ari, R. Penicillin-binding protein 2 inactivation in *Escherichia coli* results in cell division inhibition, which is relieved by FtsZ overexpression. *J Bacteriol* **175**, 6704-6710 (1993).
332. Young, K.D. Why spherical *Escherichia coli* dies: the inside story. *J Bacteriol* **190**, 1497-1498 (2008).
333. Weart, R.B. et al. A Metabolic Sensor Governing Cell Size in Bacteria. *Cell* **130**, 335-347 (2007).
334. Schaechter, M., MaalØe, O. & Kjeldgaard, N.O. Dependency on Medium and Temperature of Cell Size and Chemical Composition during Balanced Growth of *Salmonella* typhimurium. *Journal of General Microbiology* **19**, 592-606 (1958).
335. Wang, J.D. & Levin, P.A. Metabolism, cell growth and the bacterial cell cycle. *Nat Rev Micro* **7**, 822-827 (2009).
336. Weart, R.B. & Levin, P.A. Growth Rate-Dependent Regulation of Medial FtsZ Ring Formation. *J. Bacteriol.* **185**, 2826-2834 (2003).
337. Potrykus, K., Murphy, H., Philippe, N. & Cashel, M. ppGpp is the major source of growth rate control in *E. coli*. *Environmental Microbiology* **13**, 563-575 (2011).
338. Powell, B.S. & Court, D.L. Control of *ftsZ* Expression, Cell Division, and Glutamine Metabolism in Luria-Bertani Medium by the Alarmone ppGpp in *Escherichia coli*. *J. Bacteriol.* **180**, 1053-1062 (1998).
339. Tozawa, Y. et al. Calcium-activated (p)ppGpp Synthetase in Chloroplasts of Land Plants. *J Biol Chem* **282**, 35536-35545 (2007).
340. Sajish, M., Tiwari, D., Rananaware, D., Nandicoori, V.K. & Prakash, B. A Charge Reversal Differentiates (p)ppGpp Synthesis by Monofunctional and Bifunctional Rel Proteins. *J Biol Chem* **282**, 34977-34983 (2007).
341. Richter, D., Fehr, S. & Harder, R. The Guanosine 3′,5′-Bis(diphosphate) (ppGpp) Cycle. *Eur J Biochem* **99**, 57-64 (1979).
342. Rivas, G. et al. Magnesium-induced Linear Self-association of the FtsZ Bacterial Cell Division Protein Monomer. *J Biol Chem* **275**, 11740-11749 (2000).
343. Matsuzawa, H., Hayakawa, K., Sato, T. & Imahori, K. Characterization and genetic analysis of a mutant of *Escherichia coli* K-12 with rounded morphology. *J Bacteriol* **115**, 436-442 (1973).
344. Batchelor, E., Walthers, D., Kenney, L.J. & Goulian, M. The *Escherichia coli* CpxA-CpxR Envelope Stress Response System Regulates Expression of the Porins OmpF and OmpC. *J. Bacteriol.* **187**, 5723-5731 (2005).
345. Miticka, H. et al. Transcriptional analysis of the *rpoE* gene encoding extracytoplasmic stress response sigma factor σ^E in *Salmonella enterica* serovar Typhimurium. *FEMS Microbiol Lett* **226**, 307-314 (2003).
346. Kihara, M., Minamino, T., Yamaguchi, S. & Macnab, R.M. Intergenic Suppression between the Flagellar MS Ring Protein FliF of *Salmonella* and FlhA, a Membrane Component of Its Export Apparatus. *J. Bacteriol.* **183**, 1655-1662 (2001).
347. Katayama, E., Shiraishi, T., Oosawa, K., Baba, N. & Aizawa, S.-I. Geometry of the Flagellar Motor in the Cytoplasmic Membrane of*Salmonella* typhimuriumas Determined by Stereo-photogrammetry of Quick-freeze Deep-etch Replica Images. *J Mol Biol* **255**, 458-475 (1996).
348. Fraser, G.M. & Hughes, C. Swarming motility. *Curr Opin Microbiol* **2**, 630-635 (1999).
349. Pruss, B.M. & Matsumura, P. A regulator of the flagellar regulon of *Escherichia coli*, *flhD*, also affects cell division. *J. Bacteriol.* **178**, 668-674 (1996).
350. Pruss, B.M., Markovic, D. & Matsumura, P. The *Escherichia coli* flagellar transcriptional activator *flhD* regulates cell division through induction of the acid response gene *cadA*. *J. Bacteriol.* **179**, 3818-3821 (1997).
351. Schlumberger, M.C. & Hardt, W.-D. *Salmonella* type III secretion effectors: pulling the host cell's strings. *Curr Opin Microbiol* **9**, 46-54 (2006).

352. Ellermeier, J.R. & Slauch, J.M. Fur Regulates Expression of the *Salmonella* Pathogenicity Island 1 Type III Secretion System through HilD. *J Bacteriol* **190**, 476-486 (2008).
353. Lucas, R.L. & Lee, C.A. Roles of *hilC* and *hilD* in regulation of *hilA* expression in *Salmonella enterica* serovar Typhimurium. *J Bacteriol* **183**, 2733-2745 (2001).
354. Bronstein, P.A., Miao, E.A. & Miller, S.I. InvB Is a Type III Secretion Chaperone Specific for SspA. *J. Bacteriol.* **182**, 6638-6644 (2000).
355. García-Del Portillo, F., Pucciarelli, M.G. & Casadesús, J. DNA adenine methylase mutants of *Salmonella* typhimurium show defects in protein secretion, cell invasion, and M cell cytotoxicity. *Proceedings of the National Academy of Sciences* **96**, 11578-11583 (1999).
356. "Science Gateway: Protein Molecular Weight Calculator." from http://www.sciencegateway.org/tools/proteinmw.htm.
357. Ehrbar, K., Mirold, S., Friebel, A., Stender, S. & Hardt, W.-D. Characterization of effector proteins translocated via the SPI1 type III secretion system of *Salmonella* typhimurium. *International Journal of Medical Microbiology* **291**, 479-485 (2001).
358. Komoriya, K. et al. Flagellar proteins and type III-exported virulence factors are the predominant proteins secreted into the culture media of *Salmonella* typhimurium. *Mol Microbiol* **34**, 767-779 (1999).
359. Silphaduang, U., Mascarenhas, M., Karmali, M. & Coombes, B.K. Repression of Intracellular Virulence Factors in *Salmonella* by the Hha and YdgT Nucleoid-Associated Proteins. *J. Bacteriol.* **189**, 3669-3673 (2007).
360. Hindle, Z. et al. Characterization of *Salmonella enterica* Derivatives Harboring Defined *aroC* and *Salmonella* Pathogenicity Island 2 Type III Secretion System (*ssaV*) Mutations by Immunization of Healthy Volunteers. *Infect. Immun.* **70**, 3457-3467 (2002).
361. Cirillo, D.M., Valdivia, R.H., Monack, D.M. & Falkow, S. Macrophage-dependent induction of the *Salmonella* pathogenicity island 2 type III secretion system and its role in intracellular survival. *Mol Microbiol* **30**, 175-188 (1998).
362. Ibarra, J.A. et al. Induction of *Salmonella* pathogenicity island 1 under different growth conditions can affect *Salmonella*–host cell interactions in vitro. *Microbiology* **156**, 1120-1133 (2010).
363. Spratt, B.G. *Escherichia coli* resistance to [beta]-lactam antibiotics through a decrease in the affinity of a target for lethality. *Nature* **274**, 713-715 (1978).
364. Liu, X. & Matsumura, P. The FlhD/FlhC complex, a transcriptional activator of the *Escherichia coli* flagellar class II operons. *J. Bacteriol.* **176**, 7345-7351 (1994).
365. Heran Darwin, K. & Miller, V.L. InvF Is Required for Expression of Genes Encoding Proteins Secreted by the SPI1 Type III Secretion Apparatus in *Salmonella* typhimurium. *J. Bacteriol.* **181**, 4949-4954 (1999).
366. Prüss, B.M. FlhD, a transcriptional regulator in bacteria. *Recent research developments in microbiology* **4**, 31-42 (2000).
367. Coombes, B.K. & Finlay, B.B. Insertion of the bacterial type III translocon: not your average needle stick. *Trends in Microbiology* **13**, 92-95 (2005).
368. Kharraz, L. Function of the Bacterial Cytoskeleton in the Biology and Pathogenicity of *Salmonella.* Institute for Cell and Molecular Biosciences, PhD thesis (Newcastle University, Newcastle; 2008).
369. Baxter, M.A. & Jones, B.D. The *fimYZ* Genes Regulate *Salmonella enterica* Serovar Typhimurium Invasion in Addition to Type 1 Fimbrial Expression and Bacterial Motility. *Infect. Immun.* **73**, 1377-1385 (2005).
370. Kage, H., Takaya, A., Ohya, M. & Yamamoto, T. Coordinated Regulation of Expression of *Salmonella* Pathogenicity Island 1 and Flagellar Type III Secretion Systems by ATP-Dependent ClpXP Protease. *J. Bacteriol.* **190**, 2470-2478 (2008).
371. Iyoda, S., Kamidoi, T., Hirose, K., Kutsukake, K. & Watanabe, H. A flagellar gene *fliZ* regulates the expression of invasion genes and virulence phenotype in *Salmonella enterica* serovar Typhimurium. *Microb Pathog* **30**, 81-90 (2001).

372. Grant, W.D., Sutherland, I.W. & Wilkinson, J.F. Exopolysaccharide Colanic Acid and Its Occurrence in the *Enterobacteriaceae*. *J. Bacteriol.* **100**, 1187-1193 (1969).
373. Wu, J. & Xie, J. Magic spot: (p) ppGpp. *Journal of Cellular Physiology* **220**, 297-302 (2009).
374. Kimbrough, T.G. & Miller, S.I. Contribution of *Salmonella* typhimurium type III secretion components to needle complex formation. *Proc Natl Acad Sci USA* **97**, 11008-11013 (2000).
375. Wood, M.W. et al. Identification of a pathogenicity island required for *Salmonella* enteropathogenicity. *Mol Microbiol* **29**, 883-891 (1998).
376. Gerlach, R.G. et al. *Salmonella* Pathogenicity Island 4 encodes a giant non-fimbrial adhesin and the cognate type 1 secretion system. *Cell Microbiol* **9**, 1834-1850 (2007).
377. Ahmer, B.M.M., Van Reeuwijk, J., Watson, P.R., Wallis, T.S. & Heffron, F. *Salmonella* SirA is a global regulator of genes mediating enteropathogenesis. *Mol Microbiol* **31**, 971-982 (1999).
378. Potter, L.C. & Cole, J.A. Essential roles for the products of the *napABCD* genes, but not *napFGH*, in periplasmic nitrate reduction by *Escherichia coli* K-12. *Biochem. J.* **344**, 69-76 (1999).
379. Encheva, V., Shah, H.N. & Gharbia, S.E. Proteomic analysis of the adaptive response of *Salmonella enterica* serovar Typhimurium to growth under anaerobic conditions. *Microbiology* **155**, 2429-2441 (2009).
380. Berks, B.C. et al. Sequence analysis of subunits of the membrane-bound nitrate reductase from a denitrifying bacterium: the integral membrane subunit provides a prototype for the dihaem electron-carrying arm of a redox loop. *Mol Microbiol* **15**, 319-331 (1995).
381. Hussain, H., Grove, J., Griffiths, L., Busby, S. & Cole, J. A seven-gene operon essential for formate-dependent nitrite reduction to ammonia by enteric bacteria. *Mol Microbiol* **12**, 153-163 (1994).
382. Watson, N., Dunyak, D.S., Rosey, E.L., Slonczewski, J.L. & Olson, E.R. Identification of elements involved in transcriptional regulation of the *Escherichia coli cad* operon by external pH. *J. Bacteriol.* **174**, 530-540 (1992).
383. Greenacre, E.J., Lucchini, S., Hinton, J.C.D. & Brocklehurst, T.F. The Lactic Acid-Induced Acid Tolerance Response in *Salmonella enterica* Serovar Typhimurium Induces Sensitivity to Hydrogen Peroxide. *Appl. Environ. Microbiol.* **72**, 5623-5625 (2006).
384. Evans, M. et al. Analysis of the ArcA regulon in anaerobically grown *Salmonella enterica* sv. Typhimurium. *BMC Microbiology* **11**, 58 (2011).
385. Gunsalus, R.P. & Park, S.J. Aerobic-anaerobic gene regulation in *Escherichia coli*: control by the ArcAB and Fnr regulons. *Res Microbiol* **145**, 437-450 (1994).
386. Fink, R.C. et al. FNR Is a Global Regulator of Virulence and Anaerobic Metabolism in *Salmonella enterica* Serovar Typhimurium (ATCC 14028s). *J. Bacteriol.* **189**, 2262-2273 (2007).
387. Teixidó, L. et al. Control by Fur of the nitrate respiration regulators NarP and NarL in *Salmonella enterica*. *Int Microbiol.* **13**, 33-39 (2010).
388. Purcell, B.K., Pruckler, J. & Clegg, S. Nucleotide sequences of the genes encoding type 1 fimbrial subunits of *Klebsiella pneumoniae* and *Salmonella* typhimurium. *J. Bacteriol.* **169**, 5831-5834 (1987).
389. Althouse, C., Patterson, S., Fedorka-Cray, P. & Isaacson, R.E. Type 1 Fimbriae of *Salmonella enterica* Serovar Typhimurium Bind to Enterocytes and Contribute to Colonization of Swine In Vivo. *Infect. Immun.* **71**, 6446-6452 (2003).
390. Cohen, H.J., Mechanda, S.M. & Lin, W. PCR amplification of the *fimA* gene sequence of *Salmonella* typhimurium, a specific method for detection of *Salmonella* spp. *Appl. Environ. Microbiol.* **62**, 4303-4308 (1996).

391. Baumler, A.J., Tsolis, R.M. & Heffron, F. Contribution of fimbrial operons to attachment to and invasion of epithelial cell lines by *Salmonella* typhimurium. *Infect. Immun.* **64**, 1862-1865 (1996).
392. Swenson, D.L. & Clegg, S. Identification of ancillary *fim* genes affecting *fimA* expression in *Salmonella* typhimurium. *J. Bacteriol.* **174**, 7697-7704 (1992).
393. Marc, D. & Dho-Moulin, M. Analysis of the *fim* cluster of an avian O2 strain of *Escherichia coli*: serogroup-specific sites within *fimA* and nucleotide sequence of *fimI*. *J Med Microbiol* **44**, 444-452 (1996).
394. Reynolds, C.M. et al. An Outer Membrane Enzyme Encoded by *Salmonella* typhimurium *lpxR* That Removes the 3′-Acyloxyacyl Moiety of Lipid A. *J Biol Chem* **281**, 21974-21987 (2006).
395. Manabe, T. & Kawasaki, K. Extracellular Loops of Lipid A 3-O-Deacylase PagL Are Involved in Recognition of Aminoarabinose-Based Membrane Modifications in *Salmonella enterica* Serovar Typhimurium. *J. Bacteriol.* **190**, 5597-5606 (2008).
396. Raivio, T.L., Popkin, D.L. & Silhavy, T.J. The Cpx Envelope Stress Response Is Controlled by Amplification and Feedback Inhibition. *J. Bacteriol.* **181**, 5263-5272 (1999).
397. Monsieurs, P. et al. Comparison of the PhoPQ Regulon in *Escherichia coli* and *Salmonella* typhimurium. *Journal of Molecular Evolution* **60**, 462-474 (2005).
398. Lewis, C. et al. *Salmonella enterica* Serovar Typhimurium HtrA: regulation of expression and role of the chaperone and protease activities during infection. *Microbiology* **155**, 873-881 (2009).
399. Sailer, F.C., Meberg, B.M. & Young, K.D. Beta-Lactam induction of colanic acid gene expression in *Escherichia coli*. *FEMS Microbiol Lett.* **226**, 245-249 (2003).
400. Majdalani, N. & Gottesman, S. THE RCS PHOSPHORELAY: A Complex Signal Transduction System*. *Annual Review of Microbiology* **59**, 379-405 (2005).
401. Wood, T.K. Insights on *Escherichia coli* biofilm formation and inhibition from whole-transcriptome profiling. *Environmental Microbiology* **11**, 1-15 (2009).
402. Pruss, B.M., Besemann, C., Denton, A. & Wolfe, A.J. A Complex Transcription Network Controls the Early Stages of Biofilm Development by *Escherichia coli*. *J. Bacteriol.* **188**, 3731-3739 (2006).
403. Simm, R., Morr, M., Kader, A., Nimtz, M. & Römling, U. GGDEF and EAL domains inversely regulate cyclic di-GMP levels and transition from sessility to motility. *Mol Microbiol* **53**, 1123-1134 (2004).
404. Cano, D.A., Domínguez-Bernal, G., Tierrez, A., Portillo, F.G.-d. & Casadesús, J. Regulation of Capsule Synthesis and Cell Motility in *Salmonella enterica* by the Essential Gene *igaA*. *Genetics* **162**, 1513-1523 (2002).
405. Stout, V. Identification of the promoter region for the colanic acid polysaccharide biosynthetic genes in *Escherichia coli* K-12. *J. Bacteriol.* **178**, 4273-4280 (1996).
406. Lacour, S. & Landini, P. σ^S-Dependent Gene Expression at the Onset of Stationary Phase in *Escherichia coli*: Function of σ^S-Dependent Genes and Identification of Their Promoter Sequences. *J. Bacteriol.* **186**, 7186-7195 (2004).
407. Zhou, D., Hardt, W.-D. & Galan, J.E. *Salmonella* typhimurium Encodes a Putative Iron Transport System within the Centisome 63 Pathogenicity Island. *Infect. Immun.* **67**, 1974-1981 (1999).
408. Boyer, E., Bergevin, I., Malo, D., Gros, P. & Cellier, M.F.M. Acquisition of Mn(II) in Addition to Fe(II) Is Required for Full Virulence of *Salmonella enterica* Serovar Typhimurium. *Infect. Immun.* **70**, 6032-6042 (2002).
409. Kehres, D.G., Janakiraman, A., Slauch, J.M. & Maguire, M.E. SitABCD Is the Alkaline Mn^{2+} Transporter of *Salmonella enterica* Serovar Typhimurium. *J. Bacteriol.* **184**, 3159-3166 (2002).
410. Janakiraman, A. & Slauch, J.M. The putative iron transport system SitABCD encoded on SPI1 is required for full virulence of *Salmonella* typhimurium. *Mol Microbiol* **35**, 1146-1155 (2000).

411. Ikeda, J.S., Janakiraman, A., Kehres, D.G., Maguire, M.E. & Slauch, J.M. Transcriptional Regulation of *sitABCD* of *Salmonella enterica* Serovar Typhimurium by MntR and Fur. *J. Bacteriol.* **187**, 912-922 (2005).
412. Hu, W.S., Lin, J.-F., Lin, Y.-H. & Chang, H.-Y. Outer Membrane Protein STM3031 (Ail/OmpX-Like Protein) Plays a Key Role in the Ceftriaxone Resistance of *Salmonella enterica* Serovar Typhimurium. *Antimicrob. Agents Chemother.* **53**, 3248-3255 (2009).
413. Hu, W.S., Li, P.-C. & Cheng, C.-Y. Correlation between Ceftriaxone Resistance of *Salmonella enterica* Serovar Typhimurium and Expression of Outer Membrane Proteins OmpW and Ail/OmpX-Like Protein, Which Are Regulated by BaeR of a Two-Component System. *Antimicrob. Agents Chemother.* **49**, 3955-3958 (2005).
414. Felek, S. & Krukonis, E.S. The *Yersinia pestis* Ail Protein Mediates Binding and Yop Delivery to Host Cells Required for Plague Virulence. *Infect. Immun.* **77**, 825-836 (2009).
415. Kolodziejek, A.M. et al. Outer Membrane Protein X (Ail) Contributes to *Yersinia pestis* Virulence in Pneumonic Plague and Its Activity Is Dependent on the Lipopolysaccharide Core Length. *Infect. Immun.* **78**, 5233-5243 (2010).
416. Hu, W.S., Lin, Y.-H. & Shih, C.-C. A proteomic approach to study *Salmonella enterica* serovar Typhimurium putative transporter YjeH associated with ceftriaxone resistance. *Biochemical and Biophysical Research Communications* **361**, 694-699 (2007).
417. Fontana, R., Aldegheri, M., Ligozzi, M., Lo Cascio, G. & Cornaglia, G. Interaction of ceftriaxone with penicillin-binding proteins of *Escherichia coli* in the presence of human serum albumin. *J Antimicrob Chemother* **42**, 95-98 (1998).
418. Moncrief, M.B.C. & Maguire, M.E. Magnesium and the Role of *mgtC* in Growth of *Salmonella* typhimurium. *Infect. Immun.* **66**, 3802-3809 (1998).
419. Blanc-Potard, A.-B., Solomon, F., Kayser, J. & Groisman, E.A. The SPI-3 Pathogenicity Island of *Salmonella enterica*. *J. Bacteriol.* **181**, 998-1004 (1999).
420. Morgan, E. et al. Identification of host-specific colonization factors of *Salmonella enterica* serovar Typhimurium. *Mol Microbiol* **54**, 994-1010 (2004).
421. Blondel, C., Jimenez, J., Contreras, I. & Santiviago, C. Comparative genomic analysis uncovers 3 novel loci encoding type six secretion systems differentially distributed in *Salmonella* serotypes. *BMC Genomics* **10**, 354 (2009).
422. Klumpp, J. & Fuchs, T.M. Identification of novel genes in genomic islands that contribute to *Salmonella* typhimurium replication in macrophages. *Microbiology* **153**, 1207-1220 (2007).
423. Lambert, M. & Smith, S. The PagN protein of *Salmonella enterica* serovar Typhimurium is an adhesin and invasin. *BMC Microbiology* **8**, 142 (2008).
424. Folkesson, A. et al. Multiple insertions of fimbrial operons correlate with the evolution of *Salmonella* serovars responsible for human disease. *Mol Microbiol* **33**, 612-622 (1999).
425. Lambert, M.A. & Smith, S.G.J. The PagN protein mediates invasion via interaction with proteoglycan. *FEMS Microbiol Lett* **297**, 209-216 (2009).
426. Suzuki, T., Saga, S. & Sasakawa, C. Functional Analysis of *Shigella* VirG Domains Essential for Interaction with Vinculin and Actin-based Motility. *J Biol Chem* **271**, 21878-21885 (1996).
427. Phadtare, S. & Inouye, M. Role of CspC and CspE in Regulation of Expression of RpoS and UspA, the Stress Response Proteins in *Escherichia coli*. *J. Bacteriol.* **183**, 1205-1214 (2001).
428. Rowley, G., Spector, M., Kormanec, J. & Roberts, M. Pushing the envelope: extracytoplasmic stress responses in bacterial pathogens. *Nat Rev Micro* **4**, 383-394 (2006).
429. Humphreys, S. et al. Role of the Two-Component Regulator CpxAR in the Virulence of *Salmonella enterica* Serotype Typhimurium. *Infect. Immun.* **72**, 4654-4661 (2004).

430. Eriksson, S., Lucchini, S., Thompson, A., Rhen, M. & Hinton, J.C.D. Unravelling the biology of macrophage infection by gene expression profiling of intracellular *Salmonella enterica*. *Mol Microbiol* **47**, 103-118 (2003).
431. Hébrard, M., Kröger, C., Sivasankaran, S.K., Händler, K. & Hinton, J.C.D. The challenge of relating gene expression to the virulence of *Salmonella enterica* serovar Typhimurium. *Current Opinion in Biotechnology* **22**, 200-210 (2011).
432. Contreras, I., Toro, C.S., Troncoso, G. & Mora, G.C. *Salmonella* typhi mutants defective in anaerobic respiration are impaired in their ability to replicate within epithelial cells. *Microbiology* **143**, 2665-2672 (1997).
433. Paiva, J.B. et al. The contribution of genes required for anaerobic respiration to the virulence of *Salmonella enterica* serovar Gallinarum for chickens. *Brazilian Journal of Microbiology* **40**, 994-1001 (2009).
434. Löber, S., Jäckel, D., Kaiser, N. & Hensel, M. Regulation of *Salmonella* pathogenicity island 2 genes by independent environmental signals. *International Journal of Medical Microbiology* **296**, 435-447 (2006).
435. Miller, S.I., Kukral, A.M. & Mekalanos, J.J. A two-component regulatory system (*phoP phoQ*) controls *Salmonella* typhimurium virulence. *Proceedings of the National Academy of Sciences* **86**, 5054-5058 (1989).
436. Gal-Mor, O., Elhadad, D., Deng, W., Rahav, G. & Finlay, B.B. The *Salmonella enterica* PhoP Directly Activates the Horizontally Acquired SPI-2 Gene *sseL* and Is Functionally Different from a *S. bongori* Ortholog. *PLoS ONE* **6**, e20024 (2011).
437. Lehnen, D. et al. LrhA as a new transcriptional key regulator of flagella, motility and chemotaxis genes in *Escherichia coli*. *Mol Microbiol* **45**, 521-532 (2002).
438. Peterson, C.N., Carabetta, V.J., Chowdhury, T. & Silhavy, T.J. LrhA Regulates *rpoS* Translation in Response to the Rcs Phosphorelay System in *Escherichia coli*. *J. Bacteriol.* **188**, 3175-3181 (2006).
439. Zahrt, T.C., Mora, G.C. & Maloy, S. Inactivation of mismatch repair overcomes the barrier to transduction between *Salmonella* typhimurium and *Salmonella* typhi. *J. Bacteriol.* **176**, 1527-1529 (1994).
440. Huang, W., McKevitt, M. & Palzkill, T. Use of the arabinose P_{BAD} promoter for tightly regulated display of proteins on bacteriophage. *Gene* **251**, 187-197 (2000).
441. Kutsukake, K. & Iino, T. Role of the FliA-FlgM regulatory system on the transcriptional control of the flagellar regulon and flagellar formation in *Salmonella* typhimurium. *J. Bacteriol.* **176**, 3598-3605 (1994).
442. Bertin, P. et al. The H-NS protein is involved in the biogenesis of flagella in *Escherichia coli*. *J. Bacteriol.* **176**, 5537-5540 (1994).
443. Soutourina, O. et al. Multiple Control of Flagellum Biosynthesis in *Escherichia coli*: Role of H-NS Protein and the Cyclic AMP-Catabolite Activator Protein Complex in Transcription of the *flhDC* Master Operon. *J. Bacteriol.* **181**, 7500-7508 (1999).
444. Partridge, J.D., Bodenmiller, D.M., Humphrys, M.S. & Spiro, S. NsrR targets in the *Escherichia coli* genome: new insights into DNA sequence requirements for binding and a role for NsrR in the regulation of motility. *Mol Microbiol* **73**, 680-694 (2009).
445. Bender, J. & Kleckner, N. Tn*10* insertion specificity is strongly dependent upon sequences immediately adjacent to the target-site consensus sequence. *Proceedings of the National Academy of Sciences* **89**, 7996-8000 (1992).
446. Halling, S.M. & Kleckner, N. A symmetrical six-base-pair target site sequence determines Tn*10* insertion specificity. *Cell* **28**, 155-163 (1982).
447. Lee, S.Y., Butler, D. & Kleckner, N. Efficient Tn*10* transposition into a DNA insertion hot spot in vivo requires the 5-methyl groups of symmetrically disposed thymines within the hot-spot consensus sequence. *Proceedings of the National Academy of Sciences* **84**, 7876-7880 (1987).
448. Gibson, K.E. & Silhavy, T.J. The LysR Homolog LrhA Promotes RpoS Degradation by Modulating Activity of the Response Regulator SprE. *J. Bacteriol.* **181**, 563-571 (1999).

449. Sabbagh, S.C., Forest, C.G., Lepage, C., Leclerc, J.-M. & Daigle, F. So similar, yet so different: uncovering distinctive features in the genomes of *Salmonella enterica* serovars Typhimurium and Typhi. *FEMS Microbiol Lett* **305**, 1-13 (2010).
450. Lejona, S., Aguirre, A., Cabeza, M.L., Vescovi, E.G. & Soncini, F.C. Molecular Characterization of the Mg^{2+}-Responsive PhoP-PhoQ Regulon in *Salmonella enterica*. *J. Bacteriol.* **185**, 6287-6294 (2003).
451. Hengge, R. Principles of c-di-GMP signalling in bacteria. *Nat Rev Micro* **7**, 263-273 (2009).
452. Römling, U., Gomelsky, M. & Galperin, M.Y. C-di-GMP: the dawning of a novel bacterial signalling system. *Mol Microbiol* **57**, 629-639 (2005).
453. Cotter, P.A. & Stibitz, S. c-di-GMP-mediated regulation of virulence and biofilm formation. *Curr Opin Microbiol* **10**, 17-23 (2007).
454. Kulshina, N., Baird, N.J. & Ferre-D'Amare, A.R. Recognition of the bacterial second messenger cyclic diguanylate by its cognate riboswitch. *Nat Struct Mol Biol* **16**, 1212-1217 (2009).
455. Benach, J. et al. The structural basis of cyclic diguanylate signal transduction by PilZ domains. *Embo J* **26**, 5153-5166 (2007).
456. Ryjenkov, D.A., Simm, R., Römling, U. & Gomelsky, M. The PilZ Domain Is a Receptor for the Second Messenger c-di-GMP. *J Biol Chem* **281**, 30310-30314 (2006).
457. Simm, R., Morr, M., Remminghorst, U., Andersson, M. & Römling, U. Quantitative determination of cyclic diguanosine monophosphate concentrations in nucleotide extracts of bacteria by matrix-assisted laser desorption/ionization–time-of-flight mass spectrometry. *Analytical Biochemistry* **386**, 53-58 (2009).
458. Galperin, M. A census of membrane-bound and intracellular signal transduction proteins in bacteria: Bacterial IQ, extroverts and introverts. *BMC Microbiology* **5**, 35 (2005).
459. Simm, R., Lusch, A., Kader, A., Andersson, M. & Romling, U. Role of EAL-Containing Proteins in Multicellular Behavior of *Salmonella enterica* Serovar Typhimurium. *J. Bacteriol.* **189**, 3613-3623 (2007).
460. Kader, A., Simm, R., Gerstel, U., Morr, M. & Römling, U. Hierarchical involvement of various GGDEF domain proteins in rdar morphotype development of *Salmonella enterica* serovar Typhimurium. *Mol Microbiol* **60**, 602-616 (2006).
461. Galperin, M.Y., Higdon, R. & Kolker, E. Interplay of heritage and habitat in the distribution of bacterial signal transduction systems. *Molecular BioSystems* **6**, 721-728 (2010).
462. Detweiler, C.S., Monack, D.M., Brodsky, I.E., Mathew, H. & Falkow, S. *virK*, *somA* and *rcsC* are important for systemic *Salmonella enterica* serovar Typhimurium infection and cationic peptide resistance. *Mol Microbiol* **48**, 385-400 (2003).
463. Clarke, D.J., Joyce, S.A., Toutain, C.M., Jacq, A. & Holland, I.B. Genetic Analysis of the RcsC Sensor Kinase from *Escherichia coli* K-12. *J. Bacteriol.* **184**, 1204-1208 (2002).
464. Rogov, V.V. et al. A New Structural Domain in the *Escherichia coli* RcsC Hybrid Sensor Kinase Connects Histidine Kinase and Phosphoreceiver Domains. *J Mol Biol* **364**, 68-79 (2006).
465. Stout, V. & Gottesman, S. RcsB and RcsC: a two-component regulator of capsule synthesis in *Escherichia coli*. *J. Bacteriol.* **172**, 659-669 (1990).
466. Girgis, H.S., Liu, Y., Ryu, W.S. & Tavazoie, S. A Comprehensive Genetic Characterization of Bacterial Motility. *PLoS Genet* **3**, e154 (2007).
467. Majdalani, N., Heck, M., Stout, V. & Gottesman, S. Role of RcsF in Signaling to the Rcs Phosphorelay Pathway in *Escherichia coli*. *J. Bacteriol.* **187**, 6770-6778 (2005).
468. Majdalani, N., Hernandez, D. & Gottesman, S. Regulation and mode of action of the second small RNA activator of RpoS translation, RprA. *Mol Microbiol* **46**, 813-826 (2002).

469. Gervais, F.G. & Drapeau, G.R. Identification, cloning, and characterization of *rcsF*, a new regulator gene for exopolysaccharide synthesis that suppresses the division mutation ftsZ84 in *Escherichia coli* K-12. *J. Bacteriol.* **174**, 8016-8022 (1992).
470. Paolo, L. Cross-talk mechanisms in biofilm formation and responses to environmental and physiological stress in *Escherichia coli*. *Res Microbiol* **160**, 259-266 (2009).
471. Beloin, C. et al. Global impact of mature biofilm lifestyle on *Escherichia coli* K-12 gene expression. *Mol Microbiol* **51**, 659-674 (2004).
472. Waters, C.M., Lu, W., Rabinowitz, J.D. & Bassler, B.L. Quorum Sensing Controls Biofilm Formation in *Vibrio cholerae* through Modulation of Cyclic Di-GMP Levels and Repression of vpsT. *J. Bacteriol.* **190**, 2527-2536 (2008).
473. Sinha, K., Mastroeni, P., Harrison, J., de Hormaeche, R.D. & Hormaeche, C.E. *Salmonella* typhimurium *aroA*, *htrA*, and *aroD* mutants cause progressive infections in athymic (nu/nu) BALB/c mice. *Infect. Immun.* **65**, 1566-1569 (1997).
474. Johnson, K.S. et al. The role of a stress-response protein in bacterial virulence. *Res Microbiol* **141**, 823-825.
475. Lowe, D.C. et al. Characterization of candidate live oral *Salmonella* typhi vaccine strains harboring defined mutations in *aroA*, *aroC*, and *htrA*. *Infect Immun* **67**, 700-707 (1999).
476. Wagner, J.K., Galvani, C.D. & Brun, Y.V. *Caulobacter crescentus* Requires RodA and MreB for Stalk Synthesis and Prevention of Ectopic Pole Formation. *J. Bacteriol.* **187**, 544-553 (2005).
477. Popham, D.L. & Young, K.D. Role of penicillin-binding proteins in bacterial cell morphogenesis. *Curr Opin Microbiol* **6**, 594-599 (2003).
478. Nakayama, S.I. et al. Activation of *hilA* expression at low pH requires the signal sensor CpxA, but not the cognate response regulator CpxR, in *Salmonella enterica* serovar Typhimurium. *Microbiology* **149**, 2809-2817 (2003).
479. Todar, K. (2008). "Todar's Online Textbook of Bacteriology." from http://www.textbookofbacteriology.net/index.html.
480. Paul, W. Role of the cell envelope in bacterial adaptation to growth in vivo in infections. *Biochimie* **70**, 987-1011 (1988).
481. Seltmann, G. & Holst, O. The bacterial cell wall. (Springer, 2002).
482. Osborne, S. & Coombes, B. RpoE fine tunes expression of a subset of SsrB-regulated virulence factors in *Salmonella enterica* serovar Typhimurium. *BMC Microbiology* **9**, 45 (2009).
483. Domka, J., Lee, J., Bansal, T. & Wood, T.K. Temporal gene-expression in *Escherichia coli* K-12 biofilms. *Environmental Microbiology* **9**, 332-346 (2007).
484. Sledjeski, D.D. & Gottesman, S. Osmotic shock induction of capsule synthesis in *Escherichia coli* K-12. *J. Bacteriol.* **178**, 1204-1206 (1996).
485. Magnusson, L.U., Farewell, A. & Nyström, T. ppGpp: a global regulator in *Escherichia coli*. *Trends in Microbiology* **13**, 236-242 (2005).
486. Costanzo, A. & Ades, S.E. Growth Phase-Dependent Regulation of the Extracytoplasmic Stress Factor, σ^E, by Guanosine 3',5'-Bispyrophosphate (ppGpp). *J. Bacteriol.* **188**, 4627-4634 (2006).
487. Castanie-Cornet, M.-P., Cam, K. & Jacq, A. RcsF Is an Outer Membrane Lipoprotein Involved in the RcsCDB Phosphorelay Signaling Pathway in *Escherichia coli*. *J. Bacteriol.* **188**, 4264-4270 (2006).
488. Erickson, K.D. & Detweiler, C.S. The Rcs phosphorelay system is specific to enteric pathogens/commensals and activates *ydeI*, a gene important for persistent *Salmonella* infection of mice. *Mol Microbiol* **62**, 883-894 (2006).
489. Taghbalout, A. & Rothfield, L. New insights into the cellular organization of the RNA processing and degradation machinery of *Escherichia coli*. *Mol Microbiol* **70**, 780-782 (2008).
490. Khemici, V., Poljak, L., Luisi, B.F. & Carpousis, A.J. The RNase E of *Escherichia coli* is a membrane-binding protein. *Mol Microbiol* **70**, 799-813 (2008).

491. Taghbalout, A. & Rothfield, L. RNaseE and the other constituents of the RNA degradosome are components of the bacterial cytoskeleton. *Proceedings of the National Academy of Sciences* **104**, 1667-1672 (2007).
492. Taghbalout, A. & Rothfield, L. RNaseE and RNA Helicase B Play Central Roles in the Cytoskeletal Organization of the RNA Degradosome. *J Biol Chem* **283**, 13850-13855 (2008).
493. Danese, P.N. & Silhavy, T.J. The σ^E and the Cpx signal transduction systems control the synthesis of periplasmic protein-folding enzymes in *Escherichia coli*. *Genes & Development* **11**, 1183-1193 (1997).
494. Heusipp, G., Nelson, K.M., Schmidt, M.A. & Miller, V.L. Regulation of *htrA* expression in *Yersinia enterocolitica*. *FEMS Microbiol Lett.* **231**, 227-235 (2004).
495. Danese, P.N., Snyder, W.B., Cosma, C.L., Davis, L.J. & Silhavy, T.J. The Cpx two-component signal transduction pathway of *Escherichia coli* regulates transcription of the gene specifying the stress-inducible periplasmic protease, DegP. *Genes & Development* **9**, 387-398 (1995).
496. Baranova, N. & Nikaido, H. The *baeSR* two-component regulatory system activates transcription of the *yegMNOB* (*mdtABCD*) transporter gene cluster in *Escherichia coli* and increases its resistance to novobiocin and deoxycholate. *J Bacteriol.* **184**, 4168-4176 (2002).
497. Yoon, H., Lim, S., Heu, S., Choi, S. & Ryu, S. Proteomic analysis of *Salmonella enterica* serovar Typhimurium *fis* mutant. *FEMS Microbiol Lett.* **226**, 391-396 (2003).
498. Iwai, N., Fujii, T., Nagura, H., Wachi, M. & Kitazume, T. Structure-activity relationship study of the bacterial actin-like protein MreB inhibitors: effects of substitution of benzyl group in *S*-Benzylisothiourea. *Biosci. Biotechnol. Biochem.* **71**, 246-248 (2007).
499. Ferrières, L., Aslam, S.N., Cooper, R.M. & Clarke, D.J. The *yjbEFGH* locus in *Escherichia coli* K-12 is an operon encoding proteins involved in exopolysaccharide production. *Microbiology* **153**, 1070-1080 (2007).
500. Weintraub, A. Immunology of bacterial polysaccharide antigens. *Carbohydrate Research* **338**, 2539-2547 (2003).